The Connectome of the Larval Brain of *Ciona intestinalis* (L.).

by

Kerrianne Ryan

Submitted in partial fulfilment of the requirements
for the degree of Doctor of Philosophy

at

Dalhousie University
Halifax, Nova Scotia
December 2015

Dedication

To Science
To Art
To Music
To the pursuit of understanding of everything around us
To Learning
To Sharing
To Life

Table of Contents

List of Tables

List of Figures

Abstract

The anatomical substrate for animal behaviour is founded on the circuits of synaptic connections formed by the brain's neurons. Small nervous systems allow us to examine the entirety of a nervous system in comprehensive detail, revealing details of both the neurons' ultrastructure and their synaptic networks. This study uses serial-section EM (ssEM) as an anatomical connectomic approach to analyze the number and distribution of synapses within the networks of the larval brain of the ascidian *Ciona intestinalis*. There are 166 neurons in a single larva studied. These form at least 32-50 cell types, and 8,390 synapses. Instances of sidedness include stronger connections for left-side neurons and the lack of left-side neurons corresponding to those on the right.

Neurons are mostly monopolar with <25% having dendrites, and their axons usually form an obvious terminal. Dense reconstruction of the entire CNS reveals all cells, unlike studies that use reporter genes to reveal morphological forms of selected neurons in their entirety, but fail to identify unlabelled neighbours, which are a majority. The completed larval connectome reveals that Cajal's Dynamic Law of Polarization is widely violated, many synapses forming between axons (axo-axonic synapses) and terminals (axo-terminal synapses), especially among relay interneurons, rather than onto dendrites or somata. Thus, presynaptic sites are most commonly located over axons or their terminals, while dendrites and somata are heterodoxically presynaptic. In contrast, terminals of sensory neurons bear most of the neurons' presynaptic sites. Synaptic structure is sometimes unpolarised, with synaptic vesicles situated opposite each other, neurons so connected forming both reciprocal and serial synapses.

Larval responses to environmental cues rely on the network of underlying neuronal connections that translates these cues into motion. The anatomical connectome reveals the components and connections of pathways for sensory integration of visual, gravity, and peripheral information both to and from pathways of other sensory systems. These sensory pathways feed into motor networks reported here that are involved in central pattern generation and a putative escape response. The network complexity of the larval brain of *Ciona intestinalis* is considerable compared with the reported simplicity of larval behaviour and the number of neurons.

List of Abbreviations and Symbols Used

°	Degree (angle)
°C	degrees celsius
5HT	5-hydroxytryptamine (serotonin)
aaIN	anaxonal arborizing interneuron
aATEN	anterior Apical Trunk Epidermal Neuron
ACh	acetylcholine
ACIN	Ascending Contralateral Inhibitory Neuron
ant	antenna neuron
antIN	antenna interneuron
antRN	antenna relay neuron
ASNET	Ascidian Dendritic Network in Tunic
AVG	ascending motor ganglion interneuron
BV	Brain Vesicle (also known as sensory vesicle)
C	Canal
Ca2+	Calcium
ChaT	Choline acetyltransferase
CNC	Caudal Nerve Cord
CNS	Central Nervous System
cor	coronet cell
DA	Dopamine
DCEN	Dorsal Caudal Epidermal Neuron
ddN	descending decussating paired MG interneuron
DNA	Deoxyribonucleic acid
Emx	Family of homeobox transcription factor genes
Ep	Ependymal cell
EST	Expressed sequence tag
FGF	Fibroblast Growth Factor
GABA	Gamma-Aminobutyric Acid
GAD	Glutamate decarboxylase
GJ	Gap junction
Glut	Glutamate
Gly	Glycine
Hb9/Mnx	Motorneuron and pancreas homeobox 1 gene
Hh	Hedgehog gene
Hoxb1	Homoeobox gene b1
hpf	hours post fertilizations
Hz	Hertz
ISL	Islet (insulin enhancer) gene
L	the left side of the animal
Lhx	Lim/Homeobox gene (containing Lim domain)
MAGUK	Membrane-associated guanylate kinase gene family
MASC	N-methyl-d-aspartate receptor complex/MAGUK associated signalling complex
MG	Motor Ganglion (also known as visceral ganglion)

ml	millileters
mmIN	multimodal interneuron (receiving input from multiple sensory neuron types)
MN	Motor neuron of the motor ganglion
mt	mid-tail paired descending motoneuron
Nkx2.2	Homeodomain gene
nm	nanometers
Not	Notochord
Not	A homeodomain gene
NT	neurotransmitter
oacc	Otolith associated ciliated cell
Oc	Ocellus
Olig	Oligodendrocyte transcription factor gene
Ot	Otolith
pATEN	posterior Apical Trunk Epidermal Neuron
Pax	Paired box homeodomain gene
Phox	Paired-like homoeobox gene
Plan	Planate neuron (also known as Bipolar tail neurons)
PNS	Peripheral Nervous System
pr	photoreceptor
prIN	photoreceptor interneuron
PSD	Postsynaptic density
PVGN	posterior unpaired right-side interneuron at the motor ganglion/tail boundary
R	The right side of the animal
RN	relay neuron
RNA	Ribonucleic acid
RTEN	Rostral Trunk Epidermal Neuron
Rx	Retinal homeobox gene
ssEM/ssTEM	serial section transmission electron miscroscopy
TALEN	Transcription activator-like effector nuclease
TEM	Transmission Electron Microscope
TH	Tyrosine Hydroxylase
trIN	photoreceptor tract interneuron
vAChT/vAChTP	Vesicular acetylcholine transporter
Vax	Ventral anterior homeobox gene
VCEN	Ventral Caudal Epidermal Neuron
VG/VGN/VIN	Descending ipsilateral paired MG interneuron
vGAT	vesicular GABA transporter
vGLUT	vesicular glutamate transporter
µm	micrometers

Acknowledgements

I would first and foremost like to thank my supervisor Ian Meinertzhagen for his mentorship throughout my PhD, and for encouraging me to be independent and to think in new ways to challenge myself. Next, this project would not have been possible without the tremendous skills of Zhiyuan Lu, who worked tirelessly in cutting the extensive series and was always ready to discuss approaches, techniques and future directions in the field of anatomical connectomics. Jane Anne Horne also provided invaluable technical support throughout the course of my program, and prevented many possible meltdowns over technical glitches. Several undergraduates in the Meinertzhagen lab also contributed to the project through tracing and cataloguing efforts, foremost among these was Ms Carlie Langille who was always quick to problem solve and was both diligent and timeless in her work ethic. I would also like to thank all members of the lab who supported and encouraged me throughout this long arduous process.

I would next like to acknowledge my family and friends who were with me through this entire journey, and my boyfriend who helped me survive the last few years. In particular, I want to thank my mother for being an endless font of encouragement, support, knowledge, and understanding, and for being an amazing role model.

Finally, I must thank all the *Ciona* that contributed to this massive undertaking, and all members of the ascidian community for being supportive, encouraging and engaging when welcoming me into their research network.

Chapter 1 : Introduction

1.1 General Introduction

1.1.1 *Ciona intestinalis*:

Model animal species allow us to explore accessible biological systems to gain a deep understanding of their processes. That understanding is enabled by genomic information and associated molecular methods and is applied to cell populations in which the architecture, development and physiology are already well characterized. Model species include in particular two model invertebrates, *C. elegans* and *Drosophila melanogaster*, both species of protostomes. Traditional metazoan phylogeny classifies vertebrates as a subphylum of the phylum Chordata, which share tadpole-type larvae containing a notochord and hollow nerve cord, together with two other subphyla, the Urochordata (Tunicata) and the Cephalochordata. A recent revision to this scheme now elevates vertebrates to their own phylum, with Urochordates and Cephalochordates as sister phyla (Satoh et al., 2014). A member of the Urochordata, *Ciona intestinalis* (L.) is an invertebrate deuterostome that provides us with a third model species.

Ciona intestinalis, is an invasive species of sea squirt, which is hermaphroditic but self-sterile (Kawamura et al., 1991). The sessile adult filter feeder releases eggs and sperm into the surrounding seawater where non-self external fertilization and development occurs in the water column (Fig. 1.1). Cleavage and early development are both rapid and temporally and spatially determinate, resulting in a fixed lineage of cells that arises by radial cleavage (Conklin, 1905), making the embryo an attractive model for experimental embryology. The lineage of the CNS from the neural plate has been traced

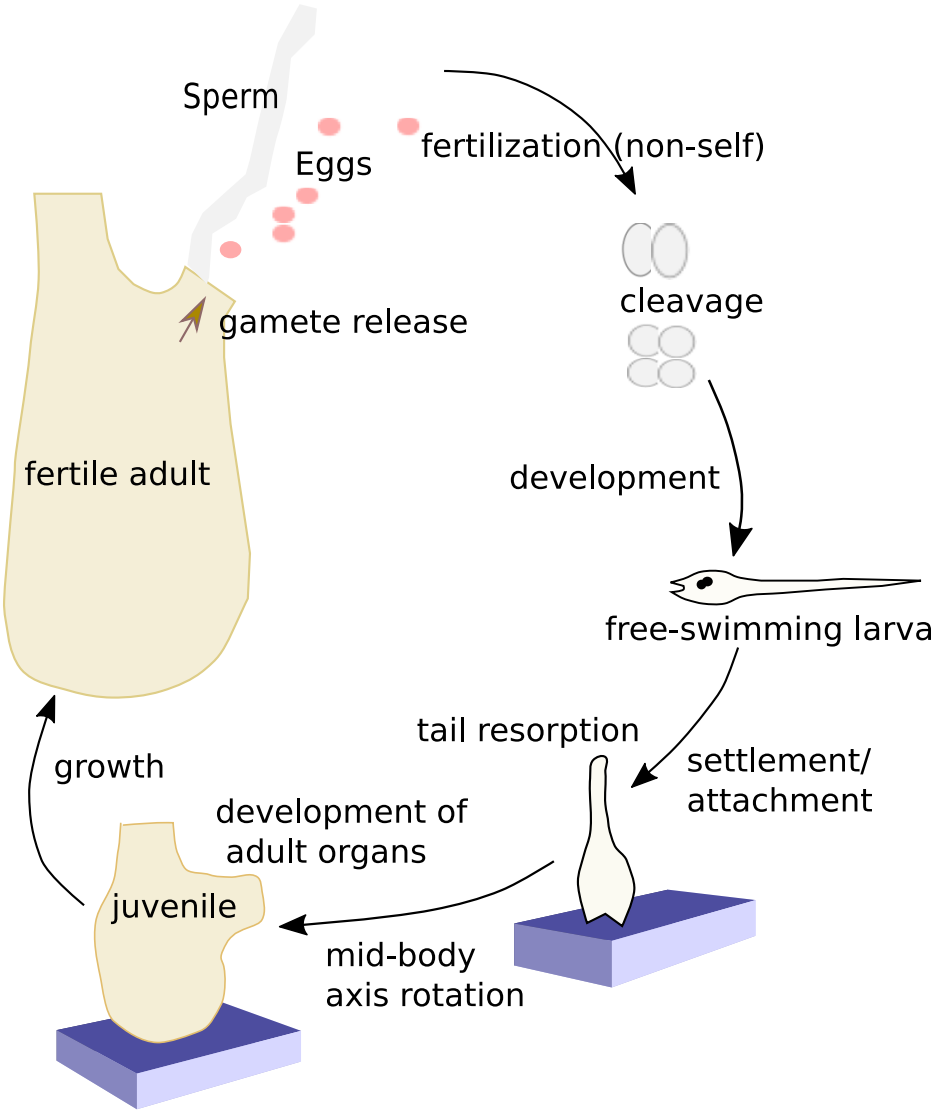

Figure 1.1. The life cycle of *Ciona intestinalis*. Adult *Ciona* release gametes that mix in the water column with gametes from other individuals, and undergo fertilization, cleavage and development to form the free-swimming larva. Larvae swim for 1-3 days until they undergo settlement trunk down on an appropriate substrate, at which point their tails are resorbed, adult organs develop, and the body axis rotates producing the juvenile form. Juveniles then begin to filter-feed and grow into adults.

to the 14th generation, one or two generations before the larval neurons are generated (Cole and Meinertzhagen, 2004), although the lineage of most larval neurons has still not been followed from the preceding final division.

As a urochordate, *Ciona intestinalis* is a member of a sister group of vertebrates (Graham et al., 2004) (Fig. 1.2), sharing homologies with many vertebrate features in both its larval and adult stages (Bone and Ryan, 1978; Shimeld and Holland, 2000; Manni et al., 2001; Lemaire et al., 2002; Meinertzhagen et al., 2004; Deyts et al., 2006; Manni et al., 2006; Stolfi et al., 2011). In particular, the ascidian larval form follows a typical chordate body plan, with a dorsal hollow nerve cord overlying its notochord. Although ascidians are diverse, and their phylogenetic relationships remain unresolved (Fig. 1.1), they share these vertebrate features and many similarities in the composition of their nervous systems, described later in this thesis.

In addition to the phylogenetic position of *Ciona intestinalis* (Fig. 1.2), its genome was sequenced and reported early (Dehal et al., 2002), and has allowed a thorough examination of the *Ciona* transcriptome, producing an extensive cDNA library (Satou et al., 2002) and large-scale EST (expressed sequence tag) (Satou et al., 2003) in situ hybridization screens (Satou et al., 2001b). The combination of these data with methods for: high throughput electroporation of promoter and enhancer constructs (Corbo et al., 1997) into eggs; mutation by morpholino injection (Satou et al., 2001a); more recent proteomic (Inaba et al., 2007) and targeted knock-down studies using both TALEN (Treen et al., 2014) and CrispR-Cas9 (Sasaki et al., 2014; Stolfi et al., 2014); as well as reversible methods employing channel rhodopsin (Nagel et al., 2003; Horie et al., 2015,

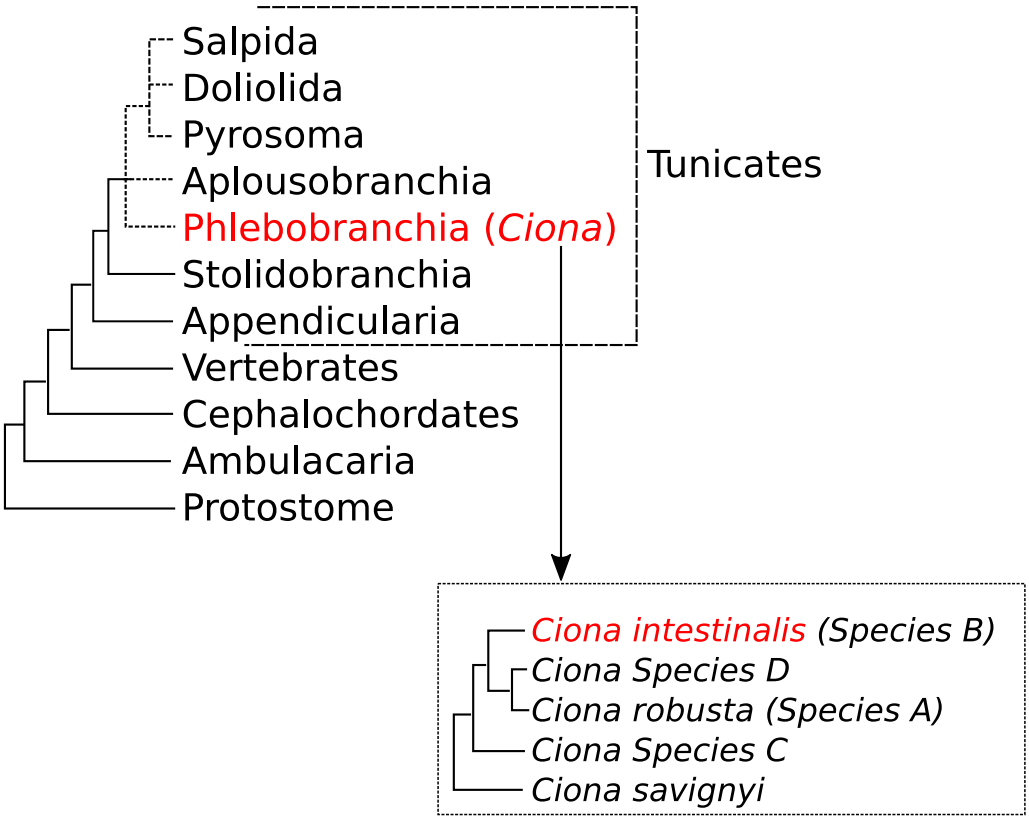

Figure 1.2. Phylogenetic cladogram (adapted from Lemaire, 2011) showing position of *Ciona intestinalis* in relation to other animal groups. Note the common ancestry of tunicates and vertebrates, and the tentative relationships among tunicates (indicated by dashed lines). A cladogram of relationships within Phlebobranchia (adapted from Zhan et al., 2015), illustrates that *Ciona intestinalis* (L.) shares a common ancestor with other members of its species complex (now defined as unique species), all of which share a common ancestry with *Ciona savignyi*.

pers comm.), make *Ciona intestinalis* a powerful model organism (reviewed in Stolfi and Christiaen, 2012). Thus, underwriting a rapidly expanding literature on this species. Of its many advantages as an experimental animal, the ascidian larva of the urochordate subphylum provides us with an opportunity to examine a tiny nervous system with relatively few neurons, one that nevertheless shares its form of central nervous system (CNS) with the much larger and more complex vertebrate CNS (Meinertzhagen et al., 2004). Like vertebrates, ascidians' dorsal hollow nerve cord has an anterior sensory region, and a more posterior motor component and caudal nerve cord overlying its notochord, which is flanked on either side by muscle cells (Fig. 1.3). Despite containing only a reported ~300 cells in its CNS (Nicol and Meinertzhagen, 1991), the tadpole larva of *Ciona intestinalis* exhibits behavioural responses to light (Kawakami et al., 2002; Tsuda et al., 2003; Inada et al., 2003; Zega et al., 2006), gravity (Tsuda et al., 2003; Zega et al., 2006), mechanical (Brown et al., 2005; Brown, pers. comm.) and chemical (Svane and Young, 1989) cues during its free-swimming period of 1-3 days. The lecithotropic larva uses these cues to identify and settle on an appropriate substrate, and then undergoes metamorphosis into its adult form, which retains little of the larval CNS and lacks the typical chordate form (Cloney, 1978; Horie et al., 2011).

The development time and larval period vary with temperature, but a high percentage of fertilization and hatching occur at 18°C (Patanasatienkul et al., 2014), the standard experimental rearing temperature in the lab. The larvae hatch 18 hours after fertilization at 18°C and swim for 4-5 hours before becoming competent to settle and undergo metamorphosis into their adult form (Horie et al., 2005; Nakayama et al., 2005). Although Svane and Havenhand (1993) report no requirement for a pre-competence

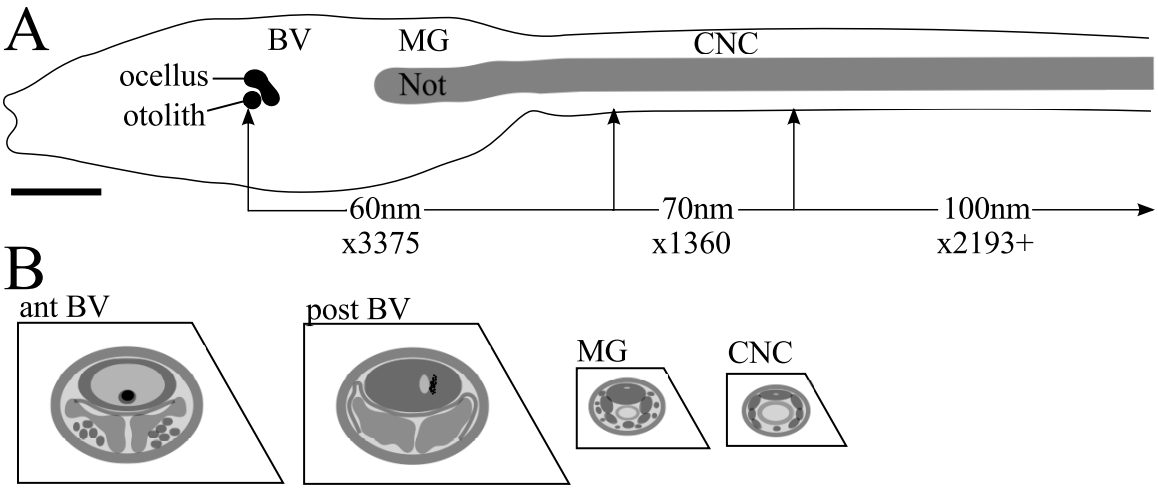

Figure 1.3. Sectioning of *Ciona intestinalis* larva, its CNS and notochord. A) Diagram of larva illustrating major landmarks and sectioning thickness along its A-P axis, indicating the number of sections of each thickness (60-100nm). BV: brain vesicle; n: neck; MG: motor ganglion; Not: notochord; CNC: caudal nerve cord. Scale bar: 50μm. B) Diagrams of representative sections through the different regions of the larva, scaled in proportion to each other.

period in *Ciona intestinalis* larvae before they are able to settle, laboratory experiments reveal that a period of several hours before metamorphosis is retained even in mutant larvae in which normal cues for metamorphosis are forced at earlier stages (Matsunobu, 2015, pers. Comm.). In the wild, larvae can live as long as 1.5 days before undergoing metamorphosis (Svane and Havenhand, 1993). During their free-swimming period, the swimming behaviour of such larvae includes single-sided tail flicks that turn larvae 90° (Bone, 1992) at 10Hz (Zega et al., 2006), spontaneous symmetrical alternating tail contractions in a whip like motion at 15-50Hz (Bone, 1992), later recorded for spontaneous swimming as either 20 Hz (Zega et al., 2006), or faster 30Hz alternating symmetrical tail contractions in response to the dimming of incident light (Kawakami et al., 2002; Zega et al., 2006). The latter so-called shadow response behaviour begins 1.5 hours post hatching (Zega et al., 2006) at 20°C and 3-4 hours post hatching at 18°C (Tsuda et al., 2003; Horie et al., 2005), corresponding to the time when the larva's photoreceptor terminals undergo expansion (Horie et al., 2005). Behaviour related to orientation of larvae has also been reported in response to ablation or mutation experiments that have an impact upon the otolith (Tsuda et al., 2003; Sakurai et al., 2004) and in response to chemical or physical settlement cues (Svane et al., 1987).

The motor system driving this swimming behaviour utilizes cholinergic transmission (Ohmori and Sasaki, 1977), resulting in tail contractions driving swimming behaviour that occur practically simultaneously in all muscle cells of each side (Bone, 1992). These comprise 36 cells in total (Katz, 1983) that are not segmented; all cells on each side are connected via gap junctions (Bone, 1992). Input from motor neurons to muscle occurs on the dorsal and medial muscle cells (Bone, 1992), where nicotinic acetylcholine receptors

may provide a mechanism for graded excitation-contraction (Nishino, 2011). Taken together, the evidence indicates that excitation of the muscle cells of these larvae occurs via cholinergic motor neurons of the Motor Ganglion (MG). Although the networks integrating the sensory information into behaviour are not yet characterized, the small size of *Ciona intestinalis* larvae make it an excellent candidate for such analysis, for which a comprehensive anatomical analysis of its neural networks using serial section electron microscopy (ssEM) is first required. The resulting anatomical 'connectome' mapping all synaptic connections between cells of the larval CNS, would as a result join that of *C elegans* as only the second complete connectome of any nervous system.

1.1.2 Connectomics:

Brain functions have long been postulated based on partial or theoretical data that in many cases reveal only the ultimate outcome of circuits rather than the actual network of circuits that generate such outcomes. Models of how brains function often assume a simple designer-centered structure that ignores the fact that the brain's networks and biological functions are products of evolution that have arisen through adaptation and co-option, not by de novo design. Thus, knowing the actual structure of neural circuits in its entirety enables us to see what the brain's true networks comprise rather than what an intelligent engineer would put there if s/he were trying to achieve the same outcome. In response to this need, the field of connectomics has recently been identified, so as to identify structural circuits not only by identifying neurons and their connections, but also by creating a map of their locations and orientations (Lichtman, 2008). Although this is not a new idea (see Horridge, 1968), it is now enabled by new digital technologies, especially for imaging.

Anatomical connectomics is delimited by the fact that most synapses can only be observed at the EM, and so this level of resolution is required to catalogue neurons and their synaptic connections (Lichtman et al., 2008). Neurons can then be identified and reconstructed either or sparsely, as single elements, or can be reconstructed densely, as one of an entire volume of the brain. Although both dense and sparse reconstruction and annotation can be undertaken using serial-section TEM, ssTEM (or emerging techniques of block-face and Focused Ion Beam milling), sparse reconstruction methods, although more rapid, may misassign or miss branches and may provide only partial information about pre- or postsynaptic partners. In contrast, dense reconstruction allows us to collect and catalogue data on all cells and connections in a brain or brain region. "No cell can hide" in dense reconstruction, which allows us to not only propose functional circuits, but to falsify predicted circuits that lack a structural substrate (Denk, 2012). Although sectioning, imaging, aligning, tracing and annotating even a single connectome is time-consuming, the method is exhaustive and not only provides a substrate for future comparisons, but even a single connectome is valuable in ascertaining which circuits are present in a functional brain, permitting evaluation of existing theoretical models or predicted computational outcomes (Denk, 2012). Of course, an anatomical network does not alone reveal function; it lacks all information in the temporal realm. Its significance is twofold, in being interpretative, enabling the interpretation of data on network function, and predictive, in identifying possible interactions for which a pathway may exist but no interaction yet sought. The benefit of small brains, like that of larval *Ciona intestinalis*, is that it is feasible to generate a connectome for multiple animals, especially with the recent advances in techniques related to all steps in the process of image

collection and annotation (Lichtman, 2008; Denk, 2012; Plaza et al., 2014). Multiple connectomes of the same circuits then allow us to identify the level of precision in network wiring (Takemura et al., 2015).

1.1.3 *Ciona intestinalis* as a connectome model species:

Once thought to be like 'a chordate *C. elegans'* mostly because of its invariant pattern of early cleavage (Meinertzhagen and Okamura, 2001; Meinertzhagen et al., 2004), *Ciona intestinalis* larva are now known to exhibit plasticity and characteristics that suggest some variability. With respect to its nervous system, this phenotypic plasticity means that the rearing conditions and sensory exposure may affect neuronal connectivity and numerical composition. While such phenotypic plasticity may seem disadvantageous, it better reflects the state of many other known nervous systems, and allows a documented substrate for studying such plasticity. Furthermore, *Ciona*'s simple canonical larval behaviours can be readily observed and manipulated in the lab. Although calcium imaging is now a working functional method in larval *Ciona* (Horie, 2015, pers comm.), we still await a method that offers millisecond resolution of neuronal activity underlying these behaviours. Anatomical connectomics provides us with the important knowledge of where to target examination of ascidian neural circuits because it not only resolves the diversity of cell types it does so at a resolution compatible with their physical dimensions at synapses, as well as revealing all connections in all pathways (Lichtman and Denk, 2013). Thus, unlike the standard ''hypothesis-driven'' research with a focus on analyzing biological mechanisms over phenomenon, the work presented here, as in other connectomic studies, is primarily ''hypothesis generating'' and more in the tradition of systems biology (Varshney et al., 2011).

The methods that apply to all sections of this thesis are presented directly below, and are not repeated in subsequent chapters. This thesis first addresses the ultrastructural and anatomical synaptic properties revealed through ssEM. Cells and cell types identified in the connectome are then compared with reports in the literature to identify putative neurotransmitter phenotype where possible. The proceeding three chapters (Chapters 5-7) discuss the three main sensory input pathways in the larval nervous system: visual, gravity sensing, and mechanosensory/chemosensory. After addressing sensory pathways and integration, Chapters 8-10 address the cell types and networks of the motor ganglion and tail, with particular focus on the distinction between reticulospinal and spinal neurons, the identification of a putative central pattern generator controlling swimming behavior, and a putative startle-response pathway through a Mauthner-like neuron. Finally, general conclusions are presented, emphasizing the future of the field of connectomics and of our understanding of the nervous system of *Ciona intestinalis* larvae.

1.2 **Methods**

1.2.1 Animals:

Adult animals, *Ciona intestinalis* (L.), were collected by Peter Darnell from Mahone Bay, Nova Scotia. Adults were kept under constant illumination in tanks at the Aquatron facility of Dalhousie University, with water flow (between 5 and 6 L/min) at ~18 ^{o}C. Adults kept for 1-5 days were removed from the tank and dissected to expose the oviduct and sperm duct. Eggs were collected from the oviduct using a pipette and placed in Petri dishes containing seawater filtered through a Nalgene 0.2 μm syringe filter. Animals were then washed with seawater and the sperm duct pierced with a pipette and sperm

sucked directly into the pipette and placed in a microcentrifuge tube. Sperm from one hermaphrodite parent was added two drops at a time into a Petri dish containing eggs from a different hermaphrodite parent and the dish was gently swirled to distribute the sperm to ensure cross-fertilization. Eggs and sperm were left for 15 min for fertilization to occur, and then eggs were rinsed several times with filtered seawater and placed in a Petri dish with filtered seawater, wrapped in aluminum foil, and placed in an incubator at 18^{o}C.

1.2.2 Fixation:

Larvae were removed from the incubator after 20 h, and two-hour larvae (21 h post fertilization) reared at 18^{o}C in the dark were fixed at 4^{o}C for 2 h in 1% OsO_4 in 0.2M Na_2PO_4 (phosphate buffer) adjusted to pH 7.2 with HCl. This stage was chosen based on the previously reported timing of larval behaviours and to retain consistency with previous studies from the Meinertzhagen laboratory that counted and characterized the cells of the CNS (Nicol, 1987; Stanley McIsaac, 1997). Likewise, the fixation method was the same as that used for those previous studies because other fixation protocols that were attempted and checked resulted in poor penetration. Animals were then transferred to a post-fixation solution containing 2% glutaraldehyde in 0.2M phosphate buffer for 1 h at 4^{o}C. Fixed specimens were then dehydrated in an ethanol series (as shown in Appendix A). After dehydration, specimens were placed in a dish containing equal parts of propylene oxide (PO) and Epon 812 overnight at room temperature. Sibling larvae were then transferred to 100% Epon for 3 h and then placed in fresh dish containing 100% Epon and placed in a 60^{o}C oven for 48 h to polymerize.

1.2.3 Sectioning:

Larvae were sectioned and checked for acceptable fixation, then a single larva within a block of Epon was cut from the disc containing sibling larvae and an ultrathin series of 60-nm cross sections starting at the level of the otolith pigment (Fig. 1.3) was cut by Mr. Zhiyuan Lu using a Leica EM UC7 and then a Leica Ultracut UCT ultramicrotome using a 2 mm Diatome diamond knife. This series extended to the posterior motor ganglion (Fig. 1.3), and was later extended by additional cross sections cut through the tail at a thickness of 70 nm in the anterior, and then 100nm to the tip of the tail (Fig. 1.3). All sections were post-stained for 5-6 min in freshly prepared aqueous uranyl acetate followed by 2-3 min in lead citrate.

1.2.4 Imaging, Montaging and Alignment:

Sections were viewed using an FEI Tecnai 12 electron microscope operated at 80kV and images were captured using initially a Kodak Megaview II camera with software (AnalySIS: SIS GmbH, Münster, Germany), and later a Gatan 832 Orius SC1000 CCD camera using Gatan DigitalMicrograph software. High magnification sections with a resolution of 260 pixels per μm (3.85 nm per pixel) were collected for the neuropil region of each section. The profile area encompassing neuropil ranged from five 5x5 montages per section at the largest areas in the posterior BV to single 2x2 montages per section in the tail. In addition, lower magnification images with a resolution of 72 pixels per μm (13.9 nm per pixel) of the entire CNS and overlying epidermis were collected for every section in the anterior BV, and for every fourth section through the posterior brain vesicle, neck, motor ganglion and anterior tail (Fig. 1). In the tail because the entire CNS

was visible in the high magnification series, only the first and last sections on each grid were imaged at low magnification.

Montages were obtained using image shift-beam shift and compiled automatically with the Gatan DigitalMicrograph software or with AnalySIS. Maximum automatic montage dimensions for Gatan DigitalMicrograph software were 5x5 (consisting of 25 single-frame images), which did not cover the entire area in some regions, so that software-generated montages were manually compiled in Adobe Photoshop. All images were also converted to gray scale and adjusted to appropriate resolution using Adobe Photoshop to ensure accurate calculations and alignment when importing into the Reconstruct software (version 1.1.0.0 publicly available at http://synapses.bu.edu/) used to render cells in three dimensions (Fiala and Harris, 2001). Images were imported into either a high magnification or low magnification series in Reconstruct, and every section manually aligned using this software.

1.2.5 Tracing and Annotation:

All profiles in every third section were then traced completely, except in sections where traces could not be confirmed from the traces of previous sections, in which case every section was then traced. In the high magnification series traces were hidden and all sections were then blindly annotated for synapses, putative gap junctions, dense-core vesicles, multivesicular bodies, autophagosomes and cilia. Specific examples of these are illustrated in Figs. 2.3 and 2.4 of Chapter 2. Traces were then made visible and annotated elements were assigned to specific pre- and postsynaptic elements. Blind annotation was duplicated in 100 section blocks by an independent annotator (Ms Carlie Langille). Most annotations of each viewer duplicated existing synaptic contacts seen by the other, but

neither viewer annotated a synapse between two partners that did not replicate a synapse formed elsewhere by the same two cells. Of the differences observed, 95% were simply differences between the numbers of sections in which a synapse was observed at existing annotated synapses. Synapses from pairs of neurons, and neurons of the same class were also compared, but these provided unreliable comparisons in a single specimen. Synapses were identified based on the criteria established in *C. elegans* (White et al., 1986) of a cluster of vesicles concentrated at a presynaptic membrane. Although postsynaptic densities were observed at some synapses (Gray, 1959; Peters and Palay, 1996) these were not present at all, so did not provide an exclusive criterion. Synapse validity and quantification was established by comparing the total number of sections in which a synapse was observed between partners (Fig. 1.4). Putatively identified gap junctions were annotated where apposing membranes approached each other with densities present on the membranes of both sides, except where these contacts were directly adjacent to the neural canal. This excluded junctions provisionally interpreted as desmosomes or adherens junctions around the neural canal.

1.2.6 Network analysis:

Network graphs were created using Cytoscape 3.0.1. Synaptic and gap junction data were imported from standard .csv files including all connections, with both direction of synapse, total number of connections and total number of sections in which connections were observed. Nodes representing neurons and edges representing synapses or gap junction were coloured by cell type, and edge thickness was associated to either total number of synapses or gap junctions, or total number of sections in which synapses or gap junctions between partners were observed in ssEM (as indicated in figure legend).

A

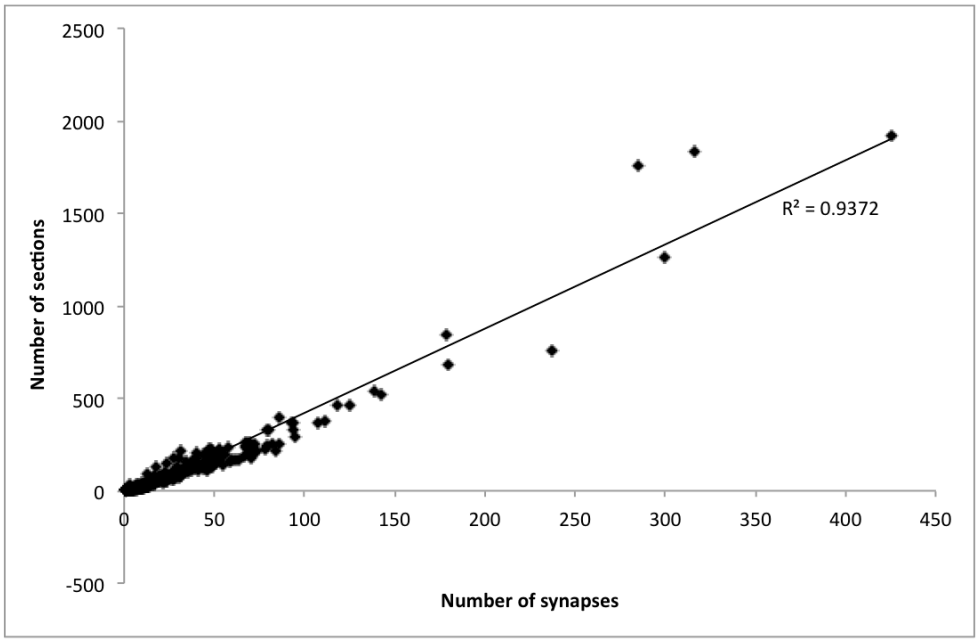

B

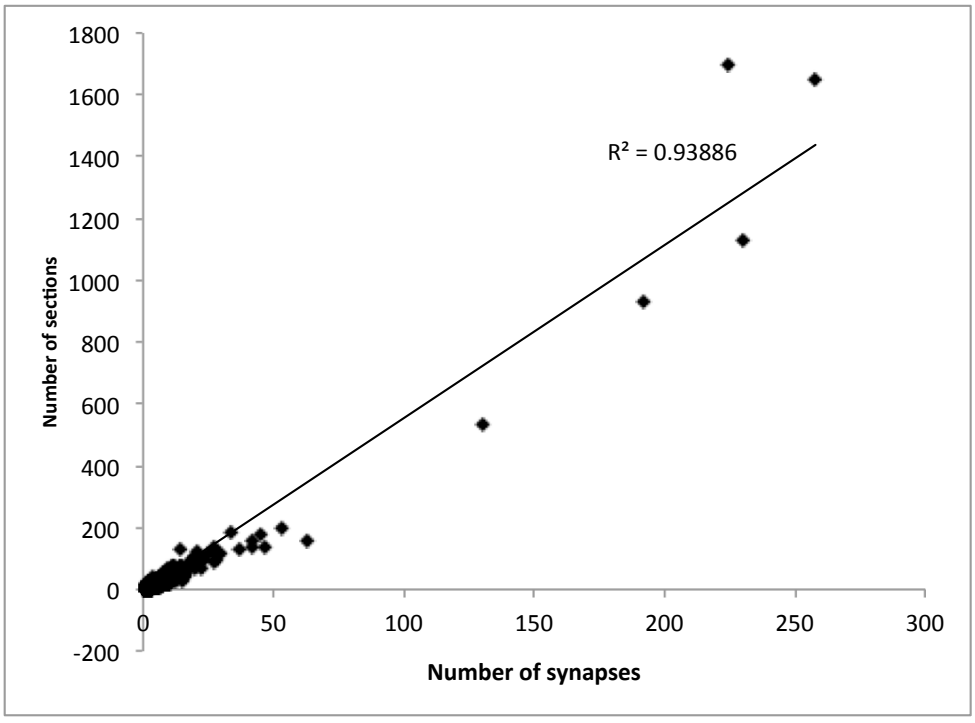

Figure. 1.4. Linear relationship between the numbers of synapses and the number sections in which each synapse was observed for: A) Each presynaptic neuron and B) Each synaptic partnership. R-squared values for each plot both equal 0.94.

Chapter 2 : Synaptic Structure

2.1 **Introduction**

Sites of chemical synaptic contact have well-recognized structural features (de Camilli et al. 2001). These comprise a presynaptic element containing a cumulus of synaptic vesicles filled with neurotransmitter, which is released into a synaptic cleft, and from there diffuses onto a postsynaptic element that expresses receptors to the neurotransmitter on its membrane surface. Some synapses, such as some of those in *Drosophila* (Prokop and Meinertzhagen, 2006) or the vertebrate retina (Dowling and Boycott, 1966), are divergent and may have multiple postsynaptic elements at each release site. Many structural details have been reported since the first discovery of synapses (Palade, 1954; Palay 1954, 1956). Presynaptic vesicles and various associated organelles, and postsynaptic specializations, including so-called postsynaptic densities have been reported in numerous studies and are now accepted structural proxies for sites of physiological transmission, visible in both 2D (e.g. Couteaux and Pecot-Dechavassine, 1970) and 3D (Harlow et al., 2001; Szule et al., 2015) reports from studies of ultrathin EM sections. Such anatomical criteria allow synapses to be identified and the synaptic partners to be traced to specific cells (Palay and Chan-Palay, 1976). In vertebrate brains, the propagation of impulses in neurons travels in one direction, from dendrites toward the cell body, and from the cell body through the axon toward the terminal, according to the historical law of dynamic polarization (Cajal, 1891; van Gehuchten, 1891). Thus, presynaptic sites typically occur at terminals, which possess calcium channels that facilitate the influx of Ca^{2+} when the membrane is depolarized by the presynaptic action

potential (Delaney and Stanley, 2009). The momentarily increased concentration of Ca^{2+} in the terminal then leads to the release of transmitter into the cleft (Delaney and Stanley, 2009), where it binds to postsynaptic receptors, which are of two types, either ligand gated, that cause an ionic conductance change in the postsynaptic cell (Monaghan et al., 1989; Nicoll et al., 1990), or G-protein coupled (GPC) receptors, that for example activate inwardly rectifying K^+ channels in postsynaptic neurons (Lüscher et al., 1997).

Violating the orthodoxy of the law of dynamic polarization, in some cell types, for example amacrine neurons of the vertebrate retina, synapses can be both pre- and postsynaptic on the same neurite, and thus show features of both an axon and a dendrite (e.g. Dowling and Boycott, 1966). Elsewhere, presynaptic sites can also originate at parts of the neuron other than its terminal (Peters and Palay, 1996; Pinault et al., 1997; Maxwell and Riddell, 2008). Presynaptic sites have been identified on axon initial segments, axon branches, and along the length of an axon (Peters and Palay, 1996; Pinault et al., 1997). Axosomatic and axodendritic synapses originate from presynaptic sites on axons, but postsynaptic elements are typically polarized to the cell body or dendrites of the postsynaptic cell, as in canonical synapses. In contrast, axoaxonic synapses originating from axons onto other axons, axon hillock regions, axon initial segments, or terminals, have different functional implications (Pearce and Govind, 1993; Pinault et al., 1997; Mitchell et al., 1993; Maxwell and Riddell, 1999). Axo-axonal synapses are often considered the substrate for presynaptic inhibition, especially within the vertebrate spinal cord (Rudomin and Schmidt, 1999). Excitatory axoaxonic contacts also exist, but these are mostly reported between interneuron axons and are proposed to function to synchronize firing (Pinault et al., 1997). By contrast with their paucity in

vertebrate and complex invertebrate brains, axoaxonic synapses dominate the synaptic relationships in basal nervous systems (Westfall, 1996).

Although uncommon in nervous systems, somato-dendritic, somato-axonic, and somato-somatic synapses have also been identified (Peters, 1991; Peters and Palay, 1996), but are reported to be more common in basal nervous systems (Westfall, 1996). For such numerical comparisons to be valid, however, careful neurite identification criteria and sampling procedures are required. Presynaptic contacts can also originate from dendrites, which are more usually or even exclusively postsynaptic in vertebrate neurons, and can form onto other dendrites, axons, or cell bodies (Rall et al., 1966; Gobel, 1976; Groves and Linder, 1983; Peters and Palay, 1996). Of these, dendro-dendritic synapses appear to be more common (Peters and Palay, 1996; Peters et al., 1991; Pinault et al., 1997), but the relative frequencies have not been carefully evaluated, so it is unclear whether differential rates of detection might contribute to the more informal assessment of the relative rates of occurrence that appear in the literature. The presynaptic dendrites that have been reported comprise those that release both GABA (Peters, 1972; Palay and Peters, 1996; Pinault et al., 1997; Lagier et al., 2007) and are thus presumed to be inhibitory, and those that release dopamine (Wilson et al., 1977; Groves and Linder, 1983) and may therefore be excitatory (Rall et al., 1966). While the locations of these synapses with respect to their cells' morphology may deny the law of dynamic polarization, in some cases the synaptic structure is itself also unpolarised, forming reciprocal and serial synapses that deny a simple pre- and postsynaptic dichotomy (Rall et al., 1966; Gobel, 1976; Peters and Palay, 1996; Westfall, 1996).

2.1.1 Polarity of Synapses:

Chemical synapses are structurally asymmetrical; their polarity depends on the release of neurotransmitter from a presynaptic cell and its action on a postsynaptic target cell. Presynaptic sites are identified most consistently by the presence of a cluster of synaptic vesicles near the cell membrane, the active zone. In some cases, this active zone occurs in both cells juxtaposed at a synaptic contact site (Jessel and Kandel, 1993). Even though such reciprocal synapses are not unidirectional, they may still be polarized if different neurotransmitters or receptors are expressed in each cell (Isaacson and Strowbridge, 1998). If each neuron at a reciprocal synapse releases the same neurotransmitter and expresses receptors for that transmitter, then each should also be presynaptic to itself. Such an arrangement may provide a substrate for self-regulation at the presynaptic site if it would express receptors to its own neurotransmitter, or as more commonly reported, if dendrites or axon branches of a single neuron contact each other at a so-called autapse (Ikeda and Bekkers, 2007). Autapses can most usually be inhibitory, providing potential regional control of a neuron's action or for self-regulating the timing of its firing (Bacci et al., 2003; Ikeda and Bekkers, 2007), or excitatory, providing a means for sustaining activity (Saada et al., 2009; Bekkers, 2009). Sustained release requires a constant and readily available supply of vesicles at the active zone, which can be maintained by specialized presynaptic structures. It also requires careful adjustment of the excitatory feedback to ensure that the discharge is stable over longer periods than the more short-lived forward transmission.

2.1.2 Presynaptic Specializations:

In some of these presynaptic terminals, vesicles are held in pools around a particular organelle, such as a ribbon (in photoreceptor or hair-cell neurons: Raviola and Gilula, 1975) or T-bar (in many synapses of fly neurons: Prokop and Meinertzhagen, 2006), which are readily identified in cross sections from EM (Zhai et al., 2004). These structures ensure that a large pool of vesicles is docked at the presynaptic site, which is important for sustained release (Sterling and Matthews, 2005). Along with holding vesicles at or near the active zone, structures such as presynaptic ribbons appear to guide vesicles to the presynaptic membrane (Peters et al., 1991). On some presynaptic membranes, a hexagonal presynaptic grid (Akert et al., 1969; Gray, 1963) consisting of dense projections also appears to guide synaptic vesicles to appropriate release loci (Triller and Korn, 1985; Peters and Palay, 1996). These specializations are apparent in serial EM because they are rich in protein, which is cross-linked into place when specimens are fixed using glutaraldehyde and is stained using uranyl acetate and lead. More recent observations from EM tomography reveal a system of ribs, spars and beams that apparently fulfill a similar function at the frog neuromuscular junction (Harlow et al., 2001; Szule et al., 2015). These structures are generally visible only after using specialized procedures not necessarily compatible with routine microscopy or in all brain regions. Thus, depending on fixation and the nature of presynaptic structures, presynaptic organelles may not be preserved during fixation, and many presynaptic sites are identified only by an accumulation of vesicles at the membrane, with no visible tethering structure (Harris et al., 2012).

The synaptic vesicles can vary in their appearance in EM depending on fixation and content. These differences are most apparent in vesicle shape, size and the electron lucence of their core (Peters and Palay, 1996). Vesicle shapes were originally linked to the polarity of transmission, inhibitory (elongate vesicles) or excitatory (round) (Uchizono, 1965) in a dichotomy no longer upheld. The two main vesicle shapes, spherical and elongate, are present in tissue fixed with glutaraldehyde (Sabatini et al., 1963). The degree of elongation depends on the molarity of the fixative (Valdivia, 1971; Nakajima, 1974 as cited in Peters and Palay, 1996), and synapses with exclusively elongate vesicles are associated with a GABA neurotransmitter (Peters and Palay, 1996). Vesicles containing neurotransmitter are typically electron-lucent, with the exception of some aminergic neurotransmitters that are often packaged in ~50 nm vesicles with a dense core (Tomlinson, 1975; Tranzer and Richards, 1976; Peters and Palay, 1996). Larger dense core vesicles with diameters of ~60-180 nm also co-populate some active zones, and may contain aminergic neurotransmitters, neuropeptides, or other peptides (Tomlinson, 1975; Peters and Palay, 1996). In nervous systems of the most basal animals, however, synaptic vesicles are typically larger than in vertebrates or protostome models, and are granular in nature, although fewer vesicles overall may populate the active zone (Westfall, 1996). Given that aldehyde fixatives take time to stabilize biological structure, perhaps up to six minutes (Macintosh and Meinertzhagen, 1995), whereas live imaging of labeled endocytic vesicles reveals that an entire cycle of a synaptic vesicle takes about 35–40 s (Schikorski, 2014), many vesicles may be shed or recycled during initial fixation and not preserved to yield faithfully their number *in vivo*.

The appearance of the postsynaptic site in electron micrographs gave rise to an early

distinction between two types of synapses: type 1 asymmetric synapses with prominent densities just inside the postsynaptic membrane, and type 2 symmetric synapses that lack such prominent postsynaptic densities (Gray, 1959). Based on the proteome of postsynaptic densities, which includes channel, receptor, scaffold, and proteins for synthesis and modification, postsynaptic densities are likely to be involved in signalling, adhesion, translation, protein synthesis and to contribute to the cytoskeleton (Gardiol et al., 1999; Sakarya et al., 2007; Ryan and Grant, 2009). Many of the proteins in the PSD gene set are highly conserved between species, and several form multiprotein complexes, which in vertebrates exist together with MAGUK associated signalling, or MASC complexes (Ryan and Grant, 2009). The PSDs of protostomes and deuterostomes share a core set of homologous proteins that has expanded divergently since their common ancestor, whereas in vertebrates the PSD and MASC complexes have additional components. Some of these multiprotein complexes are the neurotransmitter receptors responsible for functional synaptic transmission (Collins et al., 2006; Grant, 2006; Ryan and Grant, 2009). The receptors transiently bind the released neurotransmitter and this regulates ion exchange across the postsynaptic membrane, resulting in a change in membrane potential of the postsynaptic element. The magnitude of this change depends on the number and density of receptors, and the channels in the membrane these regulate (Lüscher and Keller, 2004). The direction of change depends on the equilibrium potential of the particular ion species (Nishi and Koketsu, 1960; Eccles, 1964). The sequence is more complex for metabotropic receptors that act via a GPC pathway.

Synaptic ultrastructure has been conserved over long periods of evolutionary history. Along with organelles for the synthesis and storage of neurotransmitters at the

presynaptic site, 2D electron microscopy has revealed a range of subsynaptic organelles at the postsynaptic density in a range of species from cnidarians to vertebrates (Smith and Rasmussen, 1965; Westfall, 1973; Westfall, 1996; Racca et al., 1997). Most common are subsynaptic cisternae. Some of these are smooth, while others bear apparent ribosomes (Westfall, 1996), suggesting they may be involved in protein synthesis. Furthermore, markers for both Golgi and endoplasmic reticulum, organelles involved in protein synthesis and post-translational modification, have been localized to these subsynaptic cisternae (Gardiol et al., 1999). In view of the nature and presence of these organelles at the postsynaptic site and the protein complement of postsynaptic densities, some postsynaptic sites have the potential for local protein synthesis, folding, modification and insertion of receptors into the membrane (Gardiol et al., 1999). This ability to make and integrate functional receptors and channels at the postsynaptic site affords a means for local synaptic plasticity (Gardiol et al., 1999; Grant, 2006; Ryan and Grant, 2009), particularly at asymmetric synapses with large PSDs.

In addition to their postsynaptic properties, Type 1 asymmetric synapses have presynaptic sites containing larger vesicles that retain their round shape after fixation with glutaraldehyde (Peters and Palay, 1996). Many, but not all such asymmetric synapses have been shown subsequently to be excitatory glutamatergic synapses (Peters et al., 1991; Peters and Palay, 1996; Harris et al., 2012). In contrast, symmetric synapses have smaller vesicles, which span a range of shapes in glutaraldehyde fixed tissue and are mostly inhibitory GABAergic or glycinergic synapses (Peters and Palay, 1996; Harris, Weinberg and Verrall, 2012). Although both symmetric and asymmetric synapses exist even in basal invertebrates (Horridge and Mackay, 1962; Hernandez-Nicaise, 1973;

Westfall, 1973), these structural characterizations are not exhaustive, and are mostly based on studies using vertebrate systems. In general, vesicles, which we can view as miniature osmometers, have a size and shape that is highly sensitive to the state of ultrastructural preservation and offer at best a rather poor prognosis for the identification of their vesicle contents.

The symmetry of synapses is discussed above with respect to monosynaptic connections in which a single presynaptic cell generates synaptic potentials in a single postsynaptic cell at a single synaptic contact site. However, multiple postsynaptic elements may co-populate partnerships at the same presynaptic contact site, forming divergent polyadic synapses. These polyadic synapses are found in vertebrates, but mostly in the retina (Dowling, 1970; Dowling, 1987; Fletcher et al., 2000; Lamb, 2013), and while they are also present in invertebrate visual systems (Shaw and Meinertzhagen, 1986; Lamb, 2013; Meinertzhagen, 2010), they are also observed throughout the CNS of many invertebrate species (White et al., 1986; Meinertzhagen, 2010), even in basal cestodes (Biserova et al., 1997). In such cases it is expected that all postsynaptic elements will share neurotransmitter release, although possibly not equally, but postsynaptic densities and organelles are seen more often in monadic contacts (Urwyler et al., 2015), and when they appear in polyadic synapses are not observed in all postsynaptic elements co-populating the same synapse (Koulen et al., 1998).

In addition to the symmetry described by the arrangement of the postsynaptic element(s) and its receptors, the polarity of a synapse can be bidirectional at reciprocal synapses, as evident from the distribution of vesicles. Reciprocity can occur between the same two partner neurons at separate synaptic sites (Dowling and Boycott, 1966; Dacheux and

Raviola, 1986; Isaacson and Strowbridge, 1998), or at unpolarised synapses with vesicles populating both pre- and postsynaptic juxtaposed elements (Reuter and Palmberg, 1987; McCarrager and Chase, 1985; Westfall, 1996). The latter type are most commonly reported in basal nervous systems, such as those of cnidaria, ctenophores, and other invertebrates (Westfall, 1996), but also occur in pulmonate snails (McCarrager and Chase, 1985), suggesting that although they may be a basal feature, they survived in later forms. Elsewhere, reciprocity, as with other synaptic features discussed, is a more common feature of visual, or other sensory systems (Shaw, 1984; Dacheux and Raviola, 1986; Song et al., 2005; Vigh et al., 2005). Reciprocal synapses differ in nature depending on whether the neurotransmitter of both partners is the same or differs. If both presynaptic cells use the same neurotransmitter, then release of the transmitter could also act on its own site of release, as in an autapse (Ikeda and Bekkers, 2007; Bekkers, 2009; Saada et al., 2009). In contrast, if cells use distinct neurotransmitters, the polarity of transmission may be either conserved or reversed between the two cells, which likely express distinct receptors on their postsynaptic membranes. In either case, if the action of both transmitters is excitatory, then its release should amplify excitation in both coupled neurons (Fig. 2.1). If inhibitory, the interaction should briefly inhibit the action of both cells (Fig. 2.1). In the case of distinct neurotransmitters or receptors, the interaction may be more complex, incorporating timing of synaptic delay and receptor dynamics, but ultimately leading to one active inhibitory neuron and one inactive excitatory neuron (Fig. 2.1).

Another synaptic arrangement, commonly associated with reciprocal synapses, is the serial synapse, in which a process is presynaptic to its target, which is in turn presynaptic

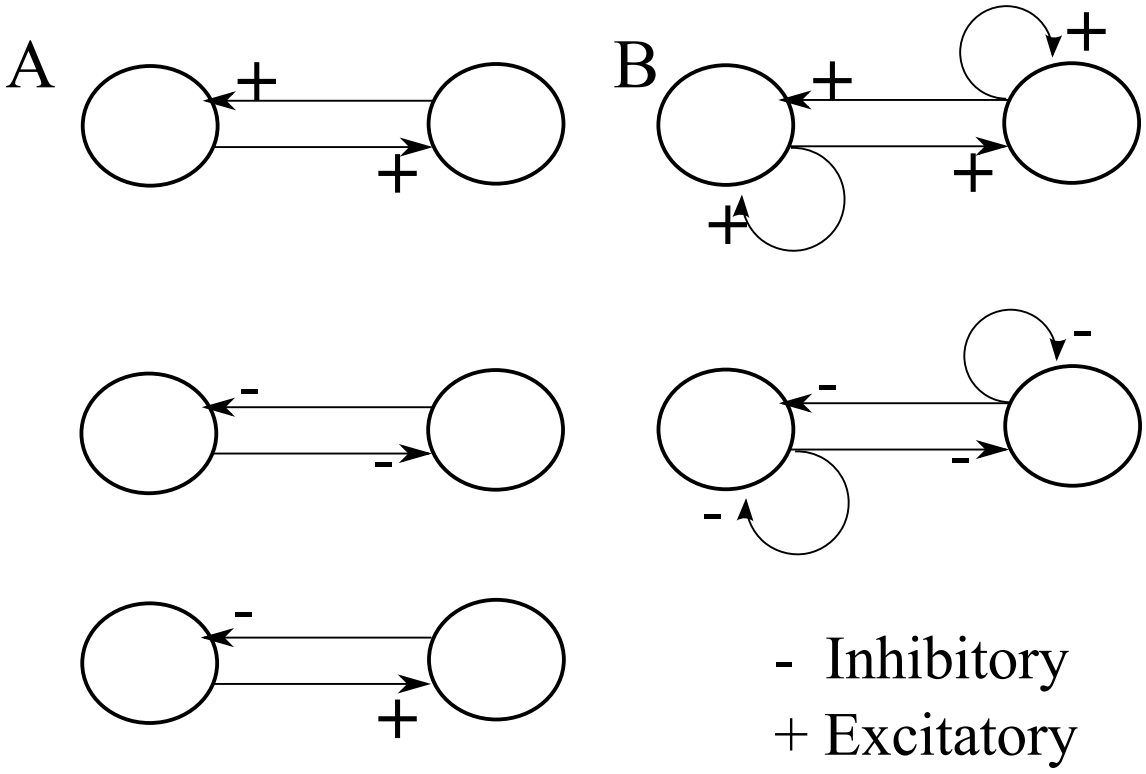

Figure 2.1. Models of simple two-cell networks. A) Simplest arrangement of reciprocal connections between inhibitory and excitatory neurons. B) Possible self-regulating networks of cells that express receptors to their own neurotransmitters. One (top, right) is self-exciting, while others are self-extinguishing and stabilizing.

to a third process, with all synapses in close adjacency (Gray, 1961; Kidd, 1962). Such arrangements are for example commonly seen in the amacrine cell networks of the inner retina, where they mediate the lateral transfer of visual signals (Dowling, 1970, 2012; Dowling and Chappell, 1972). The proximity of serial presynaptic sites is particularly relevant because it means that local changes in membrane potential can more rapidly result in neurotransmitter release at the first synapse (Dowling, 1970). This feature may allow action to be mediated by fewer synapses or provide more localized control of transmission i.e. neurotransmitter release without a full action potential. Like reciprocal synapses, serial synapses were reported early on in visual systems (Dowling, 1970; Dowling and Chappell, 1972). In invertebrates, serial synapses exist between dragonfly photoreceptor terminals (Dowling and Chappell, 1972), whereas serial and reciprocal synapses occur among amacrine cells in the vertebrate inner retina (Dowling, 1970). In both these cases, the neurotransmitters at serial and reciprocal synapses are inhibitory (Dowling, 1970; Dowling and Chappell, 1972). Serial synapses also occur at synaptic terminals, particularly in the spinal cord (Wu and Saggau, 1997), and are reported to control the localized action of afferent terminals, in presynaptic inhibition (Gray, 1962; Eccles et al., 1961). A further example of inhibitory serial synapses exists in the cat perigeniculate nucleus populated by serial GABA (GAD+) synapses (Montero and Singer, 1984). Basal Cnidaria and Hydrozoa also appear to exhibit presynaptic inhibition mediated by serial synapses, which again confirms that this type of arrangement existed even in the first nervous systems (Westfall, 1996; Westfall et al., 2002).

2.2 **Results**

2.2.1 Axo-axonal Synapses:

Within the CNS of *Ciona intestinalis* the distribution of presynaptic sites over the surface of a neuron varies by cell type. Presynaptic sites are most commonly located at either axons or terminals, although dendrites and somata are also presynaptic at some sites. In sensory neurons, such as photoreceptors, terminals bear most presynaptic sites, but axonal synapses also occur. Motor neurons, likewise, form most of their presynaptic sites on their terminals. In contrast, the interneuron classes, including relay neurons, planate neurons, and descending and ascending motor ganglion (MG) interneurons (see Chapter 4), have more sites over their axons, where they form en passant axo-axonic contacts with other neurons, than they do at sites over their terminals. Brain vesicle (BV) intrinsic interneurons are an exception, and have approximately equal numbers of presynaptic sites over their axons as their terminals, each constituting approximately 40% of their total presynaptic sites. The anaxonal arborizing neurons, a class of BV intrinsic interneuron, lack axons, so have an even greater proportion of terminal synapses; these comprise > 80% of their presynaptic sites. Thus, among all the CNS neurons of the *Ciona intestinalis* larva, sensory neurons, motor neurons, and anaxonal arborizing neurons have more synapses at their terminals, while relay interneurons of the BV, tail and MG have more over their axons, with BV intrinsic neurons possessing approximately equal proportions of both. Despite the distribution of presynaptic sites at neuron terminals, many presynaptic sites form *en passant* onto axons rather than onto the dendrites or somata of their postsynaptic target neurons.

Axo-axonal synapses constitute the greatest proportion of synapses involving relay and MG interneurons, comprising > 50% for both ascending and descending MG interneurons and > 35% for BV relay neurons. Synapses formed by BV relay neurons at their terminals also form *en passant* onto the axons and terminals of both relay and MG neuron targets, which together constitute > 20% of their total synapses. Likewise, > 50% of BV intrinsic interneurons synapses form *en passant* from their axons or terminals onto the axons or terminals of their targets. Synapses from terminal to terminal also constitute the greatest proportion of photoreceptor synapses (43%), and *en passant* synapses constitute over 60% of their contacts. Other sensory tract neurons also form synapses *en passant*, and the latter comprise at least half of the synapses of the photoreceptor tract neuron and peripheral neurons. Antenna neurons, however, only form < 20% of their synapses *en passant.* These numbers give the impression that presynaptic sites are formed at various places over the cell surface, and that each cell type may have a preferred location to form them, but that this location is neither absolute nor exclusive. Overall, the canonical vertebrate arrangement in which synapses from a presynaptic neuron form upon the dendrites or soma of its postsynaptic partner is rarely upheld by the larval neurons of *Ciona* and in some cell types is not found at all.

The abundance of *en passant* synaptic contacts in the larval CNS of *Ciona* is particularly apparent when examining the proportional distribution of postsynaptic sites. Within the CNS and among the axons of the peripheral neuropil, 68% of all neuron-neuron synapses terminate on axons or terminals. This proportion does not depend on the size of the synaptic contact, but remains the same when considering not only all synapses, but also those seen in two or more consecutive sections of the series. More synaptic contacts are

made onto axons than onto terminals, the latter constituting only 23-26% of all synapses, whereas those onto axons comprise 42-44%. The ambiguous expanded regions just distal to the cell bodies of relay neurons in the posterior BV, the region that would correspond to the spike initiation zone of a vertebrate neuron, receive an additional 3% of all synapses. While spike-initiating axon hillock regions are structurally difficult to define in the simple neurons of this nervous system, those identified receive less than 1% of all synaptic contacts and would therefore seem not to be electrophysiologically strategic.

2.2.2 Somatic and Dendritic Presynaptic Contacts:

In contrast to conventional ideas of polarity in vertebrate neurons, many presynaptic sites were identified on dendrites or cell bodies within larval CNS of *Ciona*, which were particularly common in BV intrinsic neurons. Presynaptic dendrites or somata constitute 7% of presynaptic sites for MG interneurons, 10% for AVG neurons, and 12% for BV relay neurons, but 22% for presynaptic BV intrinsic interneuron sites. Somatic synapses make up 17% of all presynaptic sites from these BV intrinsic neurons, with >10% of these being somato-somatic. No particular significance for this location is readily apparent.

2.2.3 Vesicle Types and Presynaptic Specializations:

Presynaptic vesicle pools in *Ciona intestinalis* were not uniform, and often contained multiple vesicle types. Small and large vesicles sometimes co-populated the same pools (Fig. 2.2C; 2G), although small vesicles (30-60nm in diameter) were also found alone at some presynaptic sites (Fig. 2.2A; 2B; 2D). In such exclusively small vesicle synapses the vesicles tended to cluster more closely to form a tighter active zone (Fig. 2.2A). In addition to electron lucent vesicles, large (110-140nm) (Fig. 2.3A; 3D; 3E), medium (70-

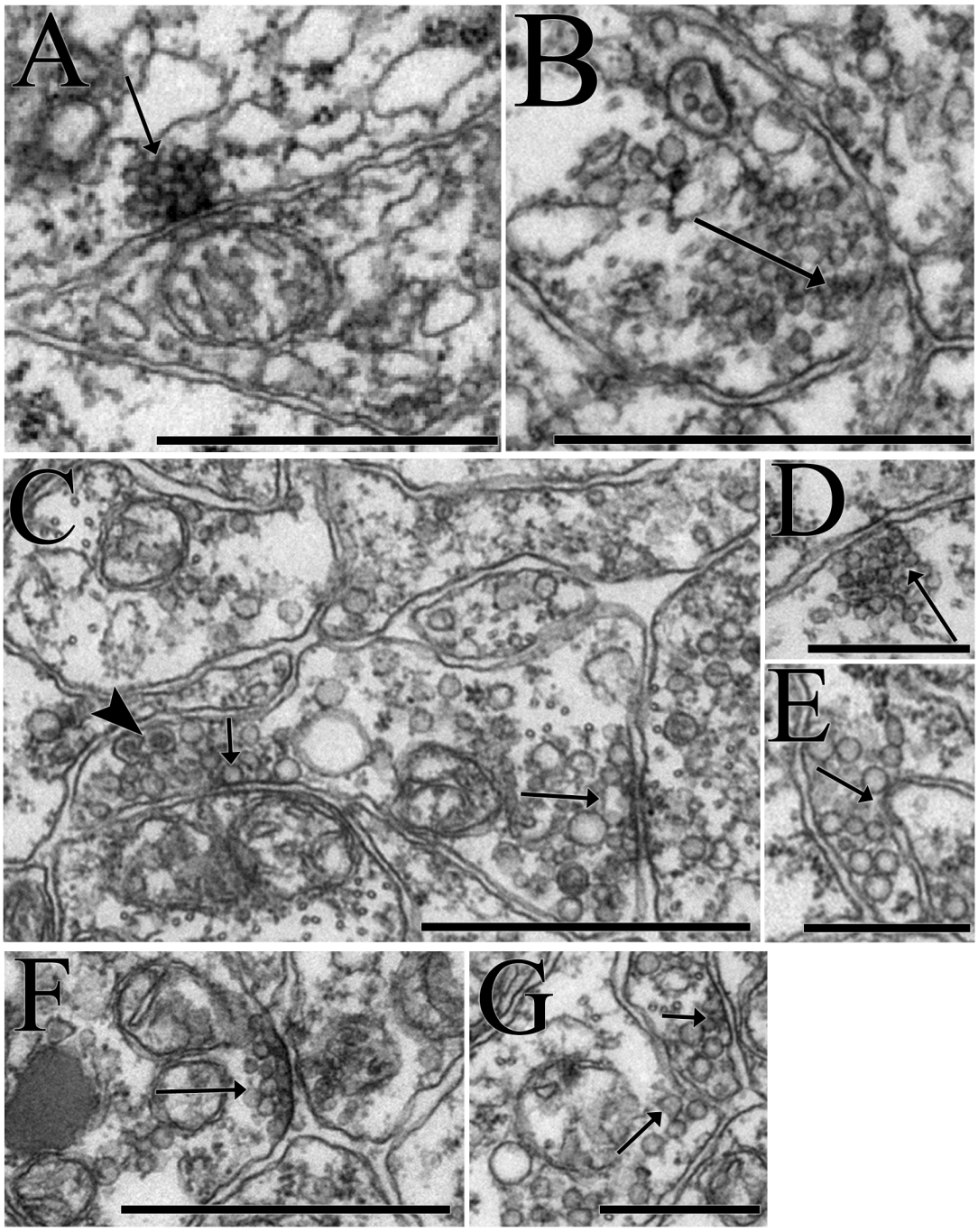

Figure 2.2. Synapses containing various sizes of presynaptic vesicles. A) Small (30-40nm) tightly packed cumulus of vesicles at a single presynaptic site (arrow). B) Small clear vesicles (30-50nm) at a single synapse forming a dispersed cumulus (arrow). C) Mixed populations of small (30-50nm) and large (70-110nm) clear vesicles (arrows) as well as dense core vesicles (arrowhead). D) Small-vesicle (30-50nm) synapse with tightly packed vesicles (arrow). E) Large (70-90nm) clear core vesicle synapse (arrow). F) Synapse with tightly packed cluster of small vesicles (30-50nm) arranged in rows (arrow). G) Synapse with moderate sized (50-60nm) dispersed vesicles at two adjacent synapses (arrows). Scale bars: 1µm (A-C and F); 500nm (D-E and G).

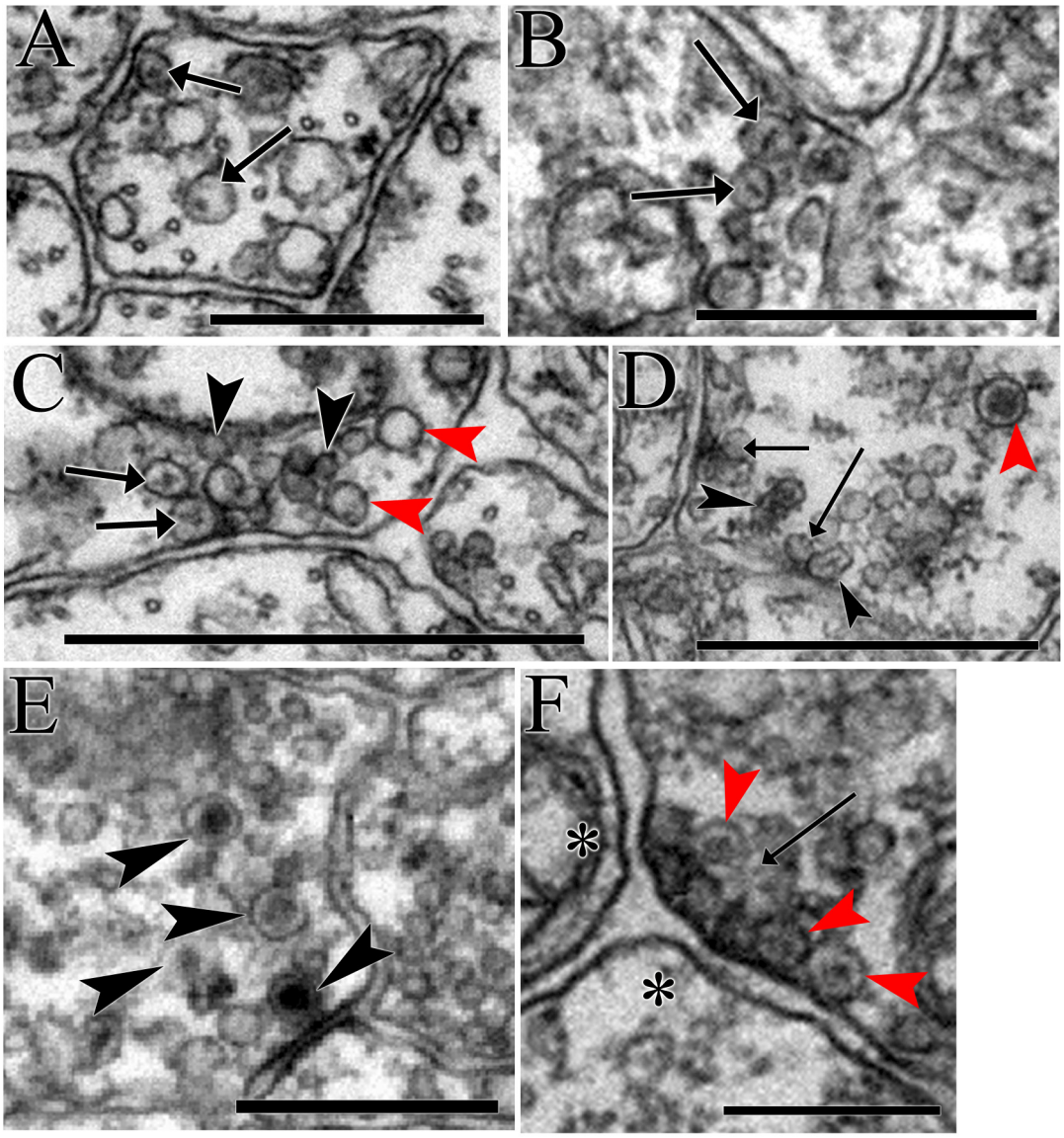

Figure 2.3. Mixed clear and dense core vesicle synapses. A-B) Medium sized dense core vesicles (70-90nm) with small cores (arrows) in cytoplasm (A) and at presynaptic site (B). C) Mixed synapse containing small (30-60nm) (black arrowheads) and medium (70-80nm) (red arrowheads) electron lucent vesicles and medium dense core vesicles (70-90nm) with small cores (arrows). D) Synapses (arrows) containing electron lucent vesicles (30-60nm) as well as medium size dense core vesicles (60nm) with elongate cores (black arrowheads). Adjacent large dense core vesicle (90nm) is shown for comparison (red arrowhead). E) Synapse containing electron lucent vesicles (30-70nm) and large dense core vesicles (100-110nm) with large dark cores (arrowheads). F) Dyad synapse (arrow) containing medium (60-90nm) dense core vesicles (red arrowheads) opposite two postsynaptic elements (asterisks). Scale bars: 500nm (A-B, E-F); 1µm (C-D).

80 nm) (Fig. 2.3A; 3C), and small (40-60 nm) (Fig. 2.3B; 3D) dense core vesicles (dcvs) were also found in presynaptic active zones (Fig. 2.3). The size of the density within these vesicles also varied so that some medium sized dense core vesicles had small cores (Fig. 2.3A-C). In an identified sample of 126 neurons with mixed synapses containing both dense and clear core vesicles, 12 were synapses from peripheral neurons. These mixed vesicle synapses were presynaptic to all regions of the neurons of all major cell types. Along with the 17 coronet cells with almost exclusively dense core vesicles populating their presynaptic sites, 42 other neurons (Appendix A), including four peripheral neurons, possessed some dcv synapses in which most, if not all vesicles contained a dense core (as seen in Fig. 2.3). The most mixed and dcv synapses (~40 each) were found in the three anaxonal arborizing interneurons (aaINs) (Appendix A). Several relay neurons, including the eminens neurons, multimodal coronet interneurons and other photoreceptor and antenna relay neurons that received much of the input from other relay neurons, also possessed a moderate number of synapses containing dense core vesicles (12-31 synapses each), as did tail planate neurons (Appendix A).

The synapses of the larval CNS of *Ciona intestinalis* lack any presynaptic specializations, such as presynaptic ribbons or T-bars. Despite lacking obvious protein structures to dock vesicles to the membrane, some synaptic sites vesicles could appear tightly clustered at the presynaptic membrane (Fig. 2A; 2B; 3F), although vesicles were more diffusely dispersed at many other presynaptic sites (Fig. 2C; 2D; 3C; 3E). The former arrangement occurred commonly with small vesicles or dense core vesicles, whereas large electron lucent vesicles tended to be less tightly packed at the active zones. Some active zones also appeared to have small vesicles arranged in several rows emanating from the

presynaptic membrane in a ray-like pattern (Fig. 2.4A). Additionally, some presynaptic sites contained multivesicular bodies (Fig. 2.4B-D), although multivesicular bodies were not exclusive to presynaptic sites. Multivesicular bodies throughout the CNS also have densities at particular points on their membranes, which are often surrounded by vesicles (Fig. 2.4D).

2.2.4 Symmetry and Polarity of Synapses:

Both symmetrical and asymmetrical synapses were present in the CNS of *Ciona intestinalis* (Fig. 2.5A-C). Many synapses in the larval CNS lacked clear postsynaptic densities, in some cases making the identification of postsynaptic elements challenging. In addition to densities at some sites, subsynaptic cisternae (Fig. 2.5D-E) populated some postsynaptic sites, but could be difficult to distinguish from other organelles or vesicles. However, subsynaptic cisternae were especially common and evident in muscle cells at approximately 500 neuromuscular junctions (Fig. 2.6). Neuromuscular junctions also had distinct postsynaptic membrane specializations that formed a thick dark protrusion (Fig. 2.6A-E;G;I-J). Along some sections of muscle, when one dorsal cell gave way to another, the muscle took on a more irregular shape at the junctions (Fig. 2.6A;C-D). At other neuron-neuron contacts with dark postsynaptic membrane staining, the presynaptic membranes also appeared darker and thicker, and a darker gray staining was often observed in the synaptic cleft compared with the lucent space usually observed between cells (Fig. 2.5C). Some synapses were also directly adjacent to other cell-cell junctions that lacked vesicles on either side of the membrane (Fig. 2.7) of the synaptic cleft along their entire length (Fig. 2.8B), while others had many vesicles populating one side over many sections, with fewer at the opposite membrane. Most unpolarised synapses

Figure 2.4. Presynaptic architecture. A) Array of vesicles at triad presynaptic site (arrow) of photoreceptor tract interneuron (trIN). B-C) Multivesicular bodies (mvb) adjacent to presynaptic sites (arrows). D) Multivesicular body membrane densities (arrowheads). E) Reconstruction of marked multivesicular body membrane densities (as seen in D) in the reconstructed BV and MG. Scale bars: 1µm (A-C); 500nm (D); 10µm (E).

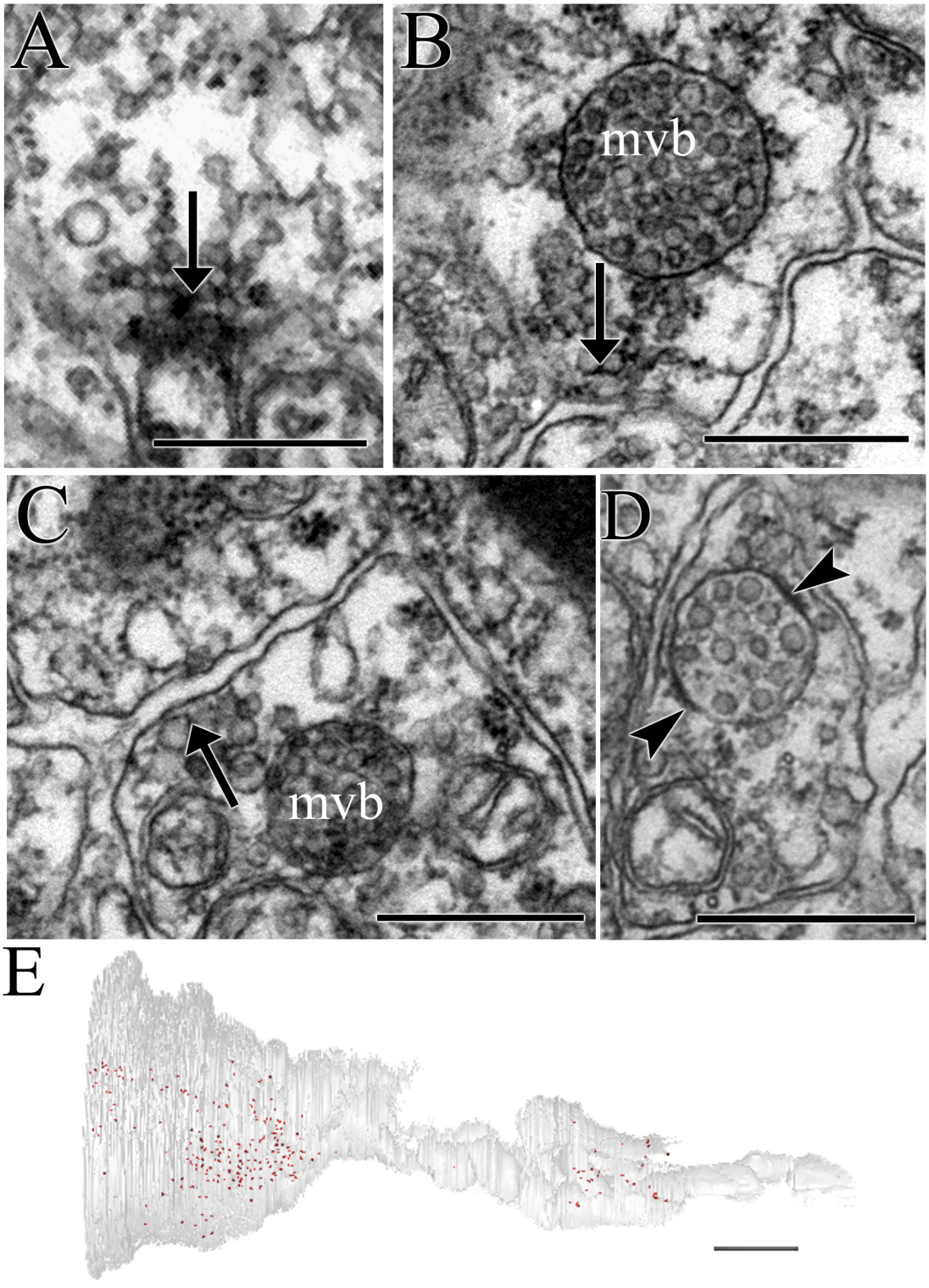
A
B
mvb
C
mvb
D
E

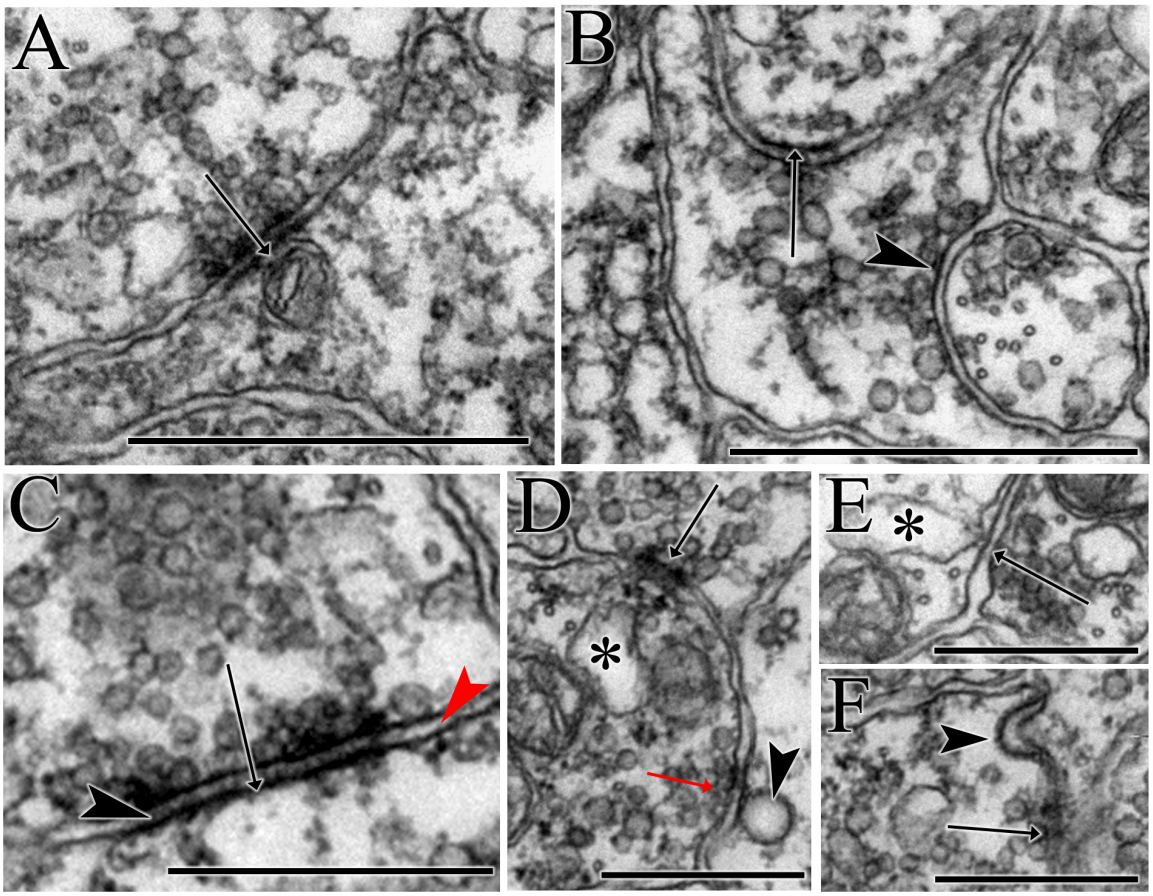

Figure 2.5. Postsynaptic specializations. A-C) Symmetrical synapses with postsynaptic densities (arrows). B) Symmetrical (arrow) and asymmetric (arrowhead) synapse from the same cell to two different postsynaptic partners. C) Synaptic cleft containing dark material (black arrowhead) compared with lucent intercellular space outside the cleft (red arrowhead). D) Postsynaptic cisterna (asterisk) at symmetrical synapse (arrow) adjacent to synapse (red arrow) with large postsynaptic vesicle (arrowhead). E) Asymmetric synapse (arrow) with postsynaptic cisterna (asterisk). F) Synapse (arrow) adjacent to invaginating vesicle (arrowhead). Scale bars: 1µm (A-B); 500nm (C-F).

Figure 2.6. Neuromuscular junctions. A) Two neuromuscular junctions from different motor neurons (arrows), one opposite two postsynaptic densities underlain by prospective subsynaptic cisternae (black arrowheads) and the other onto a branch of an adjacent dorsal muscle cell with postsynaptic density (red arrowhead). B) Neuromuscular synapse (arrow) with postsynaptic density and subsynaptic cisterna (arrowhead). Two additional postsynaptic densities on muscle (red arrowheads) do not lie directly opposite a cluster of synaptic vesicles in the motor neuron. C) Postsynaptic specialization including density and cisterna on muscle cell (arrowhead) with clear basal lamina (red arrowhead) between muscle and motor neuron, the latter lacking a visible presynaptic cumulus. D) Neuromuscular synapse (arrow) onto branch of dorsal muscle cell with both postsynaptic membrane density and membranous vesicle (arrowhead). E) Two adjacent neuromuscular junctions (arrows) with postsynaptic densities and subsynaptic cisternae (arrowheads). Membrane at postsynaptic densities is raised and curved toward the presynaptic cell. F) Two adjacent neuromuscular synapses (arrows) with postsynaptic cisternae (arrowheads), but lacking postsynaptic membrane densities. G) Single neuromuscular synapse (arrow) with multiple adjacent postsynaptic specializations (arrowheads). H) Neuromuscular synapse (arrow) with large postsynaptic cisterna (arrowhead), lacking postsynaptic density. I) Two neuromuscular junctions from a single motor neuron with postsynaptic densities and subsynaptic cisternae (arrowheads) spaced between bands of actin filaments (red arrowheads). J) Large neuromuscular synapse (arrow) across the basal lamina (red arrowhead) with long, multilobed postsynaptic membrane density on muscle cell with underlying cisternae (arrowheads). Scale bars: 10μm.

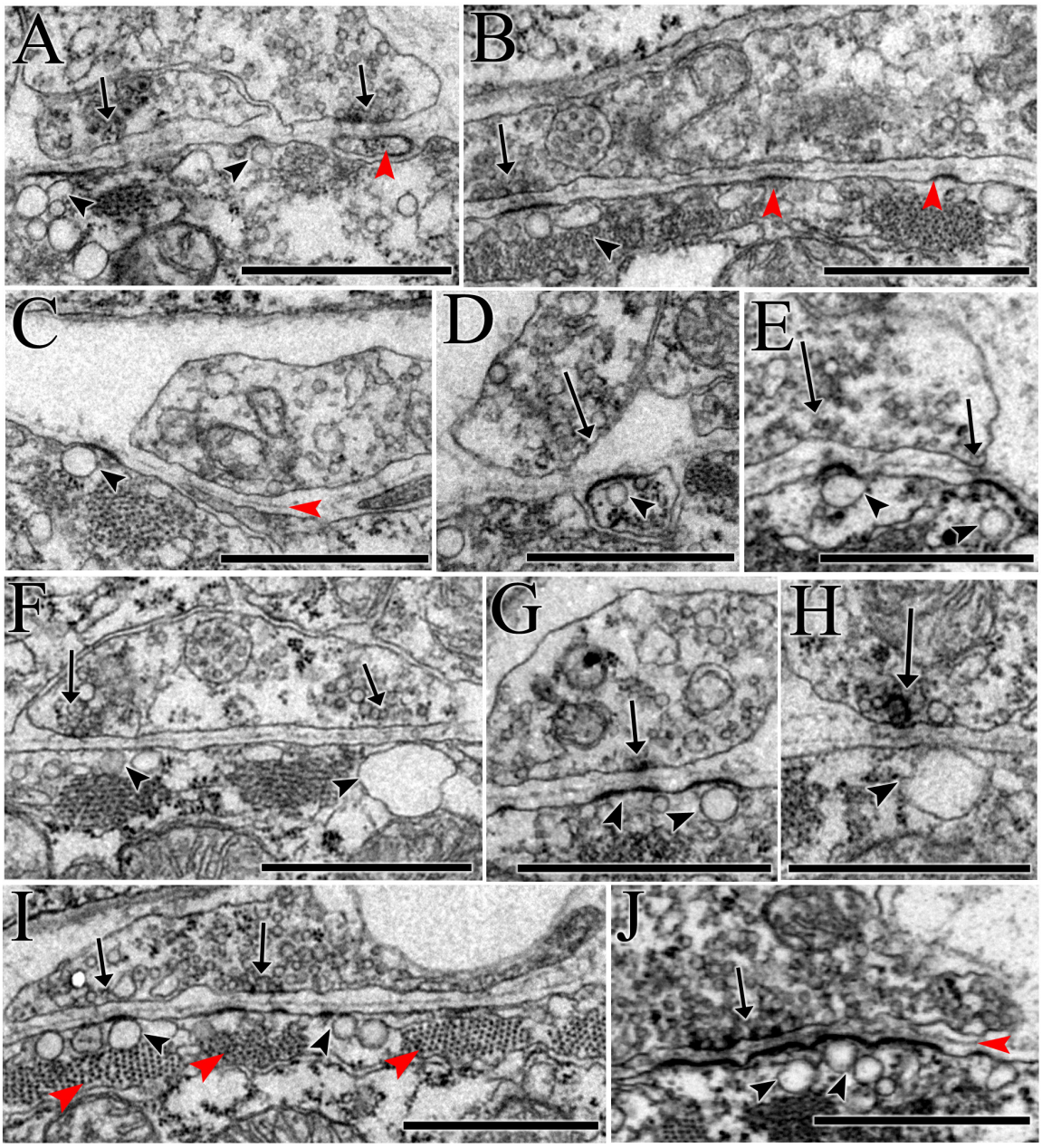
A
B
C
D
E
F
G
H
I
J

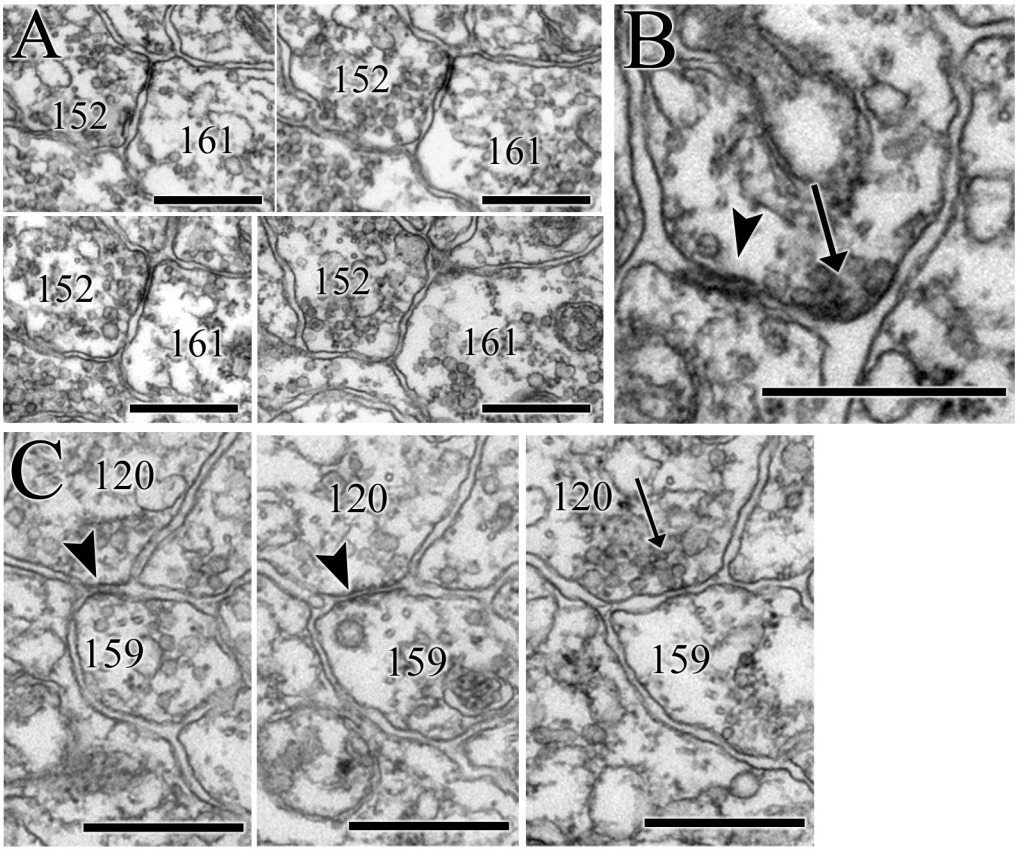

Figure 2.7. Neighbouring synapses and putative gap junctions between neurons. A) Panel of several sections through a putative gap junction membrane apposition (arrow) in which vesicles appear just inside the membrane of one of the neurons, cell 152. B) Putative gap junction (arrowhead) directly adjacent to a synapse between the same neuron pair (arrow). C) Panel of three consecutive sections illustrating the junction between two cells with densities on opposing membranes. The first two panels have no obvious synaptic vesicles and resemble putative gap junctions (arrowheads), while the last section lacks a flattened membrane with density, and instead resembles a synapse (arrow) with vesicles populating the presynaptic neuron (cell 120). Scale bars: 500nm.

involved anaxonal arborizing neurons, antenna relay neurons (cells 147 and 152), both eminens cells, AVG5, planate neurons, and the first pair of MG interneurons. Each of these neurons participated at ≥15 unpolarised synapses. In addition to these, two anterior BV neurons (cells 4 and 18), both antenna neurons, the first two right-side motor neurons, five photoreceptor relay neurons (cells 86, 96, 121, 123, and 126) and three antenna relay neurons (cells 120, 142, and 161), each participated in >10 unpolarized synapses. The unpolarised synapses were mostly *en passant* axo-axonic synapses, but also occurred at terminals and at somato-somatic contacts (Fig. 2.9).

The axo-axonal nature of many of the synapses in *Ciona* favours the formation of serial synapses. These were difficult to enumerate without establishing the extent of allowable proximity between sites, however, so most use the definition of Kidd (1962) that "a serial synapse is the process that is both pre- and postsynaptic". This limits the identification of serial synapses to those observed in single sections, but given that axon diameters range from approximately 750 to 1500 nm and sections in the current series were 60nm thick, any postsynaptic sites within 12-25 sections of a presynaptic site could be considered components of a serial synapse, as could be observed in a re-sectioned single section.

Within the *Ciona* larval nervous system there were single sections in which obvious serial synapses were visible (Fig. 2.10A-C). These serial synapses included two-step monad (Fig. 2.10B), dyad (Fig. 2.10A), unpolarized (Fig. 2.10A), and multi-step serial synapses (Fig. 2.10C). Examining reconstructed pre- and postsynaptic sites for individual neurons revealed close proximity between a high proportion of pre- and

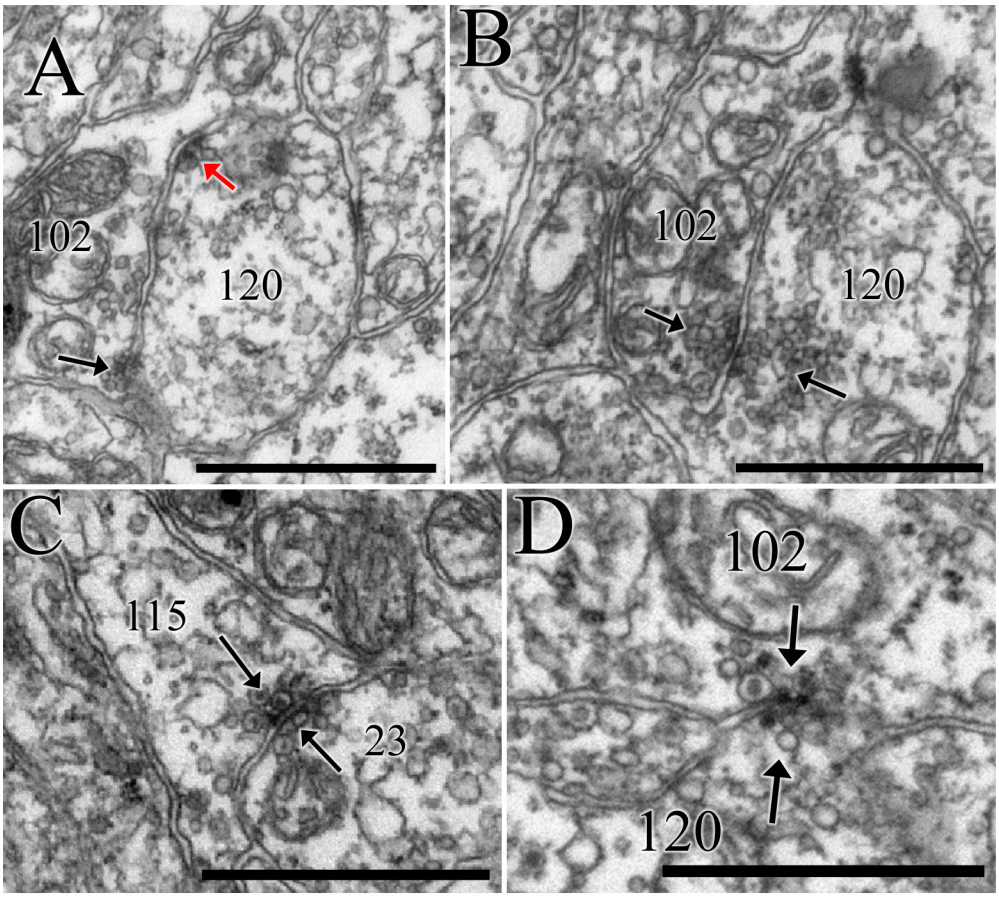

Figure 2.8. Reciprocal and unpolarised synapses. A) Single section with synapse from cell 102 to cell 120 (black arrow) and a reciprocal partner synapse from cell 120 to cell 102 (red arrow). B) Unpolarized synapse (arrows) between cell 102 and cell 120 with vesicles populating both sides of the synaptic cleft. C) Unpolarized mixed synapse (arrows) between cell 115 and cell 23 with dense core and electron lucent vesicles on both sides of the synaptic cleft. D) Unpolarized mixed synapse (arrows) between cell 102 and cell 24 with small and large dense core vesicles and electron lucent dense core vesicles on both sides of the synaptic cleft. Scale bars: 1μm.

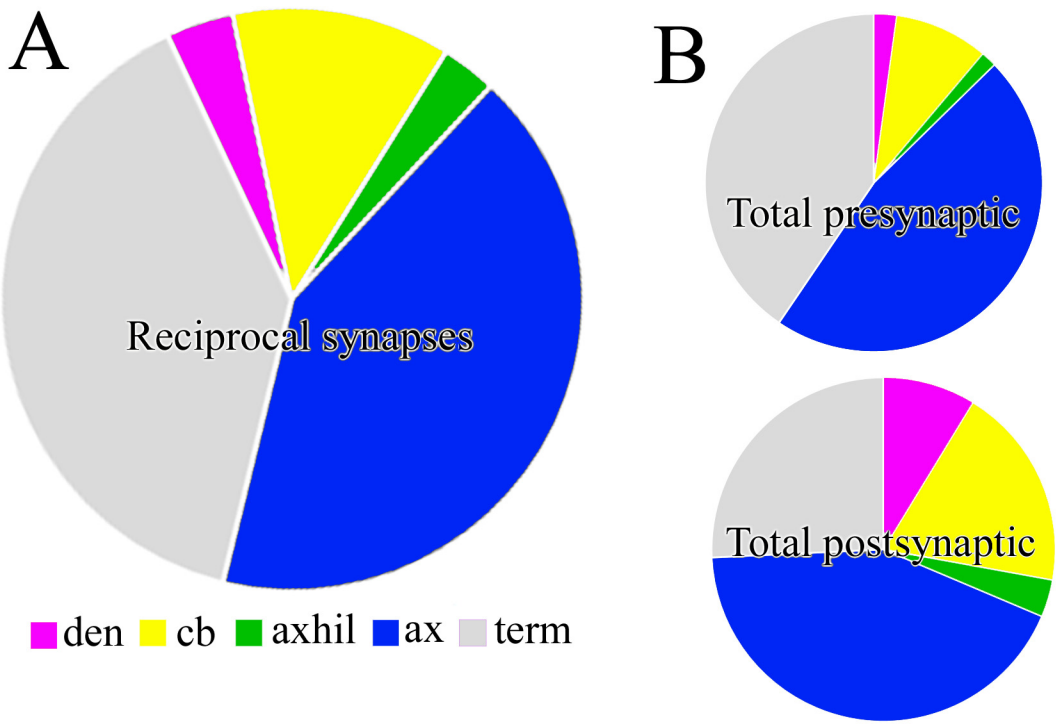

Figure 2.9. Pie charts illustrating the distribution of synapses on different parts of the cell: dendrites (den), cell body (cb), axon hillock (axhil), axon (ax), and terminal (term). A) Unpolarized synapses. B) Total pre- and postsynaptic sites.

postsynaptic synapses (Fig. 2.10D-E). Thus, serial synapses appeared to be a common occurrence, particularly within the brain vesicle, even if not quantified further.

2.2.5 Polyadic Synapses:

Of the 6618 synapses between neurons in the larval *Ciona* CNS, 921 were polyadic, having multiple postsynaptic elements. Considering only synaptic contacts between CNS cells, excluding peripheral synapses and synapses onto muscle or the basal lamina, then ~13% of the remaining 6618 synaptic contacts had multiple postsynaptic partners. Some of these synapses were polyadic for only part of the total synaptic contact (Fig. 2.11D), and these comprised approximately a quarter of all such synapses. All classes of larval *Ciona* neurons had some synapses that were polyadic. These had between two and four postsynaptic partners (Fig. 2.11), with only a single synapse of the latter type. The most common of these polyadic synapses in *Ciona* were dyads (Fig. 2.11A-D), which constituted 93% of all polyadic synapses. However, most polyadic synapses were formed by antenna neurons; antenna 1 and antenna 2 having multiple postsynaptic partners at 74 and 26 of their synapses, respectively. Several polyadic synapses also originated from motor ganglion interneurons AVG5 and VGN1L, which were each presynaptic at 20 or more polyadic synapses. Within the peripheral pathway two peripheral neurons with axons in the CNS, planate 2 and pns10, and one anterior interneuron, cell 4, also formed many polyadic synaptic contacts (>15 each). Polysynaptic contacts were also abundant between interneurons, particularly multimodal relay neurons, and these presumably facilitate the integration of antenna, coronet and photoreceptor signals (Appendix B).

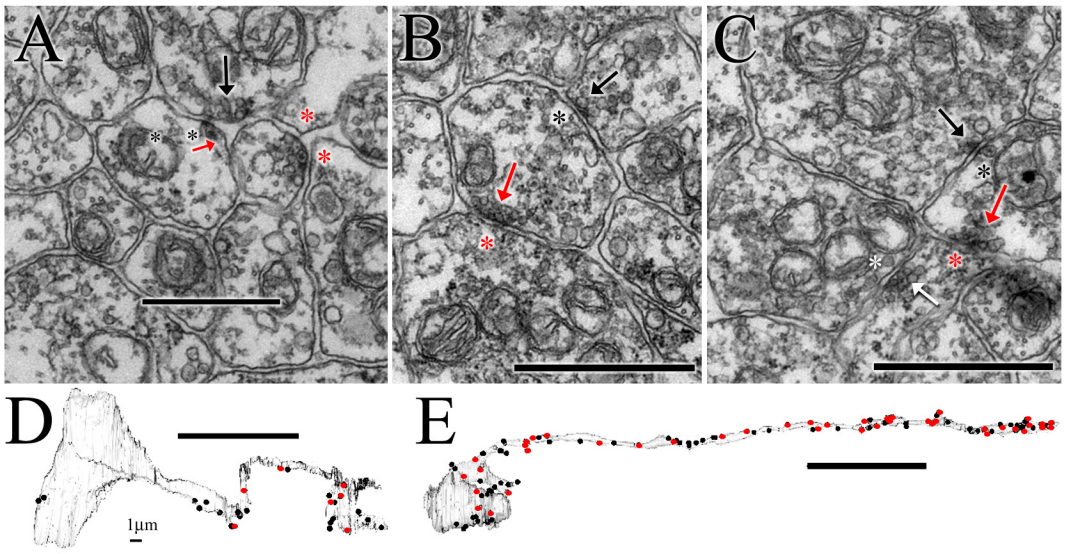

Figure 2.10. Serial synapses in the CNS. A) Serial dyad synapse (black arrow) from single neuron onto two postsynaptic targets (black asterisks), one postsynaptic target is presynaptic in the same section (red arrow) at a mixed vesicle dyad synapse (red asterisks). B) Serial monad synapse (black arrow) onto a single postsynaptic target (black asterisk) that is presynaptic at an adjacent synapse (red arrow) to a single postsynaptic target (red asterisk). C) Compound serial synapse from one neuron (black arrow) to a single postsynaptic target (black asterisk), which is itself presynaptic (red arrow) to another single postsynaptic neuron (red asterisk), which is presynaptic (white arrow) to a single postsynaptic target (white asterisk). E-F) Reconstructions marked with puncta representing pre- (red) and post- (black) synaptic sites of a brain vesicle intrinsic neuron (D: cell 42) and a relay neuron (E: cell 143). Pre- and postsynaptic sites are frequently observed within 1µm of each other. Scale bars: 1µm (A-C); 10µm (D-E); 1µm (D-E: as indicated).

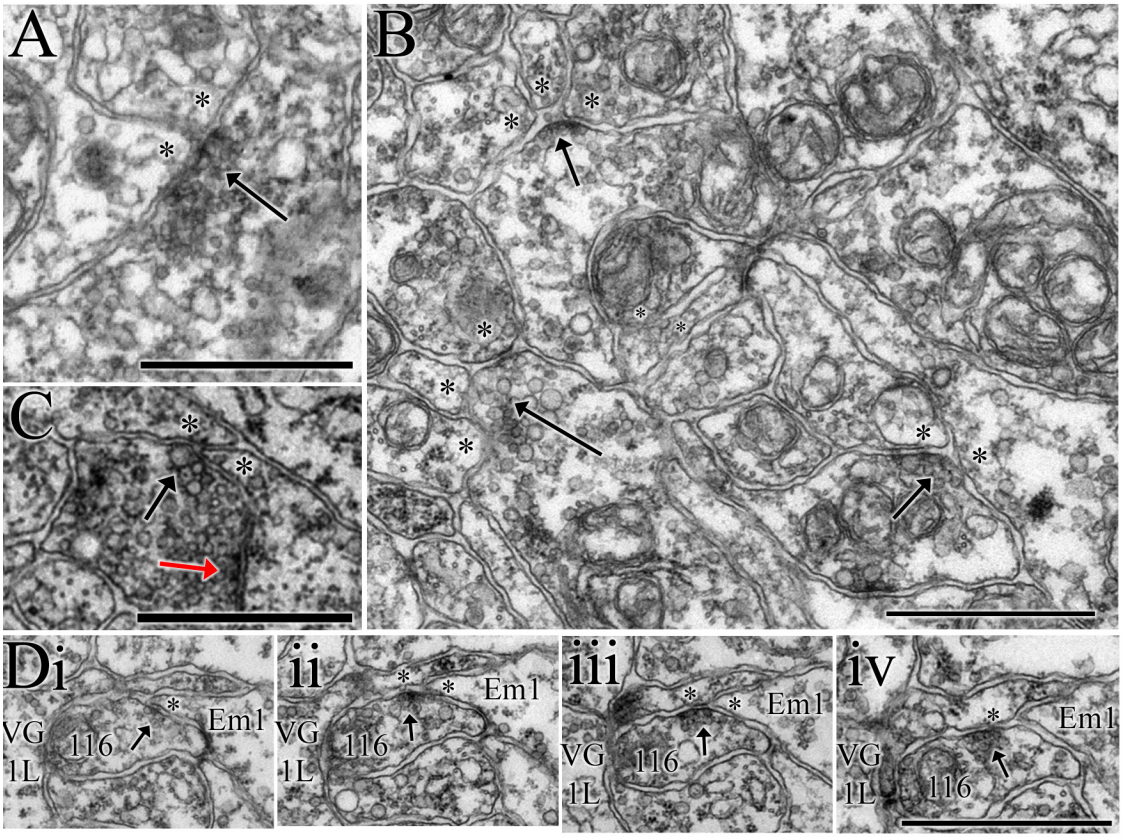

Figure 2.11. Polyadic synapses. A) Dyad synapse (arrow) with two symmetrical postsynaptic targets (asterisks) opposite a single presynaptic site. B) Three polyadic synapses (arrows)--two triad and one dyad--with postsynaptic targets indicated by asterisks. Vesicle features vary among synapses. C) Dyad synapse (black arrow) onto two postsynaptic targets (asterisks) that is directly adjacent and shares a vesicle pool with monad synapse onto one of the same postsynaptic targets (red arrow). D) Synapse through four adjacent 60-nm sections (sections 1093-1096: i-iv). I) Cell 116 is presynaptic at a monad synapse onto a single postsynaptic element (asterisk), Eminens 1 (Em1). ii-iii) Cell 116 is presynaptic at a dyad synapse onto both Em1 and VG1L (asterisks). iv) Cell 116 is presynaptic at a monad synapse onto a single postsynaptic element (asterisk), VG1L. Scale bars: 1µm.

2.2.6 Autapses:

Within the larval *Ciona* CNS some single neurons provided synaptic input onto themselves at autapses. Without molecular markers to indicate their locations, autapses must occur between neurites of a single cell, or neurites and the cell body in order to be observed in EM. Thus, I expected to observe these autapses more commonly in more highly branched neurons with extensive neurites, and in neurons with collateral axon branches (Fig. 2.12). As most of the neurons have fairly simple forms and lacked extensive branching, the autapses observed were therefore infrequent and generally small. Both cell 4 (Fig. 2.12A) and planate neuron 4 (Fig. 2.12C), which are components of the peripheral integrative network gave rise to collateral axons, as did two relay neurons, cell 100 (Fig. 2.12D) and cell 142 (Fig. 2.12B). Cell 4, cell 100, and planate cell 4 had autapses (Fig. 2.13), but each possessed only one to three of these, and only planate 4 had putative gap junctions between its collateral branches. Cell 142 lacked autapses, despite its neurites being adjacent to each other over great distances (Fig. 2.13), so clearly autapses formed with great selectivity. Other autapses occurred between short collateral branches, branches of anaxonal arborizing neurons (Fig. 2.13C), terminal sections of antenna 1 (Fig. 2.13B), between cell bodies and dendrites at dyad synapses with other postsynaptic partners, between ramifications of the MN1 terminals, and between collateral branches of RTENs and of AVG5 in the peripheral axon tract overlying the motor ganglion and tail. In addition to synaptic connections, putative gap junctions existed between dendrites of VGN1 neurons (Fig. 2.13D).

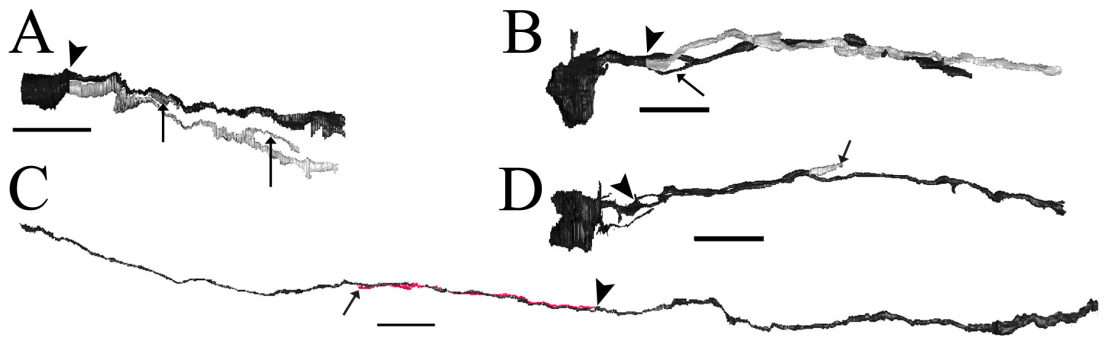

Figure 2.12. Axon collaterals. A) Anterior brain vesicle interneuron, cell 4, with two collateral neurites extending from its cell body (arrowhead). One collateral also has two of its own short collateral branches (arrows). B) BV relay neuron, cell 142, has a single axon that branches (arrowhead) to form two main collateral branches (dark gray and light gray) that braid along their lengths. One branch splits to form a short rostrally projecting neurite (arrow). C) Planate neuron 4 of the tail splits in the rostral tail (arrowhead) to form a braiding collateral branch (pink) that extends to the posterior MG (arrow). D) The axon of BV relay neuron, cell 100, branches (arrowhead) to form two collaterals that separate, then braid before the shorter branch terminates (arrow). Scale bars: 10μm.

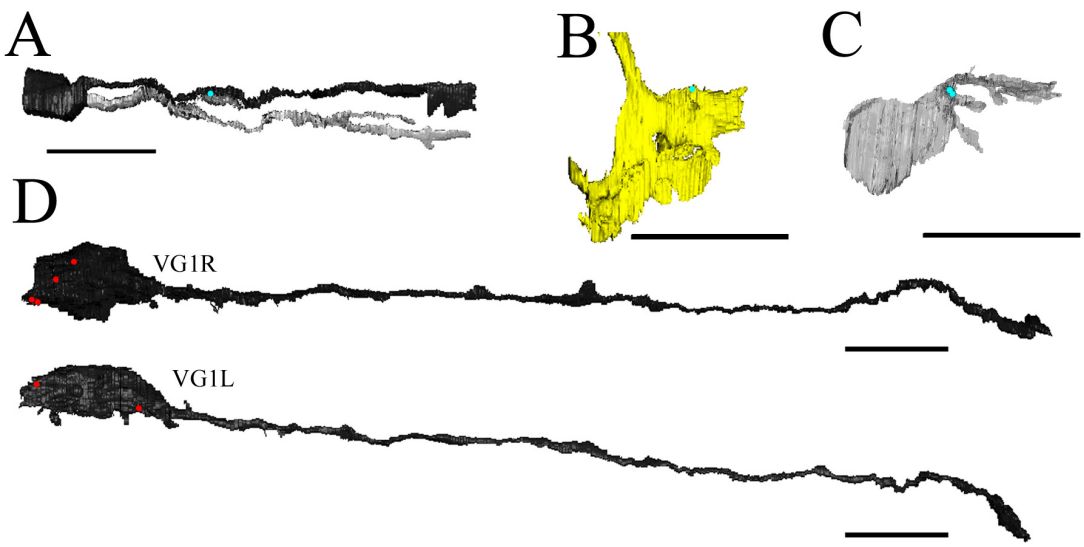

Figure 2.13. Autapses in *Ciona intestinalis* larval CNS. A) Single autapse (blue punctum) between collateral branches of brain vesicle intrinsic interneuron, cell 4. B) Single autapse (blue punctum) between branches of antenna 1 terminal. C) Two autapses (blue puncta) between branches of aaIN (cell 95) terminal. D) Inside views of left (VG1L) and right (VG1R) brain vesicle interneurons (anterior is left). Each neuron possesses putative gap junctions between its own dendrites and cell body (red puncta). Scale bars: 10μm.

2.3 **Discussion**

Synapses can be readily identified by anatomical means in ascidian larval tissue, despite the lack of visible presynaptic architecture or postsynaptic densities in many instances. Because of the poor penetration of the larval tunic by aldehyde fixatives and resulting poor fixation quality resulting from these, osmium was used as a primary fixative (Nicol, 1987). Thus, the protein cross-linking typically occurring in initial aldehyde fixative steps for conventional EM is delayed until after osmication (which initially fixes primarily lipids), and this may reduce the visibility of protein structures, such as presynaptic elements or postsynaptic densities. However, the appearance of many postsynaptic densities throughout the CNS, and other protein-rich structures suggests that these are not entirely lacking. Methods such as high pressure freezing (Studer et al, 2001) and microwave fixation (Bozzola and Russell, 1999) with reagents that increase permeability (e.g. heptane) could provide a means of resolving more clearly whether presynaptic architecture is, in fact, present. Regardless of architecture, >95% of synapses that were identified were also identified by an independent annotation of sections (undertaken by Ms Carlie Langille) to identify synapses in 100 section stacks that ran the length of the entire series. Reassuringly synapses that differed between annotations were not novel connections between neurons but merely recapitulated existing synapses, and most were annotated in an adjacent section to an existing synapse, simply increasing the reported size of the synapse. This catalogue of synapses raises as many questions as it provides grounds for solid discussion. One primary impression of the synaptic organization is that it embodies a wide range of synaptic combinants, while the left-right differences in synaptic numbers are compatible with the imprecise regulation of synaptic

number and type. A similar catalogue from sibling larvae would be needed to support this view more closely however. Particular cell types may form synapses of a particular type, but this association is neither strictly observed nor exclusive. The same is true of left-right partners, for which variation between partners could be due to a lack of precision as opposed to a specified program with functional significance. Thus the overall synaptic population, like the network it connects, seems imprecise, as does the size of individual synaptic contacts. The number of identified synapses is similar to that of *C. elegans*, with which numerically it is most easily compared. In *C. elegans* 279 somatic neurons form a connectome of 6393 chemical synapses, 890 gap junctions, and 1410 neuromuscular junctions (White et al., 1986; Varshney et al., 2011), compared with 6618 synapses formed between 177 neurons, 1772 neuromuscular synapses, and 2105 putative gap junctions (1206 with > 1 section. Each CNS neuron thus forms on average 37 presynaptic sites and 12 putative gap junctions. These are remarkably similar numbers, compared with which the neurons of *Ciona* differ chiefly in the variety of their synaptic configurations and the relative lack of stereotypy of these.

2.3.1 Polarity:

The polarity that might be predicted from Cajal's law of dynamic polarization is clearly absent in the larval CNS of *Ciona intestinalis*, suggesting that this is a feature of vertebrate neurons, or their increased numbers, and not those of basal chordates. Its rebuttal is consistent with what we know about the synaptic features of basal nervous systems, which feature unpolarised, serial, axo-axonic or even somato-somatic synapses between their simple neurons, and the lack of extensive dendritic outgrowth is associated with a high proportion of all synapses forming *en passant* onto axons or terminals of

neurons rather than on their dendrites or somata. However, the increasing reports of these atypical features in vertebrate brains (Ren et al., 2007; Crandall and Cox, 2012; Inan et al., 2013; Strowbridge, 2009) may suggest that polarization, in this sense, is not as fundamental to nervous systems as Cajal once proposed. Instead, recent studies point to cytoskeletal arrangements as the underlying elements driving the polarity of neurons (Rolls et al., 2015). However, other connectomic studies note that even presynaptic dendrites, axons or somata appear to be specialized in many cases, so that branches or regions that are presynaptic are segregated or distinct from those that are postsynaptic (Purves and Hume, 1981; Hume and Purves, 1983; Sanes and Yamagata, 2009). This segregation is not apparent in the larval nervous system of *Ciona,* however, even though some cell types -- such as motor neurons and some sensory cells -- do adhere to a more strict polarization in their synaptic roles, even though these are subject to well-known mechanisms such as presynaptic inhibition and neuronal coupling that necessitate a more complex understanding of the nature of nervous systems. For example, presynaptic inhibition requires synapses to be located between axon terminals in order for an inhibitory input to suppress locally the excitatory output. The small number of neurons and short distances between brain regions within *Ciona* may also contribute to features of its synaptic organization, leaving open the question of whether all neurons are spiking or not, as some are in fact shown to be (Bone and Mackie, 1982; Zanetti et al., 2007). Moreover, the lack of myelin allows axo-axonic synapses to form en passant between relay and motor neurons. Even so, unmyelinated axons in vertebrate brains are not reported to form en passant synapses, which therefore may be an ascidian larval feature. The lack of extensive dendritic arbors on these simple neurons would also limit the

receptive field of these simple neurons if inputs were limited to their dendrites and soma. This lack of dendrites may also contribute to the presence of presynaptic sites on the soma, as is also present in both basal and more derived nervous systems in neuronal cells lacking axons (Peters and Palay, 1996). Finally, insofar as dendrites have been interpreted as providing a means to segregate inputs from different partners (Purves, 1988) the lack of an extensive dendritic arbor may also partly reflect the paucity of partner neuron inputs to a *Ciona* larval neuron.

The abundance of synapses terminating on axons or terminals within the ascidian nervous system is critical in interpreting network dynamics. The functional significance of synaptic organization is an important consideration in anatomical connectomics (Morgan and Lichtman, 2013). Synaptic dynamics are dependent on a number of features of both the pre- and postsynaptic cell, including membrane resting potential, receptor and ion channel concentrations and properties, intracellular ion concentrations, propagation of electrotonic potentials, and the number and dynamics of neurotransmitter quanta released. Various studies have applied cable theory to model the effect of synapses based on their location on the cell, by compartmentalizing portions of cable (neurite/axon/dendrite) along the length of axons and dendrites. Cable theory estimates the spread of electrotonic potentials along the length of a neurite, which should have a higher internal resistance than its cell body because of its smaller diameter. Axo-axonal, axo-terminal, and terminal-terminal synapses can produce local current changes that influence the post-synaptic cell's local presynaptic release. However, research on *Ciona* neurons has provided neither direct recordings from neurons *in vivo*, nor knowledge of the number, density, and distribution of receptors and ion channels that are necessary to model

accurately the transmission and timing of existing synaptic connections. For this reason if none other, anatomical synaptic data could help to guide such studies to create a clearer picture of the nature of transmission in this basal chordate.

The variation between individual neurons in the number and size of synapses within the connectome of *Ciona intestinalis* likely evolved to maximize efficiency by focusing energetic effort. In nervous systems, analogue local computation is most efficient, but when there is too much noise in a system, a digital mode involving pulsate computation is required (Sterling and Laughlin, 2015). Local analogue computation occurs abundantly in *Ciona* through reciprocal connections, axo-axonic synapses, and synaptic distributions within a neuron that differ from the standard polarized design. These locations may minimize the neurons' energetic demands by localizing responses to small regions of the neuron.

Action potentials are the mechanism used in higher nervous systems to encode information transfer over what for a *Ciona* larva are long distances, and in areas with more noise. These action potentials initiate at a spike initiation zone within each neuron (Debanne et al., 2011). Among mammalian neurons, spike initiation occurs mostly at either the axon initial segment (Foust et al., 2010) or, in myelinated axons, the first node of Ranvier (Palmer and Stuart, 2006). For many actions generated by nervous systems rapid conduction is necessary for signal transfer down the length of an axon to its target. For myelinated axons, conduction velocity is proportional to axon diameter, whereas for unmyelinated axons it is proportional to the square root of axon diameter (Rushton, 1951), so that in either case for the same rapid conduction time axon diameter must increase in some proportion to axon length. Myelin increases this base speed of

conduction, which is limited by axon diameter in a naked axon, so for long axons in vertebrates myelin is necessary where speed of conduction would require axon diameters greater than approximately 0.5 μm (Sterling and Laughlin, 2015). But the ascidian larval CNS lacks myelinated axons. Axon diameters of many relay neurons in *Ciona* are >0.5 μm, but the longest axons from neurons of the larval BV of *Ciona* are less than 80 μm, although some interneurons and motor neurons in the MG and tail can extend over distances greater than 200 μm. Thus, even at slow speeds of 0.5m/sec (the lower range of unmyelinated axon conduction in vertebrate neurons), it would only take 0.4 msec for conduction from the initial segment to the terminal tip of the longest axons in *Ciona*. This comparison does, however, ignore the effects of the lower conduction velocities at the lower temperatures typical of sea-water. In vertebrate unmyelinated axons, the spike initiation zone is located 20-40 μm from the axon hillock (Debanne et al., 2011), which would encompass the entire length of the axon of some neurons in the larval CNS of *Ciona.*

Very limited recordings from cultured neurons of *Ciona* larvae suggest that after their depolarization at least some neurons (resembling relay interneurons) are capable of producing action potentials in the form of either single spikes or trains of spikes (Zanetti et al., 2007). Identifying regions of high sodium channel concentration in ascidian neurons would help to identify where such action potentials could initiate in *Ciona intestinalis* neurons. Some vertebrate neurons minimize their energetic requirements by employing axo-axonic synapses at regions of spike initiation (Sterling and Laughlin, 2015), so in *Ciona* spike initiation sites may be located where the cell is highly postsynaptic. Our anatomical synapse data reveal that postsynaptic sites are concentrated

more densely near the axon hillock of many relay neurons, although they also occur along the length of the axons, where they can form unimpeded because of the lack of myelination. Regardless of the exact site of potential spike initiation, the location of such sites caudal to the cell body means that current-induced voltage changes in the axon from axo-axonal synapses do not need to pass through the cell body to initiate a spike. Likewise, inhibition on the axon or at the terminal can act locally by depressing the local membrane potential, and if located close to the site of initiation of spikes, can depress the potential, increasing the excitation required to initiate an action potential.

The *Ciona* larval CNS has a high level of deviation from the mean total number of presynaptic sites per neuron (Mean=38; SD=52.7). In particular, neurons of the anterior BV and those of the posterior MG and tail, with axons and terminals outside the highly synaptic regions of the posterior BV, neck and anterior MG fall within the lower range of total presynaptic size and number. In contrast, sensory neurons, relay neurons, and motor neurons and their local interneurons have the greatest number of synapses. This pattern of variation in the number and size of synapses per neuron could relate to which mode of transmission a neuron primarily employs, those using more local computation possibly requiring fewer, smaller synapses. The synapse size and number may also be proportional to the ionic noise in the region of synaptic input, also reflected in the high variation in the number of postsynaptic sites on individual neurons (SD=36.3). Those neurons with the smallest and fewest synapses tend to be postsynaptic in areas of less synaptic activity, such as the isolated axon bundles of the anterior and mid-BV, while those in the same region but with axons in the peripheral bundle which has many synapses from peripheral neurons have a high number of presynaptic sites.

2.3.2 Neuromuscular Junctions:

Neuromuscular junctions share both basal chordate and vertebrate features. Large vacuolar structures resembling cisternae are frequently observed beneath the muscle membrane at neuromuscular larval junctions in *Ciona*. Similar subsynaptic cisternae are found in both invertebrate (Westfall, 1996) and vertebrate muscle (Merrillees et al., 1963), and have a proposed role in the internal Ca^{2+} release (Blanchet et al., 1996) required for muscle contraction (Campbell et al., 1974). The muscle cells in *Ciona* do not extend into the neuropil, as occurs in *C. elegans*, but instead some motor neurons extend terminals out from the neuropil to contact the muscle. These endplates are found in only one pair of motor neurons, however, while the other motor neurons remain wholly within the CNS with their axons and terminals adjacent to dorsal muscle. Insofar as the muscle does not penetrate the CNS, at both types of neuromuscular junctions motor neuron terminals are separated from muscle cells by a basal lamina, as at vertebrate neuromuscular junctions (Sanes, 1983). In basal, uncentralised nervous systems, such as in ctenophores, neural tissue is not surrounded by a basement membrane at the neuromuscular junction (Hernandez-Nicaise, 1973). Thus, the basal lamina in *Ciona* might play a role in the formation of neuromuscular synapses as it does in vertebrates (McMahan and Wallace, 1989). Thick, dark postsynaptic specializations on the muscle membrane are also found in ascidians and vertebrates, but not in basal neuromuscular junctions (Westfall, 1996). The smooth membrane of dorsal muscle cells in *Ciona* is only interrupted when one cell gives way to the next and pieces of the muscle extend, giving an appearance more similar to vertebrate neuromuscular junctions. These small pieces tend to have dark thick membranes that make up a greater surface area, whereas

the smooth portions of muscle membrane have only small protruding membrane specializations, possibly suggesting different postsynaptic mechanisms at these sites.

2.4 **Conclusions**

The larval CNS of *Ciona* widely violates Cajal's law of dynamic polarization, and exhibits a high level of reciprocity in its connections. The 177 small neurons of this system form similar numbers of synapses to those in the connectome of *C. elegans*. Based upon their relatively short distances of projection, *Ciona's* neurons should be isopotential, implying that synaptic delay is solely determined by the timing of the synapses themselves in neurons that may not spike, and lack ensheathing glia, myelin, and other features of vertebrate brains. The abundance of basal ultrastructural features of this connectome contrasts with the surprising complexity revealed in its connections.

Chapter 3 : Gap Junctions

3.1 **Introduction**

Gap junctions (GJs) directly connect the cytoplasm of two neighbouring cells, and so provide a means by which small molecules, including ions, can pass readily between cells of the nervous system that are so connected. Such junctions are formed by hexameric channel protein peptides that form a hemichannel in each cell membrane that connects across the intercellular space to form a patent channel. The intercellular cleft of a GJ is estimated at ~2nm (Bennett, 1991). The channel proteins are encoded by members of three gene families -- innexins, pannexins and connexins. In vertebrates, GJs are formed by connnexins, whereas in invertebrates GJs are typically formed by innexins (Panchina et al., 2000). A search for innexin homologues in mammals uncovered a new class of innexin homologue, the pannexins, which have been identified in Platyhelminthes, Nematoda, Arthropoda, Mollusca and Chordata (Panchin et al., 2000). Thus, in the latter, chordate-specific connexins exist alongside unrelated pannexins, the latter being expressed more ubiquitously throughout the animal kingdom. In vertebrates, GJs are formed mostly be connexins, but both pannexins and connexins can also form hemichannels (Bennett et al., 2012). Thus, the distinction between protostome innexins and deuterostome pannexin is revealed more so through the functions of the proteins themselves. Gene duplications in the protochordate lineage are proposed to have played an important role in facilitating this diversity by allowing connexins to take on an important role in GJ formation (Alexopoulos et al., 2004). As chordates, the genome of ascidians such as *Ciona intestinalis* contains sequences for both connexin and pannexin

proteins (Sasakura et al., 2003; Okamura et al., 2005). In particular, the genome of *Ciona intestinalis* contains a large number of 17 connexin-like genes and 2 pannexin-like genes (Sasakura et al., 2003).

Although they are annotated in the genome, the specific functions of these connexin and pannexin genes in *Ciona intestinalis* lack extensive investigation. Some evidence, however, suggests an important role for a connexin gene in neural plate induction, proposed to function by enabling the passage of Ca^{2+} transients through GJs between cells (Hackley et al., 2013). Insofar as the properties of resulting junctions have not been experimentally examined, it is not possible to assert the exact properties of these junctions, which could include rectifying junctions. Despite these variations, and the protein composition underlying their function, all GJs allow for passage of ions directly between associated cells, preventing their diffusion throughout the extracellular space Thus, they couple interacting cells electrically, so in neurons (in most cases) eliminating both the distinction between excitatory and inhibitory connections and the directionality of their connection. In *Ciona* GJs provide another mechanism for fast coupling of cells and combination or propagation of signals.

Bidirectional flow of positive current can occur at GJs, but rectification is common between cells of different types (Marder, 2009). In a rectifying synapse, positive current flows preferentially in one direction, facilitating a directional transfer of information. GJs are made up of channels with a contribution from each cell. In *Drosophila,* Phelan et al. (2001) established that paired cells contributing distinct subunits form rectifying junctions at these heteromeric channels. This heterotypic rectification appears to occur for both innexin (Marder, 2009) and connexin (Rubin et al., 1992) junctions, implying

that the specific expression of connexin and pannexin proteins could help to identify those junctions that could rectify in one direction.

In addition to the passage of ions, GJs also allow the passage of small signaling molecules with a low molecular weight. The pore size was first established by the ability of coupled *Drosophila* salivary gland cells to pass injected dextrans of different molecular weights, after these were injected as fluorescein conjugates (Lowenstein, 1981). In that case the GJs were formed by innexins, rather than connexins, however.

3.2 **Results**

Putative GJs observed in the CNS of larval *Ciona intestinalis* are difficult to see except in favourable section planes that cut the membrane faces perpendicularly and thus lie away from sites of membrane curvature. Such contacts vary in size from those observed in only a single section to those of putative junctions that span up to 58 sections (3.48μm) (Fig. 3.1). Likewise, the number of GJs between pairs ranges from only a single junction up to 55 GJs between a single cell pair. Those neurons with the greatest number of GJs between them are also those with the greatest total size, and also form the largest individual GJs. Assuming that each hexameric channel supports a unit conductance, and that areas of membrane contact bear a fixed average density of such channels, as has been shown at other sites (Caspar et al., 1977), the strength of electrical connections is defined in this study by the number and size of GJ membrane contacts (from the total number of 60nm sections in which a contact is observed between a given cell pair).

In general, the strongest electrical pairings occur within the motor ganglion (MG). In the MG, the motor neurons themselves are electrically connected extensively on each side of

the MG, with strong GJ contacts between the first two motor neurons (L:271, R:320), and the second and fourth motor neurons (L:188, R:117). Strong GJ contacts also exist between motor and interneurons of each side of the MG: the first motor neuron with the first interneuron (L:116, R:130) and the second motor neuron with the second interneuron (L:177, R:199). Along with these, strong electrical pairings occur across the midline of the MG between the first pair of interneurons (123), between the decussating M-cell like neurons and the contralateral MN2s (L:55, R:45), and more weakly between MN1s and the contralateral first interneurons (L to R:19, R to L: 13). On the right side of the MG, a unique descending neuron also forms many putative electrical junctions with both the second and fifth right-side motor neurons (MN2:113, MN5:69). Although these GJs are often between neurons that are also synaptically coupled, the putative strengths of GJs, both by number and size, are in many cases not proportional to chemical synapse size and number. In particular, synapses between the left and right side neurons are small and sparse, unlike GJs. Some differences between the putative strength of GJs and synapses are asymmetrical, being similar on one side, but different on the other. In these cases, such as between the second interneuron and motor neuron, the GJ connections show greater symmetry than do synaptic connections. In addition, many synaptic connections lack parallel GJ connections.

Outside of the MG, a single cell type, the Eminens interneurons, also has strong electrical connections. Eminens neurons share many large GJs between themselves, and one (Eminens2) also forms strong connections with the descending decussating MG neurons. For these Eminens neurons, unlike the motor ganglion neurons, strong GJ partnerships parallel strong synaptic connections.

Figure 3.1. Putative gap junctions in the larval CNS of *Ciona intestinalis*. A) Putative gap junction in two adjacent 60-nm sections (i and ii) illustrates membrane densities on both sides of membrane apposition (i) and closing of the gap between the two apposing membranes (ii). B) Putative gap junction through several sections (i-v). Membrane densities and absence of intercellular space at membrane apposition (arrow in i) are apparent when compared to adjacent membrane (arrowhead in ii). C) Putative gap junction with membrane densities (arrow). Intercellular space retained, but filled with electron dense material (arrowhead). D) Putative gap junction with dense thread-like densities extending into one axon (arrow).

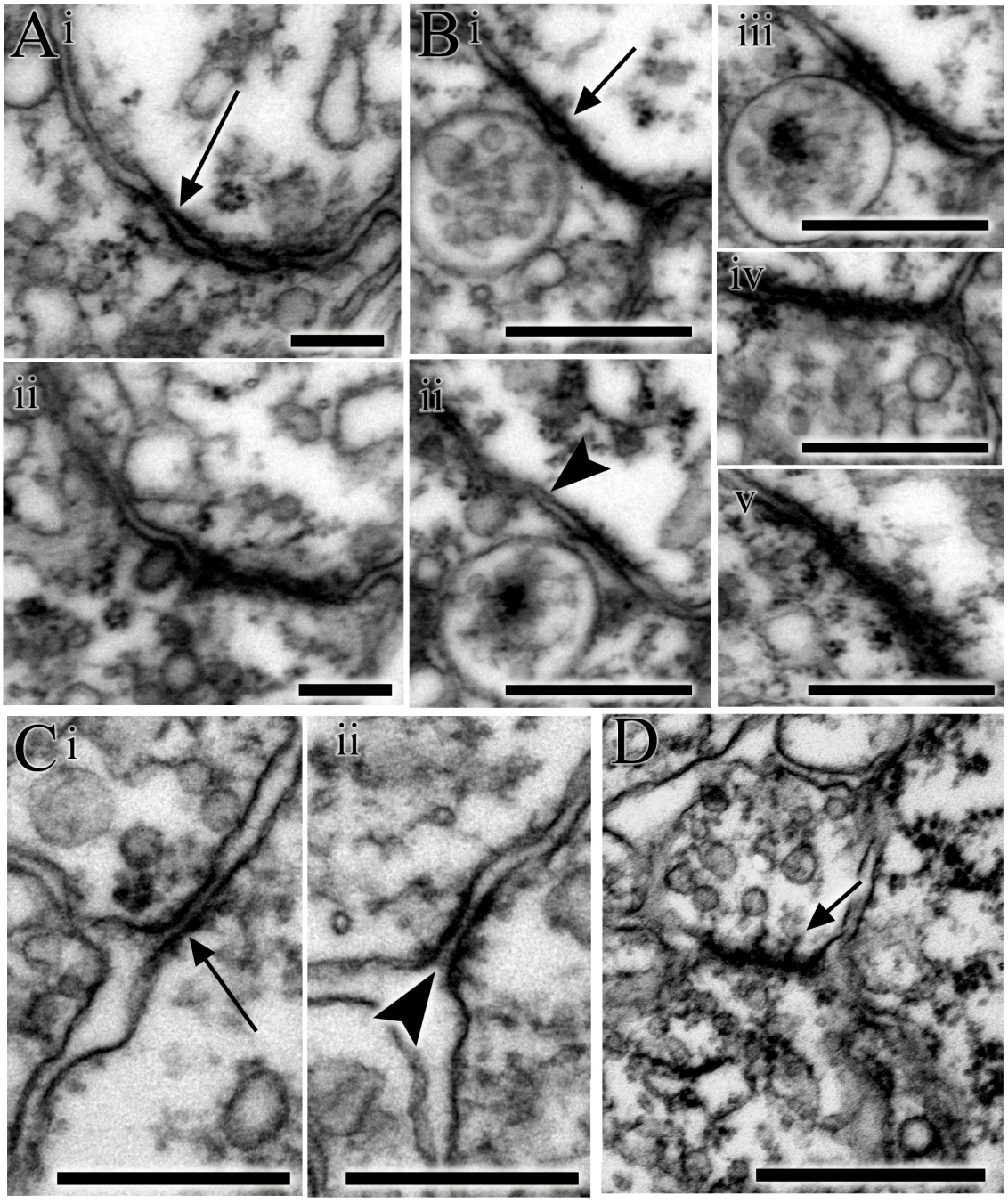
Ai
Bi
iii
iv
ii
ii
v
Ci
ii
D

Interneurons of the BV that descend to the MG to form terminals also form putative GJs along their length in addition to their axo-axonal synapses. Most of these are neurons of the antenna pathway, including both relay neurons and some BV intrinsic neurons. Together, these form a sub-network involving several types of interneurons descending from the brain ganglion to the motor ganglion, centred around a single highly connected neuron, cell 120. Indeed, only one of the interneurons in this sub-network is not connected to 120 and lacks all putative GJs. One cluster of these neurons includes interneurons that receive input from photoreceptors, coronet cells, and anterior ciliated neurons that provide synaptic input to the descending paired motor ganglion interneurons (VGNs). The second cluster includes interneurons that do not descend to the motor ganglion, rather, these anaxonal neurons have highly branched terminals in the posterior brain vesicle that are part of the retinal pathway and morphologically resemble amacrine cells of the vertebrate retina (although they also receive antenna input and are thus anatomically multimodal). These anaxonal arborizing neurons (aaINs) form GJs with the descending multimodal antenna and photoreceptor relay interneurons. In addition to this connected network, several brain vesicle interneurons form a separate sub-network of putatively electrically coupled neurons, including both intrinsic and relay neurons. These likewise are presumably multimodal neurons that interact directly with some components of the peripheral pathway, either through chemical synapses or GJs.

A total of 120 GJ partnerships exist between neurons, far fewer than those for chemical synapses between neurons. However, gap junctions lack anatomical directionality, so only half of all possible synaptic partnerships are possible. Of all existing partnerships, 8% are connected by both chemical synapses and gap junctions, with only an additional

24 partnerships (1% of all partnerships) exclusively formed by gap junctions (Fig. 3.2). Of those synaptic partners that share gap junctions, only 36 of 275 have unidirectional synaptic partnerships (Table 3.1).

Some neighbouring neurons have GJs between their cell bodies (Fig. 3.3A). In the BV many of these heterodox sites occur between neurons of the same type, particularly in the posterior BV where the cell bodies of neurons belonging to the same class are often adjacent. The dendrites of these neurons also form putative GJs with each other and with cell bodies of both their adjacent neurons and the neurons of the same class whose cell bodies are not directly adjacent. Many neurons with putative GJs between their cell bodies also possess axo-axonal GJs, but axo-axonal GJs are not exclusive to neurons with adjacent cell bodies, although those between neighbours are more common. Some relay neurons, such as cell 130, form axo-axonic GJs only with neurons that have non-adjacent cell bodies. Terminal GJs also exist between some relay neurons (Fig. 3.3B) that also have axonal, dendritic or somatic GJs. In addition to these terminal junctions within the MG, some anterior or intrinsic brain vesicle interneurons form GJs between their terminals and relay neurons. Their GJ partners often possess GJs with other neurons in addition to these brain vesicle intrinsic neurons, such as antenna relay interneurons, eminens neurons. Other terminal gap junctions occur between motor neurons near their neuromuscular junctions (Fig. 3.3C). The overall ubiquity of putative gap junctions illustrates their widespread presence throughout the neuropil, their density only dissipating in the tail (Fig. 3.3D), where only few cell profiles are present.

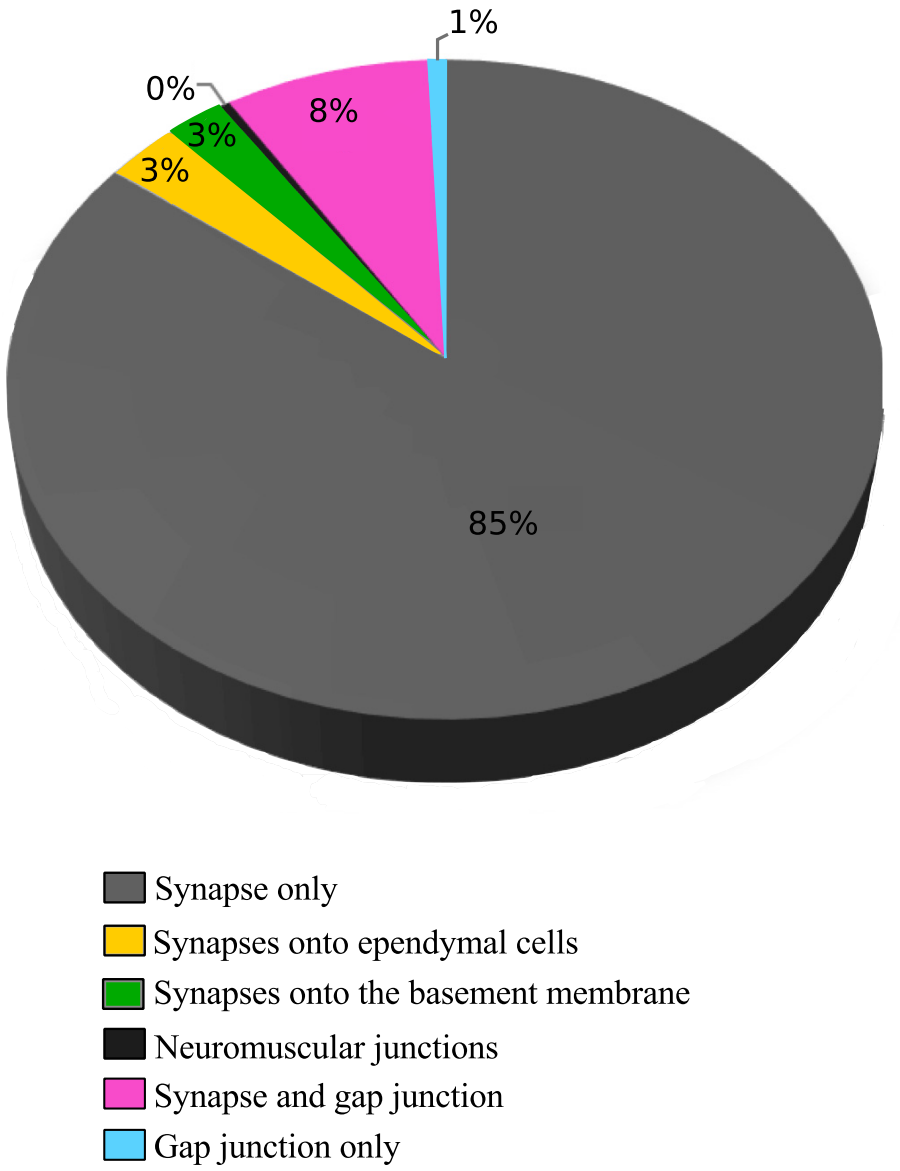

Figure 3.2. Pie chart of synaptic and gap junction partnerships in the larval CNS of *Ciona intestinalis*. Percentages of total number of partnerships are given for those connected by only chemical synapses (Synapse only, Synapses onto Ependymal cells, Synapses onto the basement membrane, and Neuromuscular junctions), those connected by both chemical synapses and gap junctions (Synapse and gap junction), and those connected only by gap junctions (Gap junction only).

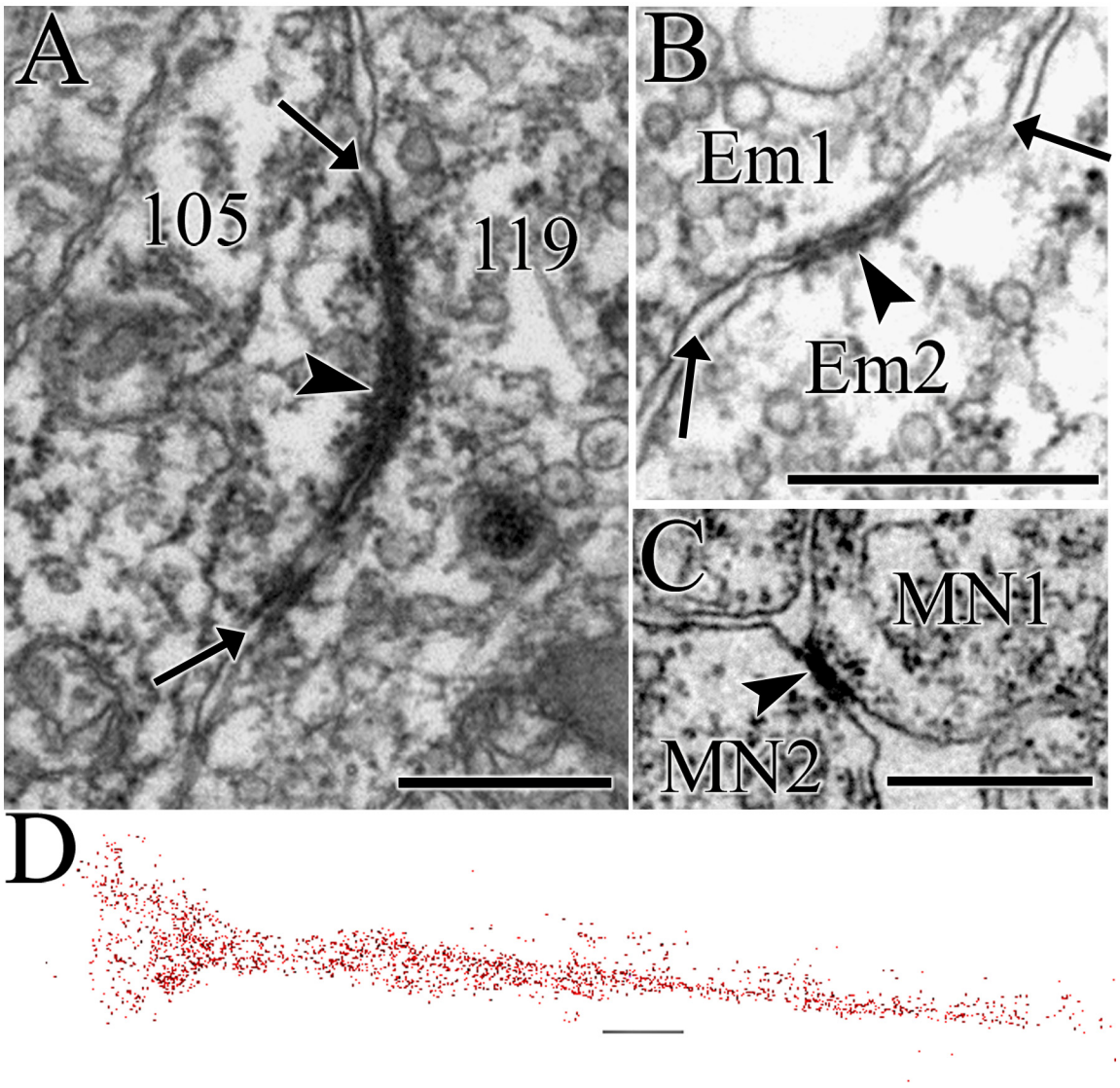

Figure 3.3. Putative gap junctions in the larval CNS of *Ciona intestinalis*. A) Putative gap junction (arrowhead) between cell bodies of two relay neurons (cells 119 and 105) with dark membranes in close apposition relative to intercellular space at adjacent portions of opposing membranes (arrows). B) Putative gap junction (arrowhead) between terminals of two eminens neurons (Em1 and Em2) with densities on both opposing membranes in close apposition in contrast to adjacent areas between arrows with wider intercellular space. C) Putative gap junction (arrowhead) between axons of two motor neurons (MN1 and MN2) near their neuromuscular terminals. D) Left lateral view of cloud showing all putative gap junctions reconstructed from the entire larval CNS. Scale bars: 500nm (A-C); 10µm (D).

Table 3.1. Number and proportion of each type of partnership within the nervous system of a *Ciona intestinalis* larva. Total number of partnerships is given for each type: Synapse only (neurons connected by only chemical synapses), Synapse to Ependymal cells (neuron-ependymal cell pairs in which the neuron is presynaptic to the ependymal cell at a chemical synapse), Synapse onto basement membrane (number of neurons with synapses onto basement membrane), Neuromuscular junctions (partnerships between neurons and muscle via neuromuscular junctions, all muscle cells grouped into single muscle on left and right), Synapse (reciprocal) and gap junction (neurons connected by both chemical synapses (both to and from each partner) and gap junctions), Gap junction only (neurons or cells connected by only gap junctions), Gap junction with non-reciprocal synapse partners (neurons connected by both chemical synapses and gap junctions for which synapses are polarized, only in one direction between cells).

Type of partnership	**Number of partnerships**	**Proportion of all partnerships**
Synapse only	2835	84.30%
Synapse to Ependymal cells	95	2.80%
Synapse onto basement membrane	83	2.50%
Neuromuscular junctions	14	0.40%
Synapse (reciprocal) and gap junction	275	8.20%
Gap junction only	24	0.70%
Gap junction with non-reciprocal synapse partners	36	1.10%
All partnerships	**3362**	

3.3 **Discussion**

From regions of membrane apposition, I identified more electrical junctions between neighbouring axons in the motor ganglion and tail regions than in the brain vesicle and neck. A number of the proposed electrical junctions between left and right components of this region provide a mechanism for coordination between sides. The many junctions between motor neurons also suggest that these function in an additive fashion. As expected, I find many GJs between neurons of the same class, which could function to coordinate and synchronize the actions of that class. The distribution of GJs along the entire length of neurons is common in the larval *Ciona intestinalis* CNS, suggesting that connexin protein expression should be seen in cell bodies, dendrites, axons and terminals. The adjacency of the cell bodies of many neurons that form GJs is expected because of clustering of cell types, especially in the brain vesicle, and suggests that developmental signals and a close cell lineage could also play an important role in determining the formation and/or functional significance of the GJs seen at those sites. However, the many exceptions to this trend suggest that adjacency of cell bodies is not necessary for GJ formation.

The asymmetries in the GJs observed in the motor ganglion network involve unique sided neurons (PVGNs) and ACIN pathways, which may both play roles in inhibition of the system. However, these would likely involve inhibitory chemical synaptic transmission, as is known for the glycinergic ACIN neurons. The convergence both of known inhibitory synapses and putative GJs on the same targets is difficult to reconcile. Rectification could allow the passage of positive current in only one direction, perhaps from an excitatory neuron to its inhibitory presynaptic partner as a mechanism for

positive feedback. However, the co-existence of putative GJs with inhibitory synaptic connections in both directions between a pair of neuron, such as occurs between eminens neurons, is still counterintuitive, and a powerful reminder that connectomic anatomy operates not by the more conventional ‘‘hypothesis-driven’’ mode of biological research, but primarily by ‘‘hypothesis generating’’ (Varshney et al., 2011). Some evidence indicates that in the leech (Hirudo) GJs precede synapse formations, so proper synaptic connections cannot form in the absence of GJs (Todd et al., 2010). A similar relationship has been proposed for photoreceptor synapses in the fly's optic lamina (Curtin et al., 2002). Investigation of both the molecular foundations and the physiological nature of ascidian GJs will be necessary in order to resolve these curiosities.

Parallels between chemical synapses and GJs between neurons support the idea that the two structures could be related developmentally. However, as many neurons connected by synapses lack GJs between them, this cannot be an invariable rule. In particular, aside from motor ganglion neurons, neurons connected by GJs do not tend to form GJs with their targets outside of their class. Thus, GJs may couple relay neurons to strengthen or coordinate their action, but do not directly facilitate their actual input to the motor ganglion. The motor ganglion neurons appear to be capable of forming GJs among themselves, so the small number of GJs between relay neurons and their motor ganglion targets may suggest the expression of different types of connexins incompatible with each other. Although connexins are known to form heteromeric channels, containing different connexin proteins, with varying properties, some combinations are incompatible for even heteromeric mixing (Beyer et al., 2001). Future studies, especially those that might enable transcript profiling of individual cells, will show whether the 17 connexin genes in

Ciona intestinalis may incorporate such pairings, and the unique expression within the larval CNS could then provide insight into this question, as well as inform us about the functional properties of GJs having specific connexin combinations.

Finally, I must acknowledge that structural criteria for GJs are suggestive more than definitive. Membrane appositions may have a different significance at some or all such contacts, and some appositions may be entirely missed unless the sectioning plane and imaging are both propitious. Clearly some means to label connexins at EM level, for example using immuno-EM as has been reported in the retina (e.g. Dorgau et al., 2015), would be required to provide the necessary assurance that sites of membrane apposition are indeed sites of candidate exchange between *Ciona* larval neurons.

3.4 **Conclusions**

Gap junctions are present in the larval CNS of *Ciona intestinalis*, and are most abundant between neurons of the MG and between certain subsets of relay neurons. Between these partners, GJs occur at many sites of contact and over many sections. In general, most gap junctions occur between synaptic partners, especially those with reciprocal synaptic relationships. In some cases, these GJs seem heterodox given the directionality of the synaptic relationships they mirror, suggesting that some GJs in *Ciona* may be rectifying.

Chapter 4 : Neurotransmitter Expression in Identified Cells of the Ascidian Larval Brain

4.1 **Introduction**

To progress from an anatomical connectome to a functional network requires, first, information on the sign (whether excitation or inhibition) and dynamics of transmission at the synapses between identified neurons in the network. Identification of the neurotransmitter phenotype of identified neurons requires evidence at many levels: the cell must possesses the enzymes to synthesize the neurotransmitter and machinery to pump it into vesicles. Indeed, further evidence is required to demonstrate that the neuron uses the transmitter in question, and thus to be rightfully accredited with the title GABAergic (for GABA) etc. it must have mechanisms to release it, must do so under physiological conditions, and the neurotransmitter in question must then act at a postsynaptic site with the requisite receptors to respond to it. The historical debate in the 1960s established these criteria (Eccles, 1963; McLennan, 1963), but they are, in fact, a minefield that has actually been successfully navigated by very few neurons and their neurotransmitters. In the current literature, the expression of reporters for specific neurotransmitter genes, especially synthetic enzymes and transporters, is often taken as a sufficient proxy for neurotransmitter phenotype and is used to attribute the title "ergic" to neurons for which other evidence may be lacking. To deal with this ambiguity, this thesis will refer to such studies and in particular cases such neurons as putatively "ergic" or as using a particular putative neurotransmitter. Otherwise, reference is made directly

based on expression, as positive for particular promoters through reporter genes, or for neurotransmitters through antibody expression.

A detailed survey of the literature identifies some cell types with putative neurotransmitter phenotypes that can be identified quite clearly in the comprehensive map of cells reported in this thesis from a ssEM series of a single *Ciona intestinalis* larva. Using such morphological criteria, it was thus possible to match cells found in this series to those expressing markers for particular neurotransmitters. For this, direct identification of the neurotransmitter itself by means of immunocytochemistry would have been ideal, but in larval *Ciona* antibody labelling studies for the neurotransmitters themselves are unfortunately limited. Many neurotransmitter antibodies fail to detect ascidian larval CNS neurons (Vorontsova et al., 1997), even though in *Ciona* the synthetic enzymes for those antibodies exist in the genome (Dehal et al., 2002). The reasons for this discrepancy are not clear but possibly have to do with either the tiny reserves of neurotransmitter in individual cells or the ease with which these are discharged during initial fixation, and so become depleted to below the immunodetection threshold. Thus, most available images are of reporter constructs for neurotransmitter synthesis or transport gene promoters. In addition to images reported in the literature, original image stacks for more detailed analysis were kindly provided by Dr. Takeo Horie (Shimoda Marine Research Center, University of Tsukuba, Japan).

4.2 **Results**

4.2.1 Sensory Neurons:

Starting with the sensory neurons in the brain vesicle, most photoreceptors express vGLUT reporters and antibodies (Horie et al., 2008a). However, a subset of

photoreceptors, identified based on the expression of arrestin and opsin (Horie et al., 2008b), do not express glutamate. The different types of photoreceptors are characterized in greater detail in the next chapter. The 23 photoreceptors found here to have outer segments projecting into the pigment cup correspond to the Group I photoreceptors, which express arrestin immunoreactivity in combination with a vGLUT reporter (*Ci-VGLUT* promoter) and immunoreactivity to a Ci-VGLUT antibody (Horie et al., 2008a; Horie et al., 2008b, Horie et al., 2010). A further seven photoreceptors identified here with outer segments projecting directly into the canal reside anterior to Group I photoreceptors and correspond to Group II photoreceptors. These express a ci-GAD reporter (Zega et al., 2008) as well as double labelling with arrestin and v-GAT reporter (Horie, unpublished as cited in Horie et al., 2010), and so exhibit evidence of a GABA phenotype.

Nestled among these photoreceptors are a few previously uncharacterized cells. Two of these are vacuolated, and project along the Group II photoreceptor tract. When compared with sectioned Ci-GAD *in situ* sections, these appear to correspond to a region of Ci-GAD mRNA expression (Fig. 6c in Zega, 2008) and thus also would exhibit evidence of a GABA phenotype. With cell bodies located anterior to the photoreceptors, the vacuolated photoreceptor-tract neurons correspond to two elongate vGAT expressing neurons, with vacuole-like "holes" (Horie, 2010: 5-x63-1). In addition to these, a dorsal photoreceptor-tract associated neuron occupies the non-arrestin region of vGLUT expression (Horie et al., 2010: 1-x63-2). Thus, this neuron appears to be a putative glutamatergic photoreceptor-associated interneuron.

Glutamate reporter (vGLUT) expression is also present in the other main identified sensory organ, the otolith pigment cell, and its associated neurons (Horie et al., 2008a). The associated antenna neurons, located next to the otolith pigment root, and in direct contact with ciliated otolith-associated cells, extend axons toward the photoreceptor-tract, alongside the Group II photoreceptors to the PSV, where they expand to form large terminals. These axons and terminals correspond to expression patterns also observed from vGLUT reporter expression (Horie et al., 2008)

Neurotransmitter expression in coronet cells has been soundly asserted using promoter-driven TH reporter along with dopamine antibody (Moret et al., 2005). In addition, studies using reporters for neurotransmitter receptors indicate that these neurons also express GABA-R1 and -R2 receptors on their bulbous protrusions (Zega et al., 2008), while the cells themselves co-express reporters for TH yet are capable of taking up serotonin and express a *SERT* promoter (Razy-Krajka et al., 2012), the latter indicating a serotonin phenotype. Although in the literature these cells have been presumed to be non-neuronal, I have identified presynaptic sites populated with dense-cored vesicles, likely therefore to contain dopamine or possibly serotonin (5-HT), which form onto some postsynaptic interneurons at many sites (Fig. 4.1A-B), but predominantly onto other coronet cells (Fig. 4.1C) and the basal lamina (Fig. 4.1C). The latter site is functionally enigmatic.

Most reports in the literature suggest that peripheral neurons have a phenotype that is putatively glutamatergic. Confirmed among these are papillar neurons, RTEN and ATEN trunk epidermal neurons, and DCEN and VCEN caudal epidermal neurons, all of which express vGLUT-Kaede in transgenic lines (Horie et al., 2008a; Horie et al., 2011).

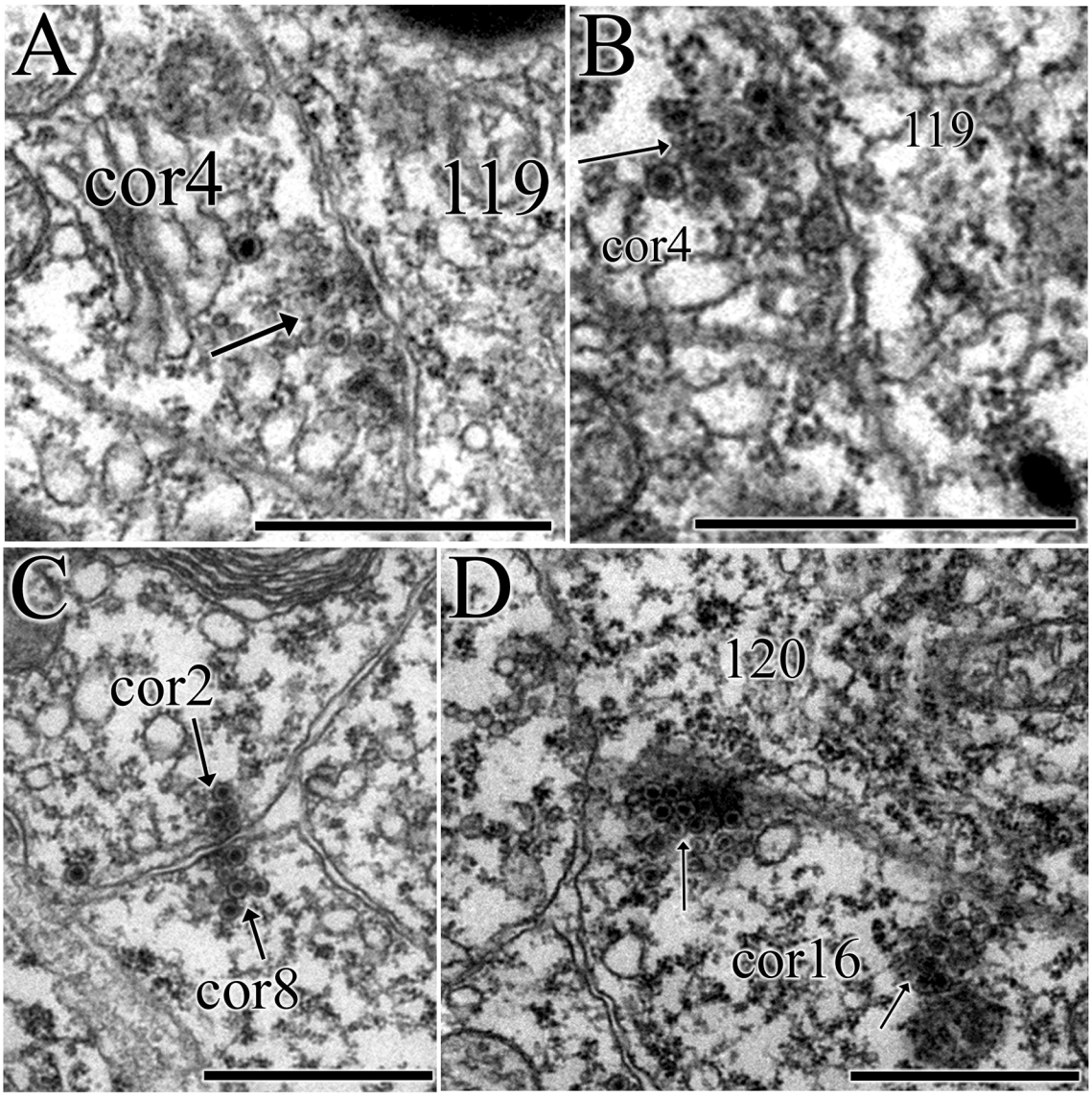

Figure 4.1. Coronet cell dense core vesicle synapses. A-B) Dense core vesicle (60-90nm) synapse (arrows) from coronet cell 4 onto multimodal coronet relay neuron, cell 119, visible in sections through a combined thickness of >240nm. C) Unpolarised synapse between two coronet cells with dense core vesicles (60-70nm) on both sides of the synaptic cleft (arrows). D) Synapses at adjacent sites from a single coronet cell (cor16) onto the same relay neuron (cell 120). Scale bars: 1μm.

In addition, GABA antibody labels neurons in the palps (Brown et al., 2005: their Fig. 4b; Zega et al., 2008: their Fig. 7d), as does Ci-GAD mRNA and a Ci-GAD reporter (Zega et al., 2008; Takamura et al., 2010: their Fig. 11a), and vGAT reporter (Horie et al., 2010: their Fig 3a). Takamura et al. (2010) propose that these putative GABAergic papillar neurons represent a peripheral neuron subset that transmits signals via glutamatergic RTEN trunk epidermal neurons at the base of the papillae, identified in previous studies with a pan-neuronal antibody (Takamura et al., 1998). Finally, Pennati et al. (2007) have demonstrated that mRNA for TPH, which is involved in the synthesis of serotonin, appears to express in the DCEN and VCEN neurons, in addition to the glutamatergic phenotype these cells also express.

4.2.2 Interneurons:

The left and dorsal quarters of the anterior brain vesicle are also populated by previously undescribed neurons (Appendix C), many of which are ciliated. Zega et al. (2008) demonstrated Ci-GAD mRNA expression, a GABA phenotype, in the dorsal cells of this region, which appears to correspond to interneurons with non-emergent cilia that do not extend from the cells into the canal. These include cells 4, 6, 16, 20, 29 and 30. GABA-R2 in situ probes demonstrate the transcription of this GABA receptor mRNA in this dorsal left region of the anterior brain vesicle, as evident in histological sections (Zega et al., 2008). All but one of these putatively GABAergic interneurons are extensively involved in peripheral pathways, and have more presynaptic sites than other cells in the anterior brain vesicle (Appendix D). The remaining neurons, all of which are small primary ciliated neurons of the anterior brain vesicle, have few synapses (8-35) (Appendix D), and may express insufficient neurotransmitter associated genes to be

visible in normally fixed tissue in whole-mount preparations at the larval stage. Possibly, their expression pattern might differ at earlier developmental stages, and neurotransmitters at these stages may also act in non-synaptic roles (Buznikov et al., 1964).

Many invertebrate larvae and embryos possess an anterior ciliated apical organ (Lacalli, 1994), populated with serotonergic ciliated neurons (Byrne et al., 2007; Ruiz-Jones and Hadfield, 2011). Although they lack a definitive counterpart in vertebrates (Lacalli, 1994), many vertebrate ciliated neurons contact the CSF, and express monoamines (Vigh and Vigh-Teichmann, 1998). Thus, the fact that these anterior ciliated neurons in *Ciona* larvae contact the canal and extend cilia within the CSF may support a serotonergic phenotype, and the ability to synthesize 5-HT may contribute to their role as stem cells for adult neurons (Benninghoff et al., 2012), a role proposed for cells in this region of the larva (Horie et al., 2011).

Despite the lack of *in situ* expression of the mRNA for TPH, a serotonin synthesis gene (Pennati et al., 2007), the equivalent region labels with 5-HT fluorescein isothiocyanate-conjugated antibody in *Phallusia mammilata* (Pennati et al., 2001). Although the sensitivity of antibodies and reporters is variable, these neurons should express promoter-driven constructs sufficiently to observe their phenotype in sectioned material. It is of course possible that they did so at an earlier developmental stage and that expression then declined, but it seems unlikely that any such decline could have happened completely over the few hours required for larval development. There are also many technical issues with antibody reagents that might preclude the detection of low levels of transmitter.

These contradictions are typical of a number that surround the neurotransmitter phenotypes of identified neurons.

Within the posterior and mid brain vesicle, reports demonstrate expression of several neurotransmitter markers, including reporters for VACHT, vAChTP, and ChAT, all cholinergic markers; vGLUT, a glutamate marker; and vGAT, GADGCH, alpha2R, and antibody label for GABAergic synapses. Of these, the latter provides clear evidence for the neurotransmitter content of larval neurons, because the antibody is directed to the transmitter, GABA, itself, and because GABA occurs only in the nervous system, and not in other cells (Olsen and DeLorey, 1999, p.335). Even detailed analysis of double-labelled image stacks does not allow confident determination of phenotype for most cell types. This would require multi-reporter studies employing sectioning techniques, or promoter driven expression of reporters visible from EM, or immuno-EM studies. However, some cell types can be firmly identified because of their unique locations, shapes, or structural features. These include eminens neurons, large ventral interneurons, and some photoreceptor interneurons.

Since the original identification of eminens neurons by Imai and Meinertzhagen (2007a), they have been or can be identified in a range of light microscopy studies (Zega et al., 2008; Takamura et al., 2010; Horie et al., 2010) because of their unique dorsal posterior location in the brain vesicle, their large cell volumes, long axons terminating in the proximal tail, and because these are conserved features across different specimens (Imai and Meinertzhagen, 2007a). These features are now confirmed in the present study (Fig. 4.2), which supplements the original descriptions with synaptic connectomic data, confirming that eminens neurons lie in the peripheral integration pathway. In previous

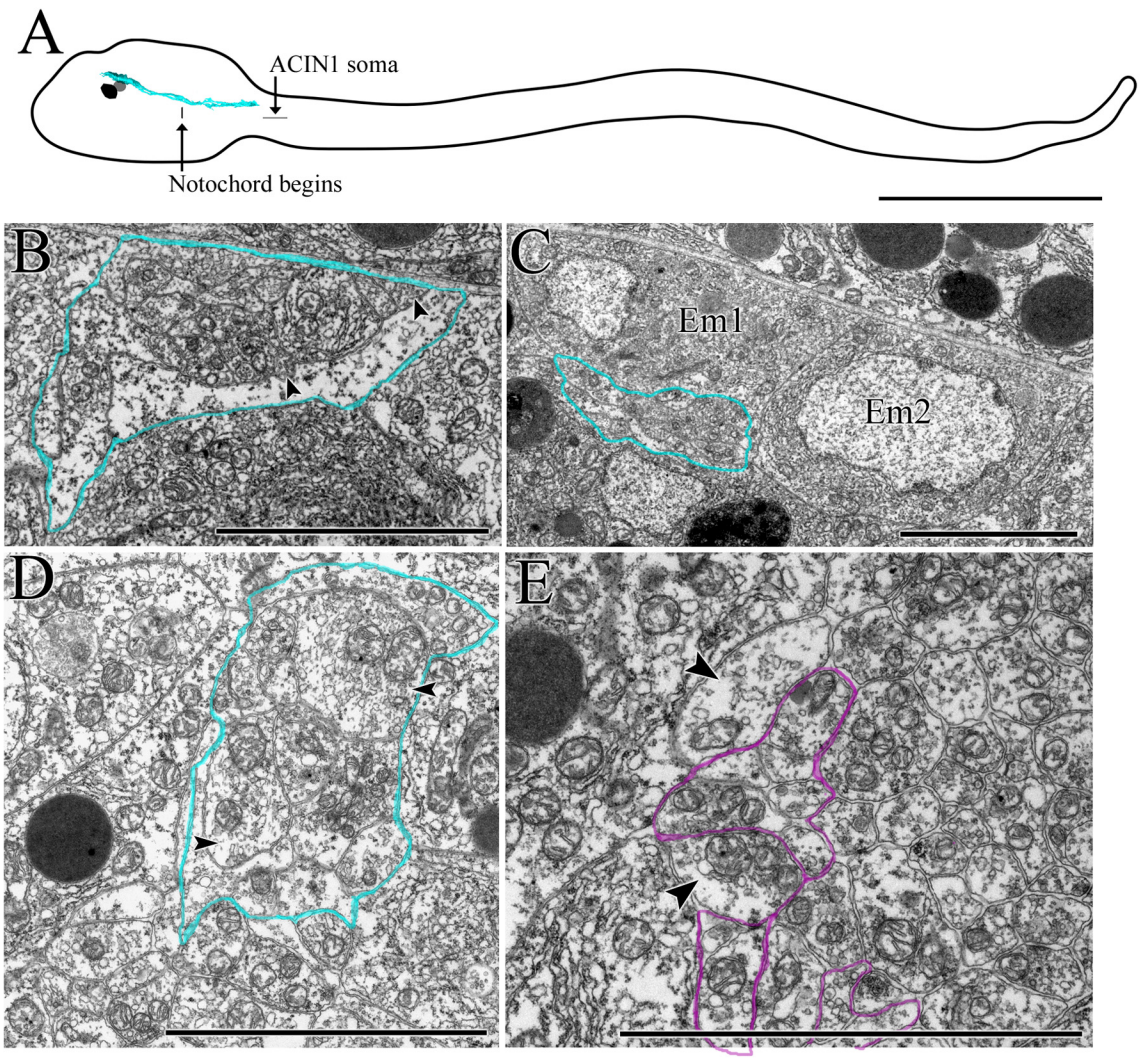

Figure 4.2. Eminens neurons. A) Reconstructed eminens neurons in a representative larval outline shown relative to landmarks. B) Anterior dorsal peripheral neuropil (outlined in blue) contains eminens neuron dendrites (arrowheads). C) Two eminens neuron cell bodies adjacent to the dorsal peripheral neuropil (outlined in blue). D) Eminens neurons (arrowheads) bundled with other peripheral axons in the posterior brain vesicle (outlined in blue). E) In the neck, eminens neurons (arrowheads) lie adjacent to the axon bundle including AVG peripheral MG interneurons and planate tail interneurons (purple outline). Scale bars: 100µm (A); 5µm (B-D).

studies, eminens cells were shown to express reporters for GABA, Ci-GAD and vGAT (Zega et al., 2008; Takamura et al., 2010; Horie et al., 2010), although Takamura alone identifies the cells as Eminens cells at the confocal level (Fig. 5d in Takamura et al., 2010). These neurons lie along the glutamatergic tract of rostral and apical trunk epidermal neurons, RTENs and ATENs, that cross the basal lamina to travel within the brain vesicle. This is consistent with our observations of the contributions of eminens cell dendrites, cell bodies and axons to the peripheral bundle (Fig. 4.2B-E).

The eminens-like cell with an additional rostral projection identified by Takamura et al. (2010) compares most closely to the cell Eminens1 in our study. Confocal studies examining the projection patterns of eminens neurons indicate that they terminate in the proximal tail (Imai and Meinertzhagen, 2007a). Our results are consistent with these findings (Fig. 4.2A), although unlike Takamura (2010) I see no dorsal projection in the motor ganglion, which may originate instead from other putative GABA positive neurons that exist in that region.

At least some of the large ventroposterior sensory interneurons identified by Imai and Meinertzhagen (2007a) appear to express cholinergic markers, Ci- VACHT (Horie et al., 2010) as well as ChAT and Ci-vAChTP (Takamura et al., 2010). However, additional Ci-vGAT positive neurons located on the left ventral as well as the central region of the posterior brain vesicle extend neurons beyond the motor ganglion toward the tail. Thus, along with putative cholinergic large ventroposterior sensory interneurons, several Ci-GAD positive neurons also bear similar morphological resemblance to large ventroposterior sensory neurons, with projections extending dorsally, then bending to project to the posterior motor ganglion or tail (Takamura, 2010: his Fig. 5e, f, h). Despite

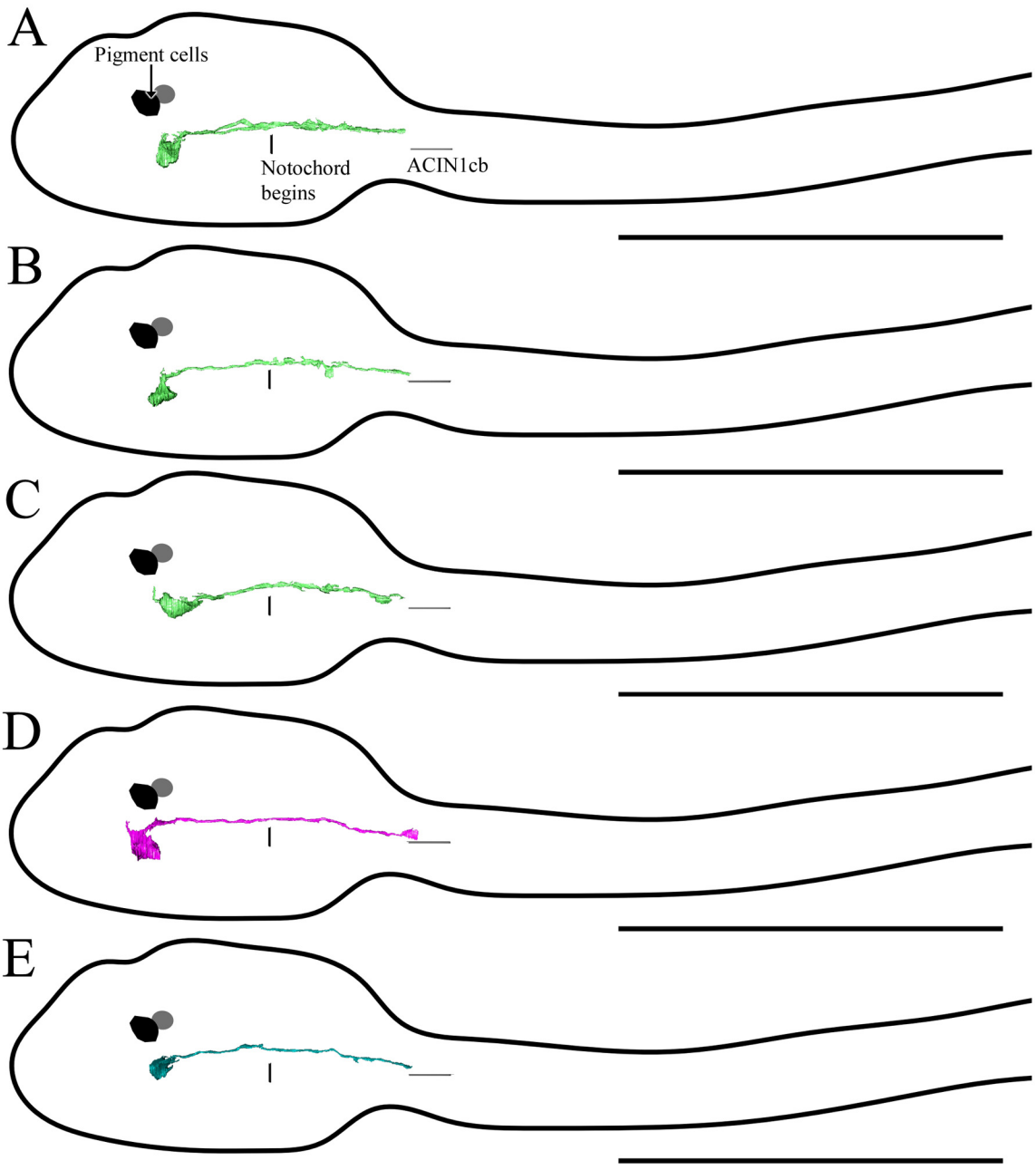

Figure 4.3. Reconstructed large ventral interneurons of the posterior brain vesicle shown relative to landmarks in a representative larval outline. A-C) Antenna interneuron cells 142 (A), 120 (B), and 147 (C). D) A photoreceptor interneuron, cell 105. E) Multimodal photoreceptor/peripheral network interneuron, cell 130. Scale bars: 100µm.

identifying cells matching the morphological phenotype of these cells (Fig. 4.3), resolution from the 2-D confocal image stacks does not allow us to distinguish amongst the individual cells seen in our dataset, seven of which share this morphological phenotype (Appendix E). The multiplicity of neurotransmitter phenotypes found in each broad interneuron category within the posterior brain vesicle is compatible with the presence of multiple phenotypes when resolved at single-cell level, and this possibility is also suggested by their variable patterns of connections. Given their simple shapes, however, morphological criteria may not be sufficient to resolve each exact neuron described in the connectome, for which the connections alone must arbitrate final identity. Discussion on this point is extended below.

In addition to eminens and large ventral posterior sensory neurons, Takamura et al. (2010) identified at least 13 dorsal, 8 middle, and 11 ventral brain vesicle cell bodies with varying nuclear sizes, all expressing LacZ under a Ci-GAD promoter. The ssEM series also revealed varying neuronal and nuclear sizes of posterior brain vesicle interneurons (Appendix E), but these cannot be matched exactly with Takamura's report. According to Takamura et al. (2010), the axon bundle originating from these neurons projects to either the middle or dorsal motor ganglion, yet I find no true dorsal projection of axons within the motor ganglion or tail (Fig. 4.4). Both the bipolar Ci-GAD LacZ neurons identified by Takamura et al. (2010) were absent in our analysis. While these may represent inconsistencies between individuals, I suggest that their bipolarity may have been misassigned, and ascending branches may instead derive from tail or dorsal motor ganglion neurons, as discussed below.

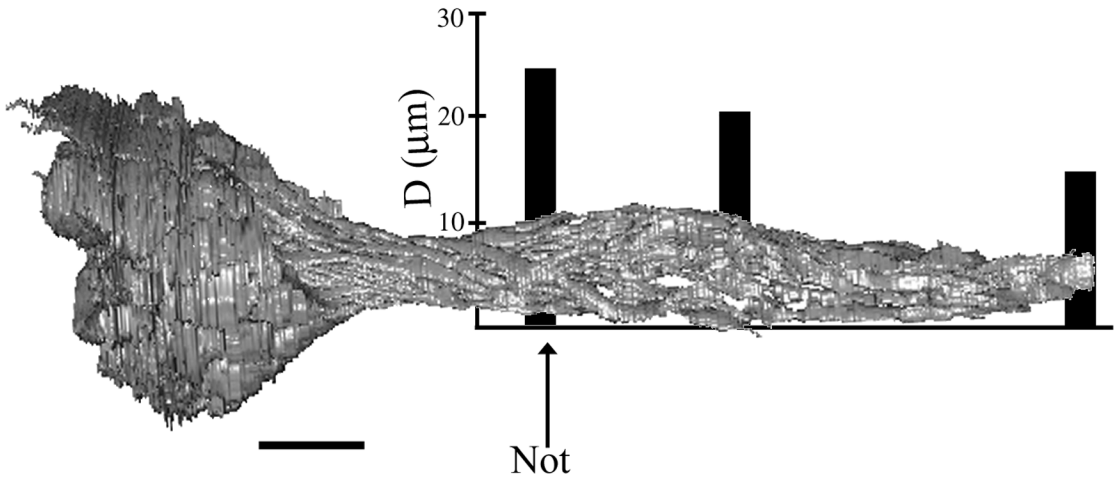

Figure 4.4. Reconstruction of all relay neurons of the posterior brain vesicle with terminals in the ventral and mid-motor ganglion or the tail, overlain on a histogram of the total diameters (in µm) of the CNS at three points in the motor ganglion. Not: anterior extent of notochord (with arrow), also indicating anterior extent of motor ganglion.

4.2.3 Motor Ganglion Neurons:

In the anterior motor ganglion (MG), the longstanding view that five pairs of motor neurons (MNs) constitute the ventral region of the MG was challenged by reports from Stolfi and Levine (2011). Their findings demonstrated expression of various orthologues for developmental genes expressed in vertebrate interneurons, and revealed these developmental reporters in at least two out of five pairs of cells examined in that study. As discussed, I find nine pairs of descending neurons in this region, only five of which exhibit the presynaptic contacts directly onto muscle that would confirm them to be actual motor neurons (Fig. 4.5A-B). The nature of these contacts is discussed in the chapter on reticulospinal neurons (Chapter 8), but contrary to assertions of motor neuron innervation of anterior-most ventral muscle cells by Bone (1992), represented only by schematic diagrams, our series confirms the lack of direct innervation of the ventral muscle cells noted in other more recent studies (Stanley McIsaac, 1999; Okada et al., 2001; Imai and Meinertzhagen, 2007a; Horie et al., 2010).

With respect to neurotransmitters, MNs in *Ciona intestinalis* are considered to be cholinergic, based on pharmacological evidence examining the effects of D-tubocurarine on muscle (Ohmori and Sasaki, 1977). The rectifying nature of ascidian nicotinic acetylcholine receptors, which are expressed on dorsal muscle bands, later established that ascidian muscle can respond proportionally to the levels of acetylcholine at neuromuscular junctions (Nishino et al., 2011). While this graded control is critical to achieve swimming in the context of the non-segmented muscle of ascidians, other recent reports by Nishino et al. (2010) demonstrate inhibitory glycine receptor expression on the muscle, especially in the anterior region (in muscles V1, M1, D2 and V2). The lack of

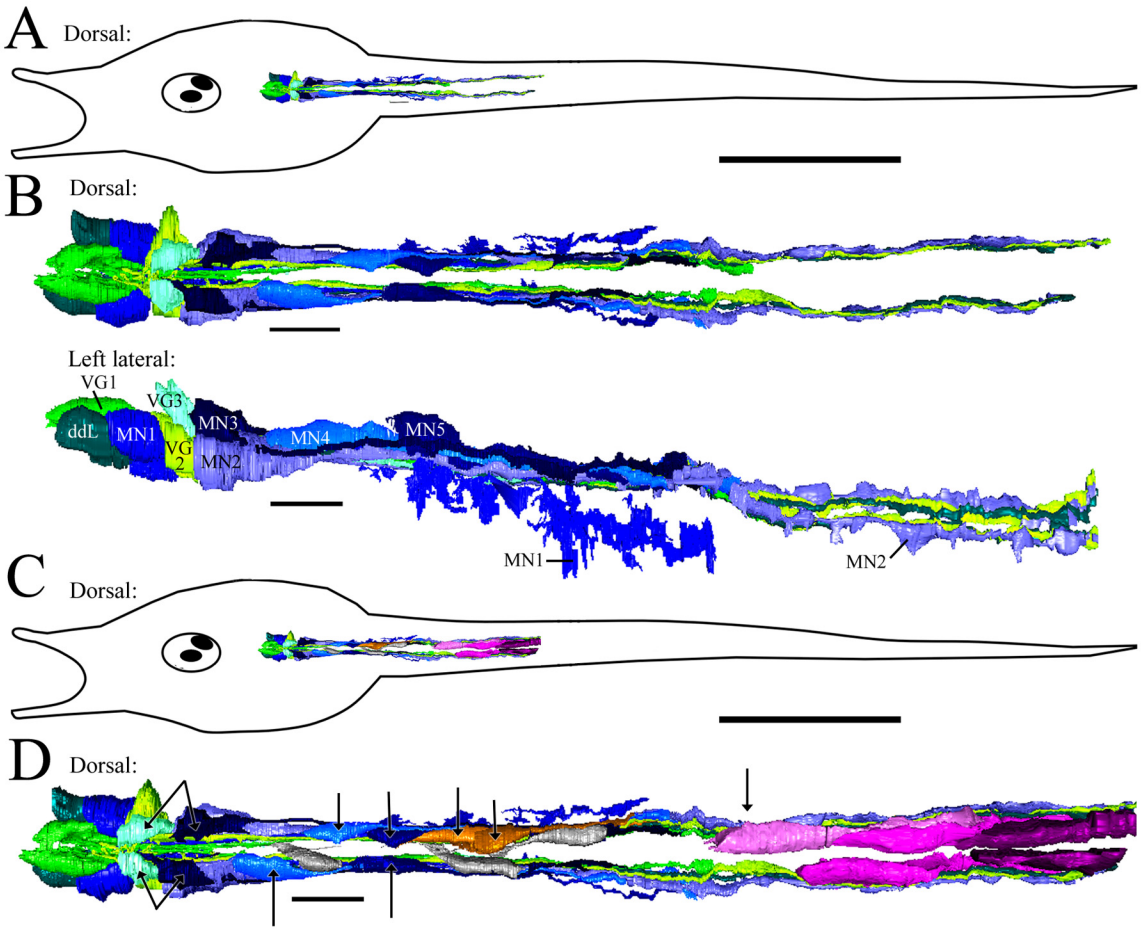

Figure 4.5. Neurons of the motor ganglion. A) Reconstructions of paired motor ganglion neurons relative to a profile of the entire larva , dorsal view. B) Paired MG neurons from dorsal and left-lateral views (with a representative neuron of each pair labelled in the latter), including: descending decussating neuron (ddN), descending MG interneurons (VG1-VG3), and motor neurons (MN1-MN5). C) Reconstruction of paired and unpaired neurons of the motor ganglion and rostral tail relative to the entire larva. D) Enlarged view from C. Neurons of uncertain neurotransmitter (those not matched to neurons from confocal studies) are indicated with arrows. Scale bars: 100µm (A, C); 10µm (B, D).

direct innervation of ventral muscle cells suggests that glycine may act as a tonic neuromodulator, rather than synaptically. While there is no strong evidence for the presence of any other neurotransmitters in the anterior ventral MG, there is evidence for glycinergic neurons at the trunk tail border as well as some evidence of dorsal expression of both Ci-GAD and vGAT, two GABA reporters, in the anterior motor ganglion (Takamura et al., 2010; Horie et al., 2010). Additionally, at least one large ventral anterior MG neuron expresses the Ci-GAD promoter in some preparations (Takamura et al., 2010). Thus, while MG interneurons may express acetylcholine, like their neighbouring motor neuron targets, it is possible that some express GABA instead, and so are likely to be inhibitory.

Although Horie et al. (2010) report five pairs of MG neurons in the motor ganglion, their VCNs 1-5, close examination of the original image stacks from these authors suggests that there may be more than five pairs of neurons expressing VACHT. Takamura et al. (2010) report fewer than ten neurons expressing vAChTP reporter in each image stack, although these differ in their arrangement and pairing, both studies together suggesting the existence of more than ten cells in total.

Tentative matches to putative cholinergic neurons identified in this region can be distinguished by their location and morphology, more easily than in the posterior brain vesicle. No. 1 and VCN1 cells correspond to ddVG neurons, also called A12.239 (Stolfi and Levine, 2011). Consistent with suggestions based on confocal studies (Takamura et al., 2010; Stolfi and Levine, 2011), these neurons decussate, and extend axons into the tail, but never contact muscle or provide direct synaptic input to the muscle (Fig. 4.5). No. 3 and VCN2 (or A11.118) neurons appear to correspond to MN1s, large endplate

primary motor neurons (Fig. 4.5). This identification is based on their large endplates, and round cell bodies. Cells No. 5, No. 4, VCN 4, and A10.57 all appear to be large and elongated, with bulbous terminal regions formed along their length down the tail. These correspond to our description of large elongate primary MN2s (Fig. 4.5), which contact the dorsal muscle in the MG alongside other MNs, but also provide extensive neuromuscular junctions down the length of the tail (Fig. 4.5). No.4 and VCN3 neurons are reported to localize to a more dorsal position than the first two pairs of cells, which is similar to both MN3 and VGN3 pairs identified in our series (Fig. 4.5B,D). Although both Horie et al. (2010) and Takamura et al. (2010) employed double label, the resolution and labelling within the MG, combined with the mosaicism of expression make conclusive analysis impossible. Without the full complement of MG neurons as a background, it is difficult to ascertain which of the two pairs these neurons represents, although it is likely to be the MN3 pair, insofar as these contact the muscle.

No. 2 neurons may be VGN1 neurons or VGN2 neurons, because both are located between ddNs and MN1s. These, in turn, correspond to A13.474 and A11.117 neurons (Stolfi and Levine, 2011), respectively. Of these, VGN1 neurons terminate in the proximal tail and may represent the second type of No. 2 neurons described by Takamura et al. (2010), whereas VGN2 neurons extend well into the tail. Both of these pairs of neurons lack direct synaptic contact to the muscle, so are considered interneurons rather than motor neurons, regardless of their neurotransmitter phenotype. Corresponding neurons were not described by Horie et al. (2010) when using an alternative vesicular acetylcholine transporter reporter, VACHT.

Takamura et al. (2010) identified other long, flat putatively cholinergic neurons in the ventral posterior motor ganglion, No. 6 and No. 8, which could correspond to the posterior MNs in our series. Like No. 6, the MN4 and MN5 pairs in our series extend axons into the tail past the level of the ascending contralateral inhibitory neuron (ACIN) and posterior MG unpaired right-side (PVGN) neurons, terminating just anterior to the first set of paired mid-tail neurons (Fig. 4.5C-D). Close examinations of image stacks from Horie reveals cells expressing ChAT-Kaede, with propidium iodide for nuclear label, along the axon tract in the posterior motor ganglion overlying the MN1 terminals. These appear to correspond to MN5 neurons in our study.

Ovoid neurons described by Imai and Meinertzhagen (2007a; 2007b) appear to correspond to three different cell types, two of which are not actually located within the MG, but in the proximal tail, caudal to the motor neuron terminals. The ovoid visceral ganglion neuron in their report that is located in the MG, along with those described by Takamura et al. (2010), extended long, fine axons into the tail, which is a feature not observed for posterior motor ganglion neurons or caudal tail neurons in the current series. The only axons I observe from the MG or proximal tail that extend well into the tail are those of anterior motor ganglion neurons: ddNs, VGN2s, and MN2s (Fig. 4.5C-D). The location of the visceral ganglion ovoid neuron in Figure 9 of Imai and Meinertzhagen (2007a) appears instead to correspond to that of MN2, which is just anterior to the first endplates of MN1 (Fig. 4.5). Likewise, the location and morphology of the paired putative cholinergic neurons described as visceral ganglion ovoid neurons by Takamura et al. (2010: Fig. 8g) suggest that they are also MN2 neurons (Fig. 4.5). These paired neurons extend axons deep into the tail with expansions at terminal regions along their

length. The other identified ovoid neurons are actually located in the tail, and are discussed below.

These comparisons between the several accounts of the different motor ganglion neurons are summarized for clarity in Table 4.1.

4.2.4 Dorsal Motor Ganglion:

Whereas Horie et al. (2010) did not report vAChT expression in the dorsal motor ganglion, Takamura noted four dorsal cells expressing GFP driven by the vAChTP promoter. One apical bipolar cell with its axon extending "along the ATEN pathway" (Takamura et al., 2010) to the proximal tail in the posterior direction corresponds to AVG5 in our study (Fig. 4.6A-B). Likewise, in vAChT and vGAT co-labelled stacks from Horie et al. (2010), a cell body and a descending dorsal axon in the dorsal caudal region of the motor ganglion express reporter driven by vAChT. Our EM data reveal that this neuron also extends two axons ventrally on the left and right sides of the CNS to extend both anteriorly and posteriorly in the main ventral neuropil (Fig. 4.6), making this a multipolar cell of particular note. Three other putative cholinergic dorsal cells identified by Takamura et al. (2010) all extend single axons ventrally and anteriorly, although the axons in the images provided in their publication are not distinguishable from each other (Fig. 9, 10 in Takamura et al., 2010). The medially located cell among this group may correspond to ascending motor ganglion interneurons AVG4, AVG2, or AVG1, all centrally located in the dorsal motor ganglion in our series (Fig. 4.6C-D). Of these, AVG4 is the most likely candidate, because it underlies AVG5 and extends not

Table 4.1. Neurons of the motor ganglion, with comparison of different naming classifications and distinguishing features. Names used in this study (connectome name) and their abbreviations (Abbr.) are given and other naming classification systems are listed and specified by author, and distinguishing features are identified from observations from TEM series that correspond to noted attributes in the literature. Putative neurotransmitter (NT) is given for each neuron pair, as acetylcholine (ACh), GABA or glycine. Cases where neurotransmitter expression or identity is ambiguous are indicated by ?, and alternate possibilities are indicated where appropriate by /. Neurotransmitter is based on reporter gene expression in cell type identified in corresponding studies, and lineage name is noted where available.

Connectome Name	Abbr.	Lineage name	Cell-specific promoter	Horie et al., 2010	Takamura et al., 2010	NT	Imai and Meinertzhagen, 2007a	Defining feature
descending decussating neurons	ddN	A12.239	Dmbx	VCN1	No. 1	ACh	motor neuron	decussates
visceral ganglion interneuron pair 1	VGN1	A13.474	Vsx		No. 2	ACh	motor neuron	close cell body pairs, axons to proximal tail
motoneuron pair 1	MN1	A11.118	Nk6	VCN2	No. 3	ACh	caudal neuron	large frondose endplates
visceral ganglion interneuron pair 2	VGN2	A11.117	Vsx/Pitx	VCN4	No. 4	ACh	VG ovoid neuron	dendrites toward midline
motoneuron pair 2	MN2	A10.57	Islet	VCN5	No. 5/VG ovoid neuron	ACh	motor neuron	large elongate cell bodies and long bead-on-string axons far into tail
visceral ganglion interneuron pair 3	VGN3			VCN3 ?	No. 4?/cells dorsal to No. 2?	ACh? GABA?		small more dorsal cell bodies rotated toward midline
motoneuron pair 3	MN3			VCN3 ?	No. 4?/cells dorsal to No. 2?	ACh? GABA?		small more dorsal cell bodies with lateral then posterior axon projection
motoneuron pair 4	MN4				No. 6/No. 8?	ACh?		elongate oval cell body
ascending contralateral inhibitory neuron 1	ACIN1			ACIN1		glycine	Planate neuron?	long descending dendrite, ascending decussating axon
motoneuron pair 5	MN5				No. 6/No. 8?	ACh?		more dorsal cell body dorsal to anterior MN1 frondose endplates
posterior visceral ganglion interneurons	PVGN 1				cell posterior to No. 5?/neurons in proximal tail?	ACh? GABA?		right side only, at location of ACIN cbs, long neurite with simple terminal
	PVGN 2							right side only, dorsal, opposite ACIN2L, short neurite
midtail neuron pair 1	mt2/4			Fig. 1F-H	No. 9?	ACh	Planate neuron	elongate flattened cell body in tail
midtail neuron pair 2	mt			Fig. 1F-H	No. 9?,	ACh	Planate neuron	elongate flattened cell body in tail
ascending MG neurons	AVG			VCN3 ?	multipolar dorsal ascending cells	ACh and GABA	contrapelo cells	dorsal, with ventral ascending neurites

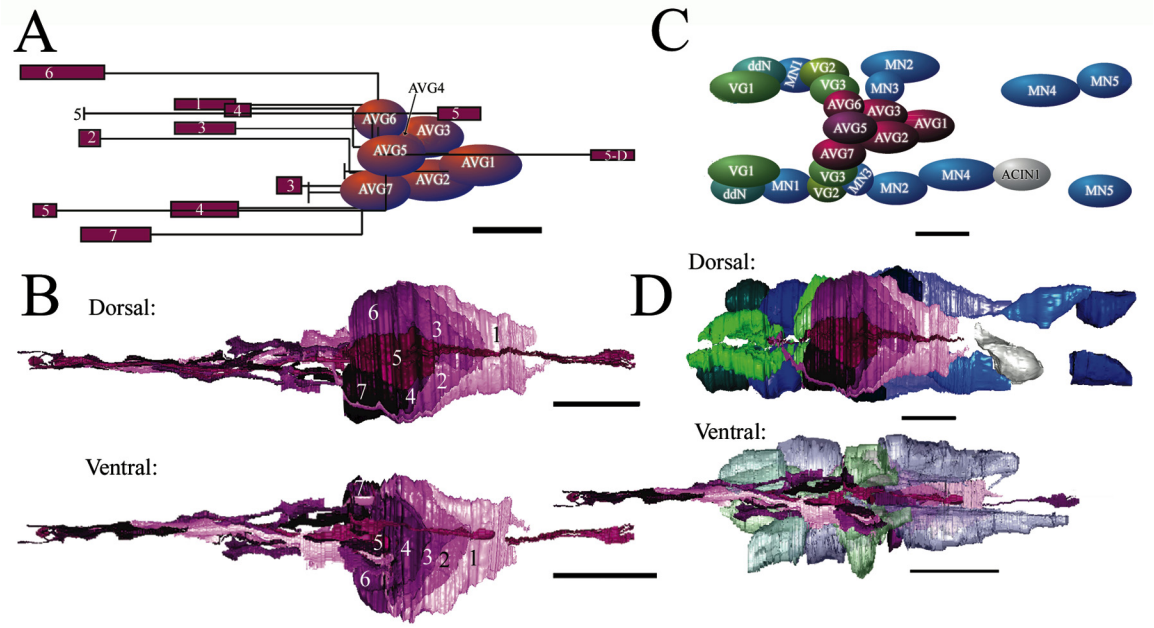

Figure 4.6. Ascending interneurons of the dorsal motor ganglion (AVGs). A) AVG neuron positions and projections. Cell bodies labelled with cell name, terminals labelled with corresponding number. Note that anterior lies to the left and that most cell axons are ascending. B) Compiled reconstructions of AVG neuron cell bodies (from low magnification series) and neurites (from high magnification series) colour-coded and labelled by number on cell bodies, from dorsal and ventral views. C) Cell bodies of all motor ganglion neurons illustrating relative sizes and locations, labelled with cell names: descending decussating neurons (ddN), descending motor ganglion interneurons (VG1-3), motor neurons (MN1-5), AVGs 1-5, and the first, left side, ascending contralateral inhibitory neuron (ACIN1). D) Reconstructed AVG neurons and ventral motor ganglion neuron cell bodies, dorsal and ventral views. Ventral motor ganglion neurons made transparent in ventral view to reveal AVG neurites. Scale bars: 10µm.

one, but two axons ventrally then anteriorly (Fig. 4.6A-B). The remaining two lateral (left and right) putative cholinergic dorsal neurons likely represent AVG6 on the right and AVG7 on the left. Each of these neurons in our series extends an axon ventrally and anteriorly through the motor ganglion and neck to form terminals in the brain vesicle. Though these descend initially on the right and left sides, they turn at the midline ventral to the cell bodies of VGN1s and extend toward the brain vesicle along the central neuropil rather than ending near MN1 (No. 3) (Fig. 4.6D), as suggested by Takamura et al. (2010). Close examination of image stacks collected by Horie et al. (2010) suggests that the dorsal regions of the larvae are not always included within the collected region, so it is not possible to rule out vAChT expression in this region. The AVG neurons are unusual in several respects: a) the cell bodies of some emit dendrites, which most *Ciona* neurons lack; b) AVG3-AVG5 have two axons arising from the cell body; and c) AVG5 has an axon that splits to yield two daughter axons. These features are heterodox either for neurons in general or Ciona neurons in particular, and their organization will be considered in greater detail later on (see Chapter 7).

Takamura et al. (2010) also report specific instances of other vAChTP expressing cells in this region, which may correspond to those identified in our study, but absent elsewhere in the literature. GFP expression, driven by the promoter for the vesicular ACh transporter Ci-vAChTP, was observed in three small cells dorsal to No. 2, one cell posterior to No. 5, and one small cell, No. 7, dorsal to No. 5 and near the midline. These three small dorsal putative cholinergic cells are in the similar locations to VGN3 and MN3 neurons. However, I find that both of these cell types are paired. The dorsal AVG neurons described above, also occupy this region, though they tend to lie dorsal to the

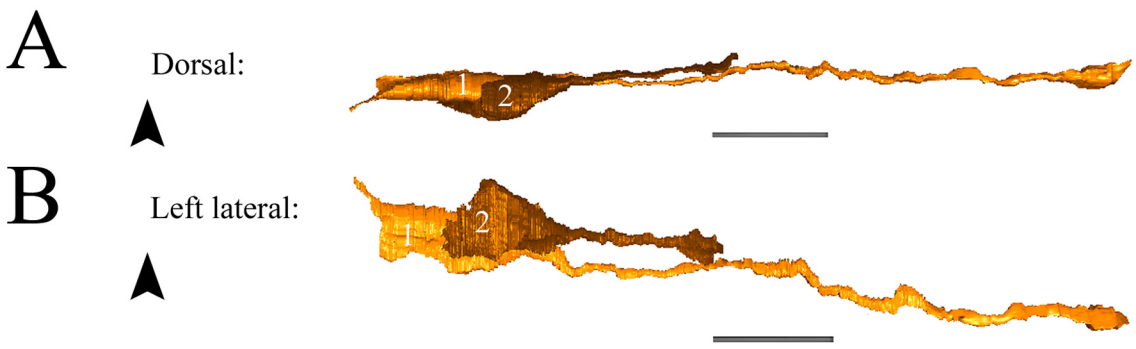

Figure 4.7. Unpaired right-side posterior visceral ganglion neurons (PVGNs) at the motor ganglion-tail border. A) Dorsal view of PVGN 1 and 2. B) Corresponding left-lateral view. Arrowheads: location of ACIN1L cell body. Scale bars: 10µm.

canal and are likely not the cells in question. The slender cell posterior to No. 5 may be the PVGN1 or PVGN2 neuron, both exclusive to the right side of the animal in our series with a more dorsal location than other motor ganglion counterparts (Fig. 4.5C-D; Fig. 4.7).

Cholinergic markers have been reported to express in many individual cells of the ventral motor ganglion, but do not account for all MG cells identified in our study. *In situ* expression patterns for Ci-GAD, and less explicitly for Ci-vGAT suggest that GABA is either synthesized in terminals of brain vesicle neurons or some MG neuronal cell bodies in the anterior ventral and dorsal motor ganglion (Zega et al., 2008; Yoshida et al., 2004). However, based on promoter-driven reporter constructs, only Takamura et al. (2010) identified a single bipolar cell in the ventral anterior motor ganglion expressing LacZ driven by the Ci-GAD promoter. I find no such bipolar ventral motor ganglion neuron, but the axon between the brain vesicle and motor ganglion may be a descending relay axon from one of the labelled brain vesicle relay neurons (Fig. 4.8). The location of the cell body of the bipolar neuron is similar to that of VGN2s, with a descending axon extending from the dorsal posterior edge of the cell body (Fig. 4.8). Additionally, the dorsal motor ganglion contains cells reported to express Ci-GAD driven LacZ (Takamura et al., 2010). While vGAT reporter expression is not described by Horie et al. (2010), the image stacks reveal weak expression in the dorsal motor ganglion. Furthermore, the same promoter used to drive Kaede in transgenic lines reveals dorsal expression recapitulating the patterns observed by Zega et al. (2008) and Takamura et al. (2010). Detailed analysis of the expression observed by Takamura et al. (2010) reports that some fibers extending from a cluster of five or more cells reached the posterior brain vesicle,

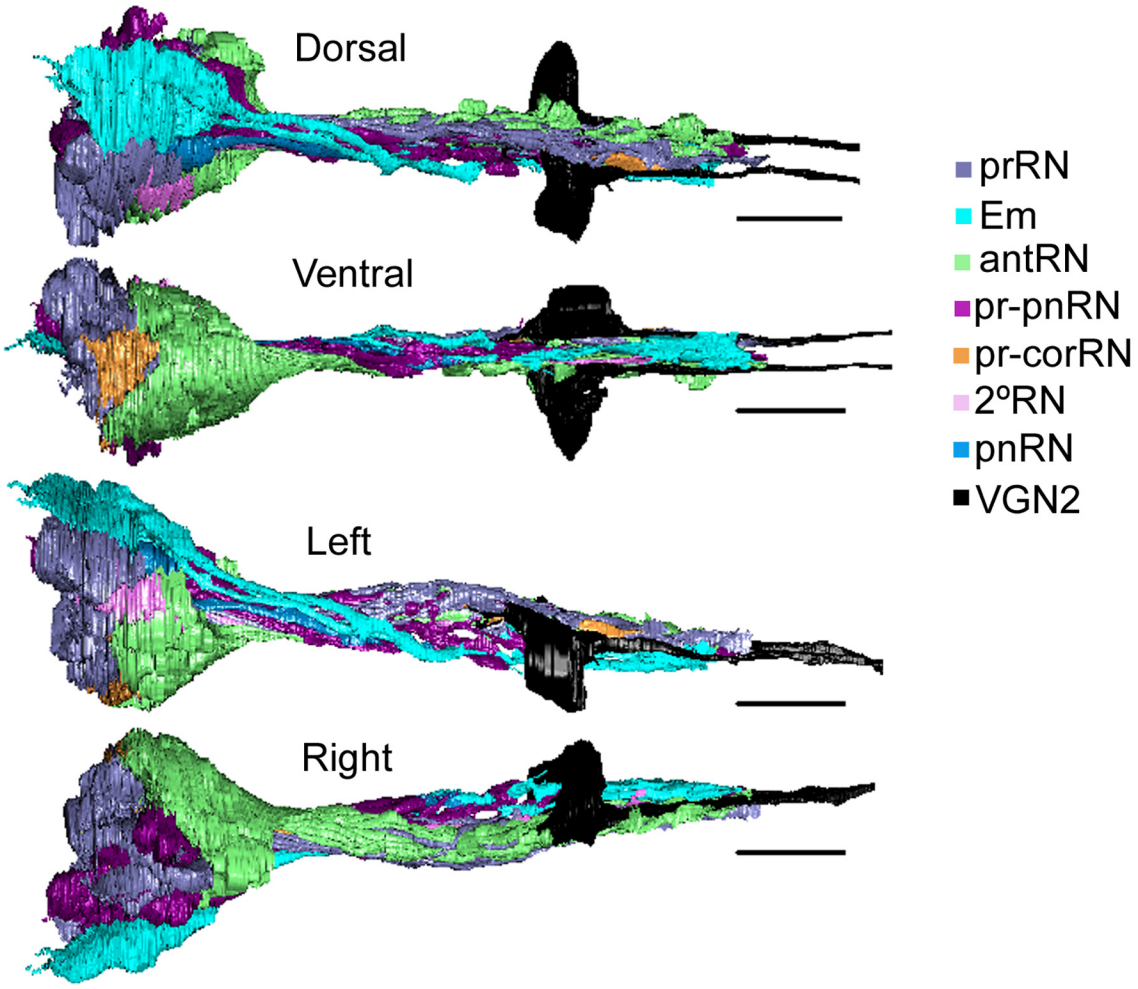

Figure 4.8. Rotated views of reconstructed brain vesicle relay neurons and paired VGN2 neurons of the motor ganglion. Cell types are colour-coded for: photoreceptor relay neurons (prRN); eminens neurons (Em); antenna relay neurons (antRN); photoreceptor/peripheral relay neurons (pr-pnRN); photoreceptor/coronet relay neurons (pr-corRN); relay neurons lacking direct sensory input (2ºRN); peripheral relay neuron (pnRN); and motor ganglion descending interneuron pair 2 (VGN2). Scale bars: 10µm.

while others projected posteriorly. Among these, some were identified as multipolar or bipolar neurons. The three more posterior AVG neurons, AVG1, AVG2, and AVG3 identified in our serial EM image stack are likely to be among these dorsal GAD expressing neurons (Fig. 4.6B-D). All three are located centrally, with axons projecting to the dorsal left side, passing by cell bodies of MN3L and VGN3L en route (Fig. 4.6C-D. These axons then branch, or turn ventrally to ascend in the ventral neuropil (Fig. 4.6). These neurons do not, however, account for the GAD expression observed in descending axons of dorsal neurons (Takamura et al., 2010). Of the AVG neurons, only the AVG5 neuron (Fig. 4.6) extends an axon caudally in the ventral motor ganglion, so other identified dorsal neurons expressing Ci-GAD driven LacZ may be VGN3 neurons, which have dorsal cell bodies with respect to the rest of the ventral anterior motor ganglion and descend to the posterior MG (Fig. 4.5; Fig. 4.9). Overall, the AVG interneurons fall into four broad categories, based on morphological characteristics (summarized in Figure 3.9).

4.3 **Discussion**

Is there a possibility that MN3 and VGN3 have different neurotransmitters between left and right partners? Reported expression data does not resolve paired neurons dorsal to the identified ventral motor complex in the motor ganglion, but our study reveals two pairs of neurons, one pair with synaptic input to muscle, that terminate in the proximal tail (Fig. 4.5B-D). Each of these pairs should derive from a common mother cell, so mosaic expression ought not to explain differences in their reporter gene expression on either side of the neuropil. Thus, it is possible that VGN3 or MN3 pairs may express

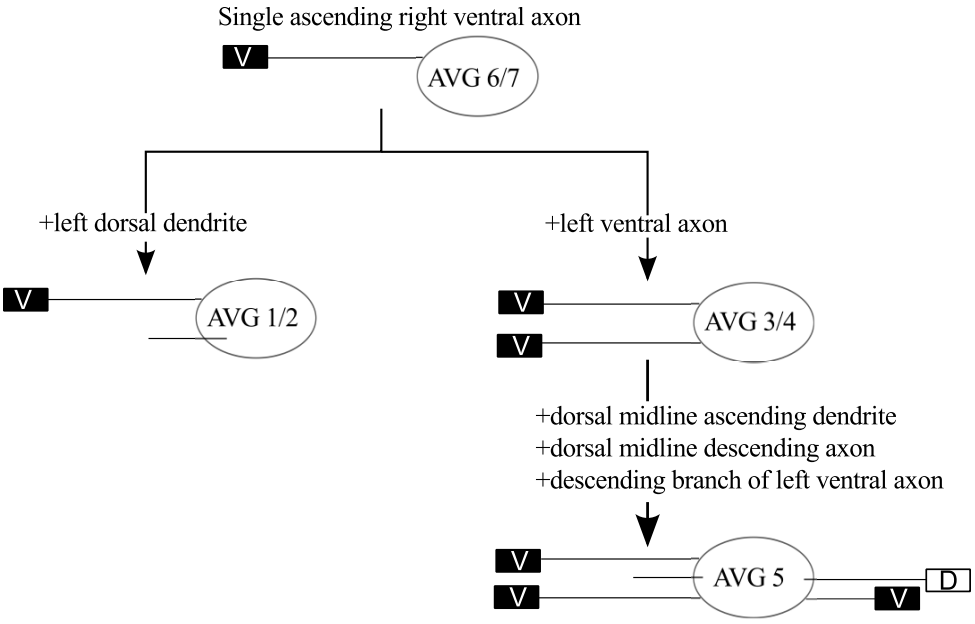

Figure 4.9. Chart illustrating morphological types of ascending dorsal motor ganglion (AVG) interneurons. AVG neurons are given names for each morphological type, with additional features indicated by + followed by description of the additional character.

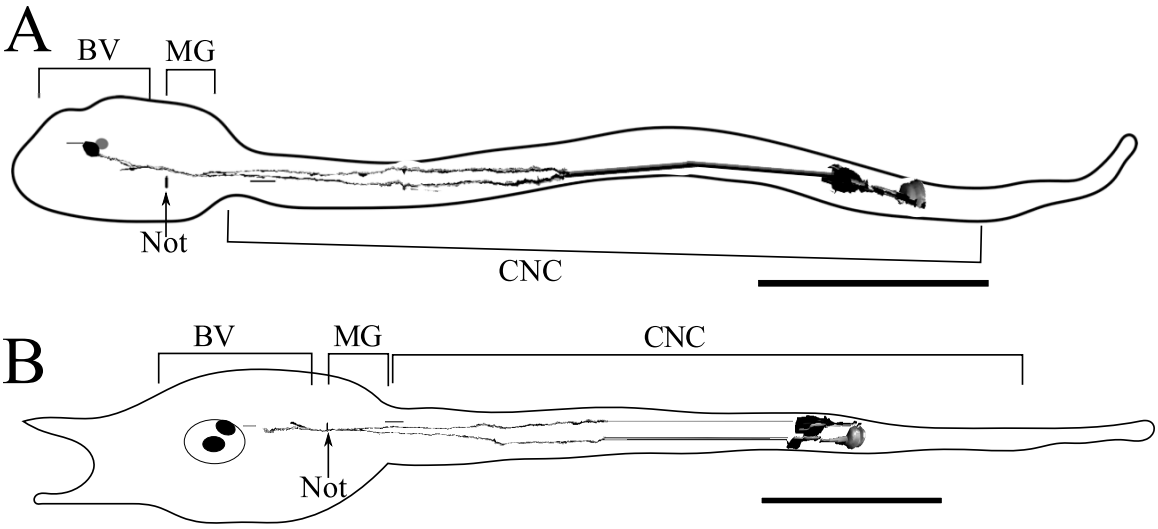

Figure 4.10. Planate neurons of the tail reconstructed relative to a profile of the entire larva, dorsal view. Caudal third of the tail is not reconstructed. Scale bar: 100µm.

different neurotransmitters between left and right partners. Alternatively, these pairs may not show any expression for the transmitters examined in the literature.

4.3.1 Tail Neurons:

Two types of neuron in the tail correspond to ovoid tail neurons described by Imai and Meinertzhagen (2007a), but only the anterior of these has ventral cell bodies. Mid-tail neurons identified in our study (Fig. 4.5C-D) exist in a similar arrangement and location as those depicted in Figure 8d of Imai and Meinertzhagen (2007a), while those in Figure 8e correspond more closely to the location of planate tail neurons (Fig. 4.10), distinguished as bipolar neurons by Imai and Meinertzhagen (2007a; 2007b). This latter type has cell bodies located in the peripheral tissue in our study (Fig. 4.10) (see Chapter 7), and their neurotransmitter expression is discussed below. The ovoid-like mid-tail neurons I find in our study have shorter descending axons within the tail (Fig. 4.5C-D), like the second ovoid cell type described by Takamura et al. (2010), which terminate only a short distance from their cell bodies. Thus, these short descending mid-tail neurons are likely these same ovoid neurons. It should be noted that these also resemble the planate neurons described by Imai and Meinertzhagen (2007a; 2007b), although I instead refer to the deeper tail neurons as planate neurons.

Cholinergic reporters are expressed in these paired descending neurons in the tail with short descending axons (Horie et al., 2010; Takamura et al., 2010). This label occurs in cells, corresponding to the paired mid-tail neurons present in this ssEM series, which extend ipsilateral descending axons along the two axon tracts of the tail (Fig. 4.5C-D). These neurons provide synaptic input to muscle (see Ryan, 2015: Chapter 8), so may be

akin to spinal motor neurons, which are cholinergic in vertebrates (Dale et al., 1936). As with the putative cholinergic neurons in reporter studies (Horie et al., 2010; Takamura et al., 2010), the pairing of these mid-tail MNs is not precise, and their cell bodies lie on either side of the canal abutting the left and right axon tracts (Fig. 4.5C-D). These cells are located in the place of ependymal cells of the tail, but at least one pair differs from ependymal cells in that it has cilia that do not enter the canal. In addition to these paired neurons, some ciliated ependymal cells on the right side appear to extend short neurites that bear presynaptic sites onto the basement membrane, but these fail to provide input to muscle.

All descriptions of axon projection from confocal stacks are complicated by the four ascending planate neurons that I identify with cell bodies in the tail and with axons that extend rostrally up the length of the tail, through the motor ganglion, to terminate in the brain vesicle (Fig. 4.10). For example, their axons may have been mistaken themselves by Imai and Meinertzhagen (2007a) as descending axons from the VG ovoid neurons, and may instead be descending brain vesicle relay axons. The neurotransmitter phenotype of these neurons is unclear; however, GABA expression (Brown et al., 2005) and GAD promoter driven LacZ expression in cells at these locations in the tail have both been reported (Brown et al., 2005, Takamura et al., 2010). While not discussed, images obtained by Horie et al. (2010) demonstrate weak immunoexpression of anti-Ci-vGAT at the same locations in the tail. However, in images obtained by, but not discussed in Horie et al. (2010), expression driven by the VACHT promoter is also evident in the tail at sites corresponding to locations near these cell bodies; long anterior axonal projections from these cells are not evident however. Another interesting aspect of light microscopic

reports is that both GABA antibody and Ci-GAD *in situ* data identified three tail cells in different animals (Zega et al., 2008), whereas Takamura et al. (2010) identified four cells, one of which appeared smaller, with shorter axonal projections. In contrast, reports or images showing the expression of cholinergic markers in caudal tail neurons reveal only a single neuron (Horie et al., 2010).

Interestingly, a terminal from a descending axon is reported just anterior and ventral to the location of one of these tail cells (Horie et al., 2010), consistent with our observation that descending neurons of the motor ganglion terminate anterior to the cell bodies of the four ascending tail neurons. Yet Ci-GlyR promoter drives GFP expression in axon projections beyond this point in the tail (Nishino et al., 2011). This expression could intimate phenotypic diversity, or may indicate that glycine receptors exist on these tail neurons, as well as descending neurons of the motor ganglion, and may respond to the long-range tonic actions of glycine. The tail neurons themselves are bipolar, so any expression within these neurons could extend to the tip of the tail.

4.3.2 Co-transmission in *Ciona* Larval Neurons:

Mounting evidence suggests that fast neurotransmitters can be both co-expressed and co-released within individual neurons. At other locations acetylcholine is reported to co-release with ATP, glutamate, monoamines, and GABA (Hnasko and Edwards, 2012). Co-release of glutamate with monoamines or GABA, and GABA with glycine also occurs in mammalian nervous systems (Hnasko and Edwards, 2012). Some fast transmitters appear to release from single vesicles (June et al., 1998) or single vesicle pools (Onoa et al., 2010), whereas evidence suggests that other transmitters are released from distinct vesicle pools (Lee et al., 2010). The mosaic nature of reporter expression in

Ciona intestinalis and the small number of double label studies support the possibility that fast neurotransmitters may be co-expressed in ascidian neurons, despite the lack of prior consideration of this topic. Co-expression or co-release could have particular relevance to the function of this tiny CNS, especially within integrative regions such as the posterior brain vesicle. This is a particularly relevant consideration when attempting the difficult task of interpreting the functional organization of the larval connectome.

The dynamics of co-release of multiple fast transmitters from individual neurons depends on the packaging and arrangement of transmitter at synapses, and on transporter dynamics. In the case of starburst amacrine cells of the vertebrate retina, GABA release is more sensitive to Ca^{2+} than ACh release (Lee et al., 2010). Thus, the threshold of these neurons for a GABA releasing action potential would be lower than that for acetylcholine, which in the case of starburst amacrine cells enables the two transmitters to function in different roles (Lee et al., 2010). However, the particular machinery of the synaptic vesicle release mechanism may not be the same in all neurons co-expressing these two neurotransmitters. Co-storage of glutamate and acetylcholine functions to promote the vesicle filling of presynaptic acetylcholine, and the co-release of the two neurotransmitters results in postsynaptic actions on different timescales (Hnasko and Edwards, 2012). The more rapid action of glutamate could be mediated by a number of factors, including organization, as well as synaptic and postsynaptic protein compositions (Hnasko and Edwards, 2012). Yet another possibility arises from recent findings that in vertebrate neurons GABA and glutamate are co-released (Noh et al., 2010; Beltrán and Gutiérrez, 2012; Shabel et al., 2014). Thus, even without considering peptide

transmitters, all combinations of neurotransmitters identified in *Ciona* larvae have potential to be co-released.

In the *Ciona* larva, several neurons in the brain vesicle are co-labelled for both vAChT reporter expression and VGAT antibody (Horie, unpublished raw data). These neurons are located in the mid-dorsal posterior brain vesicle, just ventral and slightly anterior to the eminens neurons, a location that corresponds to the region containing the photoreceptor relay neurons that form synaptic contact with neurons of the peripheral network (Fig. 4.11). Of these, the highest level of expression of VGAT immunoreactivity exists in a cell that seems to correspond in location to cell 74 (Fig. 4.12A). The presynaptic sites of these neurons contain mixed pools of vesicles, including dense and clear cored vesicles of varying size (Fig. 4.12B). GABA and acetylcholine are each packaged into small electron lucent vesicles at synaptic terminals (De Rijk et al., 1990; Weihe et al., 1996). However, phosphorylation can target vAChT expression to large dense core vesicles (Krantz et al., 2000), and ACh has been identified in dense core vesicle fractions (Schubert and Klier, 1977; Agoston and Whittaker, 1989). Assuming that, like starburst amacrine cells, GABA release occurs at lower Ca^{2+} concentrations than acetylcholine release, the network involving cell 74 illustrates how this could enable photoreceptor response to produce different effects on peripheral-motor coordination (Fig. 4.12C).

Other neurons, such as AVG5, VGN2, VGN3, MN3, PVGN, and the planate neurons of the tail seem to correspond to neurons expressing different neurotransmitters in reporter and antibody studies. These neurons may co-express GABA and acetylcholine or GABA and glutamate, but confirmation would require co-labelling studies with strong

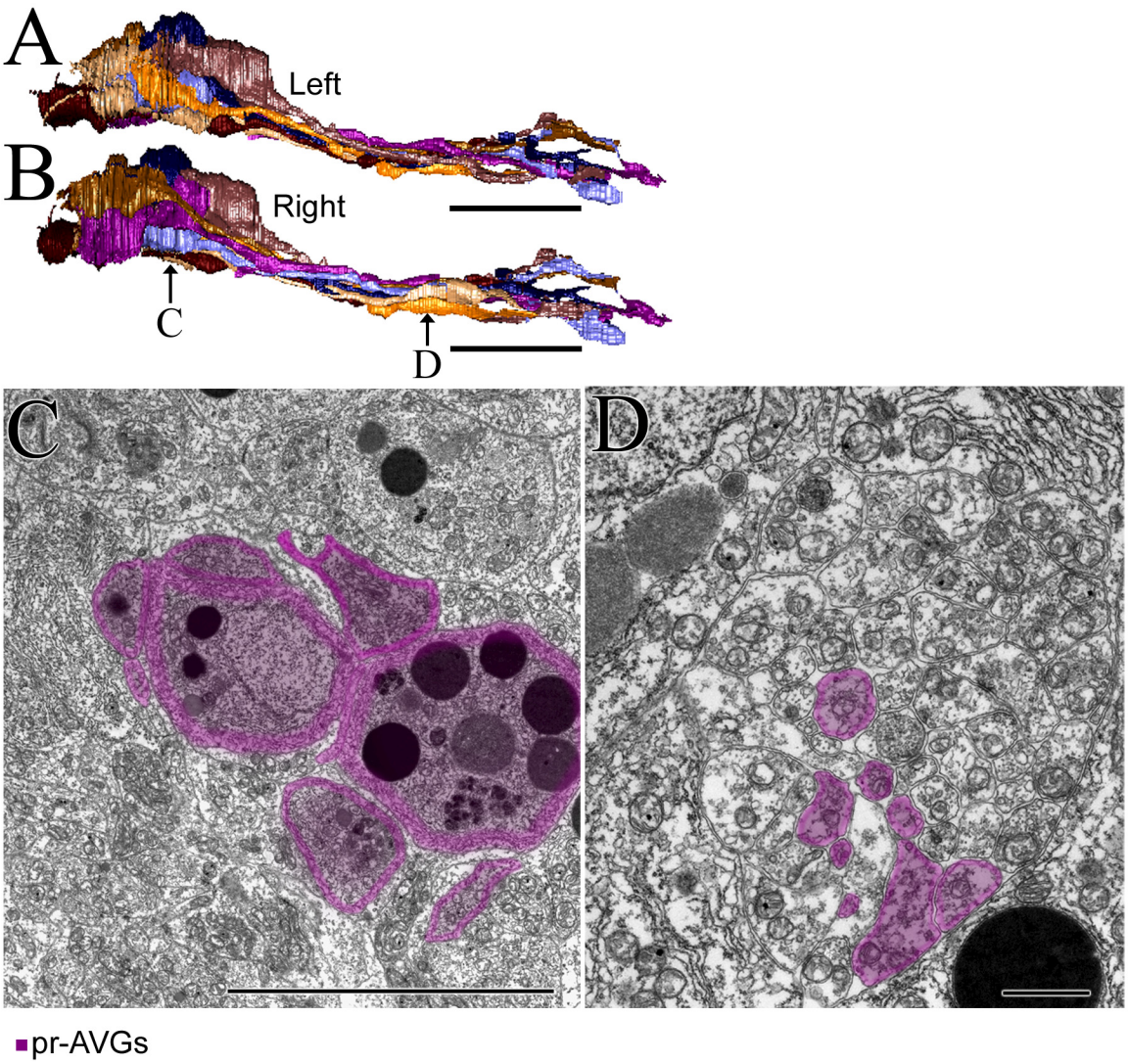

Figure 4.11. Photoreceptor-AVG relay neurons of the posterior brain vesicle. A) left lateral view of reconstructed pr-AVG neurons. B) Right lateral view of reconstructed pr-AVG neurons labelled with section locations for panels C and D. C-D) EM sections showing pr-AVG neurons viewed as if from caudal to rostral (dorsal is up, left to the larva's left). C) Section in the posterior BV illustrating clustering of pr-AVG cell bodies and axons. D) Section in the neck showing ventral-right location of pr-AVG axons. Scale bars: 10µm (A-B); 1µm (C-D).

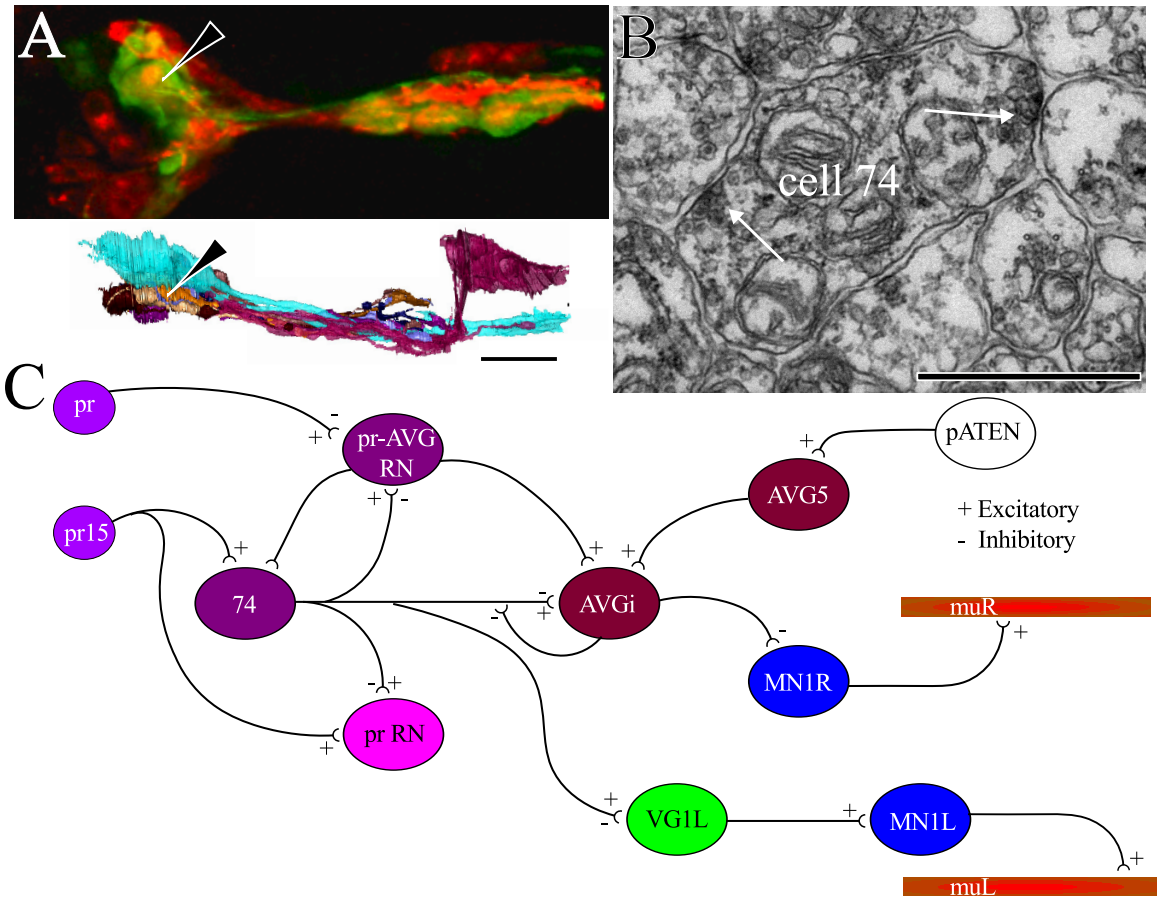

Figure 4.12. Relay neurons with putative co-expression of neurotransmitters. A) Side-by-side comparison between confocal image stack with reporter labels for vGAT1 (red) and vAChT (green) (Horie et al., 2010; raw data) and reconstruction of the proposed counterparts reconstructed from serial EM, including eminens (blue) and AVG cells (for reference), and photoreceptor-AVG interneurons located in the region with putative co-expression (black arrowhead). B) Mixed synapses of candidate neuron with putative co-transmission, cell 74. C) Diagram of potential pathway of neuron with proposed co-expression of acetylcholine and GABA neurotransmitters: cell 74. Nodes represent neurons or classes of neurons: photoreceptors (pr); photoreceptor15 (pr15); photoreceptor relay neurons (pr RN); photoreceptor and AVG relay neurons (pr-AVG RN); inhibitory ascending MG interneurons (AVG); ascending MG interneuron 5 (AVG5); posterior apical trunk epidermal neuron (pATEN); right motor neuron 1 (MN1R) and left (MN1L); MG descending interneuron 1 (VG1L); left muscle (muL); and right muscle (muR). Scale bars: 10µm (A), 1µm (B).

Figure 4.13. Diagram of neuronal cell bodies in the CNS with putative neurotransmitters. A-B) Dorsal views of representative cell bodies mapped to 3-D location and sized by length on A-P axis. A) Neurons coloured by cell type (key): Ocellus PR (ocellus photoreceptors), Canal PR (canal photoreceptors), trIN (photoreceptor tract interneuron), vacIN (vacuolated photoreceptor tract neurons), Ant (antenna neurons), PN IN (peripheral interneurons of the brain vesicle), Cor (coronet cells), PR/Ant RN (relay neurons with photoreceptor and antenna inputs), RN (relay neurons lacking direct sensory input), PR RN (photoreceptor relay neurons), BV IN (brain vesicle intrinsic interneurons), mm RN (multimodal relay neurons), Eminens, Neck (neck neurons), ddN (descending decussating neurons), VGN (descending paired motor ganglion neurons), MN1&2 (motor neuron pairs 1 and 2), AVG (ascending dorsal motor ganglion neurons), MN3-5 (motor neuron pairs 3-5), ACIN (ascending contralateral inhibitory neurons), PVGN (descending right-side posterior motor ganglion interneurons), midtail (paired descending midtail neurons). B) Neurons coloured by putative neurotransmitter where known (key): ACh (acetylcholine), GABA, Glut (glutamate), DA (dopamine), Gly (glycine), Unknown (neurons lacking putative neurotransmitter identification based on comparisons between EM series and confocal studies). C) Territories of putative neurotransmitters (key) based on reporter gene or antibody expression mapped to dorsal view of CNS outline.

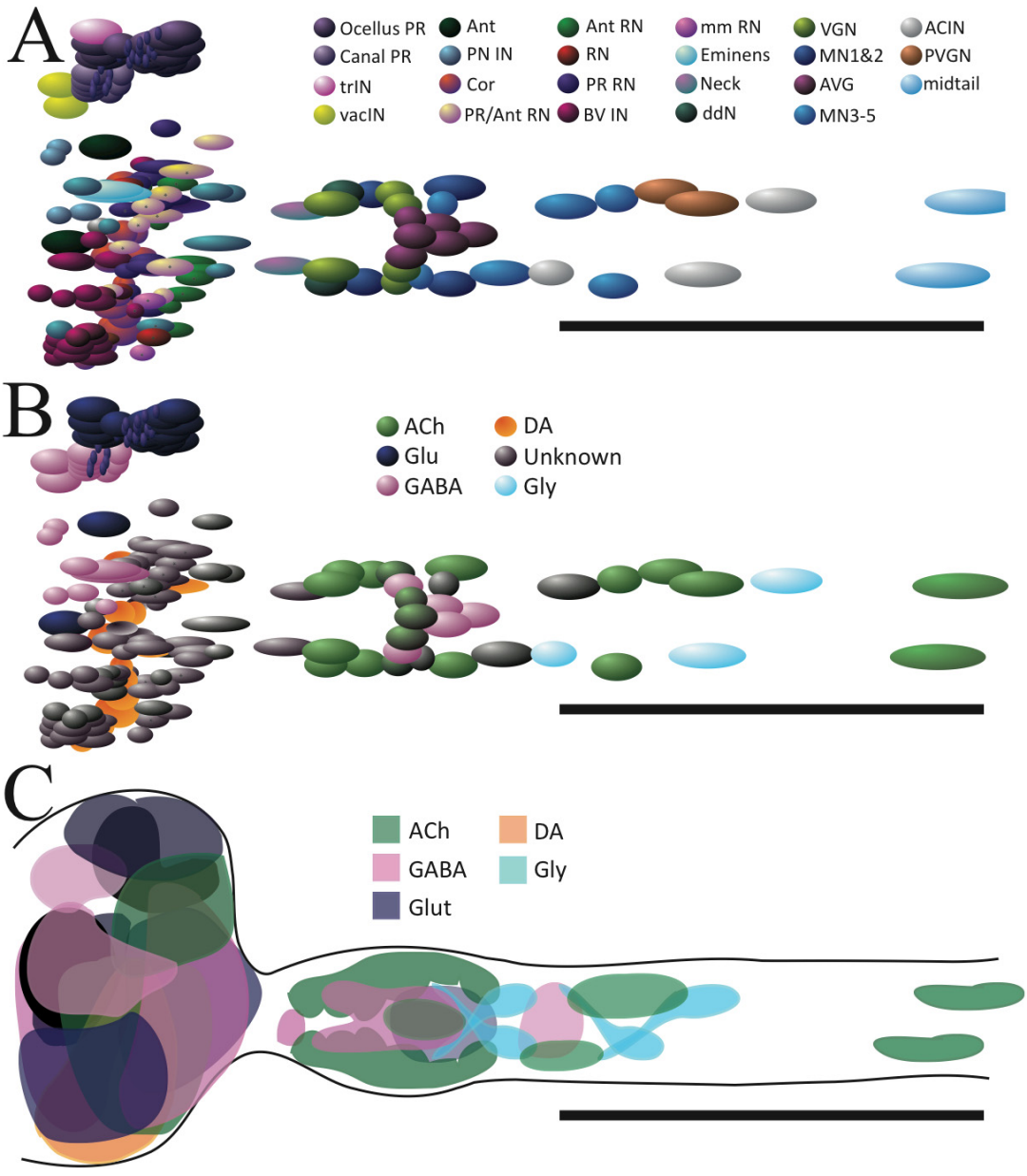
A
Ocellus PR
Canal PR
trIN
vacIN
Ant
PN IN
Cor
PR/Ant RN
Ant RN
RN
PR RN
BV IN
mm RN
Eminens
Neck
ddN
VGN
MN1&2
AVG
MN3-5
ACIN
PVGN
midtail
B
ACh
Glu
GABA
DA
Unknown
Gly
C
ACh
GABA
Glut
DA
Gly

expression of both reporters in each type of neuron. Examining these neurons using molecular tools and immuno-EM could potentially resolve their neurotransmitters and the possibility of co-expression. Overall, difficulties in antibody staining and identification of reporter constructs for many receptors limit interpretation of neurotransmitter action, even where reporters for synthetic proteins are expressed. The map of putative neurotransmitters itself is limited, especially in areas of high neuronal density (Fig. 4.13). Even in cases where receptor

antibodies exist, as for CiCBR (the *Ciona* cannabinoid receptor), high levels of background label can prevent interpretation of whole-mount labeling in larvae (Egertová and Elphick, 2007). The resolution of individual cells, furthermore, is limited in whole-mount imaging, especially in regions of dense neuropil. Examining sectioned material will be a critical next step, and is used in very few existing studies on *Ciona*. Molecular tools at the EM level and immuno-EM would both also resolve more accurately the relatively small numbers of synapses and fine neurites in the anterior brain vesicle, as well as the close proximity of cells in the posterior brain vesicle. The larval connectome provides a basis on which to interpret such future studies, while they in turn will help interpret the function of this network, which still labours under difficulties when based on morphological comparisons alone.

4.4 **Conclusions**

The neurotransmitter phenotypes can be resolved for several neurons, especially within the MG and tail, but the full complement of CNS neurons revealed in this study challenges many assumptions underlying previous assertions about the larval CNS. The neurotransmitter phenotypes of interneurons in the BV are particularly

important to resolve, especially for cases in which these differ in their sign or polarity. Network data can help us to identify particular neurons of interest, such as cell 74, which may use multiple neurotransmitters. More detailed data on neurotransmitters and their receptors in the *Ciona* larval CNS will allow networks to be modeled to predict behavior from underlying circuits.

Chapter 5 : Visual System

5.1 **Introduction**

Although adult ascidians are filter-feeding sessile invertebrates, their larval forms possess a chordate body plan, in which a dorsal central nervous system (CNS) overlies a notochord. This CNS is divided into three regions: the brain vesicle (brain vesicle), containing two pigmented organs; the motor ganglion (MG); and a caudal nerve cord in the tail (CNC) (Crowther and Whittaker, 1984) (Fig. 5.1). One of the pigmented organs in the brain vesicle is a light sensing ocellus, comprising a single pigment cup cell with many pigment granules (Eakin and Kuda, 1971) and 30 photoreceptors (Horie et al., 2005), overlying three glycogen containing lens cells (Eakin and Kuda, 1971). The photoreceptors themselves, like those of vertebrates, are of the ciliary type, and extend a stalks that contains a basal body and expands to form ciliary outer segments in the ocellus pigment cup (Dilly, 1962; 1969; Eakin and Kuda, 1971). The lamellae of these outer segments are orientated parallel to the cilium (Eakin and Kuda, 1971) in contrast to the perpendicular arrangement found in vertebrate rods (Lamb et al., 2007). Eakin and Kuda (1971) propose that this arrangement allows photoreceptors of both *Ciona* larvae and vertebrates to detect light at an angle perpendicular to the lamellae to facilitate maximum light absorption by photopigments.

Sequencing the genome of *Ciona intestinalis* has, amongst many other things, facilitated our understanding of the visual system's homologies with those of vertebrates, perhaps most clearly for the phototransduction pathway. The photoreceptors of *Ciona intestinalis*

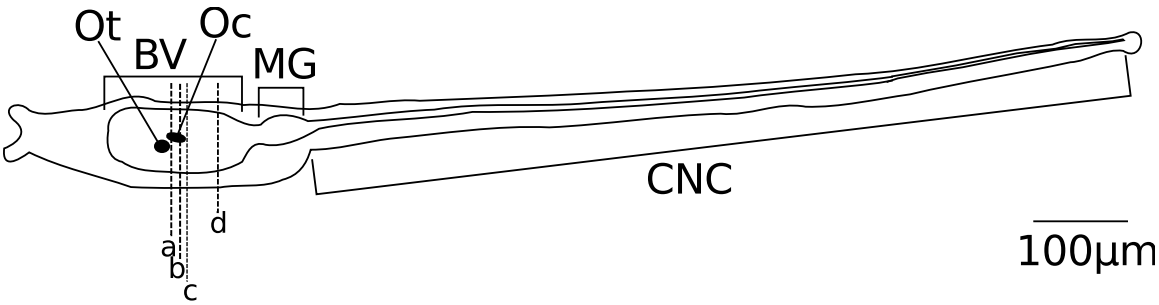

Figure 5.1. *Ciona intestinalis* larva including the following CNS components (left lateral view, dorsal to the top): brain vesicle (BV) containing the sensory pigment organs, the otolith (Ot) and ocellus (Oc); motor ganglion (MG); caudal nerve cord (CNC). Vertical lines represent approximate locations of section planes for subsequent figures: (a) Fig. 2B; (b) Fig. 2A, Fig. 2D, Fig. 4, Fig. 5A, and Fig. 9; (c) Fig. 6B-D; (d) Fig. 16.

express *Ci-opsin1* (Kusakabe et al., 2001; Inada et al., 2003; Horie et al., 2008b), which works as a light sensor by binding with a chromophore to form the photopigment (Wald, 1953; Fain et al., 2010) and arrestin (Nakagawa et al., 2002; Horie et al., 2005; Horie et al., 2008b), a phototransduction component that deactivates opsin (Lamb, 2013). While the mechanism of action is similar to vertebrate phototransduction, enabling photoreceptors that hyperpolarize to light, the underlying structural components lack the complexity observed in vertebrate eyes. Using an Anti-Ci-Opsin1 antibody, Horie et al. (2005) identified 10 outer segments outside of the pigment cup (Tsuda et al., 2003b) and 20 inside the pigment cup. Further analysis using this antibody revealed that photoreceptors fall into three main classes I, II and III, with the first two of these constituting the 30 known ocellus pigment cup associated photoreceptors, 18-23 in group I and 8-11 in group II (Horie et al., 2008b). These numbers differ from previous reports of 15-20 cells by Eakin and Kuda (1971) and 17 or 18 in four larvae, by Nicol (Nicol, 1987; Nicol and Meinertzhagen 1991). It is likely that these counts constitute only group I photoreceptors, but also notable that they differ. Together with limitations of sectioning employed in previous studies, "regulatory mode" of this cell type is posed as an explanation for this variation (Horie et al., 2008b). Recent confirmation of multiple species of *Ciona intestinalis* (Suzuki et al., 2005) may also underlie this variation, since the Japanese workers used *Ciona robusta* (Brunetti et al., 2015; Manni et al., 2015) not *intestinalis*. However, there is evidence (Brown, pers comm.) suggesting that cell number may depend on the light conditions under which larvae are raised, which may, in particular, have an impact on the number of group I photoreceptors. These group I outer segments are arranged in rows inside the pigment cup, while the hitherto unexplored

outer segments of group II photoreceptors occur anterior to the pigment cup, within the lumen of the brain vesicle (Horie et al., 2008b). Their placement meant that these photoreceptors were probably overlooked in previous studies. These outer segments appear to contain photopigment, as Horie et al. (2008b) report specific EM immunodetection of Ci-opsin1 on the lamellar membranes of these outer segments, although confirmatory images were not provided.

Along with ultrastructural details, many studies (Nakagawa et al., 1999; Tsuda et al., 2001; 2003a; 2003b; Kawakami et al., 2002; Inada et al., 2003; Zega et al., 2006) characterized behavioural responses to light during the larval phase of the *Ciona intestinalis* life cycle. The ease of manipulation of this stimulus, and field observations of larval behaviour led to the elucidation of a shadow response, which elicits symmetrical swimming of larvae in response to a step-down of light starting at 1.5 hours post hatching (Zega et al., 2006). This response has been the foundation of further experiments that demonstrate sensitization, habituation (Kawakami et al., 2002), and loss of function with both genetic loss and physical destruction of phototransduction components (Tsuda et al., 2003b; Inada et al., 2003). Expression of Arrestin and Opsin genes within ciliary photoreceptors, and the requirement for a pigmented ocellus (Tsuda, 2003; Inada et al., 2003) for normal behaviour suggest a similarity to the vertebrate visual system. However, in *Ciona*, the resulting behaviour exploits non-segmented tail muscle and a simplified motor system (Grillner et al., 1998; Burighel et al., 1977). The frequency of muscle field potentials (i.e. of contractions) increases with age, starting at a frequency close to that of spontaneous swimming (20Hz) at 1.5 hours post hatching, and increasing to 30Hz from 2 hours post hatching onward, possibly indicating a release from inhibition

somewhere within the motor pathway (Zega et al., 2006). A frequency change, apparent when spontaneously swimming larvae are stimulated by a step-down of light, suggests that the photoreceptive pathway can override spontaneous swimming (Zega et al., 2006). The photoreceptor terminals ramify, extending their spread, three hours post hatching (Horie et al., 2005) implying that connections to interneurons may continue to be established through the first three hours of larval life. These terminals are evident in the posterior brain vesicle (PBV), and evidence for direct monosynaptic photoreceptor input to motor neurons is lacking. The density of interneurons in the posterior brain vesicle makes resolution of the interneurons of the photoreceptors challenging using light microscopy alone. Thus, the actual pathway between the visual and motor systems is unknown. I identified the neurons involved in this pathway and their network of connections.

The developmental genes involved in retinal induction, including pax6, Rx, Wnt, Frizzled, and Six3 are all expressed in cells within the brain vesicle of *Ciona intestinalis*, but beyond the region in which the photoreceptors themselves are located. The *in situ* evidence available is currently of insufficient resolution to determine the precise cellular expression pattern, however, and this will require sectioned specimens, and ideally reporter constructs, to determine the accurate localization. All retinal cell types present in vertebrates derive from retinal progenitor cells, which are multipotent cells capable of forming amacrine cells, rod and cone photoreceptors, bipolar neurons, Müller cell glia, retinal ganglion cells, and horizontal cells. The timing of development in the vertebrate retina, which generates amacrine cells, rods, bipolar cells and glia late, compared with retinal ganglion cells, horizontal cells and cones (Rapaport, 2006), may possibly mirror

the developmental establishment of populations of retinal cells in ascidians, however without detailed expression data this cannot be easily ascertained. Thus, understanding this region in the ascidian larva can only be based, at present, upon the degree of stratification, and on a comparison of the connections between cell types rather than on developmental expression patterns.

Beyond photoreceptors, the only neural cells implicated at present in the visual pathway are the dopamine-synthesizing coronet cells, which have been proposed to share properties with vertebrate amacrine cells (Razy-Krajka et al., 2012). Although these rather enigmatic cells were initially thought to function in pressure detection because of the structure of their modified cilia (Eakin and Kuda, 1971), no influence of pressure was evident on either the period or frequency of larval swimming under controlled experimental conditions (Tsuda et al., 2003b). While coronet cells are not photoreceptors, as they were first proposed to be (Dilly, 1969), they develop within the visual field and are nevertheless capable of modulating the larva's photic response (Razy-Krajka et al., 2012). Razy-Krajka et al. (2012) propose that the amacrine cell-like coronet cells lie in close relation to a population of putatively cholinergic neurons, and send processes toward glutamatergic and GABAergic neurons. Analysis of these coronet cells and their possible connections will help resolve whether they are anatomically qualified to be involved in synaptic transmission, strengthening the relevance of their proximity and projections. The projections and connections of their postsynaptic partners are likewise of interest, and both will be discussed below in relation to coronet cells' fine structural characteristics and connectivity.

5.2 **Results**

5.2.1 Photoreceptor Classes:

Three populations of photoreceptors were identified based upon their possession of modified cilia that to a greater or lesser extent -- depending on the photoreceptor type -- resemble outer segments (Fig. 5.2A,B,D). Of these photoreceptors, the most anterior are those that project outer segments directly into the lumen of the canal, rather than into the ocellus pigment cup. These seven Type II photoreceptors, are in contact with lens cells and extend axons toward the posterior brain vesicle along the main photoreceptor axon tract, on the right ventral border of the CNS. There are two rows of these Type II photoreceptors, one row of three photoreceptors (TypeII-i) anterior to the pigmented portion of the ocellus pigment, and one other row of four (Type II-ii) photoreceptors that lie more posteriorly (Fig. 5.2C). From ultrastructural analysis, it is clear that the outer segments of the Type II-ii photoreceptors lie between the lens cells and ocellus pigment cup, and come into contact with the ocellus pigment cup itself (Fig. 5.2C).

The second population of photoreceptors, Type I, lie adjacent to the Type II photoreceptors on the dorsal right side, but extend their outer segments into the ocellus pigment cup through its lateral edge (Fig. 5.2A). These Type I photoreceptors are grouped in five rows (I-i to I-v) of 5, 5, 4, 4, and 5 cells respectively (Fig. 5.3A-B). All of these photoreceptors also project their axons to the external edge of the CNS on the right side, then toward the posterior brain vesicle along the photoreceptor axon tract.

The third group of photoreceptors lies more caudally and ventrally. These six Type III photoreceptor cells have modified cilia that resemble, if not exactly, outer segments (Fig.

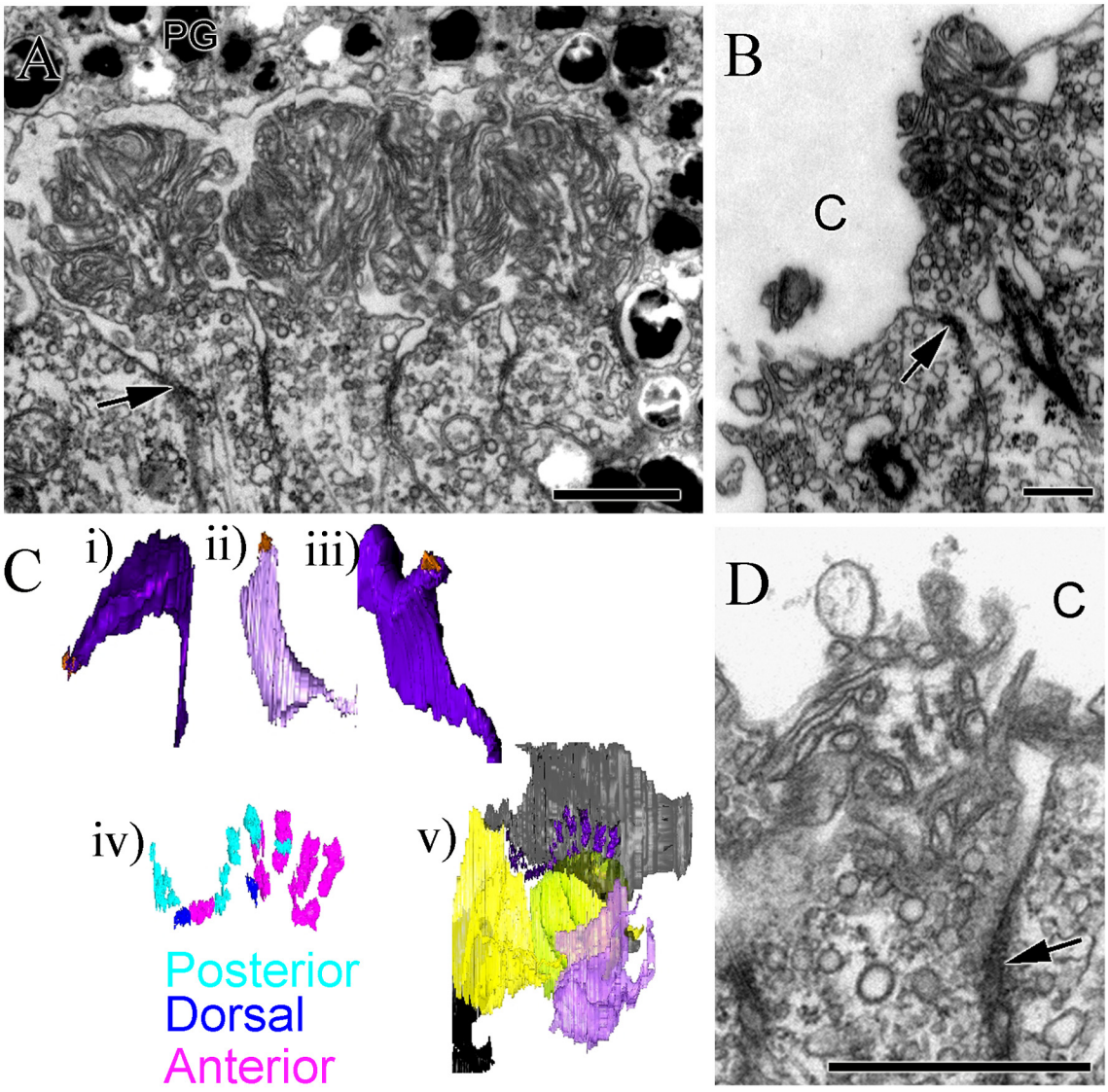

Figure 5.2. Larval photoreceptor outer segments in *Ciona*. A) Type I outer segments emerge from narrow stalks connected by desmosomes (arrow) into the ocellus pigment cup containing pigment granules (PG). B) Type II outer segments emerge from stalks connected by desmosomes (arrow) directly into the neural canal (C). C) Type I and II outer segments (orange) extend from either anterior (i), dorsal (ii), or posterior (iii), edges of photoreceptors (purple). Complete reconstruction of the series of rows of Type I and II outer segments (iv) with colour-coded orientations of outer segments. Reconstruction of outer segments with vacuolated and pigment cells (v), left lateral view. D) Type III modified ciliary outer segment emerging directly into canal (C) through stalks connected by desmosomes (arrow). Scale bars: 1µm.

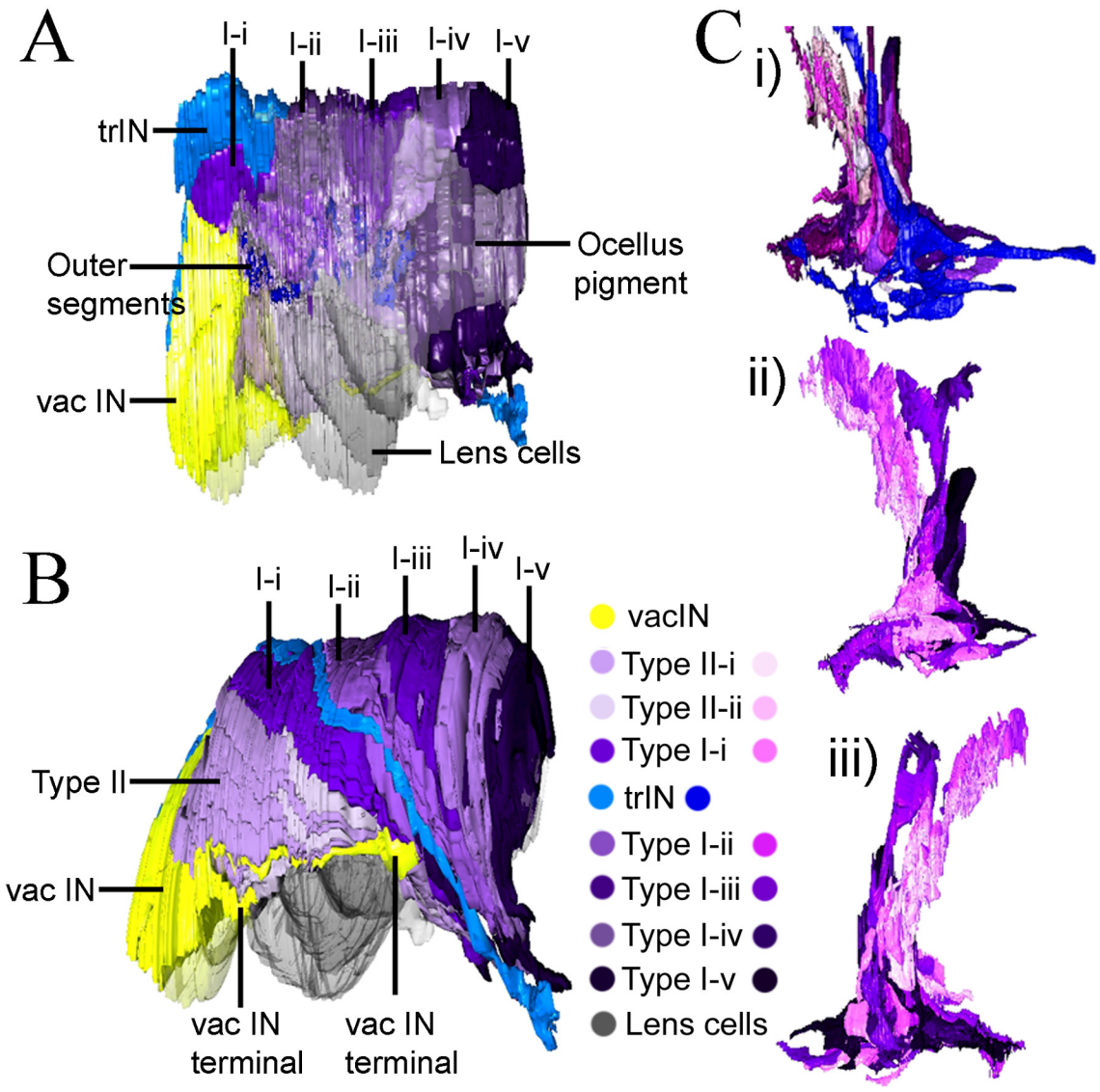

Figure 5.3. Reconstructions of visual system components (excluding photoreceptor and photoreceptor tract interneuron (trIN) terminals) from left lateral (A) and right lateral (B) views. Lens cells and ocellus pigment are rendered transparent to allow outer segments to be visible. vacIN: two anterior vacuolated photoreceptor tract interneurons that terminate within the PR axon tract. C) Type I and II photoreceptor terminal reconstructions, with (i) and without (ii) trIN terminal from ventral (i and ii) and dorsal views (iii).

4.2C; Fig. 5.4). Although these do not contact the lens cells or the ocellus pigment cup directly, they are themselves vacuolated in the same way as are lens cells, with mitochondria but no membrane, lining the vacuole (Fig. 5.4B-C). A subset of these also directly contacts coronet cells, and/or antenna neurons, though there is no EM evidence of junctions of any kind between them and either of the other cell type. Furthermore, this class of photoreceptor extends only short axons at 2hph.

5.2.2 Novel Photoreceptor Tract Neurons:

Along with the photoreceptors themselves, other hitherto undescribed neurons form close spatial associations and connections with photoreceptors. These are as follows: a) A single associated neuron (cell 36) lies dorsal to the Type I-i ocellus photoreceptors, and extends an axon to the right border of the CNS, then ventrally along the photoreceptor tract to form a terminal in the posterior brain vesicle (Fig. 5.3A-C). b) Two additional neurons caudal to the photoreceptors have vacuoles that resemble those of lens cells, and although these contribute to the single cell layer of the CNS surrounding the canal, a thin cellular extension from adjacent cells prevents them from forming any direct contact with the canal. These cells also lack cilia or microvilli, so are not candidate photoreceptors. The axons of these two neurons extend along the photoreceptor tract, however, alongside antenna and canal photoreceptors, and both terminate anterior to the tract entry into the main posterior brain vesicle neuropil. A single ciliated neuron lies between Type III photoreceptors and both lens cells and the ocellus pigment cup (Fig. 5.4B). This cell directly contacts both of the former cell types, and its primary cilium is not modified.

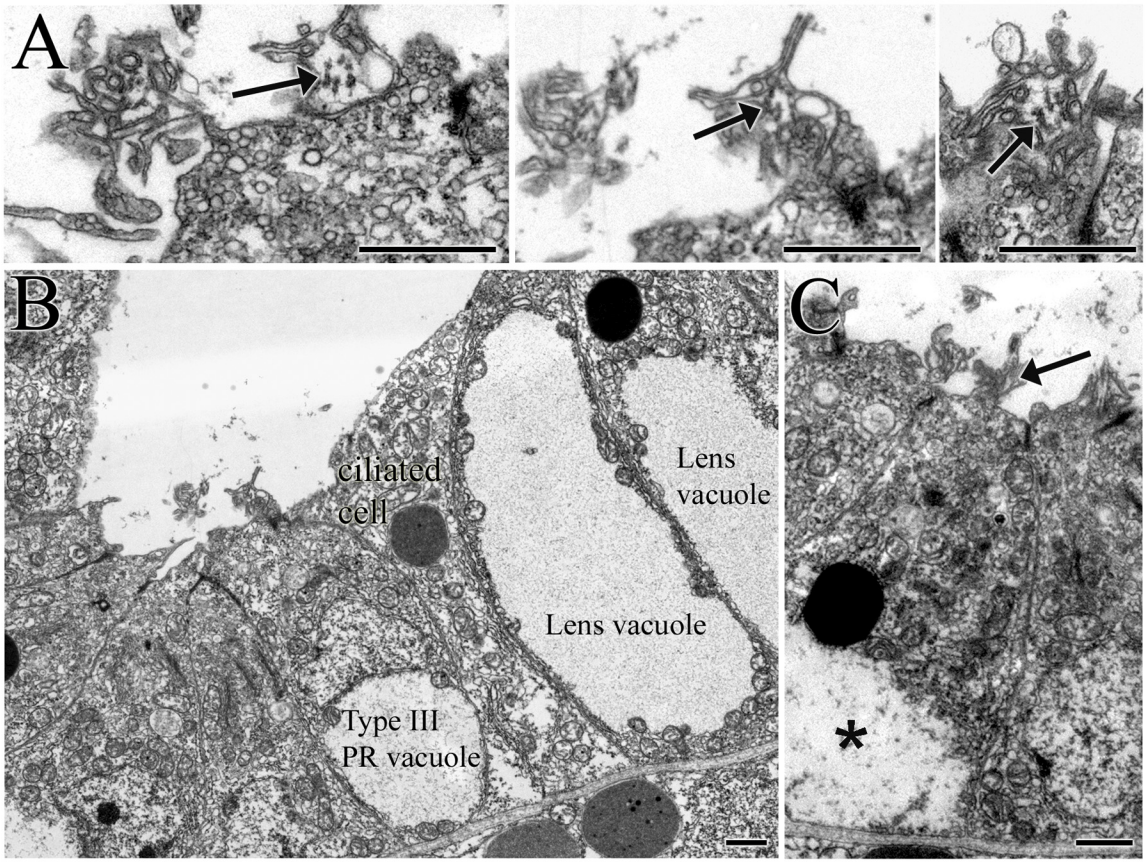

Figure 5.4. Type III photoreceptors in the ventral mid-brain vesicle of the *Ciona* larva. A) Three Type III outer segment-like modified cilia with ciliary microtubule arrangement (arrow). B) Vacuoles of lens cells and Type III photoreceptors (PR) appear similar in structure and staining in EM. A ciliated cell lies between Type III photoreceptors and lens cells. C) Vacuoles (asterisk) and modified cilia (arrow) are present in each Type III photoreceptor. Scale bars: 1μm.

Two antenna cells thought to mediate directional information of the gravity sensing otolith organ project axons ventrally underneath the anterior portions of the lens cells toward the right side of the brain vesicle, near the photoreceptors. Their axons travel in a small bundle along with two other groups: a) photoreceptor-associated vacuolated neurons mentioned above (lens 1 and lens 2 cells); and b) the Group II Photoreceptors in the right ventral region of the brain vesicle between the photoreceptor cell bodies and the lens cells. Synaptic inputs and outputs of the antenna neurons are located almost exclusively in the terminal regions of these cells. The majority of these large and plentiful synapses form upon cell bodies of interneurons in the posterior brain vesicle (cells 142, 147 and 161) that are not postsynaptic to photoreceptors. Only three antenna relay neurons (cells 135, 152, and 159) are postsynaptic to photoreceptors at 1-3 synapses, but these synapses are few and small. Both antenna neurons receive direct feedback from their postsynaptic partners and they form reciprocal connections between each other. One highly branching posterior brain vesicle intrinsic neuron (cell 115) is anaxonal and receives input from both antenna neurons, in addition to being postsynaptic to photoreceptors and many other interneurons. Although most connections from the second antenna cell target the same subset of descending postsynaptic brain vesicle interneurons as the first antenna neuron, the second antenna neuron (cell 63) also provides fewer or smaller input contacts onto many intrinsic brain vesicle neurons.

5.2.3 Photoreceptor Outer Segment Arrangements:

The functional components of the photoreceptors, their outer segments, exhibit differing arrangements with respect to the photoreceptor cell bodies that bear them. Although all extend from the dorsal side of the cell, the portion of the dorsal surface from which they

extend varies between anterior, dorsal or posterior (Fig. 5.2C). These arrangements do not correspond to specific types of photoreceptors, however. Instead, the 3-D arrangement of all outer segments along a single path appears to dictate the direction in which the outer segments project. As a result, the more anterior photoreceptors, Type II-i, all but one I-i, and the two of the most anterior dorsal photoreceptors of I-ii project outer segments in a posterior direction (Fig. 5.2C; Appendix F). Three Type II-ii photoreceptor slightly posterior to these, pr-e, pr-f and pr-g, project outer segments dorsally. The rest of the photoreceptors, except for pr1, have outer segments arising from the anterior sides of their somata.

5.2.4 Photoreceptor Axon Projection Patterns:

All of the photoreceptor axons follow a single tract toward the posterior brain vesicle alongside the antenna neurons' axons. The photoreceptor axon tract comprises several distinct fascicles before these turn to enter the main posterior brain vesicle neuropil. The fascicles contain the following axons: a) Type II-i, Type II-ii, antenna and lens; b) Type I-I and 36; c) Type I-ii; and d) Type I-iii. The Type II and Type I-i photoreceptor axons are thereby separated from other photoreceptors by photoreceptor associated neuron 36, into a group containing antenna and anterior vacuolated neurons (Fig. 5.3A-B). One of the anterior vacuolated neuron axons lies between antenna and photoreceptor axons in the fascicle, and terminates near the Type III photoreceptors. The second fasciculates with antenna axons and terminates only a short distance from the cell body (Fig. 5.3B). The ventral-most photoreceptors of each row of Type I neurons extend their axons directly along a ventral path to join the photoreceptor tract as it extends into the main posterior brain vesicle neuropil, rather than projecting a lateral extension before turning toward the

brain vesicle (Fig. 5.3B). The photoreceptor tract does not contact other neuronal cell types until it turns to enter the main neuropil of the posterior brain vesicle, just posterior to the lens cells and Type III photoreceptors. The photoreceptor bundle there extends into the main neuropil alongside several ventral posterior brain vesicle interneurons to intertwine with the axons and dendrites in this region. Along the length of these axons, photoreceptors form a surprising number of presynaptic contacts onto other photoreceptor axons, other axons in this bundle from anterior vacuolated, photoreceptor associated, and antenna cells, and onto the basal lamina (Fig. 5.5).

5.2.5 Photoreceptor Terminals:

Type I and Type II photoreceptors form terminals in the main neuropil of the posterior brain vesicle, where they establish synaptic partnerships with a variety of interneurons. Type II canal photoreceptors appear to have less elaborate terminals, and extend over only small fields. In particular, the Type II-i photoreceptor terminals extend just into the outer edges of the neuropil. Two of the Type II-ii terminals are likewise short, but the other two terminals are larger, and extend club-shaped terminals along the antero-posterior axis of the CNS, perpendicular to their entering axon. Ocellar photoreceptor terminals are generally larger [mean 11.02±6.38 μm^3 for the ocellus and 5.26±2.01 μm^3 for the canal], and extend over greater distances [152.74±66.2 nm and 71.29±35.5 nm], the volumes derived from the product of section number and thickness, and although all extend axons into the posterior brain vesicle neuropil, some lack expanded terminals there. In fact, only half of the ocellar photoreceptor terminals are branched, only one has extensive terminal branching, seven have only short fine branches, and six of these only have two branches (Appendix F). Among each row of Type I photoreceptors, there are

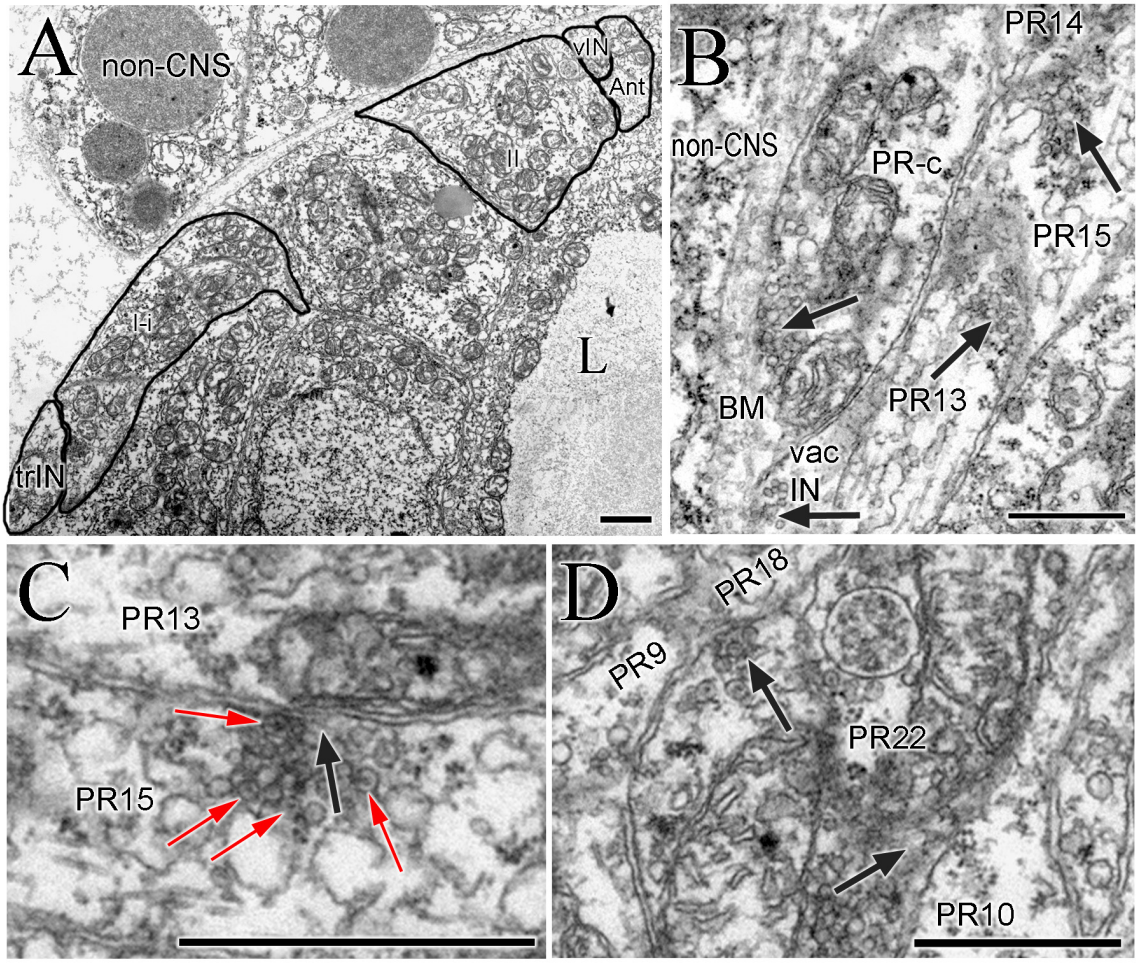

Figure 5.5. The photoreceptor axon tract. A) Arrangement of axon bundles (outlined) of Type I-i and Type II photoreceptors, the photoreceptor tract interneuron (trIN), antenna neurons (Ant), and vacuolated photoreceptor associated interneurons (vIN) on the outer right ventral edge of the mid brain vesicle outside a lens cell (L) and photoreceptor cell bodies. B-D) Synaptic contacts (arrows within the photoreceptor tract). B) Serial synaptic contacts between photoreceptors (PR), and synapses from a photoreceptor and an anterior vacuolated interneuron onto the basement membrane between CNS and non-CNS tissues. C) Synapse (black arrow) with vesicle pool containing both clear and dense-core (red arrows) and small vesicles. D) Axo-axonal dyad synapses from one photoreceptor onto other photoreceptor axons within the photoreceptor tract. Scale bars: 1μm.

various terminal shapes. Based on projection shape and region of the terminal I have classified each photoreceptor terminal's field. Several photoreceptors (pr1,6,8,9,16,19,21,22) extend single terminals toward the anterior, where they expand along their longitudinal axes (Appendix F). Along with other morphological similarities, these constitute the terminals that extend most anteriorly (Appendix F, Fig. 5.6D), and span the range of terminal volumes. Differing from the anterior projecting terminals, several photoreceptors (pr3,5,10,12,17,18,23), extend axons along the photoreceptor entry tract directly into the posterior brain vesicle neuropil, where they expand into club like terminals (Appendix F; Fig. 5.6B). These terminals are amongst the most posterior of the photoreceptor terminals (Fig. 5.6D; Appendix F), and span a range of volumes. There are two distinct types of branched terminals, the first of which, as seen in pr 4,7,11,13**,** consists of an expanded portion, from which extend two arms in different directions, each with its own expanded terminal. The other two photoreceptors with branched terminals, pr15 and pr20, have branches extending from their two main branches (Fig. 5.6C; Appendix F). All fall in the upper range of terminal volumes, and three of the branched neurons extend the furthest of any the photoreceptor terminals along the anterior-posterior axis (Fig. 5.6D).

5.2.6 Photoreceptor Interneurons:

Insofar as the photoreceptor terminals all terminate in the posterior brain vesicle, the next level of processing depth begins in this region, which is host to all first-order photoreceptor interneurons. A subset of these first-order interneurons that receive direct photoreceptor input do not extend beyond the posterior brain vesicle. Instead, these synapse onto target interneurons within the posterior brain vesicle, which contains a

Figure 5.6. Photoreceptor terminals. A-C) Reconstructions of representative photoreceptor terminals. A) Expanded terminal region that extends in an anterior direction. B) Club-like terminal ending perpendicular to the long axis of its axon. C) Bifid terminal with expanded branches toward anterior and posterior. D) Representation of photoreceptor terminal range from anterior (left) to posterior (right) for each photoreceptor sorted by row reveals no clear pattern. Scale bars: 5 μm.

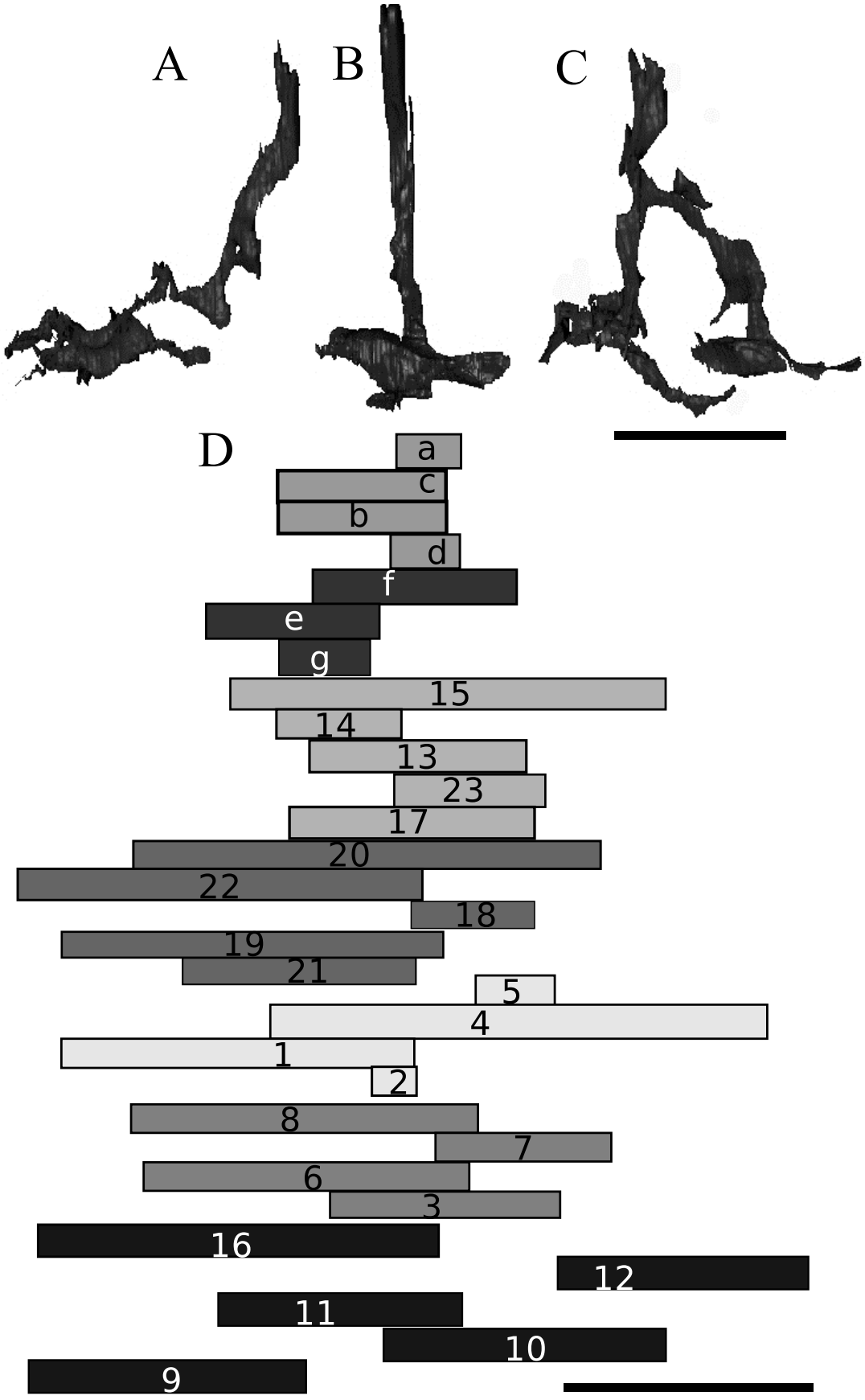
A
B
C
D
a
c
b
d
f
e
g
15
14
13
23
17
20
22
18
19
21
5
4
1
2
8
7
6
3
16
12
11
10
9

number of second- and third- order interneurons. However, many target interneurons also receive direct input from photoreceptors, and many, in turn, provide synaptic input onto other interneurons, most of which are relay neurons that extend down into the motor ganglion. Thus, the retinal network that exists within this specific region of the *Ciona* posterior brain vesicle provides an integrative system that permits lateral spread of signal to the 13 extrinsic photoreceptor relay neurons as well as to multimodal relay neurons.

The cell bodies of the first subset of photoreceptor interneurons are themselves located caudal to the retina, and their forked terminals extend toward the retinal integrative region (Fig. 5.7A). These ciliated neurons (cells 13, 17, 18, 22) are each from different axon fascicles anteriorly, but join a single axon fascicle before extending within the posterior brain vesicle. These interneurons are all rather sparsely connected, and receive input from only one or two photoreceptors each (Table 5.1) onto their terminal regions. All of these, in turn, provide input from their terminals onto different extrinsic and intrinsic photoreceptor interneurons (Fig. 5.8B-D). The second group of interneurons in the retina are brain vesicle intrinsic interneurons with somata lying just rostral to the posterior brain vesicle. Five of these neurons (cells 50, 62, 68, 70, 78) are ciliated, and many of their cilia come into contact with the bulbous protrusions of the coronet cells. These neurons have terminals with a distinctive V-shape, having a bend at their caudal end to form a caudally projecting arm (Fig. 5.7B). The cell bodies of these neurons lie in the mid-left brain vesicle and they receive inputs from a subset of photoreceptors onto their axons or terminal regions. These, in turn, provide synaptic input onto both intrinsic and extrinsic (relay) photoreceptor interneurons (Fig. 5.8B-C). Though more highly connected than their caudal counterparts, these neurons do not provide widespread or

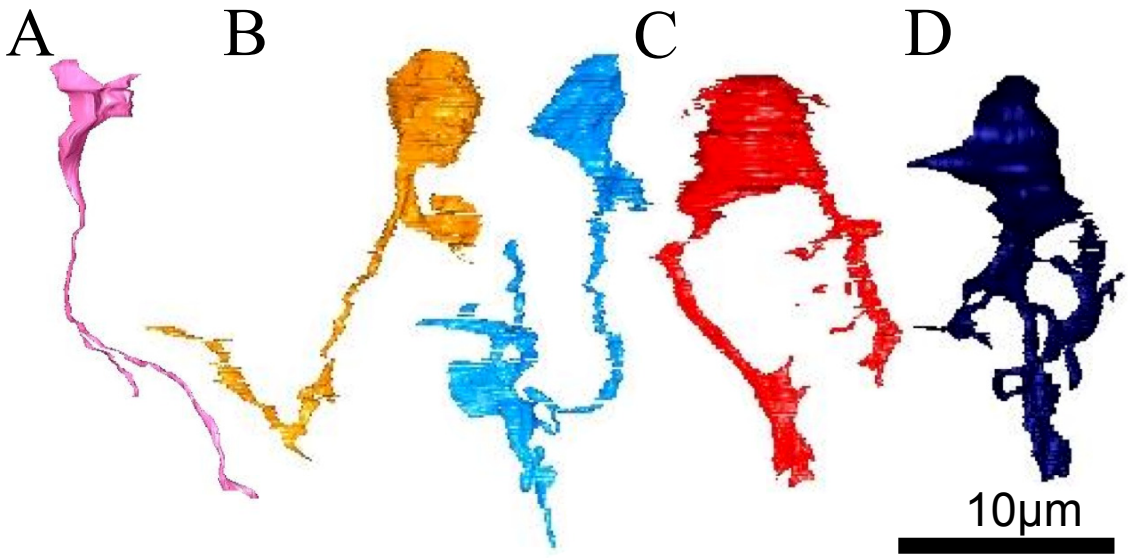

Figure 5.7. Reconstructed brain vesicle intrinsic photoreceptor interneuron types; anterior to the top, rotated to depict distinctive features of each cell type. A) Bifid terminal neuron. B) Simple and branched V-shaped terminal interneurons. C) Bipolar interneuron. D) Anaxonal arborizing interneuron with large branched terminal. Scale bar: 10µm.

Figure 5.8. Photoreceptor relay pathways in the larval *Ciona* brain vesicle (BV). A) Synaptic connections between photoreceptor rows i-v and Type II canal photoreceptors, II. Relative strengths illustrated by arrowhead size. B) Photoreceptors, BV intrinsic photoreceptor interneurons (PRINs) and relay photoreceptor interneurons are interconnected with information flow in both directions between most pairs of cell types. C) Expanded network illustrates two classes of photoreceptor relay interneurons, black and white. The first (black) provides no input to brain vesicle intrinsic interneurons. The second (white) is connected as in the first, with an additional feedback pathway through another subset of BV intrinsic photoreceptor interneurons. D) Photoreceptors can be divided into three groups based on their direct synaptic connections with brain vesicle interneurons. The first group PR_1 provides direct synaptic input only to relay interneurons, the second, PR_2 provides reciprocal synaptic input to both relay and intrinsic BV interneurons, and the third, PR_3 receives direct synaptic input from BV intrinsic interneurons and provides reciprocal synaptic input to relay interneurons.

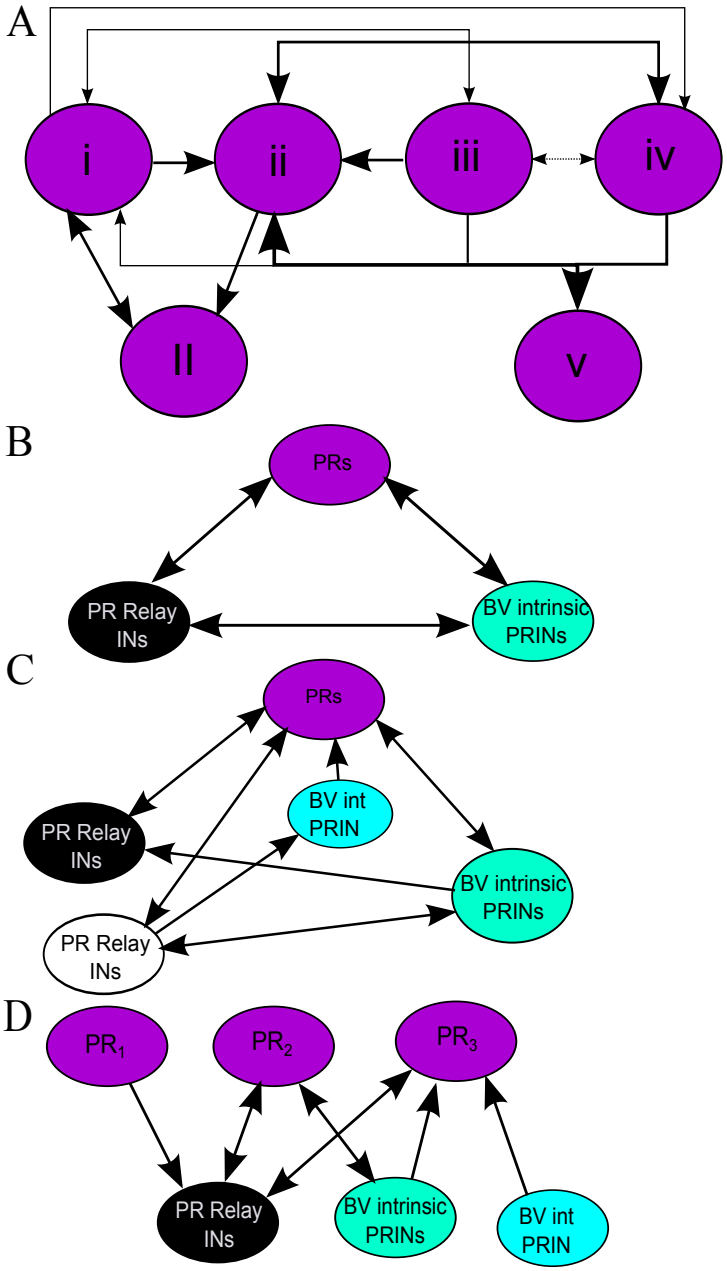
A
i
ii
iii
iv
II
v
B
PRs
PR Relay INs
BV intrinsic PRINs
C
PRs
BV int PRIN
PR Relay INs
BV intrinsic PRINs
PR Relay INs
D
PR1
PR2
PR3
PR Relay INs
BV intrinsic PRINs
BV int PRIN

abundant synaptic outputs. All but one of these neurons terminate in the same rostro-caudal region, the other terminating earlier in the posterior brain vesicle. In addition to these more sparsely connected photoreceptor interneurons, two bipolar neurons (one ciliated, one uncertain) (Fig. 5.7B) also receive direct photoreceptor input; one of these is vacuolated, but exhibits no differences in its connectivity from that of the ciliated group.

Along with the ciliated neurons in this region, one other neuron receives direct input from photoreceptors, but does not extend its axon to the motor ganglion. It forms a highly branched terminal in the posterior brain vesicle, which extends into the neck region, more caudally than the other interneurons. This neuron (cell 102) is more widely connected, and has postsynaptic targets that include a wider range of cell types (non-prINs). Two similar neurons (95 and 115) in the same region receive little direct photoreceptor input (1-3 synapses), but connect the intrinsic and extrinsic photoreceptor interneurons and the remainder of the posterior brain vesicle. Based upon their shape and extensive branching I call these three neurons anaxonal arborizing neurons. They together form a brain vesicle intrinsic network that connects interneurons of various classes, and is anatomically qualified to provide additional control to the photoreceptor pathway.

In the posterior brain vesicle of *Ciona*, an outpocketing of the canal arises on the left dorsal side, opposite the ocellus photoreceptors. This fluid filled pocket is lined by the cell bodies of photoreceptor interneurons and their dendrites as well as two posterior coronet cells (Fig. 5.9). This portion of the canal contains no bulbous protrusions of the coronet cells, and few other cilia, though non-emergent cilia contact the canal from several photoreceptor interneurons. The pocket has an area of $60um^2$ and initiates at the level of the anterior-most ocellus photoreceptors. The wall between this canal and the

main persistent canal comprises the two bipolar brain vesicle intrinsic interneurons as well as a single ependymal cell (Fig. 5.9). These bipolar photoreceptor interneurons appear vacuolated, but these vacuoles are neither surrounded by a membrane nor well defined by a border of mitochondria as in lens and Type III photoreceptors. The fluid region contains some fixed material, and differs in appearance from the vacuoles of the lens or Type III photoreceptors (Fig. 5.4B).

5.2.7 Photoreceptor Relay Neurons that connect the Brain Vesicle to the Motor Ganglion:

Twenty-three first-order posterior brain vesicle interneurons receive photoreceptor inputs onto their dendrites, cell bodies or axons, and extend axons into the neck region to terminate in the motor ganglion. Based on their morphology and connections these neurons fall into various cell types (Appendix G). Morphologically, the cells are categorized by their soma, the shape and size of the terminal, and the attachment and projection of the axon, by the presence of an expanded terminal (or BVterm) region just posterior to the soma, in a position corresponding to that of the axon hillock in a vertebrate neuron, and finally the depth of the terminal (Fig. 5.10). Some interneurons with a spherical soma have an axon that emerges from its ventral surface, and send either a long axon in an axial direction toward the motor ganglion, or a shorter axon that projects diagonally in a ventral direction to the proximal motor ganglion (Fig. 5.10A). Two interneurons with spherical somata extend axons dorsally within the posterior brain vesicle, that form branches as they turn to descend through the posterior brain vesicle and into the neck and motor ganglion (Fig. 5.10B). In yet other interneurons, axons also emerge from the dorsal region of an oval shaped soma that have expanded regions on their proximal axons, within the posterior brain vesicle (Fig. 5.10C). Three of these

Figure 5.9. Canal out-pocketing in the mid-brain vesicle surrounded by photoreceptor interneurons (PRIN) and vacuolated interneurons (vacIN). A and C) Outlines of cell tracings within slices of the mid-brain vesicle coded by colour and nuclei marked with squares (yellow: neurons; blue: ependymal cells), with canal (C) in white and vacuoles (V) in gray at the initial outpocketing (A) and persistent pocket (B). Pocket lies opposite right side photoreceptors (PRs) and dorsal to coronet cells (Cors), which extend bulbous protrusions (BPs) into the canal ventral and anterior to the constriction of the pocket. B) reconstruction of the region containing the canal pocket with canal (Ca), surrounded by cells in black. Photoreceptor interneurons (PRIN) appear transparent to show outpocket.

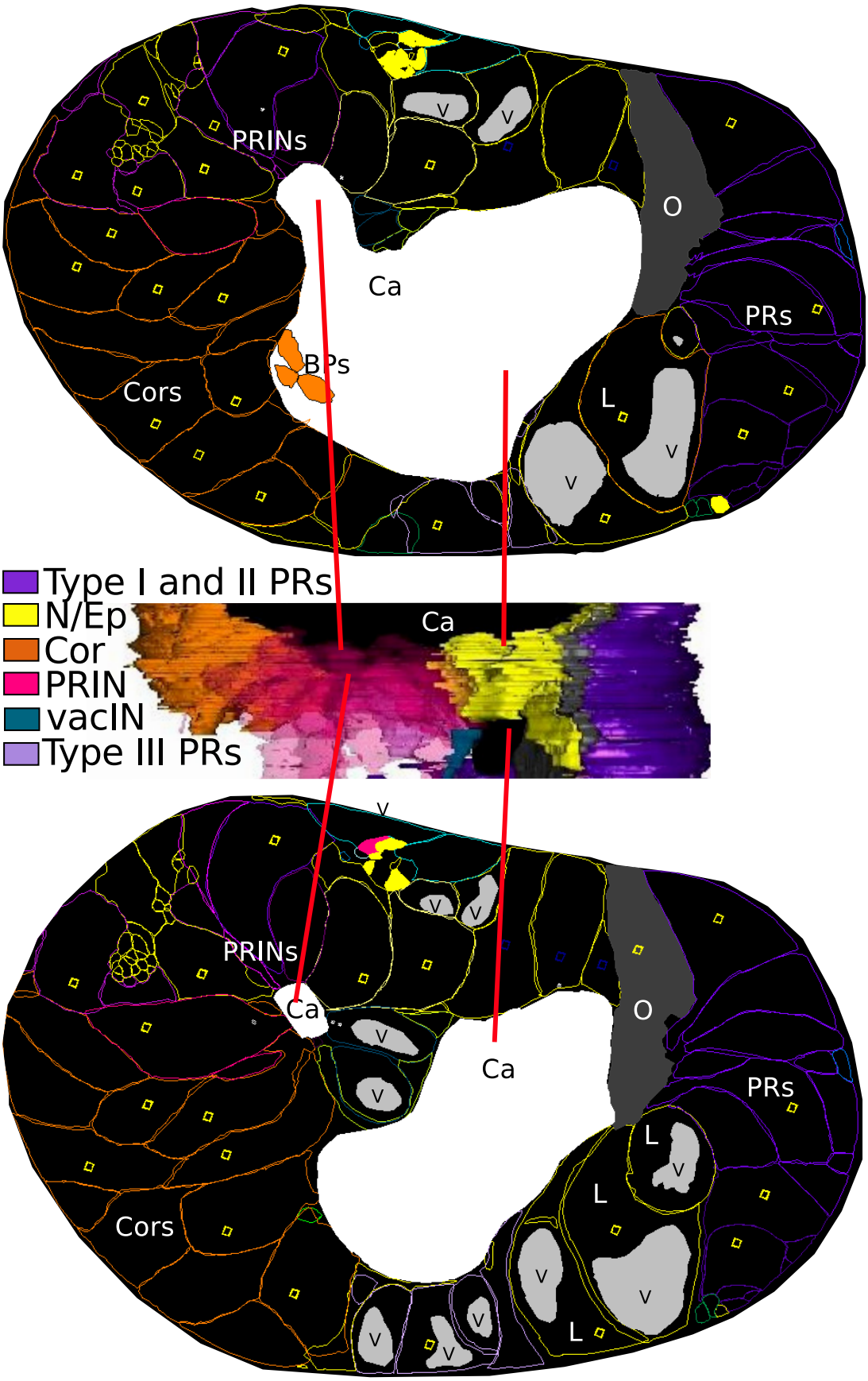
PRINs
V
V
O
Ca
PRs
BPs
Cors
L
V
V
Type I and II PRs
N/Ep
Cor
PRIN
vacIN
Type III PRs
Ca
V
V
V
PRINs
Ca
O
V
Ca
PRs
L
V
L
Cors
V
V
V
V
V
L

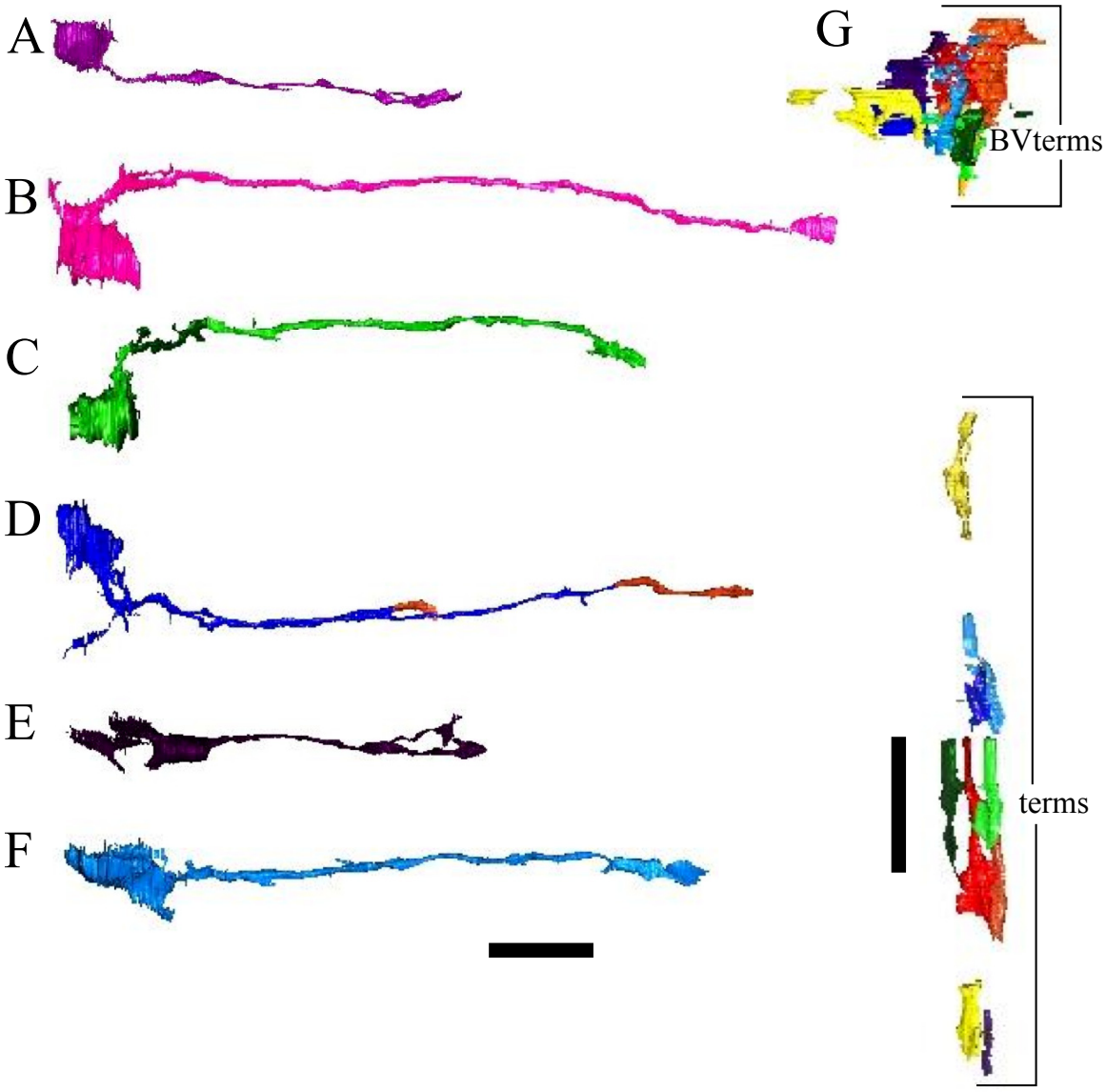

Figure 5.10. Reconstructions of photoreceptor relay neurons in the posterior brain vesicle. A) Ventral extending axon with elongate terminal (cell 74). B) Dorsal extending axon with club terminal (cell 105). C) Dorsal extending axon with expanded BV terminal region (cell 112, dark green). D) Dorsal extending collateral axons rotated to distinguish two terminal regions (cell 100, orange). E) Short bifid neuron with anterior dendrite (cell 157). F) Medially extending axon with elongate terminal (cell 126). G) Reconstructed dorsal view of brain vesicle (BVterm) and motor ganglion (VGterm) terminal regions of all photoreceptor relay neurons (cells 74, 86, 94, 96, 112, 116, 121, 126, 130) anterior to top. Scale bars: 10μm.

Table 5.1. Photoreceptor postsynaptic partners, with photoreceptor input organized by group and row. Presynaptic input from each photoreceptor row indicated with y for antenna neurons (ant1 and ant2), basement membrane (bm), and interneuron targets (by cell number). Total number of presynaptic photoreceptor partners, total number of synapses postsynaptic to photoreceptors, and number of those that are observed in more than one adjacent section is also given for each postsynaptic target. Rows are coloured by number of postsynaptic sites from photoreceptors from red (least) to purple (most): red (1-2), orange (3-5), yellow (6-8), green (10-12), blue (15-19), purple (>20).

Postsynaptic element	Input from Photoreceptor Group-Row							Number of presynaptic pr partners	Number of pr presynaptic sites	Number of pr synapses >1 section
	II-i	II-ii	I-i	I-ii	I-iii	I-iv	I-v			
bm	y	y	y	y	y			10	16	13
10	y	y						3	4	2
13			y					1	1	
16					y	y		1	3	2
22						y		1	5	3
30				y				1	1	1
36	y	y	y	y	y	y		8	15	10
42			y	y				2	5	2
50				y	y			2	2	
63			y		y	y	y	4	4	2
68			y		y		y	3	6	2
70			y	y	y	y	y	12	20	7
74			y					1	3	2
78			y	y				2	3	3
80			y	y	y	y	y	10	25	17
86						y	y	5	10	8
90			y					2	2	2
92						y	y	2	3	2
94			y	y	y		y	5	10	4
96				y		y	y	9	17	12
100				y		y	y	4	8	6
101			y					1	1	
102			y	y	y	y		6	11	8
105	y	y	y	y	y	y	y	13	30	22
108			y	y		y		5	5	4
112		y	y	y	y	y	y	7	12	9
115			y		y			2	3	
116		y	y	y	y	y	y	14	31	21
119			y		y	y	y	5	8	7
121			y	y	y	y	y	11	40	29
123		y	y	y		y	y	12	23	17
124		y	y	y	y			4	4	2
126			y	y	y	y	y	8	22	15
127		y	y	y	y		y	5	15	10
130	y	y	y	y	y	y	y	17	62	33
135							y	1	1	1
138	y						y	2	2	2
140		y	y	y	y			5	16	8
143						y		1	1	
152			y			y		2	2	
157		y	y	y			y	6	11	7
159							y	1	1	
162				y				1	1	1
167			y	y				2	3	1
lens1	y		y					3	4	2

neurons have a bi-lobed soma, and one extends two collateral axon branches toward the motor ganglion (cell 100; Fig. 5.10D), thus violating the general rule of neurons in most nervous systems, that the axon is unitary. While most of the descending brain vesicle-motor ganglion photoreceptor relay interneurons have only short dendrites extending from their soma, the expanded and branched portions of several proximal terminals (Fig. 5.10G) receive inputs and may function in the place of a dendritic arbor. Given the historical importance attached, especially by Cajal (1891), to the dynamic polarization of vertebrate neurons, I will return to the question of the polarization of larval neurons in *Ciona*. In addition to the foregoing interneurons, two brain vesicle-motor ganglion photoreceptor relay neurons (cells 152, 94) have long thin anterior dendrites and four have longer ventral anterior dendrites that give them a teardrop appearance as well as branched terminals, two with short branches, and two with bifurcated terminals each having two main branches (Fig. 5.10E). Like the ventral diagonal neurons mentioned above the axons of these teardrop shaped neurons project ventrally in a diagonal direction, and terminate in a more anterior region of the motor ganglion. Three other interneurons have simple oval shaped somata with medially emerging axons that project into the motor ganglion to form club-shaped terminals (Fig. 5.10F). A summary of these interneuron types appears in Appendix G.

Aside from the synapses between photoreceptors, those from photoreceptors to the brain vesicle-motor ganglion relay interneurons have the largest and most numerous synaptic contacts. These all originate from photoreceptor terminal regions, but vary in their locations. Twelve relay interneurons receive photoreceptor input to an expanded proximal portion of their axons, BVterm, of which two receive exclusive photoreceptor

input to this region. Nine relay interneurons have photoreceptor postsynaptic sites on their dendrites, while sixteen receive input onto their cell bodies, with only two receiving exclusive photoreceptor input to the cell body.

For those neurons with expanded BVterm regions adjacent to their somata, these regions receive numerous photoreceptor inputs. While large single-input connections from photoreceptors occur onto cell body regions, there are also single synaptic inputs to both brain vesicle terminal and dendrite regions that span many sections. However, the aggregate size of synaptic contact does not correspond closely to synapse number because several partners with only few synaptic contacts have large contact sites.

Each photoreceptor provides input to a distinct set of relay interneurons (Fig. 5.11; Appendix H) that relay this signal to the motor ganglion. Many of these neurons receive synaptic input from multiple photoreceptors that do not segregate in any obvious way, neither by group (Table 5.1), by dorso-ventral arrangement, nor by projection pattern. Relay neurons integrate significant synaptic input (those greater than one synapse that extends over more than one section) from one (cell 74) to nine (cell 121) photoreceptors. Each photoreceptor provides such input to up to eight relay neurons, with a mean of only 2.17 target relay neurons, and so is relatively specialized. Four Type II and three Type I photoreceptors provide no significant input to relay interneurons at all, and the greatest diversity of relay neuron input originates from photoreceptor 12 (Type I-v) (Appendix H). Relay neurons with most photoreceptor input partners (greater than five) are cells 105, 116, 121, 126, and 130, which include five of the six relay neurons with brain vesicle terminal regions. Direct feed-forward pathways also contribute to input through brain vesicle intrinsic interneurons, as follows: 22 and 50 to relay neuron 96; 16 to relay

Figure 5.11. Network graphs for individual photoreceptors colour-coded for cell type. Each neuron is a single node, labelled with its cell ID. Lines represent chemical synaptic contacts. Arrows indicate direction of transmission, and total size of synaptic contacts between cells is represented by the line thickness (key). A) Type II photoreceptor-a network includes two relay neurons to the MG as well as synaptic connections with other photoreceptors and the intrinsic BV photoreceptor antenna network. Also shown is synaptic contact onto the basement membrane (BM), indicated by a single node. B) Type I-iii photoreceptor network including several BV intrinsic interneurons, photoreceptors, antenna pathway connections, and relay neurons to the MG. C) Simplified network with only direct pathways from pr15 (Type I-i) through relay neurons to MG neurons. Contacts from relay neurons involved in the peripheral pathway are depicted in the colour of the AVG neurons. Abbreviations: PRs photoreceptors, PR Ins: photoreceptor interneurons, Ant neurons: antenna neurons, MG INs: interneurons of the MG, MNs: motor neurons: AVGs: ascending MG neurons of the peripheral pathway, ddL: descending decussating neuron of the left MG.

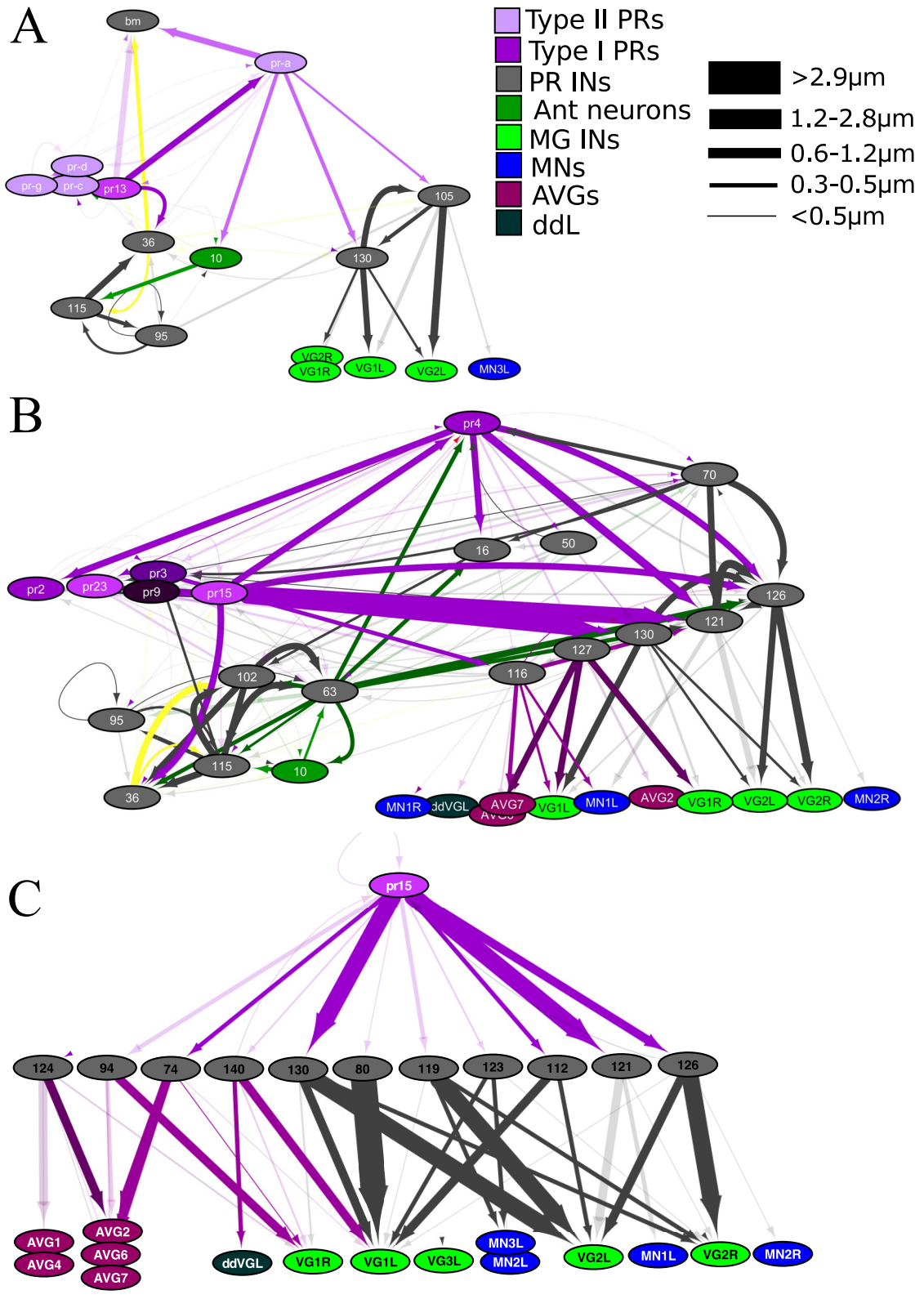
A
bm
pr-a
pr-d
pr-g
pr-c
pr13
36
10
105
130
115
95
VG2R
VG1R
VG1L
VG2L
MN3L
Type II PRs
Type I PRs
PR INs
Ant neurons
MG INs
MNs
AVGs
ddL
>2.9µm
1.2-2.8µm
0.6-1.2µm
0.3-0.5µm
<0.5µm
B
pr4
70
16
50
pr2
pr23
pr3
pr9
pr15
126
121
130
127
116
102
63
95
115
10
36
MN1R
ddVGL
AVG7
VG1L
MN1L
AVG2
VG1R
VG2L
VG2R
MN2R
C
pr15
124
94
74
140
130
80
119
123
112
121
126
AVG1
AVG4
AVG2
AVG6
AVG7
ddVGL
VG1R
VG1L
VG3L
MN3L
MN2L
VG2L
MN1L
VG2R
MN2R

neuron 112; and 70 to 121, 80, 86, 126, or 105.

Analysis of a single descending brain vesicle-motor ganglion photoreceptor interneuron's connections reveals the richness of microcircuit connections that can exist. Photoreceptor input occurs mostly to the expanded brain vesicle dendrite region, with additional inputs to the anterior axon of this neuron. This particular interneuron (cell 112) in turn then provides input from its BVterm region to terminals of anterior photoreceptor interneurons, photoreceptors, and an antenna neuron. It also provides synaptic input from its cell body onto the soma of a single coronet cell. Synaptic contacts with other descending brain vesicle-motor ganglion interneurons, most of which are other photoreceptor interneurons, are regionally restricted for some, and throughout the length of the neuron for others. The anterior synapses between these interneurons in the brain vesicle make up a greater proportion of total synaptic contact size, and those with only anterior input have a similar or larger total size of synaptic connections than connections occurring throughout the length of the cell, and larger than those with only terminal connections. Thus, from all presynaptic partners, most of cell 112's postsynaptic sites (both by number and total size) occur onto its BVterm region (Fig. 5.12A). Examination of the output distribution illustrates that more than half of the total synaptic contact size originates from the brain vesicle terminal and axon regions of this neuron, with approximately one quarter from the cell body, dendrite and terminal regions combined (Fig. 5.12B). This skewed distribution of synaptic outputs to the axon and brain vesicle terminal regions of photoreceptor brain vesicle-motor ganglion interneurons holds across neurons, except for those lacking a brain vesicle terminal, in which axonal outputs take over most of the total synaptic contact size (Fig. 5.12C).

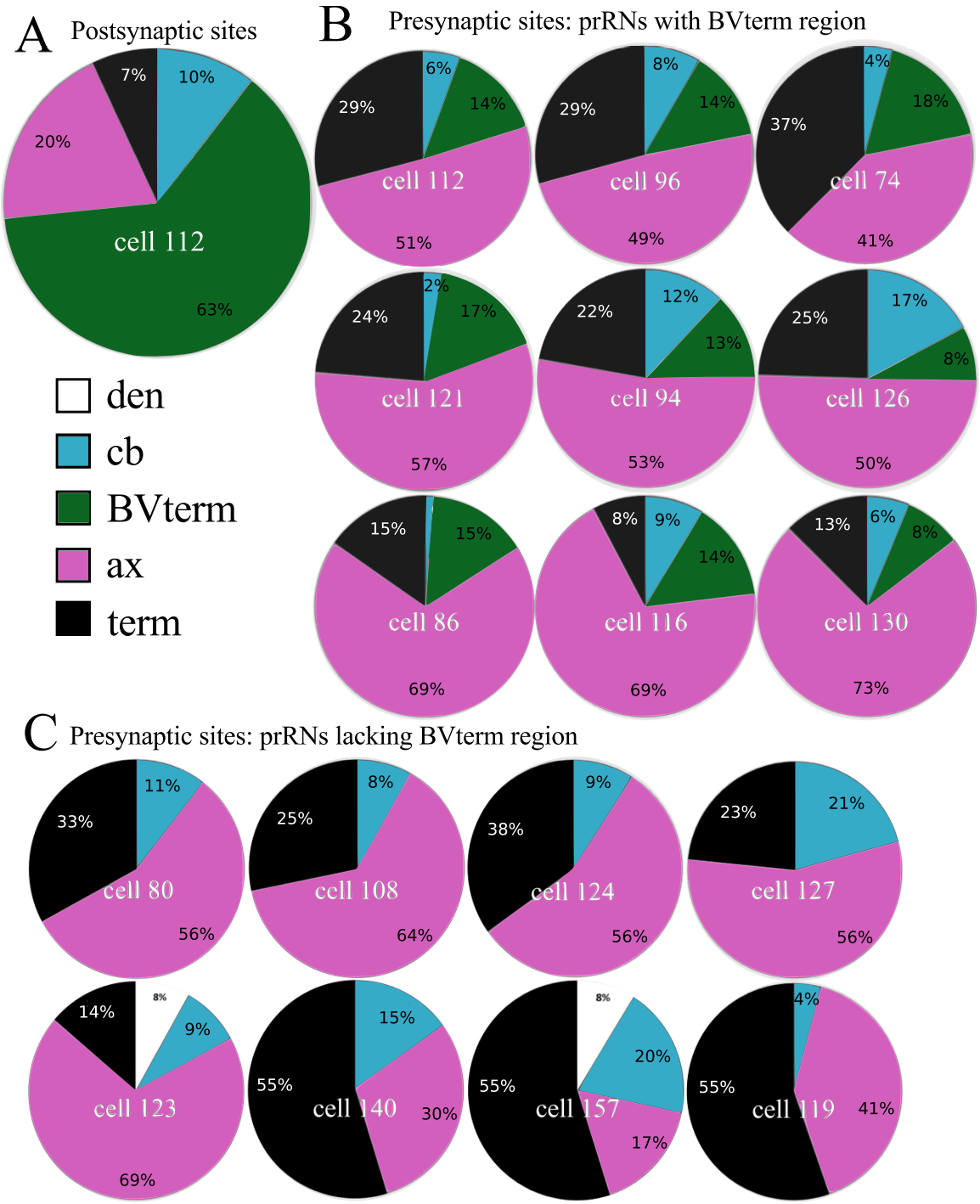

Figure 5.12. Photoreceptor relay neuron (prRN) synapses by cell region: dendrite (den), cell body (cb), expanded brain vesicle terminal adjacent to cell body (BVterm), axon (ax) and terminal (term). A) Proportions of all postsynaptic sites over different regions of cell 112 by number (angular subtense, reported as %) (which mimics proportions of total synapse sizes). Note that most synaptic sites form on the axon. B-C) Proportions of presynaptic sites from different regions of photoreceptor relay neurons (B) possessing BVterm regions and (C) and those without BVterm regions.

5.2.8 Other Sensory Pathways:

5.2.8.1 Antenna Integration:

From the preceding, it is apparent that there are many types of interneuron receiving input from photoreceptor neurons. Some interneurons are dedicated, receiving exclusive input from photoreceptors or their pathways, but most are multimodal, shared with antenna neurons or their pathways (Fig. 5.13). Some brain vesicle-motor ganglion photoreceptor interneurons integrate more directly with these pathways than others.

There are two levels at which integration of photoreceptor and antenna pathways occurs: between brain vesicle neurons that relay their terminals in the motor ganglion and in pathways between multimodal brain vesicle intrinsic sensory neurons (Fig. 5.13). Integration of antenna and photoreceptor networks can occur within the motor ganglion between the axons and terminals of brain vesicle-motor ganglion interneurons from each pathway. In all but a single case the output to the antenna network from descending photoreceptor interneurons occurs onto the descending antenna brain vesicle-motor ganglion interneurons as axo-axonal synaptic connections. This integration originates from both multimodal and dedicated monosynaptic photoreceptor interneurons. Some of the photoreceptor interneurons that provide input to the antenna pathway do not themselves receive synaptic input directly from antenna neurons (cells 80, 119, 108, 96, 123, 130, 157, 94, 86), however others (cells 121, 126, 135, 153, 159, and 152) do receive some direct antenna input from antenna neuron 2 (Fig. 5.13). Of these, cell 152 receives only minimal photoreceptor input, but also receives direct antenna input from antenna neuron 1, and is the only photoreceptor interneuron to provide input to cell bodies or dendrites of antenna interneurons. Likewise, cell 152 is the only photoreceptor

Figure 5.13. Network of photoreceptor and antenna interneuron connections with nodes grouped by cell type. Lines represent chemical synaptic contacts, colour-coded by cell type, with arrows illustrating direction of synaptic polarity (multiple arrowheads represent synapses onto multiple postsynaptic partners of postsynaptic cell type). Note combined photoreceptor and antenna input occurs onto multimodal interneurons (mmIN) as well as two brain vesicle intrinsic cell types, the photoreceptor tract neuron (trIN) and anaxonal arborizing neurons (aaINs). A) Photoreceptors (pr) grouped into single node. B) Photoreceptors separated into those receiving input from antenna 2 input (pr**), those providing input to antenna 1 (pr***), those with input to photoreceptor tract interneuron (trIN) and anaxonal arborizing interneurons (aaIN) (pr*) and those with input to only other photoreceptors, photoreceptor interneurons (prIN) and multimodal interneurons (mmIN).

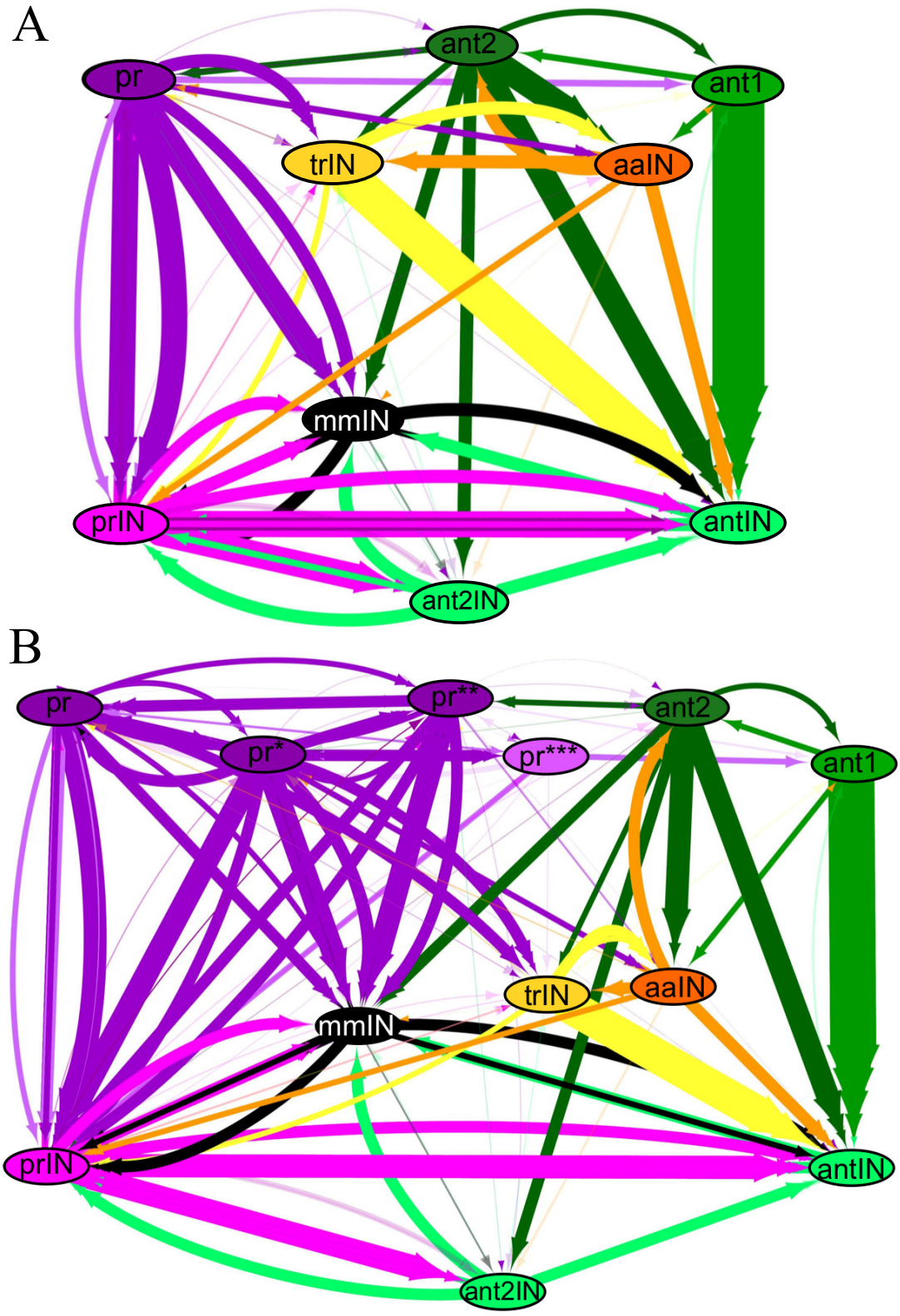
A
ant2
pr
ant1
trIN
aaIN
mmIN
prIN
antIN
ant2IN
B
pr
pr**
ant2
pr*
pr***
ant1
trIN
aaIN
mmIN
prIN
antIN
ant2IN

brain vesicle-motor ganglion interneuron that provides input to all antenna brain vesicle-motor ganglion interneurons, and itself receives input from both antenna neurons, perhaps suggesting that it is an antenna relay interneuron rather than a photoreceptor relay interneuron. The other antenna relay interneurons each receive input from between four and twelve photoreceptor interneurons, at 7 to 28 synaptic sites each. The average size of these synapses (total number of synaptic contact sections/number of synapses) for each brain vesicle-motor ganglion antenna interneuron is equal (approximately four 60nm sections each). Photoreceptor interneurons have between 1 and 15 synapses onto antenna brain vesicle-motor ganglion interneurons, with most synaptic contacts originating from cells 126, 135, 96, 86, 123 and 152. The latter include two neurons with no direct antenna input (cells 86 and 96), which share morphological similarities as detailed above, but do not share target motor ganglion neurons. Not all direct photoreceptor brain vesicle-motor ganglion interneuron partners of antenna neurons are included among these, suggesting that antenna input does not necessarily dictate the number of synaptic contacts onto other members of the antenna pathway. Thus, integration of antenna and photoreceptor network can occur within the motor ganglion at axons and terminals of the brain vesicle-motor ganglion interneurons of each pathway.

A secondary integrative network is restricted to the brain vesicle itself, and involves two types of previously undescribed brain vesicle intrinsic interneurons: the photoreceptor tract neuron (trIN) and the three brain vesicle intrinsic interneurons, cells 95, 102, and 115 with large terminals, anaxonal arborizing neurons (aaINs) (Fig. 5.7D; Fig. 5.14). Both of these pathways integrate direct input from photoreceptors and antenna neurons and provide output to the interneurons of each pathway. The most anterior integration

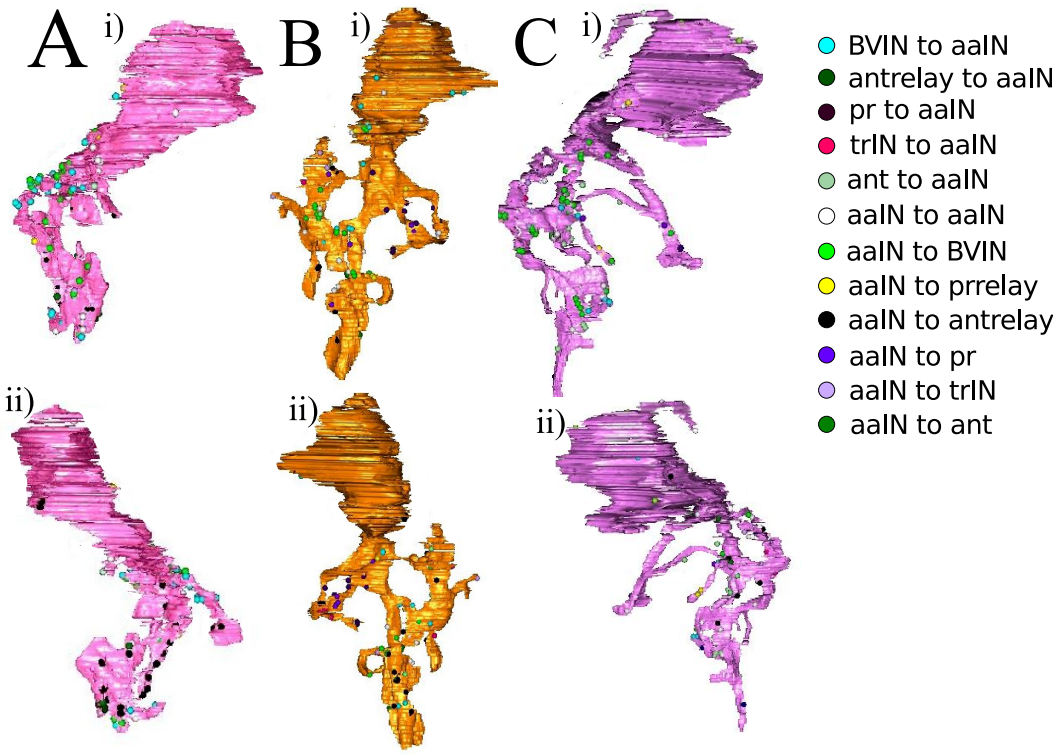

Figure 5.14. Reconstructions of anaxonal arborizing neurons (aaINs) of the posterior brain vesicle, marked with pre- and postsynaptic contact sites coded by colour. Anterior is to the top. A) Cell 95, ventral (i) and dorsal (ii) views. B) Cell 102, ventral (i) and dorsal (ii) views. C: Cell 115, ventral (i) and dorsal (ii) views. Abbreviations: interneurons of the brain vesicle (BVIN); antenna relay neurons (antrelay); photoreceptors (pr); photoreceptor tract interneuron (trIN); antenna neurons (ant); and photoreceptor relay neurons (prrelay).

through the photoreceptor tract neuron is initiated by the photoreceptor and antenna axons, which form axo-axonal synaptic inputs to trIN. These synaptic contacts form along the photoreceptor tract before it enters the posterior brain vesicle. In particular, antenna cell 2 and photoreceptor Type I-I neurons provide input to trIN, whereas antenna cell 1 and Type I-ii, I-iii, and II-I photoreceptors provide only minimal such input. In the posterior brain vesicle, the trIN forms a large elaborate terminal that provides input to some photoreceptor interneurons that is reciprocated, but also forms large and numerous presynaptic contacts onto antenna interneurons, in particular cells 142, 147, and 161. Two of these with the greatest input from trIN also receive large and numerous input from antenna cell 1. The trIN also provides reciprocal input to the three highly branched posterior brain vesicle intrinsic interneurons in the posterior brain vesicle. These neurons also receive synaptic input within the posterior brain vesicle from photoreceptors, and although all three receive some reciprocal input from antenna cell 2, cell 115 is the only one of these that receives numerous inputs from both antenna cells. The brain vesicle intrinsic neurons of the photoreceptor network also provide synaptic contact to these neurons, which themselves are synaptically connected, so that they form a fully connected network (i.e. one in which all possible connections are filled). These highly branched brain vesicle intrinsic interneurons form presynaptic contacts onto antenna brain vesicle-motor ganglion interneurons and some photoreceptor brain vesicle-motor ganglion interneurons. As with the trIN, the inputs to antenna interneurons, particularly cells 142, 147 and 161, tend to be larger and more numerous. The distribution of synaptic contacts on the branches of the brain vesicle intrinsic interneurons is not segregated in any way, neither by type nor input nor output regions (Fig. 5.14).

The resulting circuits provide overlapping pathways for integration of photoreceptor and antenna networks (Fig. 5.13; Fig. 5.15). In particular, both pathways have direct input to multimodal relay interneurons, and receive tertiary input that is integrated from photoreceptor and antenna pathways through intermediary brain vesicle intrinsic interneurons, with the input to the antenna relay neurons being stronger than that to the multimodal photoreceptor relay neurons.

5.2.8.1.1 A Note on Terminology

Before embarking on the task of itemizing all the synaptic circuits constituted by photoreceptor and antenna cell neurons, and as an introduction to the cells of the brain vesicle and motor ganglion themselves, a note on two aspects of cell terminology is appropriate. First, the divisions of the CNS, which were originally referred to as the sensory vesicle and visceral ganglion, have been renamed the brain vesicle (Satou et al., 2001b) and motor ganglion (Dufour et al., 2006; Lacalli, 2008; Nishino et al., 2011), respectively. While this change may reflect a marginal increase in scientific accuracy it also invalidates the names of cells previously assigned to these regions. Thus descending paired motor ganglion interneurons were originally attributed to the visceral ganglion as VGNs. Second, as cells became recognized individually on morphological and reporter expression grounds, they were given descriptive names reflecting these properties, which became progressively more complex as the criteria for their recognition increased. Possibly because these names were in some cases assigned by authors for whom English was a second language, or possibly because they were contrived by a generation more familiar with text messaging than writing in complete English, these names have become gradually converted to acronyms. As a result, in some cases these now incorporate

Figure 5.15. Photoreceptor antenna pathway integration at various levels through relay neurons to the motor ganglion (MG) on the left side (MG_L), right side (MG_R), or bilaterally ($MG_{L/R}$). A) Photoreceptor (pr) input to relay neurons (prR) occurs directly and indirectly through intrinsic brain vesicle interneurons (prIN). B) Some photoreceptor relay neurons (prR) form pre- and post- axo-axonal synaptic connections with antenna relay neurons (antR). Some photoreceptor relay neurons receive additional direct input from antenna neurons (ant). C) Additional integration occurs through input from photoreceptors (pr) and antenna neurons (ant) to the photoreceptor tract interneuron (trIN) and other multimodal intrinsic BV interneurons (IN) that in turn feed back to trIN and antenna neurons and feed forward into relay neurons (prR and antR). D) Combined integrative pathways of photoreceptor and antenna signals, summing pathways depicted in A-C.

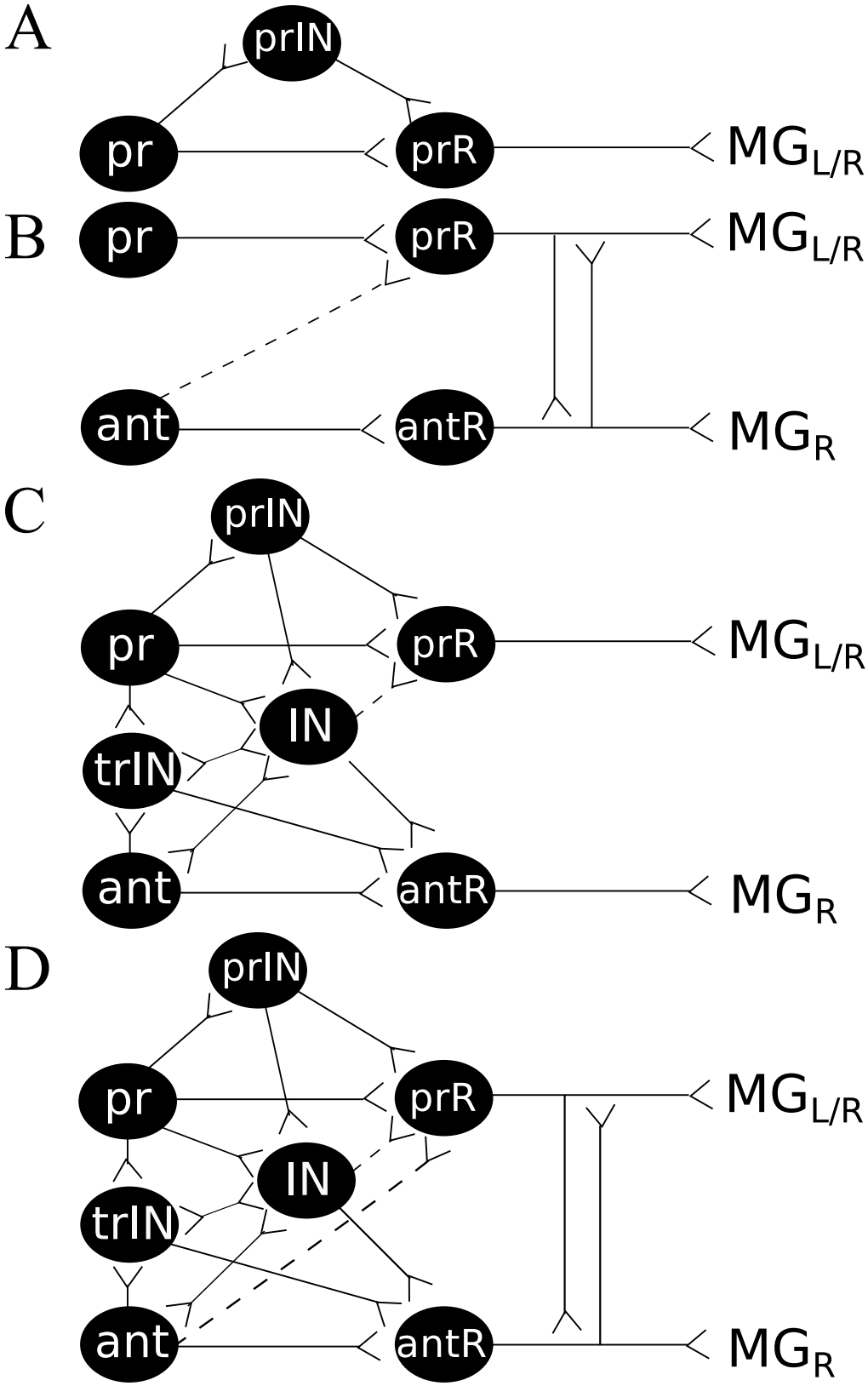
A
prIN
pr
prR
MG$_{L/R}$
B
pr
prR
MG$_{L/R}$
ant
antR
MG$_R$
C
prIN
pr
prR
MG$_{L/R}$
IN
trIN
ant
antR
MG$_R$
D
prIN
pr
prR
MG$_{L/R}$
IN
trIN
ant
antR
MG$_R$

abbreviations for the outdated names of brain regions, so that for example descending paired MG interneuron remain VGN cells even though the visceral ganglion they were once said to occupy has now become the motor ganglion. In a further development that removes their name further from its origins, acronyms are now often pronounced as single words. Against this wall of prospective confusion, this thesis will retain the full name for each cell type, although individual cell names/signifiers use acronyms, and substitute acronyms only when meaning would not be sacrificed by doing so.

5.2.8.2 Peripheral Integration:

Another class of seven photoreceptor interneurons incorporates inputs from the peripheral nervous system pathway. Photoreceptor relay interneurons that connect with the peripheral pathway do so largely through axo-axonal inputs to ascending visceral ganglion (AVG) interneurons and ascending tail neurons. The morphological features of these photoreceptor-AVG relay neurons, described above, include their shorter axons, anterior dendrites, and some with bifurcated terminals. Those neurons with a single terminal branch form reciprocal synaptic contacts with AVG neurons, with more numerous input to AVG1, AVG2, and AVG4. These receive the most feedback in turn from AVG2 (to cells 74 and 124) and AVG4 (to cell 94), at invaginated synapses onto their terminal regions (Fig. 5.16). At their terminals in the motor ganglion, all provide synaptic input to cell VGN1R, and one possesses an additional single small synapse onto cell VGN1L. Those neurons with bifurcated terminals also form reciprocal synaptic connections with AVG neurons, but one of these -- cell 157 -- forms many additional synaptic contacts with the ascending tail neurons. Thus, while strongest feedback from the peripheral pathway originates from the AVG interneurons, additional feedback occurs

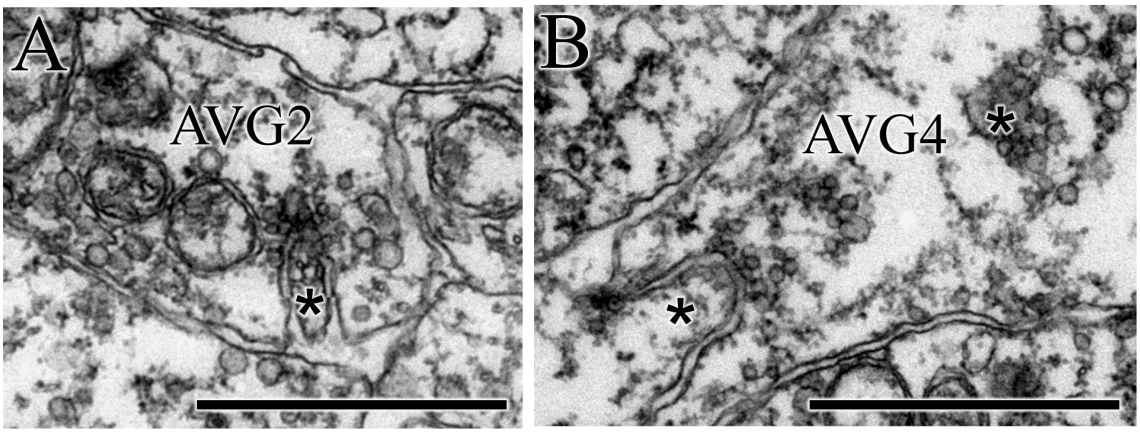

Figure 5.16. Electron micrographs of invaginated chemical synapses from ascending motor ganglion (AVG) neurons to pr/AVG relay neurons (asterisks). A) Single synapse from AVG2 to invaginated terminal branch of cell 74 (*). B) Synaptic contacts from AVG4 onto two invaginated portions of the terminal of cell 94 (*). Scale bar: 1µm.

through cell 157 from tail neurons. All three bifurcated terminal relay neurons provide additional input to both left and right VGN1 neurons, and a single member of the class, again cell 157, provides a single synaptic input to the first motor neuron on the right side. The two members of this class with more definitive bifurcation, cells 140 and 157, also provide some synaptic input to the left descending decussating neuron of the motor ganglion. Overall, input from these relay neurons to the AVG neurons occurs to all but cell AVG5, which is unique among its class, with the greatest input to cells AVG1 and AVG2. One neuron of the photoreceptor-AVG relay neuron class, cell 157, is unique in its connections, and extends furthest into the motor ganglion.

5.2.8.3 Photoreceptor Pathway Input to the Motor Ganglion:

Relay interneurons can also be grouped by their respective inputs to the motor ganglion. A few neurons have input exclusively to the left motor ganglion. For inputs to left-side motor ganglion interneurons, three relay neurons are exclusive to the first (cells 80, 108, and 116), two to the second (cells 100 and 121), and two provide input to both on the left side only (cells 105 and 112). Some members of the first two of these groups (cells 116, 100, and 121) also provide minimal input to the first motor neuron on the left side. MGIN1 input partners include two photoreceptor relay neurons involved in peripheral integration, and one other. Only two photoreceptor relay neurons, both of which also integrate inputs from the periphery, provide exclusive input to the first right-side motor ganglion interneuron. One additional neuron, cell 86, provides input exclusively to cell MGIN1R and the second motor neuron on the left side, and may be the partner of another relay neuron with similar inputs on the opposite sides of the motor ganglion, cell 96. Several other neurons provide bilateral input to the motor ganglion, to either the first or

second pair of motor ganglion interneurons. Relay neurons with input to the first pair of interneurons include the remaining photoreceptor relay neurons involved in peripheral integration, which also provide input to the left decussating interneuron and the first motor neuron on the right side (MN1R). One additional multimodal antenna neuron provides input to both members of this pair as well as to cell MN1R. The second pair receives input from the antenna relay neuron with photoreceptor input, cell 152, and the photoreceptor neuron that receives direct synaptic input from coronet cells, cell 119, both of which also provide input to the third motor neuron on the left side.

A more detailed analysis of the connections of these relay neurons reveals that those inputs to the second pair of interneurons of the motor ganglion originate from interneurons that integrate antenna signal either directly (through cells 121 and 126), or through secondary inputs from the antenna relay neurons (Fig. 5.15). While many photoreceptors are connected through this pathway, photoreceptor 4 is unique in providing exclusive synaptic contacts to the direct antenna integrative relay neurons, cells 121 and 126, to provide motor ganglion input that is restricted to the second pair of motor ganglion interneurons along with a left-side motor neuron (Fig. 5.11B). Extending this sensory integration, one of these antenna and photoreceptor integrative neurons (cell 119) also receives both direct and indirect coronet cell input and forms synaptic contacts onto all other relay neurons of this class (cells 121, 100, 112, 130) except for one (cell 126). Two photoreceptors (cells pr5 and pr22) relay their signals exclusively through these relay neurons to the left side only, and five (cells pr-a, pr2, pr18, pr11, pr7, and pr16) exclusively through these relay neurons converge on both left and right sides of the motor ganglion. The coronet integration is apparent in the outputs to the motor ganglion as

synaptic input to the third motor neuron on the left side of the motor ganglion. The greatest of these inputs exists in pathways with direct coronet integration, in which photoreceptor input passes through cell 119 itself (cells pr8 and pr12). These photoreceptors both provide additional input to peripheral integrative relay neurons, resulting in additional input to the AVG interneurons. Another set of photoreceptors (cells pr3, pr9, pr10, pr15, and pr-f) relay through interneurons that integrate both antenna and peripheral input. The last group of photoreceptors (cells pr19 and pr23) that relays through these integrative neurons provides additional input to the sole photoreceptor-exclusive relay neuron, cell 80.

The photoreceptor-exclusive interneuron is unique in providing large directed input in the motor ganglion exclusively to cell VGN1L. One photoreceptor, pr1, provides synaptic input to this and one other relay neuron (cell 140) directly, both of which then converge upon VGN1L (Fig. 5.17A). Additional input from this pathway to the left decussating descending neuron (ddN) and minimal input to VGN1R may represent a functional two-pass mechanism for sided initiation of symmetrical swimming. This left ddN cell also receives input from photoreceptor pathways that combine peripheral neuron, but not antenna input. Thus, these three photoreceptors, pr-e, pr13 and pr20, provide input to both partners of the first interneuron pair, AVG neurons (both types discussed above), and the left ddN (Fig. 5.17).

Even though the ocellus is on the larva's right side, the photoreceptor input through its relay neurons is generally greater onto left partners of motor ganglion neurons, including interneurons VGN1L by cells 80,108,112, and 116 (which share five photoreceptors as

Figure 5.17. Photoreceptor (pr) input to motor ganglion (MG) components through relay neuron subtypes. A-C) prL photoreceptors provide tertiary (third-order) input through relay neurons (IN) to the left side neurons of the MG. A) prLd provide input to left MG interneurons (VGL) and descending decussating neuron (ddL) through INLs. B) prLa provide input to left motor ganglion and left side motor neurons (MNL) through INLas. C) prLb provide inputs to VGL, MNL and ascending neurons of the MG (AVG) through INLbs. D-E) prB photoreceptors provide tertiary (third-order) input to both left and right side neurons of the MG. D) prB provide input to left and right VGNs as well as left side motor neurons (MNL) through INcs. E) prBd provide input to left and right VGNs, left MNs, AVG neurons, and some provide additional input to ddL through INds.

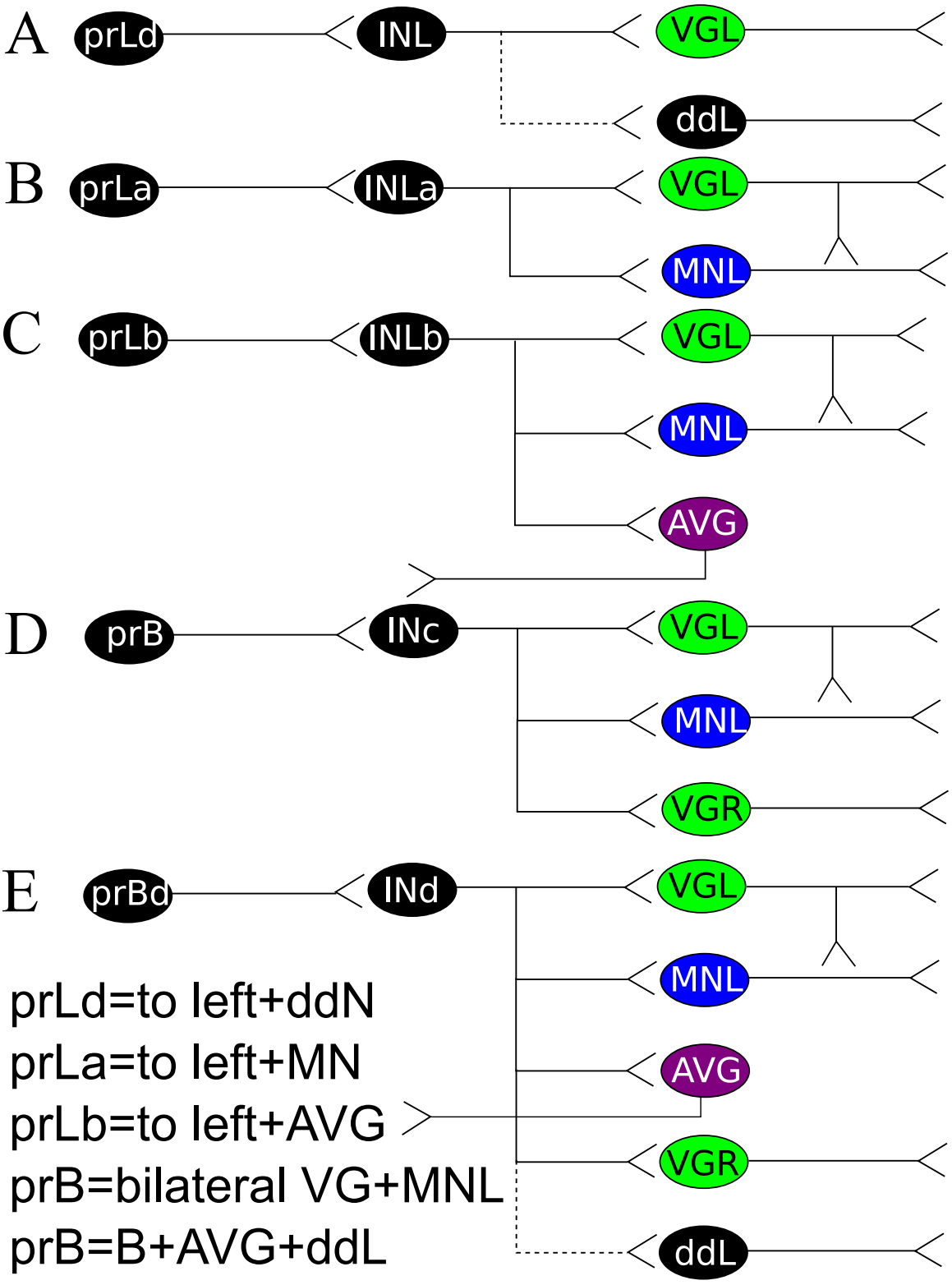
A
prLd
INL
VGL
ddL
B
prLa
INLa
VGL
MNL
C
prLb
INLb
VGL
MNL
AVG
D
prB
INc
VGL
MNL
VGR
E
prBd
INd
VGL
MNL
AVG
VGR
ddL
prLd=to left+ddN
prLa=to left+MN
prLb=to left+AVG
prB=bilateral VG+MNL
prB=B+AVG+ddL

input partners), cells 127, 130, 159, 96, 74, 157; and VGN2L by cells 105 and 130 (which also share five photoreceptors as input partners, four of which are the same as those to VGN1 interneurons). This input is coincident with their locations in the motor ganglion neuropil because the axons of photoreceptor interneurons for the most part are located dorsally, on the left side of the neuropil within the motor ganglion. However, one subtype of those photoreceptor relay interneurons that receive input from the peripheral integration system, INd neurons (Fig. 5.17E), remains in a bundle in a more ventral location where their axons intertwine with those of ascending motor ganglion (AVG) neurons. These INd neurons terminate a short distance within the motor ganglion, however, where AVG axons turn to leave the neuropil. Thus, only a single INb/INd axon belongs to the ventral bundle and terminates more posteriorly than the other INd axons, and although it branches into short dorsally projecting extensions, these do not extend far, and the axon itself does not turn to join the remaining INb axons that belong to the bundle of other photoreceptor relay neurons. The single INL (Fig. 5.17A), cell 80, also projects branches ventrally, but does not enter the ventral neuropil in the motor ganglion, and instead terminates at the same level as the INd neurons. Other regional exceptions exist, in which the axons of interneurons 86 and 126 alternately extend their axons toward the right neuropil in the motor ganglion to form presynaptic contacts to right-side interneurons (Fig. 5.18). The axon of cell 86 then returns to the left dorsal PR bundle. Within the dorsal left photoreceptor axon bundle, there are also axons of a few secondary interneurons (cells 93 and 106), which receive no direct input from sensory neurons. Most photoreceptor relay interneurons form terminals in the more anterior motor ganglion, and do not extend toward the trunk-tail boundary. INLa neurons (Fig. 5.17B)

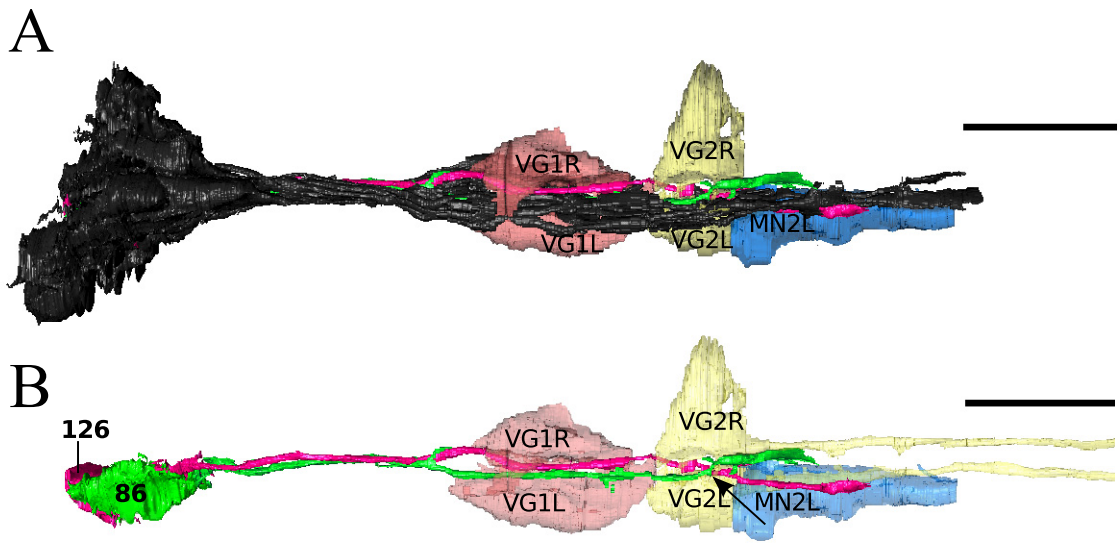

Figure 5.18. Reconstruction of photoreceptor relay neurons relative to their major postsynaptic motor ganglion targets. A) All photoreceptor relay neurons (black) with neurons 86 (green) and 126 (pink) coloured to illustrate their projection to the second right-side interneuron (VG2R) of the motor ganglion (MG). B) Cells 86 and 126 reconstructed without other relay neurons illustrating their crossing at the midline in the mid motor ganglion (arrow). VG1: first descending interneuron pair of the MG; VG2: second descending interneuron pair of the MG (L: left, R right); MN2L: second motor neuron on the left side. Scale bars: 10µm.

extend furthest into the motor ganglion and are the exception, terminating alongside the terminal of the first ACIN (Fig. 5.19).

Photoreceptor input to the motor ganglion through their relay neurons is extensive and widespread. All but four canal photoreceptors and three ocellus photoreceptors have secondary input to the motor ganglion through these relay neurons. Substantial second-order input to the motor ganglion from photoreceptor relay neurons occurs onto left and right partners of the first two motor ganglion interneurons, left and right partners of the first and second pairs of motor neurons and the left partner of the third pair, the left descending decussating neuron, and AVGs 1, 2, 6 and 7. Six photoreceptors (pr1, pr5, pr8, pr9, pr22, and pr-a) have exclusive left-side motor ganglion input through their relay neurons. Five other photoreceptors (pr16, pr18, pr19, pr23, and pr-f) have only minimal input to the right side of the motor ganglion through their relay neurons, but extensive input to the left side. The remaining photoreceptors provide substantial input to both sides of the motor ganglion through their relay neurons. This distribution of connections corresponds neither to morphological criteria nor to the organization of photoreceptor outer segments, cell bodies, nor to their terminals. For most photoreceptors, the input from their relay neurons to the interneurons of the motor ganglion is far greater in size and number than that to motor neurons or decussating descending neurons. Pr11 is an exception in that its target relay neurons have only 7 synaptic inputs to both interneurons and motor neurons. Five photoreceptors (pr1, pr3, pr20, pr-e, and pr-f) provide secondary input to the left descending decussating motor ganglion neuron through relay neurons 140, 157, and 116, all of which are multimodal PR-AVG relay neurons.

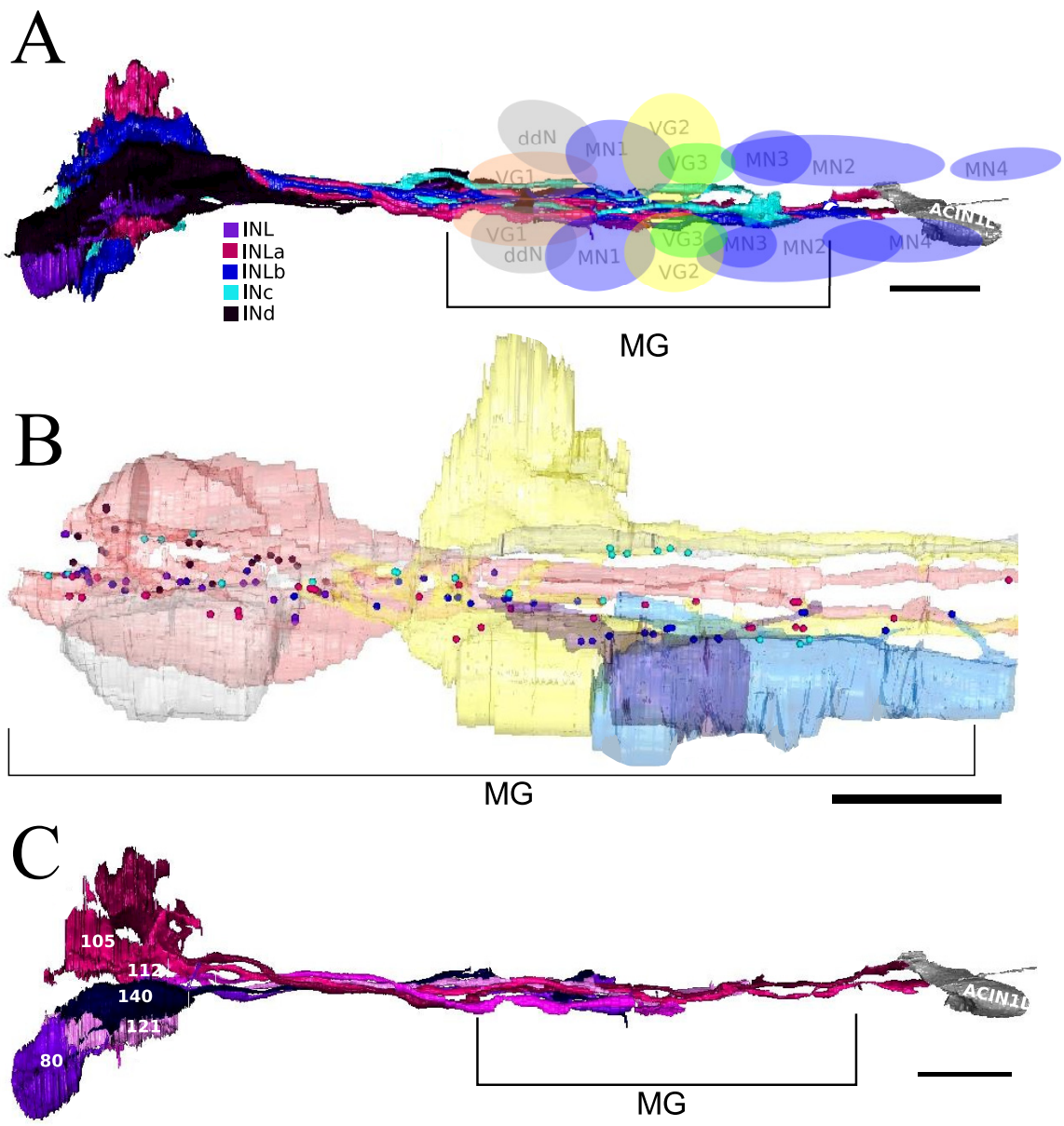

Figure 5.19. Reconstructions of photoreceptor relay neurons with the left ascending contralateral inhibitory neuron (ACIN1L). Terminals of relay neurons lie in the motor ganglion (MG), except for those of three neurons. A) All relay neurons, coloured by type. INc, INLa, and InLb neurons extend furthest through the MG toward the tail. Some bundling and spatial organization among axons and cell bodies of each type is evident. B) INL and INLa relay neurons labelled by cell body terminate before the mid-MG, except for two neurons, cells 105 and 130, which extend into the proximal tail. Scale bars: 10µm.

5.3 **Discussion**

5.3.1 Photoreceptor Characteristics:

The identification of *Ciona* larval photoreceptors has occurred in a stepwise fashion. Two classes of photoreceptor are distinguished by their location and the projection of their outer segments. The first class, projecting ciliary outer segments through the pigmented ocellus cell into the lumen of the neural canal, appears to be identified by Horie et al. (2008b) as expressing reporters for glutamate and Arrestin in their cell bodies and Ci-Opsin in their outer segments. However, the most posterior of these ocellus photoreceptors apparently lack glutamate reporter expression, although they express both Ci-opsin and arrestin reporters (Horie et al., 2008b; Horie et al., 2010). These 23 cells send axons into the region of the posterior brain vesicle where they form terminals that contact many interneurons, especially intrinsic brain vesicle interneurons, in more anterior regions, which in turn contact interneurons projecting to the motor ganglion. The synaptic pathways of this first group are in general unidirectional and monosynaptic.

A second group of photoreceptors project outer segments directly into the lumen of the canal. This class was also identified by Horie as expressing Arrestin and Opsin (Horie et al., 2008b). At lease some of these photoreceptors also appear not to express Glutamate, like the posterior class of the ocellar photoreceptors. Instead of Glutamate reporters, *in Situ* sectioning suggests widespread expression of Ci-GAD in these photoreceptors (Zega et al., 2008), which is confirmed by reporter studies using Ci-VGAT reporter with a photoreceptor specific marker (Horie, 2010 unpublished data). Photoreceptors of this canal type also project to the posterior brain vesicle and form fewer, but similar types of synapses onto a subset the same interneurons as Type I photoreceptors. All

photoreceptors are located dorsal to the three vacuolated lens cells on the right side of the brain vesicle and follow the same axon pathway laid down by the photoreceptor associated neurons (cells lens1, lens2 and trIN).

Group I Photoreceptors in *Ciona intestinalis* larvae are arranged in rows of 4-6 anterior to posterior with outer segments projecting into a space between the photoreceptor cell bodies and the ocellus pigment cup. There are five layers of 5, 4, 4, 5, and 5, respectively. Among these, the posteriormost three groups, I-iii, I-iv, and I-v all project their outer segments from the anterior portion of their cell body, whereas group I-ii have anterior, dorsal and posterior projecting outer segments, and group I-i project outer segments posteriorly. Group II photoreceptors also fall into two groups, a more anterior set of three with anterior outer segments and another set of four with dorsal outer segments. Although the anterior and posterior locations of photoreceptors roughly distinguish Type I and Type II photoreceptors, corresponding with their outer segment projection, I-i are actually anterior to II-ii. The outer segment polarity in fact tends to reflect the anterior to posterior layering of these photoreceptors. Taking into account both Type I and Type II photoreceptors, anterior layers project outer segments from the posterior portions of their cell bodies, then middle layers project outer segments dorsally, with the most posterior photoreceptors projecting their outer segments from the anterior portions of their cell bodies.

However, comparing the actual reconstructions of these photoreceptors and their associated interneurons with reporter expression studies reveals that all Type II photoreceptors appear to express glutamate reporters although I-i do not. The more posterior section lacking glutamate expression could correspond to I-v photoreceptors,

but the lack of glutamate reporter expression in this region is less clear. Thus, it seems that I-i, I-ii, I-iii, I-iv and possibly I-v photoreceptors express reporters for glutamate, whereas II-i, II-ii, and possibly I-v express reporters for GABA. The axo-axonic synapses from Type I photoreceptors with other photoreceptors, antenna axons or pr associated neurons contain vesicles with a characteristic structure, a small vesicle having a tiny dark core (Fig. 5.5C-D). These axons also appear to release neurotransmitter onto the basement membrane of the CNS (Fig. 5.5B). Analyzed row-by-row, I can now see that the networks of these layers differ (Table 5.1).

All layers appear to be fully connected (Fig. 5.8A), although the strengths of these connections vary (Table 5.2). Anatomically strongest interactions amongst rows of photoreceptors are bidirectionally between Type I-i and I-iv, I-i and I-iii, and I-i and I-v. In contrast, Type II photoreceptors receive input from both Types I-iv and I-v. Thus, it seems that layer I-i may function as an integrator of other photoreceptor signals. This is interesting, given that this layer consists entirely of photoreceptors with outer segments that extend posteriorly from their somata, and is the anteriormost layer of Type I photoreceptors. Thus, their outer segments extend into the anterior portion of the pigment cup and their axons travel for some distance along the right wall of the CNS alongside the antenna and photoreceptor associated anterior interneurons. With the exception of those synaptic contacts from Type I-v, these should all release glutamate at their synaptic contacts onto each other, in a sign-conserving manner. Thus, when light is off, the glutamatergic photoreceptors will reinforce each other's release of glutamate, whereas a light on response will prevent release by all photoreceptors.

Table 5.2. Matrix of photoreceptor synapses from presynaptic (left column) to postsynaptic (top row) photoreceptors (Pr). Cells are colour-coded by total size of synapses: 1-3 sections (yellow); 4-5 sections (orange); 6-9 sections (red); >10 sections (brown). Underlines indicate synapses that have a reciprocal synaptic counterpart from postsynaptic photoreceptor. Total number of sections (Tot) of presynaptic and postsynaptic photoreceptor synapses and number of partners (# pr) given for each photoreceptor Total numbers of reciprocal postsynaptic partners for each photoreceptor appear in final column.

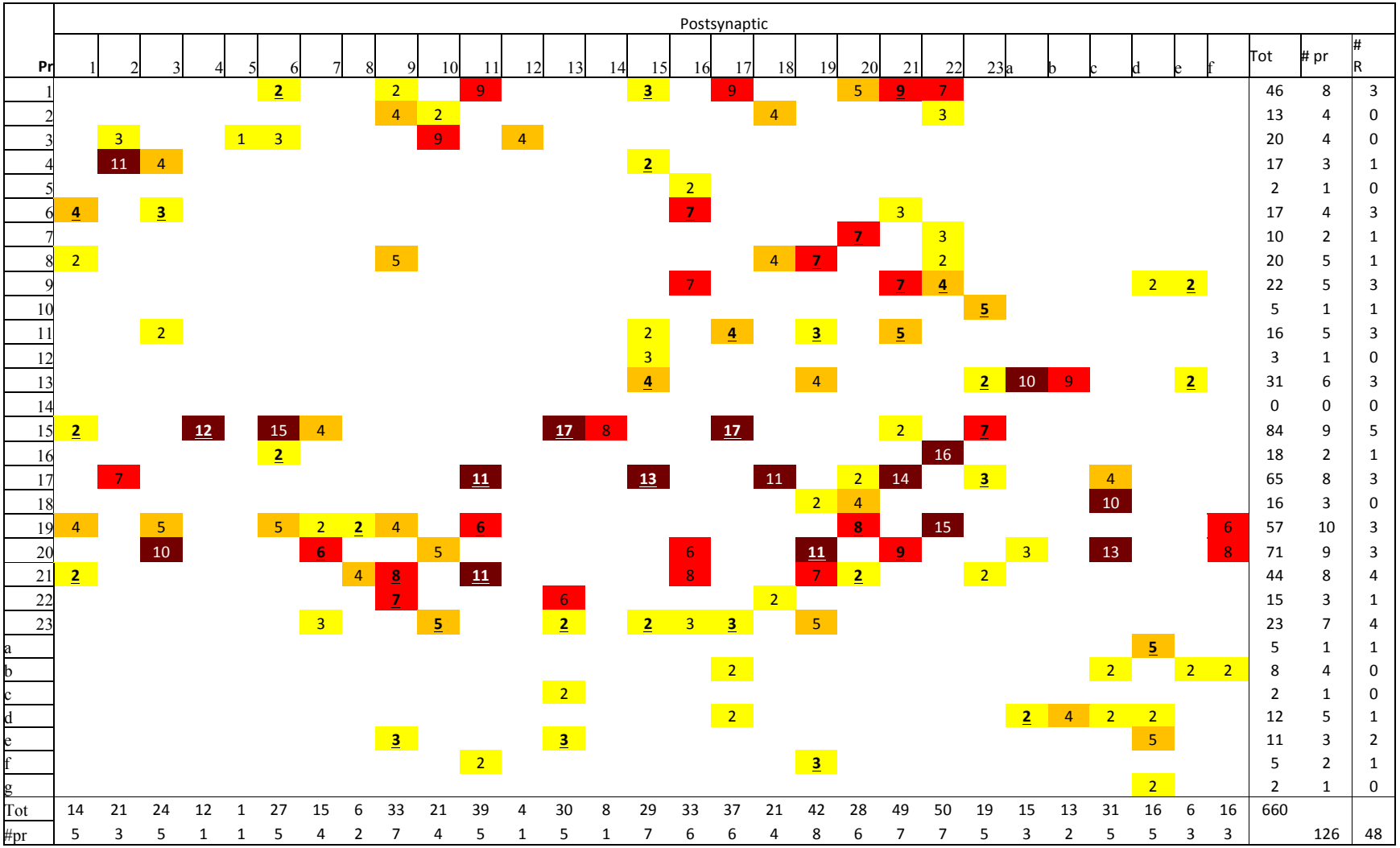
Postsynaptic
Pr
1 2 3 4 5 6 7 8 9 10 11 12 13 14 15 16 17 18 19 20 21 22 23 a b c d e f
Tot
pr
R
1 2 3 4 5 6 7 8 9 10 11 12 13 14 15 16 17 18 19 20 21 22 23 a b c d e f Tot # pr # R
1 2 9 2 9 3 9 5 9 7 46 8 3
2 4 2 4 3 13 4 0
3 3 1 3 9 4 20 4 0
4 11 4 2 17 3 1
5 2 2 1 0
6 4 3 7 3 17 4 3
7 7 3 10 2 1
8 2 5 4 7 2 20 5 1
9 7 7 4 2 2 22 5 3
10 5 5 1 1
11 2 2 4 3 5 16 5 3
12 3 3 1 0
13 4 4 2 10 9 2 31 6 3
14 0 0 0
15 2 12 15 4 17 8 17 2 7 84 9 5
16 2 16 18 2 1
17 7 11 13 11 2 14 3 4 65 8 3
18 2 4 10 16 3 0
19 4 5 5 2 2 4 6 8 15 6 57 10 3
20 10 6 5 6 11 9 3 13 8 71 9 3
21 2 4 8 11 8 7 2 2 44 8 4
22 7 6 2 15 3 1
23 3 5 2 2 3 3 5 23 7 4
a 5 5 1 1
b 2 2 2 8 4 0
c 2 2 1 0
d 2 4 2 2 12 5 1
e 3 3 5 11 3 2
f 2 3 5 2 1
g 2 2 1 0
Tot 14 21 24 12 1 27 15 6 33 21 39 4 30 8 29 33 37 21 42 28 49 50 19 15 13 31 16 6 16 660
#pr 5 3 5 1 1 5 4 2 7 4 5 1 5 1 7 6 6 4 8 6 7 7 5 3 2 5 5 3 3 126 48

If Type I-v and Type II photoreceptors are GABAergic, and still hyperpolarize to light, then they should inhibit their photoreceptor targets, which express GABA receptors according to Zega et al. (2008). The I-v photoreceptors have more numerous synaptic inputs to their photoreceptor partners than the other putative GABAergic Type II photoreceptors, but these converge on more anterior Type I ocellus photoreceptors. The main targets of all putative GABAergic photoreceptors are four Type I-i and four I-ii photoreceptors. These represent anterior, posterior, and dorsal outer segment bearing photoreceptors. This means that synaptic input to trIN, antenna neurons, and the basement membrane originate exclusively from putatively GABA positive photoreceptors or their photoreceptor targets. Thus, the sign-converting signal to the antenna pathway from this subset of photoreceptors is preserved.

A third group of prospective photoreceptors was identified by Horie et al. (2008b) that express Opsin in their "outer segments" as well as Arrestin (with expression that increases throughout the larval phase). These six cells certainly project modified ciliary elements into the lumen of the canal. They are located more posteriorly and ventrally than the other photoreceptors and have minimal association with the lens cells. Interestingly, five of the six cell bodies possess their own large vacuoles. Although these cells express arrestin at later stages of tadpole development, there are no visible axonal processes extending from these cell bodies when viewed in confocal image stacks (Horie et al., 2008b; personal observation), nor at the earlier stage examined in this study (2hph). Interestingly, some of the few inputs onto these cells are from antenna neurons, or coronet associated neurons, whereas none receives inputs from photoreceptors. There are also two cells with non-modified cilia that seem to contact the modified cilia, both of

which have cell bodies located in the same approximate region, one with a vacuole and one without.

5.3.2 Photoreceptor Tract Interneurons:

The single trIN neuron has a similar cell body location and axonal projection pattern to those of photoreceptors but lacks an outer segment. From its shape (Fig. 5.3A-B), this cell was initially thought to be the third antenna cell (Imai and Meinertzhagen, 2007a). However, the location of this cell at a distance from the otolith pigment and cell, and its lack of ciliary projection combine to indicate that it is phenotypically distinct and does not make any contact with the otolith cell. The location, size, and appearance of this cell match moreover with a vGLUT positive, Arrestin negative cell visible in reporter studies (Horie et al., 2008b). This cell may therefore represent a novel phenotype associated in the photoreception pathway, and its projection pattern implicates a role in pathfinding or axonal guidance along with two other vacuolated cells the axons of which do not reach the posterior brain vesicle (Fig. 5.3A-B). However, this neuron also makes many synaptic contacts, and may further function in sensory pathway integration. The synaptic partners of the axon tract neuron include both photoreceptors and antenna cells. This cell receives axo-axonal inputs from Type II, I-i and I-ii photoreceptors, along with terminal inputs from some photoreceptors and some antenna interneurons of the posterior brain vesicle. As discussed above, this photoreceptor input constitutes putative GABA and Glutamate signals, the latter also subject to the former. trIN also receives input from intrinsic brain vesicle and relay interneurons of both photoreceptor and multimodal varieties, as well as both antenna neurons. This photoreceptor tract neuron is a target of several brain vesicle intrinsic photoreceptor interneurons, which have few synaptic

targets. However, most of the input to this neuron comes from photoreceptors, antenna neurons, and the highly branched brain vesicle intrinsic anaxial arborizing antenna2 interneuron, cell 115.

Postsynaptic partners of the trIN include photoreceptors (in the terminal and axonal regions), but despite its association with photoreceptor neurons, the major synaptic targets of this neuron are the large relay interneurons of the antenna pathway (cells 142, 147, and 161). These presynaptic sites of the photoreceptor tract interneuron to antenna interneurons are largest (5-10 synapses with an average diameter of ~0.4μm each), spanning many sections (up to 15 60-nm sections for a single synapse). These antenna relay neurons send their axons to the motor ganglion where they synapses onto other interneurons as well as the first two pairs of VGNs, with much stronger input to the right partners of both pairs. One of these antenna interneurons also forms minimal inputs directly to the right partners of motor neuron pairs 2 and 3. Thus, depolarization of this putatively glutamatergic trIN could, along with glutamate synapses from antenna neurons, initiate strong right side motor activation and resulting muscle contractions. Additional synaptic targets of this neuron include intrinsic anaxial arborizing multimodal interneurons, 102 and 115, and to a lesser extent other photoreceptor interneurons.

The two additional vacuolated photoreceptor tract neurons caudal to the photoreceptors appear to be GABA (GAD and vGAT) positive (Zega, 2008; Horie, unpublished data). A function for pathfinding, axonal guidance, or photoreceptor-antenna segregation is reasonable for these neurons given their location and projection, but cannot be confirmed in this study. The axon track and termination within the photoreceptor tract limit the synaptic connections of these neurons to only photoreceptors, antenna neurons, the other

photoreceptor tract neuron, and each other. These vacuolated neurons, particularly lens1, also release GABA at approximately ten synapses onto Type II photoreceptors, six onto Type I-i and I-ii photoreceptors, and both photoreceptors and six onto antenna neurons. However, these neurons have far more synaptic sites that appear to release onto the basement membrane adjacent to the endoderm. This endoderm appears to express Ci-$GABA_BR2$ as illustrated by its *in Situ* expression (Zega et al., 2008).

5.3.3 Focusing Light to the Eye:

Beyond the photoreceptive cells and their interneurons, vertebrate vision requires the refractive power of a lens, especially in an aquatic environment. In the vertebrate eye, light is focused onto the retina by the lens and cornea. Along with the so-called lens cells in *Ciona,* many cells in the brain vesicle associated with the visual pathway, including neurons, contain vacuoles. In vertebrates, lamprey, and hagfish larvae (Lamb, 2013), a lens placode forms in the ectoderm overlying the developing retina, and although the lens is involved in inductive signaling, retina formation in vertebrates proceeds in the absence of lens tissue (Valleix et al., 2006; Eiraku et al., 2011; Lamb, 2013). Lamb (2013) proposes that the ectodermal lens placode evolved after the lateral invaginated eye cups, and functions to establish the initial orientation of the retina with respect to the retinal pigment epithelium, in part through FGF signalling. As in vertebrates, FGF signalling is found to play a role in initial determination of pigment cell fate in *Ciona* (Racioppi et al., 2014). The source of this FGF signalling is Row I or II 5-8 blastomeres at 6 hpf and includes A8.7 and A8.8, which give rise to lens and photoreceptor cells in *Halocynthia*, but are restricted to ventral fates in *Ciona* (Cole and Meinertzhagen, 2004; Meinertzhagen, 2005). Although Type I and II photoreceptors are thought to arise from

a-line cells in *Ciona* (Cole and Meinertzhagen, 2004; Meinertzhagen, 2005), the lens cells and Type III photoreceptors are located ventrally, so may be progeny of these FGF producing A-line blastomeres. According to Racioppi et al. (2014), this FGF signalling persists ventrally to A11.193 past Stage 55 (Cole and Meinertzhagen, 2004). Confirmation of lens cell and Type III photoreceptor lineage would provide interesting insight into their potential role in this induction of pigment cell fate in *Ciona*.

Ciona lens cells are located within the CNS, not in the ectoderm, so their homology to the lens of vertebrates is weak. Furthermore, the transparency of the refractive lens of vertebrates is in part due to β-crystallin, which although present in *Ciona* otolith and palps, is paradoxically reported to not be contained in lens cells (Shimeld et al., 2005). However, Ci-βγ-crystallin promoter-driven, expression present in cells near the ocellus does coincide with lens cell vacuole locations (Shimeld et al., 2005; Riyahi and Shimeld, 2007), although Shimeld et al. (2005) attributes some ocellus expression to absence of necessary repressor regions in the promoter. Duncan et al. (1998) suggested that Pax6 expression inhibits β-crystallin synthesis in early lens epithelial cells in vertebrates. This inhibition may explain why β-crystallin mRNA may also absent in *Ciona* lens cells, which are located in an area of Ci-pax6 expression (Irvine et al., 2008). Other transcription factors involved in β-crystallin formation in the vertebrate lens, such as Sox2 and Maf family proteins, are not expressed in domains containing *Ciona* lens cells (Tassy et al., 2010). Instead, the so-called lens cells in *Ciona* contain glycogen (Eakin and Kuda, 1970; 1972), which is also found in the lens (Eakin et al., 1961; Castillo et al., 1992; Shivalingappa et al., 1996) and cornea (Malinin and Bernstein, 1979) in some vertebrates. Where it is present in vertebrates, glycogen is thought to increase the

refractive index of these structures (Rabaey, 1963). Thus, the larval CNS lens cells in *Ciona*, despite being internal to the animal, may indeed share some characteristics of the vertebrate lens.

Lenses of other invertebrate species offer another possible explanation for the structure and composition of the *Ciona* lens cells and for vacuolated cells of the visual system. Some species of flatworms are known to concentrate glycogen in the cells of each eye (Lanfranchi and Bedini, 1988), as do crystalline cones of copepods (Wolken and Florida, 1969). Many other species of flatworms have what are referred to as mitochondrial lenses (Sopott-Ehlers, 1996; Rohde et al., 1999; Sopott-Ehlers et al., 2001). These structures are formed from mitochondria, as illustrated by the cristae present along the periphery of the lens. Although they are separate cells from the pigment cell, the vacuoles of the glycogen-containing lens cells of *Ciona* are surrounded by mitochondria and contain fragments that could be considered to resemble cristae, although the vacuolar region lacks a surrounding membrane. While the composition of the mitochondrial lenses in flatworms is unknown, glycogen is also reported in these lens-forming cells (Roemer and Haas, 1984; Sopott-Ehlers, 1996).

Unlike lens fiber cells in vertebrate eyes, the lens cells of *Ciona* have nuclei and organelles. The lining of lens vacuoles of *Ciona* with mitochondria is a notable feature that may have functional implications. Molecular switches involving components of the mitochondrion-induced apoptotic pathway initiate lens differentiation in vertebrates (Weber and Menko, 2005). The mitochondria of these lens cells have high levels of alpha-crystallin, a small heat shock chaperone protein, which preserves mitochondrial function under conditions of oxidative stress (McGreal et al., 2012). *Ciona* has a gene at

LOC100184261, which contains and alpha-crystallin domain (CDD:260235). Interestingly, in fish, the content of alpha-crystalline in the lens decreases with increasing ocean depth, and is found in only small amounts in the lenses of degenerate eyes in the rice eel and other bathydermal species (Lin et al., 2013). The chaperone role of alpha-crystallin is proposed to contribute to this reduction in deep water fish species (Lin et al., 2013). In fish, the corneal contribution to refraction is negligible, and fish lenses are rigid, so refractive index is mostly dependent on lens protein concentration (Kröger, 2013). Likewise, the refractive index of the lens of *Ciona* is likely to depend on its protein composition. Thus, the presence or absence of alpha-crystallin in the lens cells of *Ciona* could be assessed immunocytochemically, and would provide additional insight into *Ciona* lens function. If present in the lens cells, alpha-crystalline may enhance refraction as well as playing a role in preservation and cell survival.

Why does the *Ciona* lens use glycogen? In *Ciona*, there is no muscle surrounding the ocellus, so the glycogen-containing lens is thought to be simply refractive. However, *Artemia* alters the glycogen bodies in their crystalline cones while increasing or decreasing the lens curvature during light or dark adaptation, respectively (Nilsson and Odselius, 1981). Could the glycogen in *Ciona* lens cells alter the conformation of the lens? The location of this molecule is unknown in *Ciona*, but in mammals it is present in the lens at a very high concentration of 35% (Horwitz, 2003).

In addition to its role in transparency and refraction, alpha-crystallin also has small heat shock protein function, and interacts with unfolded proteins as well as cytoskeletal elements (Horwitz, 2003). Among these interactions, alpha-crystallin domain interacts with glycogen phosphorylase to raise the rate of phosphorylase inactivation (Meremyanin

et al., 2008) and, *in vitro*, can alter the activity level of GSK-3 kinase, a regulatory protein of glycogen synthase (Björkdahl et al., 2008). Thus, alpha-crystallin could increase inactivation of the glycogen breakdown pathway and decrease inactivation of glycogen synthesis, so that alpha-crystallin binding could play a role in regulating glycogen content. In addition to altering protein concentrations, alpha-crystallin interactions with cytoskeletal elements could also permit changes in the shape of lens structures. Thus, the presence of alpha-crystallin in *Ciona* lens cells could lead to a reinterpretation of its visual capacity.

5.3.4 Vertebrate Comparisons:

5.3.4.1 Photoreceptors and Retinal Cell Types:

Three populations of photoreceptors have been identified based upon their expression of arrestin and opsin antibodies (Horie et al., 2008b). The first two are discussed in detail in terms of their connections, but Type III photoreceptors lack many synapses or typical neuronal shapes at this point in the larva, although Horie et al. (2008) have suggested that these photoreceptors may have a function later in development. The late birth, glycogen content (Eakin and Kuda, 1972; Pfeiffer et al., 1994), and anatomical composition, including possession of cilia, vacuoles, and junctional connections, along with their location between the photoreceptors and the rest of the photoreceptor interneurons likens Type III photoreceptors in some ways to Müller cell glia (Goldman, 2014). The ability of the Type III cells to act in photoreception at later stages of development (Horie et al., 2008b) may also be consistent with the ability of Müller cell glia to produce new photoreceptors after injury (Goldman, 2014). Careful examination of their complement of signal molecules and transcription factors would be necessary to confirm this

suggestion however. Their contribution to the adult brain would also provide insight into their pluripotency and potential role.

Three of the known vertebrate retinal cell types, horizontal, amacrine, and retinal ganglion cells, express melanopsin (Arendt, 2003). Based on this expression, Arendt (2003) has proposed that these are sister cells that evolved from rhabdomeric precursors. Koyanagi and Terakita (2008) investigated the genomes of bilaterians for Gq-coupled melanopsin-like rhodopsins and concluded that although present in echinoderms (Raible et al., 2006) and amphioxus (Koyanagi et al., 2005), no melanopsin-like gene could be found in ascidians, so must have been lost in the ascidian lineage. Thus, it is unlikely that these cell types would exist in the *Ciona* visual system. However, additional C-opsin expression in some horizontal and ganglion cells (Davies et al., 2010), and co-expression of R- and C- opsins led Lamb (2013) to suggest that the actual ancestral cell had characteristics of a multipurpose visual cell. In this case, the lack of melanopsin expression in *Ciona* may allow for the possibility that these cell types exist in ascidians, but that they lack expression of melanopsin, along with any associated function. Certainly, the synaptic and morphological characteristics of *Ciona* photoreceptors are consistent with this multifunctional photoreceptor hypothesis.

In contrast, bipolar neurons are proposed to derive from ciliary photoreceptors (Lamb, 2013). However, hagfish lack bipolar neurons, and instead contain only photoreceptors and projection neurons in their pineal-like eye. Although present in the retina of adult lampreys, bipolar cells are not identified even in the ammocoete larval eye (Lamb, 2013). As these are the last layer to form in the vertebrate retina, it is possible that they only appear in the adult lamprey because of the prolonged delay in differentiation. *Ciona* eyes

are more akin to lateral eyes based on their outer segments projection inward, not toward the outside world (Lamb, 2013), with a proximal ocellus and distal multilayered retina (of photoreceptors) -- an orientation that is proposed, in vertebrates, to be signalled from the lens placode (Lamb, 2013). However, the retinal arrangement of *Ciona* coincides more closely with that of the pineal eye, in which photoreceptors provide synaptic input directly to OFF projection neurons (RGCs) (Lamb, 2013). In the frontal eye of amphioxus, Vopalensky et al. (2012) suggest that layers of photoreceptors themselves correspond (are homologous) to different retinal cell types. Thus, layers of photoreceptors in the retina of *Ciona* may themselves undertake the roles of both photoreceptors and their retinal interneurons, with a division of labour among individuals or groups of cells.

Lamb (2013) proposes that ciliary and microvillar photoreceptors sat adjacent to each other in the chordate ancestor, the microvillar photoreceptors that projected axons into the growing CNS/brain then evolving to receive signal from the photoreceptors, and subsequently becoming their projection neurons, retinal ganglion cells (RGCs). The case in *Ciona* seems to contradict this scenario, in that the ciliary photoreceptors themselves send axons into the brain. Furthermore, while the *Ciona* visual system does share the aspect of photoreceptor-photoreceptor synaptic contact, the Type III photoreceptors that have modified cilia and possible microvilli, and most closely resemble microvillar photoreceptors, do not project axons far into the brain at early stages, although they do receive some input from photoreceptor neurons. Only three interneurons co-populate the expanded retinal region in *Ciona*: trIN and the two vacuolated anterior interneurons. The vacuolated interneurons form synaptic relationships exclusively with photoreceptors and

antenna neurons, but trIN projects into the CNS to provide input to intrinsic photoreceptor interneurons as well as the relay neurons. Based on its connections, however, trIN seems to function to facilitate information transfer from visual to orientation pathways including the antenna relay neurons and ciliated neurons of the anterior brain vesicle. Thus, it seems this neuron may possibly coordinate orientation/roll rather than a shadow response.

5.3.4.2 *Ciona* Photoreceptors as Multifunctional Precursors of Vertebrate Retinal Cell Types:

If we consider photoreceptors as multifunctional precursors of neurons of the various retinal cell types, their detailed interactions may reveal subtypes or functional roles. Photoreceptors vary in their degrees of input to their interneurons, from no direct input to relay neurons, to input onto a large number of interneuron targets. Likewise, photoreceptors receive input from a range of other photoreceptors, with some photoreceptors providing a great deal of input to each other. Most photoreceptor inputs to a given photoreceptor are reciprocal to their own target photoreceptors, however, only one quarter of all photoreceptor-photoreceptor synaptic partnerships are reciprocal, with fewer than half of those being of equal strength in both directions (Table 5.2). Five photoreceptors have the strongest synaptic partnerships with the greatest number of photoreceptors, all of which are Type I-i or I-ii. Of those strongly connected photoreceptors, photoreceptors 17, and 21 have only a few inputs to relay neurons, whereas photoreceptors 15, 19, and 20 have numerous postsynaptic relay neuron partners. Two of those with many relay neuron targets have bifurcated terminals, photoreceptors 15 and 20 (Appendix F), and may represent a separate class of photoreceptors. Some

photoreceptors receive many strong photoreceptor inputs (pr9 and pr22), so these may collect information to distribute to interneuron targets. Others (pr1, pr13, and pr23) provide outputs to many photoreceptor targets, and may function further upstream in visual information processing. In contrast, photoreceptor 12 has few synaptic connections with other photoreceptors, but provides presynaptic contact to many relay neurons.

5.3.4.3 Comparisons between *Ciona* Photoreceptor Interneurons and Vertebrate Retinal Interneurons:

The region in which all photoreceptors form terminals contains a number of neurons, axons, the terminals of other neurons, and hosts the photoreceptor interneurons, which appear to express reporters only for acetylcholine and glutamate (Horie et al., 2008a; 2010), but not those for inhibitory neurotransmitters GABA/glycine. Input to cell bodies of first-order interneurons is limited to a subset of neurons. The first of these, based upon their targets and the location of their terminals could be considered similar to ganglion cells. These provide synaptic input to other interneurons, both photoreceptor and antenna interneurons.

The brain vesicle intrinsic photoreceptor network of *Ciona* consists of interconnected neurons that process information from photoreceptors and feed into the relay neurons in the deeper brain. However, unlike vertebrates, the direct input of photoreceptors to those relay neurons complicates direct comparisons with retinal neuronal types. The pathway processing visual information is nonetheless layered in *Ciona*, so that many brain vesicle intrinsic photoreceptor interneurons feed into the three highly branched interneurons.

These branched intrinsic interneurons form an interconnected network along with the single photoreceptor tract interneuron, trIN (Fig. 5.13; Fig. 5.14), and all connect to relay neurons. Thus, these three highly branched cells appear to collect processed information and to transmit this intrinsic network's output to relay neurons in the deeper brain, much like ganglion cells of the vertebrate retina. The intrinsic processing network of the sensory brain vesicle that feeds into these ganglion cell-like projection neurons has a layered organization, with some similarities to the vertebrate retina, in terms of its synaptic organization.

In the vertebrate retina, horizontal cells collect information from numerous photoreceptors, and converge on each other, along with bipolar neurons (Dowling, 1970; Masland, 2012). Of the intrinsic brain vesicle photoreceptor interneurons, cell 70 has the most photoreceptor input partners, originating from dorsal members of four different photoreceptor rows, the only member of its class receiving input from both putative GABA and glutamate expressing photoreceptors. Like horizontal cells, this neuron does not provide direct input to the ganglion cell-like neurons, but instead to a series of other intrinsic photoreceptor interneurons that feed into ganglion cell-like neurons and relay neurons, as well as providing direct input to several relay neurons (most targets of its downstream intrinsic interneuron partners). Unlike horizontal cells, however, cell 70 provides feedback input to photoreceptors, both its direct input partners, and partners of its own downstream interneuron targets. Thus, this horizontal cell-like cell facilitates both feedback (as for cell 22) and feed-forward (as for cell 16) loops that include photoreceptors and brain vesicle intrinsic interneurons. These interneuron targets include the two bipolar-cell like interneurons in the *Ciona* visual system, which differ in their

synaptic relations to photoreceptors. One of these, cell 92, shares two photoreceptor input partners with cell 70, and provides feedback input to photoreceptors, some of which are other presynaptic partners of cell 70. The other bipolar cell also shares its presynaptic photoreceptor partner with cell 70, along with several other interneurons, but does not provide feedback to the photoreceptors. Unlike the vertebrate retina, the network bypasses the layered arrangement because bipolar-like cells also provide input to peripheral integrative photoreceptor relay neurons.

5.3.5 Processing Depth of the *Ciona* Larval Visual System:

The visual system of the *Ciona* larva is more complex than may have been anticipated by simply watching its observed behavioural outcomes. The resulting visual circuit, like many of the ancestral circuits present in the ascidian larval nervous system, exhibits some degree of redundancy and perhaps a lack of specification. It also represents a network that could be further specialized to generate the range of specialized circuits seen in the vertebrate retina. In reality, without a full description of all connections within the vertebrate retina, it is not entirely clear that there is not some overlap in function of the various retinal cell types, however, the main functional actors in the vertebrate retina are discussed here with respect to their possible counterparts in the basal retina of *Ciona*.

The vertebrate visual system comprises a distributed hierarchical network of interconnected processing pathways (Van Essen et al., 1992). The primary processing occurs in the retina, signal integration occurs in various regions in the brain, and results in convergence upon motor systems. In basal vertebrates such as hagfish the secondary processing occurs mostly in a region in the midbrain, the optic tectum, from which input

extends to motor components in the hindbrain region (Iwahori et al., 1996). Both the retina and optic tectum are layered structures with many neurons constituting few specific cell types. Most vertebrate retinal neurons, including photoreceptors, bipolar, horizontal, amacrine, and Müller cell glia, are restricted to the retina. Retinal ganglion cells are the ultimate relay neuron targets of this retinal network, and are unique among retinal cells in extending axons into the brain through the optic nerve, to provide synaptic input to integrative regions (Kolb, 2014). Although the *Ciona* larval CNS and visual system is very much reduced, and the correspondence of its elements to those in vertebrates weak, it also comprises two distinct classes of interneurons, intrinsic neurons that are confined to the sensory brain vesicle, and tectum-like posterior brain vesicle relay neurons that project to the motor ganglion, where they contact reticulospinal-like and motor neurons (see Ryan, 2015: Chapter 8). Unlike vertebrates, however, the small size and simple structure of the *Ciona* brain together result in overlap between interneuron and photoreceptor contacts with other sensory systems. Furthermore, compared with vertebrate visual processing (Lamb, 2013), the direct input from photoreceptors to the integrative relay neurons is unlike any case in more advanced chordates.

5.3.6 Comparisons between the Eye in *Ciona* and those in Ancestral Vertebrates:

Although the adult lamprey has an eye and retina very similar to the vertebrate eye (Holmberg, 1977; Lamb, 2007), its larva lacks photoreceptive capacity and has an undifferentiated retina. Like the lamprey larva, the hagfish shares many basal characteristics with ascidian larva in that their photoreceptors connect directly to "output neurons", ganglion cells, however it lacks bipolar and amacrine cells (50-53). Unlike the ascidian photoreceptors, the hagfish eye is not required for light response, and seems

instead to function in regulating a circadian rhythm (Lamb, 2007). Thus, it seems that ascidian larval visual pathways represent a sort of intermediate with both direct connections from photoreceptors to the ganglion relay cells, and the apparent presence of other brain vesicle intrinsic interneurons that may be required for light responses.

5.3.7 Sidedness of the *Ciona* Ocellus and the Evolution of Bilateral Eyes:

In all well studied invertebrate eyes, photoreceptors arise from the ectoderm, and connect with their interneurons which arise from the brain, whereas in vertebrate eyes, photoreceptors and their interneurons arise together from an outpocketing from the brain (Meinertzhagen and Hiesinger, 2004). *Ciona* exhibits features of both types of development. Thus, along with vertebrates both photoreceptors and their interneuron in *Ciona* originate from neural ectoderm, whereas like invertebrates, this study shows that photoreceptors are regionally separated from their interneurons, which reside in the brain. Although photoreceptor interneurons, their axons and terminals are grouped within the posterior brain vesicle, they are located centrally, surrounded ventrally, laterally, and dorsally by non-retinal cell types. This segregation could be seen to frustrate the possibility that these cells could ever contribute retinal photoreceptor interneurons to form the outpocketing that in later forms could become the vertebrate retina. Unclear at this point is whether the laterality of the visual system in *Ciona*'s precursor retina is an ancestral or derived feature: either a one-sided eye must have been somehow duplicated to have given rise to the vertebrate visual system, or a bilateral visual system reduced to a unilateral design of the sort found in *Ciona*. This topic is ripe for further consideration (Esposito et al., 2015). However, the more anterior end of this proposed retina is centred

around the mini-canal, where the large lumen of the brain vesicle becomes filled in with cells and leaves a resulting pocket of CSF (Fig. 5.9).

Early determination of the optic cup by pax6 in vertebrates occurs as a single domain at the midline. The splitting of this initial determined midline domain in vertebrates occurs because of Hedgehog (HH) signalling from underlying midline medoderm and endoderm (Ekker et al. 1995; Macdonald et al. 1995). The bilateral eyes are thereby split by midline *hh* expression and *shh* mutants are cyclopic, with only a single medial eye (Belloni et al., 1996; Chiang et al., 1996). In *Ciona,* a CiPax6 transcript is expressed bilaterally in the dorsal brain vesicle, as seen in wholemount in-situ preparations at the mid-tailbud stage (Irvine, 2008 in Aniseed). Later in development, transverse sections of Ci-hh2 *in situ* in the larva indicate expression in the ventral left side of the brain vesicle at the level of the ocellus (Islam, 2010). However, sidedness of the retina appears to be determined by the late tailbud stage (Cole and Meinertzhagen, 2004).

Although *Ciona* only has a single photoreceptive organ, it is unilateral rather than medial. The ocellus pigment forms at the midline in the early tail bud stage, and migrates to the right side by the late tail bud stage (Cole and Meinertzhagen, 2004) in the presence of normal Nodal signalling in the left brain vesicle (Yoshida and Saiga, 2011). This left-side Nodal expression represses a critical ocellus development transcription factor, Rx, which determines asymmetrical right-side ocellus development (Yoshida and Saiga, 2011). Nodal acts upstream to hh genes, and in fish, nodal pathway mutants also result in cyclopathy (Feldman, 1998). Zebrafish Vax1 and 2 expression, under combined control of hh, Nodal and FGFs, is necessary for retinal partitioning from forebrain tissue (Take-uchi et al., 2003). Interestingly, no *Vax* gene could be found in the *Ciona* genome,

although *Not* and *Emx* genes, which are thought to derive from duplications of a single *Vax, Not, Emx*-like ancestral gene (Hallonet et al., 1998), are present (Wada et al., 2003). Taken together, the interactions of *Nodal, Rx,* and *hh* expression in the absence of any *Vax* gene in *Ciona* provide a mechanism for generating the unilateral, unpartitioned retina of *Ciona*.

5.3.8 Visuomotor Coordination:

Despite its small size and inherent simplicity, there is little direct input to the *Ciona intestinalis* motor system from primary sensory neurons. If we consider the vertebrate brain, by contrast, even though considerable knowledge about the circuitry of the retina (e.g. Kolb, 2014; Dowling, 2012) is matched by a similar level of knowledge about the spinal cord (Grillner and Manira, 2015; Voogt et al., 1998), very little is known about the integration between these regions. In the larval brain of *Ciona*, the various sensory signals are integrated within the posterior sensory vesicle and, to some extent, the motor ganglion itself. Thus, the necessity of that integration for encoding their environment shaped even the most simple nervous systems, so as to exclude a role for simple monosynaptic relays between sensory receptor and motor neuron. It is therefore essential to acknowledge the role played by such integration in considering sensorimotor pathways not only in vertebrates but also *Ciona*. The difference between the two of course lies in the relative magnitudes of the task required to reveal these, and the manageable proportions of that task in the tadpole larva of *Ciona*, for which this thesis will mostly consider the visuomotor pathways. Additional consideration will also be given to this topic in the section on peripheral mechanoreceptors (see Ryan, 2015: Chapter 7).

Various types of sensory pathways are anatomically qualified to produce the ultimate regulation of motor output. Further, the photoreceptor network graphs reveal that the first-order network from photoreceptors is extensive, but closely clustered, whereas the second-order network is expansive and includes less connected or clustered neurons (Fig. 5.20). Despite this rapid network expansion, the restriction of one node/single pass information flow from the photoreceptors to motor neurons does exist, but only for a few interneurons, cells 86, 105, 121, 123, with only a total of six synaptic inputs directly onto motor neurons, suggesting that although this may be a functional pathway, it is unlikely to be a major one for visuomotor control. Despite this qualification, it is interesting to note that all of these inputs are restricted to left-side motor neurons. Similarly, most input from photoreceptor relay neurons to interneurons of the motor ganglion occurs onto left-side partners. When we examine inputs onto motor neurons, the largest number and greatest size of synaptic inputs come from the planate neurons, eminens cells, and other neurons of the motor ganglion. Similarly, the more caudal interneurons as well as the decussating interneurons and planate neurons receive minimal input from brain vesicle interneurons, except for the eminens neurons. Thus, the integration of most signals coming from the sensory systems within the brain vesicle occurs via their own interactions and their synaptic inputs onto the first two interneurons of the motor ganglion. The complement of photoreceptor relay neuron input to these interneurons is distributed as illustrated alongside inputs from multimodal, antenna and coronet relay neurons (Fig. 5.21). Photoreceptor relay neuron input to VGNs falls into several categories: symmetrical single-pass input (INc: Fig. 5.17D), symmetrical tertiary input (INd: Fig. 5.17E), left-side input, left-side VGN1 input and right-side VGN1 input.

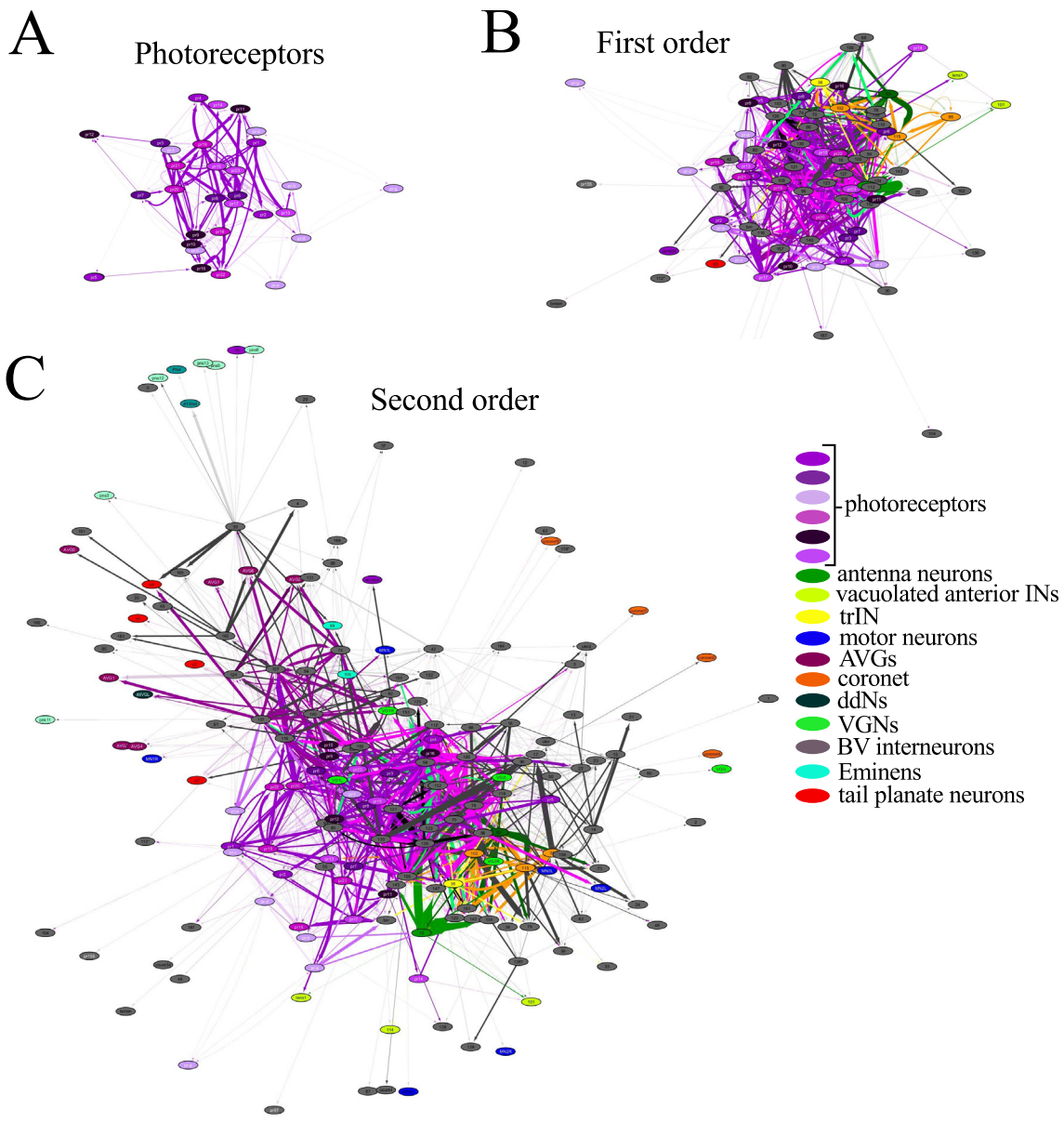

Figure 5.20. Cluster analyses of cell types. Edge-weighted spring embedded network graphs of photoreceptors (A), photoreceptors with their first-order synaptic targets (B), and photoreceptors with both their synaptic targets (first-order) and those target neurons' (second order) synaptic targets (C). Cells are colour-coded (key): trIN (photoreceptor tract interneuron), AVGs (ascending MG interneurons), ddNs (descending decussating neurons), VGNs (descending paired MG interneurons), BV interneurons (intrinsic and relay interneurons of the brain vesicle). Graphs created using Cytoscape using total synapse size for weighting of synaptic contacts. Note the expansion of the network and lack of clear or cohesive clustering among neurons, suggesting that photoreceptor interneurons are highly integrative with other neurons in the total network.

Figure 5.21. Reconstructions of motor ganglion neurons populated with photoreceptor and antenna relay neuron synaptic input sites, colour-coded by relay neuron type (key). All synaptic sites are marked by $4nm^3$ circles regardless of their actual size. prR: photoreceptor relay neuron; pr/trINR: relay neurons with input from photoreceptors and photoreceptor tract interneuron; pr/AVGR: relay neurons with inputs from photoreceptor and peripheral pathway; pr/cor/antR: relay neuron with inputs from photoreceptor, coronet cells, and antenna 2 neuron; pr/ant2R: relay neurons with inputs from photoreceptors and antenna 2 neuron; ant2R: relay neurons with inputs from antenna 2 neuron; ant1/2R: relay neurons with input from both antenna neurons. Anterior is to the left. A) Dorsal view of all target neurons in the MG, B) Target motor ganglion neurons in (A) populated with postsynaptic sites from relay neurons, paired where appropriate. Each neuron is rotated to show synaptic sites along inside edge Scale bars: 10µm.

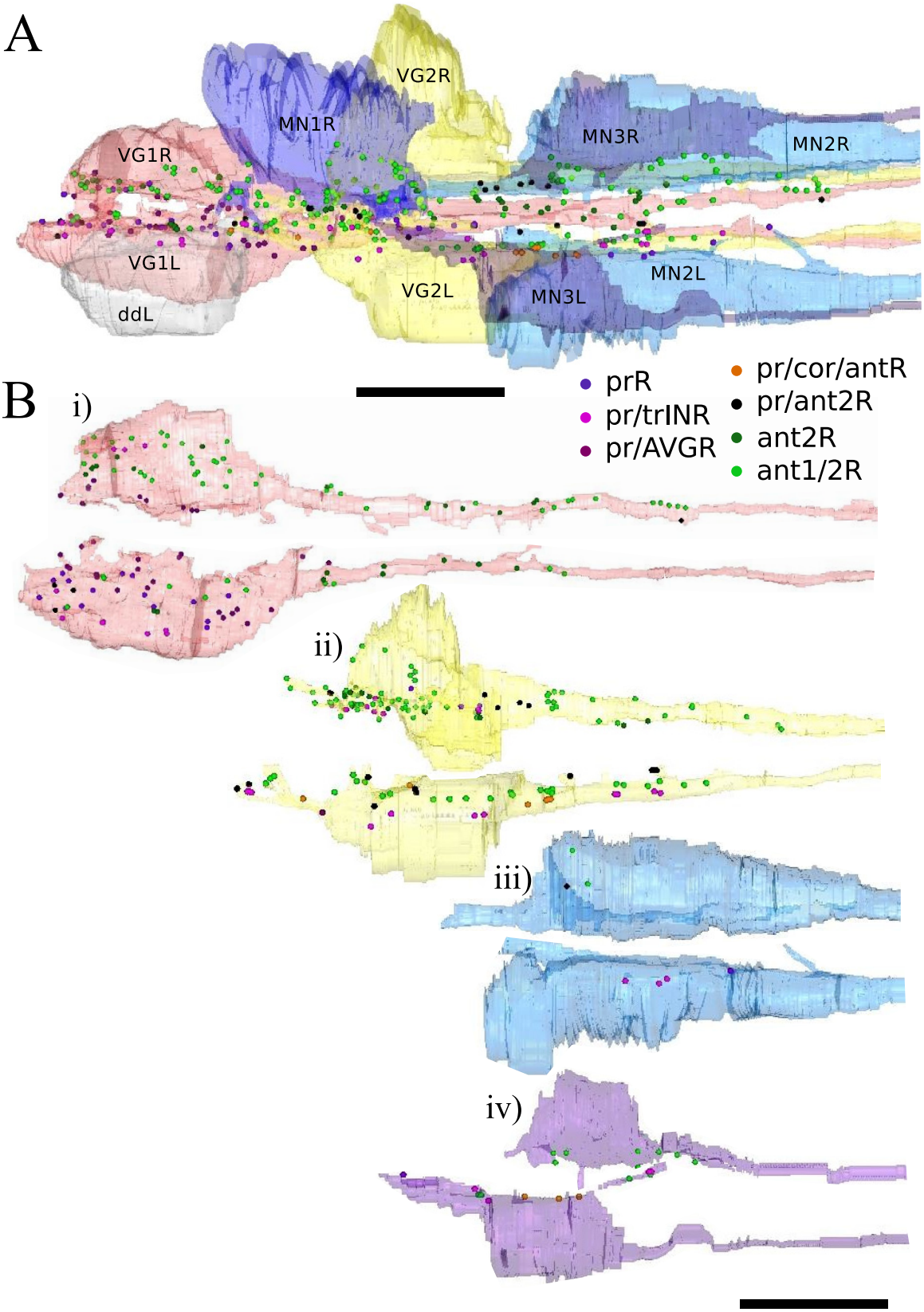
A
VG2R
MN1R
MN3R
MN2R
VG1R
VG1L
ddL
VG2L
MN3L
MN2L
B
i)
ii)
iii)
iv)
prR
pr/trINR
pr/AVGR
pr/cor/antR
pr/ant2R
ant2R
ant1/2R

5.3.9 Swimming and Photoreceptors:

The input from photoreceptors to the motor pathway involves at least three steps, through interneurons of the brain vesicle to interneurons VGN1 and VGN2 of the motor ganglion to motor neurons (MNs). This input to the motor ganglion is greater on the left than the right, and may be required to overcome the state of inhibition imposed by eminens neurons (see Ryan, 2015: Chapter 7 and Chapter 9). The connections in the motor ganglion itself are also asymmetrical, such that excitation of the left side, but not the right, could initiate bilateral contractions (see Ryan, 2015: Chapter 9). Thus, the asymmetry of photoreceptor input to the motor ganglion supports a sidedness and consistency in the initiation of symmetrical swimming after a light-off stimulus on the left side of the animal. Numerically, most of this input forms onto the first (and second) left interneuron(s), which in turn provides synaptic input to ipsilateral motor neurons MN1, MN2, and onto motor ganglion interneuron VGN2. A simple mechanism allowing coordinated swimming after this initiation could be provided by exciting the left inhibitory ascending contralateral inhibitory neuron, ACIN1L, which in turn would inhibit contralateral excitatory interneurons that also receive some input from the visual interneurons.

The input from photoreceptor relay neurons that does occur onto the right motor ganglion is all from multimodal relay neurons. Peripheral-photoreceptor relay interneurons provide input to the right side through the first interneuron, VGN1R and the decussating descending left-side neuron. Right-side inhibition could then be overcome by combined direct excitation of the right side by the first interneuron, VGN1L onto its partner, VGN1R. In conjunction with this, both the peripheral-photoreceptor relay interneurons

and the left-side motor ganglion neurons could control right-side excitation by providing input to the contralateral ddNL. Further inhibition could be achieved by the direct ipsilateral feedback from the first inhibitory ACIN to the first motor neuron on the left side. While this provides a mechanism for initiation and for coordinate activation across the left and right sides of the animal, it does not offer an explanation for the cyclical contraction of the muscle on each side during this behaviour, which is discussed in the section on central pattern generation (see Ryan, 2015: Chapter 9)

The existing sidedness of input to the motor ganglion is consistent with photopositive behaviour of early larvae, as described first by Mast (1921). As a larva swims, it spirals, so the ocellus is alternately shaded and illuminated in the presence of light, regardless of the cause of swimming. Mast (1921) suggested that during the swimming period photopositive larvae swim toward light by bending their tails toward the abocular side when shaded and ocular side when illuminated. Dybern (1963) suggested that early *Ciona intestinalis* larvae were photopositive, however subsequent reports (Svane and Young, 1989; Tsuda et al., 2003a; Tsuda et al., 2003b) deny the existence of this early photopositive period. Whether photopositive or photonegative, in the case of *Ciona intestinalis* larva with the ocellus on the right side, Mast's hypothesis would imply a bend to the right side caused by a right side muscle contraction during periods of illumination or shading while swimming. More recently, video observations revealed that during long swimming bouts larvae swim with a right-handed spiral (Watanabe and Nishino, 2015), so enhanced contractions on the right side could alter direction with less disruption of forward momentum. Thus, a swimming larva should have some light responsive input to its right motor ganglion that either directly or indirectly excites right-side motor neurons.

However, in order for this action not to disturb the coordination of left-right contractions required for symmetrical swimming, it should not alter the initiation of contraction at the trunk-tail boundary. Instead, such alterations must rely on the neuromuscular junctions along the tail. Thus, the candidate motor neurons involved include MN2 and tail MNs (see Ryan, 2015: Chapter 8 and Chapter 9).

In contrast, the gravity responsive behaviour suggests a flick to change orientation, which may or may not be associated with a following period of symmetrical swimming. A mechanism by which this may also find a pathway in our synaptic data, which reveal an intrinsic right-side network that has inhibitory feedback mechanisms to ensure only short-term excitation of motor neurons. Unlike photoreceptor input, most input from brain vesicle interneurons associated with the proposed antenna pathway for gravity perception provide input to right-side motor ganglion interneurons. Both of these first two interneurons provide excitatory input to the first and second motorneurons, respectively. In the case of the second interneuron, VGN2R, the inhibitory feedback from its target, iMN4 onto both the interneuron and its excitatory MN2 target, should shut down excitatory input to the muscle, causing this contraction to be short-lived. Similarly, the first interneuron, VGN1, excites VGN3 along with MN1, and ACIN2 along with VGN2; thus generating an inhibitory feedback system by which VGN3 inhibits the activity of MN1 and ACIN2 inhibits the activity of MN2 via its inhibition of VGN2, and its subsequent pathway inactivation, as described above. This again limits the excitation of the right muscle, resulting in a short period of contraction. As there is no feedback from the right to the left side of the motor ganglion, the implication would be that this would not initiate a swimming behaviour directly. However, there is also some input from

antenna interneurons to both left side excitatory interneurons, which could, if sufficiently strong, elicit symmetrical swimming.

These mechanisms and hypotheses assume, however, an excitatory phenotype for the descending brain vesicle neurons, which is accurate for only a subset of them. Many others express reporters for GABA, which would imply that they act in an inhibitory capacity. Coronet cells modulate the light-off motor response through alpha2-like adrenergic receptors (Razy-Krajka et al., 2012) on photoreceptors, coronet cells, glutamatergic neurons, and on vGAT positive neurons, including those near the photoreceptors. These receptors act in an excitatory capacity, and while the neuromodulatory function of dopamine is proposed, the presence of direct synaptic contact onto photoreceptor interneurons may provide an additional means of control. If these targets are indeed GABA-ergic and bear alpha-adrenergic receptors, the dopamine input from coronet cells would function to inhibit their targets in the motor ganglion. Two such neurons, cells 112 and 119, receive coronet cell synaptic input along with input from both putative GABA positive and putative glutamate positive photoreceptors. However, without knowing the receptors for dopamine on coronet interneurons, it is not possible to ascertain whether dopamine plays an inhibitory or excitatory role.

The sidedness of input to the motor ganglion from photoreceptor relay neurons may reflect their neurotransmitter phenotype. Only five photoreceptor relay neurons provide synaptic input exclusively to the left side: cells 80, 105, 123, 112 and 116. A sign-conserving (excitatory) role for these neurons fits with the above hypotheses. All of these relay neurons also receive mixed photoreceptor input. Four other relay neurons, cells 130, 121, 100, and 119, have far greater input to the left motor ganglion than to the

right, so may also be sign-conserving, providing minimal excitatory input to the right. Interestingly, a few of these neurons also provide direct input to the third left motor neuron, with input only to muscle and the second contralateral inhibitory neuron. Several photoreceptor relay neurons (cells 86,96,126,74, 140,127,157), including some that participate in the peripheral pathway, have significant input to the right motor ganglion neuropil, with three, cells 94 and 124, and 108, having input only to the right motor ganglion or the ascending motor ganglion, AVG, interneurons. Plotting these outputs onto the locations of the relay neurons' cell bodies reveals only that the latter tend to be roughly toward the middle of the brain vesicle whereas those with predominantly left side input to the motor ganglion are located nearer to the outer walls of the brain vesicle. This contrasts with the obvious spatial groupings of peripheral associated relay neurons and antenna relay neurons.

5.3.10 Peripheral Integration of Photoreceptor Signals:

Cell bodies of photoreceptors involved in the peripheral pathway are spatially grouped around the left outpocketing of the canal in the dorsal left brain vesicle, which corresponds to an area of intense expression of GABA reporters, Ci-GAD and vGAT (Zega et al., 2008; Takamura et al., 2010; Horie et al., 2010). Analysis of the photoreceptor input to these neurons reveals a possible pattern in which photoreceptors with anterior outer segments provide input through these relay neurons to ascending motor ganglion cells AVG 6 and 7, which are putative acetylcholine positive peripheral interneurons, whereas photoreceptors with posterior outer segments provide additional input through their relay neurons to AVG2 (and AVG1), which are putative GABA positive peripheral interneurons. It is interesting that cell 157 is unique in its connections

to ddL and MN1R, because it is also a target of the putative GABA photoreceptors, and so may be sign-converting, depending on its own neurotransmitter.

The terminal shape and size of peripheral associated photoreceptor relay neurons limits their input exclusively to anterior components of the motor ganglion, and the bifurcated terminals of some allow for input to the left and right sides of the motor ganglion. Their extensive interactions with ascending motor ganglion, AVG, neurons occur near these motor ganglion inputs at axo-axonal or axo-terminal synapses.

Visual input to the posterior portion of the peripheral network occurs only at the tertiary level. The only AVG neuron lacking input from photoreceptor-ascending motor ganglion (pr-AVG) relay neurons is AVG5, which receives direct synaptic input from ATENs (see Ryan, 2015: Chapter 7). AVG3, which receives only minimal input from pr-AVG relay neurons, is also postsynaptic to ATENs. The feed-forward nature of the visual network input to the tertiary AVG neurons illustrates the common convergence of multiple pathways, and suggests potential redundancy and reinforcement (Fig. 5.22). This feed forward mechanism can also have functional implications for coordinating vision and peripheral input to the motor system. Some photoreceptors with input into this pathway, pre, prf, and pr10, all of which converge on relay neuron 116, and feed into AVG7 (Fig. 5.22B-C), are putative GABA positive neurons. Thus, a light-off response may be sign-converting through these interneurons, and may provide a means to silence input to part of the peripheral pathway. Through the pr-AVG relay neurons, the visual system can influence peripheral signal input to the other AVG interneurons, including AVGs 3,4,and 5. Input to this network of AVG neurons will also have more direct impact on the peripheral input from this pathway to the first pair of motor neurons from AVG2 on the

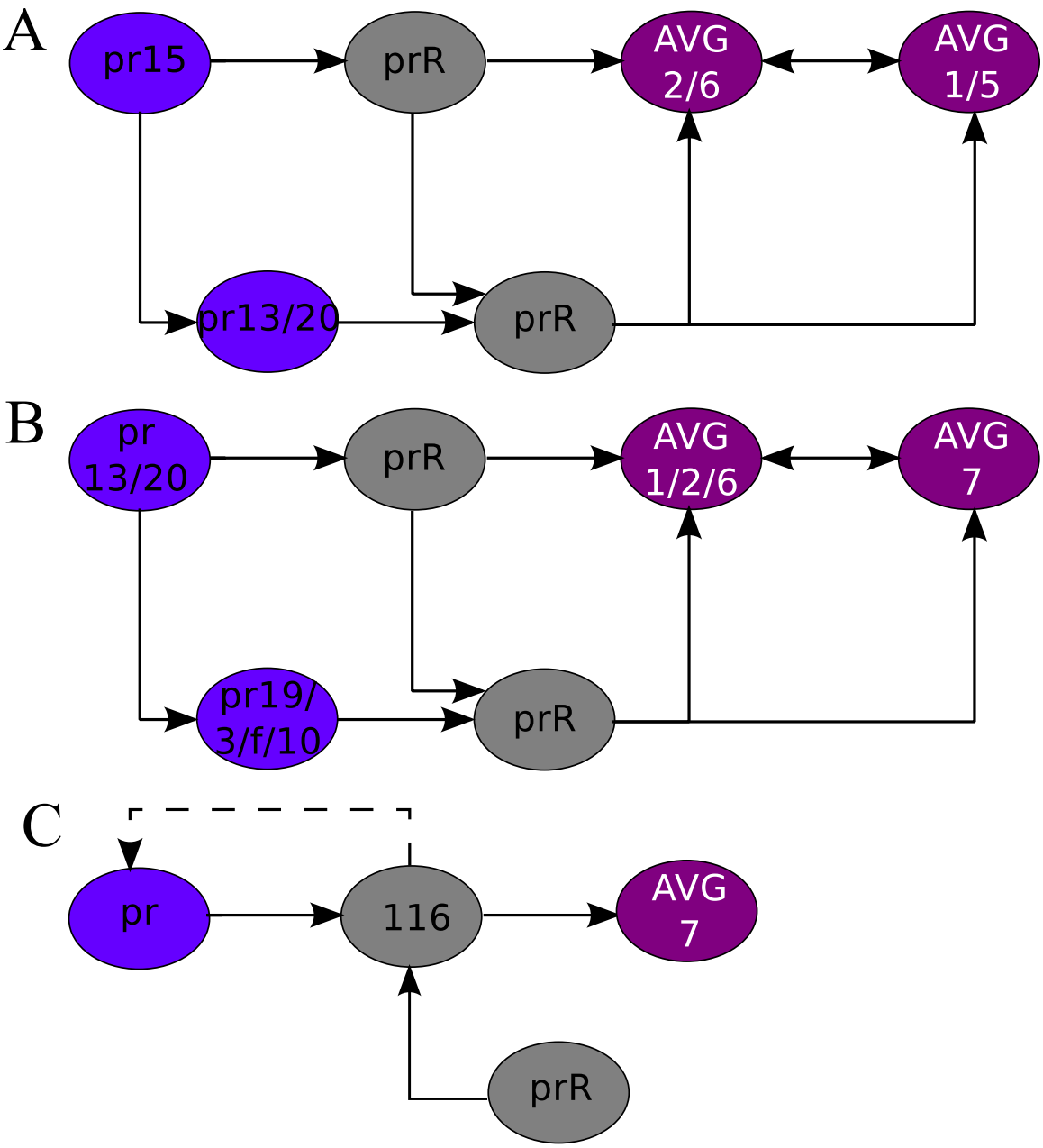

Figure 5.22. Network of photoreceptor (pr) inputs to ascending motor ganglion peripheral interneurons (AVG) through photoreceptor-peripheral relay neurons (prR). A) Downstream relay neurons of Type I-I Photoreceptor15 provide synaptic input to AVG2 and AVG6 in conjunction (not shown) with a parallel pathway through pr13 and pr20 and other photoreceptor relay neurons, cells 124, 127, and 157 and a single peripheral interneuron, 162. Additional synaptic input occurs through the AVG target neurons and relay neurons to AVG1 and AVG5. B) Type I-I and I-ii photoreceptors, pr13 and pr20 relay through their relay neurons to AVG1, AVG2, and AVG6, with a feed-forward pathway (not shown) through relay neuron synaptic connections with cells 94, 108 and 124 into AVG2 and AVG1. pr13 and pr20 provide additional synaptic input to pr19, pr3, pr-f, and pr10, the main relay neuron target of which, cell 116, provides input to AVG7 (shown in C).

right and AVG7 on the left; the visual inputs to these neurons originate from different subsets of photoreceptors, the former feeding into the latter.

The relay neurons of the first pathway receive input from putative glutamatergic photoreceptors. If the photoreceptor relay neurons of this first pathway are inhibitory, then they could inhibit their right side motor ganglion interneuron targets directly, and indirectly inhibit putative GABA input to MN1 on the right by AVG2. However, some of these putative glutamate photoreceptors feed forward to putative GABA photoreceptors, and their relay neurons also feed forward into the targets of those GABA photoreceptors' relay neurons. Likewise, two relay neurons of this pathway also receive input from putative GABA and glutamate photoreceptors. Thus, their input to the AVG interneurons, along with the first interneurons of the left and right motor ganglion, and left descending decussating neuron is unclear. Further, their downstream neuron, 124, provides synaptic input to putatively GABAergic AVG2, but is connected by putative gap junctions to both AVG6 and AVG7, which are putatively cholinergic. Thus, if inhibitory, activation of this neuron could inhibit peripheral inhibition, but activate excitatory components of this peripheral pathway. The relay neuron of the second major pr-AVG pathway, 116, inhibits or excites MN1 on the left side both directly through synaptic contacts, and indirectly, through its inputs to the putatively cholinergic AVG7. Thus, GABA input to relay neuron 116 from its photoreceptor inputs in response to a decrease in light would release AVG7 from inhibition or excitation, allowing independent activation of MN1L by the peripheral pathway through AVG7. However, neuron 116 also receives some putative glutamate photoreceptor input, and its putative gap junctions with AVG7 do not support an inhibitory action of 116. If cell 116 is excitatory, then its

inhibition by GABA photoreceptors would eliminate its excitation of MN1 on the left, and allow AVG7 to function based on its inputs from the peripheral pathway alone.

An additional integrative network between the visual and peripheral systems exists within the brain vesicle. The brain vesicle intrinsic targets of the photoreceptor pathway feed forward to AVG neurons as well as a single peripheral relay neuron, cell 131 (Fig. 5.23). These peripheral interneuron targets are themselves direct synaptic partners of anterior peripheral neurons. Of these, the posterior brain vesicle intrinsic peripheral interneurons feed forward to AVG6, but also provide direct input to the direct ATEN target, AVG5. Thus, the visual input is again integrated to the posterior peripheral network only at a tertiary level. In contrast, cell 30, which is a direct target of photoreceptor 20, appears to release neurotransmitter onto the basement membrane, adjacent to ATENa axons. This neuron may therefore integrate visual information to provide input to these peripheral neurons, but these are the only set of peripheral neurons that are synaptically isolated from the rest of the peripheral network (see Ryan, 2015: Chapter 7). The peripheral relay neuron, cell 131, receives input from several pr-AVG relay neurons directly, as well as their postsynaptic partners, again feeding into AVG neurons, but also providing some synaptic input to motor ganglion interneurons on the left and right sides. Together, all these also provide input to the eminens neurons, which are highly synaptic relay neurons of the peripheral network. All peripheral relay neurons with direct input to eminens neurons receive some input from putative GABA photoreceptors. Thus, the interneurons, could either inhibit or excite eminens neurons at their axons and terminals, under putative inhibitory control of photoreceptors, reducing or eliminating this input with a step-down of light.

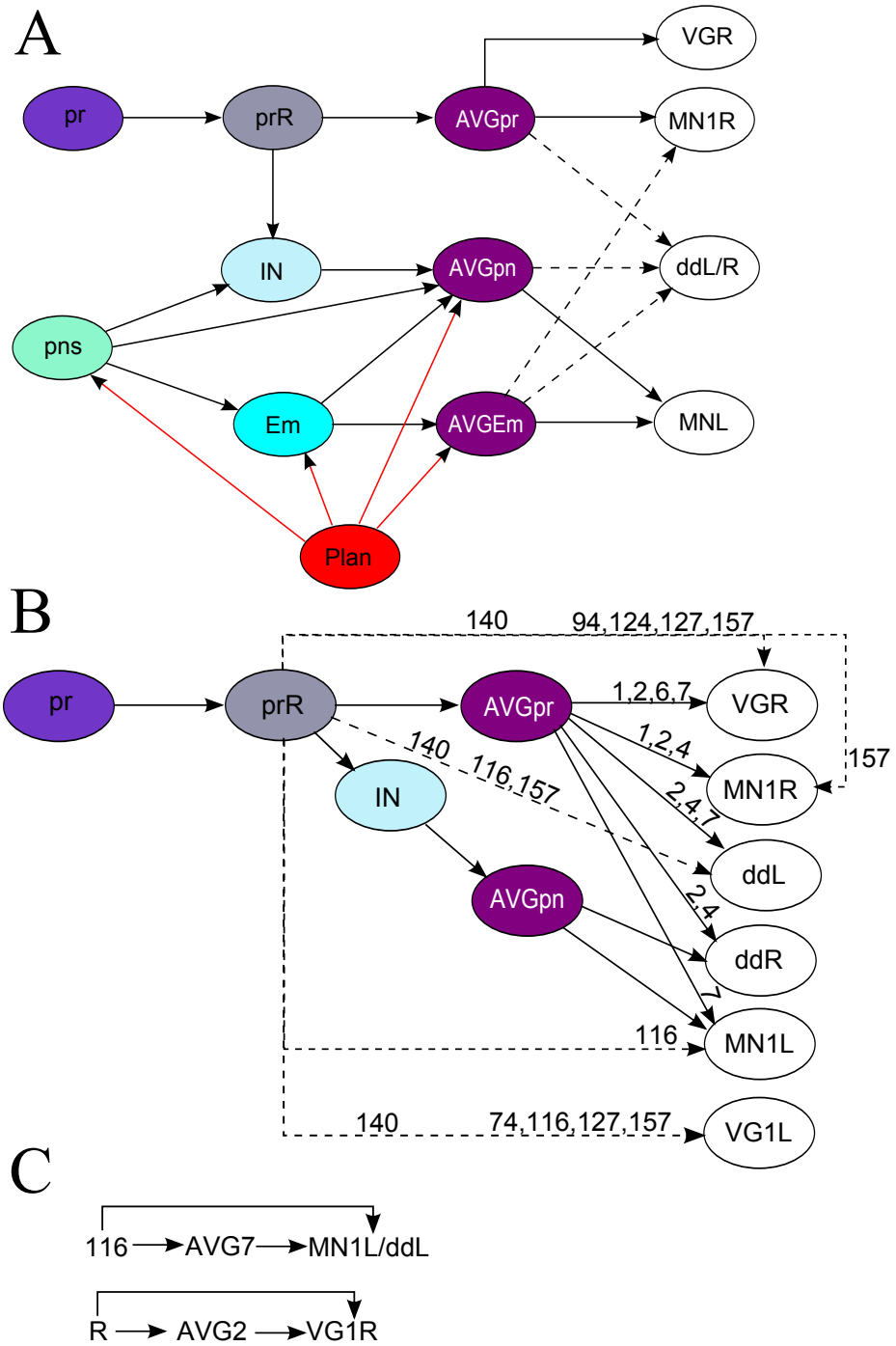

Figure 5.23. Photoreceptor network integration with peripheral pathways. A) Network illustrating input from the visual pathway and anterior peripheral pathway to the motor ganglion via the ascending motor ganglion interneurons, AVGs. B) Photoreceptor/AVG (prR) relay neuron synaptic network through AVGs (solid lines) and directly onto motor ganglion targets (dashed lines). Photoreceptor/AVG relay neurons (74, 94, 116, 124, 127, 157, 140), and specific AVGs (1, 2, 4, 6, 7) listed for each relevant connection. C) Summary of feed-forward networks from neuron 116 through AVG7 to MN1L and ddL and from relay neurons (R) through AVG2 to VG1R.

5.3.11 Interpreting Visual Circuits:

It is evident from the circuits presented here that there are numerous overlapping pathways with multiple levels of modulation between visual input and motor output. The current uncertainty about neurotransmitter phenotypes means that many interpretations can be asserted, but these all await functional dissection. Certainly, the relay neurons of the photoreceptors function in collaboration with each other, with an organization that appears to be independent of photoreceptor groups, rows, or connections. Their anatomical circuits, while providing a means for generating or rejecting hypotheses, also indicate the need for caution in designing and interpreting functional studies. Even targeted studies should not neglect the existing anatomical connections in favour of a simple model; activity in a single neuron or neuron class after exposure to light does not imply that the relay is direct or exclusive. In particular, resolving the issues of sidedness and pathway strength will be critical, especially in light of the putative differences in photoreceptor neurotransmitter phenotype, which complicated even the simple relay network.

This report illuminates the circuits underlying the observed light-responsive behaviours of larval *Ciona intestinalis* and provides a basis to both formulate and test hypotheses of visual function. There is obviously a great deal of integration between sensory modalities that has hitherto not been suspected, and which suggests the existence of a large body of behavioural response repertoire that hitherto has been undocumented. The extent of the contributions from interneurons intrinsic to the brain vesicle and connections between photoreceptors themselves were also unexpected, and provide intriguing insights into debates about the evolution from a simple visual system to the complex vertebrate retina.

Perhaps most surprising, the ability to examine all cells in this simple system illustrates that visuomotor control cannot be seen as a simple two-step process, but must occur through a more complex network involving circuits of interneurons within the motor ganglion. These must now await detailed functional documentation, but are discussed in coming sections with respect to their anatomical connections.

5.4 **Conclusions**

The visual system of *Ciona intestinalis* larvae is layered, with integration between and among first-order, second-order, and third-order components. The photoreceptors are interconnected by synapses, along with specialiazed photoreceptor associated interneurons (vacIN and trIN) identified for the first time in this study. Thus, photoreceptors seem to be like multifunctional precursors taking on many of the specialized roles of retinal neurons to distribute, modulate, and propagate visual signals. The interneurons of this pathway comprise both intrinsic and relay BV neurons, which form a complex network that also integrates coronet, antenna, and peripheral inputs. The input from visual relay neurons to the motor network occurs onto various components on both sides, but is greater to the left side, and to the first and second descending MG interneurons. Photoreceptor relay input to motor neurons is minimal, but does occur for the third left dorsally located motor neuron, MN3L.

Chapter 6 : Otolith and Otolith Pathways

6.1 **Introduction**

The otolith is a single sensory cell that protrudes into the brain vesicle lumen, with a foot in the vesicle's ventral wall (Dilly, 1962). This protrusion contains both the cell's nucleus and a large dense mass of dark pigment. The two portions of the cell, protrusion and foot, are connected by a narrow neck, with the foot portion extending toward the left side in the CNS. The neck itself is filled with endoplasmic reticulum vesicles and is surrounded by a collar formed from a folding of the otolith cell membrane (Dilly, 1962: his Fig. 3). The otolith expansion may in fact be a modified cilium, as suggested by the fibrous nature of the collar region (Dilly, 1962: his Fig. 3).

The otolith cell and ocellus pigment develop from bilaterally symmetrical a-line precursor blastomeres (left and right a8.25 cells) (Nishida, 1987; Nishida and Satoh, 1989), and depending on developmental signalling their precursors are both competent to form either cell of the sensory organ (Nishida, 1987; Darras and Nishida, 2004). Like the ocellus pigment, the otolith pigment is initially arranged as many smaller pigment granules surrounded by individual membranes (Dilly, 1962). These granules merge into a single large pigment mass before the swimming larva hatches (Dilly, 1962). The pigment is melanin (Minganti, 1957; Whittaker, 1966; Nishida and Satoh, 1989) synthesized by tyrosinase and its related protein (Sato and Yamomoto, 2001), which are expressed in pigment cells, patterned by fibroblast growth factor driven BMP signalling (Esposito et al., 2012, 2015; Racioppi et al., 2014). The melanin in *Ciona* has a high specific gravity, favouring the otolith's proposed function as a gravity receptor (Dilly, 1962). In addition to melanin, metals (Sakurai et al., 2004), as well as Ci-βγ-crystallin

are expressed in the otolith (Shimeld et al., 2005). In the late larva, Ci-βγ-crystallin has been detected in the otolith by antibody and reporter expression, although mRNA *in situ* expression was obscured by the otolith melanin pigment. The crystallin expression contrasts with that in the photoreceptive region, which expresses GFP under control of the Ci-βγ-crystallin promoter, but does not label with antibodies to the protein itself (Shimeld et al., 2005).

6.1.1 Spatial orientation:

Given its morphology and melanin content, the otolith has long been proposed as a gravity-sensing organ (Dilly, 1962; Eakin and Kuda, 1971). This role was proposed based on the observed behaviour of larvae, which swim up in the early stage, then down as they approach settlement (Grave, 1920), so exhibiting negative and positive geotaxis at different times during development (Svane and Young, 1989). The high specific gravity of the melanin provided early support for such a role of the otolith (Dilly, 1962), which was later confirmed by laser ablation of the otolith itself (Tsuda et al., 2003b). When the otolith was detached by laser ablation within one hour after hatching, larvae that previously demonstrated negative geotaxis exhibited no upward swimming behaviour, but still showed normal swimming patterns in response to a step down of light (Tsuda et al., 2003b). Observation of the larval swimming paths also revealed an increase in random swimming behaviour after otolith ablation (Tsuda et al., 2003b). Furthermore, ablation of the ocellus pigment did not significantly alter upward swimming behaviour, ruling out a role for the ocellus in the gravity response behaviour (Tsuda et al., 2003b). The role of melanin in the gravity response was further confirmed by altered upward swimming patterns observed after treatment of larvae with a tyrosinase inhibitor, 1-

phenyl-2-thiourea (PTU) that prevents melanin production (Sakurai et al., 2004) and in individual larvae with the tyrosinase mutation *spotless* (Jiang et al., 2005). Thus, it is clear that negative geotaxis is mediated by melanin in the otolith of early larvae, although its exact mechanism of action is unclear.

The proposed mechanism of action for the gravity receptive organ has been contentious. Dilly (1962) proposed that deformation of the neck by otolith displacement could be translated to impulses that signal the membrane relations with neighbouring cells. He suggested that at least one neighbouring cell, located where I find the antenna 1 cell, was a neuron with a long projection that may convey impulses from the otolith cell transmitted either by the neck junction or by mechanical distortion of the cell by otolith movements. The identification of putative gap junctions between the otolith foot and neighbouring cells caused Eakin and Kuda (1971) to propose an electrical coupling and transmission mechanism, questioning the neuronal nature of otolith associated cells. Protuberances found attaching the neighbouring cells to the otolith expansion in the canal led Torrence (1986) to conclude that these were receptive cells, which he claimed sent axons to the visceral (i.e. motor) ganglion, identified through semi-serial TEM of *Styela plicata* and *Diplosoma macdonaldi* (Torrence, 1986). The placement of the otolith's extensions from the ventral wall of the CNS in ascidians may certainly provide a means of sensing otolith pigment movement, but does not deny the coexistence of other mechanisms of action, as initially proposed by Dilly (1962). Sakurai et al. (2004) identified from SEM two fibres extending from the ventral CNS to either side of the neck of the otolith expansion, and reported three synaptotagmin-positive cells near the otolith neck, one ventral to the neck, and two on either side (Sakurai et al., 2004).

Synaptotagmin antibody label appears to extend into the canal at the location of the otolith neck, and the authors report that the two fibres also express synaptotagmin, suggesting a synaptic mechanism of action for some of the cells of the gravity organ.

The antenna cells are now acknowledged as the neuronal components of this sensory organ (Imai and Meinertzhagen, 2007a; Takamura et al., 2010; Horie et al., 2010). In another ascidian (*Diplosoma macdonaldi*), two neurons were described as bipolar sensory neurons associated with the otolith (Torrence, 1986). Similar neurons were identified in *Ciona intestinalis*, bearing two neurites extending from a round cell body, with some neurites projecting to the posterior brain vesicle (Imai and Meinertzhagen, 2007a). Three putative antenna neurons were identified using confocal light microscopy with a reporter for synaptotagmin (Imai and Meinertzhagen, 2007a), however all other studies in *Ciona* and other ascidians have identified only two such cells. Imai and Meinertzhagen (2007a) identify the challenge posed by this two-cell mechanism of gravity reception for orienting the larva in three planes. Yet, the positive or negative geotactic swimming pattern should only require vertical axis perception, so the resulting upward or downward swimming would only require an anterior and posterior receptor. As an alternative mechanism, Sakurai et al. (2004) suggest that perhaps the otolith itself acts as the third receptor via its neck and foot regions, proposing, as did Dilly in 1962, that the narrow neck may produce generator potentials. Thus, the protuberances extending to the otolith expansion and the neck itself may function together to convey directional information via just two associated neurons.

It is also possible that comparisons between the two identified otolith-associated cells made by ganglion (antenna) cells could orientate the larva (Tsuda et al., 2003b). This

mechanism requires a role for the ganglion cells, unlike the model proposed by Torrence (1986), but consistent with the antenna projection observed in *Ciona intestinalis* (Dilly, 1962; Imai and Meinertzhagen, 2007a). However, ganglion cells should, by their nature, be non-sensory, so this would require the observed ciliary expansions to the otolith to originate from cells other than the antenna neurons. The synaptotagmin expression in the otolith region (Sakurai et al., 2004) raises the issue of which neurotransmitters function in which cells in this organ. In fact, various studies have identified multiple neurotransmitter reporters near the otolith, including those for both GABA and glutamate. Although GAD expression was not found near the otolith (Zega et al., 2008), vGAT reporter expression identified putative anaxonal GABAergic cells around the otolith (Takamura et al., 2010). However, vGLUT reporter expression was observed in both the otolith and antenna neurons, suggesting that these are glutamatergic rather than GABAergic (Horie et al., 2008a), thus rendering the situation yet more complex.

6.2 **Results**

6.2.1 Otolith Cell:

The reconstructed otolith cell itself resembles existing descriptions (Dilly, 1962; Eakin and Kuda, 1971) with a few additions. The foot of the otolith protrudes an extension containing vesicles into the overlying antenna cell (cell 10) near the neck (Fig. 6.1A). The otolith cell itself forms various junctions with its neighbouring cells (Fig. 6.1A, Fig. 6.1D), including apparent synaptic contacts onto the first antenna neuron (cell 10) (Fig. 6.1B-C). I also identify a potential ciliary basal body near the neck of the otolith as well as a large vacuole similar to those seen surrounding basal bodies in other cells (Fig. 6.1E).

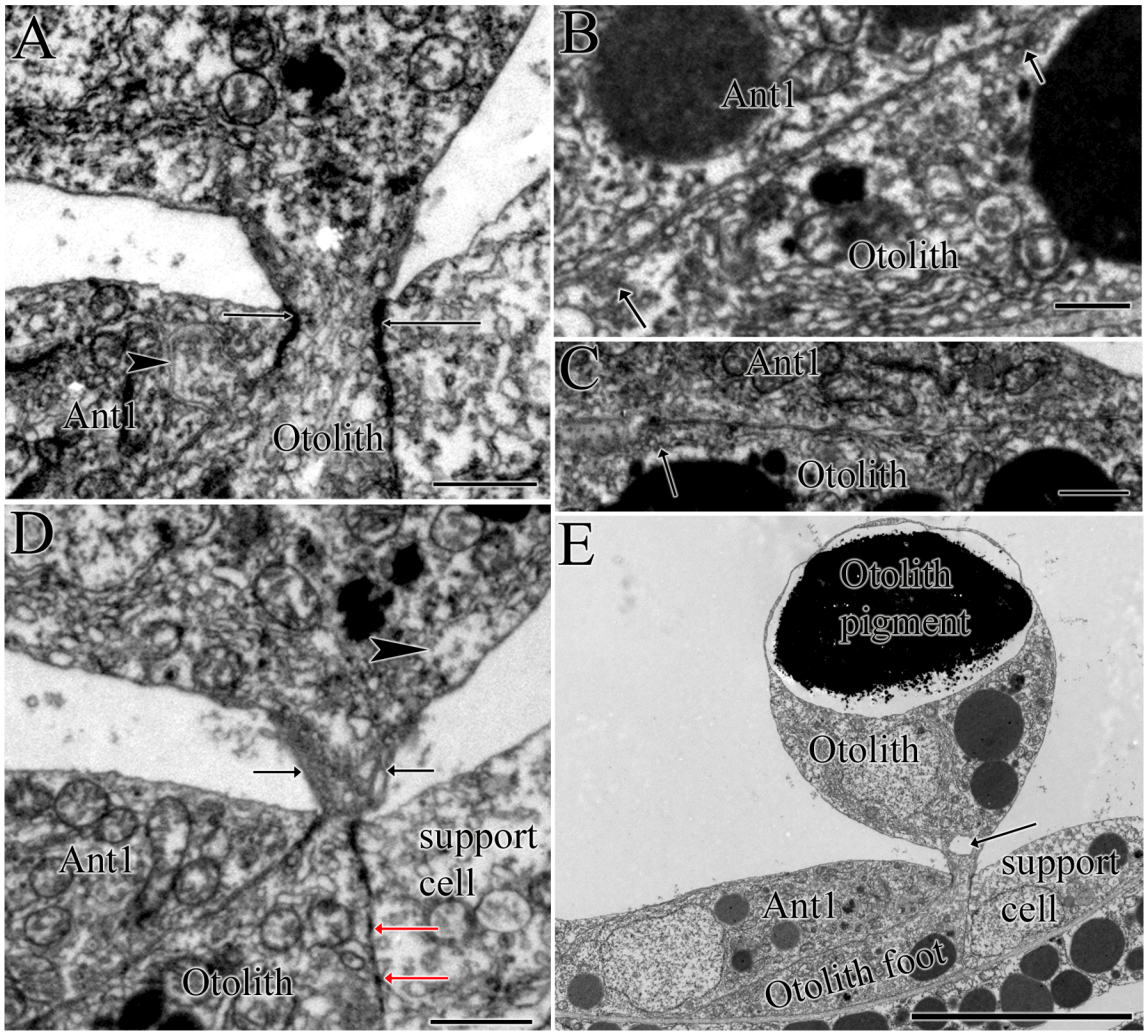

Figure 6.1. Electron micrographs of otolith cell junctions and associated cells. A) Otolith neck forms junctions with membrane densities the antenna cell on the left and support cell on the right (arrows). The otolith neck/foot region extends a protrusion containing vesicles into antenna1 cell body (arrowhead). B-C) The otolith foot forms synapses (arrows) onto the cell body of antenna cell 1. D) The neck of the otolith cell has thin modifications on either side (arrows) and its body in the canal contains a structure resembling a cilium (arrowhead) near this neck region. Junctions between the otolith foot and support cell also occur ventral to the otolith pigment (red arrows). E) The pigment and nucleus of the otolith are in the canal and are connected by the neck to the foot that extends to the left in the wall of the CNS. The otolith neck contains many small vesicle or vacuolar structures (arrows in D) as well as a larger vacuolar structure (arrow in E). Scale bars: 1μm (A-D); 10μm (E).

6.2.2 Otolith Associated Cells:

From EM data I could identify three cell types associated directly with the otolith sensory cell: the two otolith associated ciliated cells; the two antenna neurons; and a single ependymal otolith support cell. The former are anaxonal, and each contacts the pigment-containing otolith expansion in the brain vesicle cavity with its modified cilium. These modified cilia correspond to two dendrites near the otolith neck, described in the literature, that contact the pigment containing expansion anterior and posterior to the neck (Fig. 6.2A-C) (Torrence, 1986; Otsuki, 1991). Along with these contacts to the otolith expansion (2A-B), both cells abut the otolith foot on its anterior and posterior sides (Fig. 6.2C,F). Both of these cells extend their modified cilia through narrow stalks that abut the first antenna cell (cell 10), the more posterior cell's branch making additional contact with the second antenna cell (cell 63) (Fig. 6.2B).

The antenna neurons identified in this study are not bipolar as they are reported to be in *Diplosoma macdonaldi* (Torrence, 1986)., and are distinct from each other in their arrangement. Each has only a single neurite that extends alongside the other toward the right ventral wall, along the photoreceptor tract, then turns to terminate in the main neuropil of the posterior brain vesicle. The cell body of the first antenna neuron lies directly dorsal to the otolith foot in the ventral wall of the brain vesicle, to the left of the brain vesicle's otolith neck (Fig. 6.1A, Fig. 6.1D-E, Fig. 6.2C). This cell corresponds to Dilly's (1962) neuron. It contacts the foot and the neck of the otolith cell directly, and invaginates a protrusion from the otolith cell (Fig. 6.1A). A basal body in the first antenna neuron extends toward the canal, but no cilium enters the canal (Fig. 6.3A-B). The second antenna neuron is caudal to the first, and to the right side of the otolith neck,

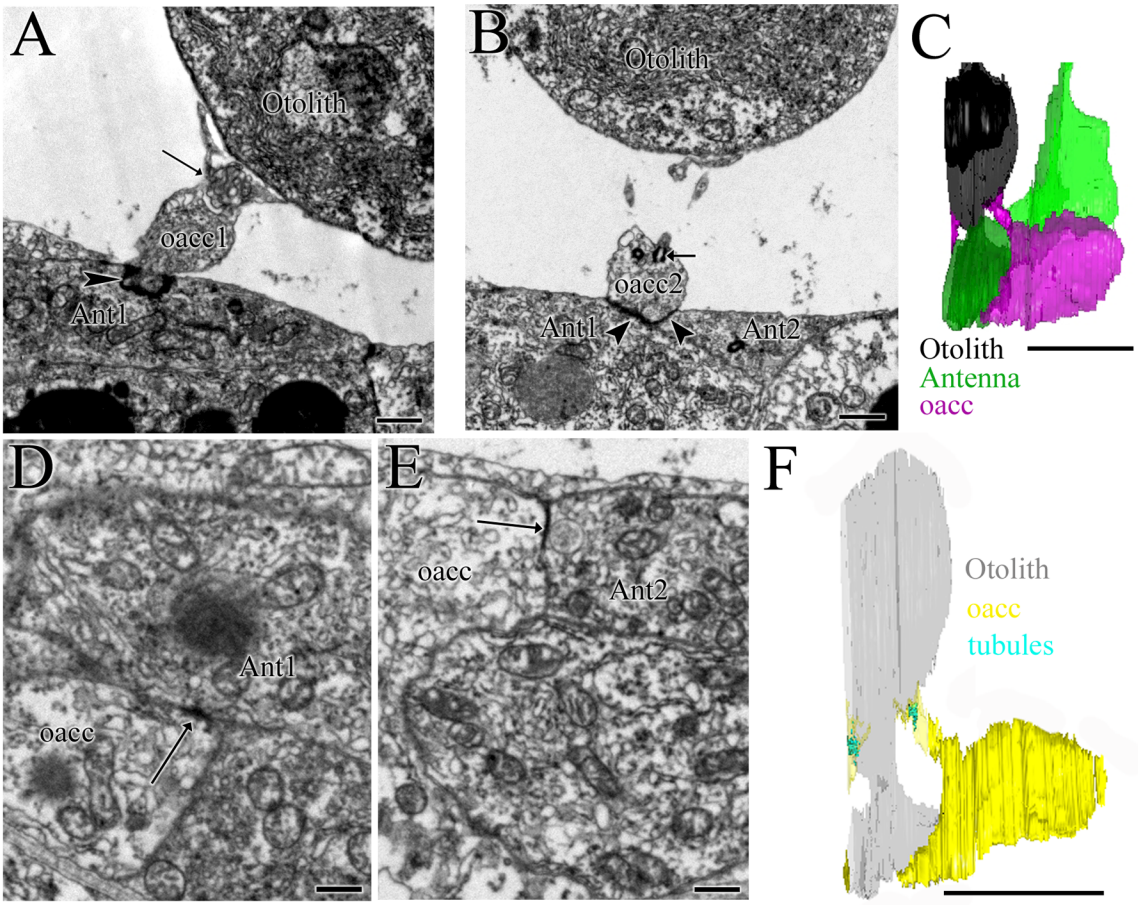

Figure 6.2. Otolith associated ciliated cells contact antenna neurons at various junctions. A) Junction of oacc1 with antenna1 (arrowhead) as it extends to contact the otolith with its modified cilium (arrow). B) Junction of oacc2 with both Antenna1 and Antenna2 neurons (arrowhead). Basal body is visible in oacc2 (arrow). C) Reconstruction of antenna neurons, otolith cell with pigment, and oaccs from left lateral view. D) Membrane apposition, signifying a putative gap junction (arrow), between oacc and Antenna1 cell body. E) Putative gap junction (arrow) between oacc and Antenna2 cell body. F) Reconstruction of oacc extensions containing tubules (as seen in A) to otolith cell from left lateral view. Scale bars: 1µm (A, B, D, E); 10µm (C, F).

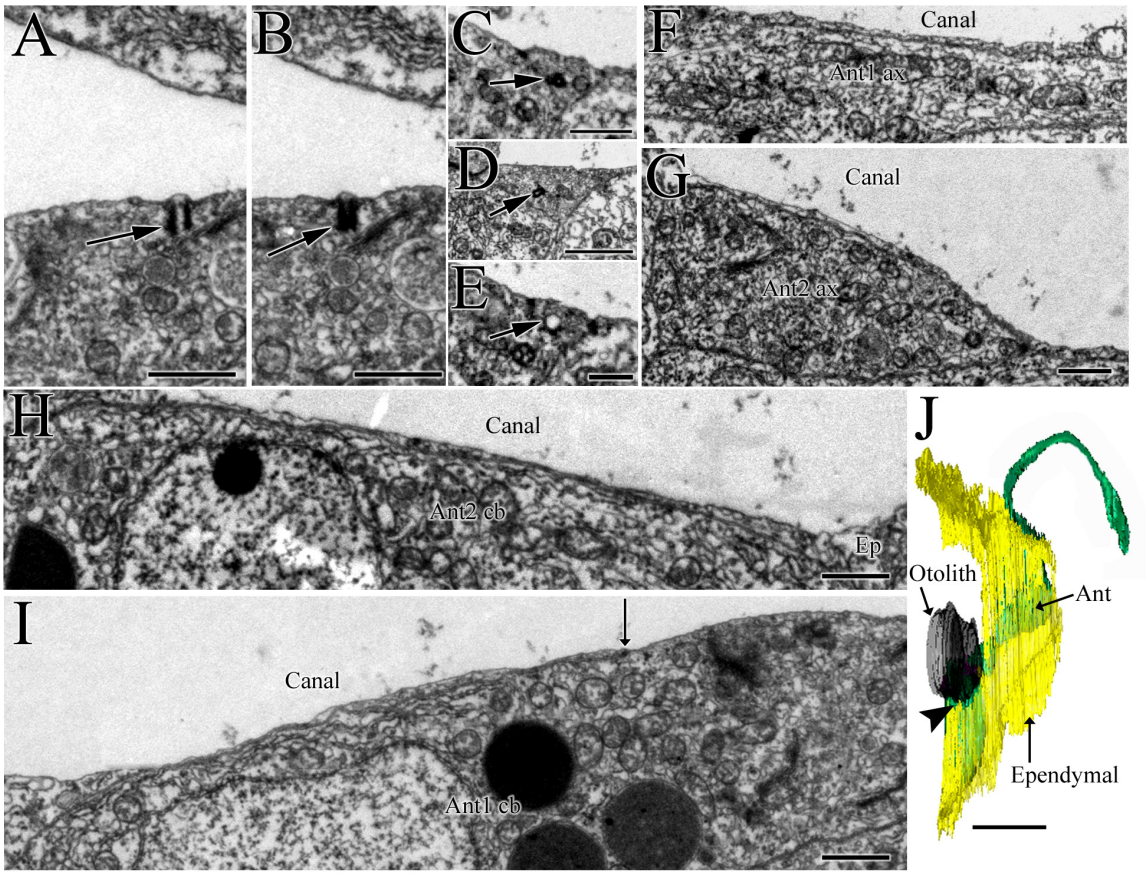

Figure 6.3. Antenna cell contacts with the neural canal. A-B) Basal body of Antenna1 neuron extends toward the canal, but does not extend outside of the cell. C-E) Basal body of Antenna2 neuron extends within the cell toward a vacuole and does not contact the canal. F-I) Axons of both Antenna1 (F) and Antenna2 (G) cells are separated from the neural canal by thin ependymal cell extensions. H) Cell body of Antenna2 neuron is also separated from the canal by thin extensions from ependymal cells (Ep). I) Ependymal extension between Antenna2 neuron cell body and canal extends only over a portion of the neuron (to arrow). J) Dorsal view reconstruction illustrating ependymal (yellow) extensions overlying antenna neurons except for the portion ventral to the otolith pigment (arrowhead). Scale bars: 1μm (A-I); 10μm (J).

making no direct contact with the otolith cell (Fig. 6.2C, Fig. 6.3J). The anterior extension of this neuron contains a putative basal body that enters a vacuole near its membrane apposition with the membrane of the other antenna neuron (Fig. 6.3C-E), but does not extend into the brain vesicle canal. Along most of the extent of their cell bodies both antenna neurons are isolated from the canal by fine cellular extensions from surrounding ependymal cells (Fig. 6.3D-I). The exceptions are regions where these neurons contact the otolith associated ciliated cells or the neck of the otolith (Fig. 6.2A-B, Fig. 6.3A-B,I).

The single otolith support cell is located to the right side of the otolith foot in the ventral wall of the brain vesicle (Fig. 6.1D-E, Fig. 6.4). This cell has a basal body that extends toward the brain vesicle canal, but no emerging cilium (Fig. 6.4A-B). Although the cell lacks a neurite (Fig. 6.4C-E) or any presynaptic sites, it does form junctional connections with the otolith cell at both the neck membrane (Fig. 6.1A) and the basal foot (Fig. 6.1D); however these may be solely structural. The only other junctions formed by this cell are apparent desmosomes with antenna neurons adjacent to the brain vesicle lumen (Fig. 6.4F).

Thick plaques or junctions, as described in previous studies (Eakin and Kuda, 1971; Torrence, 1986), exist between the basal body bearing dendrites of the otolith associated ciliated cells and antenna neurons, where cilia emerge (Fig. 6.2A, Fig. 6.2B). Membrane junctions also exist between cell bodies of the otolith associated ciliated cells and antenna neurons, and these occur over long stretches of serial sections (Fig. 6.2D, Fig. 6.2E). The first otolith-associated ciliated cell contacts only the first antenna neuron, but the second, more posterior, ciliated cell contacts both antenna neurons, albeit forming junctions over

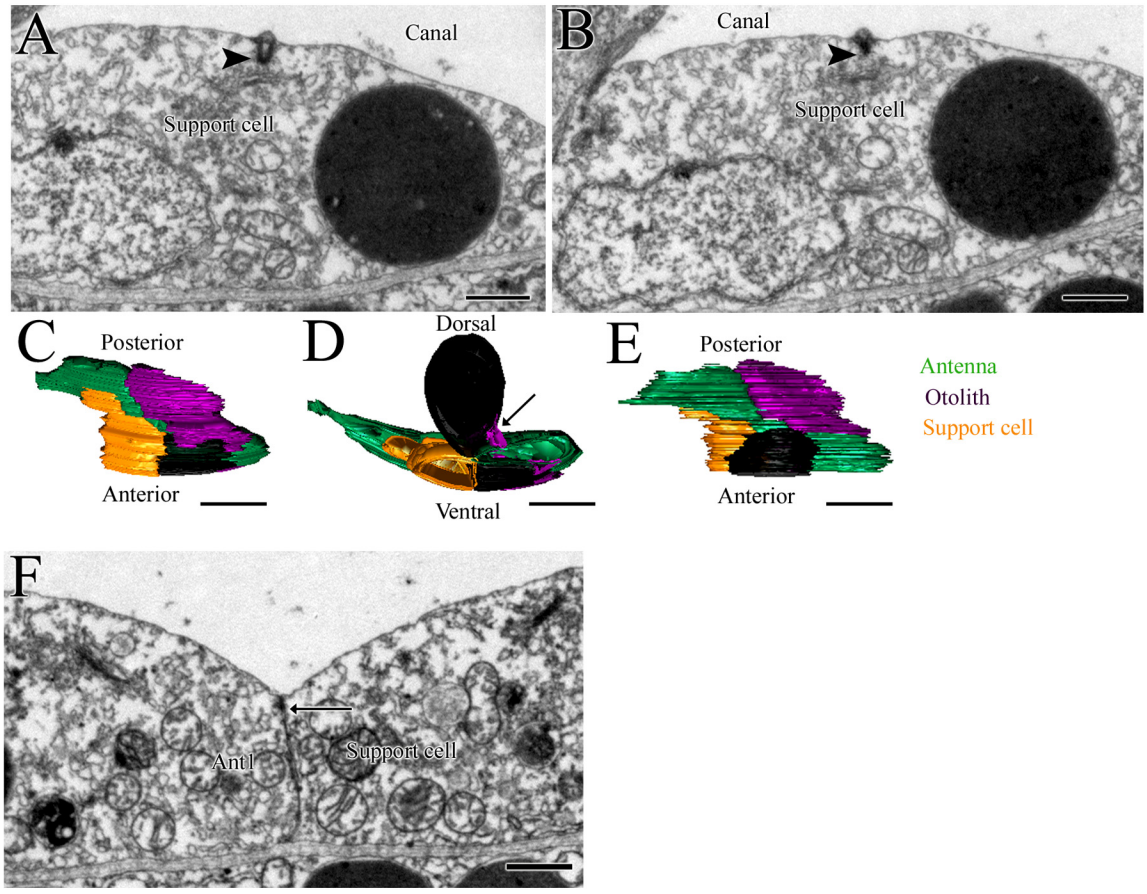

Figure 6.4. The otolith support cell. A-B) Basal body of the otolith support cell does not extend into the lumen of the brain vesicle (canal). C-E) Ventral (C), frontal (D) and dorsal (E) views of otolith associated neurons illustrating position and arrangement of support cell relative to antenna neurons, otolith cell, and otolith associated ciliated cells with modified ciliary extensions (arrow in D). F) Junction (arrow) between antenna1 neuron and otolith support cell adjacent to neural canal. Scale bars: 1µm (A-B, F); 10µm (C-E).

longer distances with the second antenna neuron. Likewise, only the first antenna neuron (cell 10) directly contacts, makes junctions, and is postsynaptic to the otolith cell itself. Thus, the two antenna neurons are likely to have distinct functions in translating otolith displacements.

The axons of the antenna neurons are adjacent along their entire lengths until their terminals expand in the posterior brain vesicle. However, there are only seven synaptic contacts between the two neurons, predominantly (six of seven) from the second antenna neuron (cell 63, presynaptic) to the first (cell 10), all of which are small (60-120nm in diameter). No putative gap junctions were observed between the two antenna neurons, and the synaptic contacts that occur are all in the region of the posterior brain vesicle in which these neurons begin to expand to form their terminals. The terminals of the antenna neurons themselves are separated by adjacent neuropil, with the exception of their axonal roots (Fig. 6.5). Aside from the inputs from antenna cell 2 to antenna cell 1, the other presynaptic partners of antenna neurons include photoreceptors, the anterior photoreceptor tract neuron (lens cell 1), anaxonal arborizing brain vesicle interneurons (**aaIN**), and a few relay interneurons of the posterior brain vesicle. Among these, Type II photoreceptors are presynaptic to the first antenna neuron at five synapses, whereas only minimal photoreceptor input occurs onto the second antenna neuron exclusively from Type I photoreceptors. Although it only receives minimal photoreceptor input, the greatest input to antenna neurons in the brain vesicle occurs from anaxonal arborizing neurons, cells 102 and 115, to the second antenna neuron, and both antenna neurons provide feedback onto these interneurons.

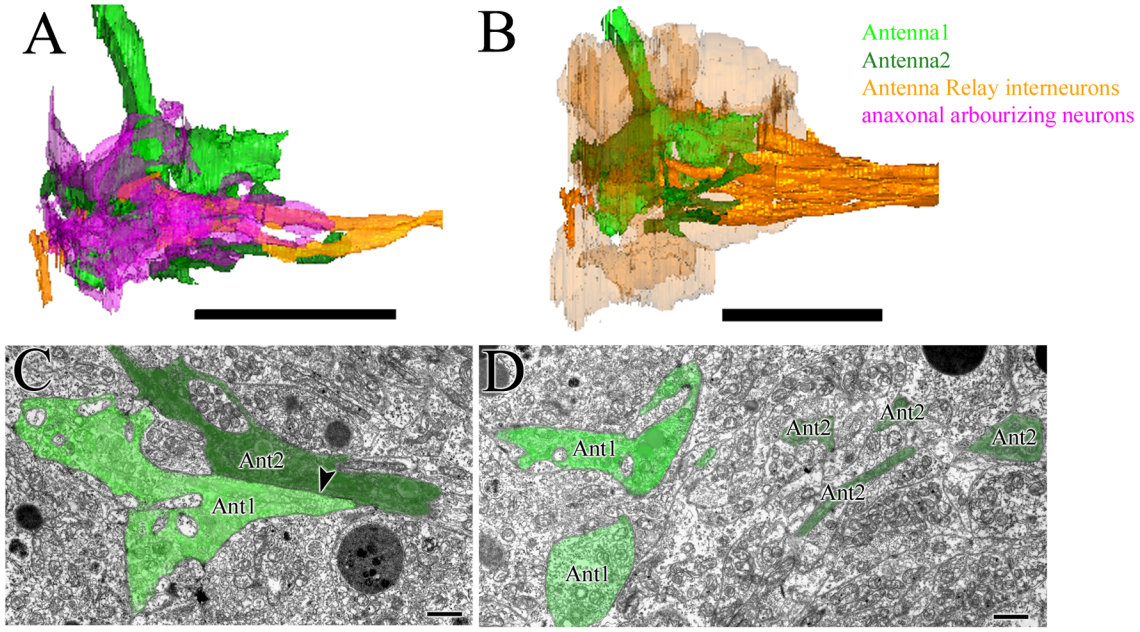

Figure 6.5. Antenna neuron terminals are intertwined with dendrites, axons and terminals of brain vesicle interneurons. A) Dendrites and axon hillock regions of antenna relay interneurons and terminals of anaxonal arborizing brain vesicle interneurons extend between terminals of the antenna neurons. B) Reconstruction of antenna relay interneuron cell bodies (transparent), dendrites and axon hillock regions surrounding antenna terminals. C-D) Antenna neurons are in contact along their axons and terminal roots into the neuropil from the ventral right side (arrowhead). Their expanded terminals in the neuropil are separated by axons and dendrites of surrounding cells. Scale bars: 10µm (A-B); 1µm (C).

6.2.3 Antenna Neuron Targets:

The terminals of antenna neurons have two defining features: a large proportion of their synaptic contacts to relay neurons are polyadic, and many synapses occur onto fully or partially invaginated dendrites of relay neurons. Approximately 40% of the presynaptic sites of the first antenna neuron are dyad or triad synapses (Table 6.1). The postsynaptic polyadic partners of the first antenna neuron co-populate up to 16 postsynaptic sites. The most common pairings of postsynaptic elements are among the descending antenna relay neurons. In particular, these include three relay neurons exclusive to the first antenna neuron, cells 143, 152 and 161, and three that receive input from both antenna neurons, cells 120, 134, and 142. These relay neurons are also the neurons that receive the most synaptic contacts from antenna neurons. For each neuron, more than 40% of their postsynaptic contacts from the first antenna neuron are at polyadic (dyad, or rarely triad) synapses, and of these, neuron 134 has the greatest proportion, 88%, of its synapses are polyadic contacts from antenna neuron 1. In contrast, the first antenna neuron has only about 25% of the presynaptic sites from antenna neuron 2 that are polyadic. Approximately 30-40% of the inputs to relay neuron targets of the second antenna neuron are polyadic, but these constitute fewer synapses in total than those of antenna 1. The composition of these synapses is also distinct from those of antenna cell 1, with fewer inputs from antenna 2 to relay neurons and far greater numbers of inputs to intrinsic brain vesicle interneurons. In addition to forming fewer total presynaptic sites (91 vs 175), contacts from antenna cell 2 to each partner are fewer and smaller than those from antenna 1 to its postsynaptic partners. The anaxonal arborizing aaIN neurons and photoreceptor tract interneuron (trIN) cell are polysynaptic at > 50% of their antenna 2

Table 6.1. Total numbers of antenna 1 (Ant1) and antenna 2 (Ant2) neuron synapses and percentages of three types of synapses: polyad (>1 postsynaptic partner), invaginated (onto invaginating dendrite), reciprocal (unpolarized synapses). Total number of synapses and percentages given in the final row.

Antenna Neurons	Total # of synapses	% Total polyad synapses	% Total invaginated synapses	% Total reciprocal synapses
Ant1	175	39	16	6
Ant2	91	25	12	7
Total	**266**	**34**	**15**	**6**

postsynaptic elements that co-populate these synapses vary for each of these neurons; trIN and aaIN co-populate each other's and antenna 1/2 relay neuron synapses, cell 102 co-populates its own and anaxonal arborizing neuron 115's synapses, and cell 95 co-populates brain vesicle intrinsic interneuron synapses.

The invaginations into the antenna terminals are not all accompanied by synaptic contacts, but are in most cases (82%), with large vesicle clouds surrounding invaginating dendrites (Fig. 6.6E-G). There are more invaginations into the first than the second antenna terminal, possibly because the shape of the second terminal comprises narrower branches (Fig. 6.6A-D). Invaginating branches within the antenna terminals originate from terminals of anaxonal arborizing interneurons, dendrites of shared antenna relay neurons, and dendrites of relay neurons of antenna cell 1. The approximate total of 50 invaginating branches have an average volume of 0.046 μm^3 ($\pm$0.035). For both antenna neurons, the proportion of their total presynaptic sites that occur onto these invaginating branches is 12-16%. Invaginated synapses constitute 6-30% of the antenna relay neurons' postsynaptic contacts from antenna 1 and up to 36% from antenna 2, although most relay neurons lack invaginating synapses with antenna 2 (Fig. 6.7). Relay neuron 120 receives among the most synaptic contacts at invaginating dendrites from both antenna 1 (29%) and antenna 2 (36%) cells. Other invaginated synaptic contacts occur from both antenna 1 and antenna 2 onto anaxonal arborizing interneuron terminals.

6.2.4 Antenna Interneurons:

6.2.4.1 Brain Vesicle Intrinsic Antenna Interneurons

Antenna neurons 1 and 2 both provide input to the photoreceptor tract interneuron, multimodal anaxonal arborizing interneurons, the vacuolated anterior photoreceptor

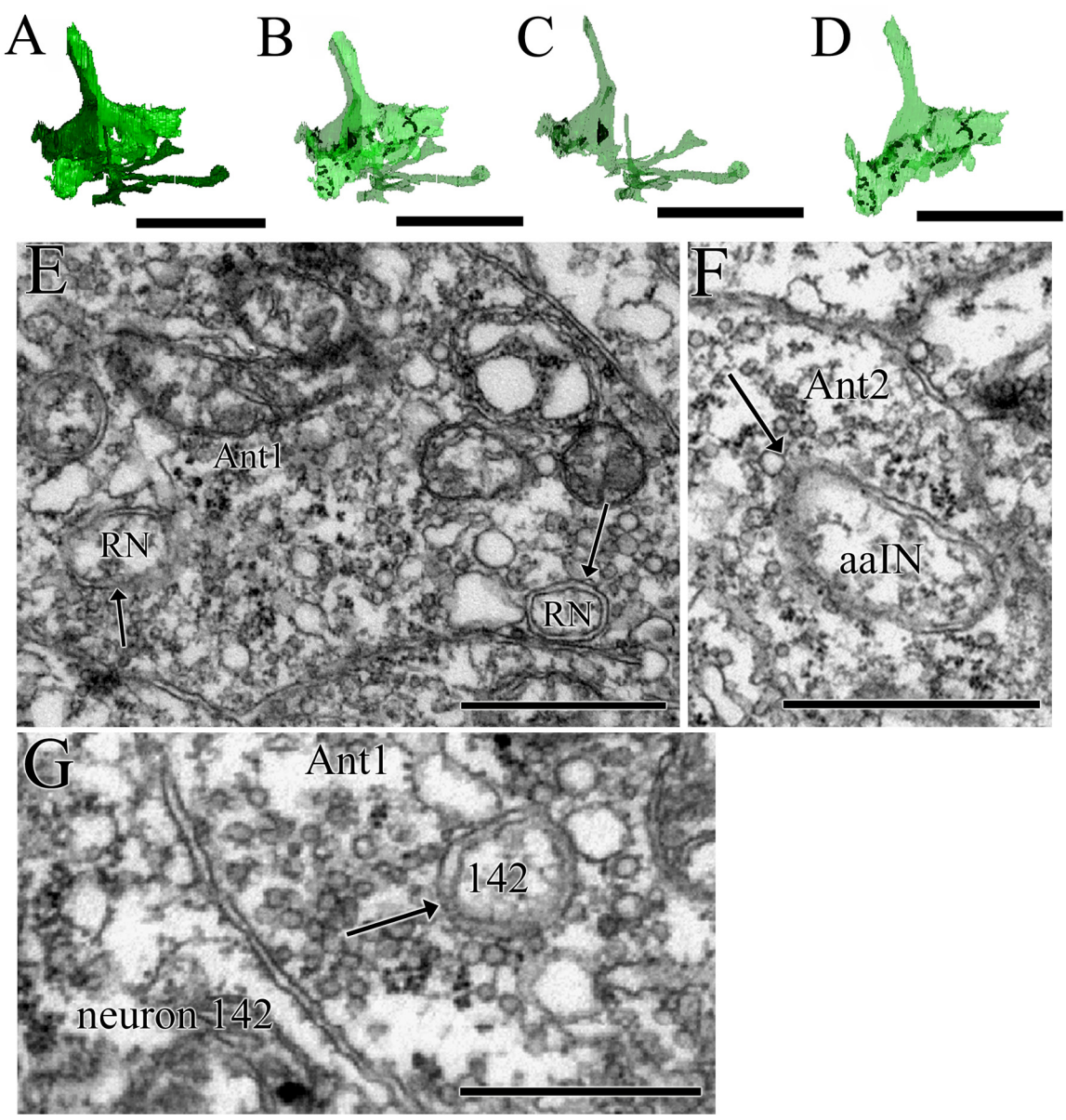

Figure 6.6. Dorsal view of reconstructed antenna neuron terminals. A) Antenna1 and Antenna2 neuron terminals extend rostrocaudally with limited branching. B) Antenna terminals receive invaginated branches of postsynaptic neuron partners (black). C) Antenna2 terminal receives invaginations in its thick anterior portion but not its thin long branched region. D) Antenna1 terminal has many invaginations distributed throughout. E-F) Invaginated synapses (arrows) of antenna neurons Ant1 onto postsynaptic relay neuron (RN) dendrites (E), Ant2 onto anaxonal arborizing neuron (aaIN) terminal (arrow in F) and Ant1 onto an invaginating dendrite of cell 142 (arrow). Scale bars: 10µm (A-D); 1µm (E-F).

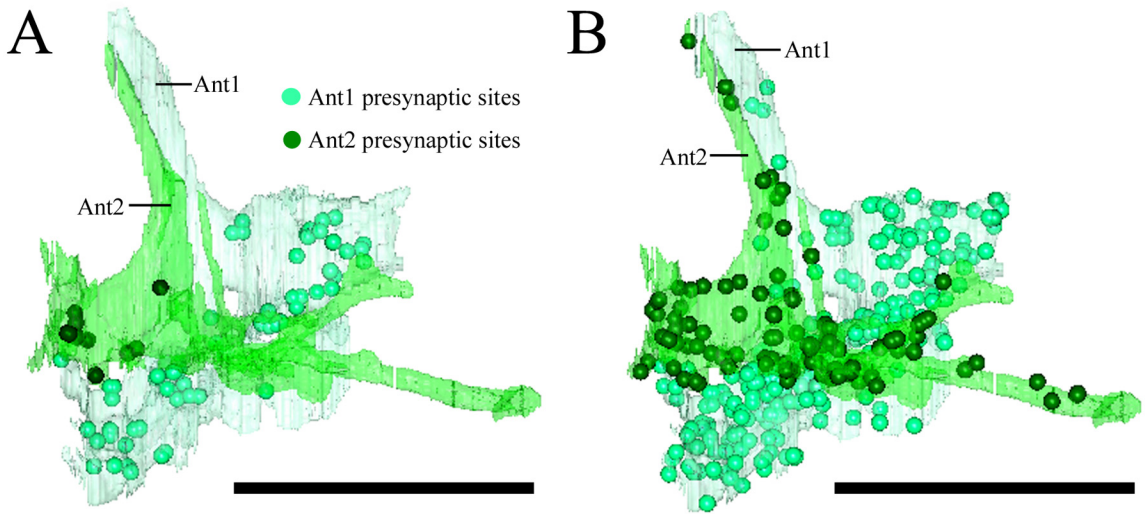

Figure 6.7. Antenna neuron presynaptic sites. A) Dorsal view of reconstructed antenna1 (Ant1) and antenna2 (Ant2) terminals with puncta representing presynaptic sites onto invaginating branches. B) Dorsal view of reconstructed antenna1 (Ant1) and antenna2 (Ant2) terminals with puncta representing all presynaptic sites. Scale bars: 10µm.

interneuron, and some Type I, II and III photoreceptors (see also Ryan, 2015: Chapter 5). In addition to these synaptic brain vesicle targets, antenna cell 2, but not antenna cell 1, provides synaptic input to several other interneurons that are intrinsic to the brain vesicle. These include a subset of anterior antenna interneurons that bear cilia. Most of these synaptic targets extend their cilia to contact the modified ciliary bulbous protrusions in the neural canal. Two such anterior ciliated interneurons, cells 38 and 79, bear single descending neurites, which split into two terminal branches in the posterior brain vesicle (Fig. 6.8A and Fig. 6.8B, respectively). Cell 38 has one posterior projecting expanded terminal branch and one perpendicular branch that extends laterally and bears several short, fine branches. Cell 79 also has perpendicular terminal branches, one longer branch extending more posteriorly and one shorter branch extending laterally. The cilium of another antenna synaptic target, cell 73, likewise contacts the coronet bulbous protrusions within the canal, but its neuronal projection is singular with a simple expanded unbranched terminal in the posterior brain vesicle (Fig. 6.8C). Two other neurons, 68 and 70, are also interneuron targets of antenna cell 2, with cilia that extend to contact the bulbous protrusions in the canal. However, these neurons are anatomically multimodal because they also receive photoreceptor input. These multimodal interneurons also have more complex terminals (Fig. 6.8D-E). Cell 68 has two neurites, with one that persists to form a branched axon with one V-shaped branch that extends back toward the anterior, and one posterior projecting branch, while cell 70 has a branched terminal that expands and branches toward the anterior and posterior, after turning laterally toward the central region of the posterior brain vesicle neuropil. Two other brain vesicle intrinsic photoreceptor interneurons, cells 16 and 90, are multimodal, receiving synaptic input

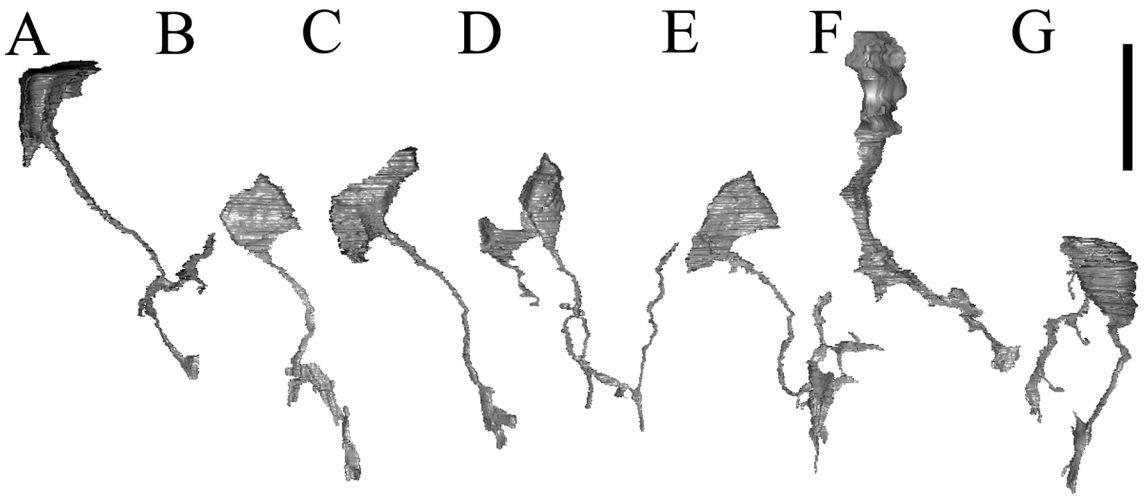

Figure 6.8. BV intrinsic antenna interneurons, shown from dorsal view. A-C) Antenna-exclusive interneurons: neuron 38 (A), neuron 79 (B), and neuron 73 (C). D-G) Multimodal interneurons with antenna synaptic input. D-E) Highly branched neurons 68 (D) and 70 (E). F) Anterior brain vesicle interneuron 16. G) Bipolar neuron 90. Scale bar: 10μm.

from antenna cell 2. The latter two neurons lack cilia that extend into the neural canal, but differ in their location and shape. Cell 16 has a thick forked terminal (Fig. 6.8F), and cell 90 is a bipolar photoreceptor neuron (Fig. 6.8G).

The brain vesicle intrinsic neuron partners of antenna relay neurons include some direct antenna neuron targets, along with other, third-order, or multimodal interneurons of the brain vesicle. The direct antenna target neurons include cells 38 and 79, described above. Other brain vesicle interneurons, cells 15, 17, and 23, are targets of the antenna pathway, but lack direct synaptic input from antenna neurons. These are likewise anterior ciliated neurons, cilia from which contact the coronet bulbous protrusions. The neurites of cells 15 and 23 are long and thin with simple thickened terminals (Fig. 6.9A). Cell 17 also has a simple thin axon, but has a more highly branched terminal (Fig. 6.9B). Another antenna relay target, cell 61, lacks a ciliary extension into the canal, and is located more dorsally than the other anterior interneurons. This neuron does, however, extend dendrites both anteriorly and posteriorly from its cell body into the canal, the posterior one contacting coronet dendrites within the canal (Fig. 6.9D). This neuron is multipolar, with one main bifurcated terminal (Fig. 6.9D). In addition, one photoreceptor interneuron with a highly branched terminal in the posterior brain vesicle, cell 78 (Fig. 6.9C), is also a target of antenna relay neurons.

6.2.4.2 Antenna Relay Neurons:

The antenna relay neurons can be divided into three classes based on their antenna neuron input: four antenna 1 relay neurons, three antenna 2 relay neurons, and three antenna 1/2 relay neurons. Of the antenna 1 relay neurons, two (cells 147 and 161) have an elongate cup-shaped cell body with short dorsal dendrites and thick axons extending from the

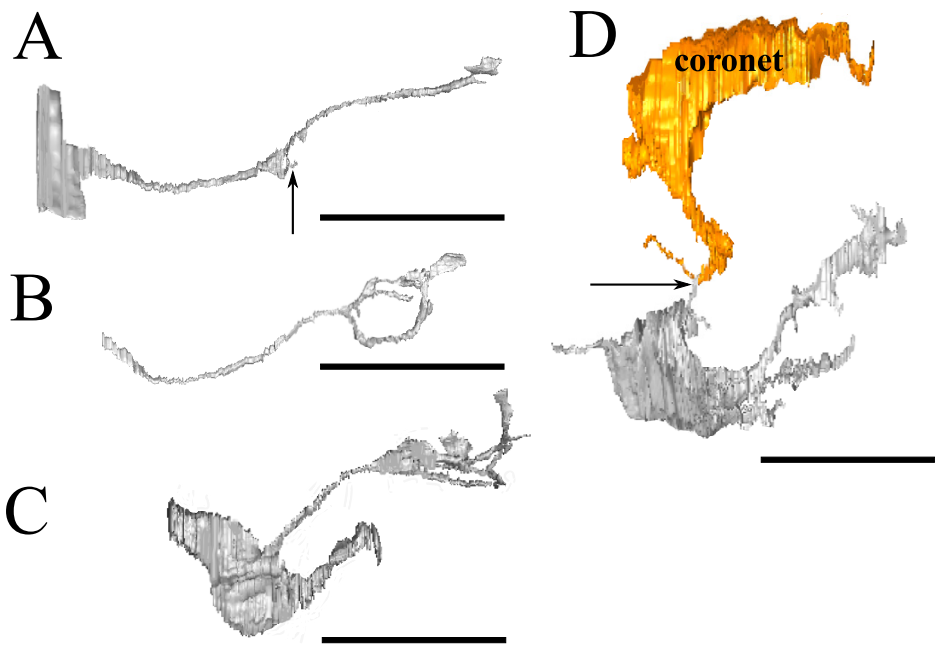

Figure 6.9. Reconstructed brain vesicle intrinsic neurons of the antenna pathway. A) Dorsal view of cell 15, bearing a long axon with a short stump at a branch point midway along its length (arrow). B) Dorsal view of the axon of cell 17 bearing a terminal with three distinct branches that do not merge posteriorly. C) Dorsal view of cell 78, a bipolar neuron with a single branched terminal in the posterior brain vesicle. D) Reconstruction of multipolar cell 61 (gray) and its associated coronet cell. In addition to an anterior dendrite, a single dendrite extends from cell 61 into the lumen of the BV where it contacts a dendrite of the coronet cell (arrow). Scale bars: 10µm.

dorso-caudal cell body and elongate unbranched terminals with multiple expanded portions (Table 6.2; Fig. 6.10A). The other antenna 1 relay neuron (cell 152) has a round cell body with a dendrite extending dorsally to the anterior and a simple descending axon originating from its dorsal surface and unbranched, elongate simple terminals in the motor ganglion (Fig. 6.10A). The antenna 2 relay neurons have small, simple, spherical cell bodies which either lack dendrites or have very short simple ones, long thin axons and simple, single, unbranched club terminals in the motor ganglion (Table 6.2; Fig. 6.10B). Two of the antenna 1/2 relay neurons have fairly spherical cell bodies, with only a few, short dendrites, and axons extending from their dorsal caudal surface that terminate in the motor ganglion (Fig. 6.10C). However, the axon of cell 120 has large expansions throughout the motor ganglion, and the axon of cell 142 branches to form multiple collateral branches, all with elongate terminals in the motor ganglion (Table 6.2; Fig. 6.10C).

The cell bodies of antenna relay neurons reside in the left-ventral posterior brain vesicle, with antenna 2 relay neurons residing more dorsally on the left side than the shared relay neurons or antenna 1 relay neurons (Fig. 6.10D). In the anterior portion of the neck between brain ganglion and motor ganglion, the axons of the antenna relay neurons constitute the ventral portion of the neuropil (Fig. 6.10D, Fig. 6.11A). This ventral bundle migrates to the right side (Fig. 6.11B), then dorsally (Fig. 6.11C-E), as it extends toward the motor ganglion. All antenna relay neurons then terminate in the dorsal right portion of the neuropil in the motor ganglion (Fig. 6.11E). A single antenna 2 relay neuron, cell 135, terminates in the anterior motor ganglion, near the cell bodies of MN1

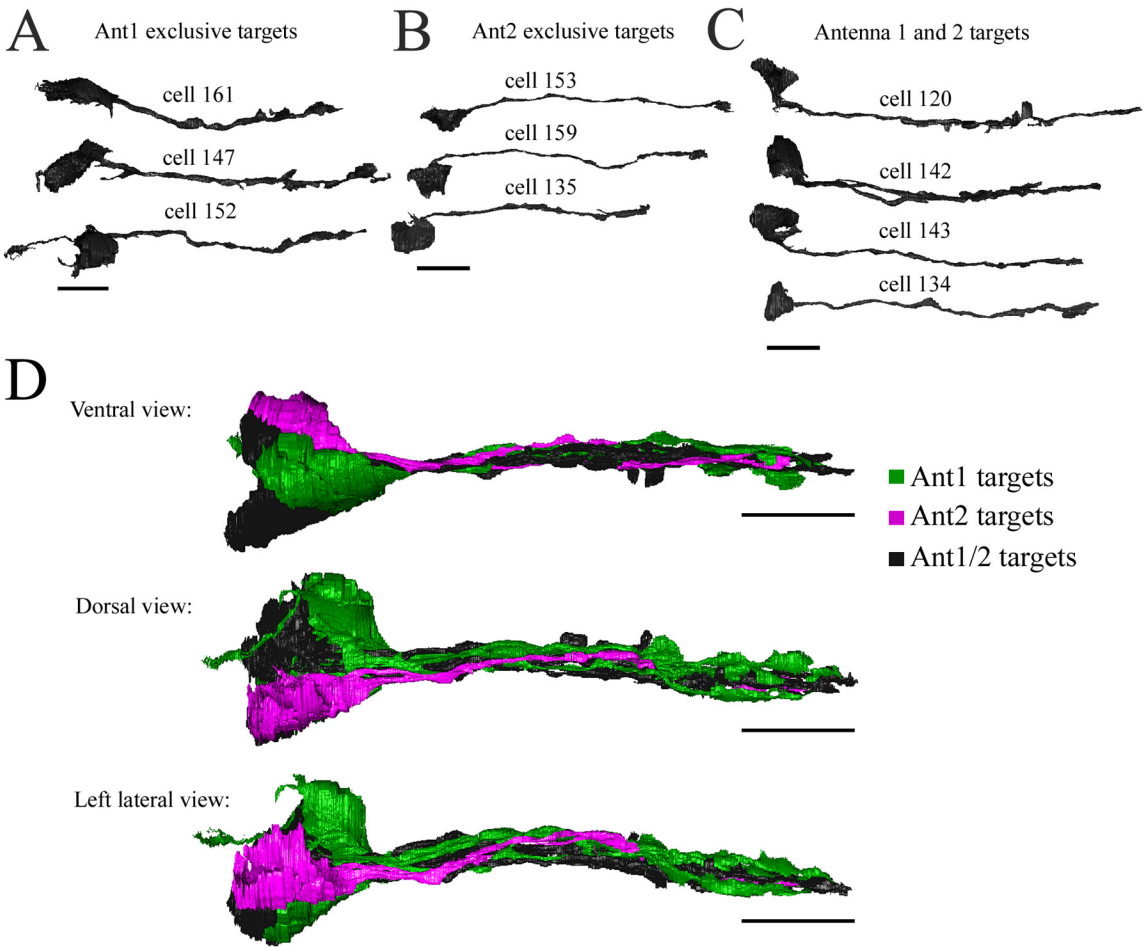

Figure 6.10. Antenna relay interneurons of the posterior brain vesicle. A) Antenna 1 exclusive relay neurons: cells 161, 147, and 152, which is also postsynaptic to photoreceptors. B) Antenna 2 exclusive relay neurons: cells 153, 159 and 135. C) Antenna relay neurons that are postsynaptic to both antenna 1 and antenna 2 neurons: cells 120, 142, 143 and 134. D) Various views of all antenna relay neurons reconstructed and colour-coded by antenna input class as indicated in key. Neurons of each class are adjacent. Scale bars: 10µm.

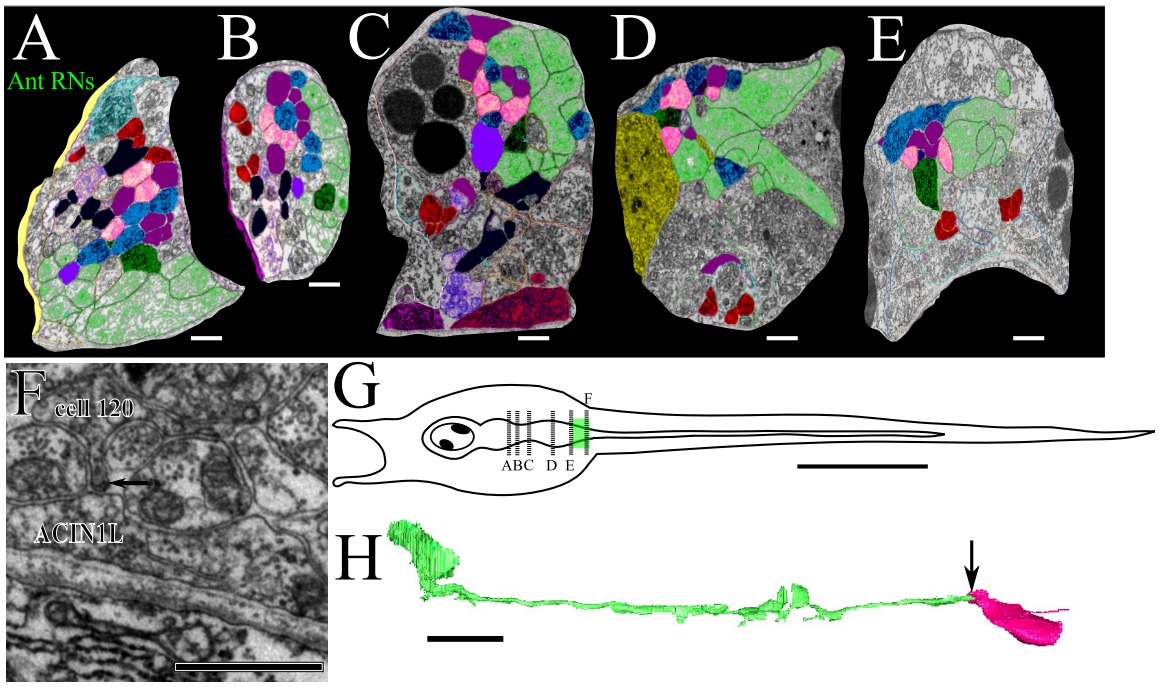

Figure 6.11. Antenna relay neuron axon bundles. A-E) Sections containing profiles of antenna relay neuron (Ant RN) axons and terminals (green) along the rostro-caudal axis. Viewed as if from the tail: dorsal is to the top, left is to the left. A) Ant RN axons are ventrally located within the posterior BV. B) Ant RN axons form the right wall of the neck neuropil. C) Ant RN axons lie in the dorsal right neuropil in the anterior motor ganglion. D) In the motor ganglion, terminals of some Ant RNs expand to cross the midline. E) Terminals of Ant RNs end in the posterior motor ganglion and rostral tail at the trunk tail border (green band in G). F) Extending most caudally into the tail, the terminal of Ant RN cell 120 contacts the crossed axon of ACIN1L (arrows in F and H). G) The locations of images in A-F from dorsal view of the larva. Green band represents the region in which ant relay neuron terminals end. H) Dorsal view of reconstruction of Ant RN cell 120 (green) showing contact with ACIN1L (pink). Scale bars: 1µm (A-F); 100µm (G); 10µm (H).

Table 6.2. Morphology of antenna relay neurons of the posterior brain vesicle, with presynaptic sensory and relay neuron (RN) input. Relay neurons (ID) sorted by sensory input: antenna cell 1 (ant1), antenna cell 2 (ant2), antenna cells 1 and 2 (ant1/2), photoreceptor (pr), Eminens peripheral relay neurons (Em), antenna relay neurons (ant 1&2 RNs), photoreceptor relay neurons (pr RN), or peripheral relay neuron (PN RN). Reconstructions aligned across cells from left lateral view.

Cell ID	Sensory input	Reconstruction	Terminal shape	RN input
147	ant1		expanded elongate term	ant1/2 RN, pr RN
161	ant1		expanded, elongate term	ant1/2 RN, pr RN
120	ant1 & ant2		expanded elongate term	ant1/2 RN, pr RN
134	ant1 & ant2		elongate term	ant1/2 RN, pr RN
142	ant1 & ant2		collateral axons, elongate term	ant1/2 RN, pr RN
143	ant1 & ant2, pr		elongate term	ant1/2 RN, pr RN
153	ant2		club term	ant1/2 RN, pr RN
159	ant2, pr		club term	ant1/2 RN, pr RN, PN RN
135	ant2, pr		elongate term	ant1/2 RN, pr RN
152	ant2, pr		elongate term	Em, ant1/2 RN, pr RN

and VGN2 on the right side. The remaining neurons terminate in the posterior motor ganglion, caudal to the cell bodies of MN2 (Fig. 6.11E). Of these terminals, cell 120 extends furthest towards the tail, terminating at the level of the trunk tail boundary, making contact with the axon of an ascending contralateral inhibitory neuron from the proximal tail (Fig. 6.11F,H).

6.2.4.2.1 Antenna Relay Neuron Synapses

The targets of the antenna interneurons span various cell types at a remarkable 753 synaptic contacts spanning a total of 2,220 individual contact sites observed in the 60nm section series. Approximately 50% of their total presynaptic contacts (both by size and by number) occur onto other relay neurons, with antenna relay neurons themselves constituting approximately 30% of all synaptic targets, and photoreceptor relay neurons constituting a further population close to 20% (Fig. 6.12A-B). Some synaptic output also occurs from these relay neurons onto interneurons intrinsic to the brain vesicle, including photoreceptor tract (trIN), anaxonal arborizing (aaIN) and other intrinsic interneurons, together comprising 8% of total synaptic contacts and 6% of total contact size (Fig. 6.12A-B). The bulk of the remaining targets are neurons of the motor ganglion, including both motor neurons and interneurons. The input to the motor ganglion neurons constitutes only approximately 30% of the total by number (Fig. 6.12A), but 40% by size (Fig. 6.12B). Of these inputs, three quarters are to the right motor ganglion, with the remaining quarter to the left side, an obvious asymmetry. The inputs to motor neurons constitute only ~10% of the motor ganglion synaptic contacts from antenna relay neurons, which represents only ~3% of the antenna relay neurons' total presynaptic contact size, whereas motor ganglion interneurons constitute ~90% of relay neuron

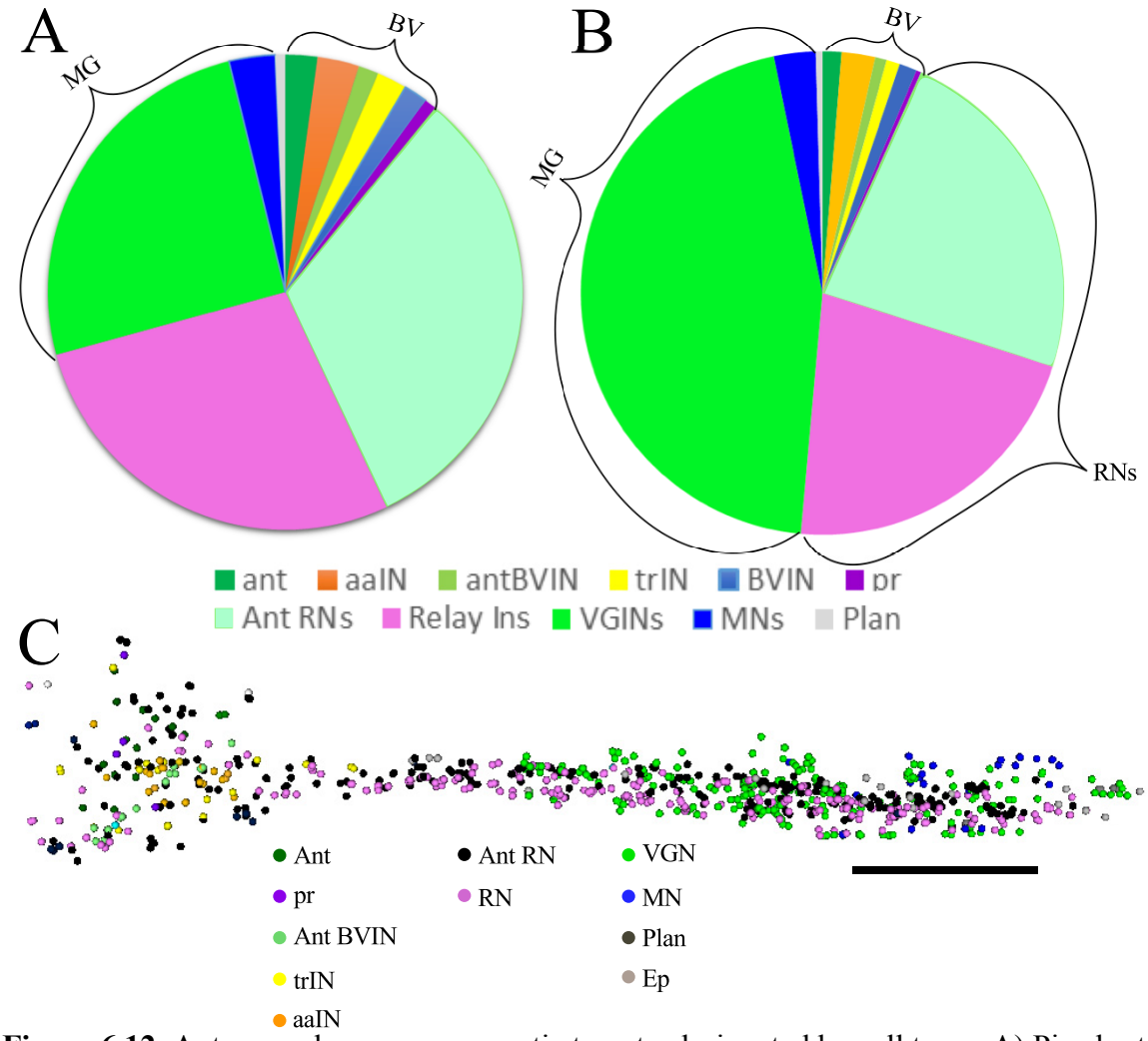

Figure 6.12. Antenna relay neuron synaptic targets, designated by cell type. A) Pie chart illustrating the distribution of antenna relay neuron synapses by number of synapses on to each target cell type. Relay neuron partners are the predominant synaptic target, with fewer synapses onto brain vesicle intrinsic partners (BV) and motor ganglion partners (MG). B) Pie chart illustrating distribution of antenna relay neuron synapses by total number of sections in which a synapse is observed between partners of each target cell type. Note approximate similarity to A (i.e. synapse sizes approximately match synapse numbers). MG interneurons and relay neurons (RNs) each make up almost half of all output, with the remainder onto other MG and tail neurons (MNs and planate neurons) and BV intrinsic neurons (BV). C) Dorsal view of the cloud of reconstructed presynaptic sites of antenna relay neurons. Each synapse is represented by a 30nm spherical punctum given the colour of its postsynaptic partner cell type. The density of presynaptic sites is greater through the neck and motor ganglion. Scale bar: 10µm.

synapses to motor ganglion partners, and ~40% of total antenna relay neuron presynaptic contact size (calculated from total number of sections in which a synapse is identified) (Fig. 6.12C).

6.3 **Discussion**

This comprehensive serial-section TEM reveals the extent to which pathways originating with the antennal cell gravity sensing organ diverge within the larval CNS of *Ciona intestinalis*. The divergence involves several cell types, and appears to incorporate multiple modalities of sensory transduction. Based on the junctional connections observed in our series, the otolith appears to be both electrically and chemically synaptic to the first antenna neuron, which is also connected by junctions with the otolith associated ciliated cells. If these junctions are electrical gap junctions, displacement of the otolith in any plane could potentially initiate signalling in the antenna neuron. Given that the otolith cell is putatively glutamatergic, the signal from otolith to this antenna neuron should result in excitation in the first, but not the second, antenna neuron (Fig. 6.13A).

The modified ciliary dendrites of otolith associated ciliated neurons are proposed to function to detect otolith movement (Torrence, 1986; Sakurai et al., 2004). The tubular structure of the modified cilia (Fig. 6.14) supports the potential spring-like function of these dendrites and the integration of complex stretch forces (Sakurai et al., 2004), rather than a simple mechanosensory function as in unmodified mechanosensory cilia (Fig. 6.13B). Whether stretch or compression results in activation of these cells would require physiological experiments using calcium indicator or dye filling experiments, which no doubt will soon be forthcoming. The proximity of these cells to a major pigmented

Figure 6.13. Summary diagram of otolith pathway connections. A) Network of connections between cell types from caudal (top) to rostral (bottom) components, as follows: otolith cell (Ot), otolith associated ciliated cells (oacc1 and oacc2), antenna neurons (Ant1 and Ant2), phorotreceptor tract interneuron (trIN), anaxonal arborizing interneurons (aaIN), antenna BV intrinsic interneurons (Ant BVIN), vacuolated BV interneurons (vac BVIN), antenna 1 relay neurons (RN_1), antenna 2 relay neurons (RN_2), and antenna 1 and 2 relay neurons (RN_{12}), motor neurons (MN), and MG interneurons 1 and 2, left and right (VG1L, VG1R, VG2L, VG2R). Arrows represent synapses with polarity from presynaptic (vesicle cloud) to postsynaptic, colour-coded by presynaptic cell type, dashed lines represent putative gap junctions. Spirals extending from oaccs represent modified tubular cilia that contact otolith cell (Ot). B) Summary illustrating two directions of otolith displacement. Anterior (A) displacement of otolith will occur when the larval trunk is tilted down, creating force on oaccs' modified dendrites. Posterior (P) displacement of otolith will occur when larval trunk is tilted up, creating an opposite force on oaccs' modified dendrites.

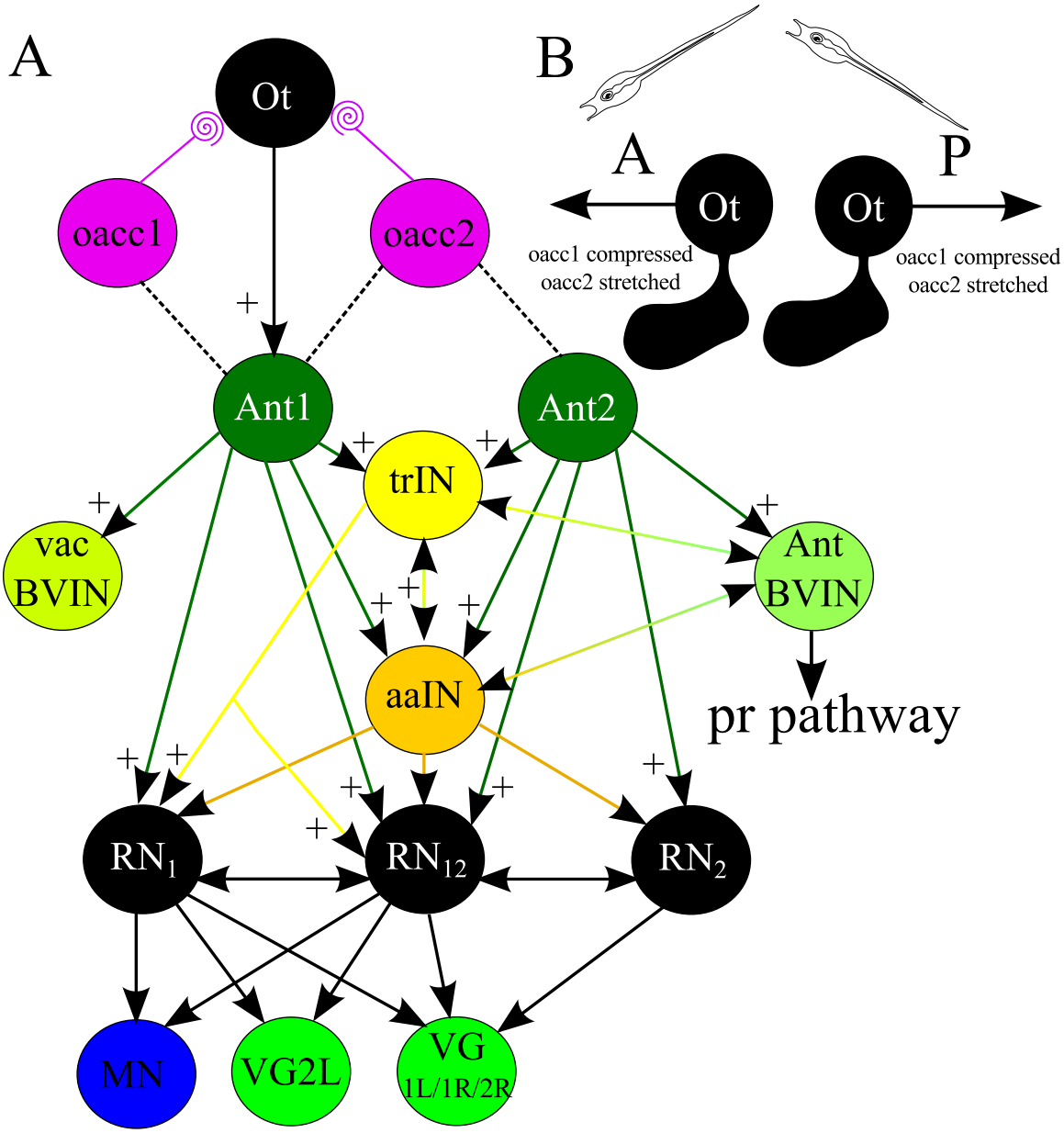
A
Ot
oacc1
oacc2
Ant1
Ant2
trIN
vac
BVIN
Ant
BVIN
aaIN
pr pathway
RN1
RN12
RN2
MN
VG2L
VG
1L/1R/2R
B
A
P
Ot
Ot
oacc1 compressed
oacc2 stretched
oacc1 compressed
oacc2 stretched

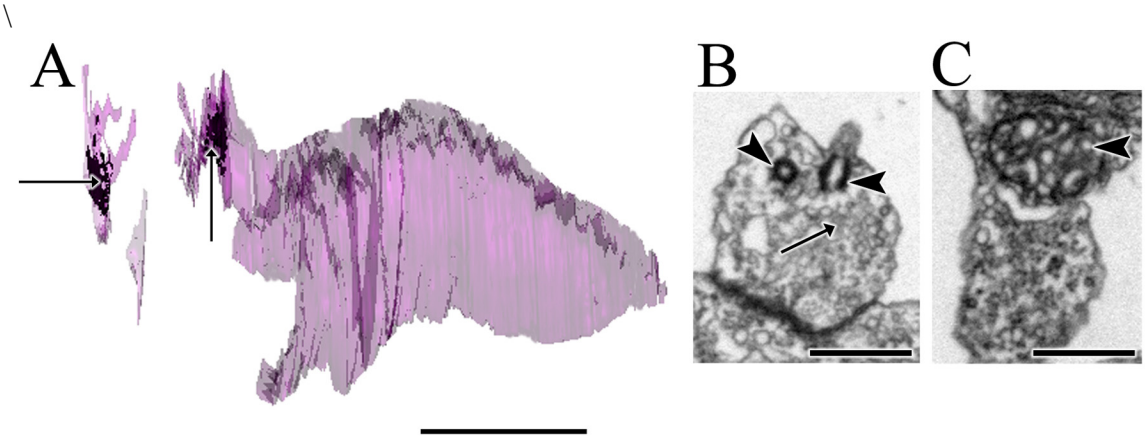

Figure 6.14. Dendrites and modified cilia of otolith associated ciliary cells (oaccs). A) Reconstructed oaccs from dorsal view to show dendrites bearing modified cilia with tubules reconstructed in black (arrows). B) Dendrite of oacc2 contains vesicles (arrow) near basal bodies (arrowheads) of modified cilia. C) Dendrite of oacc1 contains vesicles adjacent to its tubular modified cilium (arrowhead). Scale bars: 5µm (A); 1µm (B-C).

landmark in the CNS and their modified ciliated protrusions into the lumen of the brain vesicle would both also favour sharp electrode electrophysiological recordings or dye injection techniques. The Ci-GAD reporter expression in anaxonal cells surrounding the otolith is likely to correspond to these otolith associated ciliated cells, however these cells lack presynaptic sites, so the role for GABA is unclear. The dendrites of the otolith associated ciliated neurons do, however, contain many vesicles (Fig. 6.14). The junctional connections of these cells with antenna neurons, if gap junctions, would when activated offer a candidate pathway to transmit signals when activated. The potential inhibitory action of GABA is unclear from our study, but the location within the lumen of the brain vesicle could indicate a modulatory function arising from transmitter release into the canal. In addition to detecting forward and backward tilts by cilia of the otolith associated ciliary cell, the location of the antenna 1 cell on the left side adjacent to the neck in contact with the collar, and its synaptic input from the otolith cell could permit the detection of lateral movements.

The reported bipolar organisation of antenna neurons probably represents a confusion between the two otolith associated cell types, the result of limitations in the microscopy techniques used. The existence of two otolith associated cell types seen in the EM data reported here adds an additional layer of complexity to the gravity sensing organ. Thus examination of the organization and connections of these cells, and their downstream synaptic partners may help to elucidate the potential mechanism of their action. These data should also be compared with careful observations of connections at later larval stages to help understand the change that occurs from negative to positive geotaxis.

Despite extensive adjacency of the two antenna neurons, there are very few connections between these two neurons. Their few small synapses form only from the second antenna neuron to the first (Fig. 6.15B). This, along with the lack of putative gap junctions between these two neurons suggests that the antenna neurons are not tightly coupled. The existing connections are perhaps not surprising, however, insofar as neurons in *C. elegans* that are highly adjacent have a 47% chance of forming either chemical or electrical synapses (Durbin, 1987). The directionality of the connections between the neurons is also consistent with the fact that the first antenna neuron contacts all gravity organ structures, whereas the second antenna neuron contacts only the second otolith associated ciliated neuron. Thus, the second antenna neuron should retain autonomy from the first in order for directional sensitivity to be preserved.

The other synaptic inputs to antenna neurons that could modulate the signal from the otolith originate from photoreceptors, anaxonal arborizing brain vesicle interneurons, and a few relay interneurons of the posterior brain vesicle. The input from Type II photoreceptors to the second antenna neuron is putatively GABAergic (Horie et al., 2010; see Ryan, 2015: see Chapter 5), and occurs onto the axon as it enters the posterior brain vesicle neuropil. This predicted inhibition circumvents the cell body and may prevent the putative glutamatergic antenna neuron from signalling to its postsynaptic partners. The sign of the anaxonal arborizing neurons' input to the second antenna neuron remains uncertain. Aside from reciprocal input from their antenna neuron target, the input to these arborizing interneurons comes from the other antenna neuron, photoreceptors, and brain vesicle intrinsic photoreceptor interneurons, with particular input from the

Figure 6.15. Network diagram of antenna relay neurons to the motor ganglion. A) Antenna relay neurons are segregated by antenna input from exclusively antenna1 (Ant1: green), antenna 2 (Ant2: yellow), or both antenna 1 and 2 (Ant1/2: pink) cells. Node colour represents cell type, lines illustrate synaptic connections coloured by presynaptic cell type with arrow illustrating direction of synapse. Line thickness represents the total number of 60-nm sections in which a synaptic contact is observed. B) Simplified network of antenna neurons (1 and 2) to antenna 1 exclusive (a), antenna 2 exclusive (c) and antenna 1/2 (b) relay neurons illustrating connections between relay neuron classes, and their synaptic inputs to the MG components: Motor neuron 1 on the left (MN1L) and right (MN1R), 2 on the right (MN2R), and 3 on the left and right (MN3L/R); descending paired motor ganglion interneuron 1 on the left (VGN1L) and right (VGN1R) and 2 on the left (VGN2L) and right (VGN2R). Arrows represent direction of transmission, reciprocal connection illustrated by double-headed arrow. Bold MG components receive largest antenna relay neuron input.

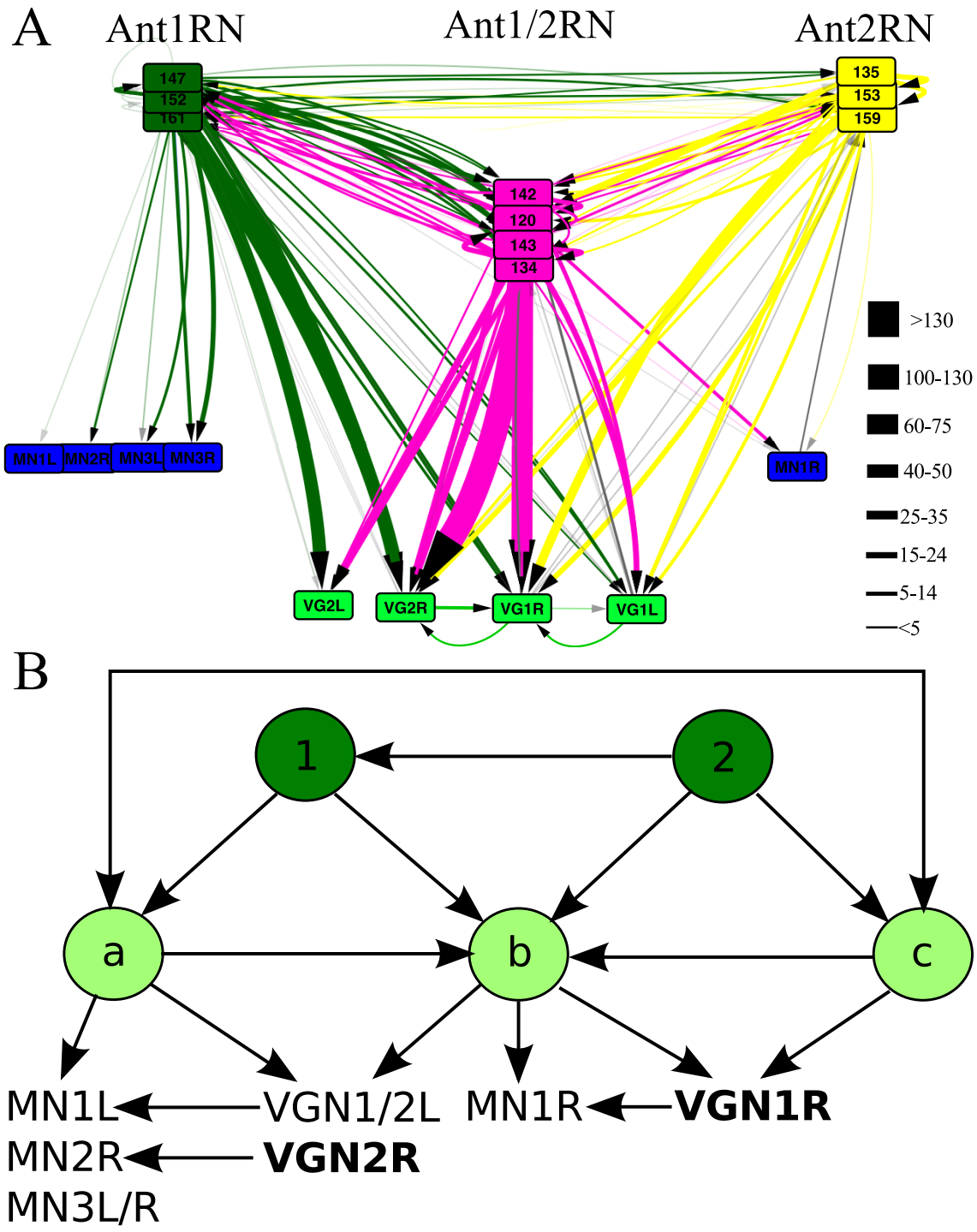
A
Ant1RN
Ant1/2RN
Ant2RN
147
152
161
135
153
159
142
120
143
134
MN1L
MN2R
MN3L
MN3R
MN1R
VG2L
VG2R
VG1R
VG1L
>130
100-130
60-75
40-50
25-35
15-24
5-14
<5
B
1
2
a
b
c
MN1L
VGN1/2L
MN1R
VGN1R
MN2R
VGN2R
MN3L/R

photoreceptor tract interneuron, trIN. Thus, the main non-sensory input to antenna cell 2 is multimodal.

The connections of the antenna relay neurons suggest that antenna cell input to the motor system follows both a direct path (Fig. 6.15), as well as acting on other pathways that converge less directly upon the motor system. Furthermore, the integration of signals from antenna 1 and antenna 2 cells occurs via these relay neurons, through those receiving input from both antenna cells, as well as through the synaptic interactions between antenna cell 1 and antenna cell 2 relay neurons (Fig. 6.15). Those relay neurons receiving input from both antenna neurons are presynaptic at many sites to both of the other types of antenna relay neurons. Antenna 1 and antenna 2 relay neurons also provide abundant input onto relay neurons of the same type; however, in accordance with the directionality of antenna neuron synapses, while some input occurs from antenna 1 relay neurons to antenna 2 relay neurons, very few small synapses are formed in the opposite direction. The other relay neuron targets of the two types of relay neurons are likely to be distinct, antenna 1 relay neurons providing input to multimodal relay neurons as well as the neuron eminens 1, whereas antenna 2 relay neurons provide some input to other photoreceptor relay neurons, but most input goes to relay neurons that receive no direct sensory input. This segregation reduces the crosstalk between these two components of the gravity sensing pathway. In the motor ganglion, however, both relay neuron pathways converge on the same postsynaptic interneuron partners, VGN1L, VGN1R, and VGN2R (Fig. 6.15). Antenna 1 relay neurons also provide synaptic input to the VGN2L interneuron as well as motor neurons 2 and 3 on the right and motor neuron 3

on the left. In contrast, an antenna 2 relay neuron, along with the antenna 1 and 2 relay neurons, provide synaptic input to MN1R (Fig. 6.15).

6.4 **Conclusions**

In the larva of *Ciona intestinalis*, the complete connectome reveals that the gravity-sensing pathway is translated through only two neurons, the antenna neurons, each forming gap junctions with otolith associated ciliated cells (oaccs). Along with the junctions from both oaccs, antenna 1 receives direct synaptic input from the otolith foot and contacts the neck of the otolith cell. These differences between antenna neurons are reflected in differences seen between synaptic connections of the three classes of antenna relay neurons to which they provide input. The synapses from antenna neurons are unique in structure within the larval CNS, forming abundant polyads and many invaginating synapses, suggesting the need to isolate these synapses from others in the posterior BV. Novel BV interneurons (trIN and aaINs) participate in this gravity-sensing pathway by forming synapses with both antenna neurons and their interneurons, and integrating synaptic inputs from visual network components. The overall input from this pathway to the motor network of the MG is greater to the right side than the left, and is greatest to the second pair of descending MG interneruons. Finally, unlike the visual pathway, there is little direct integration between the gravity-sensing pathway and neurons of the PNS pathway.

Chapter 7 : Peripheral Nervous System Integration

7.1 **Introduction**

Larval responses to environmental cues rely not only on sensory structures, but the network of underlying synaptic connections that translates these cues, communicates them to the CNS, and thereby regulates ascidian larval behaviour. Substrate preference and induction of early metamorphosis in the presence of external chemical and physical stimuli suggest that the sensory structures of neurons in the peripheral nervous system (PNS), those that bear 9+2 cilia, are capable of sensing both chemical and mechanical cues (Caicci et al., 2010; Terakubo et al., 2010). Thus, ascidian peripheral nervous systems are implicated in the function of sensory transduction of external chemical and mechanical stimuli during larval settlement (Torrence and Cloney, 1982; Svane and Young, 1989; Kimura et al., 2003; Zega et al., 2005; Caicci et al., 2010), though much of the work identifying the relevant stimuli has been conducted on species other than *Ciona intestinalis*. The anatomical composition of the peripheral nervous system has, however, been examined in *Ciona intestinalis*, in which the respective primary sensory neurons are, from anterior to posterior: papilla/palp neurons, rostral trunk epidermal neurons (RTENs), apical trunk epidermal neurons (ATENs), dorsal and ventral caudal epidermal neurons (DCENs and VCENs), and a tail tip neuron (Takamura,1998; Imai and Meinertzhagen, 2007b; Yokoyama et al., 2014). This thesis will continue to use these acronyms, which are well established in the ascidian literature.

Every peripheral neuron of the ascidian larva possesses a single cilium, contained within in a single membrane sheath that also surrounds cellular material (Terakubo et al., 2010; Konno et al., 2010), including vesicles observed in the present series. Together, these cilia constitute the reported sensory dendrites in the tunic (Imai and Meinertzhagen, 2007b) that are organized into a network of overlapping ciliated dendrites, the ascidian dendritic network in tunic (ASNET) (Yokoyama et al., 2014). Caution should be taken in ascribing network properties to these overlapping dendrites, but the projection patterns do illustrate great overlap of sensory dendrites across the larval tunic. The anteriormost neurons, the papillar neurons, have only short cilia that do not contribute to the ASNET (Yokoyama et al., 2014). However, dendrites from the RTENS and the two most anterior ATENs extend anteriorly towards, and between the papillar neurons. In the tail, the perimeter of the tunic fin is lined by overlapping dendrites of dorsal and ventral caudal epidermal neurons and a tail tip epidermal neuron. The dendrites of these neurons extend either bidirectionally or unidirectionally depending on their location along the A-P axis (Yokoyama et al., 2014). Overlap between the trunk epidermal and caudal epidermal networks also occurs between posteriorly projecting dendrites of anterior and posterior ATENs and ascending dendrites of DCENs (Terakubo et al., 2010; Yokoyama et al., 2014). The non-random organization and morphology of these ciliated dendrites is presumably suited to an underlying role in mechanosensory or chemosensory activity and the lateral extent of the dendrites provides a clear idea of each neuron's sensory field.

The sensory structures of these neurons are their ciliated dendrites, but compatible with synaptic transmission the neurons themselves express reporters for synaptic proteins (Imai and Meinertzhagen, 2007b) and classical neurotransmitters (Zega et al., 2005;

Horie et al., 2008a; Takamura et al., 2010; Horie et al., 2010), suggesting they provide synaptic input to other neurons. The anterior papillar neurons implicated in substrate recognition express reporters for both glutamate (Horie et al., 2008a) and GABA (Horie et al., 2010; Takamura et al., 2010; Zega et al., 2008; discussed in Ryan, 2015: Chapter 4). These papillar neurons extend only short axons that do not extend to the brain vesicle, but terminate adjacent to nearby left and right subsets of RTENs (Horie et al., 2008a). RTENs, in turn, extend their axons into left and right bundles that appear, at least from confocal studies, to terminate in the posterior brain vesicle (Imai and Meinertzhagen, 2007b, Horie et al., 2008a). These RTENs, and all other epidermal sensory neurons, express vGLUT reporter, and so are putatively glutamatergic (Horie et al., 2008a) (see also Chapter 4).

Two sets of four ATENs dorsal to the brain vesicle extend axons posteriorly within the epidermis, the axons of the anterior set, aATENs, terminate dorsal to the posterior brain vesicle, while the terminal locations of the posterior set, pATENs, are somewhere within the tail (Imai and Meinertzhagen, 2007b, Horie et al., 2008a). These pATEN axons appear to overlap within the tail with axons of the caudal epidermal neurons (DCENs) of the tail (Horie et al., 2008a). Later in development, reports suggest that the dorsal sensory axons extend into the motor ganglion (Burighel and Cloney, 1997). The DCEN axons, along with those of VCENs, extend along the A-P axis, and some, including the tail tip neuron, bend around the tip of the tail to join the dorsal and ventral portions of the continuous peripheral nerve of the tail (Imai and Meinertzhagen, 2007b). The caudal sensory nerve, made up of the axons of these primary caudal epidermal neurons (Torrence and Cloney, 1982; Burighel and Cloney, 1997; Terakubo et al., 2010),

comprises a reported eight axons near the middle of the tail (Burighel and Cloney, 1997). Along with the caudal epidermal neurons restricted to the peripheral nerve, axons of the caudal sensory nerve of dorsal bipolar tail epidermal neurons appear to cross into the CNS and terminate anteriorly in the motor ganglion or brain vesicle (Imai and Meinertzhagen, 2007b). Unlike the other cell bodies located in the epidermal tissue of the tail, the bipolar neurons correspond to the locations and projection patterns of cells expressing reporters for glutamate (Horie et al., 2008a), GABA (Zega et al., 2008), and acetylcholine (Horie et al., 2010). The uncertainties in past reports on PNS neurons are resolved in the present study.

The only cell type within the CNS that has been identified as a direct putative component of the peripheral integration network is the dorsal Eminens cell of the posterior brain vesicle (Imai and Meinertzhagen, 2007b; Takamura et al., 2010). From confocal microscopy, a single Eminens cell appears to receive the axons of peripheral neurons of the anterior trunk (Imai and Meinertzhagen, 2007a). Cultured cells resembling these neurons have been subjected to whole cell voltage-clamp recordings, which showed fast inward current on depolarization followed by a slowly activating and inactivating outward current, which produced trains of spikes recorded using current-clamp methods (Zanetti et al., 2007). Neurons of the same morphology and location as Eminens cells express Ci-GAD reporters, suggesting that they are GABAergic (Takamura et al., 2010). Eminens neurons terminate in the proximal tail (Imai and Meinertzhagen, 2007a; Takamura et al., 2010), so they are qualified to provide input to motor components of the motor ganglion. Further, Type A and B GABA receptor mRNA is expressed in the ventral motor ganglion (Mochizuki et al., 2003; Zega et al., 2008), suggesting that motor

components possess receptors that could mediate both fast and slow inhibitory transmission from presynaptic GABAergic partners (Bettler et al., 2004).

Aside from their role in settlement, a role for peripheral neurons in swimming behaviour was suggested in early studies by Torrence and Cloney (1982, 1983). In particular, although there is no behavioural evidence, the anatomical structure of DCENs and VCENs may indicate their potential to initiate swimming, or act in a proprioceptive capacity during swimming (Torrence and Cloney, 1982). Since these early descriptions, there has been little reported evidence for the roles of peripheral neurons in the physiology or behaviour of larval swimming aside from informal reports of rapid responses to tactile stimulation (R. A. Cloney, pers. comm. as cited in Svane and Young, 1989). Some field observations indicate that, depending on the species, settlement-related chemical cues appear to alter early larval behaviour, changing the direction of initial swimming from upward to downward, or altering the duration of swimming bouts (Bingham and Young, 1991; Stoner, 1992). However, despite the accessibility of peripheral neurons, formal behavioural experiments or physiological studies are still lacking. Thus, while much is known about the complement of peripheral neurons, their connectivity, exact projection patterns, signal integration, and synaptic properties are still largely unexplored. An anatomical perspective of these aspects of peripheral nervous networks in larval *Ciona intestinalis* will help facilitate future physiological and behavioural studies.

7.2 **Results**

To summarize the complex network to which the peripheral neurons give rise in *Ciona*, three main centres of peripheral integration exist within the CNS at the entry points of

peripheral synaptic input: Eminens and other interneurons of the brain vesicle, AVG neurons of the motor ganglion, and Planate neurons of the tail. Each centre belongs to a connected network with common input to the motor system of the motor ganglion. The synaptic nature of connections within this network varies by number and size of synaptic contacts and by number and types of input or output partners. The peripheral information is integrated with that from other sensory systems in both the posterior brain vesicle through multimodal interneurons, and in the motor ganglion through descending and ascending interneurons.

7.2.1 Rostral Peripheral Network:

The peripheral nervous system (PNS) of the ascidian larva consists of a network of neurons from the papillae of the trunk epithelium to the caudal tail. The axons of these peripheral neurons overlap to such an extent that no portion of the larva is without the peripheral axon or cell body of a sensory neuron (Fig. 7.1). In the anterior, papillar neurons extend only short axons toward RTENs (Takamura, 2010), and so in our series are not contributors to the anterior-most axon bundles of the epidermis dorsal to the brain vesicle. The anterior contributors to these dorsal nerve bundles originate instead from RTENs. In this dorsal epidermis, Apical Trunk Epidermal Neurons (ATENs) lie in groups of four and project axons that extend ventrally where they fasciculate with the RTENs and approach the ventral boundary of the epidermal tissue. Both RTENs and ATENs also extend cilia from basal bodies (Fig. 7.2), which then branch and split to extend in a net-like distribution throughout the tunic. I do not see a clear double membrane surrounding these profiles, which suggests that they could be cilia rather than

Figure 7.1. Peripheral neural network of *Ciona intestinalis* larva. A-C) PNS components, overlain on DIC Syt-GFP image (green, from Imai and Meinertzhagen, 2007b), and labeled as follows: Pap (papillar neurons), RTEN (rostral trunk epidermal neurons), ATENa (anterior apical trunk epidermal neurons), ATENp (posterior apical trunk epidermal neurons), Em (eminens neurons), ddN (descending decussating motor ganglion interneurons), AVG (ascending dorsal motor ganglion peripheral interneurons), DCEN (dorsal caudal epidermal neurons), VCEN (ventral caudal epidermal neurons), Plan (planate neurons/bipolar tail neurons). A) Overlay with peripheral neuron pathway cell body markers only. B) Overlay including axon pathways of peripheral neurons and AVGs observed from EM series. C) Overlay with background transparency reduced to highlight cell bodies, axon projections, and ciliary extensions observed in EM series. D-F) 3-D reconstructions of peripheral neural components from compiled EM profiles. D) Left lateral view of reconstructed RTEN axons and peripheral interneurons in the peripheral neuropil, ATENs, AVG4 cell body and peripheral axon, DCENs, and planate neurons (Plan) and axons from high magnification series. E) Enlarged reconstruction of ATENs and AVG5 cell from low magnification stack including ciliary dendrites of ATENs, dorsal view. F) Enlarged reconstruction of branched complex ciliary dendrites of ATENs shown midpoint trace lines extending from ATEN cell bodies (spheres). Scale bars: 100µm (A-E); 10µm (F).

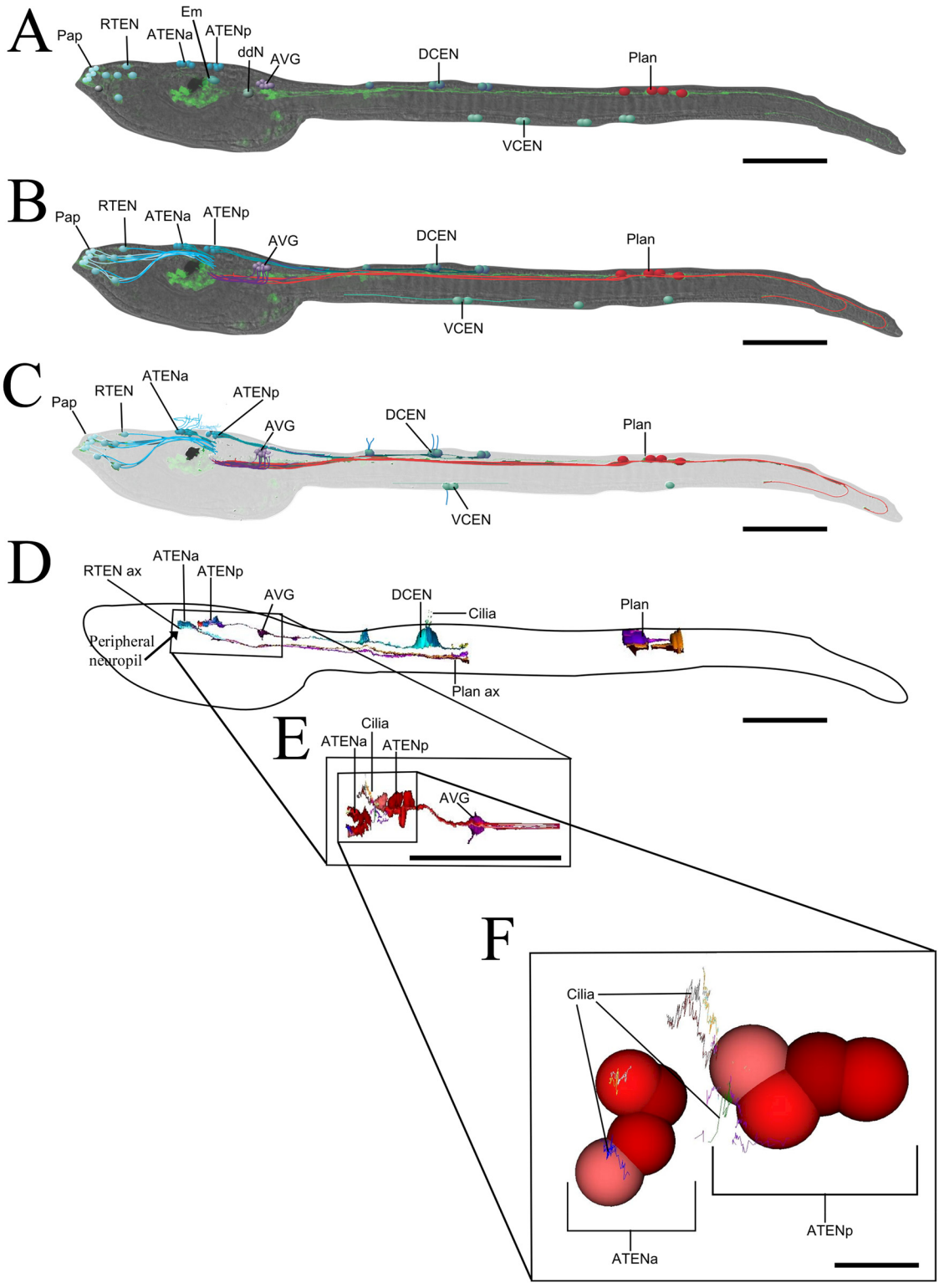
A
Pap
RTEN
Em
ATENa
ATENp
ddN
AVG
DCEN
Plan
VCEN
B
Pap
RTEN
ATENa
ATENp
AVG
DCEN
Plan
VCEN
C
Pap
RTEN
ATENa
ATENp
AVG
DCEN
Plan
VCEN
D
RTEN ax
ATENa
ATENp
AVG
DCEN
Cilia
Plan
Peripheral neuropil
Plan ax
E
Cilia
ATENa
ATENp
AVG
F
Cilia
ATENp
ATENa

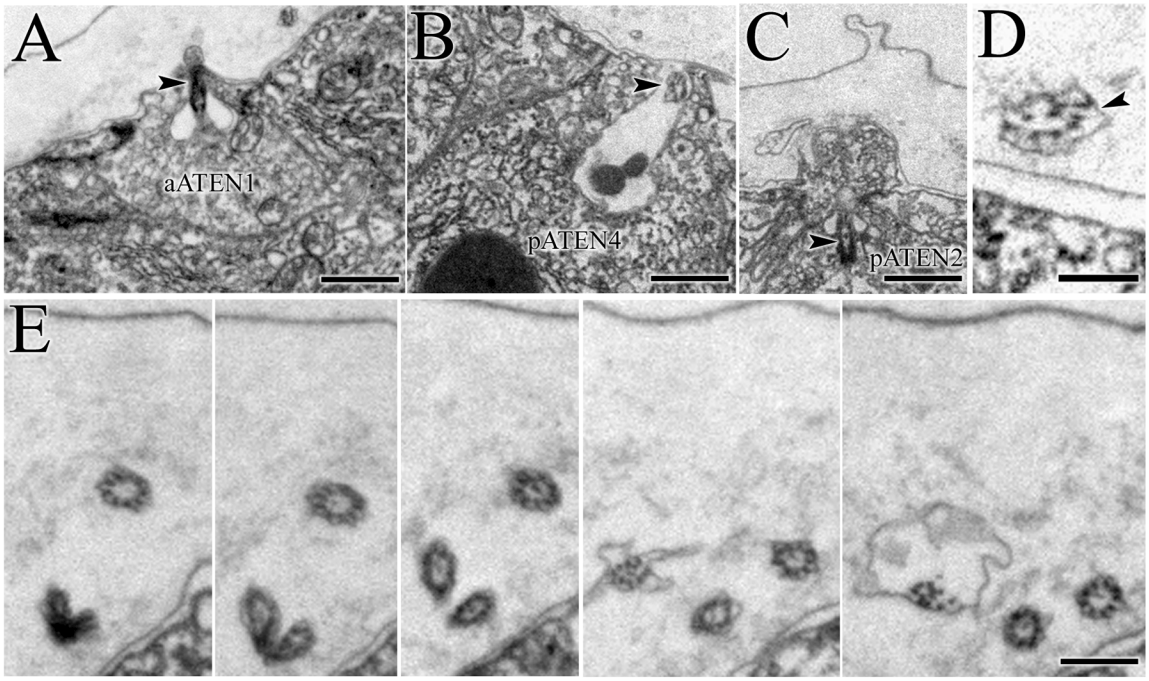

Figure 7.2. Basal bodies and cilia of peripheral apical trunk epidermal neurons (ATENs). A) Basal body emerging from an anterior ATEN neuron (arrowhead). B) Cilium (arrowhead) emerging from a posterior ATEN. Ciliary membrane and microtubule arrangement are not precise. C) Basal body of pATEN2 emerging into larval tunic. D) Cilium in larval tunic (arrowhead) has disorganized microtubules and irregular membrane shape. E) Series of sections illustrating ATEN cilia within the tunic that appear to merge and split at bend/branch points. Microtubule arrangement and membrane structure lack constancy along the length of the cilium. Scale bars: 1µm (A-C); 500 nm (D-E).

cilia within ciliated neurites, but their surrounding membrane does indeed expand at sites where the cilia branch (Fig. 7.2). The microtubule arrangement and structure of these cilia is also disorganized at more distal portions of the cilia (Fig. 7.2). Axons of several RTENs and the most rostral ATENs form two fascicles, one left and one right. Axons from each fascicle cross the basal lamina to enter the dorsal CNS, where they form a combined fascicle together with the axons of several brain vesicle interneurons. Six of these peripheral axons (three left and three right), both presumably RTENs, terminate within this fascicle, rostral to the extensive posterior brain vesicle, so are grouped into a single type: peripheral neurons, group a (pna: pns1, pns2, pns5, pns6, pns9, and pns13). The remaining six presumed ATEN axons (three left, three right) terminate in either the posteriormost brain vesicle or the neck region, and are grouped as peripheral neurons, group b (pnb: pns3, pns4, pns7, pns 10, pns 11, and pns12).

Within this axon fascicle, many of the axons or terminals contain vacuoles and related organelles. Some contain vacuoles (pns7, pns10 and pns11, Fig. 7.3), some have multivesicular bodies (pns 12, pns4, pns7, 4, Fig. 7.3A), and some have apparent secretory granules (pns10, pns4, cell 4; Fig. 7.3A-B). Several also have what are apparently autophagocytic vacuoles (pns4, psn10, Fig. 7.3B-C). These features are evident near presynaptic sites (Fig. 7.3). The pnb group of peripheral axons retains relatively consistent positions within the fascicle with only minimal braiding, running dorsal to the anterior brain vesicle interneurons in the anterior to mid brain vesicle, and ventral to the two Eminens cell bodies as they approach the posterior brain vesicle. In the posterior brain vesicle, the peripheral fascicle expands toward the main neuropil, but the

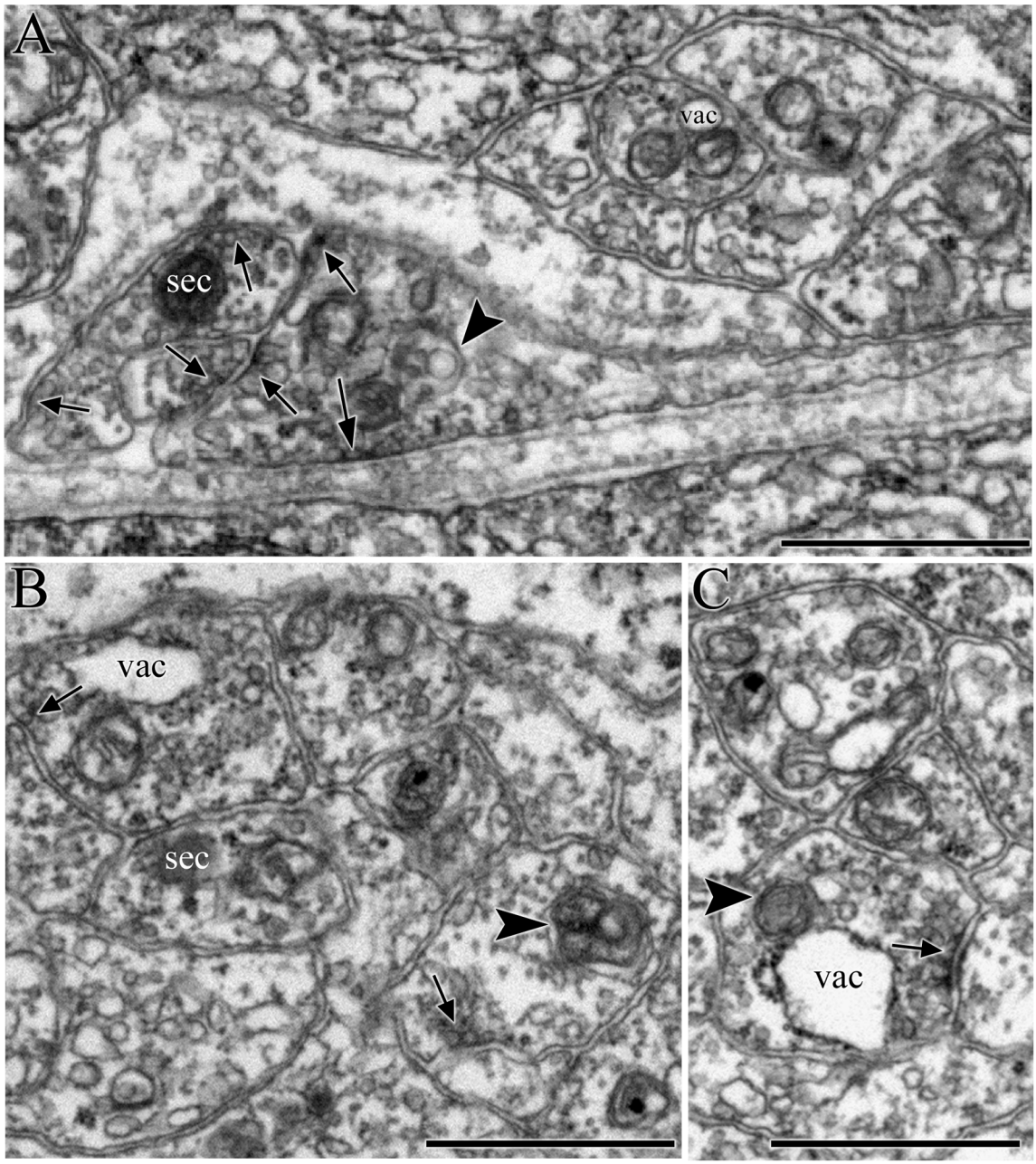

Figure 7.3. Subcellular organelles common in both peripheral neurons and CNS interneurons. A) Axons contain vacuoles (vac), secretory bodies (sec) and multivesicular bodies (arrowhead) in regions with synapses (arrows). B-C) Large vacuoles (vac) lie adjacent to synapses (arrows). Axons of the peripheral neuropil also contain putative autophagosomes (arrowheads in B and C). Scale bars: 1μm.

peripheral components remain isolated by a particular subset of peripheral and multimodal interneurons (Fig. 7.4). Thus, the peripheral axons and terminals do not contact photoreceptor or antenna neuron terminals.

After they combine in the CNS, the axons of each cell type, pna and pnb, of the left and right peripheral fascicles form synapses between themselves. The direction of anatomical transmission is for pna neurons from left (presynaptic) to right (postsynaptic), while for pnb the connections between left and right are reciprocal. These ATEN and RTEN neurons of group pna and pnb are also reciprocally connected by chemical synapses; each axon receives between 7 and 18 synapses from two to seven peripheral presynaptic partners (Appendix I). The network to which these interconnected peripheral neurons provide input involves a variety of interneurons that are anatomically qualified to integrate RTEN and ATEN signals (Fig. 7.5B). RTENs (pna) excite two sets of paired brain vesicle intrinsic interneurons, cells 4 and 6, and cells 29 and 30, which are also putatively glutamatergic (Horie, unpublished data discussed in Ryan, 2015: Chapter 4). The anterior pair of these synapse onto the posterior pair, left partner to left partner (cell 4 to cell 30), and right partner to right (cell 6 to cell 29). Cell 4 on the left and cell 29 on the right also provide synaptic output to a more posterior pair of intrinsic interneurons, cells 61 and 65. Together, these intrinsic interneurons also synapse onto other peripheral interneurons as well as the large Eminens neurons of the dorsal posterior brain vesicle. In addition, neuron 30 provides synaptic input to one of the planate neurons of the tail, planate 2. Neurons of the pnb group of peripheral ATENs provide synaptic input onto a larger number of interneurons of the peripheral integration pathway. Through their

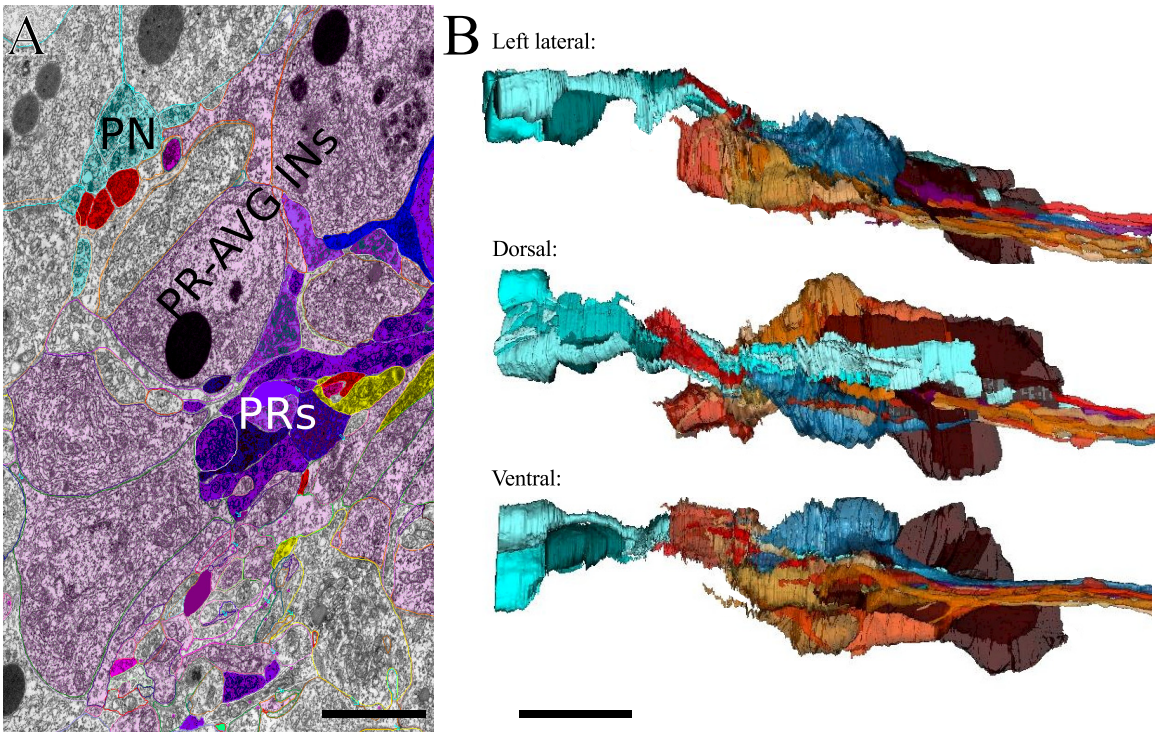

Figure 7.4. Multimodal photoreceptor/peripheral relay neurons lie between the peripheral neuropil (PN) and the photoreceptor terminals (PRs) in the posterior brain vesicle. A) Section of the posterior brain vesicle illustrating isolation of peripheral neuropil (PN) from photoreceptor terminals (PR). Dorsal to the top. Blue profiles are peripheral neurons and interneurons, red are planate neurons, pink are interneurons, and purple are photoreceptor terminals. B) Reconstructions of peripheral neurons and interneurons (blue) and adjacent PR-AVG interneurons (orange and brown) from left lateral, dorsal, and ventral views. Scale bars: 5µm (A); 10µm (B).

Figure 7.5. Network of synaptic connections in the brain vesicle from RTENs to eminens neurons. A) Synaptic inputs from anterior terminating (pna) and posterior terminating (pnb) subsets of RTENs to pairs of brain vesicle peripheral interneurons and eminens relay neurons 1 (Em1) and 2 (Em2). Arrows indicate direction of synapse; line thickness represents number of synapses shown in key. B) Network of connections among three pairs of brain vesicle interneurons of the peripheral pathway. Line without arrow between eminens neurons represents putative gap junctions. C) Differences between pnb pathways to eminens1 (Em1: top) and eminens2 (Em2: bottom). Blue lines represent RTEN synaptic inputs and red lines depict connections involved in only one of the RTEN-eminens networks.

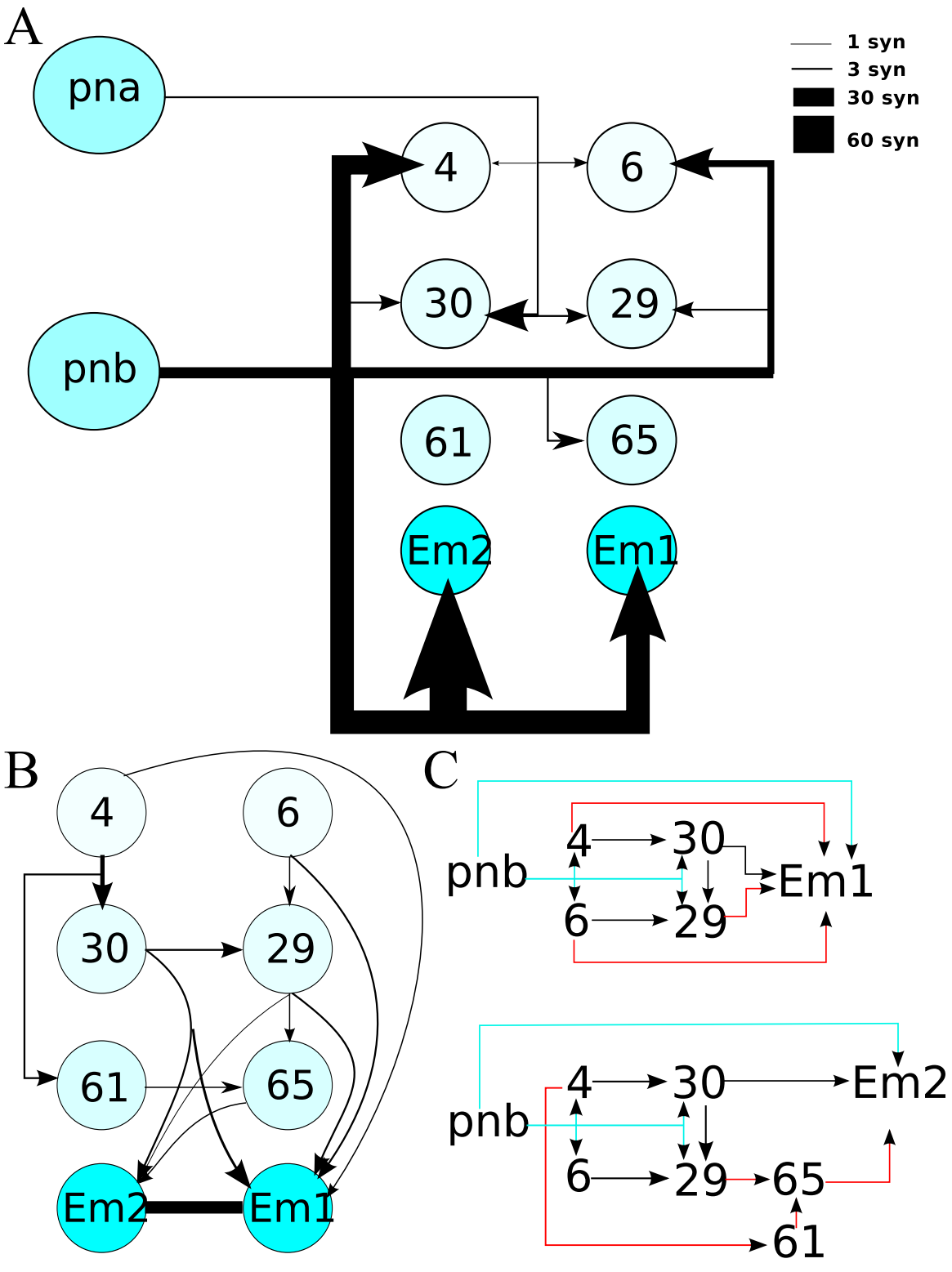
A
pna
pnb
4
6
30
29
61
65
Em2
Em1
1 syn
3 syn
30 syn
60 syn
B
4
6
30
29
61
65
Em2
Em1
C
pnb
4
30
Em1
6
29
pnb
4
30
Em2
6
29
65
61

inputs, pnb neurons putatively excite Eminens neurons both directly and indirectly (Fig. 7.5A,C). Many of these inputs are reciprocal, with the Eminens cells returning input to the pnb axons. Along with these direct reciprocal synapses, the brain vesicle intrinsic neurons also receive direct input from pnb neurons, and all form synaptic contacts onto Eminens1, while only two, cells 30 and 65, form synaptic contacts onto its partner, Eminens2 (Fig. 7.5B-C). Of these brain vesicle intrinsic neurons, the main target of pnb neurons, cell 4, receives over 30 synaptic contacts and feeds back into the pna pathway by providing synaptic input to both pna neurons and their main target interneuron, cell 30 (Fig. 7.5A).

Located in the posterior dorsal brain vesicle surrounding the peripheral axon fascicle, an additional group of brain vesicle intrinsic interneurons receives a few direct synaptic inputs from pnb neurons as well as second-order synaptic input from target interneurons of both pna and pnb neurons. These posterior brain vesicle interneurons in turn provide reciprocal input to the following: Eminens neurons, cell 4, AVG interneurons that ascend to the brain vesicle, and posterior brain vesicle relay neurons that descend to the motor ganglion. One other interneuron, cell 122, receives no input aside from a few individual synapses from the peripheral neurons, or their targets, but does provide its own input to components of this pathway.

Both groups of peripheral neurons, pna and pnb, feed forward to three groups of interneurons that send axons to the motor ganglion via the Eminens neurons, and two groups of multimodal interneurons. The existence of multiple parallel pathways to the Eminens neurons (Fig. 7.5) demonstrates clearly the redundancy of the larval peripheral nervous system, possibly illuminating the importance of this pathway in the regulation of

larval behaviour. Some other descending interneurons are synaptic targets of Eminens neurons, and do not provide feedback synapses to Eminens neurons. However, these interneurons are presynaptic to other components of the peripheral network, including ascending AVG and planate neurons that receive input from peripheral neurons of the posterior trunk and tail. As multimodal interneurons, they also receive synaptic input, directly and indirectly, from photoreceptor and antenna pathways and provide synaptic input in turn to interneurons of those pathways. Thus, these interneurons provide a mechanism to integrate peripheral information in other sensory pathways, given that the descending Eminens neurons do not provide direct widespread input to sensory pathways.

Among anterior peripheral interneurons, putative gap junctions contribute to the peripheral interneuron connections along with chemical synapses. Eminens2 has extensive putative gap junctions with anterior neuron 4, two brain vesicle intrinsic posterior interneurons, cells 163 and 164, and a multimodal relay neuron, cell 130. Eminens2 and Eminens1 are also connected by putative gap junctions, the latter having its own connections with ATENs pns3 and pns12, and photoreceptor-peripheral relay neurons, cells 108 and 116.

While the three groups of peripheral relay neurons converge upon some targets in the motor ganglion, the extent of their convergence is neither equal nor exclusive. The first pair of motor ganglion interneurons, VGN1 (the left receiving greater input than the right) are a major target of both Eminens and other peripheral interneurons descending from the brain vesicle (Fig. 7.6A-B). On the right, this motor ganglion interneuron feeds into the first motor neuron, whereas on the left it feeds mainly into the second interneuron, although both left and right VGN1 neurons also form putative gap junctions

Figure 7.6. Network of presynaptic contacts from peripheral interneurons to neurons of the motor ganglion and tail. Synaptic connections between classes of neurons are indicated by lines, with arrows representing polarity of connections. Dashed lines: synapses from peripheral interneurons' targets onto other motor ganglion and tail neurons, and muscle. A) Network of connections between peripheral relay neurons of the brain vesicle and interneurons of the motor ganglion. Asterisks indicate classes that are postsynaptic to anterior peripheral neurons (pna and pnb RTENs). B) Solid lines depict synaptic inputs from peripheral interneurons to motor ganglion components, with line colour indicating presynaptic neuron type. Connections between non-pns components are transparent grey. Open arrows: putative inhibitory synaptic contacts; black arrowheads: putative excitatory synapses. Dotted lines: partnerships with few, small synapses. C) Simplified version of A, with peripheral interneurons grouped into single representatives for each cell type: AVG, Em, and Planate. Cell types: 103 (a posterior brain vesicle PN interneuron), 160s (posterior brain vesicle intrinsic peripheral interneurons), Em (eminens relay neurons), pr-PNs (photoreceptor-peripheral relay neurons (including photoreceptor AVG neurons)), 131 (peripheral relay neuron), Plan (bipolar planate neurons of the tail), AVGs 1-7 (ascending motor ganglion neurons 1-7), and VGN1s, VGN2s, and VGN3s (descending motor ganglion interneuron pairs 1, 2 and 3), MN1-5 (motor neuron pairs 1-5), ddL/ddR (descending decussating left/right motor ganglion interneurons), ACIN (ascending contralateral inhibitory neurons), PVGN (posterior unpaired descending MG interneuron), Tail18 (tail interneuron), MT (descending paired mid-tail neurons).

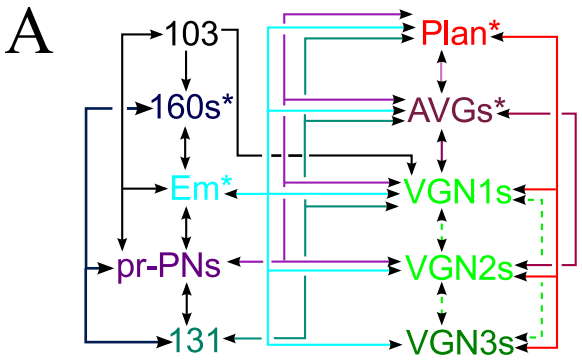
A
103
160s*
Em*
pr-PNs
131
Plan*
AVGs*
VGN1s
VGN2s
VGN3s

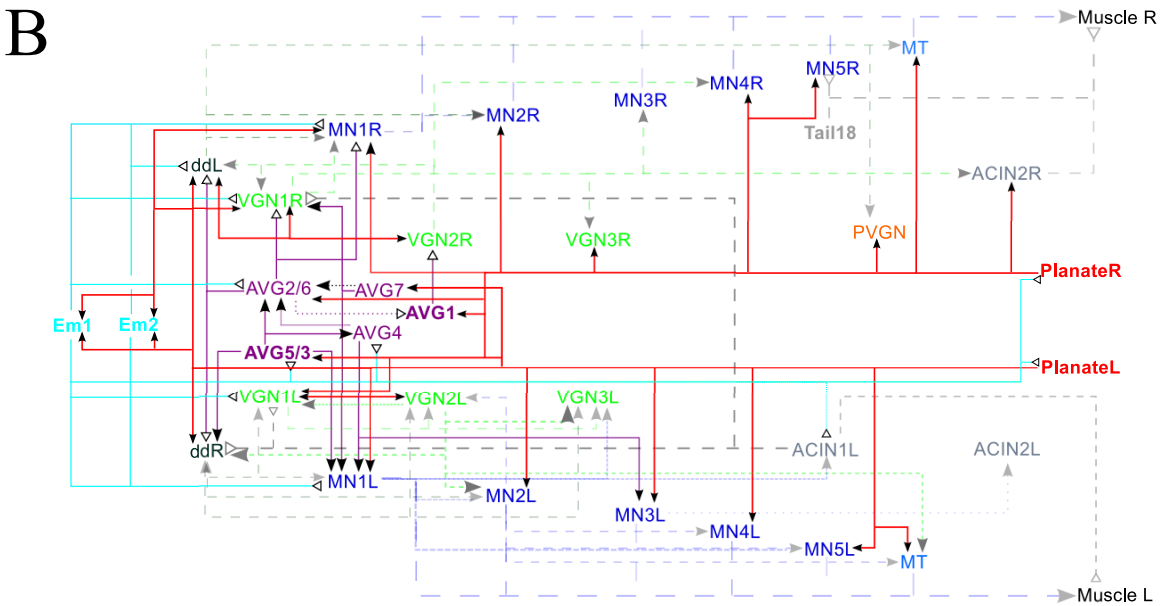
B
Muscle R
MT
MN5R
MN4R
MN3R
MN2R
MN1R
Tail18
ddL
ACIN2R
VGN1R
PVGN
VGN2R
VGN3R
PlanateR
AVG2/6
AVG7
AVG1
Em1
Em2
AVG4
AVG5/3
PlanateL
VGN1L
VGN2L
VGN3L
ddR
ACIN1L
ACIN2L
MN1L
MN2L
MN3L
MN4L
MN5L
MT
Muscle L

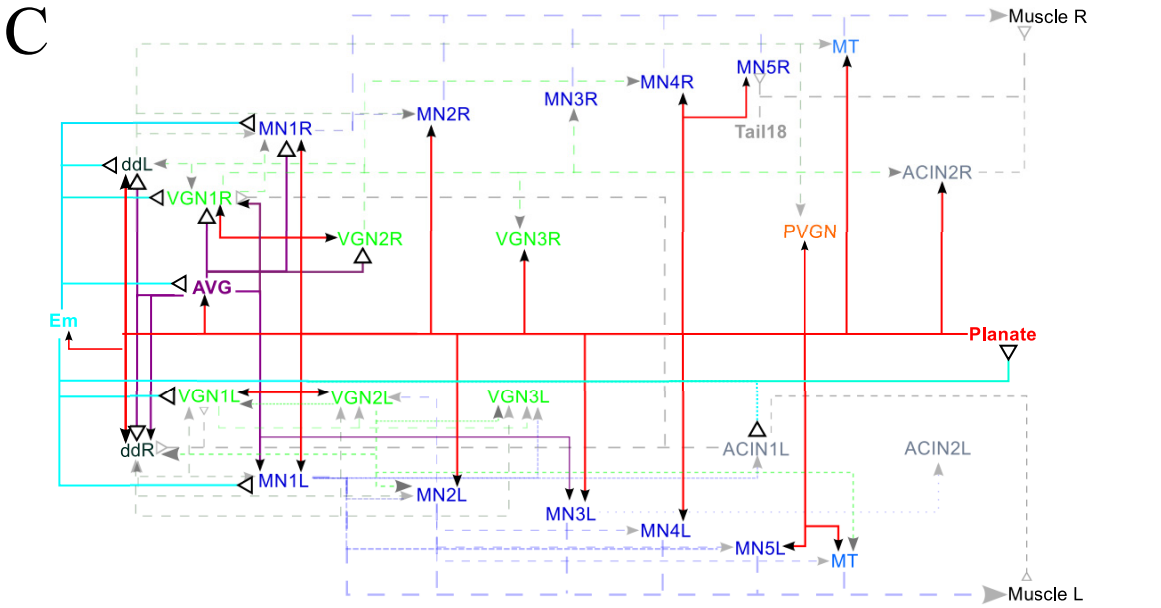
C
Muscle R
MT
MN5R
MN4R
MN3R
MN2R
MN1R
Tail18
ddL
ACIN2R
VGN1R
PVGN
VGN2R
VGN3R
AVG
Em
Planate
VGN1L
VGN2L
VGN3L
ddR
ACIN1L
ACIN2L
MN1L
MN2L
MN3L
MN4L
MN5L
MT
Muscle L

with each other and with both left and right MN1 motor neurons. The multimodal interneurons and Eminens1 provide additional input to the AVG neurons ascending from the motor ganglion (Fig. 7.6). Some of the multimodal interneurons also provide synaptic input to the left second motor ganglion interneuron, VGN2L, which receives only minimal input from interneurons, including those with photoreceptor, peripheral, and antenna input. In addition to the preceding, one of the planate neurons receives synaptic input and forms synaptic outputs onto a subset of these peripheral interneurons (Fig. 7.6).

Of the peripheral relay neurons, the Eminens neurons provide large and numerous synaptic inputs to both left and right sides of the motor ganglion. The most extensive of these synaptic partnerships are with the first VGN interneurons and motor neuron pairs. While inputs to MN1R from Eminens1 and Eminens2 are similar in size and number, Eminens1 has far greater synaptic input to both VGN1 neurons and Eminens2 provides greater synaptic input to MN1L. Eminens2 also provides large and numerous input to ddNL. Thus, these two major peripheral relay neurons have different targets, despite being connected by putative gap junctions. Nevertheless both are bilateral and project to both motor neurons and interneurons. In addition to their chemical synaptic contacts, the Eminens neurons have putative gap junctional connections with motor ganglion neurons, which augment their potential roles alongside the chemical synaptic connections. Eminens2 has extensive putative gap junctional connections with both left and right descending decussating interneurons, despite providing synaptic input to only the left partner. This provides a mechanism by which the Eminens cell could both inhibit ddNL and activate ddNR. Eminens2 has putative gap junctions with the first and second motor

neurons on the right. For motor ganglion and tail peripheral components, Eminens1 provides synaptic input to ascending neurons AVG2, AVG3, AVG4, and AVG5, and has putative gap junctions with AVG2. AVG4 and AVG3 are also postsynaptic to Eminens2 at two contact sites each. While neither Eminens neuron provides significant chemical input to Planate neurons of the tail, both receive input from Planate1 and Planate2, and Eminens1 also has putative gap junctions with both Planate1 and Planate2 cells. The feedback from Eminens neurons to those other peripheral interneurons of the tail and motor ganglion thus occurs largely through Eminens1, and not Eminens2.

7.2.2 ATEN Networks:

Two additional groups of four ATENs extend axons ventrocaudally to the boundary of the CNS and epidermis. The first of these terminates at the level of the cell bodies of the next group of ATENs, though the neurons do not make contact with each other (Fig. 7.7). Cilia of the anterior ATENs branch and extend dorsally into two extensions of the tunic (Fig. 7.7) to the tips of left and right 'horns'. These aATEN neurons may also be neurosecretory because they contain dense core vesicles and multivesicular bodies (Fig. 7.7), as well as gonadotropin-releasing hormone, GnRH (Hamada et al., 2011). In addition to their hormonal actions, the axons and terminals of these aATEN neurons and their adjacent interneurons in the peripheral fascicle of the CNS form synapses onto the basal lamina across from each other, although not upon each other directly. Even though not made upon neurons, I will nevertheless treat these as synaptic contacts, albeit that are heterodox and without clear functional explanation. Some of the partnerships formed by these synaptic interactions are reciprocal, including those with some anterior brain vesicle peripheral interneurons (cells 20 and 29). Other interneurons, a posterior brain

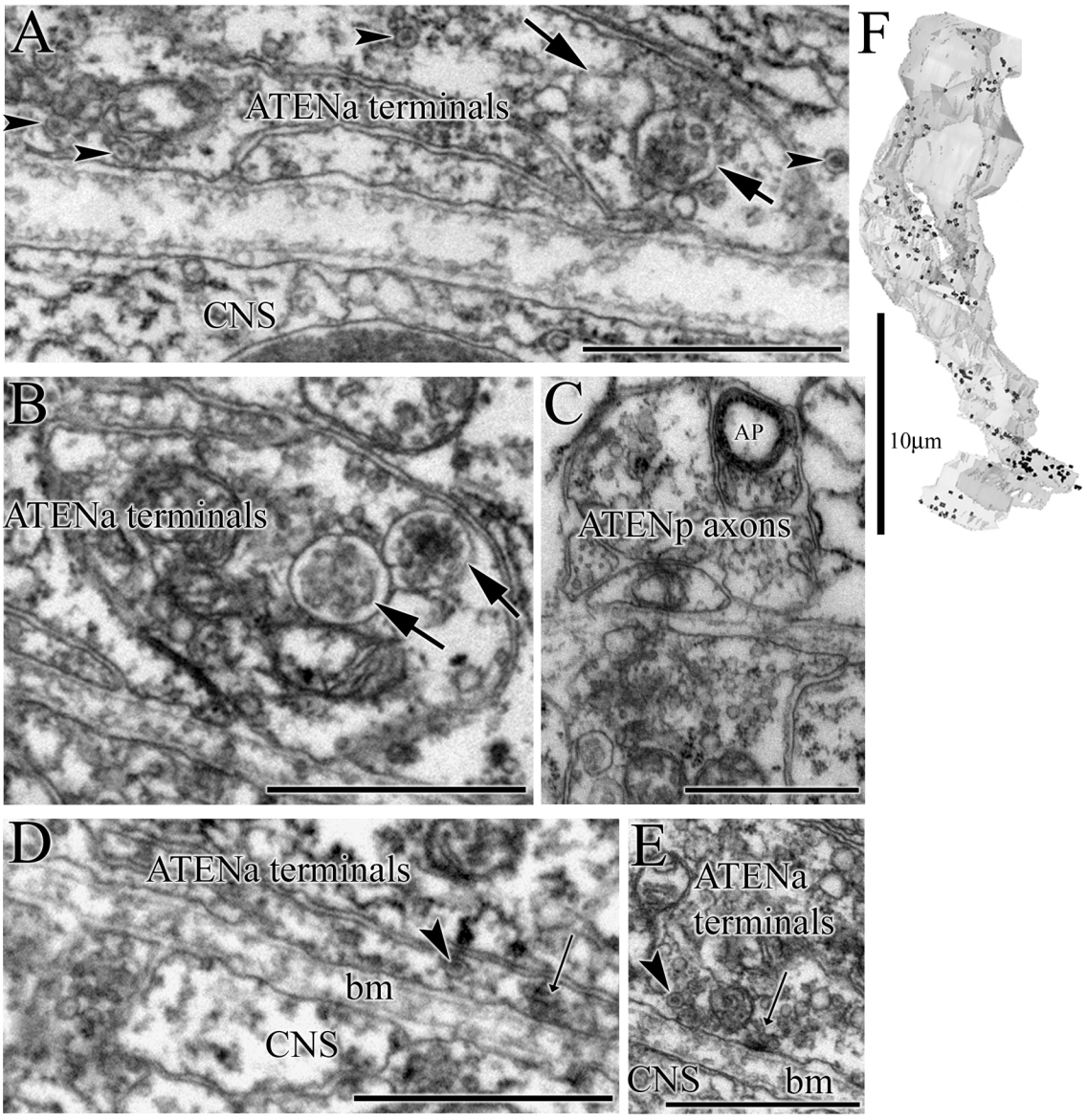

Figure 7.7. Subcellular organelles of apical trunk epidermal neurons (ATENs). A) Anterior ATEN (ATENa) axons and terminals in the epidermis overlying the CNS contain many dense core vesicles (arrowheads) and multivesicular bodies (arrows). B) Multiple multivesicular bodies (arrows) in aATEN axon. C) Putative autophagosome (AP) in ATENp axon. D-E) Dense core vesicles (arrowhead) are found near synapses of ATENa terminals (arrows) onto basement membrane (bm) opposite CNS peripheral neuropil. F) Ventral view of reconstructed ATENa neurons with puncta marking patches of dense core vesicles. Scale bars: 1µm (A-E); 10µm (F).

vesicle PN interneuron (cell 103) and the Eminens1 neuron, receive synaptic input from one ATEN, but provide input to another. In contrast, ATEN 4 forms reciprocal contacts with anterior brain vesicle peripheral interneurons (i.e. from cell 30 and to cell 6) and pna neurons (i.e. from cell pns13 and to cell pns1). Together, these connections imply a particular relationship between pna neurons and these ATENs, both directly and through feedback from interneurons (pns1, pns13, and cells 6 and 30). The anterior interneurons also feed into Eminens1 and Eminens2 by way of a weak pathway, which in turn provides only minimal synaptic input to posterior brain vesicle relay neurons, with a stronger contribution from Eminens1 than Eminens2. Putative gap junctions, however, connect Eminens neurons with photoreceptor-AVG relay neurons 116, 108, 130, and 157, multimodal relay neurons 123, 142, 105, and 130, and peripheral relay neuron 131. The second set of four ATEN neurons are located more posteriorly on the dorsal right side of the larval trunk. Their cilia emerge dorsally from basal bodies and extend into the tunic, where they converge anteriorly to extend into a single dorsal horn of the tunic. As they extend along the ventral edge of the dorsal epidermal tract to the motor ganglion the descending axons of these neurons contain expanded sections with full and empty secretory vesicles and autophagosomes. Axo-axonal synapses occur along their length between these pATEN neurons. In the motor ganglion, the basal lamina breaks down and the axons cross to embed themselves in the soma of ascending neurons of the motor ganglion (AVG5, AVG2, and AVG3) in the dorsal CNS. These pATEN neurons form presynaptic contacts in this region onto the AVG5 interneuron, the left and right CNS neurites of which project ventrally then turn rostrally and eventually terminate in the posterior brain vesicle and neck. This interneuron synapses extensively with other AVG

neurons that also ascend through the CNS neuropil. In addition, the bipolar AVG5 neuron with left and right ascending ventral neurite and descending right ventral branch, itself extends another neurite into the ATEN bundle in the epidermal axon tract. The AVG5 axon thus has additional synaptic contacts with pATENs, but also prevents direct contact between pATENs and other AVG neurons of the CNS by insulating the axon bundle. The pATEN bundle remains fasciculated and, caudally, crosses back into the epidermal tissue, where the fascicle extends further. The AVG5 neurite in question extends both rostrally to the first contact with AVG neurons and caudally. Posteriorly, the fascicle incorporates ascending DCEN neurites near the level at which the pATEN and AVG5 neurites terminate.

The aATEN neurons appear to be paired, ATEN1 with ATEN3 right and ATEN2 with ATEN4 left [one anterior one posterior on the left, one anterior one posterior on the right]. The aATEN neurons are synaptically connected among themselves, along with their output across the basal lamina to Eminens1 and other peripheral interneurons (Fig. 7.8A). ATEN1 feeds into ATEN3, both of which provide output exclusively to Eminens1 (Fig. 7.8A). ATEN4 is also presynaptic to Eminens1 across the basal lamina, but provides additional synaptic output to anterior brain vesicle interneurons, cells 6, 20 and 29 (Fig. 7.8A). ATEN2 provides input to both ATEN4 and its target ATEN1, and together ATEN2 and ATEN4 provide synaptic input to CNS interneuron 46. ATEN4 also forms synaptic contacts onto the basal lamina adjacent to the peripheral relay neuron, cell 103 (Fig. 7.8A). Thus, the right more posterior neuron with an anterior projecting cilium, ATEN1, feeds into its anterior partner with a posterior projecting cilium, ATEN3, and together these are presynaptic to Eminens1. The right posterior neuron with a

Figure 7.8. Networks of synaptic connections of anterior and posterior ATENs. A) Simplified aATEN synaptic network: RTENs (pns), brain vesicle intrinsic RTEN interneurons (BVpn), brain vesicle intrinsic interneurons (BV), aATENs (ATEN1-ATEN4), eminens1 (Em1), and peripheral relay neuron (RN103). Arrows represent direction of synaptic connections. Line thickness represents total number of 60-nm sections in which a synapse is observed (i.e. the cumulative product of synapse number and size). B) Simplified pATEN network of synapses: pATENs (pna, pnb, pnc, pnf), ascending motor ganglion peripheral interneurons (AVG1-4, AVG5), dorsal epidermal cells of the motor ganglion and tail (dEp), anteriormost dorsal caudal epidermal neuron (DCEN1).

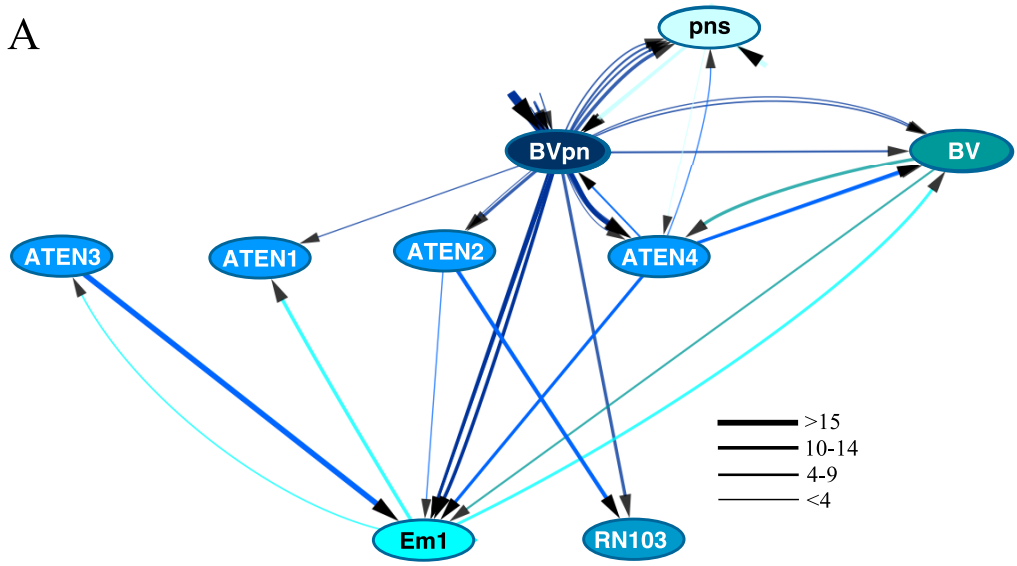
A
pns
BVpn
BV
ATEN3
ATEN1
ATEN2
ATEN4
Em1
RN103
>15
10-14
4-9
<4

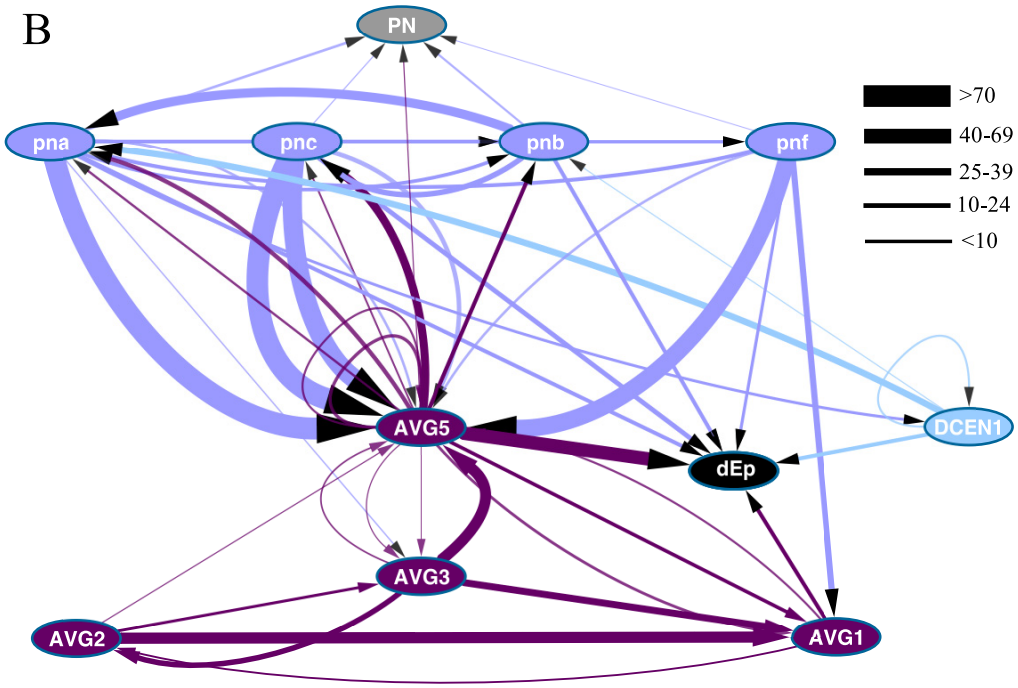
B
PN
pna
pnc
pnb
pnf
>70
40-69
25-39
10-24
<10
AVG5
DCEN1
dEp
AVG3
AVG2
AVG1

posterior projecting cilium, ATEN2, feeds into its anterior partner with an anterior projecting cilium, ATEN4, as well as ATEN1 and together both are presynaptic to anterior peripheral interneurons.

The cilia of pATEN neurons extend from cells pnf, pnb, pna, and pnc, respectively, toward the anterior. Cells pna and pnb are reciprocally connected by synaptic contacts, as are pna and pnf. However, pnb and pnf lack synaptic contact with each other (Fig. 7.8B), although pnb is the only presynaptic partner of pnc. All of these pATEN neurons provide synaptic input to AVG5 through its peripherally extending neurite, and three of these receive feedback synaptic contact from AVG5 (Fig. 7.8B). All but pnf also provide input to the soma of AVG5, where the pATEN axons lie embedded on the dorsal surface of AVG5, appearing to cross the basement membrane in the motor ganglion. Cell pna also provides synaptic input to the cell body of AVG3. Rostral to these pATEN terminals on AVG neurons of the motor ganglion, an ascending neurite from a DCEN becomes incorporated into the peripheral fascicle. The DCEN cells are paired, both members directly abutting each other rostro-caudally. The rostral cell of each pair extends a neurite anteriorly to terminate ventral to the rostral partner of the next pair of DCENs. The caudal partner extends a neurite caudally alongside the ascending neurite of the next pair, but terminates before reaching the cell bodies of that pair of DCENs (Fig. 7.9A).

Cells pna and pnb are both pre- and postsynaptic to the ascending axon of a tail dorsal caudal epidermal neuron (DCEN), DCEN1 (Fig 6.9B). The tail DCEN neurons are also interconnected by synapses, some reciprocal, as between DCEN2 and DCEN3, and some unidirectional, as from DCEN1 or DCEN5 to DCEN3 (Fig. 7.9B). Thus, while all

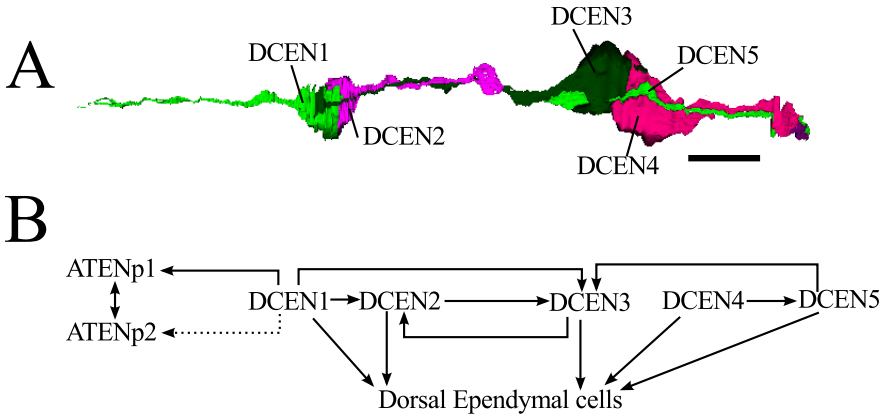

Figure 7.9. Arrangement and connections of dorsal caudal epidermal neurons (DCENs). A) Reconstruction of DCENs 1-5, illustrating overlap of axons, terminals and cell bodies, ventral view. B) Network of DCEN synaptic connections with each other, onto apical trunk epidermal neurons (ATENs) and onto basement membrane opposite dorsal ependymal cells of the tail. Arrows indicate polarity of synapse, dotted line represents synaptic connection at only a single synapse. Scale bar: 10µm (A).

pATENs provide input to the CNS via AVG5, the connections with DCENs of the tail are formed through pna and pnb.

While the dorsal location of the AVG neurons might suggest that they all receive synaptic input from the peripheral neurons, the only obvious postsynaptic partners of pATEN neurons are AVG5, and less extensively AVG3. Three parallel pathways from pATEN neurons converge upon AVG1, all of which are interconnected with each other. The first is from pATENs to AVG5 and then to AVG4 to AVG2 and to AVG1 in a serial arrangement, with additional input to AVG2 from AVG7 (Fig. 7.10). The second pathway is from pna to AVG3 to AVG6 to AVG1, also in a serial arrangement, with feedback from AVG1 to AVG6 (Fig. 7.10). Lastly, both pATENs and the pna target, AVG3, are presynaptic to AVG5, which provides direct synaptic input to AVG1. AVG2 and AVG4 are also reciprocally synaptic to AVG3, and AVG2 and AVG4 both provide synaptic input to AVG6, with feedback only from AVG6 to AVG2 (Fig. 7.10).

The pATEN targets, AVG3 and AVG5 also receive input from Eminens1, as do the AVG2 and AVG4 neurons of the first pathway. The pATEN targets, AVG3 and AVG5, receive input from other peripheral and multimodal relay interneurons, as do all AVG neurons, although sometimes at only a few synapses. Thus, all signal from the pATEN neurons is mediated through an integrated network of interneurons in the CNS (Fig. 7.10). The AVG neurons themselves have different targets in the motor ganglion. AVG5 and AVG3 provide input to the neurons of the left descending motor ganglion neuropil (Fig. 7.11A). Along with its own postsynaptic partners, AVG5 and AVG4, AVG3 provides input to MN1L, as does AVG7 (Fig. 7.11A). AVG5 provides additional input to ddR, as does the AVG5 target, AVG4, and its own target, AVG2. AVG4 is also

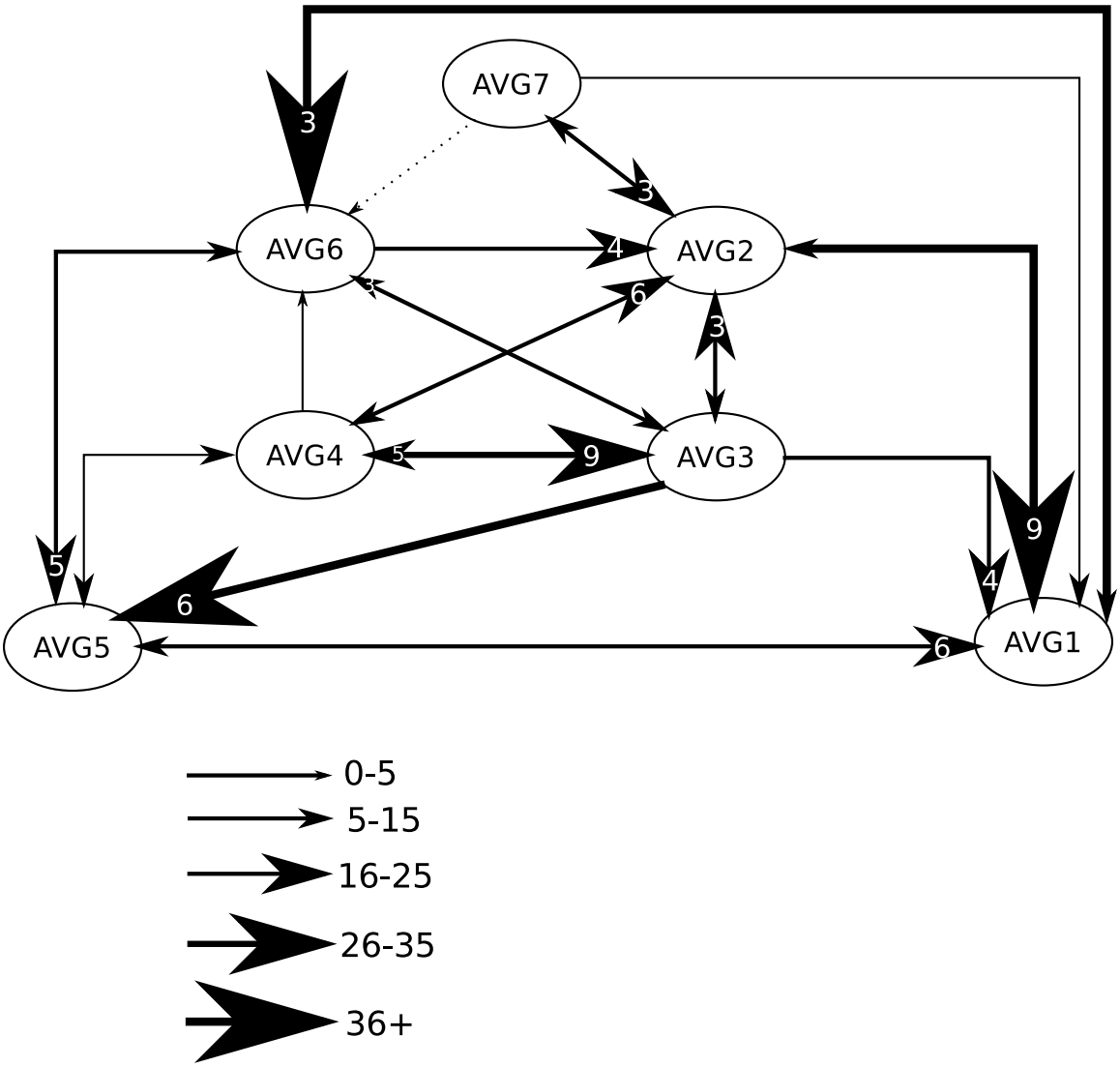

Figure 7.10. Summary of synapses between ascending motor ganglion peripheral interneurons (AVGs). Arrows represent direction of synapse, their thickness represents the number of sections in which a synapse is observed, while numbers within arrowheads indicate the number of synapses (those without a number have only a single synapse).

Figure 7.11. Total network of AVG connections to motor ganglion neurons. A) Synaptic network of AVG neurons. Dotted lines illustrate synapses between AVG neurons, solid lines illustrate synaptic connections from AVG neurons to motor ganglion interneurons and motor neurons, dashed lines indicate synapses between ventral motor ganglion neurons. B) Summary of network from both AVG and Eminens neurons to ventral motor ganglion components. Eminens inputs are shown in light blue with open triangles illustrating their putatively inhibitory synapses. AVG inputs are shown in black, with open arrows indicating putatively inhibitory inputs and solid arrows indicating putatively excitatory inputs. Synaptic connections between ventral motor ganglion components are shown, transparent lines are those connections of neurons with putative direct inhibition by AVG neurons. Neurons are as follows: excitatory ascending motor ganglion peripheral interneurons (AVG5/3, AVG4, AVG7), inhibitory ascending motor ganglion peripheral interneurons (AVG2/6, AVG3), eminens neurons (Em1 and Em2), descending decussating motor ganglion interneurons (left: ddL, right: ddR), descending paired motor ganglion interneurons (VIN1-3 L: left and R:right), motor ganglion motor neurons (MN1-5 L and R), midtail neurons (MT), asceding contralateral inhibitory neurons (ACIN1L, 2L, 2R), descending unpaired tail interneurons (PVGN1 and PVGN2), Tail18 (tail cell).

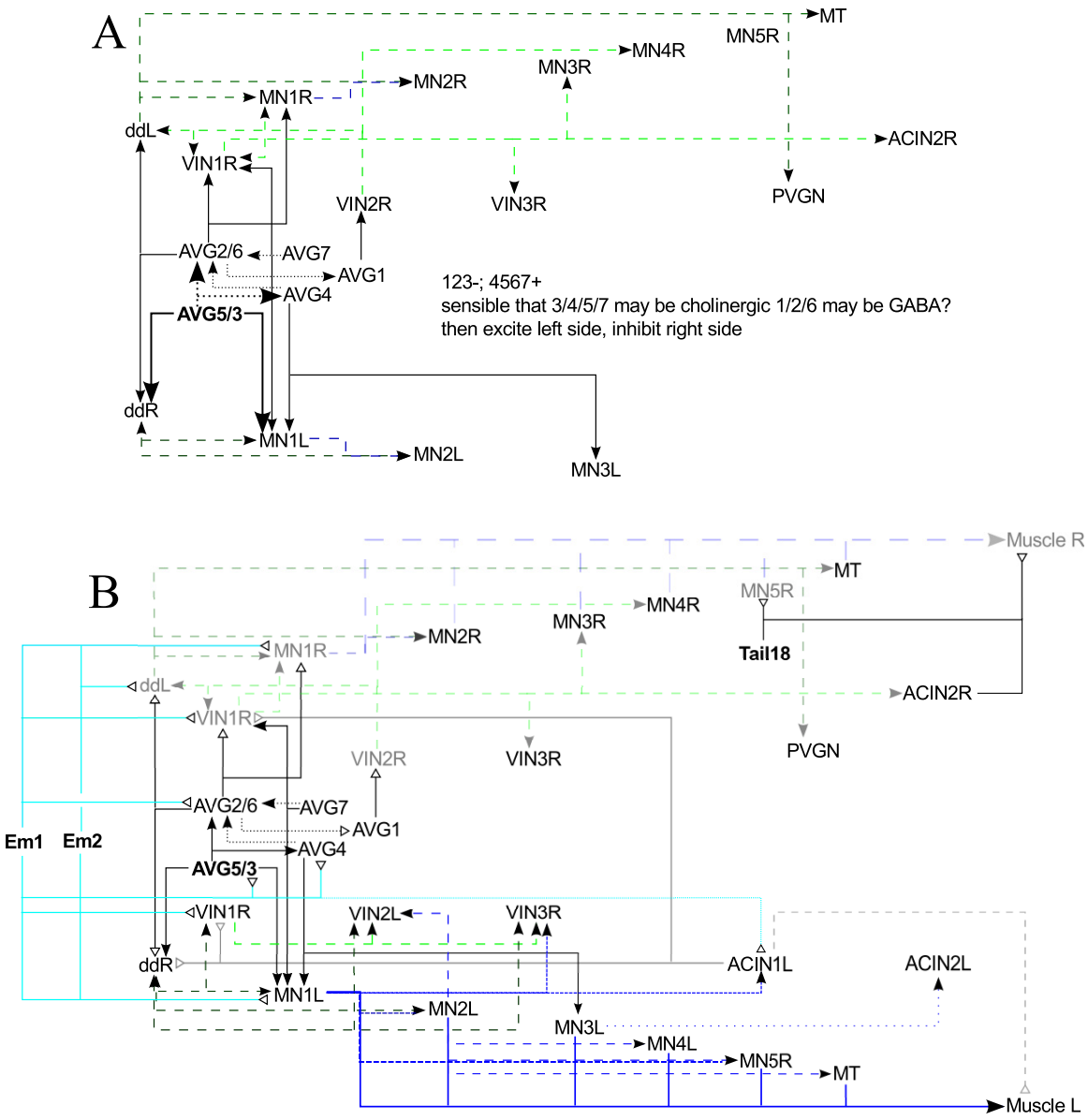
A
MT
MN5R
MN4R
MN3R
MN2R
MN1R
ddL
ACIN2R
VIN1R
PVGN
VIN2R
VIN3R
AVG2/6
AVG7
AVG1
AVG4
AVG5/3
123-; 4567+
sensible that 3/4/5/7 may be cholinergic 1/2/6 may be GABA?
then excite left side, inhibit right side
ddR
MN1L
MN2L
MN3L
B
Muscle R
MT
MN5R
MN4R
MN3R
MN2R
Tail18
MN1R
ddL
ACIN2R
VIN1R
PVGN
VIN2R
VIN3R
AVG2/6
AVG7
AVG1
Em1
Em2
AVG4
AVG5/3
VIN1R
VIN2L
VIN3R
ddR
ACIN1L
ACIN2L
MN1L
MN2L
MN3L
MN4L
MN5R
MT
Muscle L

presynaptic to ddL and MN3L. AVG4 and its downstream partners AVG2 and AVG6 provide additional synaptic input to the right-side first motor neuron (Fig. 7.11A). AVG2 is also presynaptic to the first right motor ganglion interneuron, as is its presynaptic partner, AVG7. AVG1, the ultimate target of multiple pathways from the pATENs through AVG interneurons, is unique in providing synaptic input to the second interneuron of the right side motor ganglion (Fig. 7.11A). Thus, the overall input to the motor ganglion is bilateral, however the direct input from pATEN target AVGs (3 and 5) is restricted to the left side via the right descending decussating motor ganglion interneuron and the first left side motor neuron, the former also lacking presynaptic input from inhibitory eminens neurons (Fig. 7.11B). Although AVG1, with its unique interneuron target in the right motor ganglion (VGN2), is also putatively postsynaptic to pATENs, these postsynaptic sites from pATENs are all ambiguous, occurring across the basement membrane.

7.2.3 AVG Ascending Motor Ganglion Interneurons:

The network among the AVG neurons themselves is quite complex, and functionally hard to predict, especially given the challenges in determining the precise neurotransmitter phenotypes of these cells. In general, they are highly connected. Reciprocal synaptic connections between inhibitory and excitatory subtypes exist for: AVG1 with AVG5 and AVG6; AVG2 with AVG6 and AVG4; and AVG3 with AVG4 and AVG6. Based on its GABA phenotype, AVG3 also provides synaptic inhibition from AVG5 and AVG7, which itself forms a co-inhibitory loop with AVG2. AVG7 also inhibits GABAergic AVG1. AVG7 provides putatively cholinergic synaptic input to AVG2, which inhibits AVG1. AVG7 also provides cholinergic input to AVG4 and AVG5, the former of which

also receives cholinergic input from AVG5 and provides cholinergic input to AVG6. Thus the excitatory cholinergic network forms a feed forward loop, in addition to feeding a circuit for its own inhibition. The direct peripheral synaptic input to this network is formed onto [AVG1, AVG2] AVG3, and AVG5. The most extensive pathway is onto AVG5, which extends an axon into the peripheral neuropil and forms direct synaptic contact with both ATENs and DCENs. This is also the only putatively cholinergic neuron among those directly contacting the putatively glutamatergic ATENs and DCENs. Thus, responses relating to DCEN posterior lateral line-like activity may be mediated via AVG5, whereas the inhibitory AVG1, AVG2, and AVG3 may respond to changes in the aqueous medium surrounding the rostral trunk.

Assuming that vAChT reporters identify neurons (AVG5) that are excitatory, AVG5 excites AVG4, which in turn excites AVG6. Meanwhile, AVG3, which expresses a GAD reporter, inhibits AVG5 and AVG7, and AVG1, AVG2 and AVG3 inhibit each other. AVG4, AVG5 and AVG6 provide excitatory input to AVG1, AVG2 and AVG3 and are, in turn, inhibited by these.

Some AVG neurons provide putatively excitatory input, based on their expression of a vAChT reporter, to the first pair of motor neurons, and descending decussating neurons. Of these, AVG7 is presynaptic to left neurons, and AVG5 to right side neurons. These are both postsynaptic to inhibitory Eminens2, so may differentiate between signals from the RTEN and ATEN/DCEN pathways.

Putative GABA AVGs provide widespread input within the motor ganglion to interneurons as well as motor neurons. Both AVG2 and AVG1 provide synaptic input

directly to VGN2R and MN1R, and AVG2 provides additional input to VGN1R and both ddNs. Additionally, VGN3 forms presynaptic contact upon VGN1L. Together, these putatively inhibitory connections with cholinergic motor ganglion neurons suggest a mechanism for peripheral inhibition of right-side activity in particular. It is important to note that only MN1s are directly postsynaptic to these AVGs. Thus, MN2, which is implicated in light responsive swimming, would only experience synaptic actions that lie downstream to AVG-MN1 actions. Additionally, the right-side interneurons inhibited by these AVGs are synaptic targets of antenna interneurons in the brain vesicle, so the inhibition of these interneurons by AVGs may prevent erroneous tail flicks during swimming.

Along with their connections in the motor ganglion, AVG neurons extend to the brain vesicle where they form terminals and interact synaptically with anterior neurons. In particular, a specific class of eight neurons of the brain vesicle form reciprocal synaptic connections with AVG neurons. These form a network among themselves, and also receive input from anterior PN interneurons, both directly and indirectly from photoreceptors, and from tail neurons. Thus, AVG neurons integrate mechano and chemosensory signals and photoreceptive information. There are no evident distinctions between the interactions between the AVG brain vesicle interneurons and neurotransmitter classes of AVG neurons; however, AVG2g and AVG6c receive input from most of these, whereas AVG4c and AVG5c receive minimal input and AVG3g receives none from these interneurons. In contrast, synaptic targeting of brain vesicle neurons is evenly distributed between AVG neurons.

Clustering algorithms based on all synaptic connections in the neural network group AVGs with these AVG brain vesicle interneurons and their major inputs. In particular, a large cluster includes AVG2 and AVG5 with Eminens and pns neurons and AVG interneurons along with MN1L and Planate1. Another community algorithm identifies nine communities containing AVGs. AVG1,2,3,6 and 7 are placed in a community with AVG interneurons as well as two photoreceptors, and three photoreceptor interneurons. AVG2,3,4,5,6,7 form a community with ddNs, MN1R, Planate 2,3 and 4, and a subset of AVG interneurons. In addition to predominantly AVG communities, several peripheral communities contain AVG neurons. A planate community exists wherein AVG2 and 3 are included with left side Planate neurons, MN4L, MN1R, ddNL, Eminens1, VGN1L, and interneurons including, but not limited to AVG interneurons. Another peripheral community includes AVG3 and AVG5 with Eminens2, VGN3s, MN2R, VGN1R, VGN2L, ACIN2R, PVGN, and Planate 3 and 4 as well as peripheral interneurons. Yet another community of peripheral interneurons, which includes few neurons that sparsely communicate directly with AVGs but mainly peripheral interneurons, also includes Eminens1 and Planate2. AVGs are also partial members of motor and interneuron communities of the motor ganglion, and photoreceptor interneuron communities

7.2.4 Planate Neurons:

Despite having cell bodies deep in the tail between the CNS and epidermis, four neurons from the tail extend axons as far rostrally in the CNS as the brain vesicle (Fig. 7.1). These are the planate neurons (Imai and Meinertzhagen, 2007b) and through the tail and motor ganglion their axons are paired, with two on the left and two on the right side of the larva (Fig. 7.12A,C-E). One of the right-side neurons, Plan4, has two collateral axon

Figure 7.12. Planate tail neurons in cross section at several points throughout the larva (illustrated in F). A and C) Planate profiles underlying epidermis and overlying the caudal nerve cord (CNC) in the tail shown with arrows to red (Plan 1 and 2) and blue (Plan 3 and 4) profiles. Axons of blue profiles extend caudally (A), from their cell bodies (C). B) Reconstructed planate 4 collateral axons and terminals relative to eminens cells' terminals. Continuing axon is in pink and short collateral is shown in black. Top arrow indicates collateral terminal and bottom arrow indicates collateral branch point. D and E) Paired planate axons (red and blue profiles) on the left and right sides in the CNC of the anterior tail (D) and motor ganglion (E) are separated from the tunic (Tu) by overlying epidermal cells. Axons travel along the lateral edges of the caudal nerve cord (C) and extend toward the midline in the motor ganglion (E). Axons of DCENs lie dorsal to CNC and beneath epidermal cells in the tail (C), the same position occupied by pATEN axons dorsal to the motor ganglion in the trunk (E). F) Reconstructed planate neurons with markers illustrating locations of section planes A,B,D,E. Muscle cells (Mu) and Notochord labelled for reference. Scale bars: 1µm (A-B, C, E); 10µm (D, F).

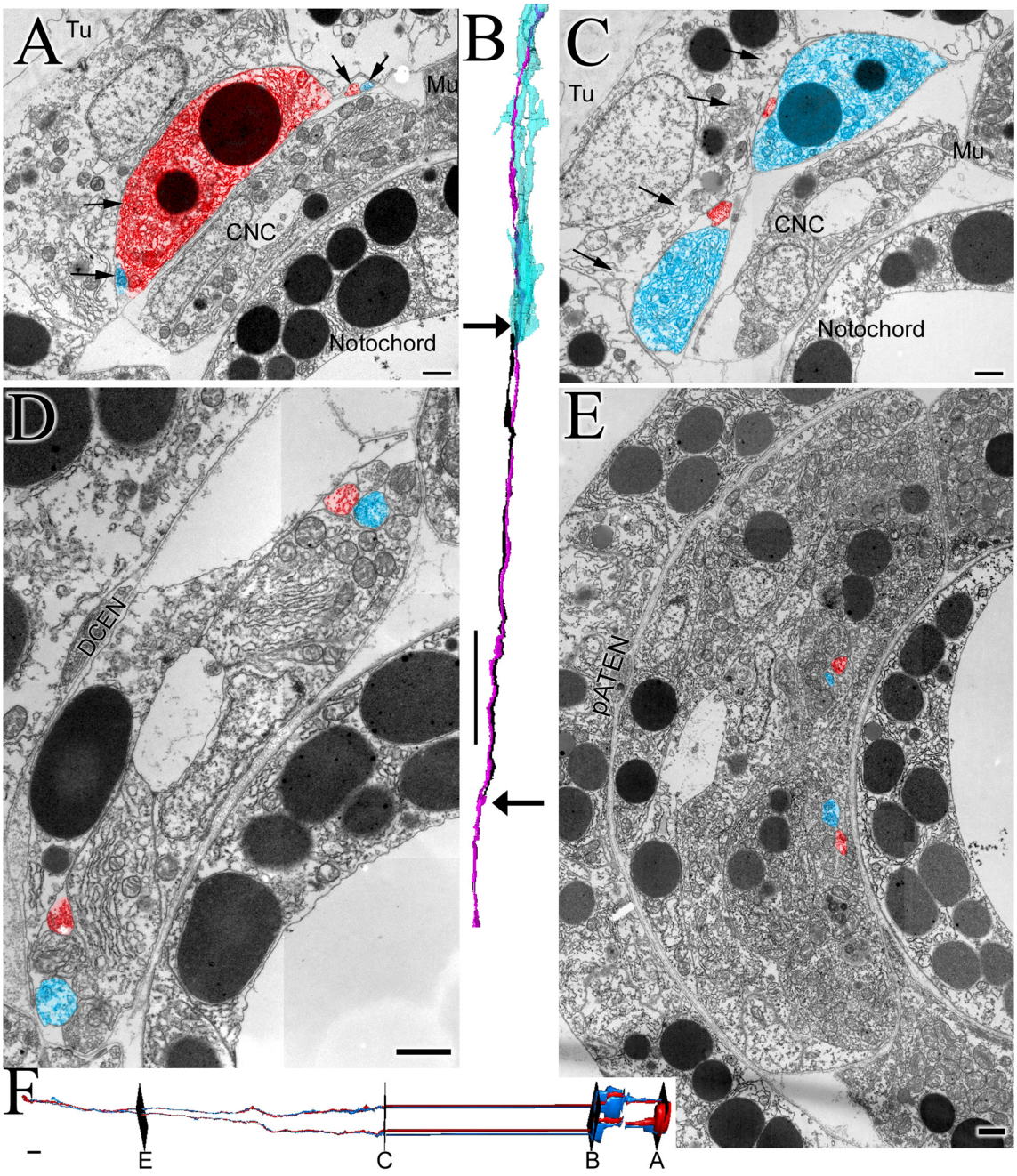
A
Tu
Mu
CNC
Notochord
B
C
Tu
Mu
CNC
Notochord
D
DCEN
E
pATEN
F
E
C
B
A

branches through the motor ganglion that split at a place where an expansion of VGN2R infiltrates their space in the proximal tail region. The second branch persists anteriorly and extends to near the terminals of the Eminens neurons (Fig. 7.12B). The remaining four planate axons, including the first from Plan4, extend further than this, up through the motor ganglion then toward the midline through the neck, where they travel alongside each other, the ascending AVG axons, and -- in the opposite direction -- the descending peripheral interneuron axons. All four planate cell axons then terminate in the brain vesicle, with one from each side, Plan1 and Plan2, extending more rostrally within the dorsal peripheral bundle. One terminal, Plan3, does not enter the peripheral bundle, but instead terminates more ventrally alongside photoreceptor terminals and the photoreceptor-AVG relay neuron axons and somata (Fig. 7.4A). The remaining axons extend within the peripheral bundle (Fig. 7.4A), all terminating at the level of the ATENa terminals, with a basal lamina separating planate axons from ATENa terminals.

7.2.5 Planate Neuron Postsynaptic Targets:

Within the tail, the targets of planate neurons are both more numerous and receive more synaptic input on the right side than on the left. Both the right-side tail interneuron, tail8 and the second ACIN on the right side receive input from both right-side planate axons. The short descending putative tail motor neurons also receive planate neuron input from Plan2 (Fig. 7.13). Likewise, Plan3 on the left side provides minimal synaptic input to the putative tail motor neuron on the left. The two posterior-most motor neurons at the trunk-tail border, MN4 and MN5, also receive some synaptic input from planate neurons on both sides (Fig. 7.13). Although these are generally few and formed by small synaptic contacts, the number of presynaptic partners, and synaptic contacts to these neurons, are

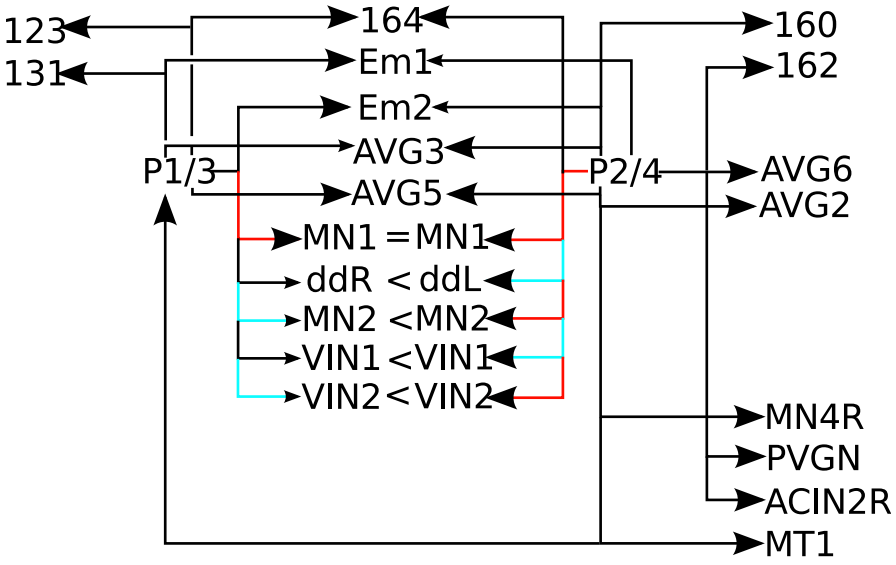

Figure 7.13. Symmetry of planate neurons' synaptic targets. Shown are: left (P1/3) and right (P2/4) planate shared postsynaptic partners (cell 164, eminens1/2, AVG3 and AVG5), inputs to paired cells (motor neurons MN1s and MN2s, decussating interneurons ddNs, and descending interneurons VIN1s, and VIN2s). Pathways reveal equal (=) or unequal (< or >) input to each partner. Partners unique to left or right side also shown. Red lines represent synaptic connections in more than 100 sections, blue lines in more than 50 sections. Arrowhead size denotes asymmetrical inputs to the same neuron from left or right planate neurons, or from left or right planate neurons to left-right neuron pairs.

likewise few and small. Their paucity and small size possibly correlate with the small number of neurons and synapses of the tail neuropil, reducing the ionic noise near the planate neurons' axon initial segments and cell bodies.

The most numerous targets of the tail planate neurons are neurons within the motor ganglion. On both sides, ddNs, motor ganglion interneurons 1 and 2, and motor neurons 1 and 2 are all postsynaptic to planate axons (Fig. 7.13). The largest and most numerous synaptic contacts occur onto the first pair of motor neurons, MN1, and are approximately the same in number (L: 48; R: 39) and size (L: 232; R: 208) on the left (L) and right (R) sides (Table 7.1). All other motor ganglion targets receive more numerous inputs from the partners of the right neuropil (ddL, MN2R, VGN1R, VGN2R) than those of the left (ddR, MN2L, VGN1L, VGN2L). Within the motor ganglion, planate axons are also presynaptic to descending brain vesicle relay neurons and ascending motor ganglion neurons (Fig. 7.13).

Aside from the motor pathway, peripheral relay neurons receive most input from planate neurons. The AVG neurons of the motor ganglion are postsynaptic to different subsets of planate neurons (Fig. 7.13). AVG3 and AVG5, which are both direct targets of ATENp neurons, are targets of all planate neurons, albeit with less input from Plan4. However, AVG2 and AVG6, which are themselves presynaptic to the right-side motor system, receive greater input from the planate axons on the right side (Plan2 and Plan4). While most feedback to planate neurons from these ascending motor ganglion peripheral interneurons comprises only single, small synaptic contacts, AVG5 provides numerous synaptic contacts to both Plan3 and Plan4.

Table 7.1. Planate tail neuron presynaptic inputs to motor neurons of the motor ganglion. Preynapstic planate partnership onto each motor neuron given with corresponding number of synapses and size of total synapses (total number of sections with synaptic profile) from each planate neuron (indicating left (L) or right (R)). Total number of synapses from all planate neurons to each motor neuron also given (Total).

Postsynaptic motor neuron identity	Preynapstic Planate partners	Number of synapses	Total number of sections with synaptic profile
MN1 Left	Plan1 (L)	27	134
	Plan3 (L)	21	88
	Total	**48**	**222**
MN1 Right	Plan1 (L)	3	14
	Plan2 (R)	22	94
	Plan3 (L)	1	4
	Plan4 (R)	11	55
	Total	**37**	**167**
MN2 Left	Plan1 (L)	10	51
	Plan3 (L)	6	30
	Total	**16**	**81**
MN2 Right	Plan2 (R)	17	90
	Plan4 (R)	10	73
	Total	**27**	**163**
MN3 Left	Plan1 (L)	1	2
	Total	**1**	**2**
MN4 Left	Plan1 (L)	2	9
	Total	**2**	**9**
MN4 Right	Plan2 (R)	2	5
	Plan4 (R)	1	2
	Total	**3**	**7**
MN5 Left	Plan1 (L)	1	3
	Total	**1**	**3**
MN5 Right	Plan4 (R)	1	3
	Total	**1**	**3**

The most prominent peripheral relay neurons, Eminens1 and Eminens2, are both postsynaptic targets of planate neurons (Fig. 7.13). While Eminens1 receives some synaptic input from all planate neurons, Eminens2 receives input from only Plan1, Plan2, and Plan3 (Fig. 7.14). Plan1 and Plan2, which are presynaptic to Eminens neurons both at their terminals in the motor ganglion and to their axons and cell bodies in the neck and brain vesicle, provide greater input to Eminens neurons than Plan3 and Plan4, which provide input only to Eminens terminals in the motor ganglion (Fig. 7.14B). Like planate neurons, Eminens2 and Eminens1 both provide input to left and right partners of the first pair of interneurons and MN1 of the motor ganglion (Fig. 7.6A). The Eminens neurons are also presynaptic to their own planate cell partners (Fig. 7.14A). In addition to the Eminens interneurons, planate neurons provide presynaptic input to another peripheral relay neuron, cell 131, and photoreceptor-peripheral relay neurons 123 and 157 (Fig. 7.13). Plan1 provides synaptic input to neuron 131 and Plan1 and Plan2 provide synaptic input to neuron 157. Plan3, which terminates alongside photoreceptor-peripheral interneurons and photoreceptor terminals, is presynaptic to neuron 123 at seven sites that span in excess of a single section. In addition to relay neurons, the posterior brain vesicle intrinsic peripheral interneurons are postsynaptic targets of planate neurons. Cells 160, 162, 163 and 164 all receive many inputs from planate neurons. These form a connected network among themselves and feed into peripheral relay neurons, including photoreceptor-AVG relay neurons and Eminens, as well as into ascending AVG neurons themselves (Fig. 7.15).

7.3 **Discussion**

Neurons of the PNS reported here have mostly been seen from light microscopy of larvae

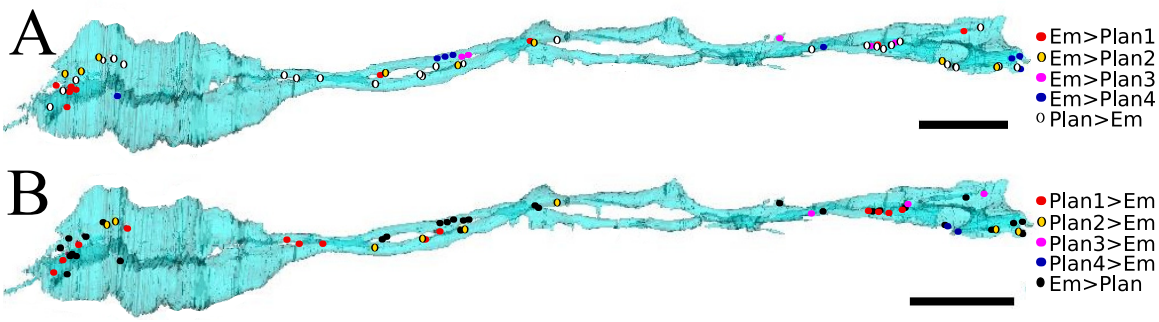

Figure 7.14. Eminens neurons' synaptic contacts with tail planate neurons. A) Reconstructed eminens neurons with puncta representing synaptic contacts onto planate neurons, colour-coded by the particular postsynaptic partner (key). Occasional postsynaptic contact sites shown in white. B) Reconstructed eminens neurons with puncta representing postsynaptic contacts from planate neurons, coloured by presynaptic partner. Presynaptic sites which receive contacts from planate neurons shown in black. Dorsal views. Scale bars: 10µm.

Figure 7.15. Neural network of posterior brain vesicle intrinsic peripheral interneurons (BVINs). A) Complete network of synaptic connections illustrating pre- and postsynaptic contacts from posterior BV intrinsic peripheral interneurons. Line widths represent synaptic strength as indicated by the number of 60-nm sections in which synapses are observed, colour-coded for the presynaptic neuron; arrows represent direction of synapse. B) Schematic diagram of synaptic network in A, by cell type. Input from all anterior peripheral components, interneurons and tail planate neurons is ubiquitous. Postsynaptic partners include relay neurons of all sensory modalities as well as photoreceptors, photoreceptor tract interneurons, and ascending motor ganglion peripheral interneurons. Lines are colour-coded only by the presynaptic partner and not the pathway strength.

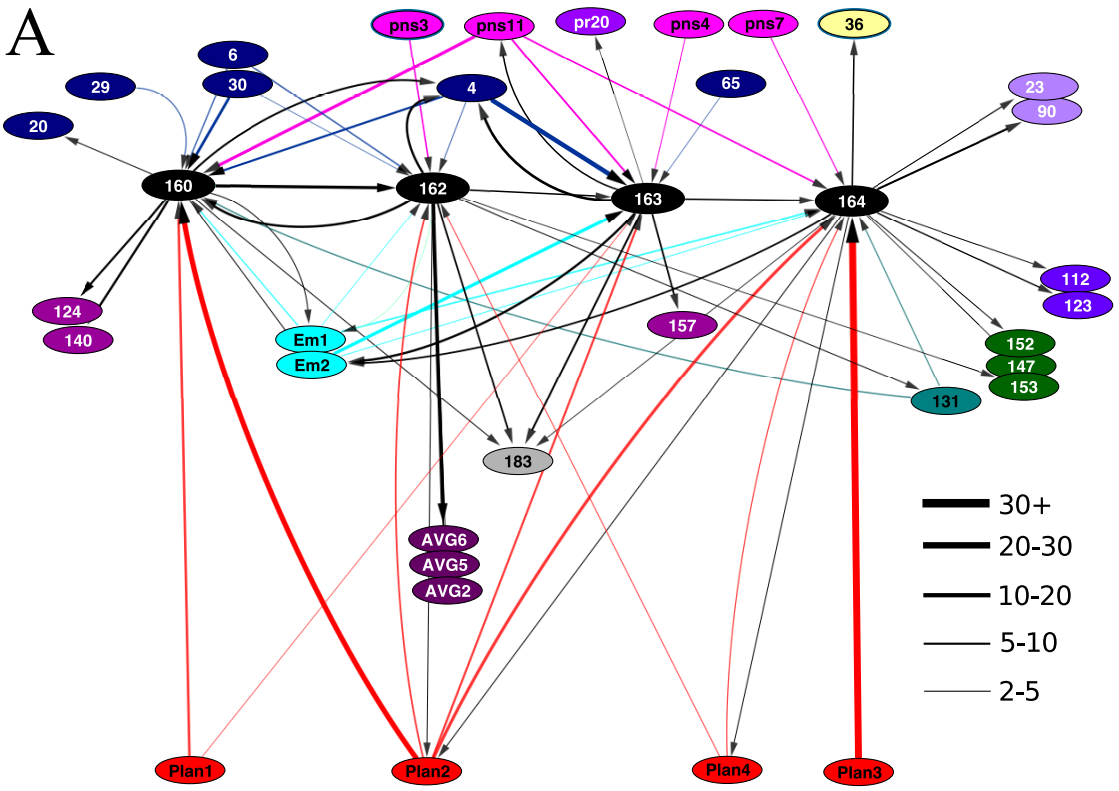
A
pns3
pns11
pr20
pns4
pns7
36
6
30
29
4
65
23
90
20
160
162
163
164
124
140
Em1
Em2
157
112
123
152
147
153
131
183
AVG6
AVG5
AVG2
30+
20-30
10-20
5-10
2-5
Plan1
Plan2
Plan4
Plan3

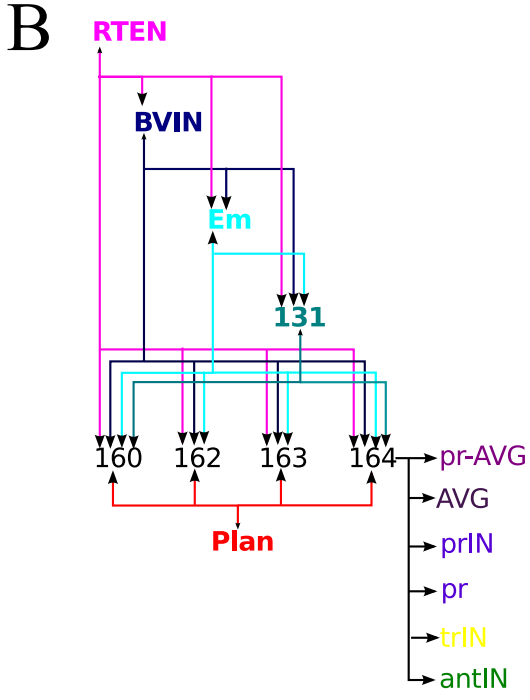
B
RTEN
BVIN
Em
131
160
162
163
164
Plan
pr-AVG
AVG
prIN
pr
trIN
antIN

by means of reporter constructs that highlight individual neuron types. These are far more sparse than the same studies of the CNS, and therefore more successful in revealing the extent of neuronal morphologies. While some of their central interneurons have been previously reported, some have not and are therefore novel in this study. More than this, the network of synaptic connections of peripheral neurons and their targets within the CNS are now revealed through detailed ultrastructural analysis (Fig. 7.16).

7.3.1 Synaptic Features of the PNS Pathways:

The synaptic features of the PNS pathway incorporate elements that are seen in other regions of the larval nervous system, and that are certainly no less complex. One additional feature is provided by an arrangement in which presynaptic terminals of ATENs abut the basal lamina of the CNS, opposite which lie the axons of several types of peripheral interneurons. This arrangement is noteworthy but without clear explanation. Although the synaptic cleft between motor neuron terminals and muscle cells are well-known to incorporate a basal lamina (Sanes et al., 1978), there has been little consideration of synapses elsewhere that similarly incorporate a basal lamina between their pre- and postsynaptic neurons. A review on basement membranes presented by Paulsson (2008) highlights their importance in directing and influencing cell behaviour, but does little to illuminate the role of presynaptic sites in larval *Ciona* that form upon a basal lamina.

These sites are interpreted here as supporting synaptic transmission, and are reciprocated at similar sites where aATENs are postsynaptic. These features are similar to those of

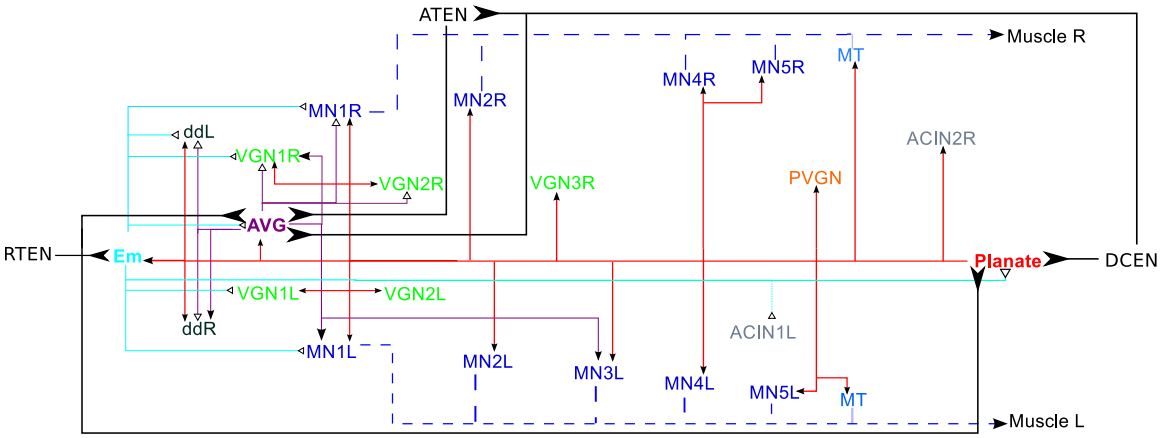

Figure 7.16. Diagram showing peripheral synaptic inputs to three main interneuron cell classes, eminens (Em), ascending motor ganglion interneurons (AVGs), and bipolar planate neurons of the tail (Plan). Peripheral neuron input shown in black, interneuron synapses to motor ganglion and tail neurons in solid lines (coloured by cell type) and synaptic contacts from motor neurons to muscle in dashed lines. Cell types: RTEN (rostral trunk epidermal neurons), ATEN (apical trunk epidermal neurons), DCEN (dorsal caudal epidermal neurons), AVG (ascending motor ganglion peripheral interneurons), Em (eminens neurons), Planate (Planate tail neurons), MN (motor neurons), ddL/ddR (descending decussating left/right motor ganglion interneurons), VGN (descending motor ganglion interneurons), ACIN (ascending contralateral inhibitory neurons), PVGN (posterior unpaired descending MG interneuron), Tail18 (tail interneuron), MT (descending paired mid-tail neurons).

pATEN, DCEN and VCEN neurons which also have a presynaptic site abutting the basal lamina but with no clear neuron opposite. These instances find very few parallels in the organization of synapses in other nervous systems. Most obvious is the neuromuscular junction, at which motor neuron terminals are separated from the muscle postsynaptic membrane by a basal lamina (Sanes et al., 1978) which is protein studded with extracellular matrix (ECM) proteins including laminins, and has signalling properties (Sanes, 2003). In addition, in the echinoderm nervous system presynaptic sites in neurons of ectoneural nerves abut hyponeural motor axons with a 40-nm basal lamina between the two (Cobb and Pentreath, 1976) across which neurotransmitter is proposed to diffuse. In the case of *Ciona*, given that the larval nervous system must undergo constant remodelling during its short life, such synapses could possibly represent the existence of synaptic sites that are regressing, prior to metamorphosis.

7.3.2 Comparisons with the Vertebrate Lateralis System:

Epidermal neurons of the larval PNS are widely presumed to play a very similar role to the vertebrate lateralis system, in detecting water displacements. A lateral line organ consists of one or more neuromasts, each containing several mechanosensory hair cells, along with mantle and support cells (Blaxter, 1987). Each hair cell possesses a single long 9+2 kinocilium and multiple microvilli, called stereocilia, that extend into the canal or surrounding liquid (Harris et al., 2003). These hair cells lack axons themselves, but provide synaptic input to afferent axons of the PNS and receive efferent input from peripheral neurons. This arrangement is that of a secondary hair cell. Neuromast organs in the lateral line systems of many aquatic vertebrates detect pressure changes and movement in the water surrounding the animal as part of the lateralis system of tactile

sense organs (Dijkgraaf, 1962). These sense organs are arranged in rows in either lateral line canals or as pit organs on the surface of the epidermis. Cyclostomes and hagfish have only the latter, suggesting that surface mechanosensory lateral line organs were the likely ancestral form. The absence of placodes and secondary sensory cells has been used to suggest that urochordates lack any ancestral lateral line system (Braun and Northcutt, 1997). In fact, there are related receptors in adult ascidians. In addition to hydrodynamic sense organs based on primary sensory neurons in the cupular organs of the adult atrial cavity, ascidians also have coronal sense organs of the oral siphon, a secondary mechanoreceptor based on anaxonal hair cells resembling those of the vertebrate acoustico-lateralis system (Burighel et al., 2003; Mackie and Burighel, 2005). Furthermore, recent work in *Ciona* has identified a proto-placodal ectodermal region containing, in the larva, ATENa (aATEN) neurons that express GnRH and are likely both chemosensory and neurosecretory (Abitua et al., 2015). As our data suggest in other sensory systems, PNS neurons of *Ciona* exhibit properties of multipotent or multifunctional progenitors, in which individual cells or cell types undertake the multiple roles designated to specific neurons or neuronal types in vertebrates.

Do secondary hair cells exist in the ascidian larva? Apparently not. The sensory cells of the *Ciona* larva bear axons and are in most cases presynaptic to CNS neurons. However, the apparent lack of anaxonal sensory cells could simply be based upon the small size and small number of cells of the ascidian larva. For example, it is possible that in vertebrates the axons of sensory cells were lost as animals grew and their energetic requirements necessitated a division between sensory and relay roles of neurons and the development of secondary sensory cells. This of course does not necessarily preclude a similar

functional or developmental origin of a system that functioned to coordinate mechanosensory signals and transmit these to the motor centre. In fact, the ATENa peripheral neurons that are located in the proposed stomodeal placodal region of the larva have only short axons, and these do not cross the basal lamina, but instead form presynaptic sites onto the basal lamina across from central neurons. Although these are supposedly neurosecretory, and do possess dense core vesicles, their synapses at these sites contain clear core vesicles, and the neurons appear to express reporters for glutamate (Horie et al., 2008a; see Ryan, 2015: Chapter 4). These cells also extend 9+2 cilia alongside multiple microvilli at their anterior contacts with the surface of the animal. Thus, ATENa neurons are both sensory and bear axons that are likely both presynaptic to CNS neurons, albeit across the basal lamina, and receive only feedback synapses from other ATENa neurons, so are in no sense secondary. In contrast, the ATENp neurons caudal to these also have microvilli surrounding their cilia, and although these extend axons toward the tail, they function in a sense as both primary and secondary sensory neurons, forming afferent and efferent synaptic contacts with tail DCENs, which themselves lack direct contact with the CNS. ATENp neurons are sensory, and provide direct input to the CNS, but are also secondary to sensory neurons of the tail, effectively functioning as both primary and secondary sensory neurons. Furthermore, while most of the identified peripheral neurons possess axons, investigation of the peripheral neuropil reveals the existence of synapses both between these axons themselves, and with the epidermal cell bodies they contact. Many of these cell bodies have obvious microvilli or short dendritic extensions from their surfaces, but although they have basal bodies, no emergent cilia are found at this stage of development. The bipolar planate axons also

contact the DCEN neuron axons, so also act as secondary sensory neurons of the peripheral system. These ascending tail planate neurons do not contact the external surface or possess cilia, despite having extramedullary cell bodies residing outside of the CNS, beneath the epidermal tissue. However, their synaptic connections and developmental signalling pathways suggest that these bipolar tail neurons (here called planate neurons) are homologous to dorsal root ganglia (Stolfi et al., in press: Appendix), which may indicate that although they function as peripheral relay neurons, they may also be sensory themselves.

7.3.3 Ascending Motor Ganglion Neurons share similarities with Rohon-Beard Neurons: The location and projection of the ascending motor ganglion neurons (AVGs) is similar to those of Rohon-Beard neurons of fish and amphibians. Cell bodies of Rohon-Beard neurons are located in the spinal cord dorsal to motor neurons (Roberts and Clarke, 1982), extending peripheral neurites into the skin and caudal neurites to the hindbrain (Bernhardt et al., 1990). This projection pattern is mirrored by AVG neurons, particularly AVG5, which extends both a dorsal peripheral neurite to contact peripheral neurons and a ventrocaudally projecting axon to the ventral motor ganglion and through the neck to the posterior brain vesicle. These Rohon-Beard neurons are sensory, and convey sensitivity to touch (Clarke et al., 1984) that leads to activation of many bilateral pairs of reticulospinal neurons, including the Mauthner cells (Gahtan et al., 2002). In *Ciona* AVGs receive peripheral neural input directly from mechanosensory pATENs and are presynaptic to both interneurons and motor neurons of the motor ganglion, including putative Mauthner-like cells.

Unlike planate neurons and dorsal root ganglion (DRG) neurons, neither Rohon-Beard, nor AVG neurons are extramedullary. Despite their shared anatomical features, individual Rohon-Beard cells and AVG neurons differ in their exact neurite projections and dorsoventral depth from the surface of the neural tube (Roberts and Clarke, 1982). In *Ciona* AVGs do not all extend peripheral axons, and are not all secondary sensory neurons, although some lacking peripheral neurites still receive input directly to their cell bodies. Rohon-Beard neurons are embryonic, and in most species undergo apoptosis after a few days, when dorsal root ganglion neurons extend their axons into similar regions as the degenerating Rohon-Beard cells (Reyes et al., 2004), although Rohon-Beard cell degeneration is not DRG neurons and AVGs like Rohon-Beard cels, planate bipolar and AVG neurons coexist in *Ciona*, even forming synaptic connections, representing a significant difference from vertebrate peripheral interneurons. The lifespan of the AVGs is not known in the ascidian larva, but TUNEL staining is not evident anywhere until 12 hours post-hatching (Cole and Meinertzhagen, 2004), and even this is limited to mesenchyme, and TUNEL staining is not seen in the CNS until shortly before settlement at 22 hours post-fertilization (Tarallo and Sordino, 2004).

7.3.4 Planate Neurons and their Relationships to other Peripheral Interneurons:

The right-sidedness of planate input to AVG2 and AVG6, combined with the sidedness of these targets, raises the question of whether there is an inherent sidedness in the signals generated by these tail neurons that must be conserved in their transmission to the right-sided motor neuron network of the motor ganglion. The inhibition of these neurons by planate neurons of the same side may allow signals from the tail to override those of the

trunk and head on the right side. However, there is additional input to left side targets, AVG3 and AVG5, from both left and right planate neurons. These targets also receive direct input from peripheral neurons, unlike their right-side counterparts. The feedback from the putatively cholinergic AVG5 to Plan3 and Plan4 is significant because AVG5 is the interneuron with the greatest input from both ATENp and DCEN neurons to its peripheral dendrite. Thus, these two planate neurons, one on each side, may be activated both directly and indirectly by peripheral neurons, allowing them distinct roles in signalling and integrating sensory information from those of the other planate neurons. Given that AVG5 provides putative excitatory input to the left motor network, its potential excitation of these potential inhibitory neurons may allow feed forward inhibition of both sides' motor networks. Of course, acetylcholine may function not only during excitation at nicotinic receptors, but also as an inhibitory neurotransmitter at muscarinic receptors (Purves, 1976). Even though the *Ciona intestinalis* genome contains a gene for muscarinic cholinoceptors (Dehal et al., 2002), expression data are currently unavailable to address this particular issue.

The putative GABA phenotype of planate neurons, as well as their peripheral relay neuron targets, eminens, and a subset of the ascending motor ganglion neurons, details a mechanism of subtractive inhibition. Planate neurons, when active, could inhibit the inhibition of the motor network from the anterior peripheral network. Likewise, Eminens neurons are presynaptic to planate neurons, so when active, would inhibit the ascending inhibition of the motor network from the tail, reducing the inhibition on motor neurons and facilitating excitation by putatively excitatory AVG MG neurons downstream of the same anterior peripheral network, but integrated with photoreceptor and antenna relay

pathways. Thus, the activity of either tail mechanosensory DCENs or head mechanosensory RTENs should be independent, allowing for more precise input to the motor pathway components.

7.3.5 Behaviour and Peripheral Integration:

Early observations of ascidian larval behaviour imply a role for chemo- and mechanosensation in larval settlement (Svane and Young, 1989), but compared with other sensory systems there are no substantial claims for the role of the peripheral nervous system in earlier phases of larval life. Apart from these instances, the very considerable network complexity of the PNS suggests a considerable processing depth, and scope for larval behaviour that remains largely unexplored, but supports a role for peripheral sensory information processing to the motor network.

Laboratory observations of larval behaviour in response to touch (Brown, pers. comm.) provide further insights when integrated together with the anatomical network information reported here (Fig. 7.16; Fig. 7.17). RTENs reside in the anterior portion of the *Ciona intestinalis* larva and provide putative glutamate-based input to the peripheral network of the brain vesicle, which is predicted to be excitatory (Fig. 7.16). When larvae are touched at the anterior of the trunk they cease swimming however (Brown, pers. comm.; Horie, pers. comm.; Fig. 7.17). The extensive putatively GABAergic input to the motor system from the ultimate brain vesicle target relay neurons, Eminens 1 and 2, provides a possible basis for this inhibition. Along with direct peripheral input to the Eminens cells, the feed-forward signals from other peripheral brain vesicle interneuron targets are putatively excitatory as well. This putative excitatory glutamatergic signalling to the Eminens cells originates from the RTENs and their target interneurons. Putative

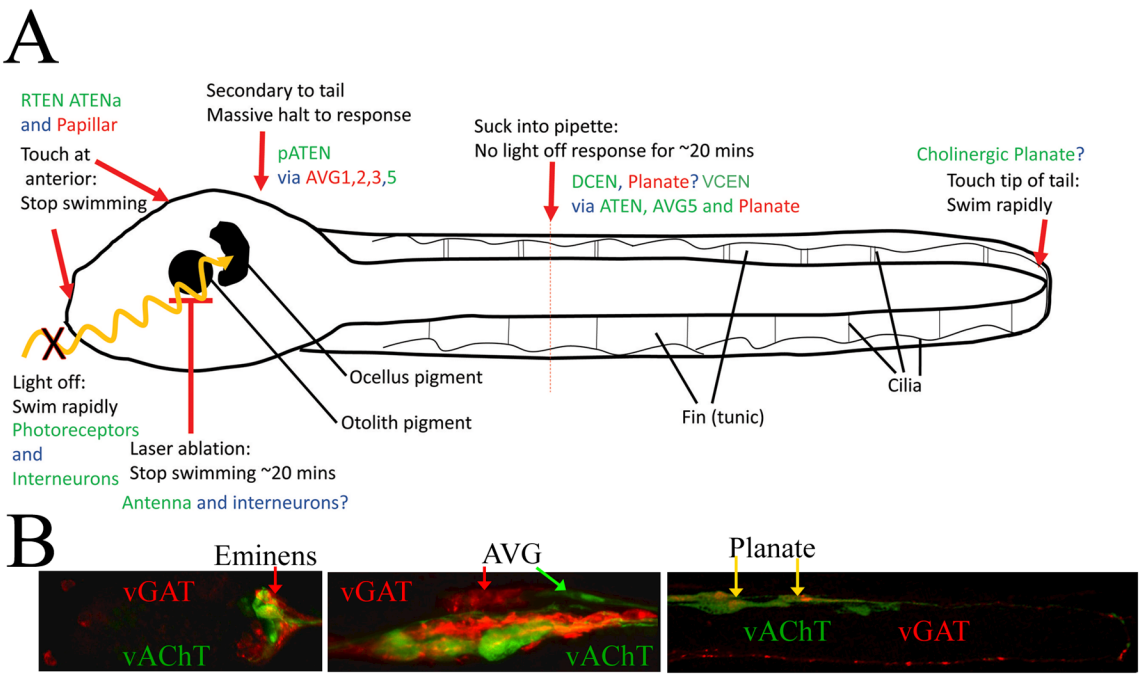

Figure 7.17. Summary of behavioural responses observed after stimulating the tadpole larva of *Ciona intestinalis* through different sensory modalities, illustrating candidate neurons and pathways involved. A) Schematic view illustrating stimuli targeted to specific places on, or pathways in, the larva (arrows), with corresponding primary neurons acting via second-order neurons that are qualified to mediate each response. Neuron names in green indicate putative excitatory neurons, and in red putative inhibitory neurons. B) Confocal images from Dr. Takeo Horie (2010) illustrating putative neurotransmitter phenotype of second-order peripheral interneurons of *Ciona* using anti-VGAT (vesicular GABA/glycine transporter) antibody and a promoter driven GFP reporter construct for vAChT (vesicular acetylcholine transporter). Note that Eminens neurons appear to be vGAT positive, suggesting an inhibitory GABA or glycinergic phenotype, while individual AVG neurons label for either vAChT reporter or vGAT antibody, and Planate neurons appear to co-express both vAChT reporter and vGAT antibody.

GABA signalling from papillar neurons is later likely to inhibit movement through anterior synaptic contacts onto RTEN neurons themselves, once an appropriate substrate for settlement is found.

When larval tails are sucked into a pipette to immobilize them, the larva responds to light only after a period of approximately 15-20 minutes (Zega et al., 2006; Fig. 7.17). The peripheral neurons of the tail, DCENs and VCENs, bear cilia that extend to the fin surface, and are putatively glutamatergic. The DCENs are synaptically connected, and the anterior DCENs are direct synaptic partners of the pATENs (and their target, AVG5). pATENs are also putatively excitatory glutamatergic neurons, and their target, AVG5, is putatively cholinergic, so also most likely to be excitatory. The targets of AVG5 include the first pair of motor neurons and the descending decussating interneuron on the right side. This excitation of the motor system would be inconsistent with the inhibition of responses to light, and relies on integration of more anterior trunk signals with those of the tail. It instead seems more likely therefore that the signal would be facilitated by the ascending planate neurons of the tail, which also contact DCENs. The planate neurons are also synaptic targets of AVG5. These neurons are putatively GABAergic, and provide widespread synaptic input to the neurons of the motor ganglion, particularly the descending decussating interneurons, and the two anterior pairs of both motor neurons and interneurons. The target motor ganglion components are the main targets of descending sensory relay neurons from the brain vesicle, and initiate swimming in response to other sensory stimuli (see Ryan, 2015: Chapter 9). It therefore seems most likely that inhibition caused by the persistent stimulation caused by drawing the tail into a pipette results from activity of the tail planate neurons.

While the planate neurons may account for the inhibitory response from tail stimulation, touching the posterior trunk also halts swimming, inconsistent with AVG5 activity, which is putatively excitatory. Although AVG5 receives direct synaptic input from pATEN neurons, it is also a synaptic target of other AVG neurons, with strong synaptic input from both AVG3 and AVG6, more than 15% of the synaptic output from each. AVG3 itself receives pATEN input, and appears to correspond to a neuron expressing a Ci-GAD reporter (Takamura et al., 2010). Along with AVG5, this putatively inhibitory neuron's other main synaptic targets include the ultimate AVG pathway target, AVG1, Eminens neurons, planate neurons, and MN1L. AVG3 also has many presynaptic sites adjacent to the basement membrane from both its dorsal cell body and ventral axon. Dorsally, these synapses are near the pATENs, and ventrally the presynaptic sites are near the anterior most dorsal muscle. Reporters for GlyR, but not GABA-specific receptors are expressed on anterior muscle cells, so it is unclear whether these synapses may have direct effects on nearby muscle, or only act through the other ventral neurons of the motor ganglion.

In contrast to the inhibitory response to mid-tail and posterior trunk contact, touching the tip of the tail results in fast swimming of the larva (Brown, pers. comm.; Horie, pers. comm; Fig. 7.17). This response would have to be mediated by mechanosensory structures in the posterior-most fin. Transmission electron microscopic images of the tail fin reveal a structure resembling a disorganized cilium (Fig. 7.18) similar to those seen elsewhere in the larva (Fig. 7.2). At the tip of the tail, *Ci-VGLUT* reporter and in situ hybridization expression is also apparent, consistent with an excitatory phenotype (Horie et al., 2008a). Thus, the signal to the motor system from this neuron should be sign-

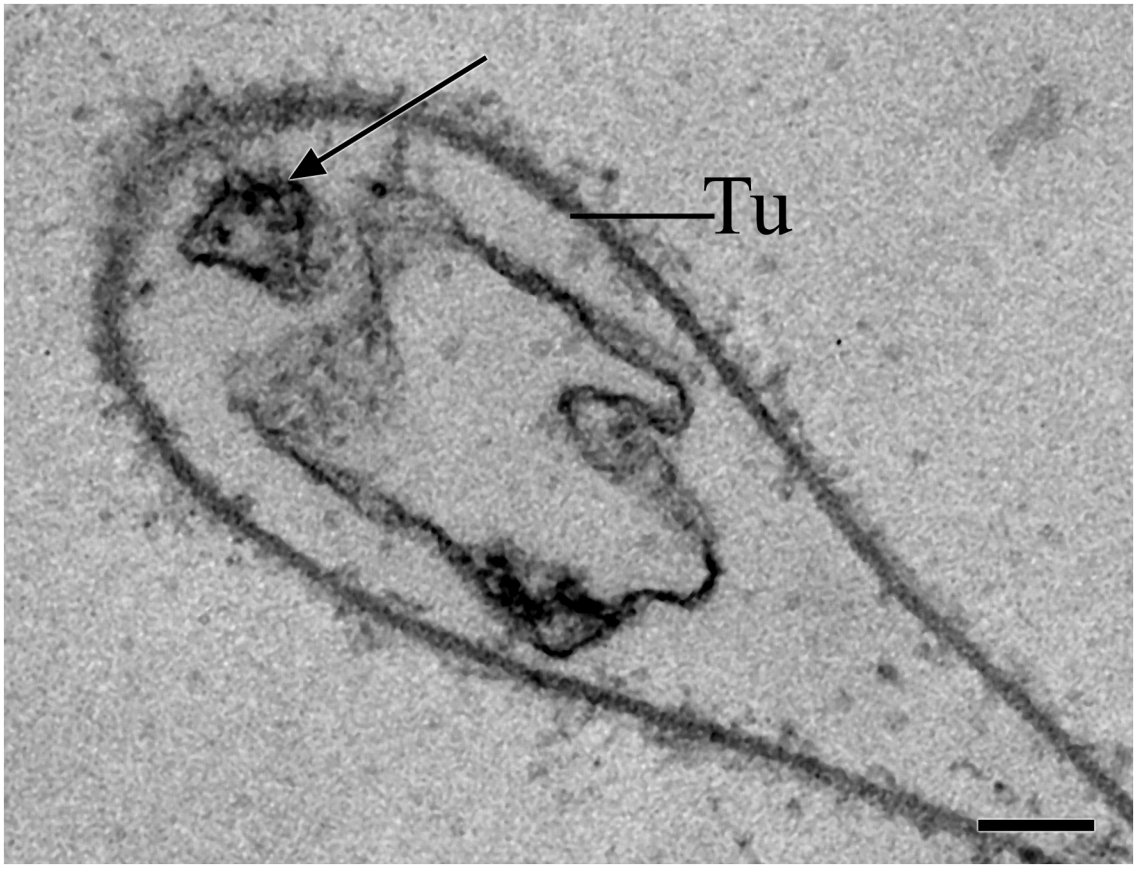

Figure 7.18. Transmission electron micrograph of tunic (Tu) at the tip of the tail of *Ciona* intestinalis larva, containing disorganized array of microtubules resembling the distal portion of a cilium (arrow). Scale bar: 100nm.

conserving. Along with the putative GABAergic neurons of the tail, an axon of a VGLUT positive neuron also appears to extend into the CNS toward the brain vesicle (Horie et al., 2008a), corresponding to the location of a planate neuron and its axon. Thus, these tail cells, both apparently planate neurons, may have different neurotransmitters. However, the interneuron targets of planate neurons do not differ from each other, except by side. Another possibility arises from recent findings that in vertebrate neurons GABA and glutamate are co-released (Noh et al., 2010; Beltrán and Gutiérrez, 2012; Shabel et al., 2014). Unfortunately, this possibility cannot be directly addressed at present because co-reporter studies in *Ciona* are lacking for GABA and glutamate. What is evident from both reporter and antibody studies is that GABA and glutamate are both expressed in cells that possess the unique properties of these tail planate neurons, so their synaptic connections cannot be treated as exclusively inhibitory or excitatory in nature. Further, a bipolar tail neuron also appears to express a reporter for Ci-VACHT (Horie et al., 2010). Although the cell bodies of planate neurons are outside the CNS they lack cilia, and receive synaptic input from DCENs. At least one of these neurons, however, wraps around the tip of the tail (Imai and Meinertzhagen, 2007b; Stolfi et al., in press), and may be a primary sensory neuron facilitating the fast swimming response from touch. This possibility, and the propitious location of these neurons, makes them ideal candidates for further study both by molecular methods, and sharp electrode electrophysiology.

7.4 **Conclusions**

The peripheral network of the *Ciona intestinalis* larva provides input to the CNS from three major points of entry: anteriorly from RTEN neurons through many BV

intrinsic peripheral interneurons and three relay neurons (PNIN and eminens neurons); to the dorsal MG from ATENp neurons through AVG neurons; and from the tail through planate bipolar tail neurons that extend their axons throughout the CNS, forming synapses onto a wide range of partners. The interneurons of these pathways overlap, forming synapses that allow integration of chemosensory and mechanosensory signals originating from head to tail. The extensive input of these interneurons to the motor network suggests that animals do indeed have behavioural responses to touch and chemical stimuli, and connectomic data reveal important targets for physiological examination.

Chapter 8 : Neurons of the Motor Ganglion and Caudal Nerve Cord: Homologies between Vertebrate Reticulospinal Neurons and Motor Neuron Subtypes in *Ciona*

8.1 **Introduction**

The motor system of larval *Ciona intestinalis* has an output that differs uniquely from other tailed chordates in that the muscle is not segmented. Instead, muscle cells on each side are connected via gap junctions. Thus the muscle cells are coupled by electrotonic signals that spread among them and produce a wave of contraction down the tail upon contraction of a single cell (Bone, 1992). With this difference from the segmental organisation of vertebrate tails, in which each myotome must be activated in consecutive sequence, the direct input to muscle in the ascidian larval motor system initiates action, and though this may be subsequently adjusted (Nishino et al., 2011), the lack of segmentation means that major input needs only to occur at the most anterior portion of the muscular tail.

Despite this obvious difference, how similar are the cell types involved in motor circuits of the larval *Ciona* CNS from those of vertebrates? The identified motor neurons of *Ciona* are located in the motor ganglion (MG), anterior to the tail. It is unclear whether this region in the ascidian larva is homologous to the hindbrain/brainstem (Wada et al., 1998; Canestro et al., 2005; Dufour et al., 2006) or alternatively the spinal cord of vertebrates, where motor neurons reside. The border between midbrain and hindbrain in craniates coincides with the rostral extent of the notochord (Glover and Fritzsch, 2009),

which in *Ciona* extends to the anterior end of the motor ganglion, suggesting homology between MG and hindbrain.

The somata of motor neurons in all chordate groups, cephalochordates, urochordates, and craniates such as lampreys, reside exclusively in the neural tube and its derivatives (Glover and Fritzsch, 2009), and exhibit distinct types of anatomical connections with their target muscles. In a similar way, the protostome *C. elegans* has motor neurons in its nerve cord that form neuromuscular junctions with tail muscle, which branches and extend toward the muscle (White et al., 1976) (Fig. 8.1A). The key difference of course is that the nerve cord is ventral not dorsal, as in *Ciona*. Like *C. elegans,* Cephalochordates possess some motor neurons that remain in the spinal cord, while axons of other so-called somatic motor neurons exit the spinal cord just as vertebrate motor neurons do (7.1B). Craniate and vertebrate motor neurons fall into two categories: branchial and somatic, both of which send axons out of the neural tube to contact muscle at neuromuscular junctions (Fig. 8.1B). In the lamprey, the brainstem contains branchiomotor neurons, whereas only somatic motor neurons are found in the spinal cord and exit the neural tube through the dorsal root. Vertebrate somatic motor neurons innervate somite-derived muscle, but the tail muscle is not segmented in larval *Ciona*, which lacks somites. Branchial motor neurons innervate the musculature of the vertebrate branchial arch, which is derived from the neural crest and lacks any obvious homologue in *Ciona* larvae (Hall and Gillis, 2013). Despite the lack of these distinct vertebrate features in ascidians, Zic genes, which are involved both in muscle segmentation (Pan et al., 2005) and the formation of neural crest in vertebrates (Elms et al., 2003; Hall and Gillis, 2013) have homologues involved in muscle and neural

Figure 8.1. Arrangement of neuromuscular junctions in various species. A) *C. elegans* motor neurons do not exit the CNS, but form neuromuscular junctions with muscle branches (or arms) that extend into the CNS. Postsynaptic specializations are light and lie beneath the muscle membrane at these neuromuscular junctions. B) Vertebrate somatic motor neurons extend myelinated axons outside of the CNS to form neuromuscular junctions at terminals on the muscle. Muscle cell membranes are highly folded with dark postsynaptic specializations at sites of neuromuscular junctions. C) Some motor neurons in *Ciona intestinalis* form neuromuscular junctions onto adjacent dorsal muscle cells without exiting the CNS, while others extend branches outside the CNS to form neuromuscular junctions at their terminal endplates on dorsal and medial muscle cells. Postsynaptic specializations on muscle cells appear thick and dark along the postsynaptic membrane and are often underlain by large membranous vacuoles that resemble subsynaptic cisternae. Between adjacent dorsal muscle cells, small branches are either embedded in the dorsal muscle surface or bare postsynaptic specializations.

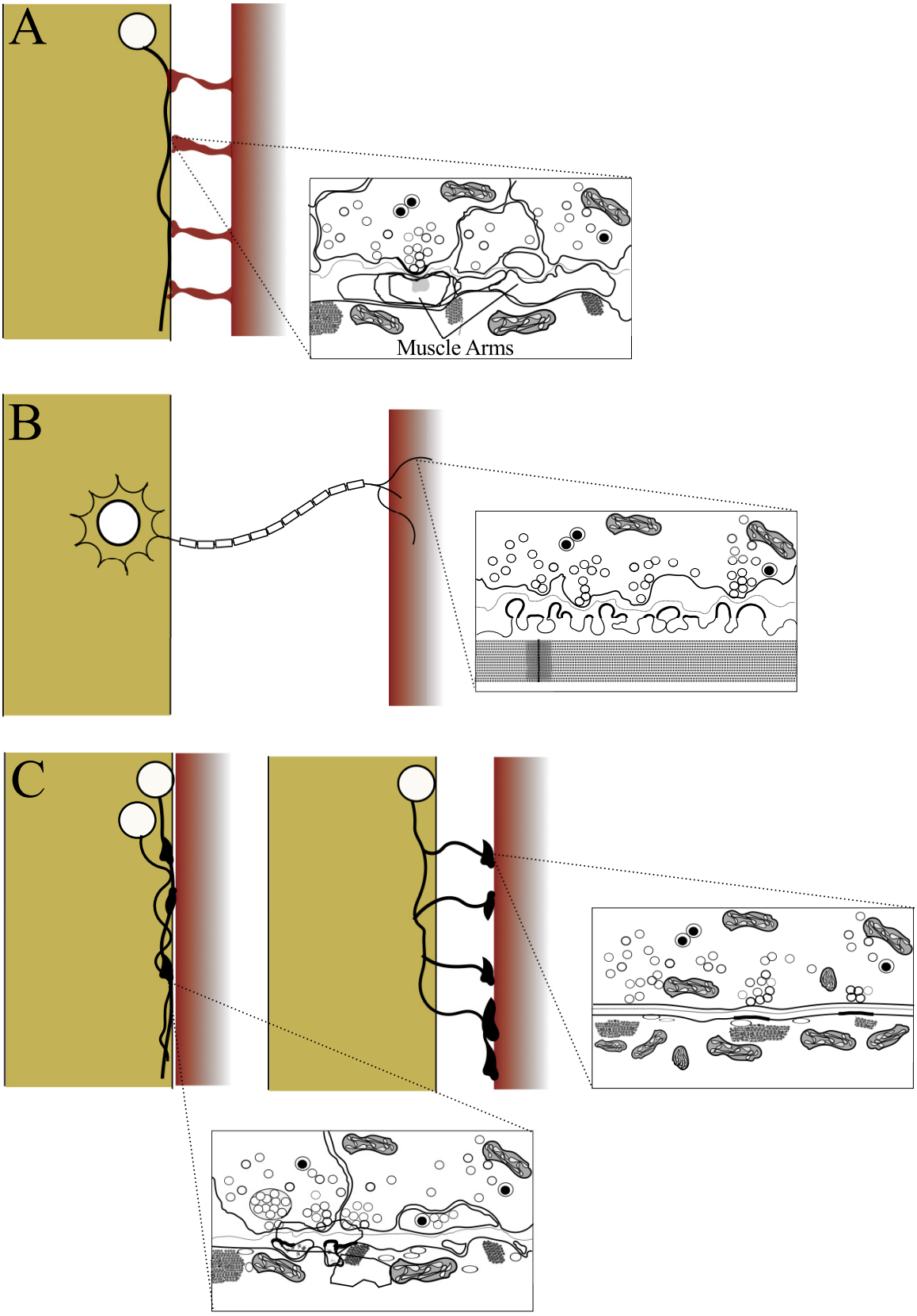
A
Muscle Arms
B
C

differentiation in ascidians. Examples include the zinc finger transcription factors *macho-1* (Nishida and Sawada, 2001; Satou et al., 2002; Imai et al., 2004; Gostling and Shimeld, 2003) and *zicL* (Wagner and Levine, 2012). Thus, the components necessary for these distinctions between different motor neuron types appear to be present already in ascidians, anticipating their function in craniate neurogenesis, and they may help to distinguish between brainstem-like and spinal-like counterparts in the motor ganglion and caudal nerve cord of *Ciona.*

Along with branchiomotor neurons, the brainstem of lampreys contains large reticulospinal neurons that extend axons into the spinal cord and provide synaptic input to motor neurons, mostly via spinal interneurons (Rovainen, 1974). Some of these large reticulospinal neurons can regulate the rate and intensity of oscillations in the spinal central pattern generator (CPG) (Buchanan and Cohen, 1982). A rhythmic CPG in *Ciona* appears to be restricted to the tail region although the motor neurons of *Ciona* have in the past been considered to reside only in the more rostral region and, until recently, possible reticulospinal neurons were, as a result, not discussed (Takamura et al., 2010). To date, identification of motor neurons has relied solely on cytological criteria rather than anatomical or physiological examinations of these cells' connections. Thus, before comparing any CPG or proposing homology with vertebrate circuits, it is important to establish the cell types that may participate in these circuits. Our data, examined in the light of recent light microscopic studies, identifies interneurons in the motor ganglion and tail regions, and suggests a more complex network of motor networks within the CNS of larval *Ciona*, one that shares characteristics with the reticulospinal network of lampreys.

The distinction between cranial-type and spinal-type motor neurons is less clear in basal chordates. The motor ganglion of *Ciona* is itself a poorly defined region, with contended landmarks and distinguishing criteria. While five pairs of motor neurons were presumed from early evidence (Nicol and Meinertzhagen, 1991), to be the only descending neurons in the motor ganglion, this now seems untenable. Along with suggestive evidence from other workers, our study confirms the co-population of this region with non-motor neurons that may, along with those motor neurons, serve to fill the roles of vertebrate reticulospinal neurons. Our evidence now reveals that the caudal nerve cord in the tail, once thought to lack neuron cell bodies (Nicol, 1987; Nicol and Meinertzhagen, 1991), in fact contains several cell types near the trunk tail boundary as well as short descending putatively cholinergic neurons along its length (Takamura et al., 2010; Horie et al., 2010). This study confirms the presence of descending tail neurons, and can be reconciled with the organisation in Appendicularians, which have motor neurons in both their motor ganglion and their caudal nerve cord (Søviknes et al., 2007). Together these new findings led us to examine the nature of cells in the reduced motor network of larval *Ciona*, compared with other chordate and vertebrate motor systems.

8.2 **Results**

Along with morphological criteria, our detailed connectomic analysis reveals that the anterior motor ganglion contains both motor neurons and interneurons that share features with vertebrate reticulospinal neurons. In *Ciona*, the identity of motor neurons among the neurons of the motor ganglion is unambiguously revealed only by their synaptic contact to muscle cells, but each pair has a distinct morphological structure and pattern of innervation, different from all the others (Fig. 8.2). Furthermore, input to muscle is

Figure 8.2. *Ciona intestinalis* motor neuron terminals and neuromuscular junctions. A) Left lateral view of larva with reconstructed terminals of motor neuron (MN) 1-5 (colour-coded, see key) in the anterior tail, with the anterior extent of notochord and pigment cells for reference. B) Dorsal view of motor neuron terminals in anterior tail relative to tail muscle. Note that motor neurons (MNs) 1, 3, 4, and 5 have relatively short axons and terminate anteriorly in the tail while MN2's terminals continue down into the tail beyond the reconstructed region shown in the figure. C-D) Enlarged views of anterior tail with reconstructed puncta representing colour-coded neuromuscular junctions of each motor neuron. C) Left lateral view (cf. A). D) Dorsal view (cf. B), arrow illustrates location of image in E. E) Electron micrograph of neuromuscular junctions (arrows) of two motor neurons, each with a different postsynaptic specialization on the muscle. Scale bars: 100µm (A-D); 1µm (E).

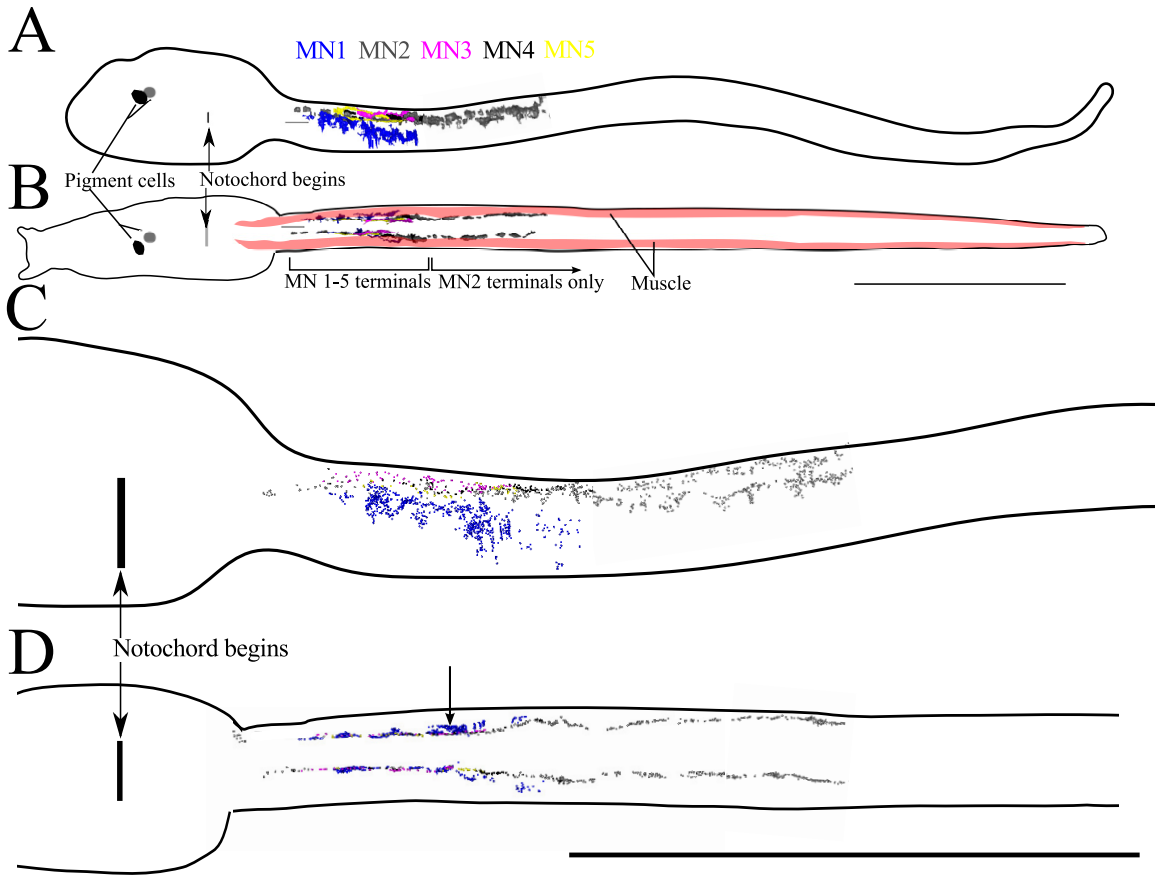
A
MN1 MN2 MN3 MN4 MN5
B
Pigment cells
Notochord begins
MN 1-5 terminals
MN2 terminals only
Muscle
C
D
Notochord begins

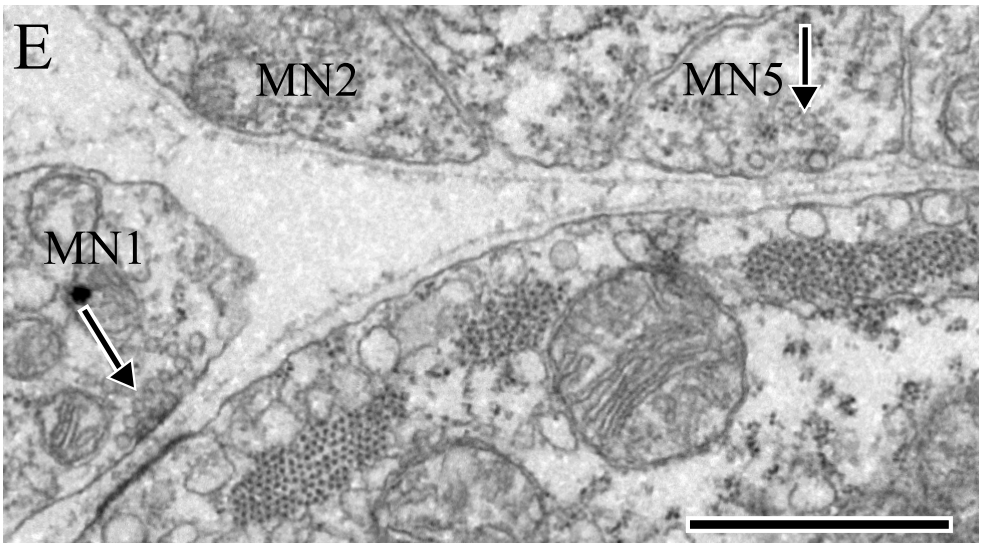
E
MN2
MN5
MN1

asymmetrical in terms of the number of synapses and their total size of synaptic contact, with neither side receiving a consistently greater input from each pair (Table 8.1). The distribution of these neuromuscular junctions is also asymmetrical between partners, with some exhibiting an alternating pattern on left and right sides (Fig. 8.2D).

Like motor neurons of cephalochordates, those of *Ciona* fall into two categories of innervation: those that leave the neural tube to innervate muscle directly (like branchiomotor neurons) (Fig. 8.1), and those that innervate muscle adjacent to the lateral edges of the neural tube without exiting the latter (like somatic motor neurons) (Fig. 8.1). Likewise, the motor neurons that exit the neural tube to innervate directly both dorsal and medial muscle are the most anterior of all motor neurons in *Ciona* and terminate in the caudal tail (Fig. 8.2A-B). I also find that the terminals of MG motor neurons in the *Ciona* larva vary by depth, so that some terminate within the motor ganglion or proximal tail while others extend down the length of the tail (Fig.7.2A-B), providing synaptic input in the tail to both muscle and other neurons.

While only one neuron actually leaves the neural tube to contact the medial muscle in the proximal tail, several other motor neurons also contact the dorsal muscle, with which they form neuromuscular junctions of varying appearance (Fig. 8.1C; Fig. 8.2E). More caudally, the second large motor neuron does expand ventrolaterally outside of the main neuropil (Fig. 8.3A-E), and other extensions from ependymal cells in this region extend dorsolaterally outside the neural tube (Fig. 8.3B,D,F). In these regions, a basement membrane is observed between ependymal and motor neuron branches and the muscle (Fig. 8.3E-F). Although a distinction between the innervating motor neurons with respect to their location and output exists in *Ciona*, the corresponding muscular innervation

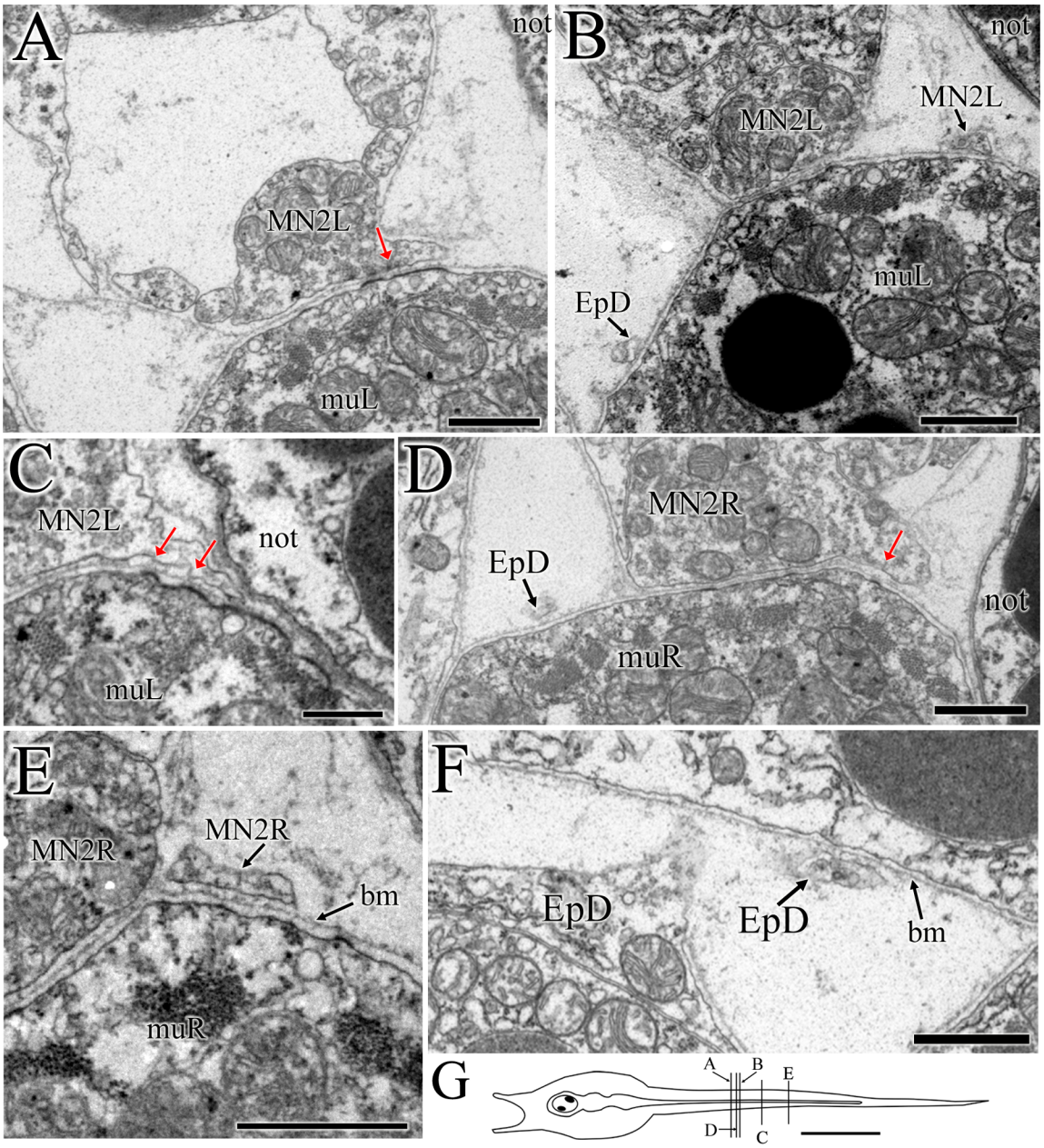

Figure 8.3. MN2 axons and dorsal ependymal cells (EpD) form extensions outside of the neuropil in the tail. A-C) Branching of MN2L terminals ventrally (to the right of the image) with (red arrow in A) and without (B) neuromuscular junctions. C-E) Branching of MN2R terminals ventrally at sites with (red arrows in C and D) and without (E) neuromuscular junctions. E-F) Basement membrane (bm) extends between MN neurites and muscle. B, D and F) Small branches extend from dorsal ependymal cells to the right and left dorsal borders of muscle and epidermal tissue (B and D). G) Diagram illustrating locations of sections A-E within the whole larva. Scale bars: 1µm (A-F); 100µm (G).

Table 8.1. Numbers and sizes of motor neuron synapses onto left and right dorsal (mul and mur) and medial (mulm and murm) muscle cells from left (L) and right (R) partners of all pairs of motor neurons (MN1-MN5) in the motor ganglion, and one pair (midtail 2 and midtail 1) in the tail. Individual and total numbers of synapses (#syn) are given alongside the total numbers of sections in which a synapse is observed (#sec) for both left and right sides. Grand totals also given for each pair and for all motoneurons.

Motor neurons	Left side						Right side							
	Dorsal muL		Medial muL		Total (L)		Dorsal muR		Medial muR		Total (R)		Grand Totals	
	# syn	# sec	# syn	# sec	# syn	# sec	# syn	# sec	# syn	# sec	# syn	# sec	# syn	# sec
midtail1	15	71			15	71	7	17			7	17	22	88
MN1L	195	948	47	140	242	1088	232	1136	130	533	452	1669	694	2757
MN2L	226	1700			226	1700	258	1648			258	1648	484	3348
MN3L	42	155			42	155	28	99			28	99	70	254
MN4L	45	181			45	181	30	115			30	115	75	296
MN5L	21	123			21	123	15	55			15	55	36	178
Total	**544**	**3178**	**47**	**140**	**591**	**3318**	**570**	**3070**	**130**	**533**	**790**	**3603**	**1381**	**6921**

which these neurons provide is not the same in vertebrates.

The interneurons in *Ciona*, one pair of descending decussating neurons (ddNs) and three pairs of motor ganglion interneurons, VGNs (Fig. 8.4), form no direct synapses onto muscle, but instead share a number of synapses with neurons in the motor ganglion and caudal nerve cord. While some of them terminate within the motor ganglion or proximal tail, two pairs, VGN2 and ddN, extend well into the tail (Fig. 8.4). In *Ciona,* the asymmetry of the motor network is obvious in the network of chemical synapses, although is less apparent in the network of putative gap junctions (Fig. 8.5).

Even though most motor neurons receive a large part of their synaptic input from these motor ganglion interneurons, the most anterior pair of motor neurons also receives substantial input from descending brain vesicle interneurons and ascending motor ganglion interneurons (discussed in detail in Ryan, 2015: Chapter 7). These motor neurons are the same pair that exit the neural tube to contact the anterior dorsal and medial muscle cells (Fig. 8.2). The more rostral pairs of motor ganglion motor neurons form synaptic connections between themselves, but receive input from different subsets of motor ganglion interneurons (Fig. 8.5). However, the more caudal descending paired motor ganglion and tail motor neurons have fewer input partners, which are limited only to those neurons that extend into the tail, including the MG interneurons, the descending decussating neurons, ddNs, ascending tail neurons and the second pair of motor neurons (Fig. 8.6). Thus, reticulospinal-like MG interneurons provide widespread input to the motor network of both the motor ganglion and tail, as do motor neurons themselves.

In addition to the motor neurons of the motor ganglion, I identify some neuromuscular

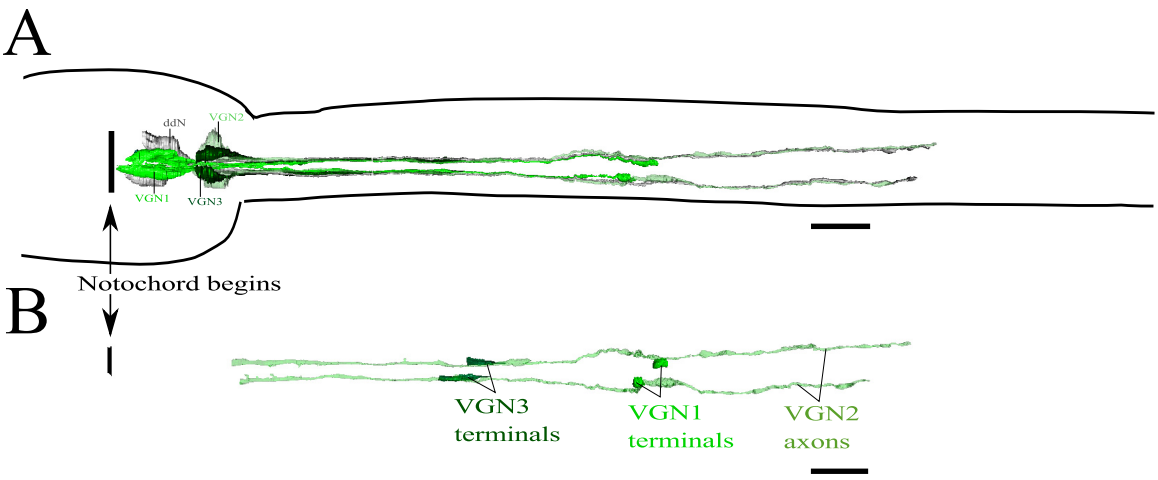

Figure 8.4. Reconstructed paired descending interneurons of the motor ganglion, dorsal view. A) paired cell bodies, axons and terminals of decussating neurons (ddN), and three anterior paired interneurons (VGN1-3). B) Terminals of VGN1s and VGN3s terminate in the proximal tail, while VGN2 and ddN axons extend far down into the tail past the reconstructed region shown. Scale bars: 10µm.

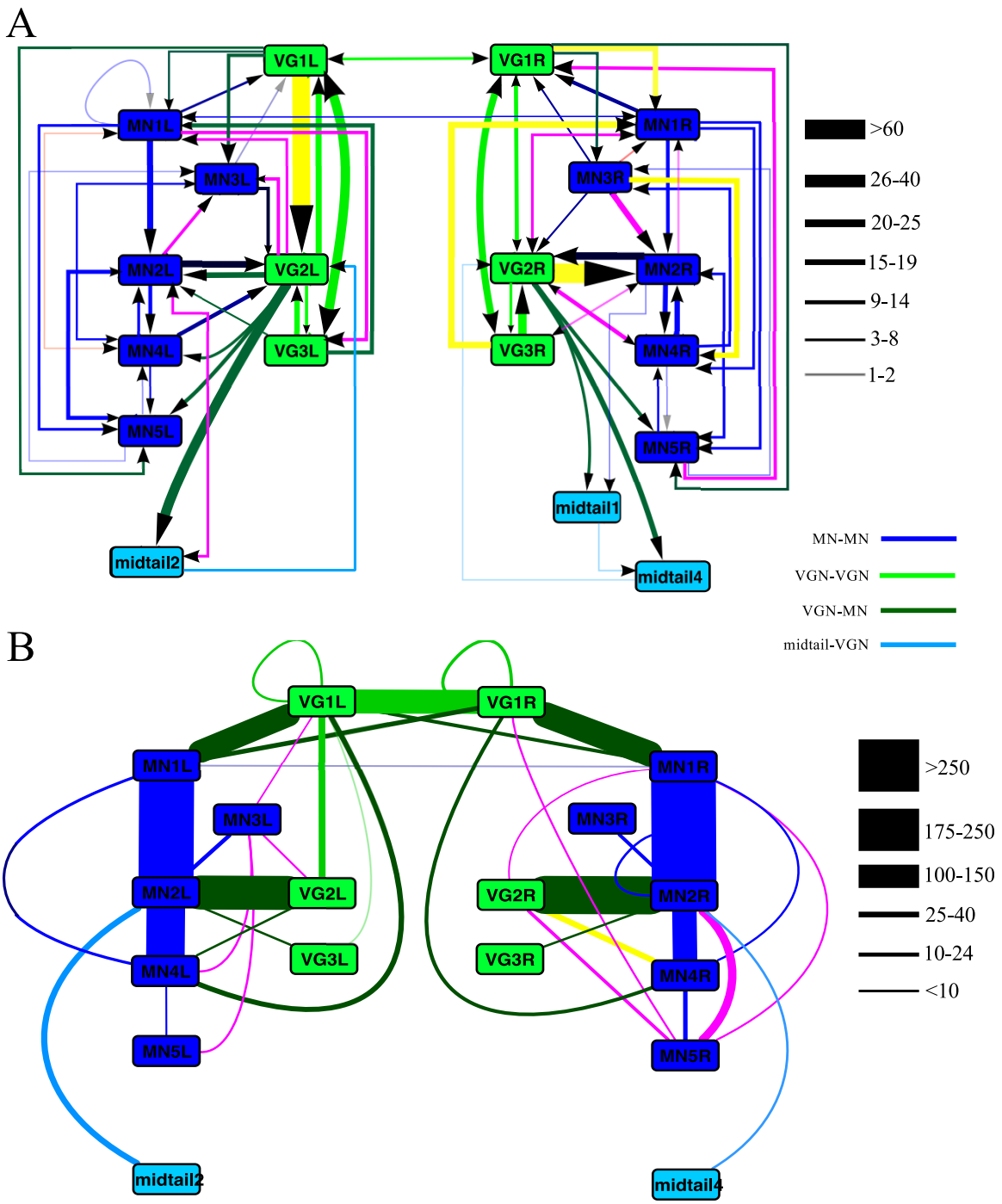

Figure 8.5. Symmetry of motor ganglion networks and paired tail neurons of larval *Ciona intestinalis*. A) Network of chemical synaptic connections. B) Network of presumed gap junctions. Line thickness in A and B represents total number of 60-nm sections in which a synaptic contact or membrane apposition is observed between partners (as defined in numbered key). Line colours of symmetrical connections according to colour key in figure. Yellow lines indicate connections that appear stronger on one side of the neuropil and pink lines indicate connections that exist on one side of the neuropil only.

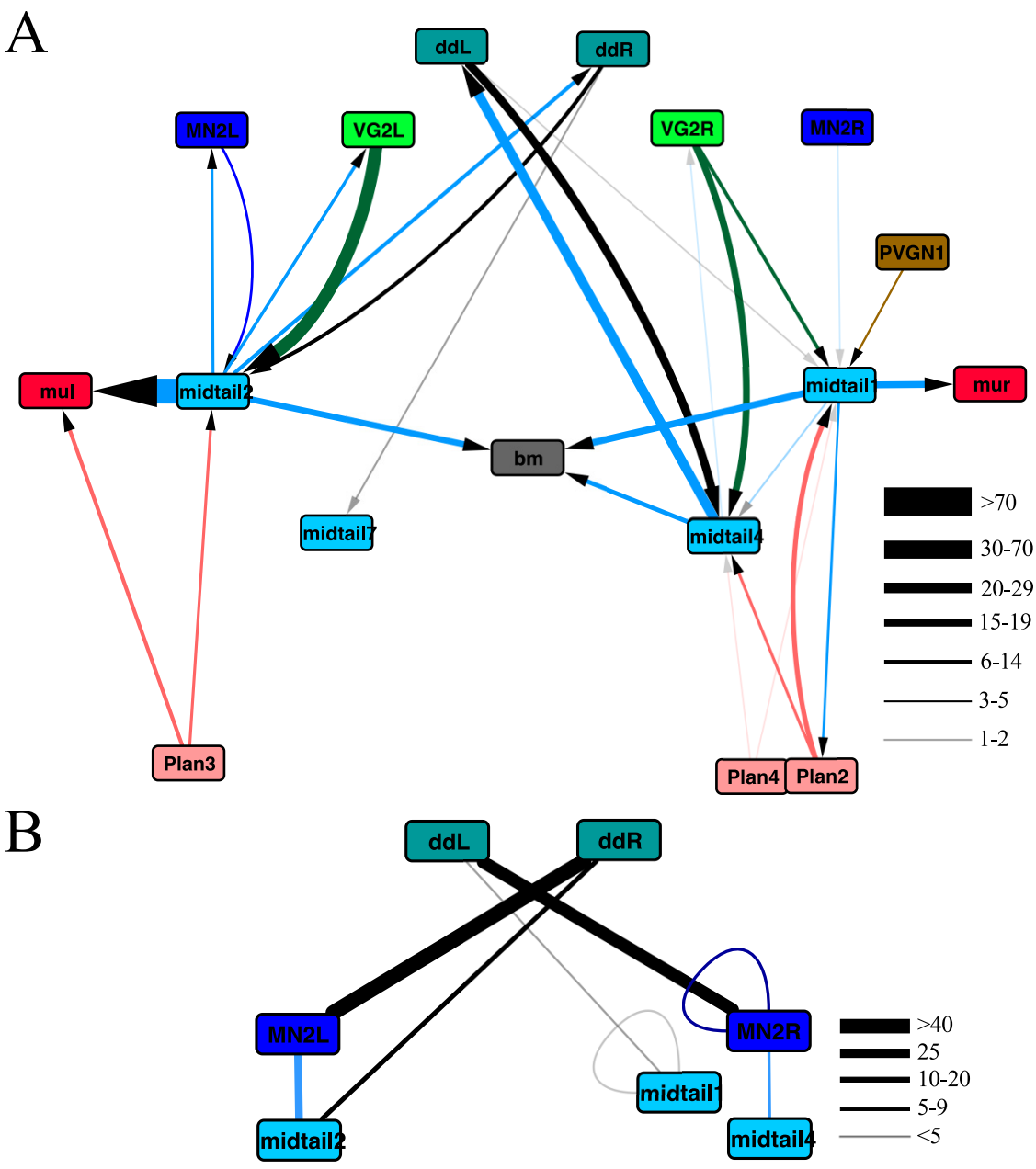

Figure 8.6. Networks of paired midtail motor neurons. A) Network of chemical synaptic connections. B) Network of midtail motor neuron putative gap junctions. Line thickness represents total size of synapse or gap junction contacts (total number of sections), as given in detail in each key.

junctions originating from short descending paired tail neurons (Fig. 8.7) that express reporters for acetylcholine (Horie et al., 2010; Takamura et al., 2010; see neurotransmitter phenotype). Like the MG motor neurons, these tail neurons are presynaptic to muscle, to basement membrane opposite the notochord, and to other neurons with axons in the tail, including descending decussating neurons, interneurons, and MN2. Both MG motor neurons and these descending tail neurons also share an increasingly asymmetrical distribution, both in terms of their cell bodies and terminals (Fig. 8.8).

8.3 **Discussion**

Reticulospinal-like interneurons, resembling those required to establish complex behaviours in the lamprey, are now identified with some anatomical assurance in the motor ganglion. Their presence is likely to be functionally relevant in conferring an ability to control motor behaviour, especially in light of their major inputs from sensory relay neurons. All descending interneurons of the motor ganglion receive input from sensory interneurons of the brain vesicle (see Ryan, 2015: Chapters 5-7), as is the case for lamprey reticulospinal neurons (Deliagina et al., 2000; 2002), and provide input in turn to motor neurons. The resulting behaviours in lamprey include the initiation of swimming, and many turning behaviours in response to different sensory stimuli (Deliagina et al., 2002). Left-right asymmetry of these connections in the lamprey reticulospinal neurons provides a basis for this diversity of movements. Asymmetry is likewise observed in the connections of the motor ganglion of *Ciona* (Appendix J), as well as the more complex inputs originating from the sensory brain vesicle (see Ryan, 2015: Chapters 5-7). However, the numerically small size of the network in *Ciona*

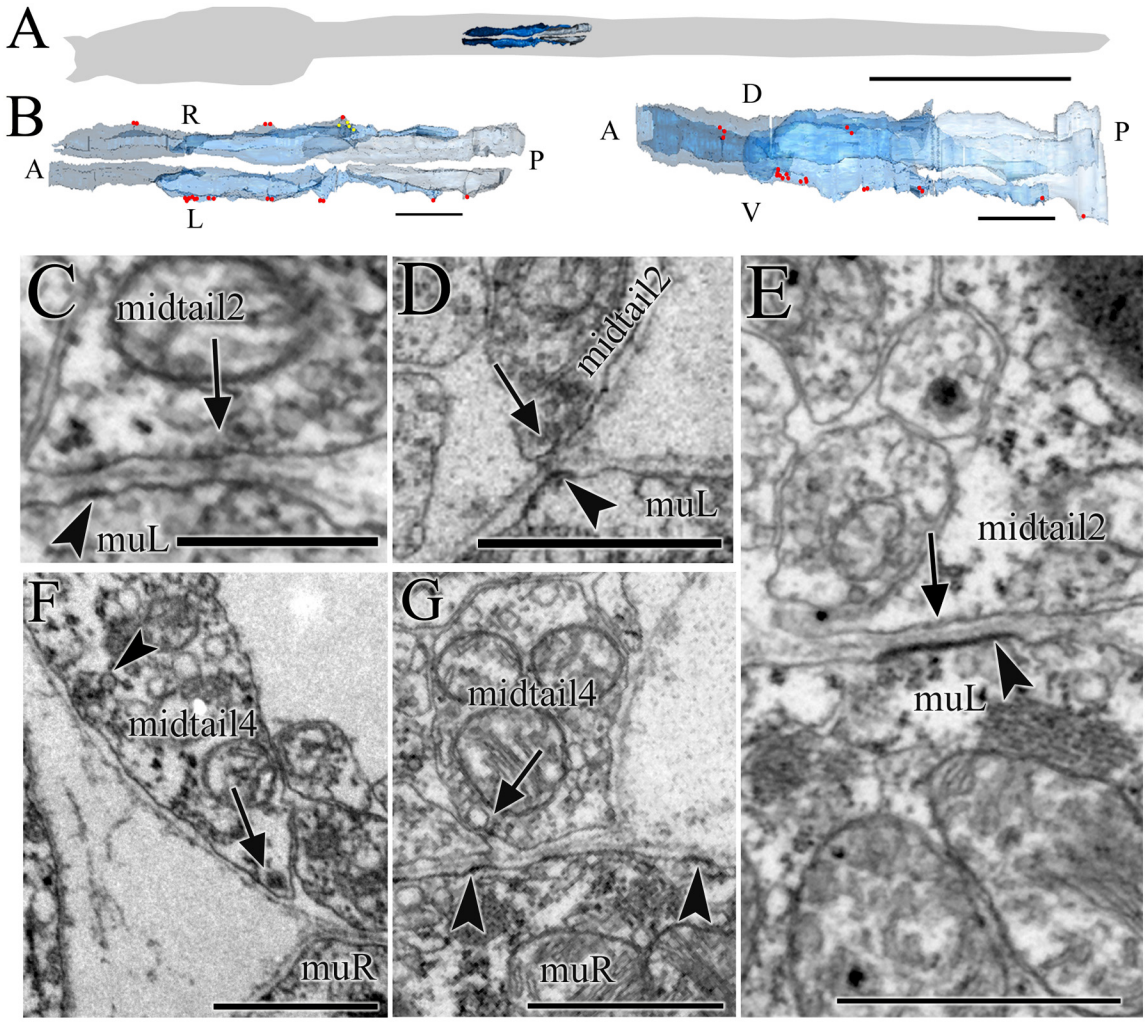

Figure 8.7. Neuromuscular junctions from paired short descending midtail neurons. Junctions form onto left and right dorsal muscle (muL, muR). A) Reconstructions of midtail neurons from dorsal view relative to larval body. B) Dorsal and left lateral views of midtail neurons with neuromuscular junctions marked by red puncta, yellow puncta represent synapses onto basement membrane. C-E) Putative neuromuscular synapses (arrows) from midtail2 onto left dorsal muscle cells. F-G) Putative neuromuscular synapses (arrows) from midtail4 onto right dorsal muscle cells. Postsynaptic densities are present on muscle cells (arrowheads in C-E; G). Some presynaptic sites have mixed vesicles (C, D and F). Synapse onto basement membrane shown by arrowhead in F. Scale bars: 100µm (A); 10µm (B); 1µm (C-G).

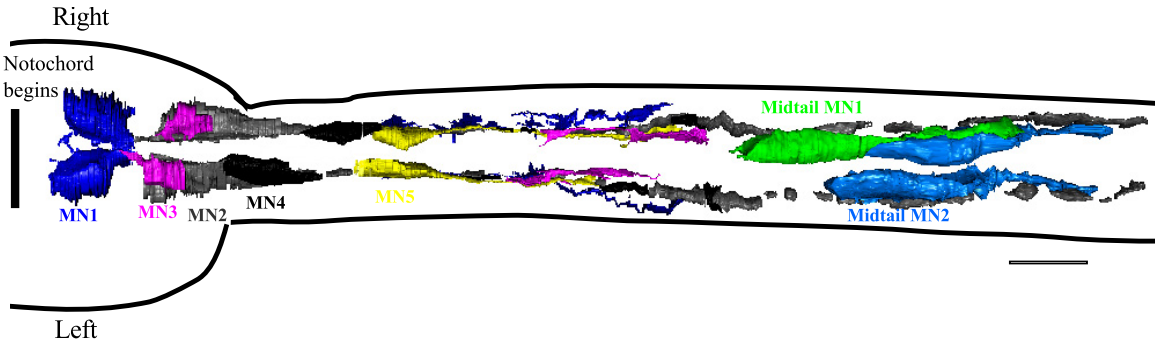

Figure 8.8. Reconstruction of motor neuron cell bodies and terminals, dorsal view relative to anterior tip of notochord (black line). Cell bodies and terminals of left partners of each pair are anterior to those of right partners. Midtail MN1 has a left-side partner cell that lacks an axon or terminal and so is excluded from the reconstruction. Asymmetry of MN4 pair is more pronounced than other pairs. Scale bar: 10µm.

reduces its capacity for controlling complex movements, even if the strong input from these neurons to the motor network implies a similar, if simpler mechanism for controlling such movements. Asymmetries among left-right partners exist, but their consistency cannot of course be confirmed in a sample from only a single larva.

In light of the reduced number of cells, neuronal roles seem to be less constrained, as is apparent from the unanticipated observation of synapses between motor neurons. Motor neurons of *Ciona* are presynaptic to each other, possibly contributing to a reticulospinal control system and suggesting a multifunctional basal neuronal state. Presumably the neurotransmitter is acetylcholine, but although nicotinic receptor subunit expression is seen in some cells of the motor ganglion (Nishino et al., 2011), this does not strictly define whether individual synapses are excitatory or inhibitory. Synaptic inhibition may function to enhance motor contrast, the more strongly excited MNs inhibiting their less strongly excited neighbours. Furthermore, the interconnection of motor neurons indicates, rather than a simple on-off mechanism, that timing and delays of input from the upstream interneurons may play an important role in this control of movement. This multifunctional state may also explain why specification of motor neurons in *Ciona* differs in some ways from that of vertebrates.

The co-population of the larval motor ganglion in *Ciona* with interneurons and obvious paired motor neurons possessing large endplates onto muscle is similar to the situation in lampreys or other basal chordates (Murakami et al., 2004). In cephalochordates, motor neurons are found along the entire length of the spinal cord, and visceral motor neurons are the anterior-most cholinergic ventral neurons in the nerve cord. However, the notochord in cephalochordates also extends along the entire length of the neural tube,

unlike the situation in *Ciona* and other ascidians, which more closely resemble the plan in other chordates (Fig. 8.9). In vertebrates the notochord does not extend under the forebrain, but lies ventral to the developing midbrain, hindbrain and spinal cord, where it is crucial for floorplate and motor neuron fate induction through Sonic hedgehog (Ericson et al., 1996). In *Ciona,* motor neurons exist in the ventral motor ganglion and, despite earlier reports (Nicol and Meinertzhagen, 1991), motor neurons are also found along the length of the caudal nerve cord, where they can be reconciled with the organisation in Appendicularians, which have motor neurons in both their motor ganglion and their caudal nerve cord. This suggests that in cephalochordates, vertebrates, and *Ciona*, ventral motor neurons are found dorsal to the notochord, but that in cephalochordates both motor neurons and notochord extend more anteriorly.

Could a muscular notochord be present in ascidians like it is in cephalochordates? Cephalochordates have a muscular notochord that is postsynaptic across a basal lamina from cholinergic neurons (Flood, 1969). During fast swimming, the notochord stiffness increases in response to neural input (Guthrie and Banks, 1970). Synapses onto notochord are thought to be unique to cephalochordates, but presynaptic sites onto the basement membrane opposite the notochord are observed from many motor ganglion and tail neurons in *Ciona*, including motor neurons of the motor ganglion and caudal nerve cord. Notochord cells in *Ciona* express Ci-zipper, a non-muscle tropomyosin (Di Gregorio and Levine, 1999), and other myosin-related genes, including *Ci-myosin Iβ* and *Ci-myosin light chain alkali*, are downstream of the *Ciona* notochord development gene, *Ci-Brachyury* (Hotta et al., 2008). However, there is no evidence of muscular function in the *Ciona* notochord, which, unlike the notochord of cephalochordates, is also

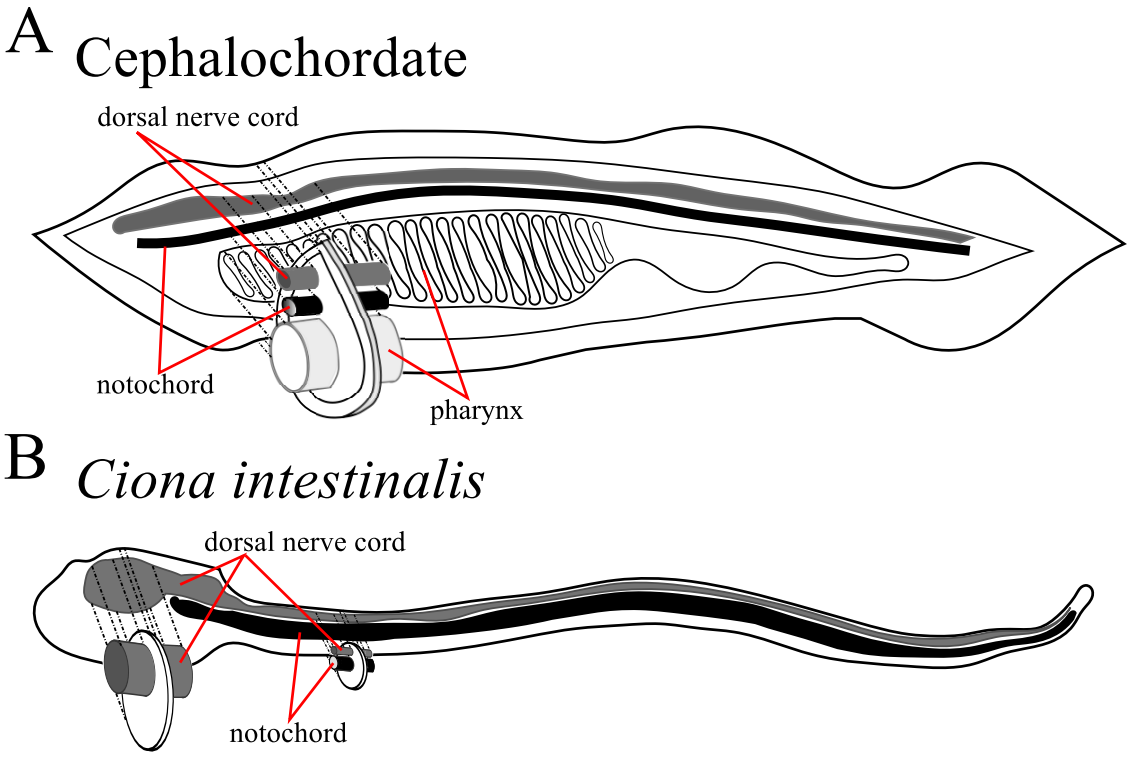

Figure 8.9. Comparison of the extent of the notochord between cephalochordates and *Ciona intestinalis*. A) Cephalochordate notochord extends along the entire length of the neural tube from anterior to posterior. B) The notochord of *Ciona intestinalis* begins caudal to the motor ganglion and does not extend further anterior to underlie the anterior CNS.

vacuolated. Nonetheless, the synapses onto the basement membrane opposite the notochord are intriguing and should prompt investigation of both neurotransmitter receptor expression by notochord cells and closer consideration of notochord function in swimming larvae.

In the lamprey, hindbrain motor neurons that exist alongside reticulospinal neurons are cranial motor neurons, which innervate the facial and branchial muscles (Glover and Fritzsch, 2009). The proposed cranial motor neuron homologues in *Ciona* are branchial basket motor neurons in adult *Ciona* that develop from the neck cells of its larva (Dufour et al., 2006), while based on their patterns of transcription factor expression motor neurons of the motor ganglion are proposed homologues of spinal motor neurons (Stolfi and Levine, 2011). However, the descending large interneurons, including the descending decussating neurons (ddNs), have proposed homology with reticulospinal neurons of the hindbrain (Takamura, 2010; Stolfi and Levine, 2011). Thus, there is some inconsistency and no doubt over-interpretation in the midbrain, hindbrain and spinal cord counterparts of *Ciona* larvae, which suggests a need to consider how these larval motor neurons are compared with those of vertebrates. This need led us to examine more closely the patterning underlying these motor ganglion and tail neurons.

Vertebrate motor neuron subtypes are specified by *FoxP1* (Dasen et al., 2008), which defines the particular expression and patterning of *Hox* genes. While *FoxP* is present in the genome of *Ciona intestinalis*, detailed expression data remain unavailable. However, *Hox1* expression is found in the hindbrain of vertebrates and the motor ganglion of *Ciona*, while *Hox5* is found in the anterior spinal cord of vertebrates and the tail of *Ciona* (Wada and Satoh, 2001). Conservation of this basic Hox gene patterning suggests that

motor neuron specification in the motor ganglion should be more similar to that in the vertebrate hindbrain than to that of the vertebrate spinal cord.

Vertebrate motor neuron specification requires a complex induction pathway comprising many genes, such as *Olig1/2, Phox2b, Hoxb1, Pax6, Nkx2.2*, and *Islet*. In vertebrates, *Islet1* is necessary for spinal motor neuron development (Ericson et al., 1992; Pfaff et al., 1996), along with the development of hindbrain branchial motor neurons, visceral motor neurons, and somatic motor neurons (Varela-Echavarria et al., 1996; Osumi et al., 1997). *Islet2* is also involved in specifying somatic motor neurons of the hindbrain (Osumi et al., 1997). Islet genes are therefore implicated in the development of motor neurons in both the hindbrain and tail. *Ciona intestinalis* has only one version of the islet gene, *ISL1/2*, which is expressed in both the motor ganglion and notochord of embryos and larvae (Giuliano et al., 1998; Imai et al., 2009). An upstream enhancer of *Islet* specifically labels A10.57, which corresponds to MN2 in our study (Imai et al., 2007; Stolfi and Levine, 2011). This suggests that the *Ciona* islet gene is involved in motor neuron specification for one motor neuron, but the single version of the gene does not allow its use to distinguish different motor neuron types. It is not helpful that MN2 is the motor neuron pair with cell bodies in the anterior motor ganglion (hindbrain) that send axons down the length of the caudal nerve cord (spinal cord), thus sharing characteristics of both reticulospinal and spinal vertebrate motor neurons.

Other motor neuron patterning genes co-expressed with *Islet* in vertebrates pattern ascidian cholinergic motor ganglion neurons, but in *Ciona* are not specific to motor neurons. Along with *Islet*, *Lhx3* is co-expressed in vertebrate motor neurons (Lee et al., 2008) and also shows transient co-expression in the same motor neuron, A10.57, as well

as A11.117 and A11.118 of *Ciona* (Katsuyama et al., 2005; Imai et al., 2009; Stolfi and Levine, 2011). These neurons in the motor ganglion of *Ciona* share cholinergic fates, but are not exclusively motor neurons. The field has been slow to comprehend the paradox that all that is cholinergic is not motor neuron. Some evidence in vertebrates for the expression of *Islet* with another gene, *Engrailed1*, suggests that motor neuron specification may be necessary to specify certain spinal interneurons (Pfaf et al., 1996). *Engrailed* expression is found in the motor ganglion of *Ciona* tailbud embryos (Jiang and Smith, 2002), and more specifically in A11.120 and A11.119, which give rise to at least two motor ganglion interneurons, the descending decussating neuron, ddN (A12.239), and a VGN descending interneuron (13.474) (Imai et al., 2009). Looking to invertebrate models, *Eve* is a motor neuron specification gene in *Drosophila* and *C elegans* (Thor and Thomas, 2002), but its orthologue in *Ciona*, *Evx*, is expressed only in epidermal receptor neurons, two populations each of the trunk epidermal neurons, rostral (RTEN) and apical (ATEN), and the caudal epidermal neurons, dorsal (DCEN) and ventral (VCEN) (Ikuta, 2004). Thus, although *Ciona* motor ganglion neurons share some gene expression patterns with vertebrates that specify neurons, these are not all specific to motor neurons. On the other hand, it appears that *Ciona*'s motor neuron specification differs from that of other model invertebrate species (Thor and Thomas, 2002), which are both protostomes.

Anterior-posterior specification may have different origins for interneurons and motor neurons, but it uses overlapping genes in the larval *Ciona* motor ganglion. In the lamprey, specifying the rostrocaudal sequence of motor neurons relies on Hox gene expression patterns, but these are independent of hindbrain reticulospinal segmentation and patterning genes (Murakami et al., 2004). Thus, Murakami et al. (2004) propose that

during evolution the early establishment of motor neuron patterning along the A-P axis preceded a later stage in the coordination of motor neuron and non-motor neuron specification, as observed in gnathostomes and other vertebrates. This pattern suggests that motor neurons may be specified by type relative to Hox gene patterning, while the patterning of interneurons into a rhombomeric segmental arrangement is specified by different genes. However, in *Ciona* both interneurons (A11.117) and motor neurons (A10.57, A11.118) are specified by some of the same patterning genes that arrange the lamprey reticulospinal neurons, including Pax6 and Eph (Stolfi et al., 2011; Murakami et al., 2004). The interactions between *Islet, Engrailed* and *Lhx3* in coupling interneuron and motor neuron fate in the *Hox1* expression domain (hindbrain) of the motor ganglion of *Ciona* would likewise be expected because these would coordinate hindbrain motor neuron and interneuron patterning.

Some evidence suggests that vertebrate fate induction pathways for motor neurons are not consistent in ascidians (Hudson et al., 2011), but the previous limited understanding of the motor ganglion limited the validity of these comparisons. In particular, hedgehog signalling is required for vertebrate motor neuron induction, but ablation of hedgehog producing floor plate cells or notochord in the 64-stage embryo of *Ciona* did not affect the *in situ* expression of *ChAT* or *vAChTP* in the larval motor ganglion region (Hudson et al., 2011). *In situ* expression of *Ci-Mnx*, a homologue of the vertebrate motor neuron specification gene *Hb9*, revealed that *Ci-Mnx* is expressed along with the RNA for acetylcholine transport and synthesis in three motor ganglion cells in both control and ablated larvae (Hudson et al., 2011). However, our anatomical analysis suggests that interneurons of this region in the *Ciona* larvae, including A11.117, which is included as

one of the three motor neurons in the study in question, express markers used to identify motor neurons. Stolfi and Levine (2011) also found that this A11.117 neuron expresses *Pitx* and Vsx, which are genes for specifying vertebrate interneurons involved in spinal motor circuits (Enjin et al., 2010; Kimura et al., 2006). Furthermore, the detection of *hh1* in *Ciona* larvae has been unsuccessful to date and *hh2 in situ* expression in the region underlying the motor ganglion is diffuse and corresponds to endoderm, but not in fact the nervous system or notochord (Islam, 2010). Instead, *hh2* in situ expression corresponds to the ventral nerve cord of the tail (Takatori et al., 2002), underlying the tail motor neurons. Additionally, hedgehog and BMP gradients specifying vertebrate spinal motor neurons act at long range, so these may in fact pattern the newly identified tail motor neurons in *Ciona*. Although hedgehog signalling is necessary for all motor neuron induction in vertebrates (Ericson et al., 1996), it is also unclear whether this is the case in all or any motor neurons in *Ciona* nor whether the roles of hedgehog signalling, and the floorplate and notochord structures, which are involved in the specification of vertebrate motor neurons, are conserved in ascidians.

The expression and presence of orthologues in *Ciona* to genes downstream of the hedgehog signalling pathway in vertebrate motor neuron specification provides further evidence for differences in the role of hedgehog signalling in motor neuron development. *Olig1* and *Olig2* genes are downstream targets of *Shh* involved in vertebrate spinal motor neuron specification (Zhou et al., 2000; Zhou and Anderson, 2002; Lu et al., 2002), but are not present in the genome of *Ciona intestinalis* (Zhou et al., 2000). *Nkx2.2* is another homeodomain protein that plays a role in the translation of *Shh* activity into ventral patterning of motor neurons in vertebrates (Briscoe et al., 1999). In *Ciona,* a single *Nkx2*

orthologue of the NK2 class is similar to vertebrate *Nkx2.1*, but no *Nkx2.2* homologous gene is present (Wada et al., 2003). In contrast to the absence of these downstream *Shh* genes, *Neurogenin* is necessary to establish motor neuron identity in both *Ciona* and vertebrates (Ma et al., 2008; Imai et al., 2009), although its pathway is dependent on *Shh* activity in vertebrates (Ma et al., 2008).

Notable spinal nerve asymmetries, an additional hallmark of many chordate nervous systems, are also present in *Ciona*. Hagfish, lamprey and cephalochordate asymmetries in the left-right distribution of spinal nerves have led to the assertion that this character is ancestral to chordates (Glover and Fritzsch, 2009). Probably the greatest of these chordate asymmetries exists in the dorsal nerves of cephalochordates, in which, from anterior to posterior, partners are increasingly caudal on the right relative to the left sides (Castro et al., 2004; Glover and Fritzsch, 2009). This pattern and increasing asymmetry is also apparent for *Ciona* motor neurons of the motor ganglion and tail. This asymmetry is less apparent in previous studies that focused only on the anterior region and includes only the first three pairs of motor neurons, which are arranged more symmetrically.

Feed-forward synaptic loops common in reticulospinal pathways are likewise found from interneurons and motor neurons in *Ciona*'s motor circuits. In the lamprey, electrophysiological studies confirm that reticulospinal neurons (RSNs) receive input from the neurons of the mesencephalic locomotor region (MLR). These then provide input to spinal motor circuits (Grillner, 2003) that consist of inhibitory, excitatory and motor neuron components. In addition to reticulospinal neurons that relay information from the MLR to the spinal network, some evidence also suggests that the motor 'on' response can be enhanced and sustained through feedforward pathway from a parallel

muscarinic pathway through glutamatergic rhombencephalic neurons (Smetana et al., 2010). This second type of hindbrain neurons also receives cholinergic MLR innervation at muscarinic synapses, and provides glutamatergic excitatory input to reticulospinal neurons that target the spinal motor network (Smetana et al., 2010). A similar feed-forward network exists in the *Ciona* motor ganglion from the posterior brain vesicle, which is compatible if this is homologized with the mesencephalon of vertebrates (Imai et al., 2009). However, *Ciona* lacks the spatial separation between the two hindbrain neuron types and both are likely cholinergic themselves rather than glutamatergic. Nonetheless, this feed-forward input from the posterior brain vesicle could provide a similarly sustained response, as observed in longer swimming bouts, but this awaits confirmation using physiological techniques. The anatomical network described here provides a basis for targeted investigation of such motor network particularities.

Ascidian motor systems seem to occupy a gap between those of cephalochordates and vertebrates. The ventral motor ganglion contains eight pairs of neurons, five of which are paired motor neurons, with two individual right side-descending neurons and three ascending (four in other studies) contralateral neurons at the trunk-tail border. The caudal nerve cord contains additional paired descending motor neurons along with the ependymal cells and axons and terminals of two interneurons, one motor neuron, and two ascending tail neurons on each side. The interneurons of the motor ganglion bear synaptic connections like those of reticulospinal neurons, and are anatomically qualified to control motor output. *Ciona* also appears to contain multiple motor neuron types, sharing some features and specification gene networks with vertebrate spinal motor neurons, but some being presynaptic at many sites to other motor neurons, making them

also anatomically qualified to function like reticulospinal neurons in motor circuits. In vertebrates, the axons of motor neurons of the ventral root leave the spinal cord, but there is no ventral root in cephalochordates, in which muscles contact ventrolateral spinal cord with processes that form synapses with motor neuron axons. In *Ciona intestinalis* there are motor ganglion (*cf* vertebrate hindbrain) motor neurons that leave the anterior caudal nerve cord (*cf* vertebrate spinal cord), but other motor neurons in both the motor ganglion and caudal nerve cord that, like cephalochordates, do not leave the nerve cord, although unlike cephalochordates the muscle in *Ciona* does not extend processes to contact these neurons. Instead, neuromuscular junctions occur between motor neurons and dorsal muscle cells, which are connected to medial and ventral muscle cells, and more posterior muscle cells, by putative gap junctions. Along with these characteristics of motor ganglion neurons, the identification of neuromuscular junctions from short motor neurons in the tail of *Ciona* and clarification of which neurons are indeed motor neurons highlights the need to revisit our understanding of ascidian hindbrain and spinal cord homologies, motor circuits, and functional roles of these neurons in directing both reported and hypothesized larval behaviour driven by motor output.

8.4 **Conclusions**

The MG of *Ciona intestinalis* contains networks and neurons like reticulospinal regions of vertebrate brains, while also having characteristics of spinal neurons. Motor neurons are not unique to the MG, but also exist in the tail, alongside axons and terminals of spinal-cord like MG motor neuron 2. This MG region, rather than a simple collection of motor neurons receiving direct relay input, represents an area of integration and complex connections that translate relayed signals into motor

outputs. The CNC itself also bears a greater number and variety of neurons than previously appreciated, further contributing to the complexity of synaptic connections underlying the seemingly simple behaviours observed in *Ciona intestinalis* larvae.

Chapter 9 : A Central Pattern Generator in the *Ciona intestinalis* Larval Brain

9.1 **Introduction**

9.1.1 Central Pattern Generators:

While sensory inputs to motor systems often initiate and modulate a complex set of behaviours, once initiated, some motor circuits function autonomously. A fictive motor pattern that can continue without sensory or descending input provides evidence of a candidate central pattern generator (CPG). Identifying such candidates has been undertaken both *in vivo* and *in vitro*, the latter by for example isolating spinal cords from their descending inputs (Stevenson and Kutsch, 1987; Dale, 1991; Grillner et al., 1991). Central pattern generation has been implicated in many rhythmical activities in vertebrate and invertebrate species: swimming (Satterlie, 1985; Dale, 1995; Grillner et al., 1991; Grillner and Wallén, 1999), walking (Cazalets et al., 1995; Cheng et al., 1998), and flying (Stevenson and Kutsch, 1987), along with other non-locomotory activities. The CPGs driving these behaviours consist of motor neurons and interneurons, and can function by a variety of mechanisms, all of which generate a rhythmic pattern of firing in the motor innervation to muscles.

In some cases, central pattern generation may rely on the pacemaker activity of either a single neuron or a group of neurons. The oscillatory patterns created by these bursting neurons then drive rhythmic motor neuron activity. When coupled, these pacemakers produce a rhythmic alternating pattern of spiking, in which the period of the rhythm is based on synaptic delays. Uncoupling of pacemaker and target neurons results in a rhythmic pattern in the pacemaker neuron, but a random pattern of activity in the targets.

This activity is driven ultimately by the endogenous bursting of particular neurons, and examples are confirmed particularly in CPGs that produce continuous activity (Marder and Bucher, 2001). The initiating bursting neurons must therefore be regulated if they are used in locomotor pattern generation because of the periodic and episodic nature of locomotion (Kandel et al., 2000). In lieu of a bursting pacemaker, some CPGs contain neurons that can sustain a depolarized state long after they are initially depolarized. In these neurons, modulation generates such plateau potentials that can be crucial to pattern generation.

Aside from rhythmicity generated by the properties of individual neurons, CPGs often also employ reciprocal inhibition to coordinate rhythmic neuronal activity. This mechanism is seen in what are called half-center oscillators (Brown, 1911), which function only when neurons are coupled to produce alternating patterns of excitation. The alternation relies on spike threshold or adaptation, and is best understood when the membrane and firing properties of the neurons involved are both known. When neurons are uncoupled in this system, both fire at random intervals, so their rhythmicity exists only because of the inhibition exerted by one element on its contralateral targets. Networks such as these are observed in many swimming behaviours, including the canonical CPG that regulates swimming in the lamprey (Fig. 9.1; Grillner et al., 1998; Grillner and Wallén, 1999).

Mechanistically, pacemaker activity requires only the excitation that results from the intrinsic periodicity of bursting neurons, whereas a half-center oscillator requires both excitation and inhibition. While the innervation to some muscles in invertebrates is

Figure 9.1. Model CPGs of the lamprey *Lampetra fluviatilis* and *Ciona intestinalis*. A) Schematic model of lamprey swimming CPG (adapted from Grillner, 1998). B) CPG model for putative inhibitory (filled circles) and excitatory (open fork) synaptic connections. B) Model of CPG network of motor neuron 1 (M_1) pair. C) Model of CPG network of motor neuron 2 (M_2) pair. Dotted lines indicate weak connections with few small synapses. Red lines indicate connections with motor neurons that exist on only one side.

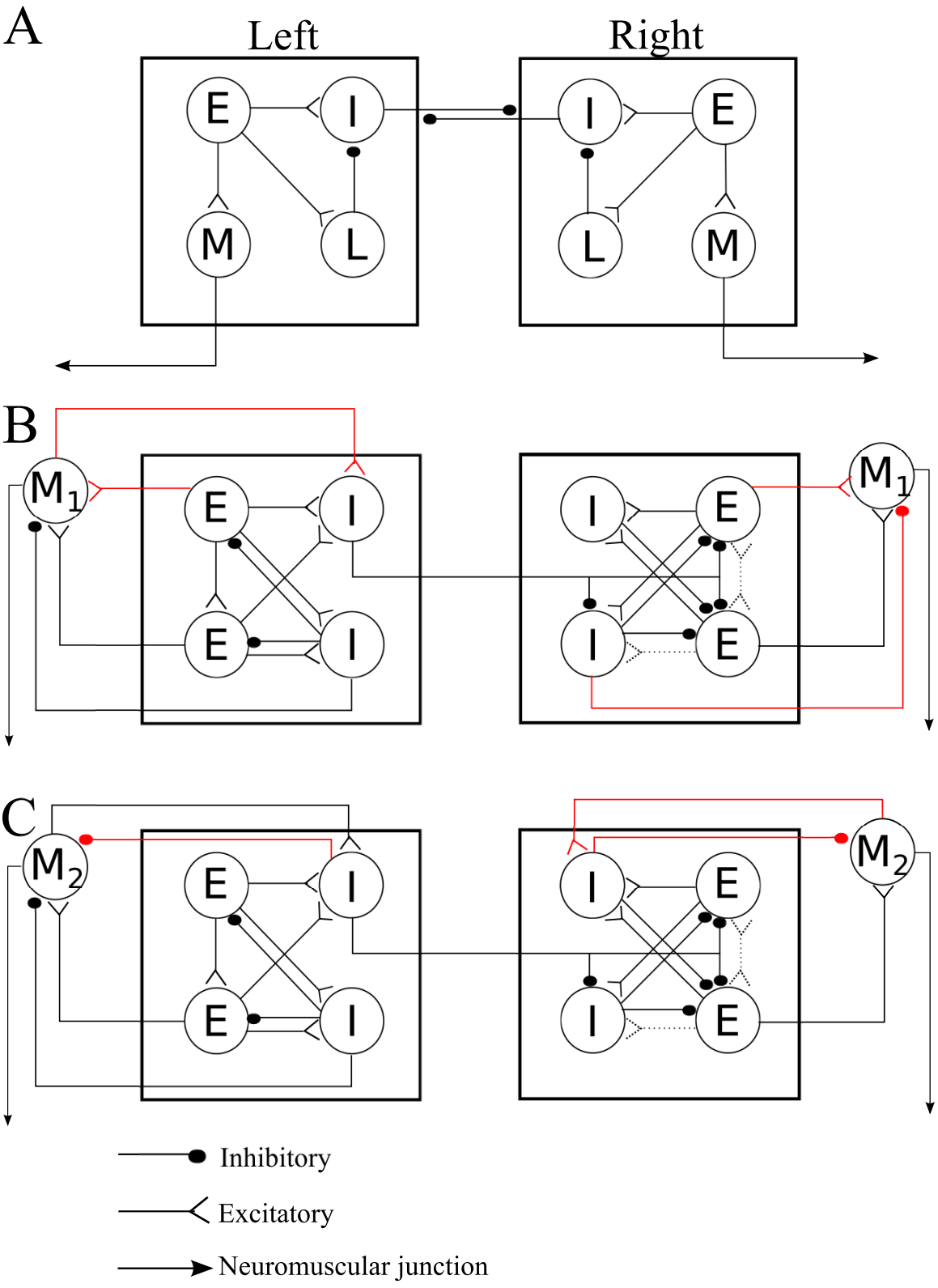
A
Left
Right
E
I
M
L
B
M_1
C
M_2
Inhibitory
Excitatory
Neuromuscular junction

inhibitory (Wolf and Harzsch, 2002), because many invertebrate and all vertebrate motor neurons are excitatory (Wolf and Harzsch, 2002; Kandel et al., 2000) the reciprocal inhibition in vertebrate CPGs must involve a series of interneurons. In the lamprey, for example, the half-center oscillating CPG controlling swimming requires an excitatory interneuron, an inhibitory neuron, a contralateral inhibitory interneuron, and a motor neuron on each side of the animal (Grillner et al., 1998). In this network, bilateral rhythmic coordination is realised through reciprocal inhibition between the inhibitory interneurons, which are themselves under the synaptic influence of both of the other interneurons on their own side (Fig. 9.1). Coordination of this inhibition relies, however, on the properties of the individual neurons and receptors involved in the CPG.

In fact, in either type of CPG the intrinsic membrane properties of each neuron involved in central pattern generation, including the motor neurons (even if these are only targets of the pattern), are important to an understanding of the particular pattern (Grillner et al., 1998; Marder and Bucher, 2001). Thus, along with knowledge of the network connections, cellular and synaptic mechanisms are of particular importance in elucidating the function of any particular CPG. This is demonstrated in even the relatively simple case of the lamprey CPG, in which synaptic depression results in a delayed excitation of the inhibitory interneuron, L, which is combined with enhanced excitability in its ipsilateral interneurons, E and I, because of postinhibitory rebound. As a result, when one side is released from inhibition by the other side, it experiences an episode of ipsilateral excitation, which leads to motor activation as well as inhibition of contralateral interneurons. This excitation is followed by the contralateral neurons being released from inhibition because of ipsilateral L cell activity. The plateau potential caused by

glutamate induced NMDA receptor activity ends as potassium channels open, resulting in a repolarization of interneurons, which are further inhibited by the now active contralateral inhibitory neuron (Grillner et al., 1998; Grillner and Wallen, 2002; Grillner, 2003).

9.1.2 Ascidian Central Pattern Generation:

The symmetrical swimming behaviour of larval *Ciona intestinalis*, and the larva's ability to retain this symmetry autonomously *a priori* intimates the presence of a CPG in the motor ganglion. This symmetrical motion requires the coordination of left and right tail flexions during both spontaneous and light-evoked swimming. Furthermore, this symmetrical motion is preserved in larvae with anterior portions of the nervous system removed (Nishino et al., 2010). The lack of segmented myotomes in ascidian larva distinguishes its motor output from that of vertebrates (lamprey, zebrafish and *Xenopus*) even though the undulatory behaviours themselves appear similar (McHenry, 2005). As in other species, it is likely that several neural networks overlap to produce the range of behaviours seen in different ascidian larvae. Deconstructing these circuits by anatomical means and exploring their interactions provide points of entry for targeted physiological studies. Identifying and classifying all morphological components of the motor ganglion will be crucial to ascertain the neural mechanisms underlying the control of ascidian larval behaviour.

Components of a CPG in *Ciona* are thought to include motor neurons and Ascending Contralateral Inhibitory Neurons (ACINs) in the motor ganglion and proximal tail (Horie et al., 2010; Nishino et al., 2010). As in vertebrates, acetylcholine acts at neuromuscular junctions where its action is blocked by a nicotinic blocker, D-tubocurarine (Ohmori and

Sasaki, 1977); and swimming activity can likewise be disrupted (Brown, unpublished as cited in Sordino et al., 2008). Putative motor neurons have therefore been identified largely based on cholinergic markers that include the expression of both promoters for, and antibodies against, cholinergic proteins (Imai et al., 2009; Horie et al., 2010; Takamura et al., 2010). Antibodies are not available that would detect acetylcholine itself. The existence of five pairs of cholinergic motor neurons is suggested by several studies, and the lack of convincing evidence for other neuronal phenotypes in the ventral portion of the motor ganglion had strengthened this classification until a study by Stolfi and Levine (2011) using enhancers from transcription factor genes to label single cells with axons that innervate the tail, differentially identified five pairs of neurons in the motor ganglion. Of these, one pair appeared to extend decussating neurites toward the tail, and another exhibited no evidence for a cholinergic phenotype (Stolfi and Levine, 2011). This report led to the important conclusion that the motor ganglion is likely to contain both cholinergic and non-cholinergic interneurons as well as motor neurons.

Among these interneurons, one type has been identified in the proximal tail and expresses glycine reporters (Horie et al., 2010; Nishino et al., 2010). The blocking of glycine receptors on cells hitherto supposed to be motor neurons and on muscle disrupts the symmetry of tail contractions in hatched larvae, but does not prevent contraction on either side (Nishino et al., 2010). Certainly, muscle and at least the branched large endplate motor neurons both express Ci-GlyR driven GFP, but as indicated above it is unwarranted to assume that all cholinergic cells are motor neurons. Thus the motor neuron identity of other GlyR expressing neurons has been inferred only by ChAT expression, and this may actually represent cholinergic interneurons not motor neurons in

the ventral motor ganglion. These labelling studies in the motor ganglion have not produced satisfactory results, and specific physiological data on CPG components are also lacking. Thus, the current EM study closely examines the connections between cells of the motor ganglion to further explore the probable CPG components and their candidate interactions. In conjunction with this anatomical connectomic analysis, I propose that the previously classified motor neurons within the motor ganglion are in many ways similar to motor neurons of the vertebrate brainstem rather than motor neurons of the vertebrate spinal cord. Other neurons of the motor ganglion share many characteristics with reticulospinal neurons that extend axons into the tail to modulate and regulate motor neuron activity. Thus, I consider these neurons, and others of the tail, to determine whether they may play a role in the intrinsic symmetrical swimming activity.

9.2 **Results**

I have confirmed distinct strong and abundant connections from two pairs of motor ganglion neurons at more than 200 sites for each neuron onto muscle (Fig. 9.2). These neurons are by definition therefore unassailably neuromuscular. The junctions occur at distinct regions along the anteroposterior axis, and the neurons themselves integrate signals from distinct partners. Among neuromuscular junctions of the first pair of motor neurons, 16% on the left and 33% on the right are onto medial muscle cells (Fig. 9.2A-C), with all other input to muscle occurring onto dorsal muscle cells. These muscles cells are themselves connected by contacts thought to be gap junctions (Fig. 9.2G-H) and thus sites of electrical transmission, compatible with the phase delay observed in muscle cell recordings (Bone, 1992). The first two pairs of motor neurons (MNs) are themselves synaptically connected asymmetrically, the most numerous of their partnerships formed

Figure 9.2. Neuromuscular junctions of the two large anteriormost endplate pairs of primary motor neurons. A-B) Reconstructed neuromuscular junctions of MN1 and MN2 of the motor ganglion from dorsal (A) and left lateral views (B) relative to the anterior extent of muscle cells (mu). C) MN1 provides the only neuromuscular synaptic input onto medial muscle cells (MN1(m) in A and B). D-F) Neuromuscular junctions onto dorsal muscle (mu-D) originate from both MN2 (D and F) and MN1 (E). G-H) Muscle cells are connected by gap junctions (arrowheads). G) Serial sections illustrating that some junctions occur alongside invaginations (astersisks) of one muscle cell into the other muscle cell. Scale bars: 10μm (A-B), 1μm (C-F), and 200nm (G-H).

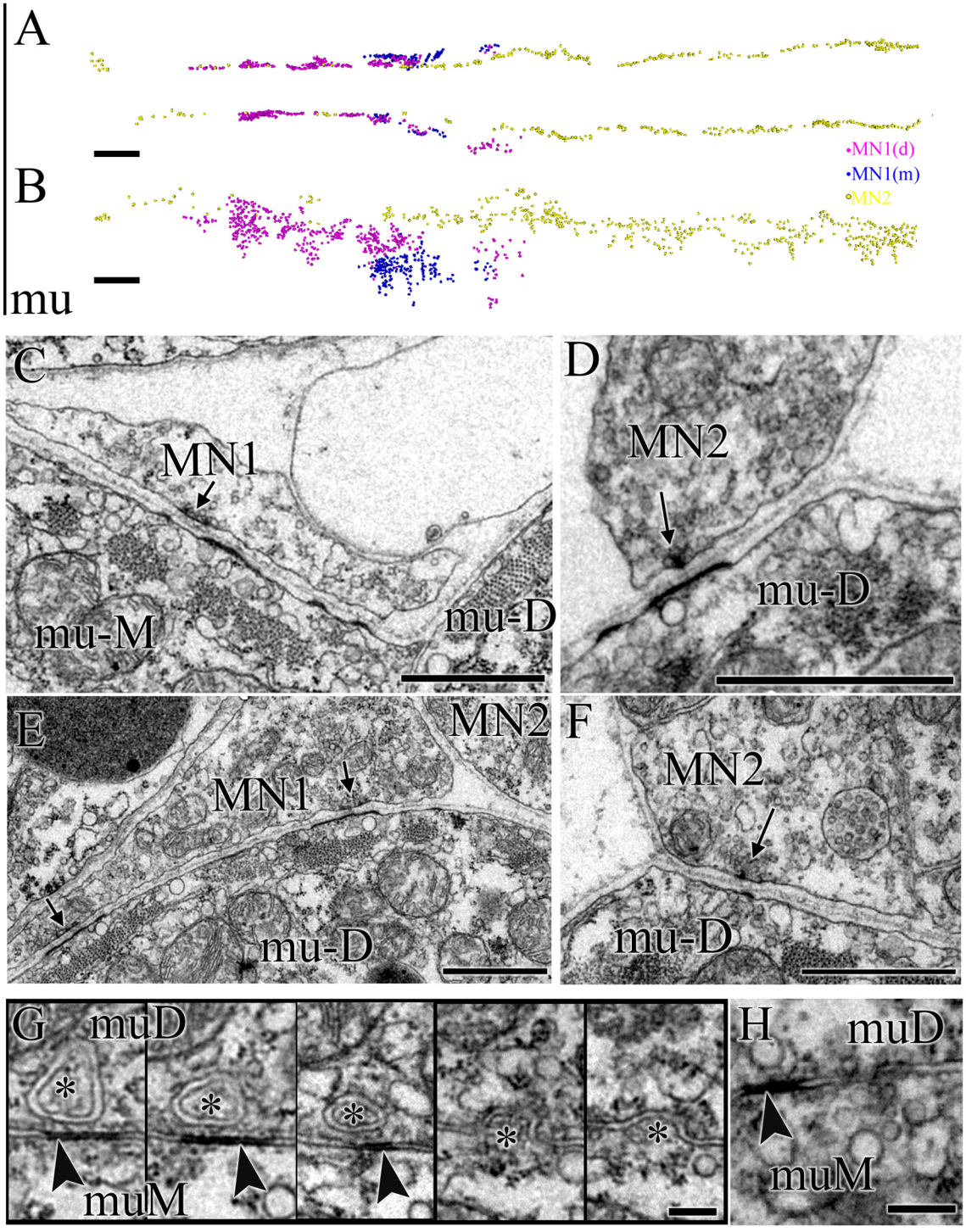
A
B
mu
•MN1(d)
•MN1(m)
•MN2
C
MN1
mu-M
mu-D
D
MN2
mu-D
E
MN2
MN1
mu-D
F
MN2
mu-D
G
muD
muM
H
muD
muM

by six synapses from MN1L to MN2L, with only three synapses from MN1R to MN2R and none back from the MN2 cells to MN1s. The two MN1 neurons also provide synaptic input to other more caudal motor neurons, with two to four synapses each. Combined, these motor neurons constitute a network of interconnected components on each side (Fig. 9.3). The other three caudal pairs of motor neurons within the motor ganglion provide input to muscle at fewer neuromuscular junctions than the first two pairs. Two of the three pairs have between 30 and 40 neuromuscular junctions each, with the most posterior pair MN5 having fewer than 20 neuromuscular junctions each (Fig. 9.4). These motor neurons are also synaptically connected with each other and with MN2s, forming one to five synapses with each (Fig. 9.3A).

The next group of proposed CPG components is that of the ascending contralateral inhibitory neurons (ACINs), which provide synaptic input to both ipsilateral and contralateral components of the motor ganglion. I identify only three such neurons near the trunk-tail boundary that decussate and ascend, two on the left and one on the right (Fig. 9.5A-C). The two left-side ACINs have neurites that are emitted from their decussating axons to ascend as invaginating fibers within the ventral ependymal cells (Fig. 9.5A, I, Fig. 9.6A). However, their synaptic contacts are received not at these fine neurites but either on their cell bodies or the axons. ACIN axons and terminals form many mysterious synapses onto the ventral basement membrane opposite the notochord (Fig. 9.5C, J-K), 13 synapses from ACIN1L, 14 from ACIN2L, and 6 from ACIN2R. Although ACINs are not presynaptic to contralateral motor neurons, they do form synaptic contacts onto ipsilateral MN2 and MN3 on both the left and right, and MN4 on the left (Fig. 9.5B, D-F, L). They also provide input to ipsilateral motor ganglion

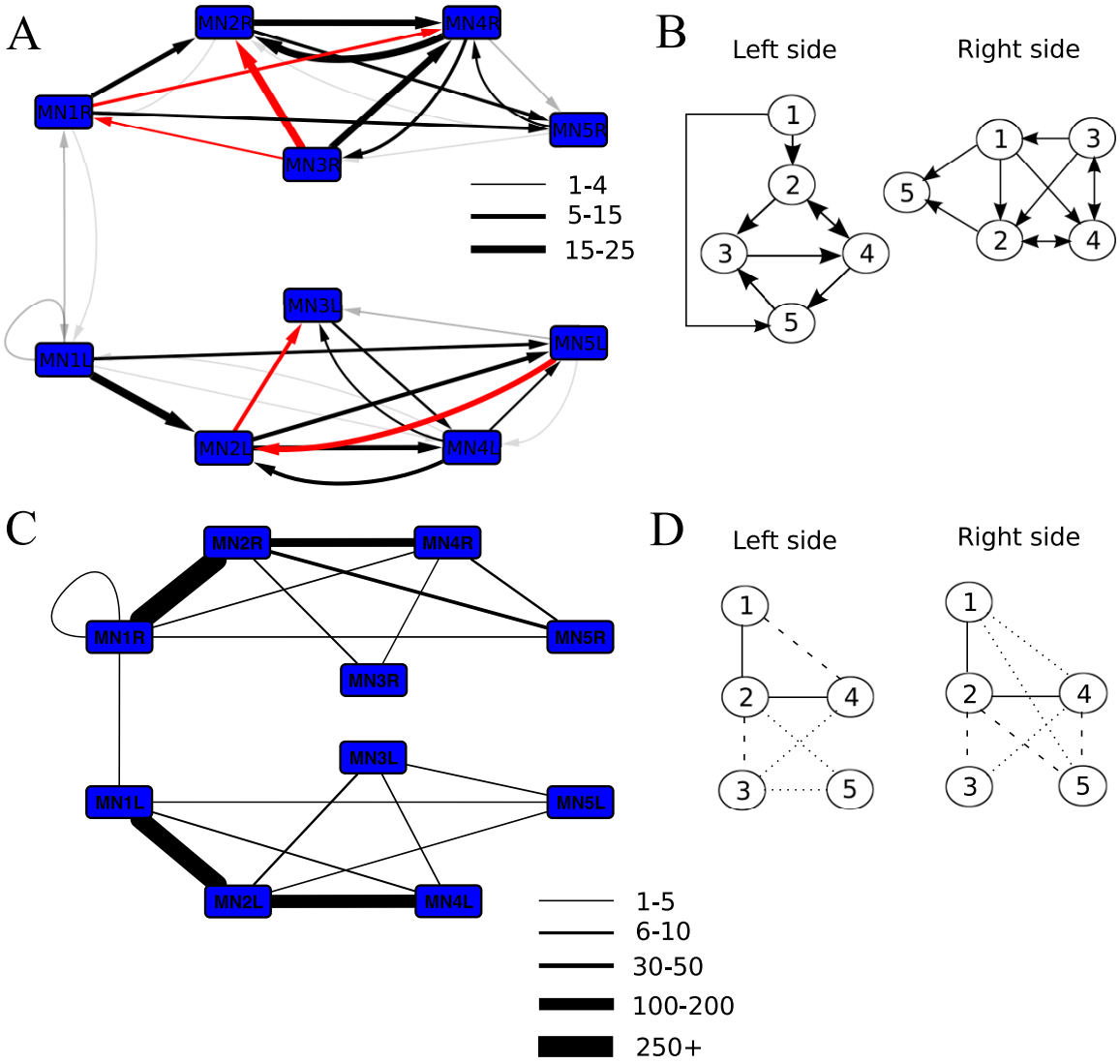

Figure 9.3. Networks of connections between motor neurons of the motor ganglion. A) Synaptic network of motor neurons 1-5 on the left (MN1-5L) and right (MN1-5R) sides. Arrows illustrate polarity of synapse, line thickness represents the total number of 60-nm sections in which a synapse is observed (key), and gray lines represent synaptic partnerships comprising only a single synapse. Red lines illustrate synaptic contacts that differ between left and right sides of the MG. B) Summary diagrams of motor neuron synaptic networks of left and right sides. C) Network of putative gap junctions between motor neurons of the MG. Line thickness represents the total number of 60-nm sections in which a putative gap junction is observed (key). D) Summary diagrams of putative gap junction network of motor neurons of the left and right sides. Dotted lines represent tentative connections, dashed lines represent minimal contacts, and solid lines represent connections with many large contact sites.

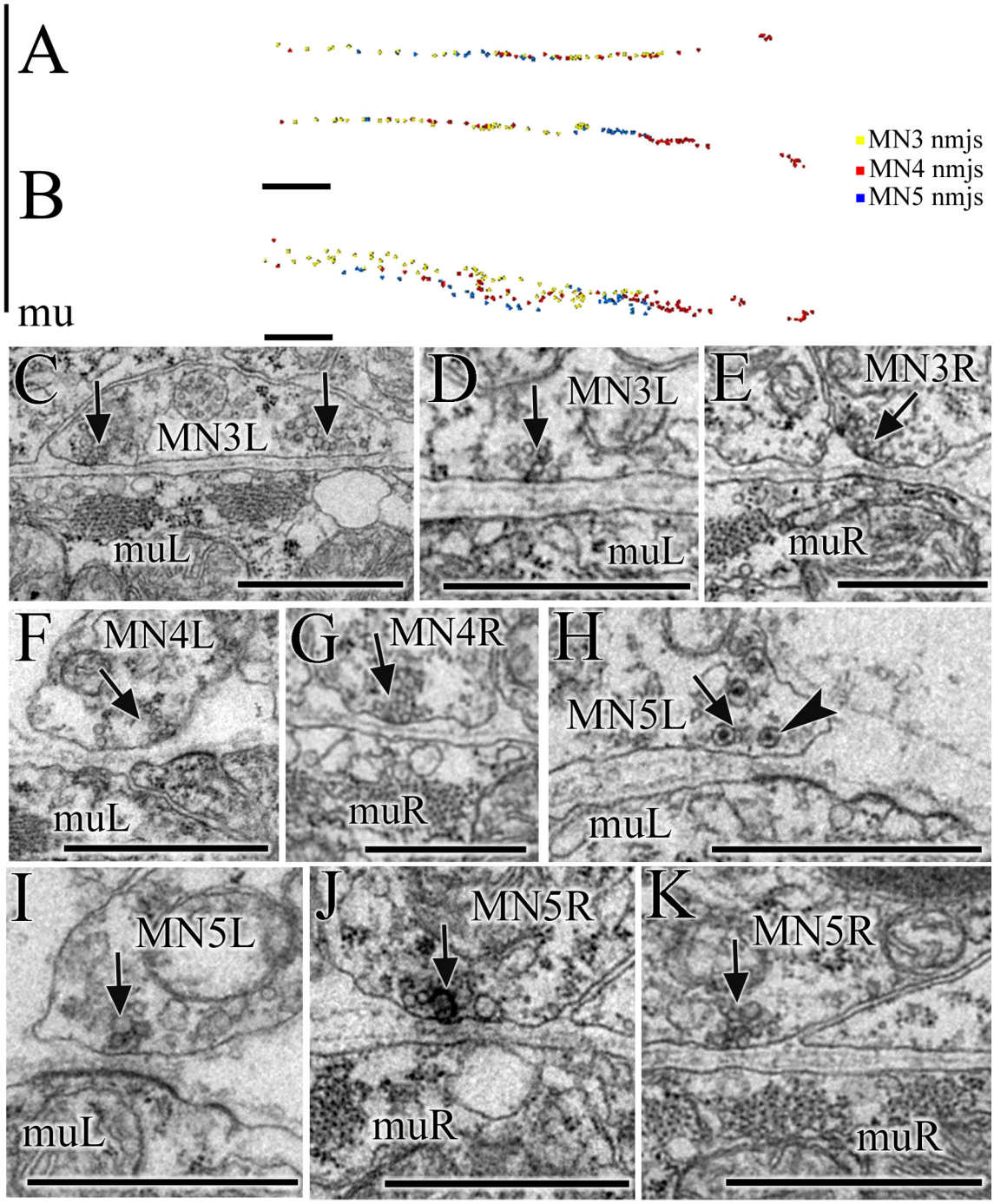

Figure 9.4. Neuromuscular junctions of three posteriormost motorneurons (MN3-MN5) of the motor ganglion. A) Reconstructed neuromuscular junctions of motor neurons, MN3, MN4 and MN5, of the motor ganglion from dorsal (A) and left lateral (B) views relative to the anterior extent of muscle cells (mu). C-K) Micrographs of neuromuscular junctions (arrows) from left (L) and right (R) partners of each pair of motor neurons, MN3 (C-E), MN4 (F-G), and MN5 (H-K) onto postsynaptic dorsal muscle cells of left (muL) and right (muR) sides. H) Some presynaptic neuromuscular sites of MN5s contain dense core vesicles (arrowhead). Scale bars: 10µm (A-B) and 1µm (C-K).

Figure 9.5. Synapses of ascending contralateral inhibitory neurons (ACIN) neurons. A) Dorsal view of reconstructed ACINs, including fine ascending and descending invaginating neurites along the midline (arrowheads). B) ACIN synapses onto ipsilateral motor neurons represented by blue puncta (ventral view). C) Reconstructions of synapses from ACIN onto basement membrane opposite the notochord are represented by white puncta (ventral view). D-F) ACIN dyad synapses (arrows) onto ipsilateral motor neurons MN2-MN4 on the right (D) and left (E-F), and an unpaired tail interneuron (PVGN2) on the right (D). G-H) ACIN contacts with ipsilateral muscle cells (arrows), either with (G) or without (H) presynaptic vesicles. Only G is a possible synapse. I-K) Synapses from ACIN2L (I) ACIN2R (J) and ACIN1L (K) onto the ventral basement membrane opposite the notochord. ACIN collateral neurite invaginating overlying ependymal cell indicated with asterisk in I. L) Network of synapses between ACINs and their ipsilateral motor neuron partners. Arrows indicated polarity of synapse and line thickness represents cumulative number of sections in which synapses are observed. Scale bars: 10μm (A-C); 1μm (D-K).

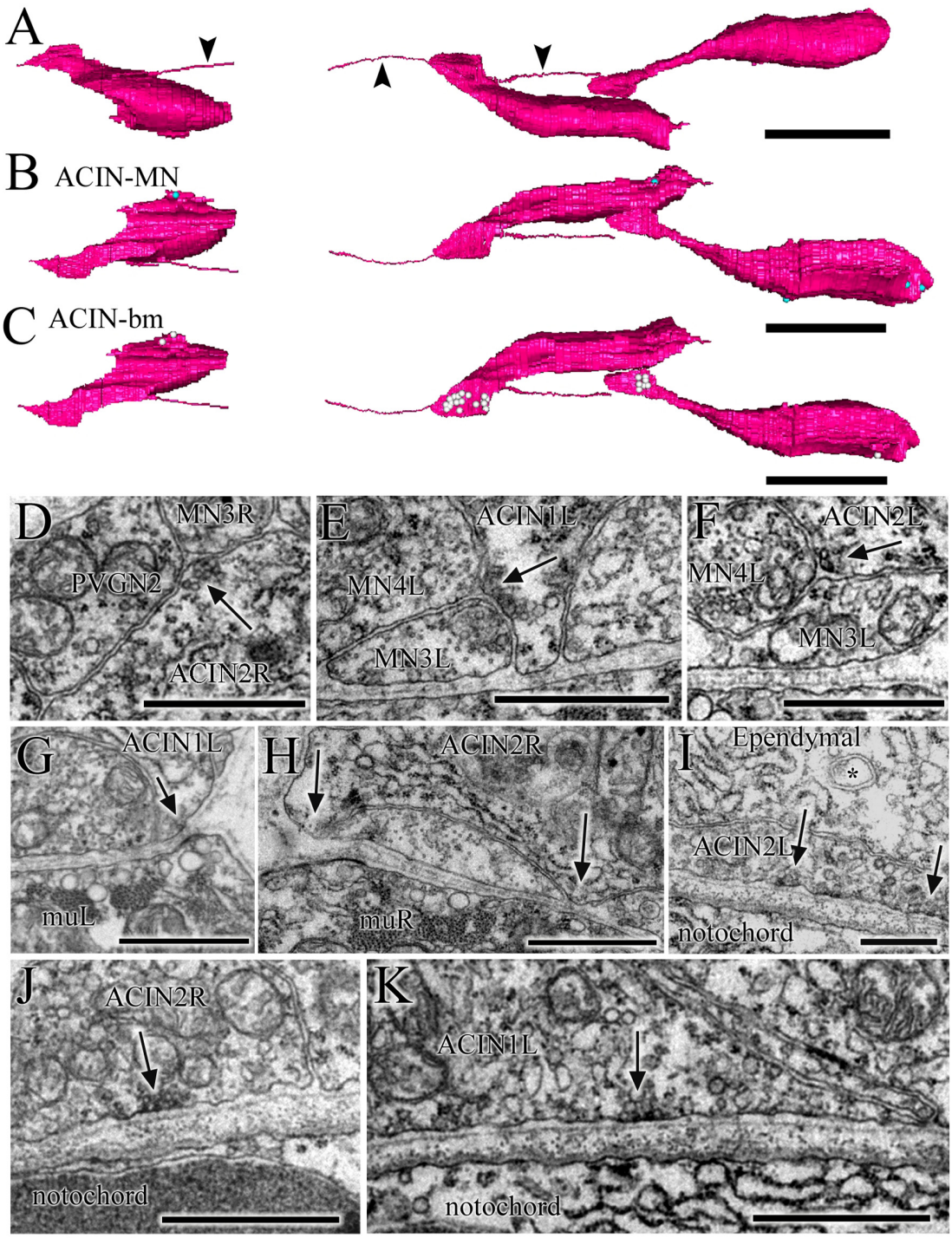
A
B ACIN-MN
C ACIN-bm
D
MN3R
PVGN2
ACIN2R
E
ACIN1L
MN4L
MN3L
F
ACIN2L
MN4L
MN3L
G
ACIN1L
muL
H
ACIN2R
muR
I
Ependymal
*
ACIN2L
notochord
J
ACIN2R
notochord
K
ACIN1L
notochord
L
MN1L
MN2L
MN3L
MN4L
ACIN1L
ACIN2L
ACIN2R
MN2R
MN3R
10-15
5-9
1-4

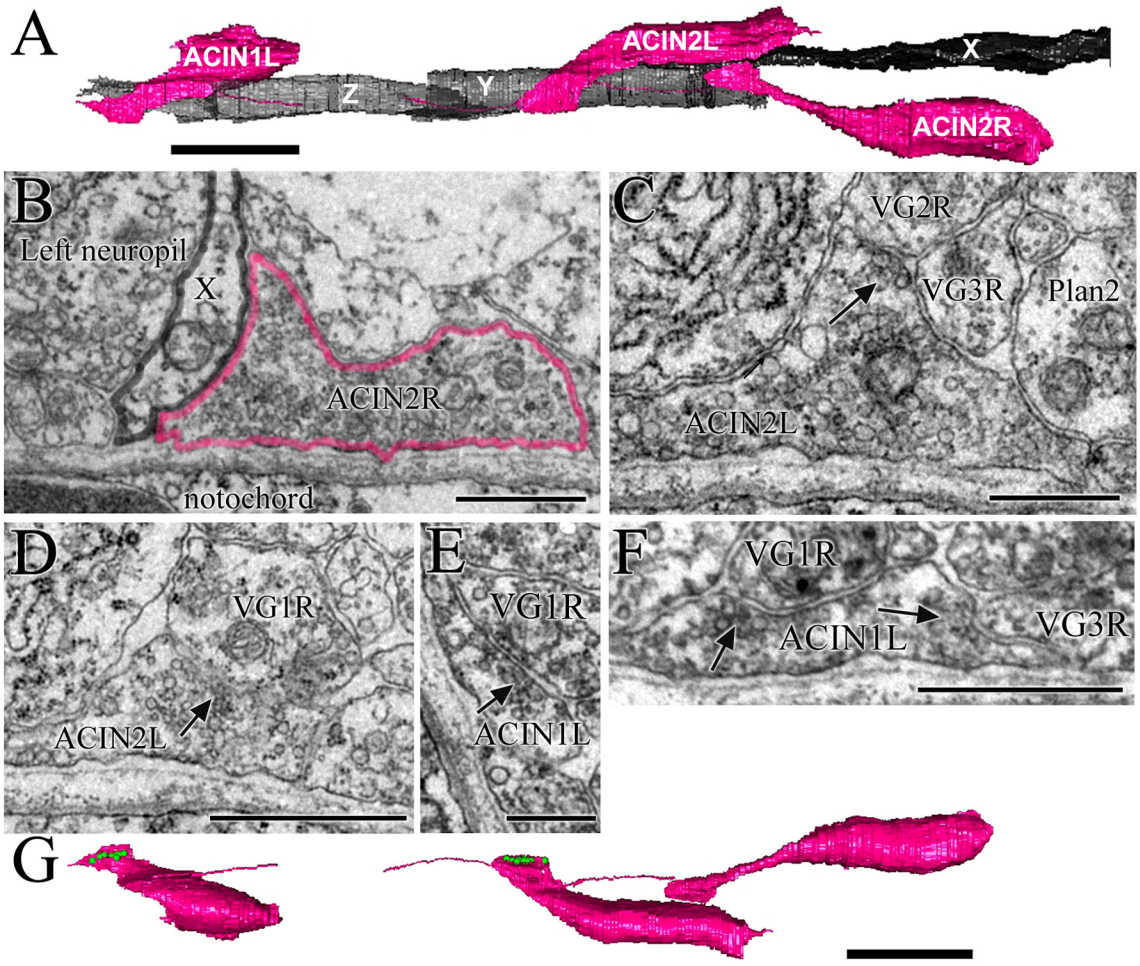

Figure 9.6. ACINs and ependymal cell contacts. A. Ventral view of ACINs (pink) and ependymal cells (black) overlying axons crossing the midline. B) ACIN2R does not contact the left neuropil, but is blocked by ependymal cell X (white arrow in A). C-F) ACIN presynaptic sites (arrows) onto contralateral VGN interneurons at dyad (C) and monad (D-F) synapses. G) Reconstructions of synapses from ACINs onto contralateral VGNs. Scale bars: 10µm (A and G); 1µm (B-D, F); 500nm (E).

interneurons VG1L, VGL and VG2R, and ACIN1L is presynaptic to the right descending decussating neuron, the axon of which forms contacts along the left side axon tract. For contralateral input, only the left side ACINs fully decussate to provide synaptic input to contralateral motor ganglion interneurons, VG1R, VG2R and VG3R (Fig. 9.6B-G), the most numerous of these being at 6 contacts and 7 contacts onto VG1R from ACIN1L and ACIN2L, respectively. The right side ACIN does not pass the left ependymal cell to reach the neuropil (Fig. 9.6A). The ACIN cell bodies are also adjacent to dorsal muscle cells at several stretches (Fig. 9.5H-I), although presynaptic vesicles are lacking at most of these sites.

The other critical elements of a presumed motor CPG are its descending interneurons. There are three descending pairs of interneurons in the ventral motor ganglion: VGN1, VGN2, and VGN3. The pair of VGN1 neurons contact each other at their cell bodies and the proximal portions of their axons, which are both on either side of the midline, alongside the descending neuropil from the brain vesicle (Fig. 9.7A, D, F). Although VGN2 cell bodies are farther apart and do not make contacts between their cell bodies, both neurons extend dendrites into the central neuropil that contact each other near the midline (Fig. 9.7A, B, F). The third pair of VGNs has cell bodies on either side of the neural canal that are more dorsal, and that extend their axons ventrally into the neuropil. This pair does not make contact, and each remains exclusively on its own side of the neuropil without approaching the midline (Fig. 9.7A, C).

Although both VG1s and VG2s contact their partners, only VGN1 partners make synaptic and putative gap junction contacts with each other (Fig. 9.7E). However, on each side the three VGN interneurons are synaptically connected, although their

Figure 9.7. Dorsal views of interneurons of the motor ganglion. A-D) Reconstructions of three anterior pairs of descending ipsilateral motor ganglion interneurons (A), comprising VGN1 (D), VGN2 (B) and VGN3 (C). Anterior is to the left. E) VGN1 partners form putative gap junctions (red puncta) at contact sites between their cell bodies and rostral axons. Dorsal view, anterior to top. F) Single section through the anterior motor ganglion illustrating proximity of VGN1 (labeled VG1L,R) left and right axons (gray) on the midline and dendritic branches of VGN2 (=VG2) neurons (white) within the neuropil of axons and terminals of brain vesicle neurons (coloured cells). Scale bars: 10μm.

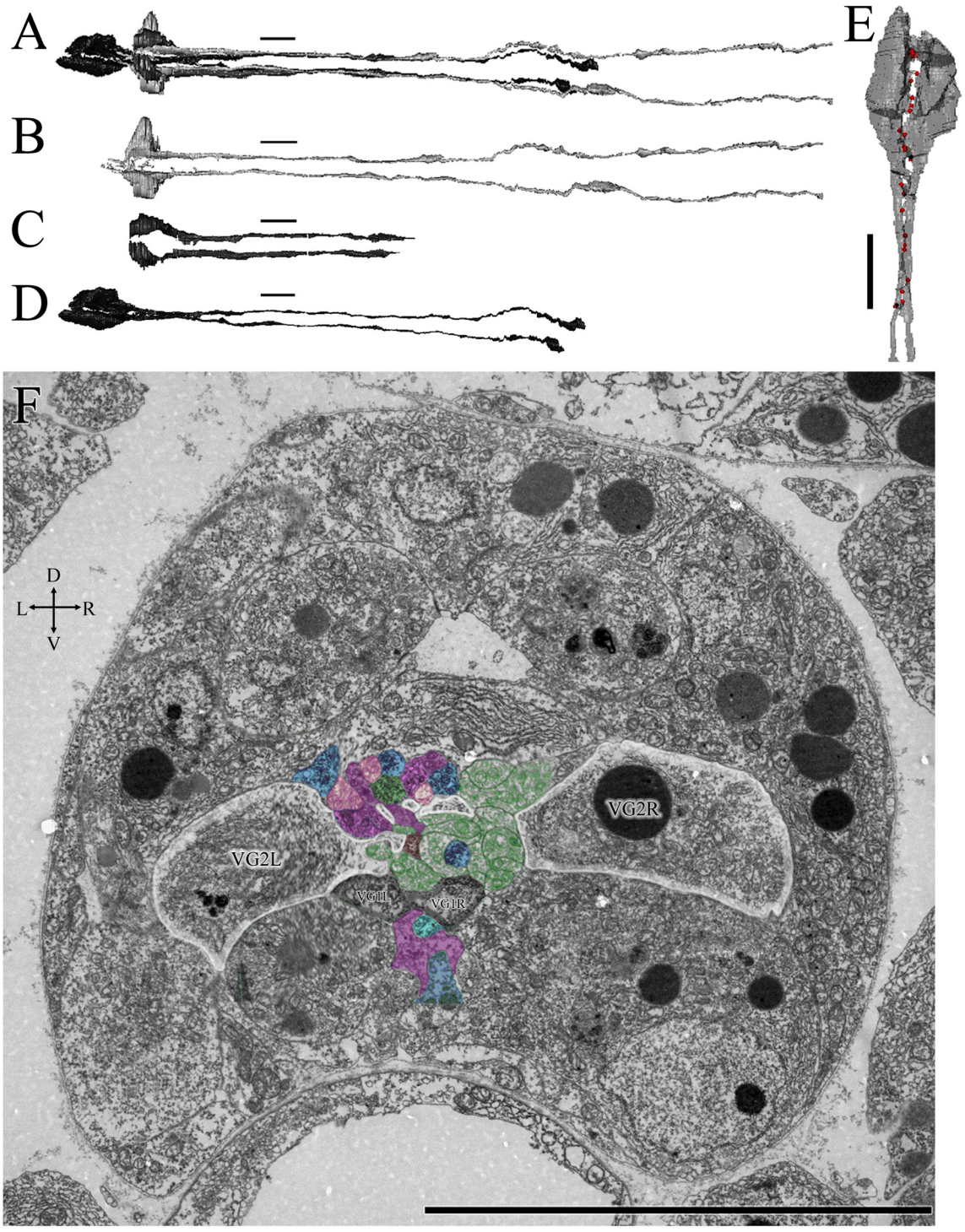
A
B
C
D
E
F
D
L
R
V
VG2L
VG2R
VG1L
VG1R

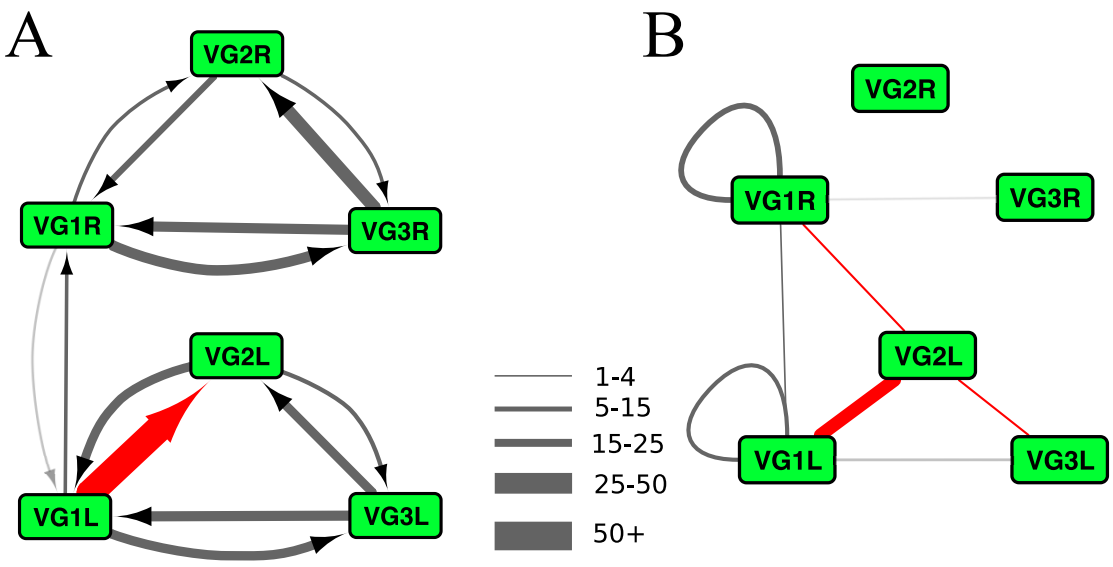

Figure 9.8. Networks of connections between descending ipsilateral motor ganglion interneurons. A) Synaptic network of descending ipsilateral interneurons (VGNs) of the motor ganglion. Arrows indicate polarity of synapses. B) Network of putative gap junctions between descending ipsilateral interneurons of the motor ganglion. Line thickness in A and B represents the total number of 60-nm sections in which a putative gap junction is observed (key). Red lines illustrate connections that differ between left and right sides of the motor ganglion.

connections differ between left and right sides (Fig. 9.8). On the left, all are completely connected, so that each is presynaptic and postsynaptic to both of the other two interneurons. On the right side, however, VG1 is only presynaptic to VG2 at a single synapse, and is not presynaptic to VG3 (Fig. 9.7A). I can only presume that these interneurons know what synapses to form, but the weak synaptic connection from VG1R to VG2R is particularly notable because on the left VG1L provides synaptic input to VG2L at 15 sites, a large number of synapses relative to other contacts in this region. Finally, VG1L and VG1R are themselves reciprocally connected by synaptic contacts, at 1 axo-axonal synaptic site from right to left and 2 (one axo-axonal and one dendro-somatic) from left to right.

Interneurons of the motor ganglion are presynaptic to motor neurons, all VGN to MN synapses being ipsilateral, occurring onto neurons of the same side. Both left and right VGN1s provide synaptic input to MN1s, with more input on the right (5 synapses) than left (1 synapse) side. This asymmetry holds for the overall inputs from VGNs to both of the first two pairs of motor neurons, with more synapses to the right than the left partner of each. VGN3 provides input to both MN1s as well as both MN2s, although the input to the latter occurs at only a single synapse on each side. VG2s form the most synaptic contacts onto motor neurons, forming connections with all but MN1L and the MN3s (Fig. 9.9). Most synapses from VGN2 occur on the right side from VG2R to MN2R at 16 contacts. The input to MN3s differs on left and right sides, originating from VGN2L on the left, but VGN1R on the right (Fig. 9.9). The two caudal-most motor neurons, MN4 and MN5, receive synaptic input only from VGN2s (of the motor ganglion interneurons, VGNs), with similar input from the left and right sides (Fig. 9.9). Several synaptic inputs

Figure 9.9. Network of synaptic connections of motor ganglion motor neurons (MNs), descending ipsilateral interneurons (VGNs) and ascending contralateral inhibitory neurons (ACINs). A) Synaptic network with arrows indicating polarity of synaptic contacts. Thickness of lines represents cumulative number of 60-nm sections in which synaptic contacts are observed (key). Dashed lines indicate synapses from contralateral ACIN neurons. B) Network summary of CPG components. Arrowhead size scales to total size of all synapses between partners. Blue lines represent synaptic inputs from motor neurons, black lines represent synaptic inputs from interneurons, dashed lines represent synaptic inputs from ACINs.

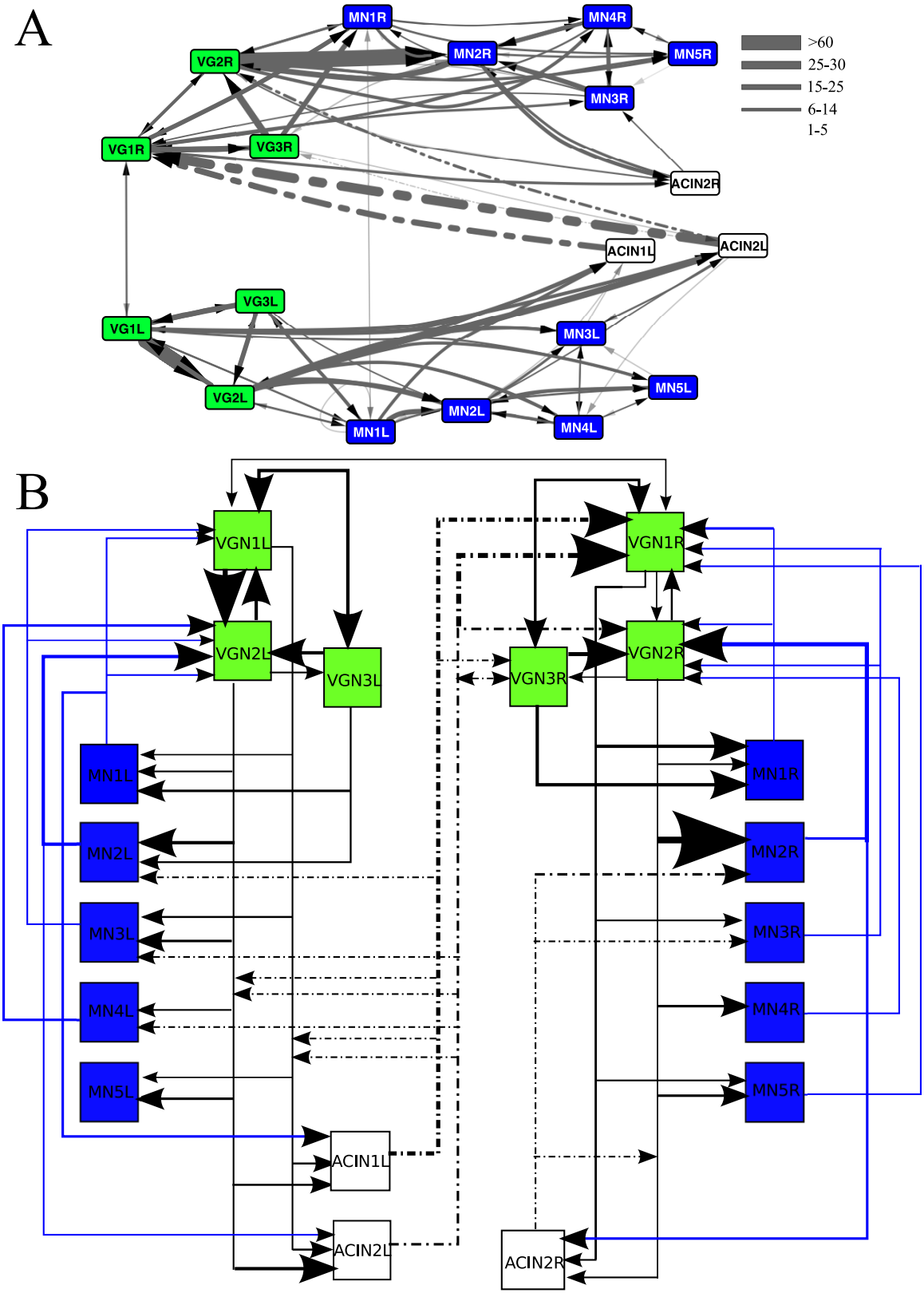
A
MN1R
MN4R
VG2R
MN2R
MN5R
MN3R
VG1R
VG3R
ACIN2R
ACIN1L
ACIN2L
VG3L
VG1L
MN3L
MN5L
VG2L
MN2L
MN4L
MN1L
>60
25-30
15-25
6-14
1-5
B
VGN1L
VGN1R
VGN2L
VGN2R
VGN3L
VGN3R
MN1L
MN1R
MN2L
MN2R
MN3L
MN3R
MN4L
MN4R
MN5L
MN5R
ACIN1L
ACIN2L
ACIN2R

from VGNs to ACINs are also observed between ipsilateral neurons. On the left, VGN1L and VGN2L are both presynaptic to both ACIN1L and ACIN2L at 3 to 4 synapses each, but these synapses vary in size, from ones spanning only two 60-nm sections to others from VG2L to ACIN2L spanning more than ten sections each (Fig. 9.9). Although there is only one ACIN on the right, ACIN2R also receives synaptic input from both VGN1R and VGN2R at 1 to 2 synapses each, that span between three and ten sections (Fig. 9.9). Only a single contralateral synapse from VGN3R occurs onto ACIN2L, which is small, spanning only two sections.

While putative gap junction connections also exist in the motor ganglion (Ryan, 2015: Chapter 8), most recapitulate the putative excitatory synaptic connections described above. The most significant of these in terms of the CPG are those between left and right sides of the motor ganglion. These occur at many contacts between VGN1 neurons, and at far fewer contacts between VGN1L and MN1R. The number of these putative junctions between this first pair of VGN interneurons is 20, compared with only three total chemical synaptic connections between the two neurons in either direction. Likewise, their total size occupies 122 60-nm sections compared with only 7 sections for their chemical synapses. Although we have cannot yet know the postsynaptic currents generated by these, from the shear numbers of contacts alone it would appear that electrical transmission could exceed that from chemical transmission.

9.3 **Discussion**

In order for a CPG to underlie symmetrical swimming in *Ciona* there must be excitation of both left and right muscle. Anatomical connections and light microscopy support the presence of excitatory components that are responsive to excitation, as suggested in larval

Ciona by symmetrical swimming movements in a reduced preparation consisting of the nerve cord and motor ganglion (Nishino et al., 2010). Excitation in the physiological experiment of Nishino et al. (2010) was achieved by application of L-glutamate, but glutamate is not reported in any motor ganglion neurons or any neurons projecting from the brain vesicle to the ventral motor ganglion. Thus, it is surprising that these neurons would possess glutamate receptors unless vGLUT reporters have failed to label existing glutamatergic input to the ventral motor ganglion. Alternatively, the dorsal ascending motor ganglion neurons that receive glutamatergic input from both the ascending trunk epidermal neurons and dorsal caudal epidermal neurons should express glutamate receptors, and provide synaptic input to the ventral motor ganglion, and so may have been responsible for the activation of motor activity. This anomaly warrants further investigation, but discussion of preliminary results suggests that some of the posteriormost brain vesicle relay neurons may express reporters for glutamate (Horie, pers. comm.). Nonetheless, the requirement to produce symmetrical swimming is for excitation to occur alternately, first on one side and then on the other, which suggests that excitation of one side alone should drive excitation of the other, although physiological confirmation of this pattern is lacking. Based on identified anatomical synapses, the candidates for this side-to-side co-activation are motor ganglion interneuron VG1 and MN1 neurons, and the small, scarce chemical synapses between the left and right sides suggests that electrical coupling at putative gap junctions, especially between VG1 neurons may function in this capacity.

Rhythmic coordination is a critical aspect of central pattern generation, so it is important to account for the symmetry of the timing of alternate flexions in the symmetrical

swimming behaviours of ascidian larvae. To explain this aspect of both the shadow response and spontaneous swimming behaviour, the proceeding discussion considers the nature of the neurons in the motor ganglion themselves. There is currently no *in vivo* record of the direct output from individual neurons, neither in *Ciona* nor any other species of ascidian larva, which limits our ability to use synaptic information to model neuronal firing. However, muscle field recordings indicate that within each side of the animal, an on-off pattern is established, which must itself be coordinated between the left and right sides of the animal.

The on-off pattern observed on each side of the *Ciona* is regular, and is retained even when symmetrical alternation is disturbed by genetic or chemical means (Nishino et al., 2010). This retention of a pattern on a single side suggests that each side of the motor ganglion has a mechanism for the alternation of motor neuron activity between an on state and an off state. One way this type of regular pattern could be generated is by an intrinsically bursting neuron. Fast rhythmic bursting neurons in other animals fire bursts at 30-50 Hz (Niedermeyer and da Silva, 2005), while the frequency of activity in *Ciona* is 10-40 Hz (Nishino et al., 2010), so falling within this range. In vertebrate neurons, this type of bursting pattern can be established by a tetrodotoxin (TTX)-sensitive persistent sodium current, INaP (Del Negro et al., 2002; Tryba et al., 2011). Such TTX-sensitive sodium currents are observed in *Ciona* oocytes (Cuomo et al., 2006), and some sodium channel genes (TuNa) are expressed in ascidian motor neurons (Okada et al., 1997). However, only one potential recording from a cultured *Ciona* motor neuron is reported in the literature, and shows only a single spike upon depolarization (Zanetti et al., 2007). Given the lack of data on rhythmic bursting in ascidians, I cannot address further whether

intrinsic bursting might result in the muscle activity pattern involved in symmetrical swimming. Techniques for observing neuronal activity could be applied to assess this possibility, especially within the motor ganglion in neurons for which we have specific reporters, such as anterior motor neurons (MN1 and MN2). This must remain a priority for future studies.

Another mechanism that could drive putative on-off alternation on one side could arise through a reciprocal feedback network between a single inhibitory neuron and a single excitatory neuron on each side. Although the neurotransmitter of the fourth pair of motor neurons is unknown, MN4 on each side forms synapses and gap junctions with the ipsilateral second, putatively cholinergic, pair of motor neurons, MN2s. Many of these connections are observed near neuromuscular junctions, although an inhibitory neurotransmitter and rectification of gap junctions would be necessary for this coupling to provide the necessary on-off pattern generation. Both means of establishing a rhythm on each side may co-exist in the *Ciona* larval motor system. *Ciona* larvae exhibit two distinct frequencies of symmetrical swimming, which imply some differences in the mechanisms underlying spontaneous vs. light-induced swimming, the frequency of the latter changing with larval age (Zega et al., 2006). While these mechanisms may explain the intrinsic rhythms of each side, in symmetrical swimming driven by a shadow response, at least, the disruption of muscle contractions when glycine receptors are blocked suggests a role for the inhibitory regulation of timing. Thus, contralateral inhibition, as suggested by the action of glycine and the presence of ascending contralateral Inhibitory neurons, ACINs, is likely to be an important component of this rhythmic coordination.

Glycinergic transmission by ACINs is implicated in the orderly coordination of the symmetrical contractions, but the underlying mechanism of action is unclear. Previous studies propose a direct inhibition by glycinergic synapses from these ACINs to contralateral motor neurons. However, our data reveal a far greater complexity in their connections, and prospectively of their mechanism of action, that does not involve any direct inhibition of contralateral motor neurons (Fig. 9.1). Likewise, ACINs are not reciprocally connected with each other, as are the inhibitory neurons in the lamprey CPG (Grillner et al., 1998). ACINs exhibit some degree of variation in their number and location (Nishino et al., 2010; Nishitsuji et al., 2012), which is exemplified in our larva, with only three such neurons. Of these, only the left side ACIN neurons provide presynaptic input to neurons of the contralateral neuropil (Fig. 9.8). Thus, our data predict that these neurons form an asymmetrical network with inhibitory input from left to right.

Detailed analyses reveal that on the left side both the first unpaired ascending contralateral inhibitory neuron, ACIN, and the second paired ACIN are postsynaptic to ipsilateral descending motor ganglion interneurons, VGN1 and VGN2. In addition to these putatively cholinergic inputs, the two ACINs on the left are postsynaptic to motor neurons, but these differ, ACIN1 being postsynaptic to MN1, while ACIN2 is postsynaptic to MN2. In turn, these ACINs provide direct feedback to both ipsilateral interneurons, and to MN2. Neither provides feedback to its ipsilateral MN1L, however. A reciprocal circuit also exists between only the first left side ACIN and the contralateral descending decussating neuron, which itself is presynaptic to targets on the left side. Although neither ACIN provides input to MN4, both are presynaptic onto the left MN4

neuron, which may also be inhibitory. Thus, while these left side ACINs both appear to be excited by the first two descending motor ganglion interneurons, they also provide inhibitory feedback to the latter. However, the differences between the inputs from the motor neurons to the first and second ACINs on the left side may reflect or suggest different roles for ACIN1L and ACIN2L, especially as these first two motor neurons differ morphologically, forming neuromuscular junctions in different regions.

On the contralateral side (R), both left side ACINs provide putative inhibitory synaptic input to the first two descending paired interneurons, VGN1 and VGN2. However, the first ACIN on the left, but not the second, is also presynaptic to VGN3 on the right side. Both of these ACIN neurons, in turn are qualified to inhibit contralateral interneurons, but not motor neurons. The neurotransmitter of the third interneuron, VGN3, is unclear, so its unique inhibition by ACIN1L may further suggest differences in the roles for the two ACIN neurons.

On the right side, the ACIN neuron receives synaptic input from the first ipsilateral interneuron, VGN1, but instead of reciprocal input to VGN1, it is presynaptic to the ipsilateral right side VGN2 neuron. This neuron is located just caudal to ACIN2 on the left side, and both (ACIN2L and ACIN2R) are postsynaptic to ipsilateral MN2s but not MN1s, lending further support to possibly unique roles for ACIN1 and ACIN2. However, in this larva no right side ACIN provides synaptic input to the contralateral left side. Without symmetrical inhibition, the feedback inhibition of the interneurons and motor neurons on the left by left-side ACINs may provide a mechanism whereby the left and right sides can be alternately inhibited ipsilaterally. It is interesting, however, that no ACIN is presynaptic to MN1, but all are presynaptic to their ipsilateral MN2, and two of

three are presynaptic to each of MN3 and MN4. Likewise, VGN1 on the right is only presynaptic to the ipsilateral ACIN, but receives no inhibitory feedback. VGN1 and MN1 neurons are the only cell pairs connected across the midline by synapses or gap junctions, and the synaptic partnership between VGN1 and VGN2 is the most apparent asymmetry in terms of both chemical synapses and gap junctions, being strongly connected on the left but not the right side. Thus, the simple network of the right-side ACIN would provide a circuit whereby activating VGN1 would lead to the inhibition of its downstream ipsilateral excitatory motor network as well as inhibition of the other major excitatory descending interneuron, VGN2, which itself receives little input from VGN1 on the right side. This proposed mechanism further implies a sidedness to the system, and an asymmetry in the ipsilateral inhibition by ACINs.

Despite the sidedness it manifests, there are several symmetrical connections, not involving ACINs, that contribute to feed forward and feedback loops within the ventral motor ganglion. On both the left and right sides, the first pair of interneurons, VGN1s, provides synaptic input to their ipsilateral interneurons and to the first pair of motor neurons, MN1s. However, as mentioned, the synapses from VGN1s to VGN2s are more numerous on the left than the right side. This second pair of interneurons, the VGN2s, provides synaptic input to ipsilateral motor neurons, MN4s, and contralateral descending decussating neurons, and interacts reciprocally with ipsilateral MN2 motor neurons. On both sides the third pair of interneurons also provides symmetrical input to ipsilateral interneurons as well as being presynaptic to the first motor neuron (although this connection is not symmetrical). The left and right motor neurons also have symmetrical synaptic connections on both sides, from the first pair to the second pair, and reciprocally

between the second and fourth pair. Contralaterally, the decussating interneuron pair provides symmetrical synaptic input to the first two pairs of MNs and reciprocal synaptic interactions with both partners of the first and third pair of interneurons, VGN1 and VGN3. Together, these symmetrical connections establish feedforward loops from interneurons to the motor neurons that exist on both sides of the animal (Fig. 9.10A). Positive feedback is also apparent in these loops (Fig. 9.10A), which could allow adjustment of their collective output and reduce sensitivity to rapid input fluctuations while maintaining sensitivity to longer term changes in input (Hornung and Barkai, 2008). Given the reciprocity in these networks, they possess both regulating loops (X and Y reciprocally connected, both feeding into Z) and regulated loops (Z regulating both X and Y, which are reciprocally connected). Putative negative feedback and feedforward loops also exist on both sides between the interneurons (Fig. 9.10B), along with a putative negative feed forward loop through the third pair of interneurons to the first motor neuron (Fig. 9.10C). Inhibitory feedback loops involving MN4s are also symmetrical, and are discussed in greater depth below.

In this way, excitation of either of the first two interneurons on either side of the larva by their upstream partners seems anatomically qualified to generate motor activity on the ipsilateral side, as follows:

[VG1→MN1, VG2→MN2/MN4], with feedforward and feedback within and between both pathways.

The foregoing analysis must of course be qualified by the lack of rigorous knowledge of the polarity of synaptic transmission, and also depends on the significance of the synaptic contacts as defined anatomically and by numerical means.

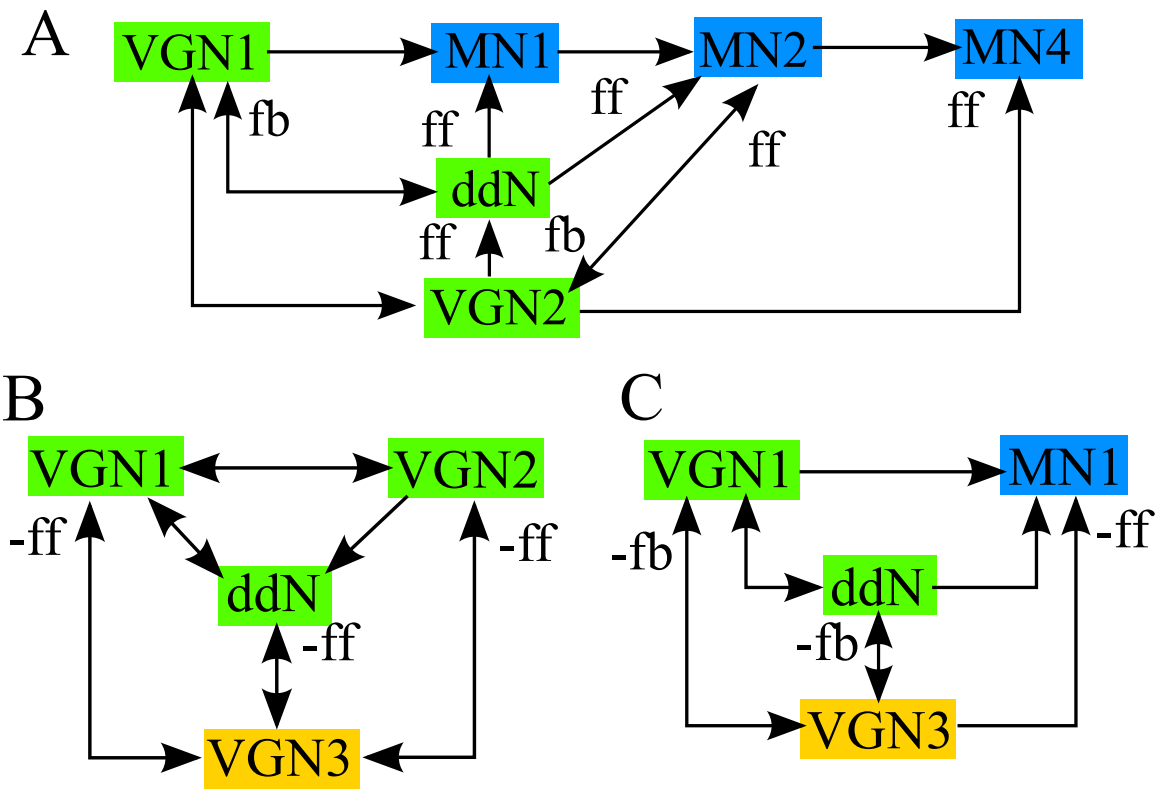

Figure 9.10. Symmetrical feedback and feedforward circuits of neurons of the motor ganglion. A) Positive feedback (fb) and feedforward (ff) circuits present on both sides of the motor ganglion. B) Negative feedback (-fb) and feedforward (-ff) circuits from putatively inhibitory VGN3 neuron within interneuron network on each side of the motor ganglion. C) Negative feedback (-fb) and feedforward (-ff) circuits from putatively inhibitory VGN3 involving interneurons and motor neuron 1 (MN1) on both sides of the motor ganglion. Arrows represent polarity of synaptic connections.

Along with these symmetrical pathways, some of the partnerships that exist on both the left and right side of the larva exhibit feedback loops on only one side. In particular, only the left second motor ganglion interneuron (VGN2) partner receives feedback from the contralateral decussating interneuron. Thus, the right contralateral descending decussating paired motor ganglion neuron, ddNR, provides feedback to VGN2L, but this is probably excitatory. Although the first two pairs of motor neurons are presynaptic to their contralateral decussating neurons on both the left and the right side, these synapses are few and small, with the exception of two larger synapses from the second motor neuron on the right MN2R, which may provide more excitatory feedback. This possibility could be used to maintain firing of the contralateral ddN, although again this is an anatomically based possibility and subject to the same qualifications as before.

In addition to the partial asymmetries and the asymmetries involving ACINs, other connections in the motor ganglion network support the presence of sidedness in the synaptic circuits of the larva's motor ganglion. These include the following:

1) Only VGN1L forms presynaptic contacts onto the ipsilateral MN2L as well as its own right side partner, VGN1R.
2) Similarly, only the left-side second interneuron, VGN2L, provides presynaptic input to its ipsilateral MN1 (L).

These again illustrate the asymmetry involving the first two pairs of interneurons and motor neurons.

Although the descending decussating neurons may have a unique role (see Ryan, 2015: Chapter 10) outside of any involvement in the CPG, the asymmetry of their synapses also contributes to our understanding of sidedness in the motor ganglion. Only the left partner

of the ddN (descending decussating interneuron) pair forms presynaptic synapses onto its ipsilateral motor neuron, MN1(L), and like VGN1 (the descending paired motor ganglion interneuron), also provides synaptic input to its own right partner. Thus, the left, but not the right, ddN could be capable of exciting its ipsilateral, left motor ganglion side. This left side of the motor ganglion is also anatomically qualified to excite the right side through the first pair of interneurons. Together, these seemingly small asymmetries indicate a mechanism for left side activity driving that of both the left side itself and the right side. Overall, the excitation of both the first two motor neurons by each of the first two excitatory descending interneurons (VGN1 and VGN2) also suggests a stronger initiation of motor control on the left side than the right. This difference may imply some role for synaptic delay allowing for fine control of the system, and together these asymmetries suggest the possibility that fast, strong left-side contractions initiate symmetrical swimming events, a possibility that, if general among all larvae, could be detected by high-speed video recording.

The networks of connections in the motor ganglion support a central pattern generator involving excitatory interneurons, motor neurons, and inhibitory interneurons (Fig. 9.1). The first pairs of both interneurons and motor neurons permit bilateral excitation, and the ACINs permit ipsilateral inhibition on both sides and contralateral inhibition from the left to the right side. The most glaring ambiguity in the CPG model for the *Ciona* larval motor system is the lack of solid evidence for a descending inhibitory interneuron. However, there is no evidence for neurotransmitter phenotype (and therefore sign) in a subset of motor ganglion neurons, including the third pair of interneurons and fourth pair of motor neurons, either or both of which may be inhibitory. Although both proposed

CPG networks involve the same neurons, the CPGs involving the first and second motor neurons differ in their connections (Fig. 9.1). This fits with the observation that there are two unique frequencies of symmetrical swimming driven by either changes in light or during spontaneous periodic bursts.

The networks of the motor ganglion present us with the same problems as do those elsewhere in the larval CNS: the polarity and strength of transmission is either not known, or is based on indirect evidence from reporters or weak evidence from immunoexpression. Even from ultrastructural evidence alone, it is hard to know whether the larval synaptic networks are simply sloppily wired, lacking precision or rigid order, or whether a core of the connections is wired in a more or less stereotypic manner, that is overlain with other connections that are either less precise, or in transit from larval morphogenesis or to metamorphosis. Larval behaviour as exhibited by directional movements or forward swimming may be more complex than has been reported, but still appears simple compared with the networks in the larval CNS, and it may be that we should concern ourselves only with pathways that exceed a particular numerical strength. Answers to these uncertainties, for which this analysis is a first attempt at a solution, albeit one that is comprehensive, will require additional studies.

9.4 **Conclusions**

I present a putative CPG within the *Ciona intestinalis* CNS that differs between the two primary motor neurons of the MG. In each case, the contralateral inhibition coordinating sided contractions is mediated not directly by ACINs, but through inputs to excitatory interneurons that are themselves presynaptic to motor neurons. These are the same interneurons that receive the sensory input from relay neurons

of the BV, and the contralateral inhibition imposed upon them occurs only unilaterally, from left to right. This suggests a sidedness to the system that is also reflected in asymmetries of the components of the motor network.

Chapter 10 : Circuits of a putative startle response and Mauthner-like pathway in the *Ciona intestinalis* larva

10.1 **Introduction**

The descending decussating feature of the descending decussating neurons (ddNs) in the larval CNS of *Ciona* has previously provided a basis to propose their homology with Mauthner cells of tailed aquatic vertebrates (Takamura et al., 2010). Along with this suggested homology, Takamura et al. (2010) have proposed that these neurons may synapse onto contralateral inhibitory ACINs concurrently identified by Horie et al. (2010), making the latter candidate homologues of commissural local inhibitory neurons (CoLos) in the zebrafish. While it is temptingly easy to make such speculative vertebrate comparisons, and while our data on synaptic connections support a Mauthner-like role for ddNs, many basal characteristics of the circuit in larval *Ciona* also exist in hagfish in which it appears they may support instead behaviour more characteristic of a withdrawal response than an escape response. The hagfish withdrawal response also depends, however, on descending decussating interneurons, so may represent the foundation of more complex escape responses as achieved through Mauthner cell pathways. In addition, the proposed interaction of *Ciona* descending decussating neurons (ddNs) with ascending contralateral inhibitory neurons (ACINs), and the synaptic interactions of these ACINs both differ significantly from the CoLos of zebrafish.

Mauthner neurons initiate vibratory or auditory induced escape behaviours in a variety of tailed aquatic vertebrates, the directionality of which is determined by the anterior lateral line. The lateral dendrite of each Mauthner neuron receives vestibular hair cell input from club endings of single-cell afferents from the glutamatergic VIIIth nerve.

Additional input from the VIIIth nerve comes from passive hyperpolarizing potential (PHP) neurons, a common Commissural PHP neuron and an ipsilateral Collateral PHP neuron. Together these provide input to the unmyelinated axon cap region at the Mauthner cell axon hillock. They facilitate feed forward inhibition and control the threshold provided by excitation from the anterior lateral line to Mauthner neurons. The Collateral PHP neurons provide a mechanism for feedback to each M-cell and facilitate inhibitory communication between the paired M-cells. The Mauthner neurons in teleosts integrate information from electrical and chemical transmission from the peripheral neurons by means of specific electrotonic coupling enabled by their axon caps, structures not present in more basal homologues of Mauthner neurons, such as those in the lamprey. The synaptic targets of Mauthner neurons include both ipsilateral and contralateral cranial relay neurons in anterior regions of the brain. Within the motor complex, Mauthner neurons provide synaptic input to contralateral descending interneurons as well as directly onto contralateral primary motor neurons. They also provide input to an ipsilateral Colo (crossed inhibitory interneuron) (Fig. 10.1A).

The best-studied input to vertebrate Mauthner neurons is that generated from hair cells. The main behavioural action of these neurons is called the C-start response, in which excitation of the Mauthner neurons on one side induces widespread activation on the contralateral side of the body. An abrupt sensory stimulus causes the pair of Mauthner neurons to fire, the first determining the initial direction of movement, to produce a characteristic C- bend, and turns the animal away from the stimulus. However, in elongate fishes, lampreys, and some amphibians a withdrawal response involving strong bilateral muscle activation occurs instead (Eaton et al., 1977; Currie and Carlsen, 1987;

Figure 10.1. Comparison between the vertebrate Mauthner escape response pathway and *Ciona* descending decussating putative startle pathway. Cells, colour-coded by cell type, are shown with synaptic connections indicated by lines illustrating gap junctions (Electrical), and excitatory or inhibitory synapses. Anterior is at the top of the page for both. A) Vertebrate Mauthner cell pathway for escape response. Motor neuron input goes to muscle of the same side. B) *Ciona* descending decussating neuron pathway for putative startle response. Descending decussating neurons lack characteristic M-cell body shape. Inputs from peripheral interneurons are shown onto cell bodies and axon hillock regions. Neurons are colour-coded by cell type to match putative homologous counterparts in the vertebrate pathway. Cell types: Mauthner cells (M-cells); VIIIth nerve (VIII nerve); collateral passive hyperpolarizing field potential neurons (collateral PHP); commisural passive hyperpolarizing field potential neurons (Commisural PHP); descending interneurons (Descending IN); motor neurons (Motoneuron); comissural local inhibitory neurons (Commisural inhibitory neurons); descending decussating interneurons (ddNs); ascending dorsal motor ganglion peripheral interneurons (AVG4/5); Eminens 2 neuron (Eminens2); motor ganglion motor neurons (Motoneuron); ascending contralateral inhibitory neurons (ACIN); unpaired right-side posterior motor ganglion interneuron (PVGN); and muscle.

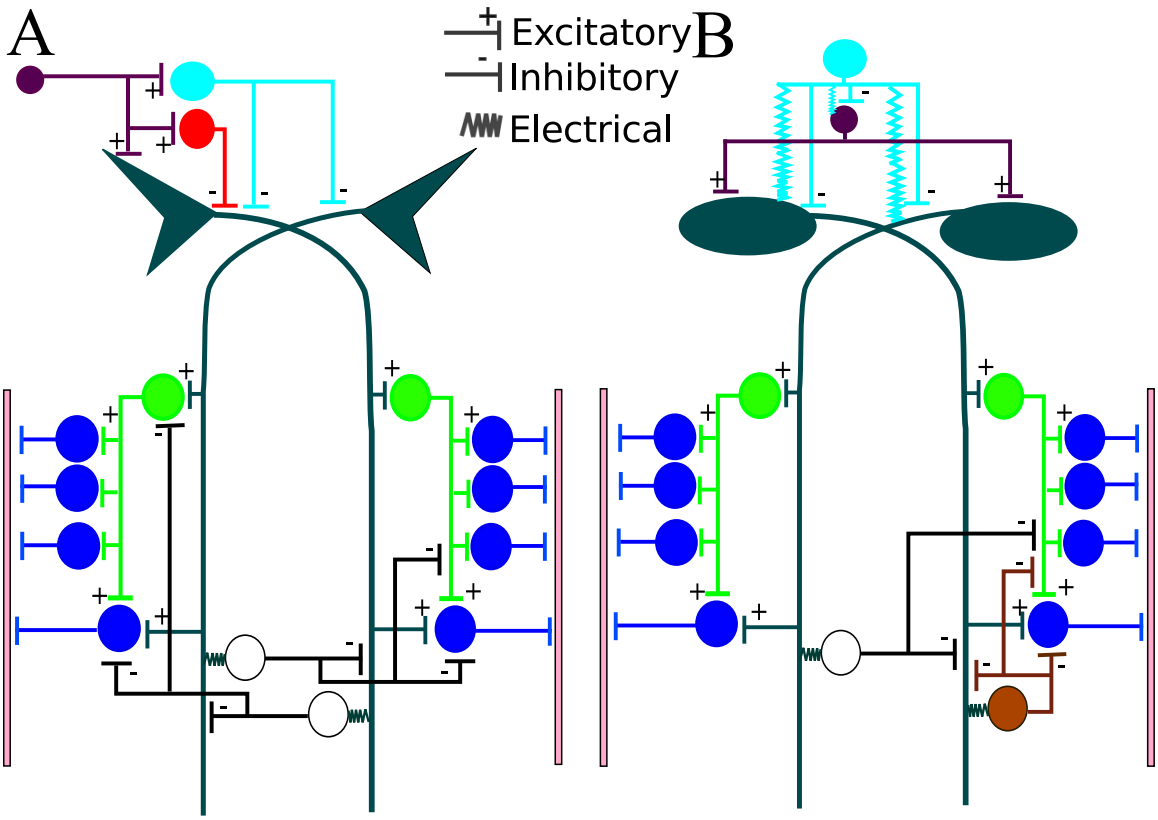

M-cells
VIII nerve
Collateral PHP
Commisural PHP
Descending IN
Motoneuron
Commisural inhibitory neurons
Muscle

ddNs
AVG4/5
Eminens2
VGN
Motoneuron
ACIN
PVGN
Muscle

Currie and Carsen, 1988; Bierman et al., 2004; Ward and Aziz, 2004), and its outcome depends on the animal's resting position (Bierman et al., 2009). This distinction in response appears to depend upon the presence of a composite axon cap structure in other vertebrates (Bierman et al., 2009). Additional fine control of signal strength of Mauthner neuron output is modulated presynaptically, determined through axonal stimulation of these neurons. Presynaptic modulation may be of particular importance in the case of a withdrawal response.

Though the Mauthner neuron is postsynaptic at chemical synapses from a number of partners, its action in vertebrates is modulated largely by electrotonic activity. In particular, the input from the VIIIth nerve occurs at club endings with mixed synapses, involving both chemical and electrical synapses (Nakajima, 1974; Tuttle et al., 1986; Pereda et al., 2003). The fast electrotonic transmission/activation of Mauthner neurons is modulated by adjacent glutamatergic chemical synapses (Pereda and Faber, 1996; Pereda et al., 1998) at gap junctions involving Connexin35 (Pareda et al., 2003). As in Mauthner pathways, in *Ciona* chemical synapses share a role in transmission with putative electrical synapses between ddNs and their partners, identified by anatomical criteria (close apposition of membranes with no associated synaptic vesicles). These electrical couplings provide a means of transmission that is faster and more reliable than at chemical synapses. The latter produce postsynaptic currents when the presynaptic neuron of the couple undergoes an action potential. With electrical transmission, the current appears instantaneously but does not involve amplification, nor can it be facilitated by prior transmission (Bennett, 1997). These types of electrical synapses are therefore frequently incorporated in escape behaviour circuits (for example at crayfish giant fibres,

where electrical transmission in the nervous system was first demonstrated: Furshpan and Potter, 1959) and they mediate fast transmission and a consequent motor response that is fast, fixed and reliable.

The connectome project undertaken in this study allows us to identify not only chemical synapses but also putative gap junctions formed by the descending ddNs in the larval CNS of *Ciona intestinalis*. From this anatomical evidence it is possible to identify the network of connections formed by the ddNs. This network, and the anatomical features of the cells and their connections, will be used as a basis to discuss similarities with and differences from the Mauthner cell networks reported in vertebrate species.

10.2 **Results**

Like Mauthner neurons, the ddNs (descending decussating neurons) of *Ciona intestinalis* receive synaptic input from major pathways that receive input from the peripheral nervous system. The peripheral input to the ddNs occurs via synaptic input from eminens interneurons of the anterior peripheral pathway, ascending motor ganglion interneurons (AVGs), and bipolar planate neurons of the tail (Fig. 10.2). The somata and proximal axon regions of ddNs are postsynaptic at many sites to the eminens and AVG neurons (Fig. 10.2B-C), along with some synaptic input from planate neurons. The eminens neurons are putatively inhibitory GABA neurons (Ryan, 2015: Chapter 4), so these are most likely to be inhibitory and not candidates for activating the ddNs by chemical transmission (as is accomplished in vertebrates via the VIIIth nerve). In contrast, two of the AVG neurons (AVG4 and AVG5) that provide input to the ddNs, appear to correspond to cholinergic neurons (Takamura et al., 2010; Ryan, 2015: Chapter 4), while one other -- AVG2 -- is putatively GABAergic (as is AVG7, which provides only a single

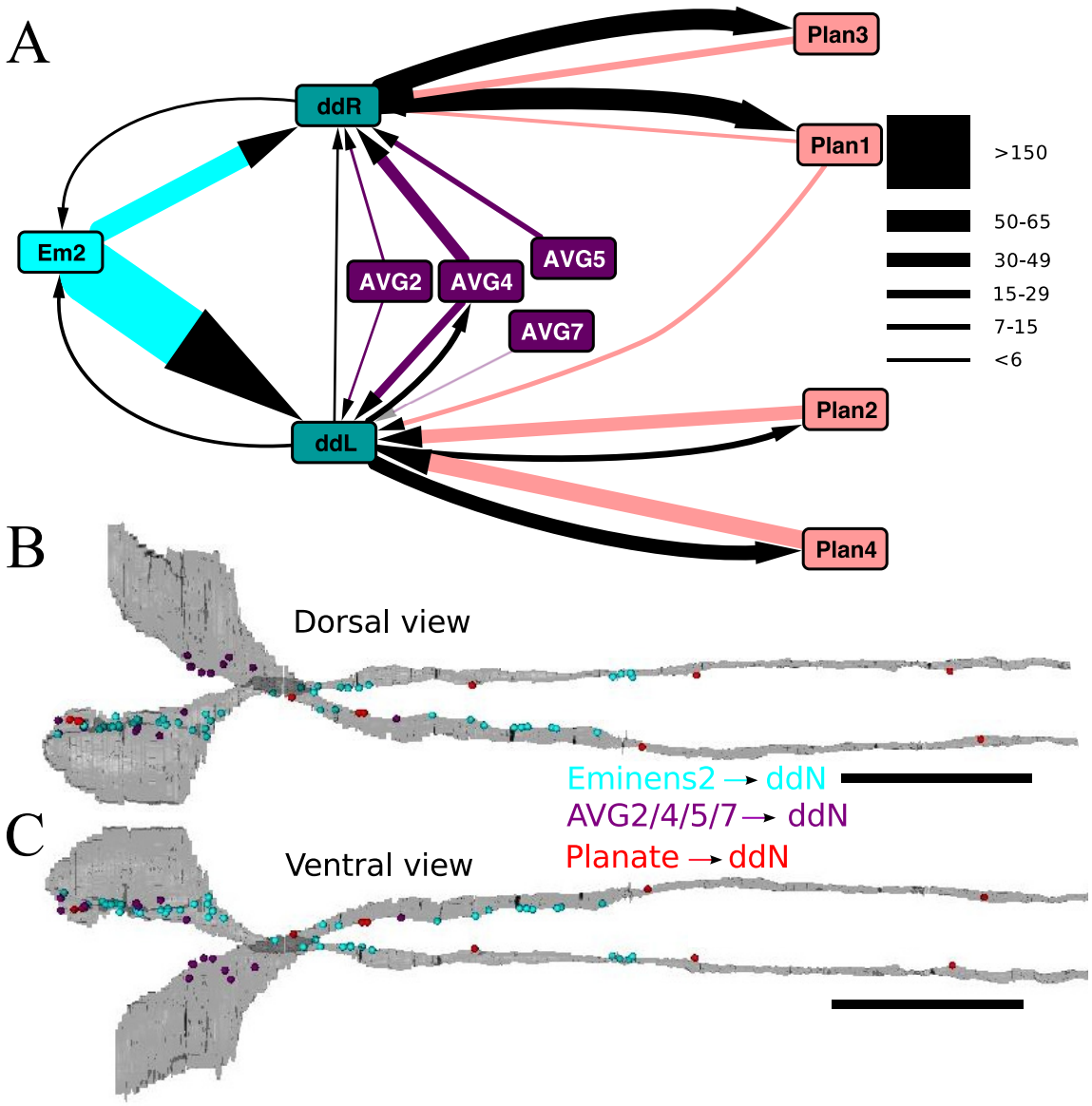

Figure 10.2. Peripheral network inputs to *Ciona intestinalis* descending decussating neurons, ddNs (ddL and ddR). A) Network diagram of ddN synapses with peripheral network components: Eminens2 (Em2), Ascending motor ganglion interneurons (AVG2-AVG7) and bipolar planate neurons of the tail (Plan1-Plan4). Nodes representing individual cells are arranged roughly anterior (left) to posterior (right) with synaptic inputs represented by arrows colour-coded for the presynaptic cell and feedback synapses from ddNs illustrated by black arrows. Line thickness reflects number of 60-nm sections in which a synapse is observed between cells (key). B-C) Locations of postsynaptic sites on descending decussating neurons from neurons of the peripheral network. Each puctum represents a single synapse, coloured by presynaptic cell type. Dorsal (B) and ventral (C) views with anterior to the left. Scale bars: 10µm.

small synaptic input to ddNL). Although AVG4 is only a secondary integrator of peripheral input to the CNS, both AVG2 and AVG5 neurons receive direct synaptic input from pATEN neurons (Ryan, 2015: Chapter 7) and these pATENs themselves also receives synaptic input from the dorsal caudal epidermal neuron (DCEN) network of the tail (like the commissural PHP in vertebrate systems). These inputs from AVGs to Mauthner-like ddNs further reflect their similarity with Rohon-Beard neurons, which are presynaptic to Mauthner cells (Low et al., 2012). The input to ddNs from the four planate (Plan) neurons in the tail is likely to be GABAergic, and is distinct between left (Plan1/3) and right partners (Plan2/4) (Fig. 10.1A), as is also the case for the vertebrate Collateral PHP. Unlike vertebrates, of course, *Ciona* ddNs are not myelinated (Fig. 10.3), myelin having arisen only among gnathostome ancestors (Waehneldt, 1990) and is lacking in both hagfish and lampreys (Bullock et al., 1984), but abundant in elasmobranches (Bullock et al., 2004). Thus, although the axon hillock regions of the ddNs cross, right over left, in contact with many axons (Fig. 10.3), they do not have a true axon cap structure.

Like Mauthner neurons, however, *Ciona* ddNs do provide synaptic input to contralateral motor neurons that is likely to be cholinergic (Fig. 10.4). On both left and right sides, the two primary motor neuron pairs with large neuromuscular terminals, MN1s and MN2s, each receive presynaptic input from the contralateral ddN (9.4A). In addition, MN1 on the left side receives synaptic input to its soma from the ipsilateral as well as contralateral ddN (Fig. 10.4B, Fig. 10.5). Other left-right symmetrical synaptic targets include the pair of MN3s (Fig. 10.4), VG3s, and descending paired tail neurons, mt2/4 (Fig. 10.6). In

Figure 10.3. Axons and axon hillock regions of descending decussating neurons illustrate orientation of crossing and lack of true axon cap structure or myelination. A) Dorsal view of reconstructed left (ddL) and right (ddR) ddNs illustrating crossing of axons, left over right, with locations of sections shown in B-F. B-F) Micrographs showing ddN axon hillock and axon regions. Dorsal points upwards. B-C) The left ddN (ddL) crosses dorsal to the right (ddR), both contacting each other as well as adjacent axons and cell bodies. D) Anterior ddN axons abut motor neuron 1 (MN1) cell bodies on one side and axons of peripheral interneuron input partners on the other. E-F) Membranes of ddN axons in the motor ganglion are naked (arrowheads), lacking a myelin sheath. Scale bars: 10μm (A); 1μm (B-F).

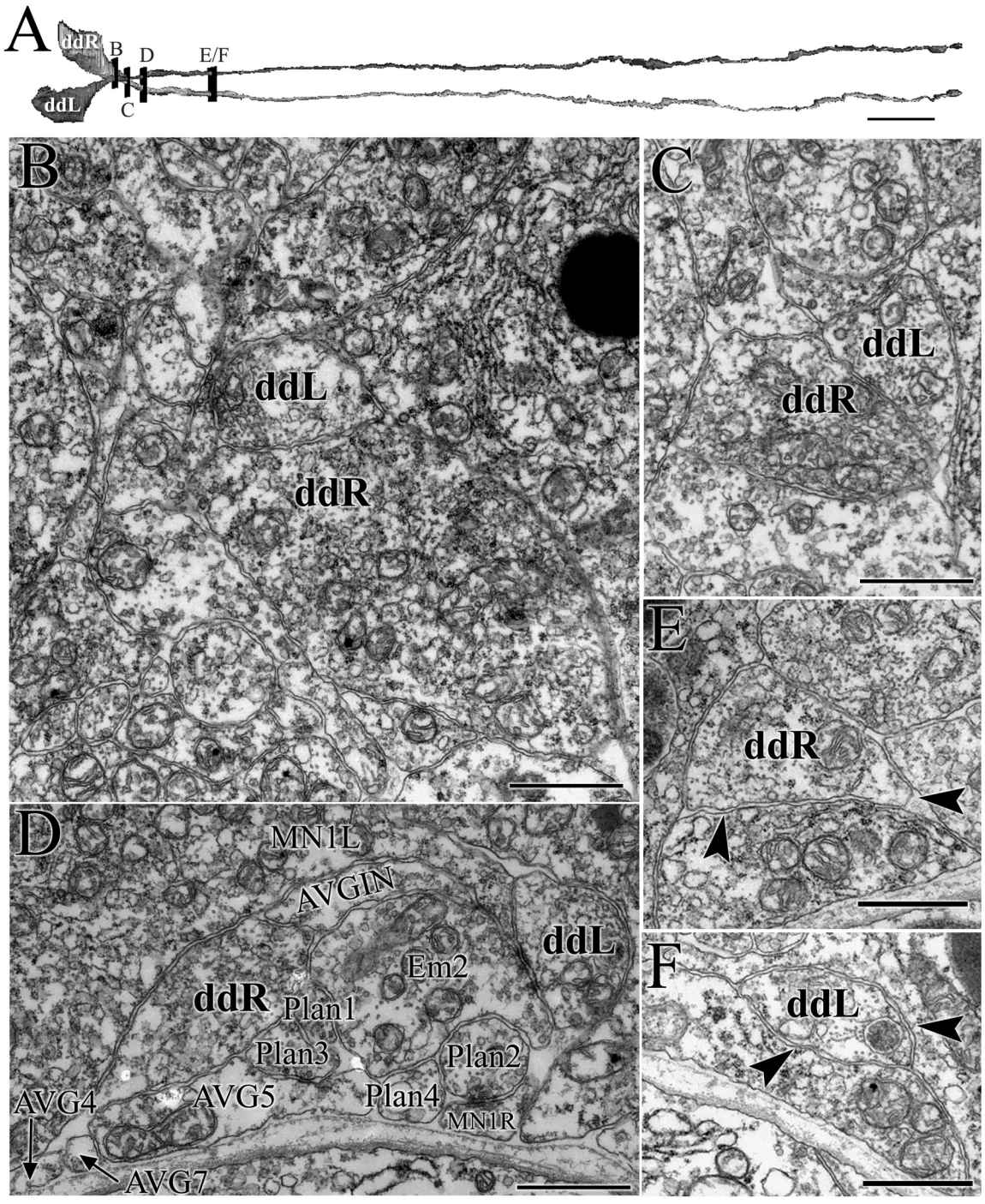
A
ddR
ddL
B
C
D
E/F
B
ddL
ddR
C
ddL
ddR
E
ddR
D
MN1L
AVGIN
ddL
Em2
ddR
Plan1
Plan3
Plan2
AVG4
AVG5
Plan4
MN1R
AVG7
F
ddL

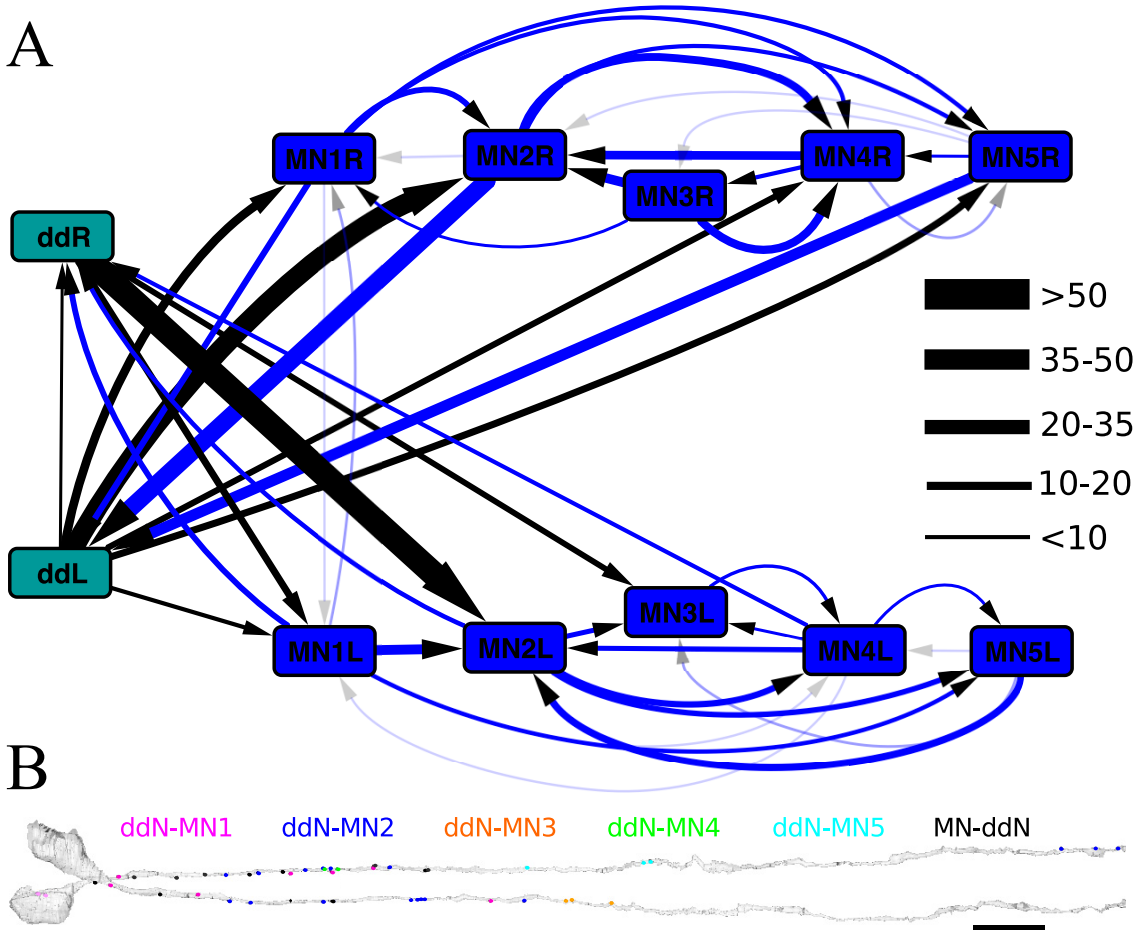

Figure 10.4. Synaptic connections between descending decussating interneurons and motor neurons of the motor ganglion (MN1-MN5). A) Network of synapses of ddNs (ddL and ddR) and MNs. Blue lines: synapses originating from MNs; black lines: those originating from ddNs; arrows indicate synaptic polarity. Nodes representing neurons are arranged by antero-posterior location of cell bodies from left (anterior) to right (posterior) with cell bodies on right (top) or left (bottom). Line thickness represents number of 60-nm sections in which a synapse is observed between cells (key). B) Locations of presynaptic sites from ddN to each MN represented by colour-coded puncta; black puncta: postsynaptic contacts from MNs to ddNs. Scale bar: 10µm.

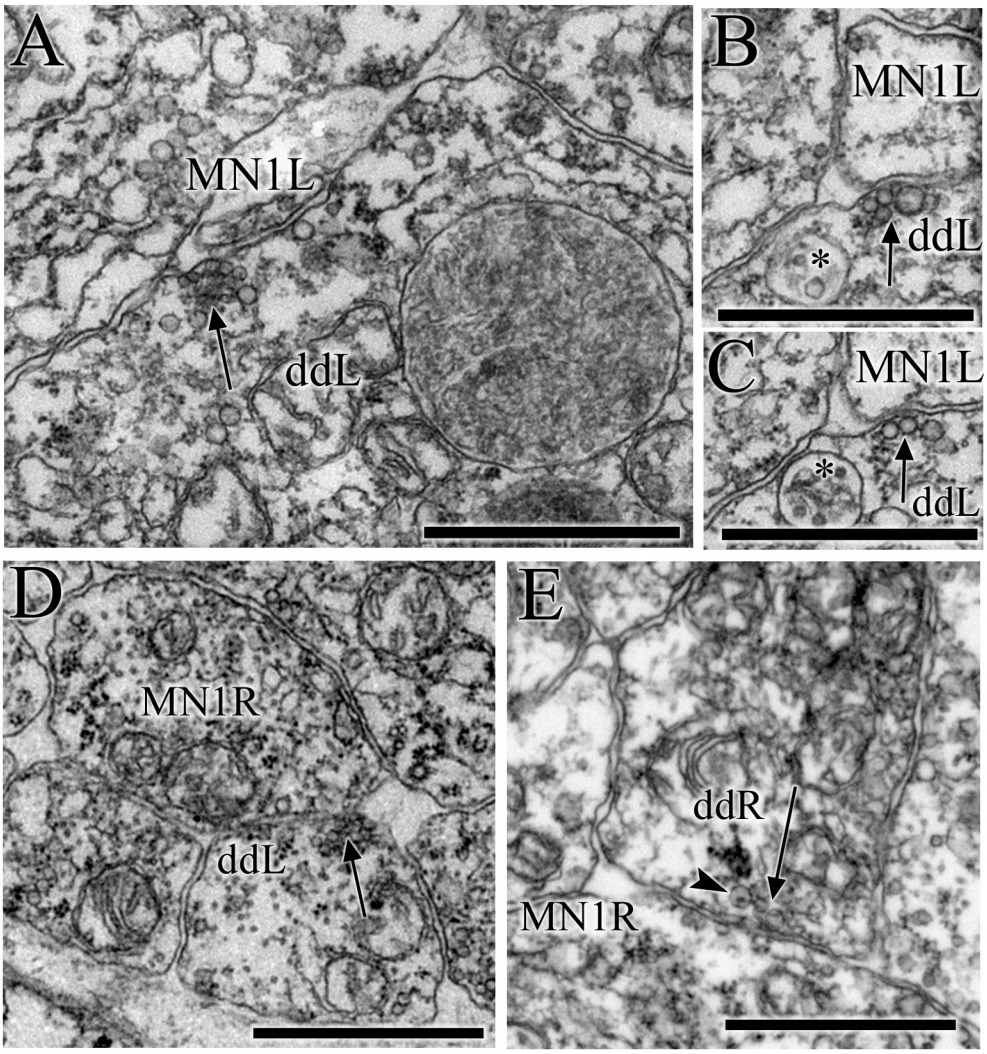

Figure 10.5. Synapses from descending descussating neurons to ipsilateral and contralateral partners of the first pair of motor neurons. A-C) Synapses (arrow) from left ddN (ddL) to ipsilateral left motor neuron 1 (MN1) dendrites. B and C are adjacent sections in which presynaptic ddL site contains a multivesicular body (asterisk). D) Synapse (arrow) from left ddN (ddL) to axon of the contralateral right motor neuron (MN1R). E) Synapse (arrow) from right ddN (ddR) onto cell body of its ipsilateral right motor neuron (MN1R) contains vesicles with small dense cores (arrowhead). Scale bars: 1μm.

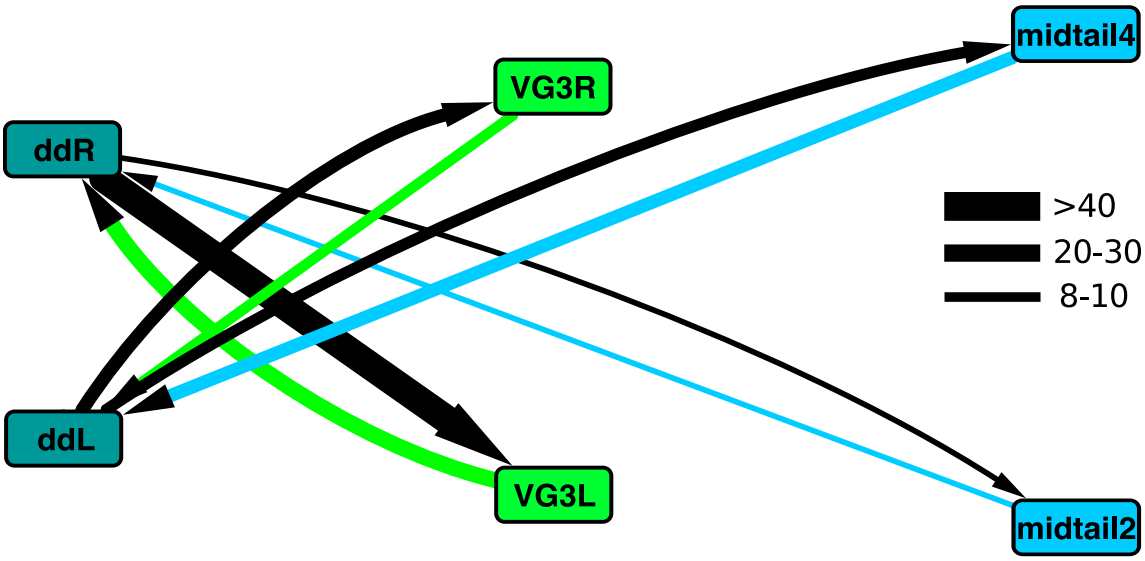

Figure 10.6. Network of synapses between left and right descending decussating neurons (ddL and ddR) and both the putatively inhibitory VGN3 interneurons (VGL and VGR) and paired midtail motor neurons 2 and 4. Line thickness represents number of 60-nm sections in which a synaptic connection is observed (key). Green lines: VGN3 presynaptic connections; blue paired midtail presynaptic connections; black ddN presynaptic connections; arrows indicate polarity of synapses.

addition to these motor ganglion targets, ddNs also provide feedback synapses to the eminens 2 neuron, ascending tail planate neurons and AVG4 (Fig. 10.2).

Even though the ddNs are paired, some of their connections are asymmetrical. The left partner alone provides unique synaptic input to the putatively inhibitory MN4R as well as MN5R (Fig. 10.4). While this left ddN is also presynaptic to the first contralateral descending interneuron (VGN1R), the right ddN is presynaptic to the second contralateral descending interneuron (VGN2L), but not VGN1L (Fig. 10.7A). Finally, the right ddN provides contralateral synaptic input to the first ascending contralateral inhibitory neuron on the left (ACIN1L) (Fig. 10.7A), which itself is presynaptic to right-side VGN interneurons (Fig. 10.7B). These putatively excitatory synapses originating from ddNs confer a candidate mechanism for a short-lived bilateral burst of activity resulting in muscle contraction (Fig. 10.8).

Although electrophysiological studies in *Ciona* have yet to confirm the role of electrical transmission between neurons, their role in Mauthner activation and the anatomical identification of putative gap junctions warrants an analysis of these connections in particular within this ddN circuit in *Ciona*. Putative electrical partners include one of the AVG interneurons of the brain vesicle (cell 116), eminens 2, AVG2, 4, 6, and 7, as well as MN1 and MN2 pairs, VGN2 and VGN3 pairs, ACINs, a posterior MG interneuron (PVGN), and tail planate neuron 2. In addition to its reciprocal chemical synaptic connection with ddNs, Eminens2 forms gap junctions with both ddNs as a major source of the contacts received from those cells (Fig. 10.9). The two ddNs themselves lack putative gap junctions at their regions of contact, but do have two, small, ambiguous connections (Fig. 10.10). In the anterior motor ganglion, a right side tail planate neuron,

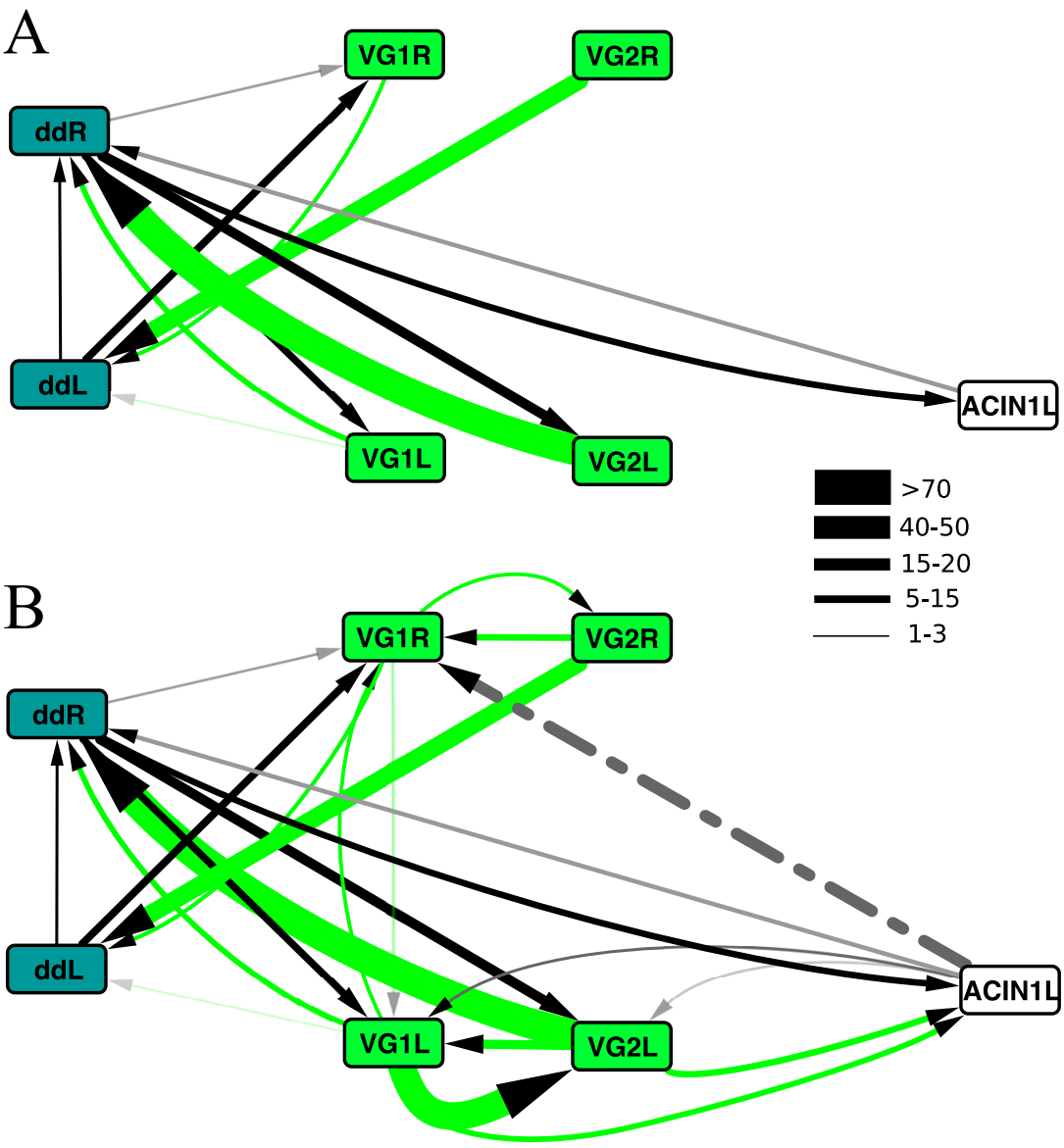

Figure 10.7. Network of synapses between descending decussating neurons (ddL and ddR) and two anterior pairs of descending motor ganglion interneurons (VG1-VG2, L and R) as well as the first left-side ascending contralateral inhibitory neuron (ACIN1L). A) Network of pre- and postsynaptic ddN connections with interneurons. B) Network of synapses including synaptic interactions between non-ddN interneurons. Dashed line from ACIN1L represents contralateral input to right side interneurons. Line colour indicates presynaptic partner: green (VGNs), gray (ACIN1L), black (ddNs). Line thickness represents the number of 60-nm sections in which a synapse is observed (key).

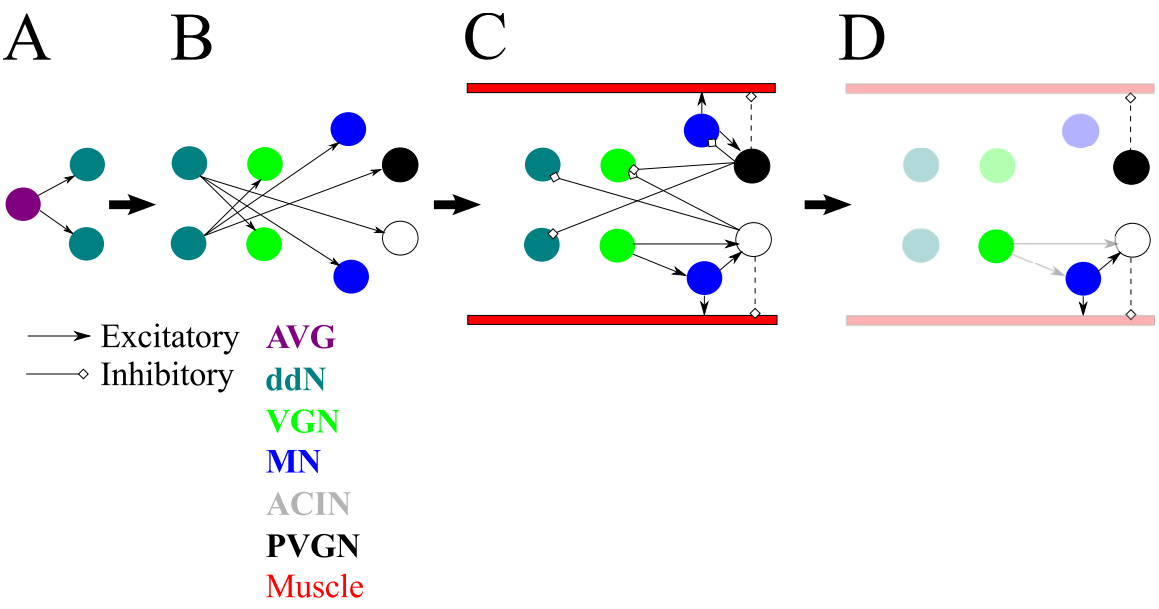

Figure 10.8. Model of short-lived bilateral muscle activation by the descending decussating neuron pathway. A) Ascending motor ganglion (AVG) neurons excite left and right descending decussating neurons (ddNs). B) ddNs next excite paired descending interneurons (VGNs), motor neurons (MNs), ascending contralateral inhibitory neuron (ACIN1L) and unpaired posterior motor ganglion interneuron (PVGN1R). C) Left and right MNs then excite ipsilateral muscle and both ACIN1L and PVGN. On the left, interneurons (VGN) also provide excitatory input to MNL and ACIN1L. ACIN1L now inhibits the right ddN and contralateral right-side interneuron (VGN). On the right side, PVGN next inhibits the left ddN, ipsilateral right-side VGN and right-side MN. Both ACIN1L and PVGN also provide putative inhibitory input directly to ipsilateral muscle (left and right sides, respectively). D) Inhibited neurons and muscles are faded to indicate inactivation. Only PVGN on the right and MN and ACIN on the left remain putatively active, with no remaining excitatory input.

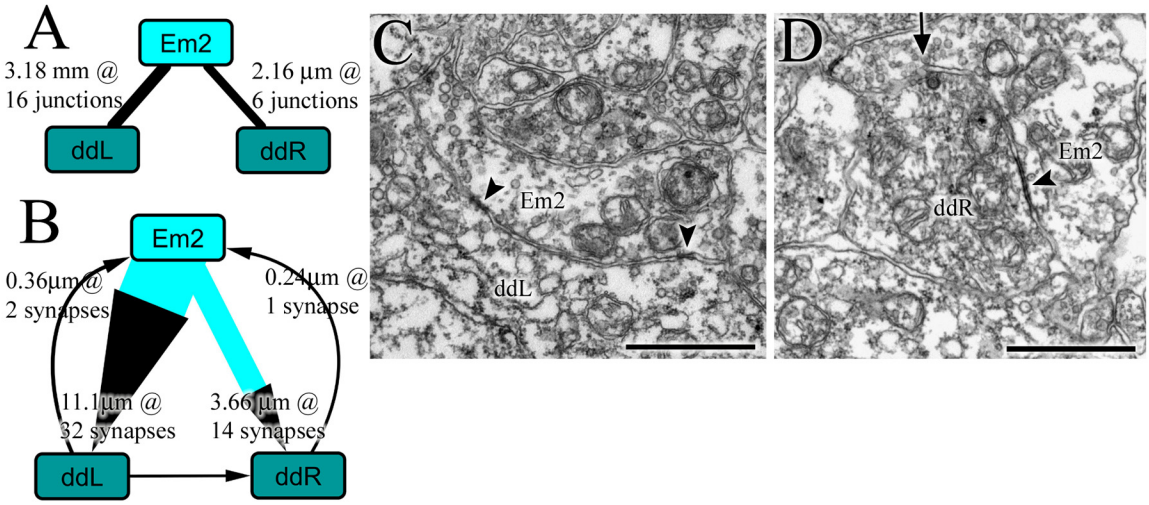

Figure 10.9. Eminens2 input to descending decussating neurons (ddL and ddR). A) Gap junctions between Eminens2 and both left (ddL) and right (ddR) partners. Total thickness through which putative gap junctions are observed is given, along with corresponding number of junctions. B) Synapses from Eminens2 to and from both ddL and ddR. Total thickness through which synapses are observed is given along with corresponding number of synapses. Inputs to ddL exceed those to ddR in both putative gap junctions (A) and synapses (B). C) Eminens2 (Em2) gap junctions (arrowheads) to cell body of the left decussating neuron (ddL). D) Eminens2 (Em2) gap junction (arrowhead) and synapse (arrow) onto right decussating neuron (ddR). Scale bars: 1µm.

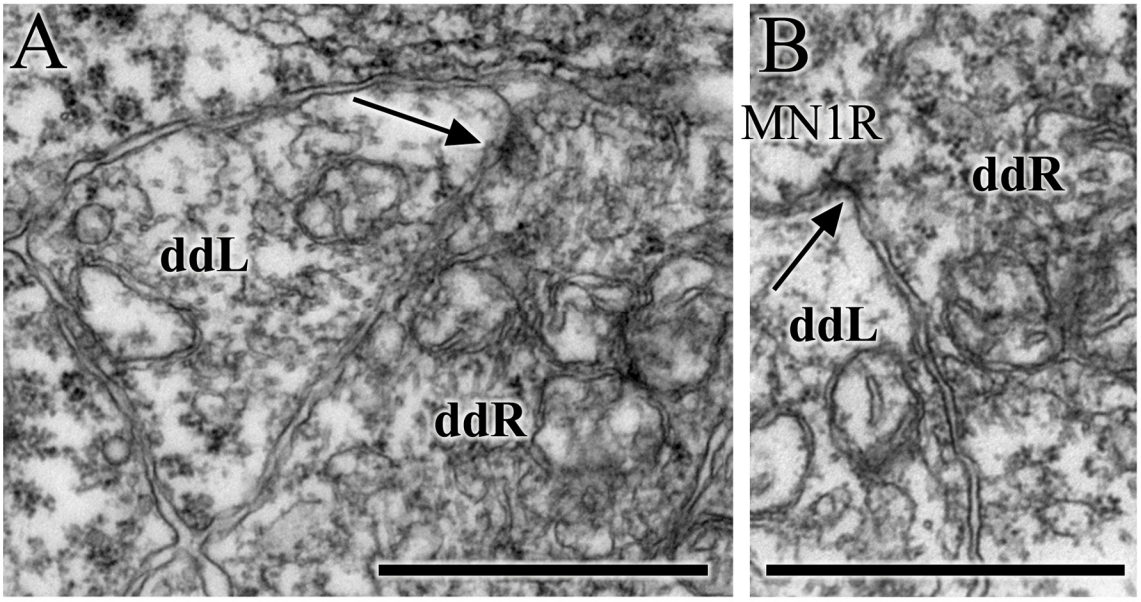

Figure 10.10. Ambiguous small junctions between descending decussating interneurons (ddN) of the motor ganglion. A) Junction (arrow) between crossing left and right ddN axons (ddL and ddR) within the motor ganglion. B) Junction (arrow) at point where

membranes of left (ddL) and right (ddR) decussating axons meet along with the cell body of the first motor neuron on the right side. Scale bars: 1μm.

Plan4, and a descending AVG interneuron both form small gap junction connections with ddNL (Fig. 10.11A,C). Although lacking chemical synapses, the left side AVG7 and right side AVG6 both form small putative gap junctions with ddNL (Fig. 10.11), whereas the bipolar ventral right side AVG2 and bipolar ventral left and right side AVG4 both form gap junctions with ddNR, along with reciprocal chemical synapses (Fig. 10.11).

Motor neurons and descending paired interneurons (VGNs) are also coupled to descending decussating interneurons by putative electrical gap junctions (Fig. 10.12). These contacts repeat the connections made by chemical synapses that are observed between the same cell types (Fig. 10.4; Fig. 10.6). Although only ACIN1L is reciprocally connected to ddNR via chemical synapses, both left side ACINs form putative electrical synapses with the right ddN (Fig. 10.13A). This connection in the left neuropil is in contrast to the right side ACIN, which does not decussate to provide input to the contralateral neuropil. The gap junctions between descending decussating neurons and left side ACINs occur on the cell bodies of ACINs (Fig. 13B). However, on the right side, a descending interneuron with no left-side partner, PVGN, is coupled by gap junctions to the left descending decussating neuron (9.13A), and provides chemical synaptic input, to the same ddN (Fig. 10.7). Both ACINs and PVGNs are also presynaptic onto the basement membrane near muscle on their ipsilateral sides (Fig. 10.14).

Of the neurons putatively coupled by gap junctions to ddNs, eminens2, AVG2 and 4, VGN2L, VGN3s, ddN, MNs, PVGN, planate2, and ACIN1L all also form chemical synapses onto the ddNs (Fig. 10.13). These include both putative excitatory and

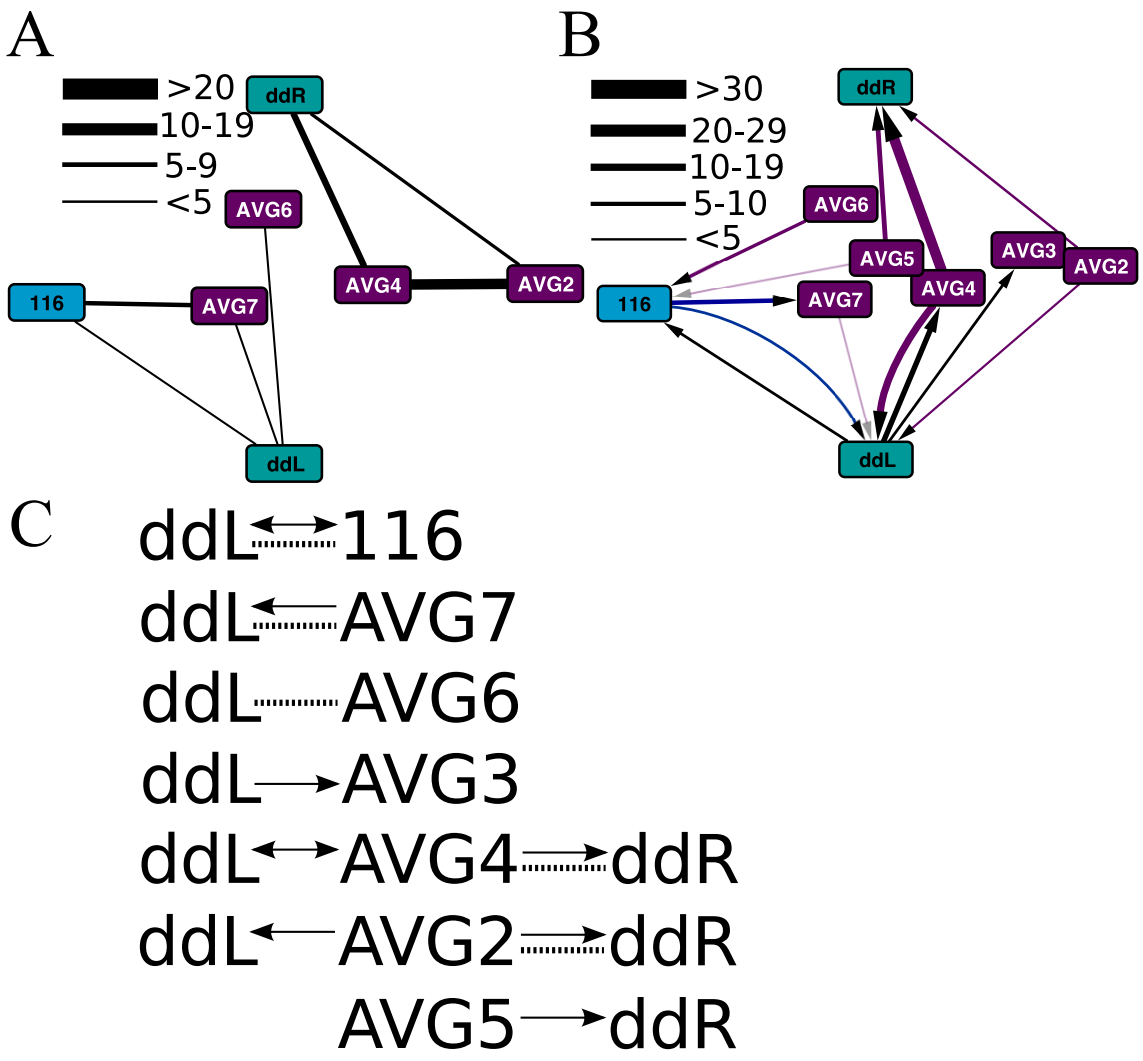

Figure 10.11. Comparison of gap junction and synaptic connections between ascending motor ganglion neurons (AVG) and the brain vesicle AVG interneuron (cell 116) and descending decussating interneurons (ddL and ddR) arranged in the relative locations of their cell bodies (distance to 116 reduced for simplicity), anterior to the left, left to bottom, dorsal view. Line thickness represents number of 60-nm sections in which a synapse is observed (keys). A) Putative network of gap junctions between ddNs, AVG neurons and AVG interneuron, cell 116. B) Network of synapses between AVG neurons/interneuron and ddNs. Arrows indicate direction of synaptic connections. Synapses between AVG neurons and cell 116 are also included. Line colour indicates presynaptic neuron. C) Summary of connections between each AVG or AVG interneuron and left (ddL) and right (ddR) decussating neurons. Arrows indicate polarity of synaptic connections, dashed lines represent putative gap junctions.

Figure 10.12. Network of gap junctions in the anterior motor ganglion. A) Network of all membrane appositions, putative gap junctions, between paired neurons in the motor ganglion, including decussating neurons (ddL and ddR), descending interneurons (VG1-VG3) and motor neurons (MN1-MN5). B) Putative gap junction network including only ddN gap junctions with paired motor ganglion neurons. Line thickness represents number of 60-nm sections in which a gap junction is observed (key). Black lines (contralateral connections), gray lines (VGNs to MNs), blue lines (MNs to MNs).

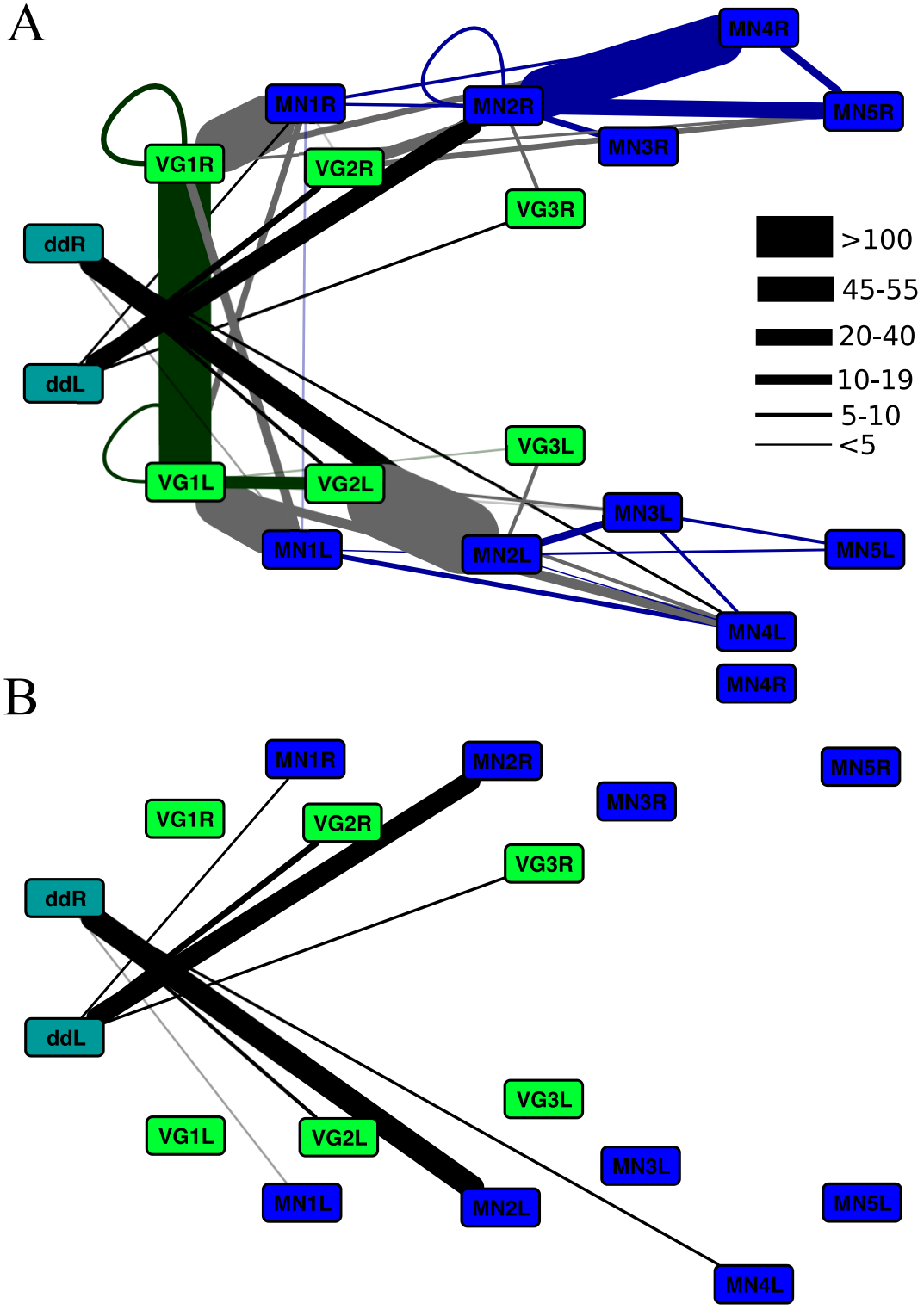
A
MN4R
MN1R
MN2R
MN5R
MN3R
VG1R
VG2R
VG3R
ddR
>100
45-55
20-40
10-19
5-10
<5
ddL
VG3L
VG1L
VG2L
MN3L
MN1L
MN2L
MN5L
MN4L
MN4R
B
MN1R
MN2R
MN5R
MN3R
VG1R
VG2R
VG3R
ddR
ddL
VG3L
VG1L
VG2L
MN3L
MN1L
MN2L
MN5L
MN4L

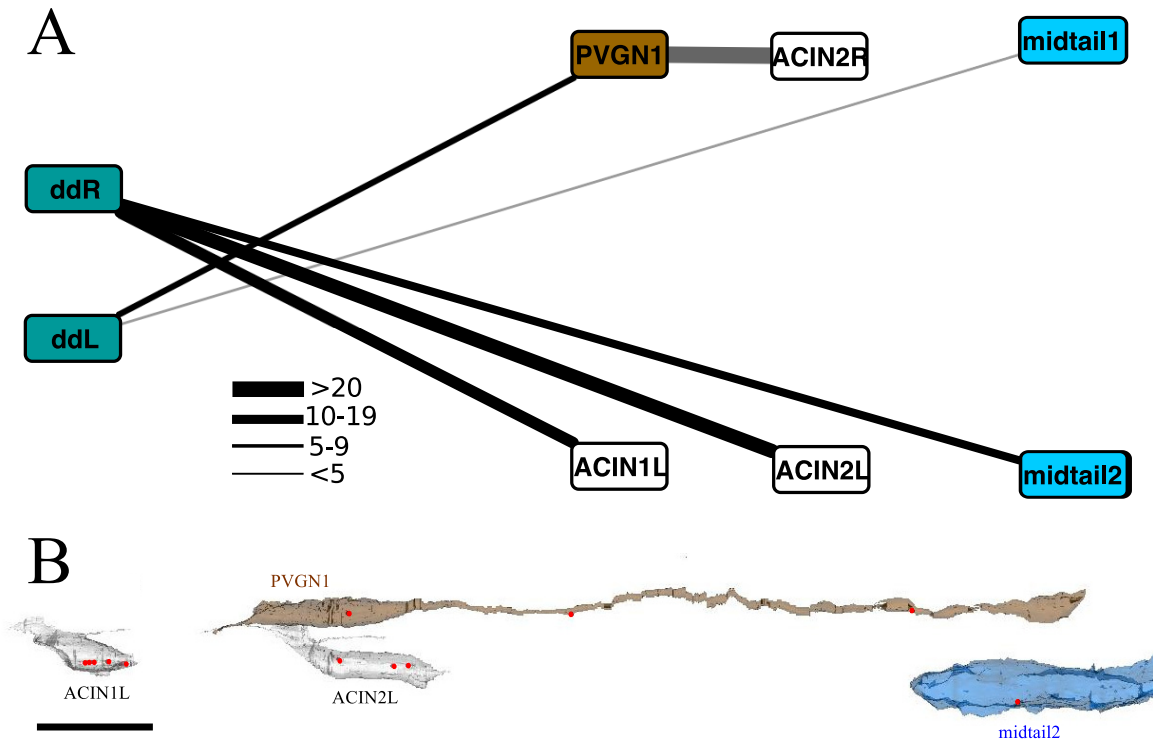

Figure 10.13. Gap junctions between descending decussating neurons and neurons at the trunk-tail border (left side ascending contralateral inhibitory neurons (ACIN1L and ACIN2L), unpaired right posterior motor ganglion neuron (PVGN1), and midtail motor neurons (midtail1 and midtail2). A) Network diagram of putative gap junctions between left (ddL) and right (ddR) decussating neurons and neurons of the anterior tail. Line thickness represents number of 60-nm sections in which a putative gap junction is observed (key). B) Reconstructed neurons of the anterior tail populated with sites of putative gap junctions with ddNs represented by red puncta. Scale bar: 10µm.

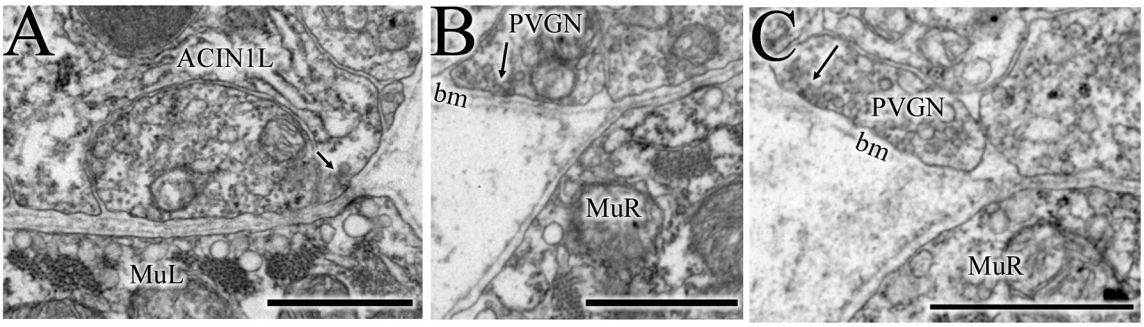

Figure 10.14. Synapses onto or adjacent to dorsal muscle from posterior neurons at the trunk-tail border. The latter include unpaired interneurons (PVGN) and the left side ascending contralateral inhibitory neuron (ACIN1L). A) Small putative synapse (arrow) from ACIN1L cell body onto ipsilateral left-side muscle (MuL). B and C) Synapses from axon of the unpaired PVGN1 (arrows) onto basement membrane (bm) adjacent to ipsilateral right-side muscle (MuR) with no evident postsynaptic specializations on muscle. Scale bars: 1µm.

inhibitory neurons. In addition, Eminens2, AVGIN, MN1L, MN2s, AVG2 and 4, VG2L, VG3s, ddNs, ACIN1L and Plan2 all receive input from chemical synapses from ddNs in addition to their gap junctions (Fig. 10.15). While these partnerships are dominated by reciprocal connections, MN1R and PVGN are presynaptic to ddNs exclusively at chemical synapses, but do exhibit evidence for electrical coupling by the anatomical gap junctions they form.

The location along the length of the ddNs of synapses, both electrical and chemical, appears to follow a distinct pattern. Contacts with AVG neurons occur on cell bodies of both the left and right ddNs. Because they contact the cell bodies directly, their axons connect to ipsilateral ddNs, although in most cases these AVG neurons themselves are multipolar and not inherently sided. While the Eminens2 neuron contacts ddNL predominantly on its cell body and decussating axon hillock region, it contacts ddNR at the axon hillock region as it decussates, and further down along the proximal axon (Fig. 10.16). Unlike these partners, the tail neurons make synaptic contacts with ddNs along their entire length, up to the cell body (Fig. 10.16). The ACIN contacts are, not surprisingly limited to the mid axon region and flank the long synapses from ddNL onto MN2Rs (Fig. 10.16). Overall, both pre- and postsynaptic sites are distributed along the length of ddN axons, but their gap junctions are more concentrated on the cell bodies and the rostral portions of the axons within the motor ganglion, with fewer putative gap junctions in the tail (Fig. 10.16).

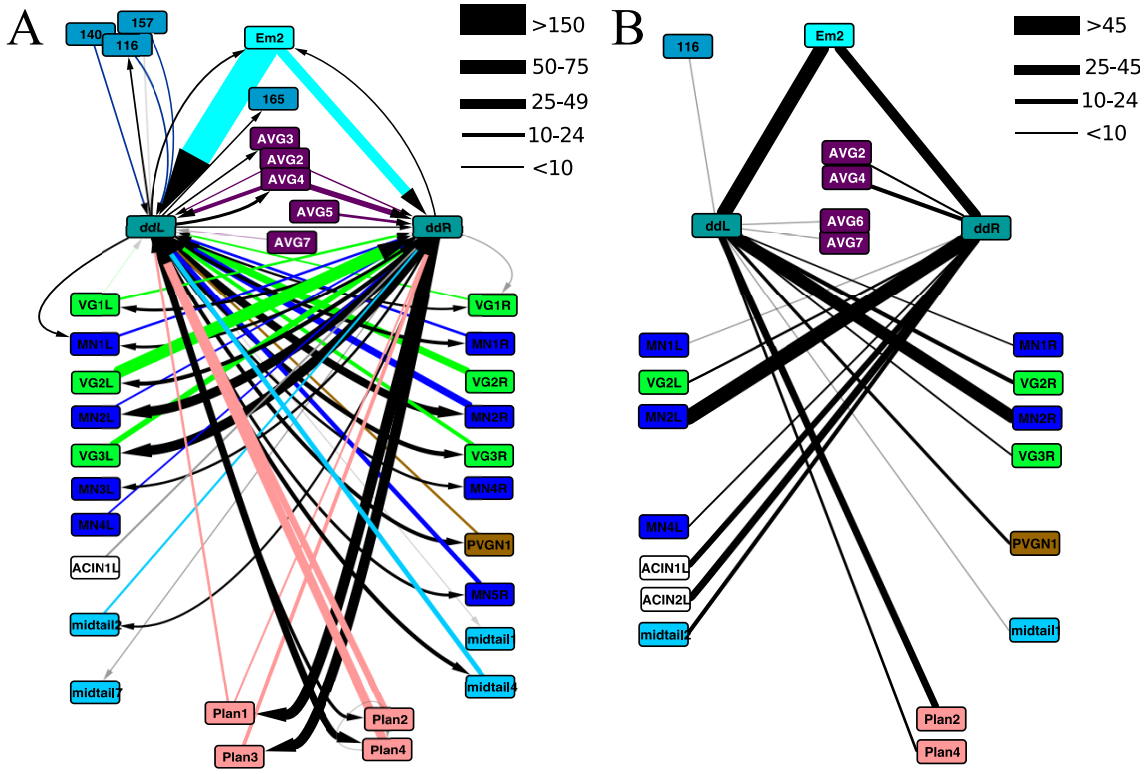

Figure 10.15. Summary of total connections of descending decussating neurons. A) All synaptic connections of left (ddL) and right (ddR) decussating neurons with cells arranged from anterior (top) to posterior (bottom). Synapses from ddNs represented in black, synapses onto ddNs represented by colour of presynaptic partner. Arrows indicate polarity of synaptic connections and line thickness indicates number of 60-nm sections in which a synapse between partners is observed (key). B) Putative gap junctions of ddNs. Line thickness indicates number of 60-nm sections in which a putative gap junction is observed (key).

Figure 10.16. Distribution of connections on reconstructed descending decussating neurons. Dorsal views, anterior to the top of the page. A) Reconstructed ddNs with their presynaptic sites marked by puncta colour-coded for the postsynaptic cell type. B) Reconstructed ddNs with postsynaptic sites marked by puncta colour-coded for the presynaptic cell type. C) Reconstructed ddNs with putative ddN gap junctions marked by puncta colour-coded for the cell type of junctional partner. Scale bar: 10μm.

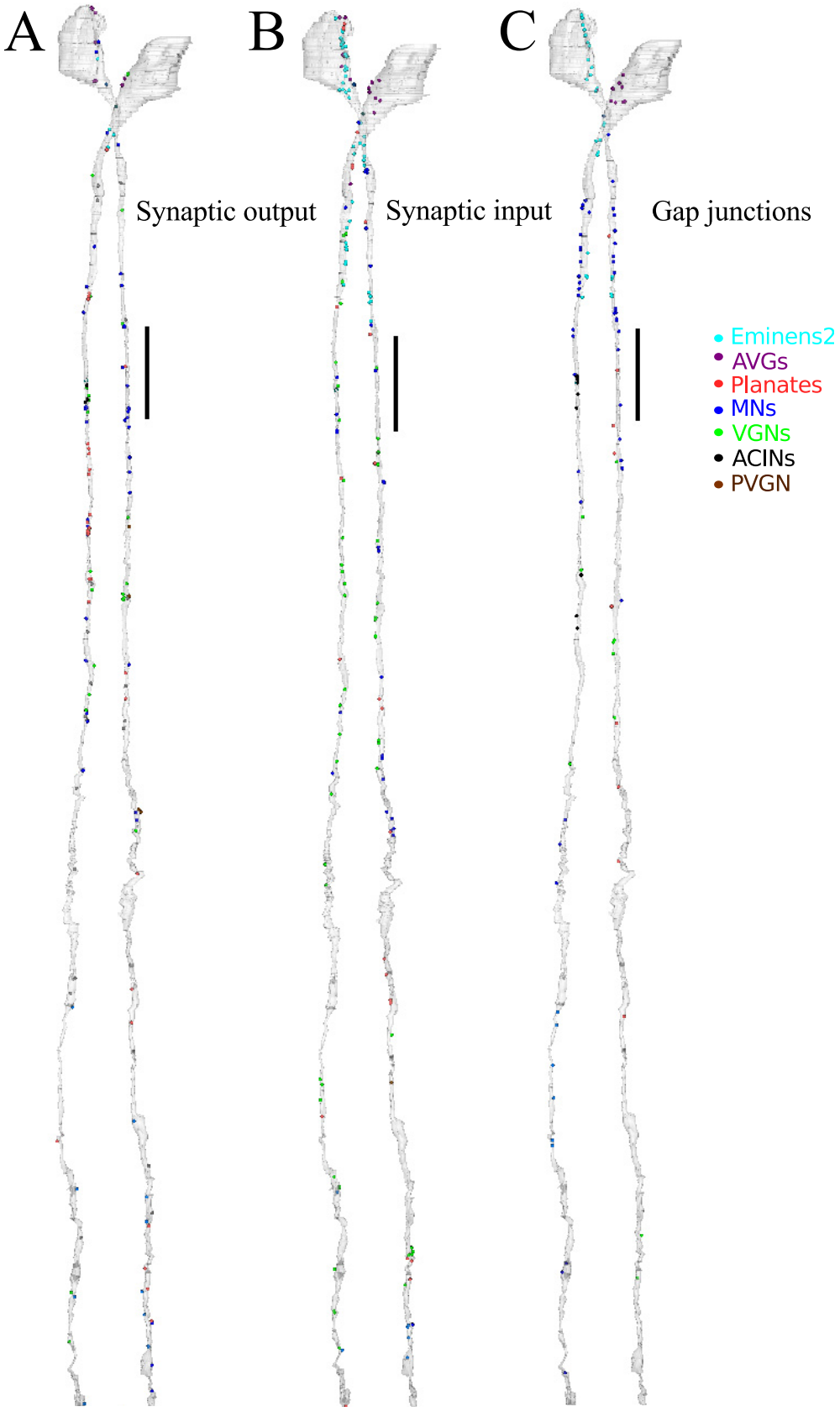
A
B
C
Synaptic output
Synaptic input
Gap junctions
Eminens2
AVGs
Planates
MNs
VGNs
ACINs
PVGN

10.1 **Discussion**

Here, as elsewhere in this report, it is difficult to infer from anatomical observations the functional interactions supported by the complex networks of neurons revealed anatomically. Given their shared inputs, however, and the direct synaptic connections between partners, both ddNs are likely to be activated simultaneously. Unlike the vertebrate startle response, in *Ciona* the inputs to the ddNs from the sensory system are themselves not sided. In fact, even the mechanosensory structures themselves are not sided, but mostly located on the dorsal and ventral midline of the animal. Obvious exceptions are RTEN neurons located on left or right sides of the anterior trunk, rostral to the brain vesicle (Imai and Meinertzhagen, 2007b; Konno et al., 2010; Yokoyama et al., 2014). However, the putative RTEN neurons of the anterior peripheral nervous system that provide synaptic input onto eminens 2 originate from both the left and right peripheral neuropil (Ryan, 2015: Chapter 7), presumably conveying information from either side. Likewise, the eminens neuron is presynaptic and makes putative gap junctions with both ddNs. However, the total synaptic pathway strength from eminens 2 is more than two times larger to the left ddN than to the right (in both the number of synapses and total contact size), and although both ddN partners receive extensive input from eminens 2, this asymmetry might suggest a greater inhibitory input to the left than the right, but does not provide an obvious means of conveying this laterality from the upstream RTEN.

Sided sensory information is also reported by Yokoyama et al. (2014), who noted that pATEN neurons, those that provide input to AVG neurons (Ryan, 2015: Chapter 7), extend their ciliary dendritic network to both the dorsal edge of the tunic and to the left

lateral side. Thus, AVG neurons may receive information from the left-side and dorsal external environment only. However, AVG2 and AVG4 neurons both provide bilateral input to ddNs, suggesting a lack of sidedness. It should be noted, however, that putative gap junctions exist between these AVG neurons and the right, but not left ddN. Additional sided chemical input to the right ddN from AVG5 is only minimal, and both the gap junction and synaptic input should lead to contraction on the left side. Such contractions driven by pATEN receptive fields on the left would turn the animal toward a stimulus, so would be poorly adaptive as a mechanism of directional escape. The planate neurons of the tail are sided in their inputs to the ddNs, but there is no evidence that their mechanosensory input neurons are sided, DCENs and VCENs projecting cilia dorsally and ventrally, and both left and right planate neurons receiving input from peripheral nervous system neurons of the anterior right peripheral neuropil.

The peripheral pathway's input to the motor network is not exclusively to ddNs, and some components may function outside the escape response. The peripheral components (AVG neurons and eminens 2 neuron) that provide synaptic input to ddNs provide additional direct synaptic input to MN1 neurons, but only minimal synaptic input to MN2 neurons, and no input at all to other motor neurons (Ryan, 2015: Chapter 7). The putative inhibition of MN1 neurons by eminens 2 suggests that they may not be easily excited through the ddN network. Planate neurons, the other presynaptic partners of ddNs, provide widespread input to most neurons of the motor ganglion, so their inhibitory action on ddNs probably coincides with inhibition of the entire motor network, allowing it to override any action of the ddNs either directly or indirectly.

Despite the likely bilateral activity of the crossed ddNs, withdrawal is an unlikely outcome in the ascidian larval nervous system, as reversal behaviour lacks either a mechanism or even any prior report. Instead, the small size of ascidian larvae, and their potential predation by filter feeders, more than active pursuit by predators, may suggest that directionality is not an important feature of their escape response. Thus, it seems reasonable that without jumping or reversing, animals would escape by initiating a tail flick to turn (or several tail flicks) or escape a current, as is observed early in their life, during larval escape from their chorion, followed by a bout of swimming. Contralateral inhibition, however, is still important to achieve a strong unilateral contraction, as demonstrated by the impaired initiation of an escape response in zebrafish after CoLos ablation (Satou et al., 2009). In such impaired escape responses, bilateral M-cell activation leads to bilateral muscle contraction in the absence of commissural inhibition (Satou et al., 2009) in a segment-specific manner. The lack of segmentation in *Ciona* makes contralateral inhibition even more critical in order to achieve any strong unilateral contraction.

Assuming acetylcholine acts as an excitatory neurotransmitter in the motor ganglion, the paired ddNs should excite VGNs and MNs bilaterally, as well as the putatively inhibitory left ACIN and right PVGN (Fig. 10.8). Based on their synaptic connections, both ACIN and PVGN are predicted to inhibit the right-side motor network. Both are presynaptic to right-side MG interneurons, but while ACIN1L is presynaptic to only the right ddN and lacks synapses onto right-side motor neurons, PVGN -- a descending right side neuron that lacks a left-side partner, provides input just to the left ddN partner, and is also presynaptic to its ipsilateral, right-side motor neurons (Fig. 10.8). The inhibition of these

neurons in the right MG would prevent excitation on the right side of the animal until the ACIN and PVGN could return to their resting potentials. However, the absence of direct inhibition of the right side motor neurons by ACINL, suggests that right-side motor neurons could still be directly excited by neurons descending from the brain vesicle. Furthermore, MN4 and MN5, which are involved in coordinating motor activity, are ddN targets on only the right side of the CNS, and this may suggest that any activity after an escape twitch would begin on the larva's right side. Bilateral ddN input to MN3, and reciprocal input to descending paired tail motor neurons, suggests alternatively the substrate for a massive contraction that is bilateral. This bilateral contraction would also be supported by the mixed synapse and gap junction inputs from ddNs to MN2s, which form many large neuromuscular junctions further into the tail than other motor ganglion motor neurons. These junctions would be compatible with tail flick activity, which is driven by action potentials throughout the tail, and unlike bilateral swimming activity can occur in even short mid portions of the tail (Bone, 1992). In addition to the putative chemical synapses, electrical coupling provided from ddNR by anatomical gap junctions is predicted to allow fast activation of left ACINs to inhibit their right-side targets, and possibly the right side muscle itself (Fig. 10.8; Nishino et al., 2010). Given that this interaction is one sided, the network may provide a mechanism to prevent bilateral muscle contractions in response to mechanical stimulation. Thus, it may be that the larva has a sided response, exhibiting the number of tail flicks necessary to achieve a directional response relative to the location of any stimulus, if it is in fact directionally sensitive at all. Alternatively, this system may serve as a mechanism to simply change direction swiftly and engage in motor activity. If this is an adaptive response to water

currents created by filter feeding animals rather than the active predator-prey responses observed in tailed vertebrates, then it would be advantageous for animals to produce strong, simultaneous contractions of all muscle cells on a single side. The putative gap junctions between ddNs and MN2s could help to drive such a fast, widespread contraction.

Unaccounted for in this model is the VGN3 pair, which is putatively GABAergic (Ryan, 2015: Chapter 4) and therefore likely to be inhibitory, and which forms synaptic feedback loops with contralateral ddNs. These interneurons also provide synaptic input to their ipsilateral VGNs and MN1 (Fig. 10.17). Both also provide synaptic input to the ddN input neuron, eminens 2. Thus, these two VGN3 interneurons provide an additional mechanism to suppress long-term activity of the ddNs directly, as well as inhibiting their pre- and postsynaptic partners. Although the right VGN3 partner receives inhibitory input from ACIN1L and eminens 2, the left does not receive inhibition from members of the putative escape/withdrawal pathway. These asymmetries in their inputs suggest a selective inhibition of the right partner, which could prevent the inhibition of right side VGNs, MN1 and the contralateral ddNL, further supporting the idea of a possible right-side initiation or ability of right-side neurons to remain responsive to other descending sensory signals.

Compared side by side, there are striking similarities between the vertebrate Mauthner and ascidian larval ddN networks (Fig. 10.1), however the complexity of inputs to Mauthner cells has been far more completely defined and functionally analysed in vertebrates, and the network exhibits less reciprocity than is seen in what may be its counterpart in *Ciona*. As with all tentative functional interpretations from the anatomical

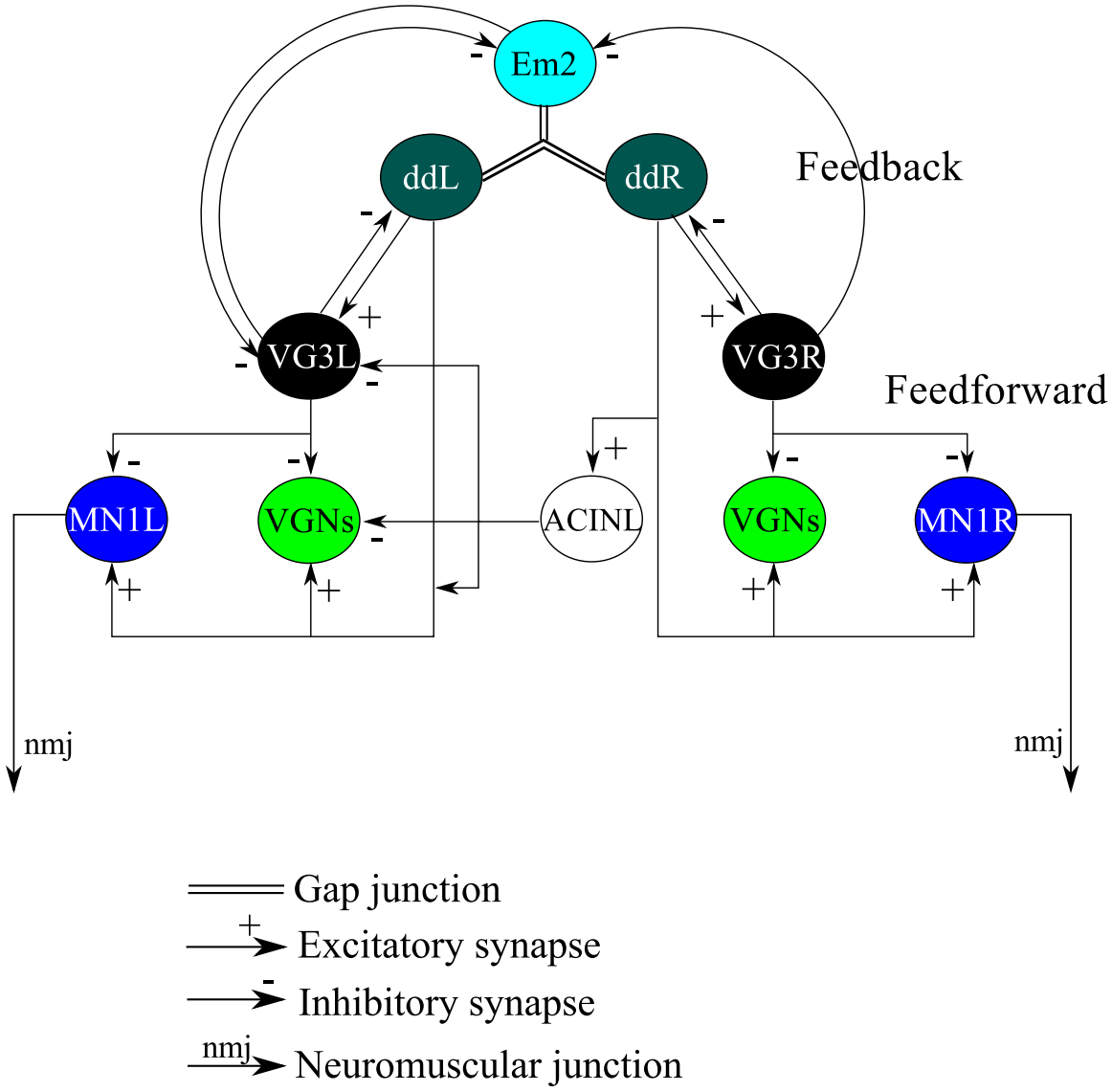

Figure 10.17. Model of descending decussating neuron pathway to the first pair of motor neurons (MN1s) with feedback and feedforward contributions from putatively inhibitory motor ganglion interneurons (VG3s). Arrows represent chemical synapses, inhibitory (-) or excitatory (+) or neuromuscular junctions (nmj).

connectome, however, the reciprocity revealed anatomically may lack a physiological counterpart within the *Ciona* larvae. Of particular importance are the physiological strengths of transmission, especially the relative strengths of postsynaptic currents at chemical synapses and gap junctions, and between feedforward and feedback synapses.

10.2 **Conclusions**

The larval CNS of *Ciona intestinalis* contains a network that resembles the startle response pathway of aquatic vertebrates. The cholinergic descending decussating neurons of the MG have similar synaptic connections to the M-cells of these vertebrates, and receive input from peripheral interneurons at GJs and synapses. Unlike the vertebrate case, the peripheral input to ddNs does not appear to be sided, and the direct contralateral presynaptic inhibition of ddNs by ACINs occurs only from left to right. Thus, like other basal vertebrates, the putative startle response pathway of *Ciona* thereby probably initiates a less directed escape response than the contralateral escape seen in many fish and amphibians.

Chapter 11 Final Discussion

The work presented in the preceding chapters describes and details the complete CNS connectome of a single tadpole larva of *Ciona intestinalis*. It represents a nervous system in an early state of pre-vertebrate evolution. Although some discussion was presented on the possible function of circuits, the anatomical connections alone do not allow for direct functional analyses nor the validation of anatomical circuits. Thus, as for any connectome, or complete synaptic wiring diagram, it is hypothesis generating rather than hypothesis-driven (Varshney et al., 2011). In particular, it does not in itself explain how behaviour is generated, because it lacks temporal information, but it lays the ascidian tadpole larva out ready for functional analyses. Current limitations in understanding the function of these anatomical circuits include but are not limited to:

1) The neurotransmitter phenotype for each class of synapse, and (more instructive) the postsynaptic receptor expression, since this reveals the polarity of transmission given that many neurotransmitters, even GABA, can be both excitatory and inhibitory in action (Staley et al., 1995; Ben-Ari, 2002). The putative co-transmission in particular neurons must also be resolved to fully explain these circuits.

2) The pathway strength. Even though this must be some combination of synapse number and size, it also depends on the postsynaptic current generated by each quantum of neurotransmitter released. A connectome only reveals anatomical measures of these. Relating the anatomical and functional strength is an essential goal of all connectomic studies (Bargmann and Marder, 2013).

For the moment there is little choice but to assume that a pathway of 10 synapses is only one tenth the strength of one that has 100, but obviously this strength will depend on the

features identified above. It is also unclear whether all anatomically identified pathways have sufficient strength to elicit a significant postsynaptic response.

How can we resolve these issues? Among many other approaches, this will require:

a) transcript profiling of single neurons (Wang and Bodovitz, 2010), to expose transcripts of neurotransmitter systems expressed in different neurons.

b) calcium signaling, which detects calcium entry during electrical activity, and has recently become a reality with improved reagents, for example those based on engineered Ca binding calmodulin proteins (e.g. Akerboom et al., 2012).

c) targeted single-cell patch clamp recordings of neurons in living animals (e.g. Lockery and Goodman, 2010).

d) dissecting circuits by disabling their single-cell elements, or rescuing their function cell-by-cell in mutants that lack function, using new genetic dissection approaches (Gao et al., 2008; Luo et al., 2008; Horie, pers. comm.). This approach is constrained by the limited means to target effector gene expression in *Ciona* and to reversibly disable gene function.

Finally, for all it may be comprehensive, the connectome reported here applies only to a single larva, now dead. Determining the stereotypy of circuits described in the current study, and thus to some extent validating these, requires that the connectome be repeated from multiple larvae. This daunting task will nevertheless be faster than the time taken for the present study, for several reasons: first, data from the present study will allow identification and alignment of neuropil regions, and their enhanced recognition; second, improvements in technology that obviate the requirement to cut ultrathin section series, especially in FIB-SEM imaging (Merchán-Pérez et al., 2009; Knott et al., 2011) or serial

block-face SEM (Denk and Horstmann, 2004); as well as in 3D reconstruction (Mishchenko, 2009; Jain et al., 2010; Cardona et al., 2012). These have all been considered within the context of larger brains as well as tiny ones (Lichtman and Denk, 2011).

Finally, given the late development of several neuronal types in *Ciona* (Nishitsuji et al., 2012), further information will be required to establish the stability of the connectome at different larval ages. The only precedent for such parallel connectomic comparisons, in columns of the medulla in the *Drosophila* visual system, suggests that pathways may have an overall error rate of synapses formed, with <1% for each pathway constituting errors, either of omission or commission (Takemura et al., in press).) It is not clear how *Ciona* would stand in comparison with the precision of the fly, but left-right differences reported in this thesis suggest that it might be far less exact. Furthermore, the phenotypic plasticity of larvae with different exposure regimes (to light, pressure, touch, or different temperatures) also warrants investigation.

Data presented in this thesis can facilitate functional analyses to address these questions, not only in the larval brain of *Ciona intestinalis* but they also address the nature and future of connectome studies in other species. Moreover, insofar as I have used dense reconstruction (Helmstaedter, 2013) I can be sure that no cell (or connection) can hide, so that although the method may be laborious it also reveals, as with genomics, the true complexity and potential redundancy of living systems. Such complete connectomes are critical in bridging the gap between form and function in the nervous system.

The larval CNS of *Ciona* widely violates Cajal's law of dynamic polarization, and exhibits a high level of reciprocity in its connections. The 177 small neurons of this

system form similar numbers of synapses (6618) to those in the connectome of *C. elegans*. The larval CNS lacks ensheathing glia, myelin, and other features of vertebrate brains, but the abundance of basal ultrastructural features contrasts with the surprising complexity revealed in its network connections.

Membrane appositions, proposed sites of gap junctions (GJs), are present in the larval CNS of *Ciona intestinalis*, and are most abundant between neurons of the MG and between certain subsets of relay neurons. In general, most GJs occur between partners that additionally form chemical synapses, especially those with reciprocal synaptic relationships, but the directionality of some of these synaptic relationships suggests that some GJs in *Ciona* may be rectifying.

The neurotransmitter phenotypes can be resolved for several neurons, especially within the MG and tail, but the full complement of CNS neurons revealed in this study challenges many assumptions underlying previous assertions about the larval CNS. Network data can help us to identify particular neurons of interest, for which data to come on neurotransmitters and their receptors will allow networks to be modeled, to predict behaviour from underlying circuits.

The visual system of *Ciona intestinalis* larvae is layered, with integration between and among first-, second-, and third-order components. The interneurons of this pathway comprise both intrinsic and relay BV neurons, which form a complex network that also integrates coronet, antenna, and PNS interneuron inputs. The input from these visual relay neurons to the motor network occurs onto various components on both sides, but is greater to the left side descending interneurons than to those of the right side.

In the larva of *Ciona intestinalis*, the complete connectome reveals that the gravity-sensing pathway is translated through only two neurons, the antenna neurons, receiving input from the otolith and its associated ciliated cells. Differences between antenna neurons are reflected in differences seen between synaptic connections of the three classes of antenna relay neurons to which they provide input. Novel BV interneurons (trIN and aaINs) also participate in this gravity-sensing pathway by forming synapses with both antenna neurons and their interneurons, and integrating synaptic inputs from visual network components. The overall input from this pathway to the motor network of the MG is greater to the right side than to the left, and is greatest to the second pair of descending MG interneurons.

The peripheral network of the *Ciona intestinalis* larva provides input to the CNS from three major points of entry: anteriorly from RTEN neurons through many BV intrinsic peripheral interneurons and three relay neurons (PNIN and eminens neurons); to the dorsal MG from ATENp neurons through AVG neurons; and from the tail through planate bipolar tail neurons that extend their axons throughout the CNS, forming synapses onto a wide range of partners. The interneurons of these pathways overlap, forming synapses that allow integration of chemosensory and mechanosensory signals originating from head to tail, and providing extensive input to the motor network, which suggests that animals do indeed have behavioural responses to touch and chemical stimuli.

The MG of *Ciona intestinalis* contains networks and neurons that resemble the reticulospinal regions of vertebrate brains, while also having characteristics of

spinal neurons. This MG region, rather than a simple collection of motor neurons receiving direct relay input, represents an area of integration and complex connections that translate relayed signals into motor outputs. The CNC itself also bears a greater number and variety of neurons than previously appreciated, including motor neurons with neuromuscular synapses.

I present a putative CPG within the *Ciona intestinalis* CNS in which the contralateral inhibition coordinating sided contractions is mediated not directly by ACINs, but through inputs to excitatory interneurons that are themselves presynaptic to motor neurons. The contralateral inhibition imposed upon these interneurons occurs only unilaterally, from left to right, which suggests a sidedness to the system that is also reflected in asymmetries of the components of the motor network.

The larval CNS of *Ciona intestinalis* contains a network that resembles the startle response pathway of aquatic vertebrates. The cholinergic descending decussating neurons of the MG have similar synaptic connections to the M-cells of these vertebrates, but the peripheral input to ddNs does not appear to be sided, and the direct contralateral presynaptic inhibition of ddNs by ACINs occurs only from left to right. Thus, the putative startle response pathway of *Ciona* probably initiates a less directed escape response than the contralateral escape seen in many fish and amphibians.

Overall, the larval CNS can be mapped to a circuit diagram that illustrates the simplest paths and overall network formed by its connections (Fig. 11.1). The network is unexpectedly complex, and suggests the presence of uncharacterized responses to sensory stimuli.

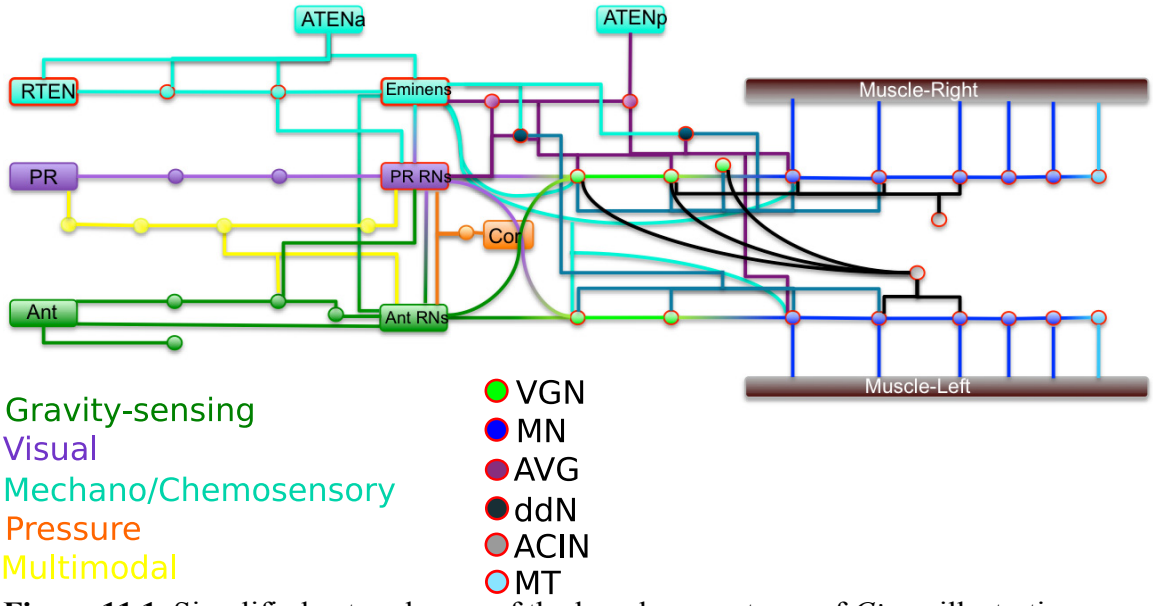

Figure 11.1. Simplified network map of the larval connectome of *Ciona* illustrating converging sensory pathways onto the motor network (VGNs and MNs). Sensory pathways are colour coded by sensory modality. Abbreviations of sensory neurons: RTEN (rostral trunk epidermal neurons), ATENa (anterior apical trunk epidermal neurons), ATENp (posterior apical trunk epidermal neurons, PR (photoreceptors), Ant (antenna neurons), and Cor (coronet cells). Relay neuron classes: PR RNs (photoreceptor relay neurons) and Ant RNs (antenna relay neurons), and Eminens (eminens PNS relay neurons). Motor ganglion and tail neurons: VGN (descending MG interneurons), MN (motor neurons), AVG (ascending MG interneurons), ddN (descending decussating neurons), ACIN (ascending contralateral inhibitory neurons), and MT (midtail motor neurons). All neurons receiving input from tail bipolar planate neurons are outlined in red.

References

Abitua PB, Gainous TB, Kaczmarczyk AN, Winchell CJ, Hudson C, Kamata K, Nakagawa M, Tsuda M, Kusakabe TG, Levine M. 2015. The pre-vertebrate origins of neurogenic placodes. Nature 524:462-465.

Agoston DV, Whittaker VP. 1989. Characterization, by size, density, osmotic fragility, and immunoaffinity, of acetylcholine- and vasoactive intestinal polypeptide-containing storage particles from myenteric neurones of the guinea-pig. J Neurochem 52:1474–1480.

Akerboom J, Chen T-W, Wardill TJ, Tian L, Marvin JS, Mutlu S, Calderon NC, Esposti F, Borghuis BG, Sun XR, Gordus A, Orger MB, Portugues R, Engert F, Macklin JJ, Filosa A, Aggarwal A, Kerr R A, Takagi R, Kracun S, Shigetomi E, Khakh BS, Baier H, Lagnado L, Wang SS-H, Bargmann CI, Kimmel BE, Jayaraman V, Svoboda K, Kim DS, Schreiter ER, Looger LL. 2012. Optimization of a GCaMP calcium indicator for neural activity imaging. J Neurosci 32:13819–13840.

Akert K, Moor H, Pfenninger K, and Sandri C. 1969. Contributions of new impregnation methods and freeze etching to the problems of synaptic fine structure. Prog Brain Res 31:223-240.

Alexopoulos H, Böttger A, Fischer S, Levin A, Wolf A, Fujisawa T, Hayakawa S, Gojobori T, Davies JA, David CN, Bacon JP. 2004. Evolution of gap junctions: The missing link? Curr Biol 14:R879–R880.

Arendt D. 2003. Evolution of eyes and photoreceptor cell types. Int J Dev Biol 47:563–571.

Bacci A, Huguenard JR, Prince DA. 2003. Functional autaptic neurotransmission in fast-spiking interneurons: A novel form of feedback inhibition in the neocortex. J Neurosci 23:859–866.

Bargmann CI, Marder E. 2013. From the connectome to brain function. Nat methods 10:483-490.

Bekkers JM. 2009. Synaptic transmission: Excitatory autapses find a function? Curr Biol 19:R296–R298.

Belloni E, Muenke M, Roessler E, Traverso G, Siegel-Bartelt J, Frumkin A, Mitchell HF, Donis-Keller H, Helms C, Hing AV, Heng HH, Koop B, Martindale D, Rommens JM, Tsui LC, Scherer SW. 1996. Identification of Sonic hedgehog as a candidate gene responsible for holoprosencephaly. Nat Genet 14:353–356.

Beltrán JQ, Gutiérrez R. 2012. Co-release of glutamate and GABA from single, identified mossy fibre giant boutons. J Physiol 590:4789–800.

Ben-Ari Y. 2002. Excitatory actions of GABA during development: The nature of the nurture. Nature Rev Neurosci 3:728-739.

Bennett MVL, Barrio LC., Bargiello TA, Spray DC, Hertzberg EL, Saez JC. 1991. Gap junctions: New tools, new answers, new questions. Neuron 6:305-320.

Bennett MLV. 1977. Electrical transmission: A functional analysis and comparison to chemical transmission. In Brookhart JM, Mountcastle VB, editors. The handbook of physiology. Section 1: The nervous system. p. 357-416. Bethesda, MD: American Physiological Society.

Bennett MVL, Garré JM, Orellana JA., Bukauskas FF, Nedergaard M, Sáez JC. 2012. Connexin and pannexin hemichannels in inflammatory responses of glia and neurons. Brain Res 1487:3–15.

Benninghoff J, van der Ven A, Schloesser RJ, Moessner R, Möller HJ, Rujescu D. 2012. The complex role of the serotonin transporter in adult neurogenesis and neuroplasticity. A critical review. World J Biol Psychiatry 13:240–247.

Bernhardt RR, Chitinis AB, Lindamer L, Kuwada JY. 1990. Identification of spinal neurons in the embryonic and larval zebrafish. J Comp Neurol 302:603-616.

Bettler B, Kaupmann K, Mosbacher J, Gassmann M, Structure M. 2004. Molecular Structure and Physiological Functions of GABA B Receptors. Physiol Rev 84:835–867.

Beyer EC, Gemel J, Martínez A, Berthoud VM, Valiunas V, Moreno AP, Brink PR. 2001. Heteromeric mixing of connexins: Compatibility of partners and functional consequences. Cell Commun Adhes 8:199–204.

Bierman HS, Schriefer JE, Zottoli SJ, Hale ME. 2004. The effects of head and tail stimulation on the withdrawal startle response of the rope fish (*Erpetoichthys calabaricus*). J Exp Biol 207:3985–3997.

Bierman HS, Zottoli SJ, Hale ME. 2009. Evolution of the Mauthner axon cap. Brain Behav Evol 73:174–187.

Bingham BL, Young CM. 1991. Larval behaviour of the ascidian *Ecteinascidia turbinate* Herdman: An in situ experimental study of the effects of swimming on dispersal. J Exp Mar Biol Ecol 145:189-204

Biserova NM, Gustafsson MKS, Reuter M, Terenina NB. 1996. The nervous system of the pike-tapeworm *Triaenophorus nodulosus* (Cestoda: Pseudophyllidea) - ultrastructure and immunocitochemical mapping aminergic and peptidergic elements. Invert Biol 115:273-285.

Björkdahl C, Sjögren MJ, Zhou X, Concha H, Avila J, Winblad B, Pei JJ. 2008. Small heat shock proteins Hsp27 or αB-crystallin and the protein components of neurofibrillary tangles: Tau and neurofilaments. J Neurosci Res 86:1343–1352.

Blanchet C, Eróstegui C, Sugasawa M, Dulon D. 1996. Acetylcholine-induced potassium current of guinea pig outer hair cells: Its dependence on a calcium influx through nicotinic-like receptors. J Neurosci 16:2574–2584.

Blaxter JHS. 1987. Structure and development of the lateral line. Biol Rev 62:471–514.

Bone Q. 1992. On the locomotion of ascidian tadpole larvae. J Mar Biol Assoc United Kingdom 72:161–186.

Bone Q, Mackie GO. 1982. Urochordata. In: Shelton GAB, editor. Electrical conduction and behaviour in "simple" invertebrates. Oxford: Clarendon Press. p 473-535.

Bone Q, Ryan KP. 1978. Cupular sense organs in *Ciona* (Tunicata : Ascidiacea). J Zool Lond 186:417–429.

Bozzola JJ, Russell LD. 1999. Electron microscopy: Principles and techniques for biologists. Sudbury, MA: Jones & Bartlett Learning.

Braun CB, Northcutt RG, Bruun CB. 1997. The lateral line system of hagfishes (Craniata: Myxinoidea). Acta Zool 78:247–268.

Briscoe J, Sussel L, Serup P, Connor DH. 1999. Homeobox gene Nkx2.2 and specification of neuronal identity by graded Sonic hedgehog signalling. Nature 398:622–627.

Brown ER, Nishino A, Bone Q, Meinertzhagen IA, Okamura Y. 2005. GABAergic synaptic transmission modulates swimming in the ascidian larva. Eur J Neurosci 22:2541–2548.

Brown TG. 1911. The intrinsic factors in the act of progression in the mammal. Proc R Soc B Biol Sci 84:308–319.

Brunetti R, Gissi C, Pennati R, Caicci F, Gasparini F, Manni L. 2015. Morphological evidence that the molecularly determined *Ciona intestinalis* type A and type B are different species: *Ciona robusta* and *Ciona intestinalis*. J Zool Syst Evol Res 53:186-193

Buchanan JT, Cohen AH. 1982. Activities of identified interneurons, motoneurons, and muscle fibers during fictive swimming in the lamprey and effects of reticulospinal and dorsal cell stimulation. J Neurophysiol 47:948–960.

Bullock TH, Moore JK, Fields RD. 1984. Evolution of myelin sheaths: Both lamprey and hagfish lack myelin. Neurosci Lett 48:145–148.

Bullock TH. 2004. The natural history of neuroglia: an agenda for comparative studies. Neuron glia biol 1:97-100.

Burighel P, Nunzi MG, Schiaffino S. 1977. A comparative study of the organization of the sarcotubular system in ascidian muscle. J morphol 153:205-223.

Burighel P, Cloney RA. 1997. Urochordata: Ascidiacea. In: Harrison FW, Ruppert EE, editors. Hemichordata, Chaetognata, and the invertebrate chordates, vol. 15. New York, NY: Wiley-Liss Inc. p.221-347.

Burighel P, Lane NJ, Fabio G, Stefano T, Zaniolo G, Candia Carnevali MD, Manni L. 2003. Novel, secondary sensory cell organ in ascidians: In search of the ancestor of the vertebrate lateral line. J Comp Neurol 461:236–249.

Buznikov GA, Chudakova IV, Zvezdina ND. 1964. The role of neurohumours in early embryogenesis. I. Serotonin content of developing embryos of sea urchin and loach. J Embryol Exp Morphol 12:563-573.

Byrne M, Nakajima Y, Chee FC, Burke RD. 2007. Apical organs in echinoderm larvae: Insights into larval evolution in the Ambulacraria. Evol Dev 9:432–445.

Caicci F, Zaniolo G, Burighel P, Degasperi V, Gasparini F, Manni L. 2010. Differentiation of papillae and rostral sensory neurons in the larva of the ascidian *Botryllus schlosseri* (Tunicata). J Comp Neurol 518:547–566.

Cajal R S .1891. Significación fisológica de las expansiones protoplásmatica y nerviosas de las células de la substancia gris. Congréso medico valenciano (cited in Cajal, 1909).

Campbell GR, Uehara Y, Burnstock G. 1974. Lanthanum nitrate in a smooth muscle membrane system. Z Zellforsch und mikroskop Anat 147:157–161.

Cañestro C, Bassham S, Postlethwait J. 2005. Development of the central nervous system in the larvacean *Oikopleura dioica* and the evolution of the chordate brain. Dev Biol 285:298–315.

Cardona A, Saalfeld S, Schindelin J, Arganda-Carreras I, Preibisch S, Longair M, Tomancak P, Hartenstein V, Douglas RJ. 2012. TrakEM2 software for neural circuit reconstruction. PLoS One 7:e38011.

Caspar DL, Goodenough DA, Makowski L, Phillips WC. 1977. Gap junction structures. I. Correlated electron microscopy and x-ray diffraction. J Cell Biol 74:605–628.

Castillo CG, Lo WK, Kuck JF, Yu NT. 1992. Nature and localization of avian lens glycogen by electron microscopy and Raman spectroscopy. Biophys J 61:839–44.

Castro A, Becerra M, Manso MJ, Anadón R. 2004. Somatomotor system of the adult amphioxus (*Branchiostoma lanceolatum*) revealed by an anticalretinin antiserum: An immunocytochemical study. J Comp Neurol 477:161–171.

Cazalets J-R, Borde M, Clarac F. 1995. Localization and organization of the central pattern generator for hindlimb locomotion in newborn rat. J Neurosci 15:4943–4951.

Cheng J, Stein RB, Jovanović K, Yoshida K, Bennett DJ, Han Y. 1998. Identification, localization, and modulation of neural networks for walking in the mudpuppy (*Necturus maculatus*) spinal cord. J Neurosci 18:4295–4304.

Chiang C, Litingtung Y, Lee E, Young KE, Corden JL, Westphal H, Beachy PA. 1996. Cyclopia and defective axial patterning in mice lacking Sonic hedgehog gene function. Nature 383:407–413.

Clarke JDW, Hayes BP, Hunt SP, Roberts A. 1984. Sensory physiology, anatomy and immunohistochemistry of Rohon-Beard neurons in embryos of *Xenopus laevis*. J Phyisiol (Lond) 348:511-525.

Cloney, R.A. 1978. Ascidian metamorphosis. Review and analysis. In Chia FS and Rice ME, editors. Settlement and metamorphosis of marine invertebrate larvae. New York, NY: Elsevier. p. 255-282.

Cobb JLS, Pentreath VW. 1976. The identification of chemical synapses in echinoderm nervous systems. Thalassia Yugoslavica 12:81-85.

Cole AG, Meinertzhagen IA. 2004. The central nervous system of the ascidian larva: Mitotic history of cells forming the neural tube in late embryonic *Ciona intestinalis*. Dev Biol 271:239–262.

Collins MO, Husi H, Yu L, Brandon JM, Anderson CNG, Blackstock WP, Choudhary JS, Grant SGN. 2006. Molecular characterization and comparison of the components and multiprotein complexes in the postsynaptic proteome. J Neurochem 97:16–23.

Conklin EG. 1905. The organization and cell-lineage of the ascidian egg. J Acad Nat Sci Phil 13:1-119.

Corbo JC, Levine M, Zeller RW. 1997. Characterization of a notochord-specific enhancer from the Brachyury promoter region of the ascidian, *Ciona intestinalis*. Development 124:589–602.

Couteaux R, Pécot-Dechavassine M. 1970. Synaptic vesicles and pouches at the level of "active zones" of the neuromuscular junction. C R Acad Sci Hebd Seances Acad Sci D 271:2346–2349.

Crandall SR, Cox CL. 2012. Local dendrodendritic inhibition regulates fast synaptic transmission in visual thalamus. J Neurosci 32:2513–2522.

Crowther RJ, Whittaker JR. 1984. Differentiation of histospecific ultrastructural features in cells of cleavage-arrested early ascidian embryos: Roux's arch. Dev Biol 194:87–98.

Cuomo A, Silvestre F, De Santis R, Tosti E. 2006. Ca2+ and Na+ current patterns during oocyte maturation, fertilization, and early developmental stages of *Ciona intestinalis*. Mol Reprod Dev 73:501–511.

Currie SN, Carlsen RC. 1987. Functional significance and neural basis of larval lamprey startle behaviour. J Exp Biol 133:121–35.

Currie SN, Carlsen, RC. 1988. Cranial components of startle behavior in larval and adult lampreys. Neurosci 24:709-718.

Curtin KD, Zhang Z, Wyman RJ. 2002. Gap junction proteins expressed during development are required for adult neural function in the *Drosophila* optic lamina. J Neurosci 22:7088–7096.

Dacheux RF, Raviola E. 1986. The rod pathway in the rabbit retina: A depolarizing bipolar and amacrine cell. J Neurosci 6:331–345.

Dale HH, Feldberg W, Vogt M. 1936. Release of acetylcholine at voluntary motor nerve endings. J Physiol 86:353–380.

Dale N. 1991. The isolation and identification of spinal neurons that control movement in the *Xenopus* embryo. Eur J Neurosci 3:1025–1035.

Dale N. 1995. Experimentally derived model for the locomotor pattern generator in the *Xenopus* embryo. J Physiol 489:489–510.

Darras S, Nishida H. 2001. The BMP/CHORDIN antagonism controls sensory pigment cell specification and differentiation in the ascidian embryo. Dev Biol 236:271–288.

Dasen JS, De Camilli A, Wang B, Tucker PW, Jessell TM. 2008. Hox repertoires for motor neuron diversity and connectivity gated by a single accessory factor, FoxP1. Cell 134:304–316.

Davies WL, Hankins MW, Foster RG. 2010. Vertebrate ancient opsin and melanopsin: Divergent irradiance detectors. Photochem Photobiol Sci 9:1418–1425.

De Camilli P, Haucke V, Takei K, Mugnaini M. 2001. The structure of synapses. In: Cowan DM, Südhof TC, Stevens CF, editors. Synapses. Baltimore, MD: Johns Hopkins University Press. p. 89-134.

Debanne D, Campanac E, Bialowas A, Carlier E, Alcaraz G. 2011. Axon physiology. Physiol Rev 91:555–602.

Dehal P, Satou Y, Campbell RK, Chapman J, Degnan B, De Tomaso A, Davidson B, Di Gregorio A, Gelpke M, Goodstein DM, Harafuji N, Hastings KEM, Ho I, Hotta K, Huang W, Kawashima T, Lemaire P, Martinez D, Meinertzhagen I a, Necula S, Nonaka M, Putnam N, Rash S, Saiga H, Satake M, Terry A, Yamada L, Wang H-G, Awazu S, Azumi K, Boore J, Branno M, Chin-Bow S, DeSantis R, Doyle S, Francino P, Keys DN, Haga S, Hayashi H, Hino K, Imai KS, Inaba K, Kano S, Kobayashi K, Kobayashi M, Lee B-I, Makabe KW, Manohar C, Matassi G, Medina M, Mochizuki Y, Mount S, Morishita T, Miura S, Nakayama A, Nishizaka S, Nomoto H, Ohta F, Oishi K, Rigoutsos I, Sano M, Sasaki A, Sasakura Y, Shoguchi E, Shin-i T, Spagnuolo A, Stainier D, Suzuki MM, Tassy O, Takatori N, Tokuoka M, Yagi K, Yoshizaki F, Wada S, Zhang C, Hyatt PD, Larimer F, Detter C, Doggett N, Glavina T, Hawkins T, Richardson P, Lucas S, Kohara Y, Levine M, Satoh N, Rokhsar DS. 2002. The draft genome of *Ciona intestinalis*: Insights into chordate and vertebrate origins. Science 298:2157–2167.

Delaney KR, Stanley EE. 2009. Calcium and neurotransmitter release. In: Encyclopedia of Life Sciences. Chichester:Wiley-Blackwell. http://www.els.net

Deliagina TG, Zelenin P V, Fagerstedt P, Grillner S, Orlovsky GN. 2000. Activity of reticulospinal neurons during locomotion in the freely behaving lamprey. J Neurophysiol 83:853–863.

Deliagina TG, Zelenin P V., Orlovsky GN. 2002. Encoding and decoding of reticulospinal commands. Brain Res Rev 40:166–177.

Del Negro CA, Koshiya N, Butera RJ, Smith JC. 2002. Persistent sodium current, membrane properties and bursting behavior of pre-bötzinger complex inspiratory neurons in vitro. J Neurophysiol 88:2242–2250.

Denk W, Briggman KL, Helmstaedter M. 2012. Structural neurobiology: Missing link to a mechanistic understanding of neural computation. Nat Rev Neurosci 13:351–358.

Denk W, Horstmann H. 2004. Serial block-face scanning electron microscopy to reconstruct three-dimensional tissue nanostructure. PLoS Biol 2:1900–1909.

De Rijk E, Jenks BG, Vaudry H, Roubos EW. 1990. GABA and neuropeptide Y co-exist in axons innervating the neurointermediate lobe of the pituitary of *Xenopus laevis*— an immunoelectron microscopic study. Neurosci 38(2):495-502.

Deyts C, Casane D, Vernier P, Bourrat F, Joly J-S. 2006. Morphological and gene expression similarities suggest that the ascidian neural gland may be osmoregulatory and homologous to vertebrate peri-ventricular organs. Eur J Neurosci 24:2299–308.

Di Gregorio A, Levine M. 1999. Regulation of Ci-tropomyosin-like, a Brachyury target gene in the ascidian, *Ciona intestinalis*. Development 126:5599–5609.

Dijkgraaf S. 1962. The functioning and significance of the lateral-line organs. Biol Rev 38:51–105.

Dilly PN. 1962. Studies on the receptors in the cerebral vesicle of the ascidian tadpole. I . The otolith. Q J Microsc Sci 103:393–398.

Dowling JE, Boycott B. 1966. Organization of the primate retina: Electron microscopy. Proc R Soc Lond Ser B, Biol Sci 166:80–111.

Dowling JE, Chappell RL. 1972. Neural organization of the median ocellus of the dragonfly. II. Synaptic structure. J Gen Physiol 60:148–165.

Dowling JE. 1970. Organization of vertebrate retinas. Investig Opthamology 9:655–680.

Dowling JE. 1987. The retina: An approachable part of the brain. Cambridge, MA: Harvard University Press.

Dowling JE. 2012. The retina: An approachable part of the brain. Revised edition. Cambridge, MA: Harvard University Press.

Dufour HD, Chettouh Z, Deyts C, de Rosa R, Goridis C, Joly J-S, Brunet J-F. 2006. Precraniate origin of cranial motoneurons. Proc Natl Acad Sci USA 103:8727–8732.

Duncan MK, Haynes JI, Cvekl A, Piatigorsky J. 1998. Dual roles for Pax-6: A transcriptional repressor of lens fiber cell-specific beta-crystallin genes. Mol Cell Biol 18:5579–5586.

Durbin RM. 1987. Studies on the development and organisation of the nervous system of *Caernorhabditis elegans*. Doctoral thesis, University of Cambridge.

Dybern BI. 1963. Biotope choice in *Ciona intestinalis* (L.): Influence of light. Zool Bidr Uppsala 35:589-602.

Eakin RM, Kuda A. 1970. Ultrastructure of sensory receptors in ascidian tadpoles. Z Zellforsch mikroskop Anat 112:287–312.

Eakin RM, Kuda A. 1972. Glycogen in lens of tunicate tadpole (Chordata: Ascidiacea). J Exp Zool 180:267-270.

Eaton RC, Bombardieri RA, Meyer DL. 1977. The Mauthner-initiated startle response in teleost fish. J Exp Biol 66:65–81.

Eccles JC, Eccles RM, Magni F. 1961. Central inhibitory action attributable to presynaptic depolarization produced by muscle afferent volleys. J Physiol 159:147–166

Eakin RM, Quay WB, Wesfall JA. 1961. Cytochemical and cytological studies of the parietal eye of the lizard, *Sceloporus occidentalis*. Z Zellforsch 53:449–470.

Eccles JC. 1964. The physiology of synapses. Berlin, Heidelberg: Springer-Verlag.

Egertová M, Elphick MR. 2007. Localization of CiCBR in the invertebrate chordate *Ciona intestinalis*: Evidence of an ancient role for cannabinoid receptors as axonal regulators of neuronal signalling. J Comp Neurol 502:660-672.

Eiraku M, Takata N, Ishibashi H, Kawada M, Sakakura E, Okuda S. 2011. Self-organizing optic-cup morphogenesis in three-dimensional culture. Nature 472:51–56.

Ekker SC, Ungar AR, Greenstein P, von Kessler DP, Porter JA, Moon RT, Beachy PA. 1995. Patterning activities of vertebrate hedgehog proteins in the developing eye and brain. Curr Biol 5:944–955.

Elms P, Siggers P, Napper D, Greenfield A, Arkell R. 2003. Zic2 is required for neural crest formation and hindbrain patterning during mouse development. Dev Biol 264:391–406.

Enjin A, Rabe N, Nakanishi ST, Vallstedt A, Gezelius H, Memic F, Lind M, Hjalt T, Tourtellotte WG, Bruder C, Eichele G, Whelan PJ, Kullander K. 2010. Identification of novel spinal cholinergic genetic subtypes disclose chodl and Pitx2 as markers for fast motor neurons and partition cells. J Comp Neurol 518:2284–2304.

Ericson J, Thor S, Edlund T, Jessell TM, Yamada T. 1992. Early stages of motor neuron differentiation revealed by expression of homeobox gene Islet-1. Science 256:1555–1560.

Ericson J, Morton S, Kawakami A, Roelink H, Jessell TM. 1996. Two critical periods of Sonic hedgehog signaling required for the specification of motor neuron identity. Cell 87:661–673.

Esposito R, D'Aniello S, Squarzoni P, Pezzotti MR, Ristoratore F, Spagnuolo A. 2012. New insights into the evolution of metazoan tyrosinase gene family. PLoS One 7:1–10.

Esposito R, Racioppi C, Pezzotti MR, Branno M, Locascio A, Ristoratore F, Spagnuolo A. 2015. The ascidian pigmented sensory organs: structures and developmental programs. Genesis 53:15–33.

Fain GL, Hardie R, Laughlin SB. 2010. Phototransduction and the evolution of photoreceptors. Curr Biol 20:R114–R124.

Famiglietti EV, Peters A. 1972. The synaptic glomerulus and the intrinsic neuron in the dorsal lateral geniculate nucleus of the cat. J Comp Neurol 144:285-334.

Feldman B, Gates MA, Egan, Elizabeth S, Dougan ST, Rennebeck G, Sirotkin HI, Schier AF, Talbot WS. 1998. Zebrafish organizer development and germ-layer formation require nodal-related signals. Nature 395:181–185.

Fiala JC, Harris KM. 2001. Cylindrical diameters method for calibrating section thickness in serial electron microscopy. J Microsc 202:468-472.

Fletcher EL, Hack I, Brandstätter JH, Wässle H. 2000. Synaptic localization of NMDA receptor subunits in the rat retina. J Comp Neurol 420:98–112.

Flood PR. 1970. The connection between spinal cord and notochord in Amphioxus (*Branchiostoma lanceolatum*). Z Zellforsch 103:115–128.

Foust A, Popovic M, Zecevic D, McCormick DA. 2010. Action potentials initiate in the axon initial segment and propagate through axon collaterals reliably in cerebellar Purkinje neurons. J Neurosci 30:6891-6902.

Funke J, Andres B, Hamprecht FA, Cardona A, Cook M. 2012. Efficient automatic 3D-reconstruction of branching neurons from EM data. Proc IEEE Comput Soc Conf Comput Vis Pattern Recognit:1004–1011.

Furshpan BYEJ, Potter DD. 1958. Transmission at the giant motor synapses of the crayfish. J Physiol 145:289–325.

Gahtan E, Sankrithi N, Campos JB, O'Malley DM. 2002. Evidence for a widespread brain stem escape network in larval zebrafish. J neurophysiol 87:608-614.

Gao S, Takemura S, Ting C-Y, Huang S, Lu Z, Luan H, Rister J, Thum AS, Yang M, Hong S-T, Wang JW, Odenwald WF, White BH, Meinertzhagen IA, Lee C-H. 2008. The neural substrate of spectral preference in *Drosophila*. Neuron 60:328–342.

Gardiol A, Racca C, Triller A. 1999. Dendritic and postsynaptic protein synthetic machinery. J Neurosci 19:168–179.

Giuliano P, Marino R, Pinto MR, De Santis R. 1998. Identification and developmental expression of Ci-isl, a homologue of vertebrate islet genes, in the ascidian *Ciona intestinalis*. Mech Dev 78:199–202.

Glover JC, Fritzsch B. 2009. Brains of primitive chordates. Encycl Neurosci:439–448.

Goldman, D. 2014. Muller glial cell reprogramming and retina regeneration. Nat Rev Neurosci 15:431-442.

Gostling NJ, Shimeld SM. 2003. Protochordate Zic genes define primitive somite compartments and highlight molecular changes underlying neural crest evolution. Evol Dev 5:136–144.

Graham A. 2004. Evolution and development: Rise of the little squirts. Curr Biol 14:956–958.

Grant SGN. 2006. The synapse proteome and phosphoproteome: A new paradigm for synapse biology. Biochem Soc Trans 34:59–63.

Grave C. 1920. *Amaroucium pellucidum* (Leidy) form constellatum (Verrill). I. The activities and reactions of the tadpole larva. J Exp Zool 30:239-257.

Gray EG. 1959. Axo-somatic and axo-dendritic synapses of the cerebral cortex. J Anat 93:420–433.

Gray EG. 1961. The granule cells, mossy synapses and Purkinje spine synapses of the cerebellum. J Anat 95:345–356.

Gray E. 1962. A morphological basis for pre-synaptic inhibition? Nature 193:82–83.

Grillner S. 2003. The motor infrastructure: From ion channels to neuronal networks. Nat Rev Neurosci 4:573–86.

Grillner S, Ekeberg Ö, El Manira A, Lansner A, Parker D, Tegnér J, Wallén P. 1998. Intrinsic function of a neuronal network - A vertebrate central pattern generator. Brain Res Rev 26:184–197.

Grillner S, Manira AE. 2015. The intrinsic operation of the networks that make us locomote. Curr Opin Neurobiol 31:244–249.

Grillner S, Wallén P, Brodin L. 1991. Neuronal network generating locomotor behavior in lamprey: Circuitry, transmitters, membrane properties, and simulation. Annu Rev Neurosci 14:169–199.

Grillner S, Wallén P. 1999. On the cellular bases of vertebrate locomotion. Prog Brain Res 123:297-309.

Grillner S, Wallén P. 2002. Cellular bases of a vertebrate locomotor system - Steering, intersegmental and segmental co-ordination and sensory control. Brain Res Rev 40:92–106.

Gobel S. 1976. Dendroaxonic synapses in the substantia gelatinosa glomeruli of the spinal trigeminal nucleus of the cat. J Comp Neurol 167:165-176.

Groves PM, Linder JC. 1983. Dendro-dendritic synapses in substantia nigra: Descriptions based on analysis of serial sections. Exp brain Res 49:209–217.

Guthrie DM, Banks JR. 1970. Observations on the function and physiological properties of a fast paramyosin muscle — the notochord of amphioxus (*Branchiostoma Lanceolatum*). J Exp Biol 52:125–138.

Hackley C, Mulholland E, Kim GJ, Newman-Smith E, Smith WC. 2013. A transiently expressed connexin is essential for anterior neural plate development in *Ciona intestinalis*. Development 140:147–155.

Hall BK, Gillis JA. 2013. Incremental evolution of the neural crest, neural crest cells and neural crest-derived skeletal tissues. J Anat 222:19–31.

Hallonet M, Hollemann T, Wehr R, Jenkins NA, Copeland NG, Pieler T, Gruss P. 1998. Vax1 is a novel homeobox-containing gene expressed in the developing anterior ventral forebrain. Development 125:2599–2610.

Hamada M, Shimozono N, Ohta N, Satou Y, Horie T, Kawada T, Satake H, Sasakura Y, Satoh N. 2011. Expression of neuropeptide- and hormone-encoding genes in the *Ciona intestinalis* larval brain. Dev Biol 352:202–214.

Harlow ML, Ress D, Stoschek A, Marshall RM, McMahan UJ. 2001. The architecture of active zone material at the frog's neuromuscular junction. Nature 409:479–484.

Harris JA, Cheng AG, Cunningham LL, MacDonald G, Raible DW, Rubel EW. 2003. Neomycin-induced hair cell death and rapid regeneration in the lateral line of zebrafish (*Danio rerio*). J Assoc Res Otolaryngol 4:219–234.

Harris KM, Weinberg RJ, Verrall AW. 2012. Ultrastructure of synapses in the mammalian brain. Cold Spring Harb Perspect Biol 4:1–30.

Helmstaedter M. 2013. Cellular-resolution connectomics: challenges of dense neural circuit reconstruction. Nat Methods 10:501–507.

Hernandez-Nicaise ML. 1973. The nervous system of ctenophores. III. Ultrastructure of synapses. J Neurocytol 2:249–263.

Hnasko TS, Edwards RH. 2012. Neurotransmitter corelease: Mechanism and physiological role. Annu Rev Physiol 74:225–243.

Holmberg K. 1977. The cyclostome retina. In: Crescitelli F, editor. Handbook of sensory physiology. Vol. VII/5: The visual system in vertebrates. Berlin, Heidelberg: Springer-Verlag. P. 47-66.

Horie T, Kusakabe T, Tsuda M. 2008a. Glutamatergic networks in the *Ciona intestinalis* larva. J Comp Neurol 508:249-263.

Horie T, Nakagawa M, Sasakura Y, Kusakabe TG, Tsuda M. 2010. Simple motor system of the ascidian larva: Neuronal complex comprising putative cholinergic and GABAergic/glycinergic neurons. Zool Sci 27:181–190.

Horie T, Orii H, Nakagawa M. 2005. Structure of ocellus photoreceptors in the ascidian *Ciona intestinalis* larva as revealed by an anti-arrestin antibody. J Neurobiol 65:241–250.

Horie T, Sakurai D, Ohtsuki H, Terakita A, Shichida Y, Usukura J, Kusakabe T, Tsuda M. 2008b. Pigmented and nonpigmented ocelli in the brain vesicle of the ascidian larva. J Comp Neurol 509:88-102.

Horie T, Shinki R, Ogura Y, Kusakabe TG, Satoh N, Sasakura Y. 2011. Ependymal cells of chordate larvae are stem-like cells that form the adult nervous system. Nature 469:525–528.

Hornung G, Barkai N. 2008. Noise propagation and signaling sensitivity in biological networks: A role for positive feedback. PLoS Comput Biol 4:0055–0061.

Horridge G, Mackay B. 1962. Naked axons and symmetrical synapses in an elementary nervous system. Q J Microsc Sci 103:531–541.

Horridge GA. 1968. Interneurons, their origin, action, specificity, growth, and plasticity. New York: WH Freeman.

Horwitz J. 2003. Alpha-crystallin. Exp Eye Res 76:145–153.

Hotta K, Takahashi H, Satoh N, Gojobori T. 2008. Brachyury-downstream gene sets in a chordate, *Ciona intestinalis*: Integrating notochord specification, morphogenesis and chordate evolution. Evol Dev 10:37–51.

Hudson C, BAM, Rouvière C, Yasuo H. 2011. Divergent mechanisms specify chordate motoneurons: Evidence from ascidians. Development 138:1643–1652.

Ikeda K, Bekkers JM. 2007. Quick guide autapses. Curr Biol 16:R308.

Ikuta T, Yoshida N, Satoh N, Saiga H. 2004. *Ciona intestinalis* Hox gene cluster: Its dispersed structure and residual colinear expression in development. Proc Natl Acad Sci USA 101:15118–23.

Imai JH, Meinertzhagen IA. 2007a. Neurons of the ascidian larval nervous system in *Ciona itnestinalis*: I. Central nervous system. J Comp Neurol 501:316-334.

Imai JH, Meinertzhagen IA. 2007b. Neurons of the ascidian larval nervous system in *Ciona itnestinalis*: II. Peripheral nervous system. J Comp Neurol 501:335-352.

Imai KS, Hino K, Yagi K, Satoh N, Satou Y. 2004. Gene expression profiles of transcription factors and signaling molecules in the ascidian embryo: Towards a comprehensive understanding of gene networks. Development 131:4047–4058.

Imai KS, Stolfi A, Levine M, Satou Y. 2009. Gene regulatory networks underlying the compartmentalization of the *Ciona* central nervous system. Development 136:285–93.

Inaba K, Nomura M, Nakajima A, Hozumi A. 2007. Functional proteomics in Ciona intestinalis: A breakthrough in the exploration of the molecular and cellular mechanism of ascidian development. Dev Dyn 236:1782–1789.

Inada K, Horie T, Kusakabe T, Tsuda M. 2003. Targeted knockdown of an opsin gene inhibits the swimming behaviour photoresponse of ascidian larvae. Neurosci Lett 347:167–170.

Inan M, Blázquez-Llorca L, Merchán-Pérez A, Anderson SA, DeFelipe J, Yuste R. 2013. Dense and overlapping innervation of pyramidal neurons by chandelier cells. J Neurosci 33:1907–1914.

Irvine SQ, Fonseca VC, Zompa MA., Antony R. 2008. Cis-regulatory organization of the Pax6 gene in the ascidian *Ciona intestinalis*. Dev Biol 317:649–659.

Islam AT, Moly PK, Miyamoto Y, Kusakabe TG. 2010. Distinctive expression patterns of Hedgehog pathway genes in the *Ciona intestinalis* larva: Implications for a role of Hedgehog signaling in postembryonic development and chordate evolution. Zool Sci 27:84-90.

Isaacson JS, Strowbridge BW. 1998. Olfactory reciprocal synapses: Dendritic signaling in the CNS. Neuron 20:749–761.

Iwahori N, Nakamura K, Tsuda A. 1996. Neuronal organization of the optic tectum in the hagfish, *Eptatretus burgeri*: A Golgi study. Anat Embryol (Berl) 193:271–279.

Jain V, Seung HS, Turaga SC. 2010. Machines that learn to segment images: A crucial technology for connectomics. Curr Opin Neurobiol 20:653–666.

Jessel TM, Kandel ER. 1993. Synaptic transmission: A bidirectional and self-modifiable form of cell-cell communication. Cell 72:1–30.

Jiang D, Smith W. 2002. An ascidian engrailed gene. Dev Genes Evol 212:399–402.

Jiang D, Tresser JW, Horie T, Tsuda M, Smith WC. 2005. Pigmentation in the sensory organs of the ascidian larva is essential for normal behavior. J Exp Biol 208:433–438.

Jonas P, Bischofberger J, Sandkuhler J. 1998. Corelease of two fast neurotransmitters at a central synapse. Science 281:419–424.

Kandel ER, Schwartz JH, Jessell TM (Eds.). 2000. Principles of neural science, Vol. 4. New York, NY: McGraw-Hill. p. 1227-1246.

Katsuyama Y, Okada T, Matsumoto J, Ohtsuka Y, Terashima T, Okamura Y. 2005. Early specification of ascidian larval motor neurons. Dev Biol 278:310–322.

Katz MJ. 1983. Comparative anatomy of the tunicate tadpole, *Ciona intestinalis*. Biol Bull 164:1–27.

Kawakami I, Shiraishi S, Tsuda M. 2002. Photoresponse and learning behavior of ascidian larvae, a primitive chordate, to repeated stimuli of step-up and step-down of light. J Biol Phys 28:549–559.

Kawamura K, Nomura M, Kameda T, Shimamoto H, Nakauchi M. 1991. Self-nonself recognition activity extracted from self-sterile eggs of the ascidian, *Ciona intestinalis*. Dev Growth Differ 33: 139-148.

Kidd M. 1962. Electron microscopy of the inner plexiform layer of the retina in the cat and the pigeon. J Anat 96:179–187.

Kimura Y, Yoshida M, Morisawa M. 2003. Interaction between noradrenaline or adrenaline and the β1-adrenergic receptor in the nervous system triggers early metamorphosis of larvae in the ascidian, *Ciona savignyi*. Dev Biol 258:129–140.

Kimura Y, Okamura Y, Higashijima S. 2006. alx, a zebrafish homolog of Chx10, marks ipsilateral descending excitatory interneurons that participate in the regulation of spinal locomotor circuits. J Neurosci 26:5684–5697.

Knott G, Rosset S, Cantoni M. 2011. Focussed ion beam milling and scanning electron microscopy of brain tissue. J Vis Exp 53:3–6.

Kolb H, Fernandez E, Nelson R, Jones B. 2014. Webvision: The organization of the retina and visual system. Available online at http://webvision.med.utah.edu

Konno A, Kaizu M, Hotta K, Horie T, Sasakura Y, Ikeo K, Inaba K. 2010. Distribution and structural diversity of cilia in tadpole larvae of the ascidian *Ciona intestinalis*. Dev Biol 337:42–62.

Koulen P, Fletcher EL, Craven SE, Bredt DS, Wässle H. 1998. Immunocytochemical localization of the postsynaptic density protein PSD-95 in the mammalian retina. J Neurosci 18:10136–10149.

Koyanagi M, Kubokawa K, Tsukamoto H, Shichida Y, Terakita A. 2005. Cephalochordate melanopsin: Evolutionary linkage between invertebrate visual cells and vertebrate photosensitive retinal ganglion cells. Curr Biol 15:1065–1069.

Koyanagi M, Terakita A. 2008. Gq-coupled rhodopsin subfamily composed of invertebrate visual pigment and melanopsin. Photochem Photobiol 84:1024–1030.

Krantz DE, Waites C, Oorschot V, Liu Y, Wilson RI, Tan PK, Klumperman J, Edwards RH. 2000. A phosphorylation site regulates sorting of the vesicular acetylcholine transporter to dense core vesicles. J Cell Biol 149:379–395.

Kröger RHH. 2013. Optical plasticity in fish lenses. Prog Retin Eye Res 34:78–88.

Kusakabe T, Kusakabe R, Kawakami I, Satou Y, Satoh N, Tsuda M. 2001. Ci-opsin1, a vertebrate-type opsin gene, expressed in the larval ocellus of the ascidian *Ciona intestinalis*. FEBS Lett 506:69–72.

Lacalli TC. 1994. Apical organs, epithelial domains, and the origin of the chordate central nervous system. Integr Comp Biol 34:533–541.

Lacalli TC. 2008. Basic features of the ancestral chordate brain: A protochordate perspective. Brain Res Bull 75: 319–323.

Lagier S, Panzanelli P, Russo RE, Nissant A, Bathellier B, Sassoè-Pognetto M, Fritschy J-M, Lledo P-M. 2007. GABAergic inhibition at dendrodendritic synapses tunes gamma oscillations in the olfactory bulb. Proc Natl Acad Sci 104:7259–7264.

Lamb TD, Collin SP, Pugh EN. 2007. Evolution of the vertebrate eye: opsins, photoreceptors, retina and eye cup. Nat Rev Neurosci 8:960-976.

Lamb TD. 2013. Evolution of phototransduction, vertebrate photoreceptors and retina. Prog Retin Eye Res 36:52–119.

Lane EB, Whitear M. 1982. Sensory structures at the surface of fish skin. II. Lateralis system. Zool J Linnean Soc 76:19-28.

Lee S, Kim K, Zhou ZJ. 2010. Role of ACh-GABA cotransmission in detecting image motion and motion direction. Neuron 68:1159–72.

Lee S, Lee B, Joshi K, Pfaff SL, Lee JW, Lee SK. 2008. A regulatory network to segregate the identity of neuronal subtypes. Dev Cell 14:877–889.

Lemaire P, Bertrand V, Hudson C. 2002. Early steps in the formation of neural tissue in ascidian embryos. Dev Biol 252:151–169.

Lichtman JW, Denk W. 2011. The big and the small: Challenges of imaging the brain's circuits. Science 334:618–623.

Lichtman JW, Livet J, Sanes JR. 2008. A technicolour approach to the connectome. Nat Rev Neurosci 9:417–422.

Lin Y-R, Mok H-K, Wu Y-H, Liang S-S, Hsiao C-C, Huang C-H, Chiou S-H. 2013. Comparative proteomics analysis of degenerative eye lenses of nocturnal rice eel and catfish as compared to diurnal zebrafish. Mol Vis 19:623–37.

Lockery SR, Goodman MB. 2010. Tight-seal, whole-cell patch clamping of *C. elegans* neurons. In: Conn MP, editor. Essential ion methods. Burlington, MA: Elsevier Inc. p. 65-80.

Low SE, Woods IG, Lachance M, Ryan J, Schier AF, Saint-Amant L. 2012. Touch responsiveness in zebrafish requires voltage-gated calcium channel 2.1b. J Neurophysiol 108:148-159.

Lowenstein, W. 1981. Junctional intercellular communication: The cell-to-cell membrane channel. Physio Rev 61:829-913.

Lu QR, Sun T, Zhu Z, MAN, Garcia M, Stiles CD, Rowitch DH. 2002. Common developmental requirement for Olig function indicates a motor neuron/oligodendrocyte connection. Cell 109:75–86.

Luo L, Callaway EM, Svoboda K. 2008. Genetic Dissection of Neural Circuits. Neuron 57:634–660.

Lüscher B, Keller CA. 2004. Regulation of GABAA receptor trafficking, channel activity, and functional plasticity of inhibitory synapses. Pharmacol Ther 102:195–221.

Ma YC, Song MR, Park JP, Henry Ho HY, Hu L, Kurtev M V., Zieg J, MAQ, Pfaff SL, Greenberg ME. 2008. Regulation of motor neuron specification by phosphorylation of neurogenin 2. Neuron 58:65–77.

Macdonald R, Barth KA, Xu Q, Holder N, Mikkola I, Wilson SW. 1995. Midline signalling is required for Pax gene regulation and patterning of the eyes. Development 121:3267–3278.

Mackie GO, Burighel P. 2005. The nervous system in adult tunicates: Current research directions. Can J Zool 83:151–183.

Malinin GI, Bernstein H. 1979. Histochemical demonstration of glycogen in corneal endothelium. Exp Eye Res 28:381-385.

Manni L, Lane NJ, Burighel P, Zaniolo G. 2001. Are neural crest and placodes exclusive to vertebrates? Evol Dev 3:297–298.

Manni L, Mackie GO, Caicci F, Zaniolo G, Burighel P. 2006. Coronal organ of ascidians and the evolutionary significance of secondary sensory cells in chordates. J Comp Neurol 495:363–73.

Manni L, Gasparini F, Stach T, Pennati R, Gissi C. 2015. *Ciona intestinalis* type A is *Ciona robusta* Hoshino & Tokioka, 1967, and *Ciona intestinalis* type B is *Ciona intestinalis* (Linnaeus, 1767) [Abstract]. In: The 8th International Tunicate Meeting: A1.

Marder E, Bucher D. 2001. Central pattern generators and the control of rhythmic movements. Curr Biol 11:986–996.

Marder E. 2009. Electrical synapses: Rectification demystified. Curr Biol 19:R34–R35.

Masland RH. 2012. The Neuronal Organization of the Retina. Neuron 76:266–280.

Mast SO. 1921. Reactions to light in the larvae of the ascidians, *Amaroucium constellatum* and *Amaroucium pellucidum* with special reference to photic orientation. J Exp Zool 34:148-187.

Maxwell DJ, Riddell JS. 1999. Axoaxonic synapses on terminals of group II muscle spindle afferent axons in the spinal cord of the cat. Eur J Neurosci 11:2151–2159.

McCarrager G, Chase R. 1985. Quantification of ultrastructural symmetry at molluscan chemical synapses. J Neurobiol 16:69-74.

McGreal RS, Lee Kantorow W, Chauss DC, Wei J, Brennan LA, Kantorow M. 2012. αB-crystallin/sHSP protects cytochrome c and mitochondrial function against oxidative stress in lens and retinal cells. Biochim Biophys Acta 1820:921–930.

McHenry MJ. 2005. The morphology, behavior, and biomechanics of swimming in ascidian larvae. Can J Zool 83:62–74.

McLennan H. 1963. Synaptic transmission. Philadelphia, PE: Saunders.

McMahan UJ, Wallace BG. 1989. Molecules in basal lamina that direct the formation of synaptic specializations at neuromuscular junctions. Dev neurosci 11:227-247.

Meinertzhagen IA. 2010. The organisation of invertebrate brains: Cells, synapses and circuits. Acta Zool 91:64–71.

Meinertzhagen IA. 2005. Eutely, cell lineage, and fate within the ascidian larval nervous system: Determinacy or to be determined? Can J Zool 83:184–195.

Meinertzhagen IA, Hiesinger PR. 2004. Visual system development, invertebrates. In Squire LR, editor. Elsevier's Encyclopedia of Neuroscience.

Meinertzhagen IA, Lemaire P, Okamura Y. 2004. The neurobiology of the ascidian tadpole larva: recent developments in an ancient chordate. Annu Rev Neurosci 27:453–85.

Meinertzhagen IA., Okamura Y. 2001. The larval ascidian nervous system: the chordate brain from its small beginnings. Trends Neurosci 24:401–410.

Merchán-Pérez A, Rodriguez J-R, Alonso-Nanclares L, Schertel A, Defelipe J. 2009. Counting synapses using FIB/SEM microscopy: A true revolution for ultrastructural volume reconstruction. Front Neuroanat 3:18.

Meremyanin AV, Eronina TB, Chebotareva NA, Kurganov BI. 2007. Kinetics of thermal aggregation of glycogen phosphorylase b from rabbit skeletal muscle: Mechanism of protective action of α-crystallin. Biopolymers 89:124–134.

Merrillees NC, Burnstock G, Holman ME. 1963. Correlation of fine structure and physiology of the innervation of smooth muscle in the guinea pig vas deferens. J Cell Biol 19:529–550.

Minganti A. 1957. Inhibition of melanogenesis in *Phallusia* embryos (ascidians). Acta Embryol Morphol Exp 1:37-47.

Mishchenko Y. 2009. Automation of 3D reconstruction of neural tissue from large volume of conventional serial section transmission electron micrographs. J Neurosci Methods 176:276–289.

Mitchell K, Spike RC, Todd AJ. 1993. An immunocytochemical study of glycine receptor and GABA in laminae I-III of rat spinal dorsal horn. J Neurosci 13:2371–2381.

Monaghan DT, Bridges RJ, Cotman CW. 1989. The excitatory amino acid receptors: Their classes, pharmacology and distinct properties in the function of the central nervous system. Annu Rev Pharmacol Toxicol 29:365–402.

Montero VM, Singer W. 1984. Ultrastructure and synaptic relations of neural elements containing glutamic acid decarboxylase (GAD) in the perigeniculate nucleus of the cat: A light and electron microscopic immunocytochemical study. Exp Brain Res 56:115–125.

Moret F, Christiaen L, Deyts C, Blin M, Joly J-S, Vernier P. 2005. The dopamine-synthesizing cells in the swimming larva of the tunicate *Ciona intestinalis* are located only in the hypothalamus-related domain of the sensory vesicle. Eur J Neurosci 21:3043–3055.

Morgan JL, Lichtman J. 2013. Why not connectomics? Nat Methods 10:494–500.

Murakami Y, Pasqualetti M, Takio Y, Hirano S, Rijli FM, Kuratani S. 2004. Segmental development of reticulospinal and branchiomotor neurons in lamprey: Insights into the evolution of the vertebrate hindbrain. Development 131:983–995.

Nagel G, Szellas T, Huhn W, Kateriya S, Adeishvili N, Berthold P, Ollig D, Hegemann P, Bamberg E. 2003. Cation-Selective Membrane Channel. Proc Natl Acad Sci 100:13940–13945.

Nakagawa M, Miyamoto T, Ohkuma M, Tsuda M. 1999. Action spectrum for the photophobic response of *Ciona intestinalis* (Ascidieacea, Urochordata) larvae implicates retinal protein. Photochem Photobiol 70:359-362.

Nakagawa M, Orii H, Yoshida N, Jojima E, Horie T, Yoshida R, Haga T, Tsuda M. 2002. Ascidian arrestin (Ci-arr), the origin of the visual and nonvisual arrestins of vertebrate. Eur J Biochem 269:5112–5118.

Nakajima Y. 1974. Fine structure of the synaptic endings on the Mauthner cell of the goldfish. J Comp Neurol 156:375-402.

Nakayama A, Satoh N, Sasakura Y. 2005. Tissue-specific profile of DNA replication in the swimming larvae of *Ciona intestinalis*. Zool Sci 22:301–309.

Nicol D. 1987. Development of the larval nervous system in the ascidian, *Ciona intestinalis*. Doctoral thesis, Dalhousie University.

Nicol D, Meinertzhagen IA. 1991. Cell counts and maps in the larval central nervous system of the ascidian *Ciona intestinalis* (L.). J Comp Neurol 309:415–429.

Nicoll RA, Malenka RC, Kauer JA. 1990. Functional comparison of neurotransmitter receptor subtypes in mammalian central nervous system. Physiol Rev 70:513–565.

Niedermeyer E, da Silva FL. (Eds.). 2005. Electroencephalography: Basic principles, clinical applications, and related fields, 5th Edition. Philadelphia, PE: Lippincott Williams & Wilkins.

Nilsson DE, Odselius R. 1981. A new mechanism for light-dark adaptation in the *Artemia* compound eye (Anostraca, Crustacea). J Comp Physiol 143:389–399.

Nishi S, Koketsu K. 1960. Electrical properties and activities of single sympathetic neurons in frogs. J Cell Comp Physiol 55:15-30.

Nishida H, Satoh N. 1989. Determination and regulation in the pigment cell lineage of the ascidian embryo. Dev Biol 132:355–367.

Nishida H, Sawada K. 2001. macho-1 encodes a localized mRNA in ascidian eggs that specifies muscle fate during embryogenesis. Nature 409:724–729.

Nishida H. 1991. Induction of brain and sensory pigment cells in the ascidian embryo analyzed by experiments with isolated blastomeres. Development 112:389–395.

Nishino A, Baba SA, Okamura Y. 2011. A mechanism for graded motor control encoded in the channel properties of the muscle ACh receptor. Proc Natl Acad Sci 108:2599–2604.

Nishino A, Okamura Y, Piscopo S, Brown ER. 2010. A glycine receptor is involved in the organization of swimming movements in an invertebrate chordate. BMC Neurosci 11:1–12.

Nishitsuji K, Horie T, Ichinose A, Sasakura Y, Yasuo H, Kusakabe TG. 2012. Cell lineage and cis-regulation for a unique GABAergic/glycinergic neuron type in the larval nerve cord of the ascidian *Ciona intestinalis*. Dev Growth Differ 54:177–186.

Noh J, Seal RP, Garver JA, Edwards RH, Kandler K. 2010. Glutamate co-release at GABA/glycinergic synapses is crucial for the refinement of an inhibitory map. Nat Neurosci 13:232–238.

Ohmori H, Sasaki S. 1977. Development of neuromuscular transmission in a larval tunicate. J Physiol 269:221–254.

Ohtsuki H. 1991. Sensory organs in the cerebral vesicle of the Ascidian larva, *Aplidium* sp.--an SEM study. Zool Sci 8:235-242.

Okada T, Hirano H, Takahashi K, Okamura Y. 1997. Distinct neuronal lineages of the ascidian embryo revealed by expression of a sodium channel gene. Dev Biol 190:257–272.

Okada T, Stanley MacIsaac S, Katsuyama Y, Okamura Y, Meinertzhagen IA. 2001. Neuronal form in the central nervous system of the tadpole larva of the ascidian *Ciona intestinalis*. Biol Bull 200:252–256.

Okamura Y, Nishino A, Murata Y, Nakajo K, Iwasaki H, Ohtsuka Y, Tanaka-Kunishima M, Takahashi N, Hara Y, Yoshida T, Nishida M, Okado H, Watari H, Meinertzhagen IA, Satoh N, Takahashi K, Satou Y, Okada Y, Mori Y. 2005. Comprehensive analysis of the ascidian genome reveals novel insights into the molecular evolution of ion channel genes. Physiol Genomics 22:269–282.

Olsen RW and DeLorey TM. 1999. GABA and glycine. In Siegel GJ, editor. Basic neurochemistry, 6th edition. Philadelphia, PE: Lippincott-Raven. P. 335.

Onoa B, Li H, Gagnon-Bartsch JA, Elias LAB, Edwards RH. 2010. Vesicular monoamine and glutamate transporters select distinct synaptic vesicle recycling pathways. J Neurosci 30:7917–7927.

Osumi N, Hirota A, Ohuchi H, Nakafuku M, Iimura T, Kuratani S, Fujiwara M, Noji S, Eto K. 1997. Pax-6 is involved in the specification of hindbrain motor neuron subtype. Development 124:2961–2972.

Palade GE. 1954 Electron microscope observations of interneuronal and neuromuscular synapses. Anat Rec 118:335.

Palay SL. 1954. Electron microscope study of the cytoplasm of neurons. Anat Rec 118:336.

Palay SL. 1956. Synapses in the central nervous system. J Biophys Biochem Cytol 2:193–202.

Palay SL, Chan-Palay V. 1976. A guide to the synaptic analysis of the neuropil. Cold Spring Harb Symp Quant Biol 40:1–16.

Palmer LM, Stuart GJ. 2006. Site of action potential initiation in layer 5 pyramidal neurons. J Neurosci 26:1854–1863.

Pan H, Gustafsson MK, Aruga J, Tiedken JJ, Jennifer JC, Emerson CP. 2011. A role for Zic1 and Zic2 in Myf5 regulation and somite myogenesis. Dev Biol 351:120–127.

Panchin Y, Kelmanson I, Matz M, Lukyanov K, Usman N, Lukyanov S. 2000. A ubiquitous family of putative gap junction molecules. Curr Biol 10:R473–R474.

Patanasatienkul T, Revie CW, Davidson J, Sanchez J. 2014. Mathematical model describing the population dynamics of *Ciona intestinalis* , a biofouling tunicate on mussel farms in Prince Edward Island , Canada. Manag Biol Invas 5:39–54.

Paulsson M. 1992. Basement membrane roteins : Structure, assembly, and cellular interactions. Crit Rev Biochem Mol Biol 27:93–127.

Pearce J, Govind CK. 1993. Reciprocal axo-axonal synapses between the common inhibitor and excitor motoneurons in crustacean limb muscles. Jounral Neurocytol 22:259–265.

Pennati R, Candiani S, Biggiogero M, Zega G, Groppelli S, Oliveri D, Parodi M, Di Bernardi F, Pestarino M. 2007. Developmental expression of tryptophan hydroxylase gene in *Ciona intestinalis*. Dev Genes Evol 217:307–313.

Pennati R, Groppelli S, Sotgia C, Candiani S, Pestarino M, De Bernardi F. 2001. Serotonin localization in Phallusia mammillata larvae and effects of 5-HT antagonists during larval development. Dev Growth Differ 43:647–656.

Pereda AE, Faber DS. 1996. Activity-dependent short-term enhancement of intercellular coupling. J Neurosci 16:983–992.

Pereda AE, Bell TD, Chang BH, Czernik AJ, Nairn AC, Soderling TR, Faber DS. 1998. Ca2+/calmodulin-dependent kinase II mediates simultaneous enhancement of gap-junctional conductance and glutamatergic transmission. Proc Natl Acad Sci U S A 95:13272–13277.

Pereda A, O'Brien J, Nagy JI, Bukauskas F, Davidson KG V, Kamasawa N, Yasumura T, Rash JE. 2003. Connexin35 mediates electrical transmission at mixed synapses on Mauthner cells. J Neurosci 23:7489–7503.

Peters A, Palay SL. 1996. The morphology of synapses. J Neurocytol 25:687–700.

Peters A, Palay SL, Webster DH. 1991. The fine structure of the nervous system: Neurons and their supporting cells. New York, NY: Oxford University Press.

Pfaff SL, Mendelsohn M, Stewart CL, Edlund T, Jessell TM. 1996. Requirement for LIM homeobox gene Isl1 in motor neuron generation reveals a motor neuron-dependent step in interneuron differentiation. Cell 84:309–320.

Pfeiffer B, Grosche J, Reichenbach A, Hamprecht B. 1994. Immunocytochemical demonstration of glycogen phosphorylase in Müller (glial) cells of the mammalian retina. Glia 12:62-67.

Phelan P, Starich TA. 2001. Innexins get into the gap. BioEssays 23:388–396.

Pinault D, Smith Y, Deschênes M. 1997. Dendrodendritic and axoaxonic synapses in the thalamic reticular nucleus of the adult rat. J Neurosci 17:3215–3233.

Plaza SM, Scheffer LK, Chklovskii DB. 2014. Toward large-scale connectome reconstructions. Curr Opin Neurobiol 25:201–210.

Purves RD. 1976. Function of muscarinic and nicotinic acetylcholine receptors. Nature 261:149-151

Rabaey M. 1963. Glycogen in the lens of birds' eyes. Nature 198:206–207.

Racca C, Gardiol A, Triller A. 1997. Dendritic and postsynaptic localizations of glycine receptor alpha subunit mRNAs. J Neurosci 17:1691–1700.

Racioppi C, Kamal AK, Razy-Krajka F, Gambardella G, Zanetti L, di Bernardo D, Sanges R, Christiaen LA, Ristoratore F. 2014. Fibroblast growth factor signalling controls nervous system patterning and pigment cell formation in *Ciona intestinalis*. Nat Commun 5:4830.

Raible F, Tessmar-Raible K, Arboleda E, Kaller T, Bork P, Arendt D, Arnone MI. 2006. Opsins and clusters of sensory G-protein-coupled receptors in the sea urchin genome. Dev Biol 300:461–475.

Rall W, Shepherd GM, Reese TS, Brightman MW. 1966. Dendrodendritic synaptic pathway for inhibition in the olfactory bulb. Exp Neurol 14:44–56.

Rapaport DH. 2006. Retinal neurogenesis. Retinal Dev:30-58.

Raviola E, Gilula NB. 1975. Intramembrane organization of specialized contacts in the outer plexiform layer of the retina. A freeze-fracture study in monkeys and rabbits. J Cell Biol 65:192–222.

Razy-Krajka F, Brown ER, Horie T, Callebert J, Sasakura Y, Joly J-S, Kusakabe TG, Vernier P. 2012. Monoaminergic modulation of photoreception in ascidian: Evidence for a proto-hypothalamo-retinal territory. BMC Biol 10:45.

Ren M, Yoshimura Y, Takada N, Horibe S, Komatsu Y. 2007. Specialized inhibitory synaptic actions between nearby neocortical pyramidal neurons. Science 316:758–761.

Reyes R, Haendel M, Grant D, Melancon E, Eisen JS. 2004. Slow degeneration of zebrafish Rohon-Beard neurons during programmed cell death. Dev Dyn 229:30-41.

Reuter M, Palmberg I. 1987. An ultrastructural and immunocytochemical study of gastrodermal cell types in *Microstomum lineare* (Turbellaria, Macrostomid). Acta Zool 68:153–163.

Roberts A, Clarke JDW. 1982. The neuroanatomy of the amphibian embryo spinal cord. Phil Trans R Soc B: Biol Sci 296:195-212.

Roemer A, Haas W. 1984. Fine structure of a lens-covered photoreceptor in the cercaria of *Trichobilharzia ocellata*. Z Parasit 70:391–394.

Rohde K, Watson N A, Chisholm L A. 1999. Ultrastructure of the eyes of the larva of *Neoheterocotyle rhinobatidis* (Platyhelminthes, Monopisthocotylea), and phylogenetic implications. Int J Parasitol 29:511–519.

Rolls MM, Jegla TJ. 2015. Neuronal polarity: An evolutionary perspective. J Exp Biol 218:572–580.

Rovainen CM. 1974. Synaptic interactions of reticulospinal neurons and nerve cells in the spinal cord of the sea lamprey. J Comp Neurol 154:207-223.

Rubin JB, Verselis VK, Bennett M V, Bargiello TA. 1992. Molecular analysis of voltage dependence of heterotypic gap junctions formed by connexins 26 and 32. Biophys J 62:183–195.

Rudomin P, Schmidt RF. 1999. Presynaptic inhibition in the vertebrate spinal cord revisited. Exp Brain Res 129:1-37.

Ruiz-Jones GJ, Hadfield MG. 2011. Loss of sensory elements in the apical sensory organ during metamorphosis in the nudibranch *Phestilla sibogae*. Biol Bull 220:39–46.

Ryan TJ, Grant SGN. 2009. The origin and evolution of synapses. Nat Rev Neurosci 10:701–712.

Saada R, Miller N, Hurwitz I, Susswein AJ. 2009. Autaptic excitation elicits persistent activity and a plateau potential in a neuron of known behavioural function. Curr Biol 19:479–484.

Sabatini DD, Bensch K, Barnett RJ. 1963. Cytochemistry and electronmicroscopy. The preservation of cellular ultrastructure and enzymatic activity by aldehyde fixation. J Cell Biol 17:19–58.

Sakarya O, Armstrong KA, Adamska M, Adamski M, Wang IF, Tidor B, Degnan BM, Oakley TH, Kosik KS. 2007. A post-synaptic scaffold at the origin of the animal kingdom. PLoS One 2:e506.

Sakurai D, Goda M, Kohmura Y, Horie T, Iwamoto H, Ohtsuki H, Tsuda M. 2004. The role of pigment cells in the brain of ascidian larva. J Comp Neurol 475:70–82.

Sanes JR. 1983. Roles of extracellular matric in neural development. Annu Rev Physiol 45:581–600.

Sanes JR. 2003. The basement membrane/basal lamina of skeletal muscle. J Biol Chem 278:12601–12604.

Sanes JR, Marshall LM, McMahon UJ. 1978. Reinnervation of muscle fibre basal lamina after removal of myofibres. J Cell Biol 78:176–198.

Sasaki H, Yoshida K, Hozumi A, Sasakura Y. 2014. CRISPR/Cas9-mediated gene knockout in the ascidian *Ciona intestinalis*. Dev Growth Differ 56:499–510.

Sasakura Y, Shoguchi E, Takatori N, Wada S, Meinertzhagen IA, Satou Y, Satoh N. 2003. A genomewide survey of developmentally relevant genes in *Ciona intestinalis*. X. Genes for cell junctions and extracellular matrix. Dev Genes Evol 213:303–313.

Sato S, Yamamoto H. 2001. Development of pigment cells in the brain of ascidian tadpole larvae: Insights into the origins of vertebrate pigment cells. Pigment Cell Res 14:428–436.

Satoh N, Rokhsar D, Nishikawa T. 2014. Chordate evolution and the three-phylum system. Proc Biol Sci 281: 20141729.

Satou Y, Imai KS, Satoh N. 2001a. Action of morpholinos in *Ciona* embryos. Genesis 30:103–106.

Satou Y, Kawashima T, Kohara Y, Satoh N. 2003. Large scale EST analyses in *Ciona intestinalis*. Its application as Northern blot analyses. Dev Genes Evol 213:314–318.

Satou C, Kimura Y, Kohashi T, Horikawa K, Takeda H, Oda Y, Higashijima S. 2009. Functional role of a specialized class of spinal commissural inhibitory neurons during fast escapes in zebrafish. J Neurosci 29:6780–6793.

Satou Y, Takatori N, Yamada L, Mochizuki Y, Hamaguchi M, Ishikawa H, Chiba S, Imai K, Kano S, Murakami SD, Nakayama a, Nishino a, Sasakura Y, Satoh G, Shimotori T, Shin-I T, Shoguchi E, Suzuki MM, Takada N, Utsumi N, Yoshida N, Saiga H, Kohara Y, Satoh N. 2001b. Gene expression profiles in *Ciona intestinalis* tailbud embryos. Development 128:2893–2904.

Satou Y, Yamada L, Mochizuki Y, Takatori N, Kawashima T, Sasaki A, Hamaguchi M, Awazu S, Yagi K, Sasakura Y, Nakayama A, Ishikawa H, Inaba K, Satoh N. 2002. A cDNA resource from the basal chordate *Ciona intestinalis*. Genesis 33:153–154.

Satou Y, Yagi K, Imai KS, Yamada L, Nishida H, Satoh N. 2002. Macho-1-related genes in *Ciona* embryos. Dev Genes Evol 212:87–92.

Satterlie R. 1985. Reciprocal inhibition and postinhibitory rebound produce reverberation in a locomotor pattern generator. Science 229:402–404.

Schubert D, Klier FG. 1977. Storage and release of acetylcholine by a clonal cell line. Proc Natl Acad Sci USA 74:5184–5188.

Shabel SJ, Proulx CD, Piriz J, Malinow R. 2014. GABA/glutamate co-release controls habenula output and is modified by antidepressant treatment. Science 345:1494-1498.

Shaw SR, Meinertzhagen IA. 1986. Evolutionary progression at synaptic connections made by identified homologous neurones. Proc Natl Acad Sci USA 83:7961–7965.

Shimeld SM, Holland PW. 2000. Vertebrate innovations. Proc Natl Acad Sci USA 97:4449–4452.

Shimeld SM, Purkiss AG, Dirks RPH, Bateman OA, Slingsby C, Lubsen NH. 2005. Urochordate betagamma-crystallin and the evolutionary origin of the vertebrate eye lens. Curr Biol 15:1684–9.

Smetana R, Juvin L, Dubuc R, Alford S. 2010. A parallel cholinergic brainstem pathway for enhancing locomotor drive. Nat Neurosci 13:731–738.

Smith CA, Rasmussen GL. 1965. Degeneration in the efferent nerve endings in the cochlea after axonal section. J Cell Biol 26:63–77.

Song S, Sjöström PJ, Reigl M, Nelson S, Chklovskii DB. 2005. Highly nonrandom features of synaptic connectivity in local cortical circuits. PLoS Biol 3:0507–0519.

Sopott-Ehlers B. 1996. First evidence of mitochondrial lensing in two species of the "Typhloplanoida " (Plathelminthes, Rhabdocoela): phylogenetic implications. Zoomorphology 116:95–101.

Sopott-Ehlers B, Kearn G, Ehlers U. 2001. Evidence for the mitochondrial origin of the eye lenses in embryos of *Entobdella soleae* (Plathelminthes, Monogenea). Parasitol Res 87:421–427.

Sordino P, Andreakis N, Brown ER, Leccia NI, Squarzoni P, R, Alfano C, Caputi L, D'Ambrosio P, Daniele P, D'Aniello E, D'Aniello S, Maiella S, Miraglia V, Russo MT, Sorrenti G, Branno M, Cariello L, Cirino P, Locascio A, Spagnuolo A, Zanetti L, Ristoratore F. 2008. Natural variation of model mutant phenotypes in *Ciona intestinalis*. PLoS One 3:e2344

SØviknes AM, Chourrout D, Glover JC. 2007. Development of the caudal nerve cord, motoneurons, and muscle innervation in the appendicularian urochordate *Oikopleura dioica*. J Comp Neurol 503:224-243.

Staley KJ., Soldo BL, Proctor WR. 1995. Ionic mechanisms of neuronal excitation by inhibitory GABAA receptors. Science 269:977-981.

Stanley MacIsaac S. 1999. Ultrastructure of the visceral ganglion in the ascidian larva *Ciona intestinalis*: Cell circuitry and synaptic distribution. Master thesis, Dalhousie University.

Sterling P, Laughlin S. 2013. Principles of neural design. Cambridge, MA: MIT Press.

Sterling P, Matthews G. 2005. Structure and function of ribbon synapses. Trends Neurosci 28:20–29.

Stevenson PA, Kutsch W. 1987. A reconsideration of the central pattern generator concept for locust flight. J Comp Physiol A 161:115–129.

Stolfi A, Christiaen L. 2012. Genetic and genomic toolbox of the Chordate *Ciona intestinalis*. Genetics 192:55–66.

Stolfi A, Gandhi S, Salek F, Christiaen L. 2014. Tissue-specific genome editing in *Ciona* embryos by CRISPR/Cas9. Development 9:4115–4120.

Stolfi A, Levine M. 2011. Neuronal subtype specification in the spinal cord of a protovertebrate. Development 138:995-1004.

Stolfi A, Wagner E, Taliaferro JM, Chou S, Levine M. 2011. Neural tube patterning by Ephrin, FGF and Notch signaling relays. Development 138:5429-5439.

Stoner DS. 1992. Vertical distribution of a colonial ascidian on a coral reef: The roles of larval dispersal and life-history variation. Amer Nat: 802-824.

Strowbridge BW. 2009. Role of cortical feedback in regulating inhibitory microcircuits. Ann N Y Acad Sci 1170:270–274.

Studer D, Graber W, Al-Amoudi A, Eggli P. 2001. A new approach for cryofixation by high-pressure freezing. J Microsc 203:285–294.

Suzuki MM, Nishikawa T, Bird A. 2005. Genomic approaches reveal unexpected genetic divergence within *Ciona intestinalis*. J Mol Evol 61:627-635.

Svane, I, Havenhand, JN, Jorgensen, AJ. 1987. Effects of tissue extracts of adults on metamorphosis in *Ascidia mentula* (O.F. Müller) and *Ascidiella scabra* (O.F. Müller). J Exp Mar Biol Ecol 110:171-181.

Svane I, Havenhand JN. 1993. Spawning and Dispersal in *Ciona intestinalis* (L.). Mar Ecol 14:53-66.

Svane I, Young CM. 1989. The ecology and behavior of ascidian larvae. Oceanogr Mar Biol 27:45-90.

Szabadics J, Varga C, Molnár G, Oláh S, Barzó P, Tamás G. 2006. Excitatory effect of GABAergic axo-axonic cells in cortical microcircuits. Science 311:233-235.

Szule JA, Jung JH, McMahan UJ. 2015. The structure and function of 'active zone material' at synapses. Philos Trans R Soc Lond B Biol Sci 370:20140189.

Takamura K. 1998. Nervous network in larvae of the ascidian *Ciona intestinalis*. Dev Genes Evol 208:1–8.

Takamura K, Minamida N, Okabe S. 2010. Neural map of the larval central nervous system in the ascidian *Ciona intestinalis*. Zool Sci 27:191–203.

Takatori N, Satou Y, Satoh N. 2002. Expression of hedgehog genes in *Ciona intestinalis* embryos. Mech Dev 116:235–238.

Takemura S, Xu CS, Lu Z, Rivlin PK, Olbris DJ, Parag T, Plaza S, Zhao T, Katz WT, Umayam L,Weaver C, Hess H, Horne JA, Nunez J, Aniceto R, Chang L-A, Lauchie S, Nasca A, Ogundeyi O, Sigmund C, Takemura S, Tran J, Langille C, Le Lacheur K, McLin S, Shinomiya A, Chklovskii DB, Meinertzhagen, IA, Scheffer LK. 2015. Multi-column synaptic circuits and an analysis of their variations in the visual system of *Drosophila*. Proc Natl Acad Sci USA (in press, accepted Sept. 18, 2015).

Take-uchi M. 2003. Hedgehog signalling maintains the optic stalk-retinal interface through the regulation of Vax gene activity. Development 130:955–968.

Tarallo R, Sordino P. 2004. Time course of programmed cell death in *Ciona intestinalis* in relation to mitotic activity and MAPK signaling. Dev Dyn 230:251-262.

Tassy O, Dauga D, Daian F, Sobral D, Robin F, Khoueiry P, Salgado D, Fox V, Caillol D, Schiappa R, Laporte B, Rios A, Luxardi G, Kusakabe T, Joly JS, Darras S, Christiaen L, Contensin M, Auger H, Lamy C, Hudson C, Rothbächer U, Gilchrist MJ, Makabe KW, Hotta K, Fujiwara S, Satoh N, Satou Y, Lemaire P. 2010. The ANISEED database: digital representation, formalisation and elucidation of a chordate developmental program. Genome Res 20:1459-1468.

Terakubo HQ, Nakajima Y, Sasakura Y, Horie T, Konno A, Takahashi H, Inaba K, Hotta K, Oka K. 2010. Network structure of projections extending from peripheral neurons in the tunic of ascidian larva. Dev Dyn 239:2278–2287.

Thor S, Thomas JB. 2002. Motor neuron specification in worms, flies and mice: Conserved and “lost” mechanisms. Curr Opin Genet Dev 12:558–564.

Todd KL, Kristan WB, French KA. 2010. Gap junction expression is required for normal chemical synapse formation. J Neurosci 30:15277–15285.

Tomlinson DR. 1975. Two populations of granular vesicles in constricted post-ganglionic sympathetic nerves. J Physiol 245:727–735.

Torrence SA, Cloney RA. 1982. Nervous system of ascidian larvae: Caudal primary sensory neurons. Zoomorphology 99:103–115.

Torrence SA, Cloney RA. 1983. Ascidian larval nervous system: Primary sensory neurons in adhesive papillae. Zoomorphology 102:111–123.

Torrence SA. 1986. Sensory endings of the ascidian static organ (Chordata, Ascidiacea). Zoomorphology 106:61–66.

Tranzer J-P, Richards JG. 1976. Ultrastructural cytochemistry of biogenic amines in nervous tissue: Methodologic improvements. J Histochem Cytochem 24:1178–1193.

Treen N, Yoshida K, Sakuma T, Sasaki H, Kawai N, Yamamoto T, Sasakura Y. 2014. Tissue-specific and ubiquitous gene knockouts by TALEN electroporation provide new approaches to investigating gene function in *Ciona*. Development 141:481–7.

Triller A, Korn H. 1985. Activity-dependent deformations of presynaptic grids at central synapses. J Neurocytol 14:177–192.

Tryba AK, Kaczorowski CC, Ben-Mabrouk F, Elsen FP, Lew SM, Marcuccilli CJ. 2011. Rhythmic intrinsic bursting neurons in human neocortex obtained from pediatric patients with epilepsy. Eur J Neurosci 34:31–44.

Tsuda M, Kawakami I, Miyamoto T, Nakagawa M, Shiraishi S, Gouda M. 2001. Photoresponse and habituation of swimming behavior of ascidian larvae, *Ciona intestinalis*. In Sawada H, Yokosawa H, Lambert CC, editors. The biology of ascidians. Tokyo: Springer-Verlag. p. 153-157.

Tsuda M, Kawakami I, Shiraishi S. 2003a. Sensitization and habituation of the swimming behavior in ascidian larvae to light. Zool Sci 20:13-22.

Tsuda M, Sakurai D, Goda M. 2003b. Direct evidence for the role of pigment cells in the brain of ascidian larvae by laser ablation. J Exp Biol 206:1409-1417.

Tuttle R, Masuko S, Nakajima Y. 1986. Freeze‐fracture study of the large myelinated club ending synapse on the goldfish Mauthner cell: Special reference to the quantitative analysis of gap junctions. J Comp Neurol 246:202-211.

Uchizono K. 1965. Characteristics of excitatory and inhibitory synapses in the central nervous system of the cat. Nature 207:642-643.

Urwyler O, Izadifar A, Dascenco D, Petrovic M, He H, Ayaz D, Kremer A, Lippens S, Baatsen P, Guerin CJ, Schmucker D. 2015. Investigating CNS synaptogenesis at single-synapse resolution by combining reverse genetics with correlative light and electron microscopy. Development 142:394–405

Valleix S, Niel F, Nedelec B, Algros M, Schwartz C, Delbosc B, Delpech M, Kantelip B. 2006. Homozygous nonsense mutation in the FOXE3 gene as a cause of congenital primary aphakia in humans. Am J Human Genet 79:358–364.

Van Essen DC, Anderson CH, Felleman DJ. 1992. Information processing in the primate visual system: an integrated systems perspective. Science 255:419–423.

van Gehuchten A. 1891. La structure de centre nerveux: La moelle épinière et le cervelet. Cellule 7:79-122.

Varela-Echavarría A, Pfaff SL, Guthrie S. 1996. Differential expression of LIM homeobox genes among motor neuron subpopulations in the developing chick brain stem. Mol Cell Neurosci 8:242–257.

Varshney LR, Chen BL, Paniagua E, Hall DH, Chklovskii DB. 2011. Structural properties of the Caenorhabditis elegans neuronal network. PLoS Comput Biol 7:e1001066.

Vigh J, Li GL, Hull C, Von Gersdorff H. 2005. Long-term plasticity mediated by mGluR1 at a retinal reciprocal synapse. Neuron 46:469–482.

Vigh B, Vigh-Teichmann I. 1998. Actual problems of the cerebrospinal fluid-contacting neurons. Microsc Res Tech 41:57–83.

Voogd J, Nieuwenhuys R, VanDongen PAM. 1998. Mammals. Chapter 22, In: Nieuwenhuys R, Ten Donkelaar HJ, Nicholson C, editors. The central nervous system of vertebrates, vol. 3. Berlin: Springer-Verlag. p. 1637-2097.

Vopalensky P, Pergner J, Liegertova M, Benito-Gutierrez E, Arendt D, Kozmik Z. 2012. Molecular analysis of the amphioxus frontal eye unravels the evolutionary origin of the retina and pigment cells of the vertebrate eye. Proc Natl Acad Sci 109:15383–15388.

Vorontsova MN, Nezlin LP, Meinertzhagen IA. 1997. Nervous system of the larva of the ascidian *Molgula citrina* (Alder and Hancock, 1848). Acta Zool (Stockh.) 78:177-185.

Wada H, Holland PW, Sato S, Yamamoto H, Satoh N. 1997. Neural tube is partially dorsalized by overexpression of HrPax-37: the ascidian homologue of Pax-3 and Pax-7. Dev Biol 187:240–252.

Wada H, Satoh N. 2001. Patterning the protochordate neural tube. Curr Opin Neurobiol 11:16–21.

Wada S, Tokuoka M, Shoguchi E, Kobayashi K, Di Gregorio A, Spagnuolo A, Branno M, Kohara Y, Rokhsar D, Levine M, Saiga H, Satoh N, Satou Y. 2003. A genomewide survey of developmentally relevant genes in *Ciona intestinalis*. II. Genes for homeobox transcription factors. Dev Genes Evol 213:222–234.

Waehneldt T V. 1990. Phylogeny of myelin proteins. Ann N Y Acad Sci 605:15–28.

Wagner E, Levine M. 2012. FGF signaling establishes the anterior border of the *Ciona* neural tube. Development 139:2351–2359.

Wang D, Bodovitz S. 2010. Single cell analysis: The new frontier in "omics." Trends Biotechnol 28:281–290.

Wald G. 1953. The biochemistry of vision. Ann Rev Biochem 22:497-526.

Ward AB, Azizi E. 2004. Convergent evolution of the head retraction escape response in elongate fishes and amphibians. Zoology 107:205–217.

Watanabe S, Nishino A. 2015. Is the spiral swimming trajectories of the larva based on the spiral configuration of myofibrils in the tail muscle cells? [Abstract]. In: The 8th International Tunicate Meeting: P35.

Weihe E, Tao-Cheng JH, Schäfer MK, Erickson JD, Eiden LE. 1996. Visualization of the vesicular acetylcholine transporter in cholinergic nerve terminals and its targeting to a specific population of small synaptic vesicles. Proc Natl Acad Sci 93:3547–3552.

Westfall JA, Elliott CF, Carlin RW. 2002. Ultrastructural evidence for two-cell and three-cell neural pathways in the tentacle epidermis of the sea anemone *Aiptasia pallida*. J Morphol 251:83–92.

Westfall JA. 1973. Ultrastructural evidence for neuromuscular systems in coelenterates. Am Zool 13:237–246.

Westfall JA. 1996. Ultrastructure of synapses in the first-evolved nervous systems. J Neurocytol 25:735–746.

White JG, Southgate E, Thomson JN, Brenner S. 1976. The structure of the ventral nerve cord of *Caenorhabditis elegans*. Phil Trans R Soc B: Biol Sci 275:327-348.

White JG, Southgate E, Thomson JN, Brenner S. 1986. The structure of the nervous system of the nematode *Caenorhabditis elegans* (The mind of a worm). Phil Trans R Soc Lond B: Biol Sci 314:1-340

White JS. 1986. Morphological and fine structural features of the basilar papilla in ambystomatid salamanders (Amphibia; Caudata). J morphol 187:181-199.

Whittaker JR. 1966. An analysis of melanogenesis in differentiating pigment cells of ascidian embryos. Dev biol 14:1-39.

Wilson CJ, Groves PM, Fifková E. 1977. Monoaminergic synapses, including dendro-dendritic synapses in the rat substantia nigra. Exp Brain Res 30:161–174.

Wolf H, Harzsch S. 2002. Evolution of the arthropod neuromuscular system. 1. Arrangement of muscles and innervation in the walking legs of a scorpion: *Vaejovis*

spinigerus (Wood, 1863) Vaejovidae, Scorpiones, Arachnida. Arthropod Struct Dev 31:185–202.

Wolken JJ, Florida RG. 1969. The eye structure and optical system of the crustacean copepod, *Copilia*. J Cell Biol 40:279–285.

Wu LG, Saggau P. 1997. Presynaptic inhibition of elicited neurotransmitter release. Trends Neurosci 20:204–212.

Yokoyama TD, Hotta K, Oka K. 2014. Comprehensive morphological analysis of individual peripheral neuron dendritic arbors in ascidian larvae using the photoconvertible protein Kaede. Dev Dyn 243:1362–73.

Yoshida K, Saiga H. 2011. Repression of Rx gene on the left side of the sensory vesicle by Nodal signaling is crucial for right-sided formation of the ocellus photoreceptor in the development of *Ciona intestinalis*. Dev Biol 354:144–50.

Yoshida R, Sakurai D, Horie T, Kawakami I, Tsuda M, Kusakabe T. 2004. Identification of neuron-specific promoters in *Ciona intestinalis*. Genesis 39:130–140.

Zanetti L, Ristoratore F, Francone M, Piscopo S, Brown ER. 2007. Primary cultures of nervous system cells from the larva of the ascidian *Ciona intestinalis*. J Neurosci Methods 165:191–197.

Zega G, Biggiogero M, Groppelli S, Bernardi FDE, Pennati R. 2008. Developmental expression of glutamic acid decarboxylase and of gamma-aminobutyric acid type B receptors in the ascidian *Ciona intestinalis*. J Comp Neurol 505:489–505.

Zega G, Pennati R, Groppelli S, Sotgia C, De Bernardi F. 2005. Dopamine and serotonin modulate the onset of metamorphosis in the ascidian *Phallusia mammillata*. Dev Biol 282:246–256.

Zega G, Thorndyke MC, Brown ER. 2006. Development of swimming behaviour in the larva of the ascidian *Ciona intestinalis*. J Exp Biol 209:3405–3412.

Zhai RG, Bellen HJ. 2004 The architecture of the active zone in the presynaptic nerve terminal. Physiology (Bethesda) 19:262–270.

Zhou Q, Wang S, Anderson DJ. 2000. Identification of a novel family of oligodendrocyte lineage-specific basic helix–loop–helix transcription factors. Neuron 25:331–343.

Zhou Q, Anderson DJ. 2002. The bHLH transcription factors OLIG2 and OLIG1 couple neuronal and glial subtype specification. Cell 109:61–73.

Appendix A

Neurons of *Ciona intestinalis* larva containing dense core synaptic vesicles in TEM series. Numbers of presynaptic sites include all sites, regardless of size in the entire larval CNS. Mixed synapses contain clear and dense core vesicles, but dcv synapses have exclusively dense core vesicles in the presynaptic vesicle pool.

Neuron	Total # presynaptic sites	# dcv syn	# mixed syn	Total # mixed and dcv syn	% mixed or dcv syn
coronet10	9	9	-	9	100
coronet5	6	5	-	5	83
coronet7	6	5	-	5	83
coronet6	5	4	-	4	80
coronet4	12	9	-	9	75
coronet3	8	6	-	6	75
coronet11	4	3	-	3	75
coronet8	10	7	-	7	70
coronet16	9	6	-	6	67
coronet2	13	8	-	8	62
coronet12	5	3	-	3	60
41	9	-	5	5	56
115	53	3	26	29	55
coronet1	13	7	-	7	54
102	64	-	34	34	53
coronet9	4	1	1	2	50
pr_158	2	-	1	1	50
95	62	-	30	30	48
13	12	-	5	5	42
23	13	2	3	5	38
74	33	1	11	12	36
50	17	1	5	6	35
MN5L	24	1	7	8	33
43	6	1	1	2	33
lens6	3	-	1	1	33
pns5	3	-	1	1	33
100	78	-	24	24	31
68	14	1	3	4	29
94	37	-	10	10	27
62	15	-	4	4	27
124	31	-	8	8	26
ATEN1	4	-	1	1	25
60	17	-	4	4	24

Neuron	Total # presynaptic sites	# dcv syn	# mixed syn	Total # mixed and dcv syn	% mixed or dcv syn
pr7	26	-	6	6	23
73	13	1	2	3	23
119	51	-	11	11	22
123	73	1	14	15	21
midtail4	10	-	2	2	20
108	46	2	7	9	20
103	47	-	9	9	19
140	37	1	6	7	19
Plan3	107	2	18	20	19
15	11	-	2	2	18
24	11	-	2	2	18
105	72	-	12	12	17
2	18	-	3	3	17
96	67	-	11	11	16
112	56	-	9	9	16
59	13	-	2	2	15
pnw	13	1	1	2	15
152	86	4	9	13	15
17	20	-	3	3	15
138	14	-	2	2	14
88	7	1	-	1	14
122	46	1	5	6	13
pr9	24	-	3	3	13
33	8	-	1	1	13
107	8	-	1	1	13
ATEN3	8	-	1	1	13
MN3R	42	-	5	5	12
midtail1	17	2	-	2	12
18	26	-	3	3	12
121	44	1	4	5	11
90	27	-	3	3	11
106	37	1	3	4	11
86	70	-	7	7	10
130	50	1	4	5	10
pr23	30	-	3	3	10
22	10	-	1	1	10
42	10	1	-	1	10
157	84	-	8	8	10
pr11	23	-	2	2	9
134	58	-	5	5	9

Neuron	Total # presynaptic sites	# dcv syn	# mixed syn	Total # mixed and dcv syn	% mixed or dcv syn
pr15	71	-	6	6	8
Ant2	95	-	8	8	8
92	24	-	2	2	8
pr4	25	-	2	2	8
Plan2	180	1	13	14	8
78	26	-	2	2	8
48	13	-	1	1	8
VG1R	79	-	6	6	8
pnb	40	-	3	3	8
AVG7	27	-	2	2	7
21	14	-	1	1	7
Em1	143	-	10	10	7
ukn2	46	1	2	3	7
Plan1	139	-	9	9	6
AVG5	93	-	6	6	6
pnc	31	-	2	2	6
pr8	31	-	2	2	6
120	125	-	8	8	6
70	48	-	3	3	6
pre	16	-	1	1	6
VG3L	49	-	3	3	6
Plan4	118	1	6	7	6
4	69	-	4	4	6
16	35	1	1	2	6
80	36	-	2	2	6
38	18	1	-	1	6
159	55	1	2	3	5
pr12	39	-	2	2	5
30	59	-	3	3	5
pr16	20	1	-	1	5
116	41	-	2	2	5
pna	44	-	2	2	5
pr21	22	-	1	1	5
pr6	22	-	1	1	5
Em2	179	1	7	8	4
6	23	-	1	1	4
61	23	-	1	1	4
pr22	23	-	1	1	4
125	48	-	2	2	4
pns7	48	1	1	2	4

Neuron	Total # presynaptic sites	# dcv syn	# mixed syn	Total # mixed and dcv syn	% mixed or dcv syn
pr3	27	-	1	1	4
VG1L	82	-	3	3	4
pr13	28	-	1	1	4
midtail2	29	1	-	1	3
pnf	30	-	1	1	3
AVG1	34	-	1	1	3
ACIN2L	37	-	1	1	3
93	45	-	1	1	2
pr20	45	-	1	1	2
VG2L	94	-	2	2	2
VG2R	94	2	-	2	2
131	47	-	1	1	2
MN4R	47	-	1	1	2
pns11	48	-	1	1	2
pns12	48	-	1	1	2
pr19	48	-	1	1	2
127	49	-	1	1	2
MN3L	51	-	1	1	2
AVG2	53	-	1	1	2
Ant1	237	2	2	4	2
126	60	-	1	1	2
143	66	-	1	1	2
36	67	-	1	1	1
ddR	79	-	1	1	1
MN1R	425	-	5	5	1
MN1L	300	1	2	3	1
142	111	-	1	1	0.9
MN2R	316	2	-	2	0.6
MN2L	285	1	-	1	0.4

Appendix B

All polyad synapses in the *Ciona* larval CNS by neuron. Neurons sorted from those with greatest to least percent of total presynaptic sites with multiple postsynaptic partners.

Neuron	Total number of presynaptic sites	Number of polyad synapses	% polyad synapses
1	5	2	40
106	37	14	38
prb	11	4	36
140	37	13	35
ukn2	46	16	35
pns10	52	17	33
29	22	7	32
Ant1	237	74	31
6	23	7	30
22	10	3	30
119	51	15	29
163	17	5	29
21	14	4	29
pr2	7	2	29
pns11	48	13	27
pr7	26	7	27
127	49	13	27
Ant2	95	26	27
AVG3	47	12	26
13	12	3	25
92	24	6	25
AVG6	38	9	24
123	73	17	23
164	13	3	23
pns12	48	11	23
2	18	4	22
pr20	45	10	22
116	41	9	22
VG1L	82	18	22
108	46	10	22
94	37	8	22
AVG5	93	20	22
86	70	15	21
74	33	7	21
105	72	15	21
pns7	48	10	21

Neuron	Total number of presynaptic sites	Number of polyad synapses	% polyad synapses
4	69	14	20
93	45	9	20
115 (aaIN)	53	10	19
AVG7	27	5	19
pns4	27	5	19
pr15	71	13	18
pr21	22	4	18
prc	11	2	18
130	50	9	18
50	17	3	18
pns3	40	7	18
61	23	4	17
122	46	8	17
AVG4	53	9	17
100	78	13	17
126	60	10	17
MN3R	42	7	17
pr4	25	4	16
160	19	3	16
78	26	4	15
pns9	13	2	15
103	47	7	15
VG2L	94	14	15
VG2R	94	14	15
90	27	4	15
pr19	48	7	15
3	7	1	14
88	7	1	14
112	56	8	14
135	49	7	14
138	14	2	14
pr17	28	4	14
80	36	5	14
pna	44	6	14
pr6	22	3	14
ukn	22	3	14
142	111	15	14
ACIN2L	37	5	14
pr23	30	4	13
AVG2	53	7	13

Neuron	Total number of presynaptic sites	Number of polyad synapses	% polyad synapses
157	84	11	13
161	69	9	13
33	8	1	13
70	48	6	13
79	16	2	13
20	17	2	12
60	17	2	12
AVG1	34	4	12
pr5	17	2	12
prf	17	2	12
18	26	3	12
ddR	79	9	11
ddL	80	9	11
159	55	6	11
147	86	9	10
36	67	7	10
96	67	7	10
30	59	6	10
42	10	1	10
101	10	1	10
coronet8	10	1	10
midtail4	10	1	10
pra	10	1	10
120	125	11	9
pnh	23	2	9
16	35	3	9
131	47	4	9
coronet4	12	1	8
pr9	24	2	8
162	25	2	8
PVGN1	51	4	8
Plan2	180	14	8
23	13	1	8
48	13	1	8
73	13	1	8
pns13	13	1	8
pr3	27	2	7
Plan1	139	10	7
pr13	28	2	7
Em1	143	10	7

Neuron	Total number of presynaptic sites	Number of polyad synapses	% polyad synapses
152	86	6	7
pr1	29	2	7
121	44	3	7
pnf	30	2	7
124	31	2	6
VG1R	79	5	6
102 (aaIN)	64	4	6
Em2	179	11	6
Plan4	118	7	6
ATEN4	17	1	6
38	18	1	6
pr12	39	2	5
pnb	40	2	5
pns1	20	1	5
MN4L	72	3	4
VG3L	49	2	4
134	58	2	3
midtail2	29	1	3
95 (aaIN)	62	2	3
pr8	31	1	3
143	66	2	3
VG3R	67	2	3
125	48	1	2
MN5R	48	1	2
153	49	1	2
MN1L	300	6	2
MN3L	51	1	2
Plan3	107	2	2
MN2L	285	5	2
MN1R	425	3	0.7
MN2R	316	2	0.6

Appendix C

Morphological and sensory input characteristics of brain vesicle intrinsic interneurons and pair of neck neurons. Reconstructions are colour-coded by major sensory input [also reported in column 2: photoreceptor (pr), antenna neurons (ant1; ant2), peripheral neurons (pns), photoreceptor relay neurons (prRN), antenna relay neurons (antRN) photoreceptor tract interneuron (trIN), anaxonal arborizing neurons (aaIN), peripheral interneurons (pns IN), and ascending motor ganglion peripheral interneurons (AVG)]. Left lateral views with 10mm scale bars at dorsal anterior and ventral anterior tail followed by descriptions of terminal (term) shape. Nuclear volumes represented as percentage of total cell body volume (vol).

Neuron ID	Sensory input	Reconstruction	Terminal shape	Cell body vol μm^3	Nuclear % of cell body vol
1	prRN		blunt	>94.72	9.88
2			elongate term	>100.9	17.16
3	prRN		branched	>24.37	2.30
4	pns		collateral axons, elongate term	>96.32	6.00
6	pns		collateral branches, expanded term	>93.17	16.46

Neuron ID	Sensory input	Reconstruction	Terminal shape	Cell body vol μm^3	Nuclear % of cell body vol
13	pr		forked	158.57	14.88
15	ant1&2 RNs		blunt	103.55	22.02
16	ant2, pr		forked	157.92	13.46
17	pr, ant2 RNs		forked	125.35	14.12
18	ukn2, trIN/ aaIN		forked	71.49	14.79
20	pnsIN		expanded term	79.81	9.99
22	pr		forked	86.72	11.76

Neuron ID	Sensory input	Reconstruction	Terminal shape	Cell body vol μm^3	Nuclear % of cell body vol
23	ant1&2 RNs		blunt	182.99	19.13
24	ant2		blunt	168.69	13.39
25	pns		no axon	98.23	
29	pns		elongate	112.17	20.66
30	pns		blunt	128.30	17.28
33	ant2		blunt	129.89	11.79
38	ant2, ant2RN		forked	267.96	11.79

Neuron ID	Sensory input	Reconstruction	Terminal shape	Cell body vol μm^3	Nuclear % of cell body vol
41			blunt	115.54	14.53
42	pr		forked	166.93	13.84
43			blunt	107.14	14.12
48	aaIN		blunt	173.49	13.54
50	pr		v term	116.54	19.22
55	prRN		blunt	123.71	12.13
59	aaIN		bent	112.67	13.52

Neuron ID	Sensory input	Reconstruction	Terminal shape	Cell body vol μm^3	Nuclear % of cell body vol
60	pnIN		elongate	121.40	12.27
61	ant2 RN		branched	173.78	12.54
62	pr		branched v term	169.98	13.06
65	pns		blunt	300.05	6.91
68	ant2, pr		branched v term	116.92	17.70
70	ant2, pr		branched v term	94.03	17.33
73	ant2		multi-lobed	145.86	12.61

Neuron ID	Sensory input	Reconstruction	Terminal shape	Cell body vol μm^3	Nuclear % of cell body vol
78	pr, ant2 RN		branched v term	214.36	11.48
79	ant1&2 RN		forked	129.34	15.00
85	pnsIN		tapered with branch	305.57	3.91
88	pr		tapered	213.89	10.75
90	ant2, pr		bipolar	278.87	8.82
92	pr		bipolar	219.18	10.77
95	ant1 & ant2, pr, ant1&2 RN		highly branched	221.89	13.39

Neuron ID	Sensory input	Reconstruction	Terminal shape	Cell body vol μm^3	Nuclear % of cell body vol
102	ant1 & ant2, pr, ant1&2 RN		highly branched	225.38	11.89
115	ant1 & ant2, pr, ant1&2 RN		highly branched	255.21	11.56
101	ant1 & ant2, pr, ant1&2 RN		expanded	140.47	13.60
160	pns		tapered	242.01	8.62
162	pr, pns, ant2 RN		tapered	137.38	12.59
163	pns		tapered	164.00	10.24
164	pns		tapered	149.17	12.77

Neuron ID	Sensory input	Reconstruction	Terminal shape	Cell body vol μm^3	Nuclear % of cell body vol
177	pns	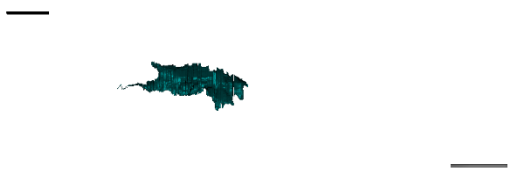	no axon	232.74	12.77
165	AVGs	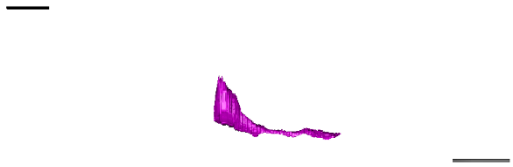	tapered	142.32	14.22
166	ant1RN		tapered	128.69	13.75

Appendix D

Synapses of brain vesicle intrinsic interneurons including number of presynaptic sites, total size of presynaptic sites (calculated from numbers of sections in which each synapse is observed) and number of presynaptic sites observed in more than one consecutive section (>1 section). Peripheral interneurons are shown in bold. Entries are sorted from greatest to least number of presynaptic sites >1 section.

Neuron	Number of presynaptic sites	Total size of presynaptic sites (mm)	Number of presynaptic sites >1 section
4	**69**	**12.66**	**54**
trIN (36)	67	14.52	52
95 (aaIN)	62	8.34	43
30	**59**	**8.16**	**46**
70	48	8.04	37
16	**35**	**5.22**	**26**
90 (bpn)	27	3.48	21
18	26	3.36	18
78	26	3.06	17
92 (bpn)	24	2.94	19
6	**23**	**4.98**	**21**
61	**23**	**2.76**	**17**
29	**22**	**3.36**	**17**
65	20	2.7	16
17	20	2.4	14
2	18	2.16	12
38	18	2.58	11
50	17	2.28	12
60	17	1.8	12
20	**17**	**2.46**	**11**
79	16	1.92	10
62	15	2.04	11
68	14	2.64	12
21	14	1.38	9
48	13	1.56	8
73	13	1.38	7
23	13	1.32	7

Neuron	Number of presynaptic sites	Total size of presynaptic sites (mm)	Number of presynaptic sites >1 section
55	13	1.38	6
59	13	1.02	6
13	12	1.56	8
15	11	1.74	8
24	11	1.32	7
22	10	0.78	5
42	10	0.6	3
41	9	1.56	8
33	8	0.54	3
85	8	0.42	3
3	7	1.38	6
88	7	0.24	2
43	6	0.3	2
1	5	0.42	2
25	5	0.24	2
46	5	0.12	1
44	3	0.12	1
71	2	0.24	2
19	2	0.18	1
82	2	0.12	1
49	1	0.24	1
12	1	0.12	1

Appendix E

Morphology of photoreceptor and antenna relay neurons of the posterior brain vesicle, including reconstructions, terminal shape, cell body volume, nuclear volmues (represented as percentage of cell body volume), and alternate name. Relay neurons sorted and reconstructions colour coded by major sensory input (also reported in column 2): pr (photoreceptor), ant1 (antenna cell 1), ant2 (antenna cell 2), ant1/2 (antenna cells 1 and 2), AVG (ascending motor ganglion peripheral intereneurons), Plan (Bipolar planate tail neurons). Postsynaptic relationship with Eminens peripheral relay neurons (Em), antenna relay neurons (ant 1&2 RNs), photoreceptor relay neurons (pr RN), or peripheral relay neuron (PN RN) is also indicated for each relay neuron. Reconstructions oriented to left lateral view and aligned across cells. Scale bars: 10mm at both dorsal anterior and ventral anterior tail.

ID	Sens-ory input	Reconstruction	Term shape	Cell body vol μm^3	Nuclear % of cell body volume	Alternate Name
80	pr	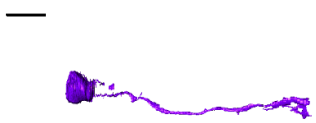	expanded	306	10.1	
86	pr	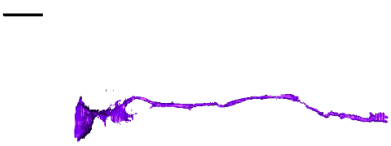	Svterm, club term	300.6	11.2	
96	pr	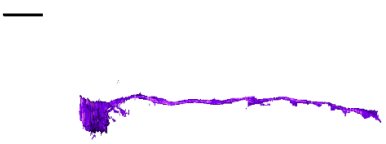	Svterm, elongate term	434.8	11.6	
100	pr	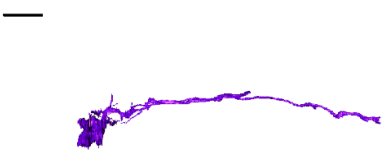	Svterm, elongate term	316.3	11.2	large ventro-posterior interneuron

ID	Sens-ory input	Reconstruction	Term shape	Cell body vol μm^3	Nuclear % of cell body volume	Alternate Name
105	pr	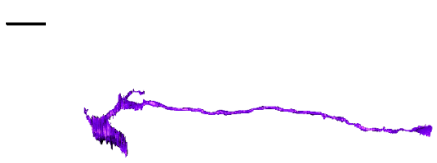	Svterm, club term	430.7	10.4	large ventro-posterior interneuron
112	pr	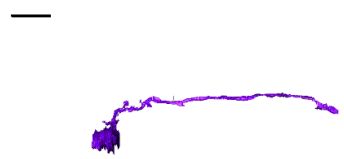	Svterm, elongate term	306.6	10.1	large ventro-posterior interneuron
121	pr	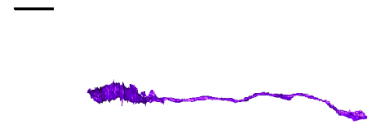	Svterm, club term	265.8	11.6	
123	pr	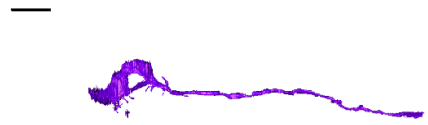	Svterm, club term	388.1	10.6	
126	pr	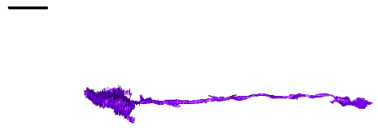	elongate term	277	11.2	
130	pr		Svterm, elongate term	286.7	13.1	

ID	Sens-ory input	Reconstruction	Term shape	Cell body vol μm^3	Nuclear % of cell body volume	Alternate Name
74	pr, AVG	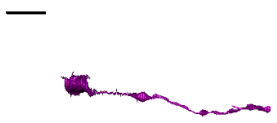	Svterm, club term	138.8	12.8	
94	pr, AVG		Svterm, elongate term	234.7	11.3	
124	pr, AVG	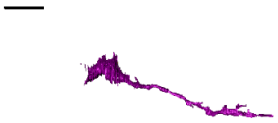	elongate term	186.5	11.1	
127	pr, AVG	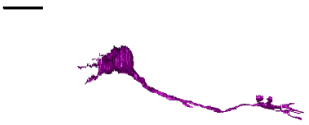	expanded branched term	203.7	14.2	
157	pr, AVG	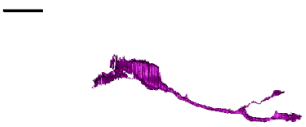	forked	139.4	21.8	
108	pr	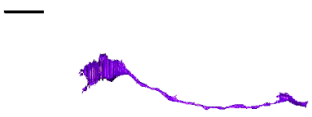	expanded	187.6	12.4	

ID	Sens-ory input	Reconstruction	Term shape	Cell body vol μm^3	Nuclear % of cell body volume	Alternate Name
116	pr		Svterm, elongate term	194.6	14.6	
140	pr	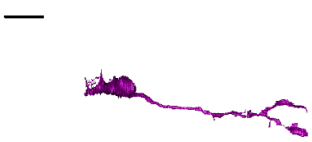	forked term	204.2	11.8	
119	pr, cor	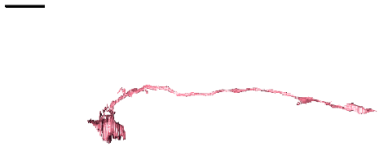	elongate term	314.5	10.2	large ventro-posterior interneuron
135	ant2, pr, ant1 &2 RNs	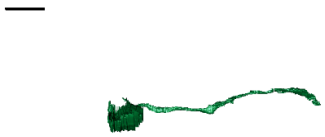	elongate term	278.4	10.8	
143	ant1, pr, ant1 &2 RNs		elongate term	349	10	
152	ant2, pr, ant1 &2 RNs		elongate term	359.4	11.7	

ID	Sens-ory input	Reconstruction	Term shape	Cell body vol μm^3	Nuclear % of cell body volume	Alternate Name
159	ant2, ant1 &2 RNs, pr	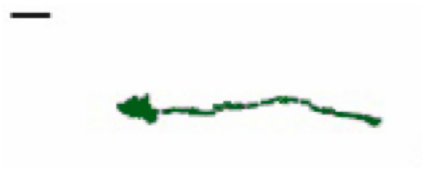	club term	140.1	18.6	
120	ant1 & ant2, ant1 &2 RNs		expanded elongate term	453.6	12.4	large ventro-posterior interneuron
134	ant1 & ant2, ant1 &2 RNs		elongate term	257.2	9.7	large ventro-posterior interneuron
142	ant1 & ant2, ant1 &2 RNs		collateral axons, elongate term	476.5	10.6	large ventro-posterior interneuron
147	ant1, ant1 &2 RNs	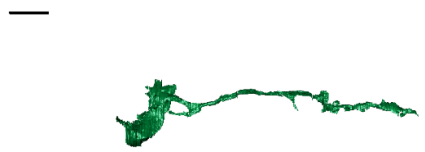	expanded elongate term	277.8	21.3	large ventro-posterior interneuron
153	ant2, ant1 &2 RNs		club term	159.6	10.4	

ID	Sens-ory input	Reconstruction	Term shape	Cell body vol μm^3	Nuclear % of cell body volume	Alternate Name
161	ant1, ant1 &2 RNs		expanded elongate term	416.5	11	
			Means	285.7	12.3	

Appendix F

Morphological characteristics of photoreceptor (PR) cells sorted by Group-row classification. Outer segment projection is described as anterior (osa) posterior (osp) or dorsal (osd) in the canal or ocellus. Reconstructed photoreceptor terminals are shown from a dorsal view and are described in the following column, with volumes and distance of extent on the anterior to posterior axis.

PR	Group-Row	Cell body volume (μm^3)	Outer segment projection	Terminal reconstruction	Terminal description	Terminal volume (μm^3)	A-P terminal distance (μm)
pr-b	II-i	255.83	canal-osp		single, blunt perpendicular	26.76	4.98
pr-c	II-i	237.43	canal-osp		single, expanded	24.79	1.92
pr-a	II-i	245.15	canal-osp		single, expanded	18.77	2.28
pr-d	II-ii	209.79	canal-osp		single, blunt perpendicular	17.92	4.2
pr-e	II-ii	253.14	canal-osd		single, expanded perpendicular	54.73	5.82
pr-f	II-ii	213.55	cana;-osa		single, expanded anteriorly	54.87	2.46

PR	Group-Row	Cell body volume (μm^3)	Outer segment projection	Terminal reconstruction	Terminal description	Terminal volume (μm^3)	A-P terminal distance (μm)
pr-g	II-ii	255.50	canal-osa		single	16.50	8.28
pr23	I-i	228.35	osp		single, expanded posteriorly	46.98	9.42
pr13	I-i	204.68	osp		2 branch, 1 dorsal 1 anterior with expasion	77.23	16.5
pr17	I-i	239.25	osd		expanded perpendicular with branching	47.49	3.06
pr14	I-i	204.21	osp		single short	11.22	4.08
pr15	I-i	352.95	osp		bifid with branching and expansions	120.38	5.52
pr21	I-ii	281.51	osa		single thick to anterior	89.17	7.74

PR	Group-Row	Cell body volume (μm^3)	Outer segment projection	Terminal reconstruction	Terminal description	Terminal volume (μm^3)	A-P terminal distance (μm)
pr19	I-ii	274.41	osa		single expanded to anterior	102.92	7.2
pr18	I-ii	219.24	osa		single, tapered to posterior	16.05	8.22
pr22	I-ii	227.32	osp		single, expanded to anterior	68.46	1.5
pr20	I-ii	344.30	osp	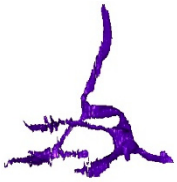	bifid, extensively branched	110.20	6.72
pr2	I-iii	254.18	osa		lateral single	14.08	9.36
pr1	I-iii	276.38	osp		single expanded to anterior	67.45	13.62
pr4	I-iii	264.81	osa	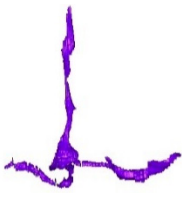	bifid, crossed branches along A-P axis	77.27	12.78

PR	Group-Row	Cell body volume (μm^3)	Outer segment projection	Terminal reconstruction	Terminal description	Terminal volume (μm^3)	A-P terminal distance (μm)
pr5	I-iii	277.95	osa		single thick	21.48	11.7
pr3	I-iv	331.85	osa		single with small branches off expansion	64.20	13.44
pr6	I-iv	294.39	osa		single with expanded 2-lobed perpendicular terminal to anterior	73.04	11.64
pr7	I-iv	301.32	osa		bifid to posterior, expansions on both branches	77.17	15.48
pr8	I-iv	289.96	osa		single, expansion to anteiror with branching	70.69	10.86
pr9	I-v	289.96	osa	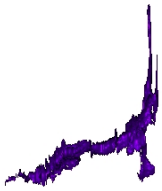	bifid, 1 branch to anterior, 1 dorsal	51.95	7.86
pr10	I-v	344.76	osa		single expanded perpendicular	91.48	5.76

PR	Group-Row	Cell body volume (μm^3)	Outer segment projection	Terminal reconstruction	Terminal description	Terminal volume (μm^3)	A-P terminal distance (μm)
pr11	I-v	270.90	osa		bifid, both branches expanded	62.88	8.34
pr12	I-v	306.64	osa		single expanded to posterior with branches	58.75	14.4
pr16	I-v	233.38	osa	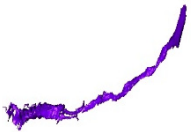	single to anterior with expansion	47.85	5.58

Appendix G

Morphology of photoreceptor relay neurons of the posterior brain vesicle, including reconstructions sorted by presynaptic sensory input: photoreceptor (pr), antenna cell 1 (ant1), antenna cell 2 (ant2), antenna cells 1 and 2 (ant1/2), ascending motor ganglion peripheral intereneurons (AVG), Bipolar planate tail neurons (Plan). Presynaptic relay neuron (RN) input from Eminens peripheral relay neurons (Em), antenna relay neurons (ant 1&2RN), photoreceptor relay neurons (prRN), or peripheral relay neuron (PNRN) is also indicated for each relay neuron. Asterisks in RN input column indicate neurons that are not themselves presynaptic to antenna relay neurons. Reconstructions oriented to left lateral view and aligned across cells.

RN ID	Sensory input	Reconstruction	RN input
86	pr		ant1/2RN, prRN
96	pr		ant1/2RN, prRN
100	pr		ant1/2RN, prRN
112	pr		prRN, *
121	pr		ant1/2RN, prRN
126	pr		ant1/2 RN, pr RN
80	pr	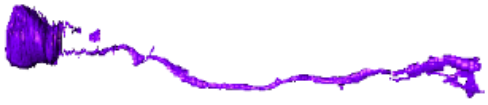	Em, ant1/2RN, prRN

RN ID	Sensory input	Reconstruction	RN input
105	pr		Em, ant1/2RN, prRN
123	pr, Plan	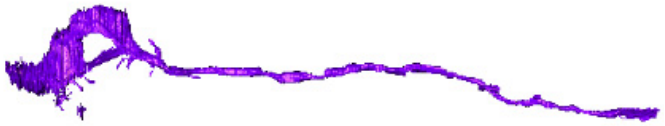	ant1/2RN, prRN
130	pr, Plan		ant1/2RN, prRN
94	pr, AVG		prRN, PNRN
127	pr, AVG	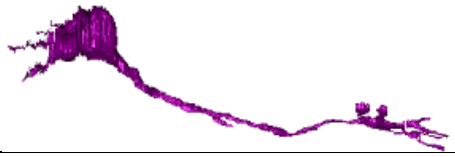	ant1/2RN, prRN, PNRN
108	pr, AVG	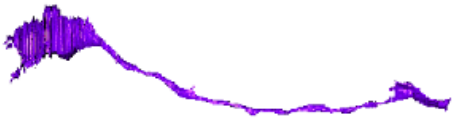	Em, pr RN
140	pr, AVG	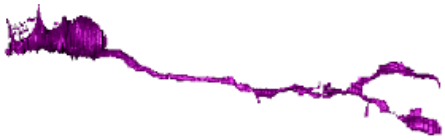	Em, ant1/2RN, prRN
116	pr, AVG, Plan	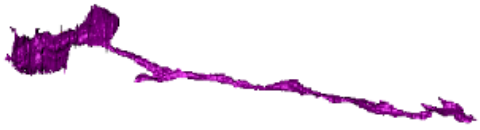	Em, prRN, *
124	pr, AVG, Plan	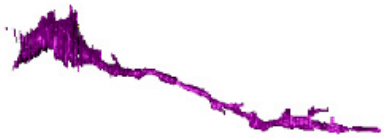	Em, prRN, *
157	pr, AVG, Plan	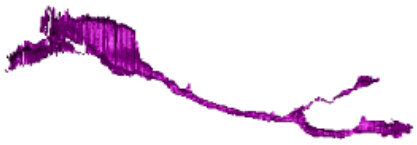	Em, ant1/2RN, prRN, PNRN

RN ID	Sensory input	Reconstruction	RN input
74	pr, AVG, Plan	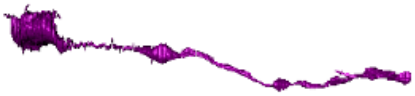	prRN, PNRN
119	pr, cor		ant1/2RN, prRN

Appendix H

Matrix of individual photoreceptor (pr) synapses with relay neurons (pr RN) given by neuron ID. Numbers represent the total number of sections in which a synapse is observed from photoreceptor to relay neuron (I, in black) and from relay neuron to photoreceptor (O, in red). Total values for given for each relay neuron (final 2 columns), and each photoreptor (final 2 rows).

pr	pr-a		pr-b		pr-c		pr-e		pr-f		pr1		pr2		pr3		pr4		pr5	
RN	**I**	**O**	**I**	**O**	**I**	**O**	**I**	**O**	**I**	**O**	**I**	**O**	**I**	**O**	**I**	**O**	**I**	**O**	**I**	**O**
74																				
80											13	3								
86															1					
94											3									
96															11	4				
100																				
103														2						
105	4								5		2				5	3			2	
108				2	7	4														
112							1			1									2	
116					9		10		8	2					7	3	2			
119																4			4	
121											14	1		5		2	20		6	
123									7						4					
124								1	2		2									
126																	10	4		
127							6	2		3							3			
130	2		3	2			3						4		2		3		11	
135																				
140						2			10	4	7	2						4		
143																1				
152																				
157							10	2	1			1		4						
Tot	**6**	**0**	**3**	**4**	**16**	**6**	**30**	**5**	**33**	**10**	**41**	**7**	**4**	**11**	**30**	**17**	**39**	**8**	**27**	**0**

prRN	pr6		pr7		pr8		pr9		pr10		pr11		pr12		pr13		pr15		pr16	
	I	O	I	O	I	O	I	O	I	O	I	O	I	O	I	O	I	O	I	O
74																	6			
80	6	1					3		3								3			
86	11		6						3		4									
94									1	2							2			
96	7		6		10		1		13		5		8							
100							5				3		10							
103																				
105	1		6		5		2						12	2					14	
108	2		4											2						
112			9					2		6			9				9			
116					6	2	4	4	11	7	2		3		2					
119					4								5			2	6			
121	10	4	8				3				6						38			3
123	4	1			18	2	1		7		17	4	7				1			
124																	1			
126	6	4			4						3	2	13	2			10	3	1	
127									1						8	3				
130	1		6						1				17				27		11	
135													2	2						
140																	2			
143			1	4																
152							1								1					
157													2		3					
Total	**48**	**10**	**46**	**4**	**47**	**4**	**20**	**6**	**41**	**15**	**40**	**6**	**90**	**8**	**14**	**5**	**107**	**3**	**26**	**3**

prRN	pr17		pr18		pr19		pr20		pr21		pr22		pr23		pr-d		Total	
	I	O	I	O	I	O	I	O	I	O	I	O	I	O	I	O	**I**	**O**
74								2									**6**	**2**
80	1				7		4				3	1	7				**50**	**5**
86																	**25**	**0**
94					1		4										**11**	**2**
96									1								**62**	**4**
100									2								**20**	**0**
103		7					3										**0**	**9**
105					8								13				**79**	**5**
108	1		2								4						**20**	**8**
112		1					2				2						**34**	**10**
116	1				17		1				11						**94**	**18**
119													4				**23**	**6**
121		3					8	2			9		8			3	**130**	**23**
123	1		3		2						6						**78**	**7**
124							1	4									**6**	**5**
126					2							1					**49**	**16**
127							22	7									**40**	**15**
130			4		7		6						6				**114**	**2**
135																	**2**	**2**
140					1	1	10										**30**	**13**
143																	**1**	**5**
152																	**2**	**0**
157					3		3										**22**	**7**
Total	**4**	**11**	**9**	**0**	**48**	**1**	**61**	**15**	**3**	**0**	**35**	**2**	**38**	**0**		**3**	**890**	**164**

Matrix of individual photoreceptor (pr) synapses with relay neurons (prRN). Numbers represent the total number of synapses from photoreceptor to relay neuron (O, in black) and from relay neuron to photoreceptor (I, in red). Total values for given for each relay neuron (final 2 columns), and each photoreceptor (final 2 rows).

prRN	pr-a		pr-b		pr-c		pr-e		pr-f		pr1		pr2		pr3		pr4		pr5	
	O	I	O	I	O	I	O	I	O	I	O	I	O	I	O	I	O	I	O	I
74																				
80											5	1								
86															1					
94											2									
96															3	1				
100																				
103														1						
105	2								2		2				2	1			1	
108				1	2	1														
112							1			1									1	
116					3		3		2	1					2	2	1			
119																2			1	
121											3	1		2		1	2		3	
123									2						1					
124								1	1		1									
126																	3	2		
127							4	2		1							1			
130	1		1	1			2						1		1		1		5	
135																				
140									6	1	3	1						1		
143																1				
152																				
157							3	1	1	1		1								
Totals	**3**	**0**	**1**	**2**	**5**	**1**	**13**	**4**	**14**	**5**	**16**	**4**	**1**	**3**	**10**	**8**	**9**	**3**	**13**	**0**

prRN	pr6		pr7		pr8		pr9		pr10		pr11		pr12		pr13		pr15		pr16	
	O	I	O	I	O	I	O	I	O	I	O	I	O	I	O	I	O	I	O	I
74																	3			
80	2	1					1		1								1			
86	2		2						1		2									
94									1	1							1			
96	2		2		1		1		1	1	3		2							
100							2				1		3							
103																				
105	1		3		2		1						3	1					2	
108	1		1											1						
112			2					1		1			3				3			
116					3	1	1	2	2	3	2		1		2					
119					2								2	1			2			
121	3	2	3				1				2						11			2
123	1	1			5	1	1		3		3		2	2			1			
124																	1			
126	3	2			2						1	1	5	1			3	2	1	
127									1						4	2				
130	1		4						1				6				8		3	
135													1	1						
140																	1	1		
143			1	2																
152							1								1					
157													1		1					
Total	**16**	**6**	**18**	**2**	**15**	**2**	**9**	**3**	**12**	**6**	**14**	**1**	**30**	**7**	**8**	**2**	**36**	**3**	**6**	**2**

prRN	pr17		pr18		pr19		pr20		pr21		pr22		pr23		pr-d		Total	
	O	I	O	I	O	I	O	I	O	I	O	I	O	I	O	I	O	I
74								1									3	1
80	1				4		2				1	1	4				22	3
86																	8	0
94					1		3										8	1
96									1								16	2
100									1								7	0
103		2						1									0	4
105					4								4				29	2
108	1		1								1						7	3
112		1					1				1						12	4
116	1				6		1				2						29	9
119													1				8	3
121		1					2	1			3		3			1	36	11
123	1		1		1						1						23	4
124							1	1									4	2
126					1							1					19	9
127							5	3									15	8
130			1		5		1						3				45	1
135																	1	1
140					1	1	3										14	5
143																	1	3
152																	2	0
157					2		2	3									10	6
Total	**4**	**4**	**3**	**0**	**25**	**1**	**21**	**10**	**2**	**0**	**9**	**2**	**15**	**0**	**0**	**1**	**323**	**82**

Appendix I

Synaptic connections between RTENs (pna and pnb neurons) sorted by postsynaptic neuron target. Number of sections in which a synapse was observed (Total # of sections), number of synapses (# of synapses) and number of synapses observed in more than one adjacent section (# of synapses >1 section) for each partnership are totaled for each postsynaptic neuron. Classification of presynaptic and postsynaptic neurons are given for each by group (pna or pnb) and its neuropil of origin (L: left or R:right).

Postsynaptic neuron	Synapse	Presynaptic Group (neuropil)	Postsynaptic Group (neuropil)	Total # of sections	# of synapses	# of synapses >1 section
pns5	pns1 (syn) pns5	pna (R)	pna (L)	4	1	1
			Totals:	**4**	**1**	**1**
pns6	pns9 (syn) pns6	pna (L)	pna (L)	14	3	1
	pns13 (syn) pns6	pna (R)	pna (L)	4	1	1
	pns7 (syn) pns6	pnb (L)	pna (L)	5	1	1
	pns10 (syn) pns6	pnb (L)	pna (L)	10	2	2
	pns11 (syn) pns6	pnb (L)	pna (L)	16	3	3
			Totals:	**49**	**10**	**8**
pns9	pns1 (syn) pns9	pna (R)	pna (L)	22	7	4
	pns13 (syn) pns9	pna (R)	pna (L)	1	1	0
	pns7 (syn) pns9	pnb (L)	pna (L)	6	2	2
	pns10 (syn) pns9	pnb (L)	pna (L)	10	3	2
			Totals:	**39**	**13**	**8**
pns14	pns9 (syn) pns14	pna (L)	pna (L)	7	1	1
			Totals:	**7**	**1**	**1**
pns1	pns13 (syn) pns1	pna (R)	pna (R)	13	3	2
	pns10 (syn) pns1	pnb (L)	pna (R)	7	2	2
	pns3 (syn) pns1	pnb (R)	pna (R)	1	1	0
	pns4 (syn) pns1	pnb (R)	pna (R)	3	1	1
	pns12 (syn) pns1	pnb (R)	pna (R)	2	1	1
			Totals:	**26**	**8**	**6**
pns13	pns1 (syn) pns13	pna (R)	pna (R)	17	4	4
	pns12 (syn) pns13	pnb (R)	pna (R)	8	3	2
			Totals:	**25**	**7**	**6**
pns7	pns9 (syn) pns7	pna (L)	pnb (L)	7	3	2
	pns10 (syn) pns7	pnb (L)	pnb (L)	9	2	2
	pns11 (syn) pns7	pnb (L)	pnb (L)	18	8	6
	pns3 (syn) pns7	pnb (R)	pnb (L)	15	5	2
	pns4 (syn) pns7	pnb (R)	pnb (L)	7	2	2
			Totals:	**56**	**20**	**14**
pns10	pns9 (syn) pns10	pna (L)	pnb (L)	1	1	0
	pns7 (syn) pns10	pnb (L)	pnb (L)	2	1	1
	pns11 (syn) pns10	pnb (L)	pnb (L)	7	2	2
	pns12 (syn) pns10	pnb (R)	pnb (L)	13	4	4

Postsynaptic neuron	Synapse	Presynaptic Group (neuropil)	Postsynaptic Group (neuropil)	Total # of sections	# of synapses	# of synapses >1 section
			Totals:	**23**	**8**	**7**
pns11	pns9 (syn) pns11	pna (L)	pnb (R)	9	3	2
	pns7 (syn) pns11	pnb (L)	pnb (L)	17	4	4
	pns10 (syn) pns11	pnb (L)	pnb (L)	27	8	4
	pns12 (syn) pns11	pnb (R)	pnb (L)	4	2	1
	pns3 (syn) pns11	pnb (R)	pnb (L)	1	1	0
			Totals:	**58**	**18**	**11**
pns3	pns1 (syn) pns3	pna (R)	pnb (R)	2	1	1
	pns13 (syn) pns3	pna (R)	pnb (R)	7	2	2
	pns7 (syn) pns3	pnb (L)	pnb (R)	10	4	4
	pns10 (syn) pns3	pnb (L)	pnb (R)	15	3	3
	pns11 (syn) pns3	pnb (L)	pnb (R)	5	2	2
	pns4 (syn) pns3	pnb (R)	pnb (R)	2	1	1
	pns12 (syn) pns3	pnb (R)	pnb (R)	10	5	3
			Totals:	**51**	**18**	**16**
pns4	pns1 (syn) pns4	pna (R)	pnb (R)	3	1	1
	pns13 (syn) pns4	pna (R)	pnb (R)	4	1	1
	pns7 (syn) pns4	pnb (L)	pnb (R)	6	2	2
	pns10 (syn) pns4	pnb (L)	pnb (R)	21	5	4
	pns11 (syn) pns4	pnb (L)	pnb (R)	2	1	1
	pns3 (syn) pns4	pnb (R)	pnb (R)	10	3	2
	pns12 (syn) pns4	pnb (R)	pnb (R)	6	3	3
			Totals:	**52**	**16**	**14**
pns12	pns7 (syn) pns12	pnb (L)	pnb (R)	6	2	2
	pns10 (syn) pns12	pnb (L)	pnb (R)	12	5	4
	pns11 (syn) pns12	pnb (L)	pnb (R)	3	1	1
	pns3 (syn) pns12	pnb (R)	pnb (R)	13	4	3
	pns4 (syn) pns12	pnb (R)	pnb (R)	4	15	3
			Totals:	**38**	**27**	**13**

Appendix J

Comparison of connections of left and right neuron pairs in the motor ganglion and tail with their postsynaptic partners. Postsynaptic partners exclude relay or sensory neurons (with the exception of Eminens neurons), and paired postsynaptic partners are designated as contralateral (co) or ipsilateral (i) where appropriate. Synapses and gap junctions are given by total number of sections with an observed synapse or gap junction between neurons, with the greater value between left and right in bold.

Presynaptic Neuron	Postsynaptic neuron	Synapses		Gap junctions	
		Left	Right	Left	Right
ddN	**Em2**	6	4	18	10
	AVG2			0	**3**
	AVG3	**5**	0		
	AVG4	**14**	0	0	**6**
	ddN (o)	**3**	0		
	MN1 (i)	**6**	0		
	MN1(co)	17	13		
	MN2 (co)	45	**57**	23	22
	MN3 (co)	0	**10**		
	MN4R (co)	**11**	0		
	MN5R (co)	**13**	0		
	VGN1 (i)	0	**2**		
	VGN1 (co)	9	14		
	VGN2 (co)	0	**21**	6	3
	VGN3 (co)	25	**58**		
	ACIN1 (i)	**12**	N/A		
	ACIN2 (co)			0	**3**
	PVGN1 (co)	**19**	N/A	**2**	0
	midtail2/4 (co)	**21**	8		
	Plan1/2 (co)	15	**60**	**8**	0
	Plan3/4 (co)	39	**58**	**2**	0
	bm	52	54		
VGN1	**Em1**	9	5		
	Em2	4	1		
	AVG6	**3**	0		
	ddN(i)	**1**	0		
	ddN(co)	10	6		
	MN1 (i)			7	5
	MN1	4	**18**	34	34
	MN3	10	8		
	MN4			5	3
	MN5	6	5		

Presynaptic Neuron	Postsynaptic neuron	Synapses		Gap junctions	
		Left	Right	Left	Right
	VGN1 (co)	5	2	27	
	VGN1 (i)			2	6
	VGN2	**60**	5	**18**	0
	VGN3	20	23		
	ACIN1	**10**	N/A	**5**	0
	ACIN2	13	9		
	Plan1/2	1	**44**		
	Plan3/4	11	**50**		
	bm	**52**	20		
VGN2	**AVG3**	0	**1**		
	ddN	**73**	41	3	6
	MN1	6	8		
	MN2	18	**73**	23	**39**
	MN3	**10**	0		
	MN4	7	12	2	6
	MN5	11	10	0	**2**
	VGN1	**19**	12	**18**	0
	VGN3	7	5		
	ACIN1	**12**	N/A	**5**	0
	ACIN2	**27**	3	7	12
	PVGN1	0	**3**	0	**4**
	Plan1/2	**34**	24	0	**2**
	Plan3/4	58	56		
	mu	**16**	8		
	bm	24	**61**		
	midtail1	N/A	**7**		
	midtail2/4	**35**	17		
VGN3	**Em2**	**9**	3		
	ddR	**31**	19		
	MN1L	12	**20**		
	MN2L	3	2	2	5
	VG1L	22	22		
	VG2L	19	**29**		
	ACIN2L	**2**	0		
	Plan3	1	**6**		
	notochord	0	**2**		
	bm	116	127		
MN1	**Em1**	4	**12**		
	Em2	3	**6**	0	**6**
	AVG2	0	**1**		
	AVG3	0	**2**		

Presynaptic Neuron	Postsynaptic neuron	Synapses		Gap junctions	
		Left	Right	Left	Right
	AVG4	0	**9**		
	AVG5	**4**	0		
	AVG7	**4**	2		
	ddN	10	**11**		
	MN1 (i)	**2**	0		
	MN1	**2**	1		
	MN2	**20**	10	28	**35**
	MN4	1	**6**	**3**	0
	MN5	**6**	**6**	0	**3**
	VGN1 (Co)			**7**	5
	VGN1	5	**11**	**34**	**34**
	VGN2	2	**7**		
	VGN3	**10**	0		
	VGN2(co)	0	**6**		
	ACIN1L	**11**	N/A		
	PVGN1	N/A	**6**	0	**2**
	Plan1	12	**25**		
	Plan3	9	**23**		
	mul	948	**1136**		
	mulm	140	**533**		
	notochord	**46**	31		
	bm	**6**	2		
MN2	**ddN**	7	**39**	22	**23**
	MN1	0	**1**	28	**35**
	MN3	**8**	0	**7**	6
	MN4	11	**15**	**55**	33
	MN5	**9**	6	0	**12**
	VGN2	17	**29**	23	**39**
	VGN3	0	**1**	2	**5**
	ACIN1 (i)			**5**	0
	ACIN2 (i)	3	**14**	**12**	8
	PVGN1	N/A	**51**	0	**37**
	PVGN2	N/A	**1**		
	Plan1/2	6	**25**		
	Plan3/4	**44**	3		
	midtail2/4	**4**	0	**8**	0
	mu	**1700**	1648		
	bm	**49**	5		
MN3	**MN1**	0	**3**		
	MN2	0	**19**	**7**	6
	MN4	4	**16**	**4**	0

Presynaptic Neuron	Postsynaptic neuron	Synapses		Gap junctions	
		Left	Right	Left	Right
	MN5			**2**	0
	VG1L	2	**3**		
	VG2L	5	**3**		
	ACIN1L	**2**	0		
	ACIN2L	**5**	0		
	PVGN1	N/A	**3**		
	PVGN2	N/A	**7**		
	Plan2/4	0	**3**		
	mul	**155**	102		
MN4	**ddN**	**6**	0		
	MN1	**1**	0	**3**	0
	MN2	8	**17**	**55**	33
	MN3	3	**6**		
	MN5	**3**	2	0	**6**
	VGN1			**5**	3
	VGN2	**12**	5	0	**6**
	ACIN2			**5**	0
	PVGN1			0	**6**
	PVGN2	N/A	**3**		
	Plan1/2	1	**2**	0	**2**
	Plan3/4	**2**	1	0	**2**
	mul	**181**	115		
	bm	**26**	12		
MN5	**ddN**	0	**23**		
	MN2	**13**	1	0	**12**
	MN3	**2**	1	**2**	0
	MN4	1	**3**	0	**6**
	VGN1	0	**8**		
	VGN2			0	**2**
	PVGN1	N/A	**15**	0	**28**
	mul	**123**	55		
	bm	0	**42**		
ACIN2	**ddN (co)**			**3**	0
	MN2 (i)	1	**9**	**12**	8
	MN3 (i)	2	**3**		
	MN4 (i)	**2**	0	**5**	0
	VGN1 (i)	**6**	0		
	VGN1 (co)	**42**	0		
	VGN2 (i)	**3**	2	7	**12**
	VGN2 (co)	**10**	0		
	VGN3	**2**	0		

Presynaptic Neuron	Postsynaptic neuron	Synapses		Gap junctions	
		Left	Right	Left	Right
	PVGN1			0	**7**
	Plan2	**10**	2		
	ep	11	**17**		
	bm	**51**	34		
Plan1/2	**Em1**	**37**	12	**7**	6
	Em2	16	**19**		
	AVG1	0	**19**		
	AVG2	5	**22**		
	AVG3	15	**23**		
	AVG4	**1**	0		
	AVG5	0	**14**		
	AVG6	0	**24**		
	ddN (i)	**10**	0		
	ddN (co)	7	**36**	0	**8**
	MN1 (i)	**134**	94		
	MN1 (co)	**14**	0		
	MN2	52	**92**		
	MN3	**3**	0		
	MN4	**9**	5	0	**2**
	MN5	**3**	0		
	VGN1 (i)	21	**44**		
	VGN1 (co)	**6**	4		
	VGN2	**40**	13	0	**2**
	VGN3	0	**6**		
	ACIN2	0	**3**		
	PVGN1	N/A	**15**		
	midtail1	0	**11**		
	midtail2/4	0	**5**		
	Plan1/2 (i)	**3**	0		
	Plan1/2 (co)	14	**15**		
	Plan3/4 (co)	0	**4**	**4**	0
	Plan3 (i)	27	**30**		
	mu	1	**34**		
	bm	**13**	0		
Plan3/4	**Em1**	3	**7**		
	Em2	**6**	0		
	AVG2	**4**	3		
	AVG3	0	**3**		
	AVG4	**3**	0		
	AVG5	**15**	8	7	**8**
	AVG6	4	**14**		

Presynaptic Neuron	Postsynaptic neuron	Synapses		Gap junctions	
		Left	Right	Left	Right
	AVG7	0	**4**		
	ddN (co)	18	**49**	0	**2**
	MN1 (co)	**4**	0		
	MN1L (i)	**88**	55		
	MN2L (i)	32	**73**		
	MN3 (i)	0	**1**		
	MN4R (i)	0	**2**	0	**2**
	MN5R (i)	0	**3**		
	VGN1 (co)	2	**7**		
	VGN1 (i)	13	**24**		
	VGN2	26	**99**		
	VGN3	0	**1**		
	ACIN2 (i)	0	**6**		
	PVGN1	N/A	**5**		
	midtail1	N/A	**1**		
	midtail2/4	**5**	1		
	Plan1/2 (i)	26	**43**	**4**	0
	Plan3/4 (co)	1	1		
	Plan3/4 (i)	0	**2**	0	**6**
	ep	**8**	7		
	mu	**8**	0		
	bm	**6**	0		